Zhen Fang
Richard L. Smith, Jr. *Editors*

Production of Biofuels and Chemicals from Lignin

Springer

Biofuels and Biorefineries

Volume 6

Aims and Scope of the Series

The Biofuels and Biorefineries Series aims at being a comprehensive and integrated reference for biomass, bioenergy, biofuels, and bioproducts. The Series provides leading global research advances and critical evaluations of methods for converting biomass into biofuels and chemicals. Scientific and engineering challenges in biomass production and conversion are covered that show technological advances and approaches for creating new bio-economies in a format that is suitable for both industrialists and environmental policy decision-makers.

The Biofuels and Biorefineries Series provides readers with clear and conciselywritten chapters that are peer-reviewed on significant topics in biomass production, biofuels, bio-products, chemicals, catalysts, energy policy, economics and processing technologies. The text covers major fields in plant science, green chemistry, economics and economy, biotechnology, microbiology, chemical engineering, mechanical engineering and energy.

Series Description

Annual global biomass production is about 220 billion dry tons or 4,500 EJ, equivalent to 8.3 times the world's energy consumption in 2014 (543 EJ). On the other hand, world-proven oil reserves at the end of 2011 reached 1652.6 billion barrels, which can only meet 54.2 years of global production. Therefore, alternative resources are needed to both supplement and replace fossil oils as the raw material for transportation fuels, chemicals and materials in petroleum-based industries. Renewable biomass is a likely candidate, because it is prevalent over the Earth and is readily converted to other products. Compared with coal, some of the advantages of biomass are: (i) its carbon-neutral and sustainable nature when properly managed; (ii) its reactivity in biological conversion processes; (iii) its potential to produce bio-oil (ca. yields of 75%) by fast pyrolysis because of its high oxygen content; (iv) its low sulphur and lack of undesirable contaminants (e.g. metals, nitrogen content) (v) its wide geographical distribution and (vi) its potential for creating jobs and industries in energy crop productions and conversion plants. Many researchers, governments, research institutions and industries are developing projects for converting biomass including forest woody and herbaceous biomass into chemicals, biofuels and materials and the race is on for creating new "biorefinery" processes needed for future economies. The development of biorefineries will create remarkable opportunities for the forestry sector, biotechnology, materials, chemical processing industry, and stimulate advances in agriculture. It will help to create a sustainable society and industries that use renewable and carbon-neutral resources.

More information about this series at http://www.springer.com/series/11687

Zhen Fang • Richard L. Smith, Jr.
Editors

Production of Biofuels
and Chemicals
from Lignin

Springer

Editors
Zhen Fang
Biomass Group, College
 of Engineering
Nanjing Agricultural University
Nanjing, Jiangsu, China

Richard L. Smith, Jr.
Research Center of Supercritical
 Fluid Technology, Graduate School
 of Environmental Studies
Tohoku University
Sendai, Japan

Preface

Lignin is the largest source of renewable aromatics in the world. Most lignins are produced as a by-product in huge quantities by the pulp-and-paper industry in the form of black liquor (ca. 50 million tonnes/a) but are also expected to be a major by-product in emerging industries related to biofuels and bioproducts (ca. 2.7–8.1 million tonnes/a). Due to the highly stable structure of lignin that consists of cross-linked phenylpropane (C6–C3) units, most lignin by-products are combusted or used as a low-grade fuel rather than being upgraded to oil or gas or recovered to produce chemicals or materials. The present text provides state-of-the-art reviews; current research and prospects on lignin production; lignin biological, thermal and chemical conversion; and lignin technoeconomics. Fundamental topics related to lignin chemistry, properties, analysis, characterisation, depolymerisation mechanisms and enzymatic, fungal and bacterial degradation methods are covered. Practical topics related to technologies for lignin and ultra-pure lignin recovery, activated carbon, carbon fibre production and materials are covered. Biological conversion of lignin with fungi, bacteria or enzymes to produce chemicals is considered along with chemical, catalytic, thermochemical and solvolysis conversion methods. A case study is presented for practical polyurethane foam production from lignin. Lignin has a bright future and will be an essential feedstock for producing renewable chemicals, biofuels and value-added products.

This book is the sixth book of the series entitled, "Biofuels and Biorefineries", and it contains 13 chapters contributed by leading experts in the field. The text is arranged into four key areas:

Part I: Lignin and Its Production (Chapters 1–3)
Part II: Biological Conversion (Chapters 4–6)
Part III: Chemical Conversion (Chapters 7–12)
Part IV: Technoeconomics (Chapter 13)

Chapter 1 introduces lignin chemistry, characterisation techniques and general applications of lignin resources with a biorefinery concept. **Chapter 2** reviews methods for isolating lignin derivatives from pulping spent liquors and gives main

challenges and perspectives in the development of viable lignin production processes. **Chapter 3** presents new technologies for recovering ultra-pure lignins from alkaline liquor streams generated either from a pulp-and-paper mill or a lignocellulosic biofuels refinery. **Chapter 4** summarises recent advances in lignin-degrading enzymes (lignin-oxidising and lignin-degrading auxiliary enzymes) produced by wood-degrading fungi and bacteria. Structural and functional aspects of lignin-degrading auxiliary enzymes are covered along with discussion on genomic studies of lignin-degrading fungi. **Chapter 5** describes bacterial lignin-oxidising enzymes, such as dye-decolorising peroxidases, bacterial laccases and beta-etherase enzyme, the current knowledge of bacterial lignin degradation pathways and current efforts to produce renewable chemicals from polymeric lignin using bacterial fermentation. **Chapter 6** offers a critical overview of the latest concepts and achievements in lignin biological degradation, focusing on fungi, bacteria and enzymes as catalysts to produce chemicals and their use for novel applications. **Chapter 7** focuses on the chemical modifications of lignin for its selective depolymerisation to monomers as aromatic feedstock chemicals and on using lignin as the starting point for novel smart materials. **Chapter 8** introduces carbon materials from lignin and discusses the characterisation and potential applications of activated carbons, carbon fibres and nanostructured, hierarchical and highly ordered carbons. **Chapter 9** deals with the fundamentals of lignin pyrolysis and catalytic upgrading and reviews significant advances in this area. **Chapter 10** gives conceptual guidelines for using solvolysis with lignin and optimisation of lignin depolymerisation process for value-added chemical production. **Chapter 11** covers molecular mechanisms associated with the thermochemical conversion of lignins and provides principles for design of pyrolysis-based lignin conversion processes to produce specific bio-oils, chemicals and biofuels. **Chapter 12** introduces major works investigating the depolymerisation mechanisms of lignin and to provide pyrolysis product formation and distribution pathways through the combination of experimental results and computational simulations. **Chapter 13** uses multi-criteria analysis to give a comprehensive assessment of integrated lignin-based biorefinery processes. An industrial case study, involving a lignin recovery rate of up to 100 tonnes/day from a softwood kraft pulping mill for the production of polyurethane foam and carbon fibre, is demonstrated and analysed.

The text should be of interest to students, researchers, academicians and industrialists who are working in the areas of renewable energy, environmental and chemical sciences, engineering, resource development, biomass processing, sustainability, materials, biofuels and pulp-and-paper industries.

Nanjing, Jiangsu, China   Zhen Fang
Sendai, Japan   Richard L. Smith, Jr.

Acknowledgements

Dr. Takafumi Sato, Utsunomiya University, Japan

Dr. Davide Savy, Università di Napoli Federico II, Italy

Prof. Eric Spinnler, Paris Institute of Technology for Life, Food and Environmental Sciences, France

Prof. Mark C. Thies, Clemson University, USA

Dr. Luvuyo Tyhoda, Stellenbosch University, South Africa

Dr. Huamin Wang, Pacific Northwest National Laboratory, USA

Prof. Shurong Wang, Zhejiang University, China

Prof. David Wilson, Cornell University, USA

Prof. Shubin Wu, South China University of Technology, China

Dr. Qingang Xiong, Oak Ridge National Lab, USA

Dr. Ying Zhang, University of Science and Technology of China, China

Special thanks and commendation from the editors are given to Dr. Xiaofei Tian (South China University of Technology) for his dedication and extensive help in the design and support of many aspects of the text and its chapters.

We are also grateful to Ms. Becky Zhao (senior editor) and Ms. Abbey Huang (editorial assistant) for their encouragement, assistance and guidance during preparation of the book.

Finally, we would like to express our deepest gratitude towards our families for their love, understanding and encouragement, which help us in the completion of this project.

June 10, 2016, in Kunming
June 10, 2016, in Sendai

(Zhen Fang)

(Richard L. Smith, Jr.)

Contents

Contributors

Olumoye Ajao Natural Resources Canada, CanmetENERGY, Varennes, QC, Canada

Xianglan Bai Department of Mechanical Engineering, Iowa State University, Ames, IA, USA

Marzouk Benali Natural Resources Canada, CanmetENERGY, Varennes, QC, Canada

Timothy D.H. Bugg Department of Chemistry, University of Warwick, Coventry, UK

Jiachuan Chen Key Laboratory of Pulp and Paper Science and Technology of Ministry of Education, Qilu University of Technology, Jinan, China

Chongbo Cheng Key Lab of Thermal Energy Conversion and Control of MoE, Southeast University, Nanjing, China

Tomás Cordero Andalucía Tech, Departamento de Ingeniería Química, Universidad de Málaga, Málaga, Spain

Zhen Fang Biomass Group, College of Engineering, Nanjing Agricultural University, Nanjing, Jiangsu, China

Pedram Fatehi Key Laboratory of Pulp and Paper Science and Technology of Ministry of Education, Qilu University of Technology, Jinan, China

Chemical Engineering Department, Lakehead University, Thunder Bay, ON, Canada

Gil Garnier Department of Chemical Engineering, Bioresource Processing Research Institute of Australia (BioPRIA), Monash University, Clayton, VIC, Australia

Banafsheh Gilani Natural Resources Canada, CanmetENERGY, Varennes, QC, Canada

Jawad Jeaidi Natural Resources Canada, CanmetENERGY, Varennes, QC, Canada

Ayyappa Kumar Sista Kameshwar Department of Biology, Lakehead University, Thunder Bay, ON, Canada

Haruo Kawamoto Graduate School of Energy Science, Kyoto University, Kyoto, Japan

Kwang Ho Kim Deconstruction Division, Joint BioEnergy Institute, Emeryville, CA, USA

Adam S. Klett Department of Chemical and Biomolecular Engineering, Clemson University, Clemson, SC, USA

Christopher S. Lancefield Department of Chemistry and Biomedical Sciences Research Complex, University of St. Andrews and EaStCHEM, St. Andrews, Fife, UK

Mingyou Liu School of Light Industry and Engineering, South China University of Technology, Guangzhou, China

Nana Liu Key Lab of Thermal Energy Conversion and Control of MoE, Southeast University, Nanjing, China

Lionel Longe School of Chemistry, Bioresource Processing Research Institute of Australia (BioPRIA), Monash University, Clayton, VIC, Australia

Rui Lou Key Laboratory of Papermaking Technology and Special Paper Development of Shaanxi Provence, Shaanxi University of Science and Technology, Xi'an, China

Gaojin Lyu Key Lab of Pulp and Paper Science and Technology of the Ministry of Education, Qilu University of Technology, Jinan, China

State Key Laboratory of Pulp and Paper Engineering, South China University of Technology, Guangzhou, China

Behrang Mansoornejad Natural Resources Canada, CanmetENERGY, Varennes, QC, Canada

Isabella Panovic Department of Chemistry and Biomedical Sciences Research Complex, University of St. Andrews and EaStCHEM, St. Andrews, Fife, UK

Wensheng Qin Department of Biology, Lakehead University, Thunder Bay, ON, Canada

Rahman Rahmanpour Department of Chemistry, University of Warwick, Coventry, UK

Goran M.M. Rashid Department of Chemistry, University of Warwick, Coventry, UK

Juan J. Rodríguez Sección de Ingeniería Química, Universidad Autónoma de Madrid, Madrid, Spain

José Rodríguez-Mirasol Andalucía Tech, Departamento de Ingeniería Química, Universidad de Málaga, Málaga, Spain

Kei Saito School of Chemistry, Monash University, Clayton, VIC, Australia

Dekui Shen Key Lab of Thermal Energy Conversion and Control of MoE, Southeast University, Nanjing, China

Richard L. Smith, Jr. Research Center of Supercritical Fluid Technology, Graduate School of Environmental Studies, Tohoku University, Sendai, Japan

Mark C. Thies Department of Chemical and Biomolecular Engineering, Clemson University, Clemson, SC, USA

Xiaofei Tian School of Bioscience and Bioengineering, South China University of Technology, Guangzhou, China

Nicholas J. Westwood Department of Chemistry and Biomedical Sciences Research Complex, University of St. Andrews and EaStCHEM, St. Andrews, Fife, UK

Shubin Wu State Key Laboratory of Pulp and Paper Engineering, South China University of Technology, Guangzhou, China

Zhenqiang Wu School of Bioscience and Bioengineering, South China University of Technology, Guangzhou, China

Rui Xiao Key Lab of Thermal Energy Conversion and Control of MoE, Southeast University, Nanjing, China

Editors' Biography

Zhen Fang is professor and leader of the biomass group in Nanjing Agricultural University. He is the inventor of the "fast hydrolysis" process. He is listed in the "Most Cited Chinese Researchers" in energy for 2014 and 2015 (Elsevier-Scopus). Professor Fang specialises in thermal/biochemical conversion of biomass, nanocatalyst synthesis and its applications and pretreatment of biomass for biorefineries. He obtained his PhDs from China Agricultural University (biological and agricultural engineering, Beijing) and McGill University (materials engineering, Montreal). Professor Fang is associate editor of *Biotechnology for Biofuels* and is serving on editorial boards of major international journals in energy.

Richard L. Smith, Jr., is professor of chemical engineering at the Graduate School of Environmental Studies, Research Center of Supercritical Fluid Technology, Tohoku University, Japan. Professor Smith has a strong background in physical properties and separations and obtained his PhD in chemical engineering from the Georgia Institute of Technology (USA). His research focuses on developing green chemical processes especially those that use water and carbon dioxide as the solvents in their supercritical state. He has expertise in physical property measurements and in separation techniques with ionic liquids and has published more than 200 scientific papers, patents and reports in the field of chemical engineering. Professor Smith is the Asia regional editor for the *Journal of Supercritical Fluids* and has served on editorial boards of major international journals associated with properties and energy.

Part I
Lignin and Its Production

Chapter 1
Properties, Chemical Characteristics and Application of Lignin and Its Derivatives

Xiaofei Tian, Zhen Fang, Richard L. Smith, Jr., Zhenqiang Wu, and Mingyou Liu

1.1 Occurrence of Lignin in Biomass

1.1.1 Source, Monolignol Constituents and Sub-unit Structures

The term 'lignin' is used to describe complicated and undefined phenolic biopolymers that bind together with cellulose and hemicelluloses to form plant cell wall structures [1]. As one of the three major constituents in lignocellulosic biomass, lignin makes up between 15 and 40 % of dry mass fraction in natural woody plants [2, 3]. With high molecular weight in the range of 100 kDa, lignin is a three-dimensional heterogeneous macromolecule containing many phenylpropanoid units that are the oxidative polymerization of three types of hydroxycinnamyl alcohol sub-units (monolignols) [3–5]. The monolignols are the *p*-hydroxyphenyl (H), guaiacyl (G) and syringyl (S) phenylpropanoid units with structural differences in the extent of methoxylation at the 3′ or 3′–5′ position of phenolic rings (Fig. 1.1). The complex inter-molecular structure of lignin is due to the combination of different

X. Tian • Z. Wu
School of Bioscience and Bioengineering, South China University of Technology,
382 Outer Ring Road East, Guangzhou University Mega Centre, 510006 Guangzhou, China
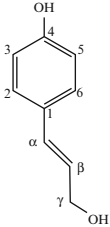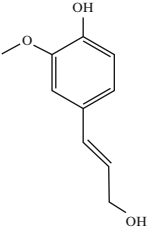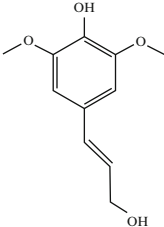
Z. Fang (✉)
Biomass Group, College of Engineering, Nanjing Agricultural University,
40 Dianjiangtai Road, 210031 Nanjing, Jiangsu, China
e-mail: zhenfang@njau.edu.cn

R.L. Smith, Jr.
Research Center of Supercritical Fluid Technology, Graduate School of Environmental Studies, Tohoku University, Aoba-ku, Sendai 980-8579, Japan

M. Liu
School of Light Industry and Engineering, South China University of Technology,
381 Wushan Road, Tianhe District, 510641 Guangzhou, China

Structure of monolignols		
4-hydroxyphenyl (H)	Guaiacyl (G)	Syringyl (S)

Source	Content (%, *w/w*) [8]		
Softwood lignin	-	90-95	5-10
Hardwood lignin	-	50	50
Grass lignin	5	75	25

Fig. 1.1 Three sub-units of lignin and their relative content in lignocellulosic biomass

amounts of monolignols and distinct substitution patterns on their phenylpropanoid units [6, 7].

Lignin biopolymers contain a variety of ether and carbon-carbon inter-molecular linkages or bonds, such as β-O-4, 5-O-4, β-5, β-1, β-β, and 5–5 (Fig. 1.2) [4, 5, 8]. The predominant β-O-4 ether linkage type (also called arylglycerol-β-aryl) has proportions of 40–60 % among all inter-unit linkages in lignin [9]. Therefore, they commonly act as the major targets for tracking structural changes that take place during lignin fractionation or de-polymerization. It has been proposed that lignin biopolymers are not random, but have a helical structure characteristic of naturally synthesized molecules [10]. Various inter-molecular linkages between different phenylpropane sub-units contribute to the heterogeneous feature of the three-dimensional network structure of lignin.

1.1.2 Distribution, Content and Chemical Structures of Lignin Sub-units

In softwoods, the average content of lignin varies between 25 and 30 % (*w/w*) [11]. Softwood lignin is predominantly composed of a large proportion of guaiacyl (G) as well as some un-methoxylated p-hydroxyphenyl (H) sub-units (Fig. 1.3). Hardwood lignin content ranges from 22 to 27 % (*w/w*) [12] and is formed from co-polymerization of G and S sub-units [4, 5] (Fig. 1.4). In grass, lignin can be
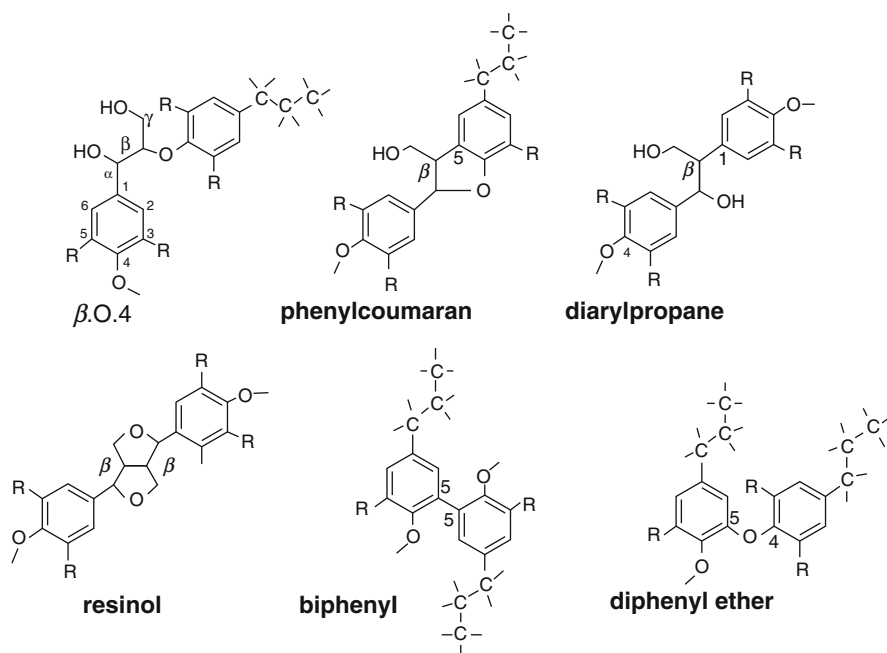
Fig. 1.2 Principal linkages between lignin sub-units R=H in hydroxyphenyl; R=OMe at C-3 and R=H at C-5 in guaiacyl; R=OMe in syringyl; Phenolic groups at C-4 may be free or etherified (Reproduced with copyright permission from Ref. [8]. Copyright © 1993 American Society of Agronomy, Crop Science Society of America, Soil Science Society of America)
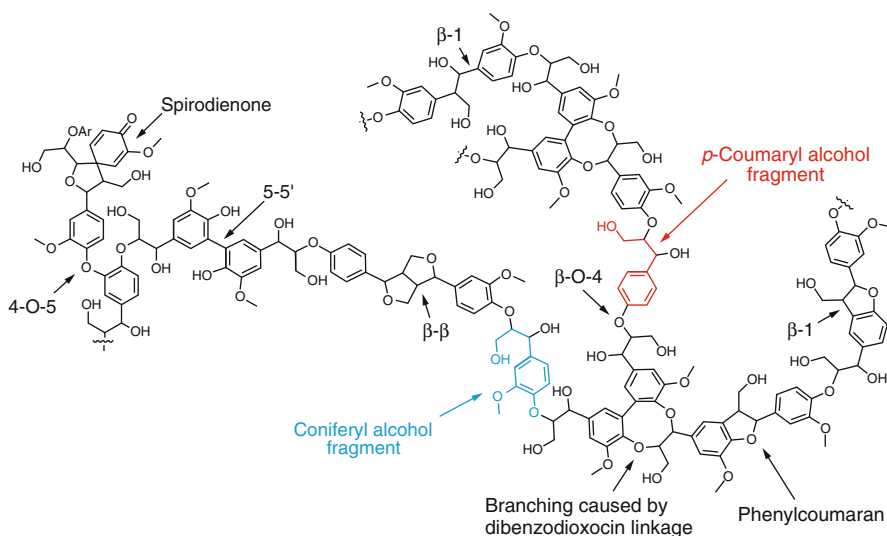
Fig. 1.3 Schematic representation of a softwood lignin structure (Reproduced with copyright permission from Ref. [19]. Copyright © 2010, American Chemical Society)
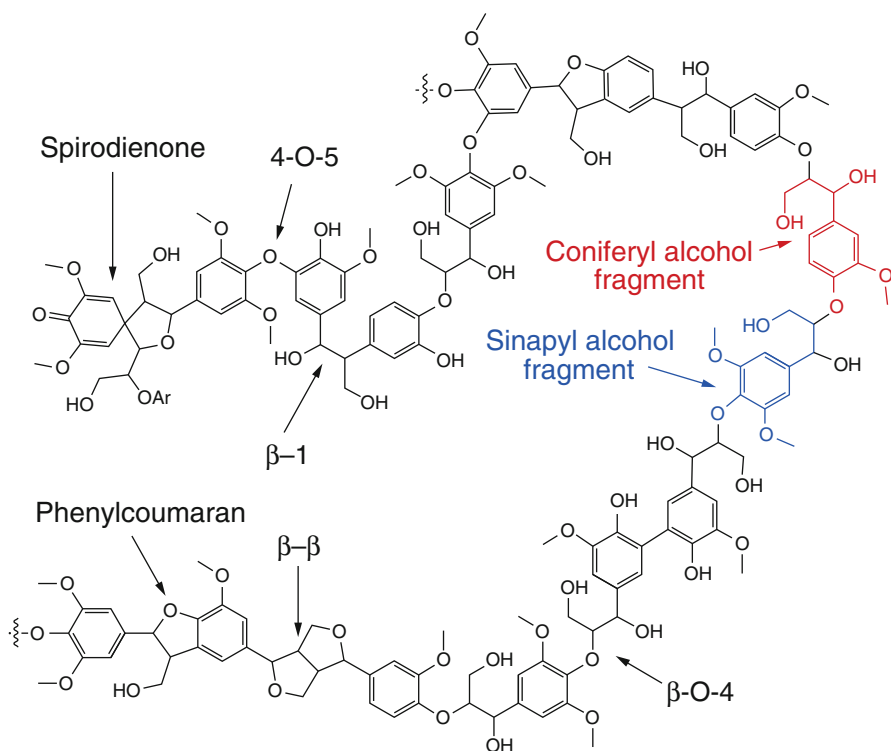
Fig. 1.4 Schematic representation of a hardwood lignin structure (Reproduced with copyright permission from Ref. [19]. Copyright © 2010 American Chemical Society)

composed of all H, G, and S sub-units and its content may vary from 1 to 19 % (*w/w*) of the total dry matter depending on plant species or growth stages [13, 14]. The chemical structure of softwood lignin does not vary much between plant species [15, 16], while hardwood lignin structures vary greatly from one plant species to another. The major inter-species difference in hardwood lignins is the S/G ratio, which influences structural features, such as amount of *β*-O-4 linkages, degree of condensation, or methoxyl content [12]. The differences between softwood and hardwood lignin also impact the application of lignin and its derivatives. For example, hardwood lignins contain more methoxyl groups than softwood lignins. The presence of methoxy groups helps to release more phenolics, methanol and CH_4 from hardwood lignin than softwood lignins in thermochemical processes [17]. Moreover, high methoxyl group content of hardwood lignins tend to give less condensed structures after pyrolysis than softwood lignins [18].

For condensed structures caused by higher proportion of H sub-units in lignin with *β*-5, *β*-1, *β*-*β*, 5–5, and 5-O-4 inter-molecular linkages, softwood has stronger recalcitrant resistance against degrading or decomposing attacks than other
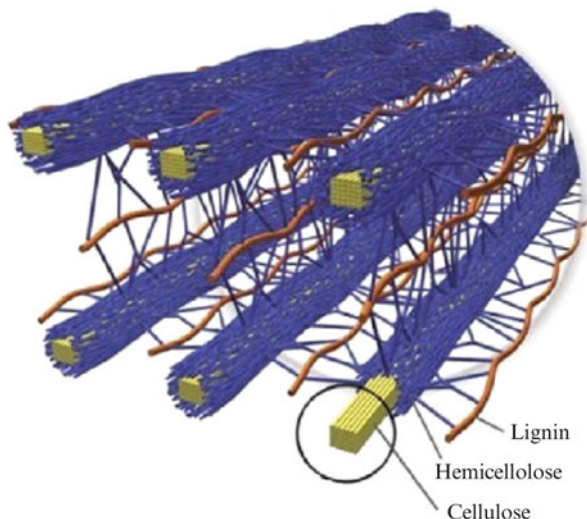
Fig. 1.5 Cellulose strands surrounded by hemicellulose and lignin (Reproduced with copyright permission from Ref. [26]. Copyright © 2010 Elsevier B.V.)

lignocellulosic biomass [8, 20, 21]. Therefore, usual pre-treatment techniques (such as, ammonia fiber explosion and dilute-acid pre-treatment methods) that work efficiently on de-structuring the hardwood or herbal biomass for subsequent enzymatic saccharification do not perform well on softwood due to its recalcitrant resistance [22, 23]. Besides the plant species, the sub-unit composition and linkage patterns in lignin vary depending on the seasons, habitat, and growth stage of the plants, as well as location of lignin in the cell wall [24]. Among these factors, the location of lignin may play a universal role. For example, wood at the top of a mature conifer tends to have higher lignin content compared with other parts of the plant [11].

In typical lignocellulosic biomass, especially woody biomass, lignin mostly deposits or condenses in cell walls, especially in the mature xylem cell walls and can form rising layers that differ in cellulose composition [25] and act as a skeleton with hemicellulose for a matrix to tightly pack the cellulose microfibrils to form ordered polymer chains (Fig. 1.5) [26]. The covalent bonds linked between lignin and carbohydrate polymers are reported as benzyl ethers and phenyl glycosides [27–29].

1.1.3 Biological Functions

It is not easy to decompose natural lignin with a single chemical, enzyme or microbiological method due to its non-regular macromolecular structure as well as the various linkage types. This feature of lignin helps it to have highly protective

capacity against degradation from mechanical, chemical and biological forces in nature. In plants, lignin functions not only as structural support but also to aid in transport of moisture and nutrients [2]. Lignin contributes to the compressive strength and hydrophobicity of cell walls of xylem in woody biomass, which are considered of importance to the physiological processes of water transport, binding and encrusting. These functions are likely to be affected by the variation in lignin localization, content and sub-unit constituents [2, 3].

1.1.4 Sources of Technical Lignin and Their Promise in Bio-refining Process

As a renewable resource, lignin and lignin derivatives have potential for producing advanced chemicals or lignin-based materials in a biorefinery. When used as raw material, lignin with or without chemical modification has several distinct advantages in industrial processes as described next. Firstly, there is wide availability of technical lignin from pulping and biofuels industries. For instance, the annual production of Kraft lignin from global pulp mills is 50 million tons approximately [1]. The cellulosic ethanol industry that uses lignocellulosic feedstock is another large producer of enzymatic lignin by-product. About 0.5–1.5 kg lignin from the enzymatically-hydrolyzed residuals is co-generated per liter of ethanol produced [1]. In the USA, 126.3 and 537.7 million liters of cellulosic ethanol were produced in 2014 and 2015, respectively [30]. An increase in the output of cellulosic ethanol will also lead to an increase in the production of enzymatic lignin. Secondly, technical lignin has advanced physicochemical features for further processing or conversion [31], such as (i) good stability and mechanical strength, mainly as the results of the presence of aromatic rings; (ii) the possibility of a broad range of chemical transformations, such as with increased phenolic OH, reduced aliphatic OH and methoxyl groups, condensed polymer fragments, or multiple polydispersity of molecular weights [32]; (iii) good reactivity for graft copolymers because of existing many reacting site on the phenolic rings (phenoxy radicals), or functional groups, such as phenolic hydroxyl and carboxyl groups [33, 34]; (iv) good solubility and compatibility with a wide range of organic solvents (e.g., alcohols, acetone, formic acid and acetic acid) for homogeneous conversions with high efficiency; (v) good distributability for blending with other materials because of the small particle size and hydrophobicity; and (vi) good rheological properties and film-forming ability for a structural component in composite materials. Thirdly, use of lignin has been demonstrated to have economic benefits on an industry scale. For example, lignin can serve directly as a substitute material additive for value-added chemicals, such as phenolic and aromatic compounds, or it can be combusted as a fuel or converted through pyrolysis to generate heat or gas.

1.2 Techniques for Determining Structural and Chemical Features of Lignin

1.2.1 Importance of Lignin Chemistry

Knowledge of the chemical structure of lignin structure and its chemistry is fundamental for developing technology for its processing and refining. Understanding lignin structure allows one to (i) determine the key time points of operation during de-lignification or lignin modification processes; (ii) develop strategies of decomposing targeted lignin structure or bonds for lignin reuse by determining changes in linkages and structures in the lignin polymers; (iii) build a gene regulation mechanism and to develop relationships between lignin structural organization and certain wood properties in plant physiology and molecular biology by screening the lignin formation and distribution during the growth of the plant; (iv) elucidate mechanisms in lignin chemistry as well as develop new characterization methods.

Nowadays, both traditional and multi-disciplinary methods are used to investigate lignin structures. Due to the complexity of lignin's heterogeneous structure, there is a continual need for suitable methods of characterization of the many types of lignin polymers. Methods should be selective, quantitative, and capable of being applied directly to the sample without destroying it [35]. With current methods, lignin can be qualitatively or quantitatively determined in situ, or in an isolated form in terms of with or without derivatization. The derivatization of lignin samples prior to analysis uses mechanical, chemical, physiochemical and biological treatment, or even their combination. However, the isolation or derivatization techniques generally cause changes in the structure of native lignin samples depending on the severity of the method employed. Changes in chemical linkages and structural representations after treatment should be considered with the proper corresponding reports [1].

1.2.2 Lignin Content

1.2.2.1 Wet Chemistry Methods

Wet chemistry methods are widely used for lignin content determination. A standard NREL analytical procedure [36] uses concentrated (72 %, *w/v*) sulphuric acid solution and its further dilution (4 %, *w/v*) to dissolve and hydrolyze cellulose and hemicellulose in wood biomass. The content of acid-insoluble lignin remaining after acid hydrolysis is determined gravimetrically by excluding the incinerated ash residual. As a low proportion of the total lignin dissolves in the acid, the content of the trace acid-soluble lignin (ASL) in the neutralized hydrolysate can be spectrophotometrically measured at 320 nm or 205 nm using literature extinction

coefficients [35, 37]. This method is generally applied to lignocellulosic biomass. Similarly, "Klason lignin" is defined as a wood or pulp constituent specifically insoluble in 72 % (*w/w*) sulfuric acid (TAPPI T222). Determination of the content of Klason lignin can be performed following an equivalent procedure according to TAPPI standards.

1.2.2.2 Spectroscopic Methods

X-ray photoelectron spectroscopy (XPS) is an effective technique to semi-quantitatively determine the content of lignin distributed on the surface of biomass[38–40]. This surface specific method detects about 5–10 nm deep into the biomass. Lignin content can be estimated based on oxygen-to-carbon atomic ratios and aliphatic carbon component acquired by XPS analysis [41]. Fourier transform infrared (FT-IR) spectroscopy coupled to chemometrics is also useful for quantitative analysis of lignin content in wood samples with proper models. Given the rapid prediction of the content of wood components, this method is suitable for on-line use during wood processing [42, 43].

1.2.3 Distribution of Lignin

1.2.3.1 Scanning Electron Microscopy and Atomic Force Microscopy Methods

To determine the deposited lignin on a material's surface after treatment, such as in Kraft pulping, dilute acid or hydrothermal pre-treatment, scanning electron microscopy (SEM) and atomic force microscopy (AFM) can be applied to directly observe the surface dispersion patterns of lignin [44–47]. Through SEM, the 3-D images of the lignin allow efficient identification of lignin shapes, like droplets, crystalline particles, flocks or regular globules that tend to have a size range from about 0.05–2 mm as precipitates on the surface of biomass [48–51]. For observing the detailed ultrastructure of lignin particles, field emission scanning electron microscopy (FESEM) is used to provide high resolution of the fractures and small openings on the lignin droplets and patches [52].

AFM imaging is a common, but efficient technique, for characterizing the topography and supra-molecular structure of solid materials. It can be used solely or even combined with other observation methods [53, 54]. Through scanning across the biomass surface with a sharp probe on a vibrating cantilever driven by multiple voltages, the height, amplitude and phase images can be captured using tapping mode under certain resonant frequencies [50]. The phase contrast images of the lignin fragments can give information on lignin distribution patterns and the proportion of particle sizes [44, 50, 55–57].

1.2.3.2   Spectroscopy and Other Microscopy Methods

With exception of the phase contract images of AFM, SEM-supplemented energy dispersive X-ray (EDX) spectra can be of help to locate the distribution of lignin based on the differences in elemental composition [58]. Hyperspectral stimulated Raman scattering microscope can be used for monitoring lignin deposition on plant cell walls by mapping the aromatic rings of lignin groups with 9 cm^{-1} spectral resolution and sub-micrometer spatial resolution. This technique allows determination of a spatially distinct distribution of functional groups such as aldehyde and alcohol groups [59].

As lignin is a predominantly ultraviolet (UV)-absorbing component, UV microscopy determination methods are sensitive and rapid for locating and for determining semi- quantitative changes in lignin composition in biomass. Under UV illumination, lignin components can be distinguished by strong and unique fluorescence. Fluorescence analysis, on the other hand, is of limited use due to the present of many unrelated fluorescencing compounds or by-products in biomass [60]. Other techniques, as confocal and regular optical microscopy may provide information on lignin particle shape and size as well as the distribution patterns on transparent surfaces of single fiber or thin fiber layers. The observed lignin particle size should be restricted to be above the limit of resolution that is practically 200 nm [51, 61].

1.2.4   Molecular Weight and Polydispersity

The molecular weight of lignin is commonly evaluated by gel permeation chromatography (GPC) [62–65]. Both the weight-average molecular weight (Mw) and number-average molecular weight (Mn) can be obtained but (Mw) is more popular, as it better describes the mass-related physical property of lignin. The polydispersity Index d (Mw/Mn) is often used for characterizing the distribution of the molar masses of lignin fragments. Smaller d values indicate a narrower mass diversity of the lignin fragments. Lignin with a high stabilization for use as additives with polymers usually possess a low Mw and narrow d [66]. GPC method requires lignin to be dissolved into a solvent for analysis. Dilute NaOH solution or THF, DMF or chloroform organic solvents are commonly used as the mobile phase depending on the properties of the column stationary phase [67, 68]. Sometimes, due to poor solubility of the most technical lignins in organic mobile phases, lignin needs to undergo acetylation or methylation pre-treatment to improve its solubility by introducing hydrogen bonds [69]. The effluent is generally monitored by a UV detector with the wavelength being between 254 and 270 nm according to typical procedures [70].

1.2.5 Functional Side-Chain Groups

In lignin, hydroxyl groups including phenolic hydroxyl and aliphatic hydroxyl, as well as methoxyl functional groups widely exist on which the linking or derivatization reactions occur that also affect aqueous solubility. These terminal functional groups serve as the candidate sites to connect with other reacting substrate through covalent bonds [71]. Quantification of the functional groups requires extensive analysis.

1.2.5.1 Nuclear Magnetic Resonance Methods

Among the available methods, nuclear magnetic resonance (NMR) spectroscopy, mostly ^{1}H NMR and quantitative ^{31}P NMR spectroscopy are efficient for characterizing the content of functional groups [72–75]. In most of NMR spectroscopy determinations, lignin has to be dissolved or derivatized in an NMR solvent as a homogeneous solution. For example, in ^{1}H NMR analysis, chloroform ($CDCl_3$) or deuterated water (D_2O) is commonly used for dissolving lignin with tetramethylsilane or p-nitrobenzaldehyde as the internal standard. To ensure the solubility of lignin in NMR solvent, the lignin must be acetylated [72, 73, 76]. In ^{31}P NMR analysis, the hydroxyl groups of lignin are selectively derivatized with organic phosphoric reagent, such as 2-chloro-4, 4, 5, 5-tetramethyl-1, 3, 2-dioxaphospholane (TMDP). The derived lignin solution can be subsequently analyzed with internal standards, such as cyclohexanol [70, 77–80]. Quantitatively estimating the hydroxyl and methoxyl functional groups refers to the intensity ratios of the integrated signals of the specific protons versus the proton signals from the internal standards. Content of phenolic hydroxyl group can also be specifically determined using modified ^{1}H NMR spectroscopy methods based on distinct integrated intensities between protons in lignin and lignin with phenolic protons exchanged by D_2O. The differences are proportional to the phenolic proton content [81].

1.2.5.2 UV and GC-FID Methods

The UV method can be applied to estimate the amount of phenolic hydroxyl groups in either milled wood lignin or Kraft lignin. In terms of the spectroscopic properties of the phenolic units carrying ionized (in alkaline solvent) and the non-ionized aromatic (in neutral solvent) hydroxyl groups, UV measures the differences in the maximum adsorption ($\Delta\varepsilon$) between the alkali solution and the neutral solvent at wavelengths ranging from 300 to 350 nm [81]. A GC-FID method can be employed to quantitatively estimate the content of methoxyl groups. In this method, the derived lignin sample is reacted with concentrated sulfuric acid under reflux. The methanol generated is then distilled off from the mixture and quantified by GC-FID. The amount of methoxyl groups in the lignin sample is considered equivalent to the methanol produced [69, 82].
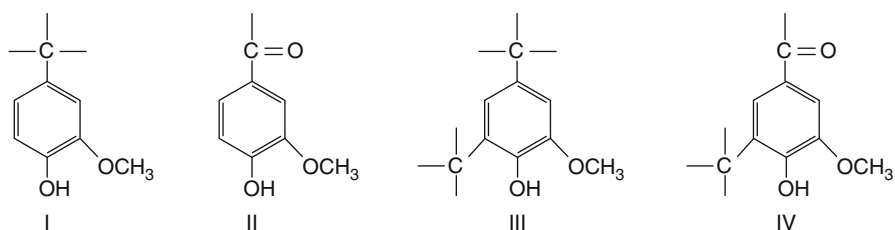
Fig. 1.6 Types of phenolic structures determined in different lignins (Reproduced with copyright permission from Ref. [69]. Copyright © 2005 Elsevier B.V.)

1.2.6   Content of Phenolic Units of Lignin

The content of different phenolic units of lignin can be estimated by the $\Delta\varepsilon$ method [69, 83]. Based on the unique maximum absorbing wavelengths between phenolic units dissolved in neutral and alkaline solvents, the content of phenolic units can be quantitatively evaluated by comparing the $\Delta\varepsilon$ values at certain wavelengths with those of the respective model types of I, II, III, and IV shown in Fig. 1.6 [69, 83].

Detailed quantitative analysis of lignin monomer compositions can be performed via pyrolysis-gas chromatography (Py-GC) method using acetylated lignin samples [84]. In the pyrolysis of the acetylated lignin, the secondary polymerization of terminal alcohol groups is prevented. On the basis of the characteristic pyrograms, lignin monomer composition can be determined with high resolution. This method works well for extractive-free plant samples [84].

1.2.7   Content of Inter-molecular Linkages

The β-O-4 ester bonds are the most frequent inter-molecular linkages present in lignin polymers. Cleavage of the β-O-4 linkages occurs more easily than other types of chemical bonds and acts an important mechanism for chemical isolation and depolymerization of lignin [70]. Elucidating the content of the β-O-4 bonds by mild, selective, and efficient methods is an important target for understanding the structural features of lignin.

1.2.7.1 ^{13}C- and ^{31}P NMR Methods

Quantitative ^{13}C NMR spectroscopy is commonly used in analysis of the bonding type for lignin dissolved in DMSO-d_6 [85–87]. To improve the sensitivity of ^{13}C NMR, two-dimensional heteronuclear single quantum coherence (HSQC) NMR analysis is used that correlates analysis of the ^{13}C and ^{1}H NMR spectra. The efficacy and usefulness of the HSQC NMR method have been well demonstrated in the characterization of lignin structures over other NMR methods [88–90]. Monitoring

Table 1.1 Spectral ranges and peak assignments of ^{13}C NMR spectral analysis of the chemical structure of woody lignin [70, 74, 85]

Range of δ (ppm)	Assignment
178.0–167.5	Unconjugated – CO_2H
167.5–162.5	Conjugated – CO_2H
154.0–140.0	C_3, C_4 aromatic ether or hydroxyl
140.0–127.0	C_1, aromatic C–C bond
127.0–123.0	C_5, aromatic C–C bond
123.0–117.0	C_6, aromatic C–H bond
117.0–114.0	C_5, aromatic C–H bond
114.0–106.0	C_2, aromatic C–H bond
90.0–78.0	Aliphatic C–O bond, C_β in β-O-4, C_α in β-5 and β-β
79.0–67.0	Aliphatic C–O bond, C_α in β-O-4
65.0–61.5	Aliphatic COR
61.5–57.5	Aliphatic C–O C_γ in β-O-4
57.5–54.0	Methoxyl-OCH_3
54.0–52.0	C_β in β-β and C_β in β-5
51.0–48.0	β-1 bond
0–49	Aliphatic C–C bond

the linkages and group changes present in lignin by ^{31}P NMR is another approach for elucidating the structure of lignin after selective derivatization. Advanced ^{31}P NMR methodology can distinguish some subtle differences in the fine structures of lignins by providing an improved resolution in NMR spectrum [91]. The principle of ^{13}C-NMR and ^{31}P-NMR analysis is the integration of chemical shift (δ) and intensity of the peaks forms to give both quantitative and qualitative information on the linkages in lignin (Tables 1.1 and 1.2) [70, 74, 80, 85, 92].

1.2.7.2 FT-IR Spectroscopy Method

Beside NMR methods, FT-IR spectroscopy is commonly used to determine changes that occur in chemical linkages and major constituents in lignin. Through FT-IR spectra, the transformed resonant absorbance at different wavenumbers assignable to various carbon linkages of the lignin skeleton can be observed (Tables 1.3 and 1.4). Because the relative content of the chemical bonds given by the intensities are comparable, changes in the lignin structure can be quantitatively inferred [8, 92, 93].

1.2.8 *Lignin-Lignin Linkages and Macromolecular Assembly*

Strategies of integrating selective or random de-polymerization of lignin with further quantitative or qualitative analysis methods are commonly used to characterize the macromolecular structure of lignin. On this basis, linkage breakdown

Table 1.2 Spectral ranges and peak assignments of ^{31}P NMR spectral analysis of the chemical structure of woody lignin [74]

Range of δ (ppm)	Assignment
150.0–145.5	Aliphatic OH
144.7–145.5	Cyclohexanol (internal standard)
136.6–144.7	Phenols
137.3–140.0	Combined *p*-OH and guaiacyl
140.0–144.7	C_5 substituted "condensed"
139.0–140.0	Guaiacyl
138.2–139.0	Catechol
137.3–138.2	*p*-Hydroxyl-phenyl
133.6–136.6	Carboxylic acid OH

Table 1.3 FT-IR absorbance of typical lignin component in biomass [92, 94]

Wavenumber (cm^{-1})	Assignment/functional group	Component
1035	C–O, C=C, and C–C–O stretching	Cellulose, hemicellulose, lignin
1215	C–C + C–O stretching	Lignin
1270	Aromatic ring vibration	Guaicyl lignin
1327	C–O stretching of syringyl ring	Lignin
1335	C–H vibration, O–H in-plane bending	Cellulose, hemicellulose, lignin
1380	C–H bending	Cellulose, hemicellulose, lignin
1425	C–H in-plane deformation	Lignin
1440	O–H in-plane bending	Cellulose, hemicellulose, lignin
1465	C–H deformation	Lignin
1500	Aromatic ring vibration	Lignin
1595	Aromatic ring vibration + C=O stretching	Lignin
1682	C=O stretching (unconjugated)	Lignin
2840, 2937	C–H stretching	Lignin
3421	O–H stretching	Lignin

usually occurs through chemical or thermal treatment, which has the advantage of being high selectivity or efficient. Chemical and thermal treatments can be applied together. Products can then be analyzed with chromatographic mass analysis, such as GPC, GC- FID, GC-MS or NMR, to identify different functional groups [96–100].

Table 1.4 FT-IR absorbance brand and assignment for Kraft lignin from hardwood and softwood [95]

Absorbance band (cm^{-1})		Assignment
Hardwood lignin	Softwood lignin	
3421	3349	O–H stretching
2937	2934	C–H stretching
2840	2840	C–H stretching
1682	1704	C=O stretching (unconjugated)
1603	1594	Aromatic skeletal vibration + C=O stretching
1514	1513	Aromatic skeletal vibration
1462	1463	C–H deformation (methyl and methylene)
1425	1427	C–H in-plane deformation with aromatic ring stretching
1327	–	C–O stretching of the syringyl ring
1269	1269	C–O stretching of the guaiacyl ring
1215	1214	C–C + C–O stretch
1151	1150	Aromatic C–H in-plane deformation in the guaiacyl ring
1116	–	Aromatic C–H deformation in the syringyl ring
–	1081	C–O deformations of secondary alcohols and aliphatic ethers
1033	1031	Aromatic C–H in-plane deformation (G > S)

1.2.8.1 Chemical Oxidation and GC-MS/FID Method

In chemo-GC-MS/FID analysis, thioacidolysis selectively cleaves aryl ether bonds to chemically degrade lignin that allows determination of the composition and portions of the uncondensed alkyl aryl ether structures. The evidence of aryl glycerol aryl ether structures in lignin can be confirmed by the characterized C_6C_3 trithioethyl phenylpropane compounds after de-polymerization [101, 102]. Alternatively, a method called, derivatization followed by reductive cleavage (DFRC), cleaves the alpha- and β- ethers in lignin, but leaves the γ-esters intact. This method is highly efficient for cleanly and completely breaking the abundant β-O-4 ether linkages existing in lignin [101, 102]. Characterization of the mono-, dimer- and trimer-lignol derivatives through GC-MS/FID can provide sufficient structural information about the polymer, especially in locating and quantifying the β-ether linkages, as well as quantifying the types of linkages at sites of the lignol γ-esters. Research shows that this method works well on both lignin model compounds and technical lignin samples [103–106].

1.2.8.2 Pyrolysis Degradation and GC-MS/FID Method

In thermo-degradation of lignin, pyrolysis, hydrothermal and organosolv treatment and are three commonly-used methods [107, 108]. Among these methods, analytical pyrolysis combined with GC-FID/MS (Py-GC-FID/MS) is a powerful analytical

tool for structural characterization of lignin and for determining monomeric proportions of S, G and H sub-units [98, 109–112]. The de-polymerization of lignin occurs at pyrolytic temperatures from 100 to 900 ° C through dehydration, depolymerization, hydrolysis, oxidation and decarboxylation reactions that produce compounds with unsaturated side chains and low molecular mass species with phenolic OH-groups [113, 114]. Generally, there are three portions, such as coke, liquid and gas generated from the pyrolysis of lignin. By directly coupling the pyrolyzer to on-line GC-FID/MS, analysis of the compounds in the gas phase and liquid phase can be performed simultaneously [8, 99, 115–117]. Due to the complex constituents in the liquid pyrolysate, only a limited number of compounds can be quantified by the GC-MS/FID method. Use of comprehensive two-dimensional gas chromatography and time-of-flight mass spectrometers (GC × GC-TOFMS)/FID can allow characterization of the complex liquid fractions [118].

1.2.8.3 Chemo-Thermo Degradation Method

The disadvantage of the Py-GC-MS/FID technique is the loss of structural information caused by extensive fragmentation as well as limited detection capacity for separation and determination of polar functional groups. The combination of pyrolysis with chemical derivatization overcomes these issues. For example, with *in situ* methylation using tetramethylammonium hydroxide (TMAH) [119], lignin fragments containing any of the carboxylic acids, alcohols or phenols can be methylated to form methyl ethers after the cleavage [96]. Another example is that, by introducing the preliminary acetylation of lignin, prevention of secondary formation of cinnamaldehydes from the corresponding alcohols is possible [84]. In this case, the lignin monomer derivatives formed can contain intact side chains that sufficiently reflect the structure of the lignin.

1.2.8.4 Enzymatic Oxidization and Resonance Raman Spectroscopy Method

As a sensitive and selective method, enzymatic probing treatments of lignin in conjunction with resonance Raman (RR) spectroscopy, combined with Kerr gated fluorescence rejection in the time domain, can be used for elucidating lignin polymer structures. After treatment of lignin through oxidation by laccases + ABTS [2,2'-azino-bis (3-ethylbenzthiazoline-6-sulfonic acid) diammonium salt] or *p*- benzoquinone adsorption, spectra of fluorescent lignin polymers that reflect the redox potential can be obtained by light laser excitation with a specific wavelength. Basic structural information, such as syringyl lignin groups can be implied. This method requires selection of the proper wavelengths for fluorescence excitation to produce satisfactory results and must be compared within certain sources of lignin [61].

1.3 Derivatization and End-Use of Lignin and Lignin Derivatives

1.3.1 Sources of Lignocellulosic Biomass for Technical Lignin Derivatives

Depending on the isolation approaches, common technical lignin produced on a large scale include Kraft or alkali lignin [120, 121], lignosulfonate [122, 123], soda lignin [31, 124], organosolv lignin [73, 125], cellulase isolated-lignin [126, 127], and lignin residuals after acid hydrolysis [126, 128]. Similar isolating mechanisms, i.e., acid-catalyzed hydrolysis (HCl or HBr), oxidation (ligninolytic enzymes, HF, CF_3COOH, $Na_3H_2IO_6$, $Cu (NH_4)_4 (OH)_2$)), and extraction (acetone, phenol, dioxane or ionic liquids), some amounts of technical lignin, such as ionic liquid-extracted lignin [129], ball-milled lignin [130, 131] and lignozyme(fungal)-degraded lignin [132, 133], are prepared for the purpose of lab-scale investigations.

1.3.2 Application of Lignin and Lignin Derivatives

Typically, Kraft and organosolv lignin as well as cellulase isolated-lignin obtained from pulping and biofuels industries, respectively, represent a significant opportunity in the market for upgrading to value-added chemicals, such as fuels and performance products of materials. Figure 1.7 shows that a wide range of renewable chemicals and materials can be produced from technical lignin [134]. As it is a challenge to identify all potential materials and chemical products from lignin due to its complex nature [135], selected examples that are representative of end-uses of technical lignin or lignin derivatives are discussed in the next section, while other extensive applications and detailed information are available by referring to reviews and books on the subject [136–140].

1.3.2.1 Energy

Due to its high-energy content, lignin that largely exists as black liquor in industry is commonly combusted for heat recovery or used as an alternative fuel [107, 141]. Burning lignin constitutes the largest source of energy derived from an industrial by-product in North America, especially in the USA [142]. Through thermochemical approaches, the black liquor rich in lignin can be separate into three products, namely, biogas, bio-oil containing low-molecular-weight compounds, and brown tar containing high-molecular-weight compounds [143]. Processing aqueous black liquor by means of catalytic gasification can produce combustible biogas [144–147] or produce hydrogen [148] through electrolysis. Fast pyrolysis lignin can yield bio-oil to allow the production of either fuel substitutes or phenolic platform
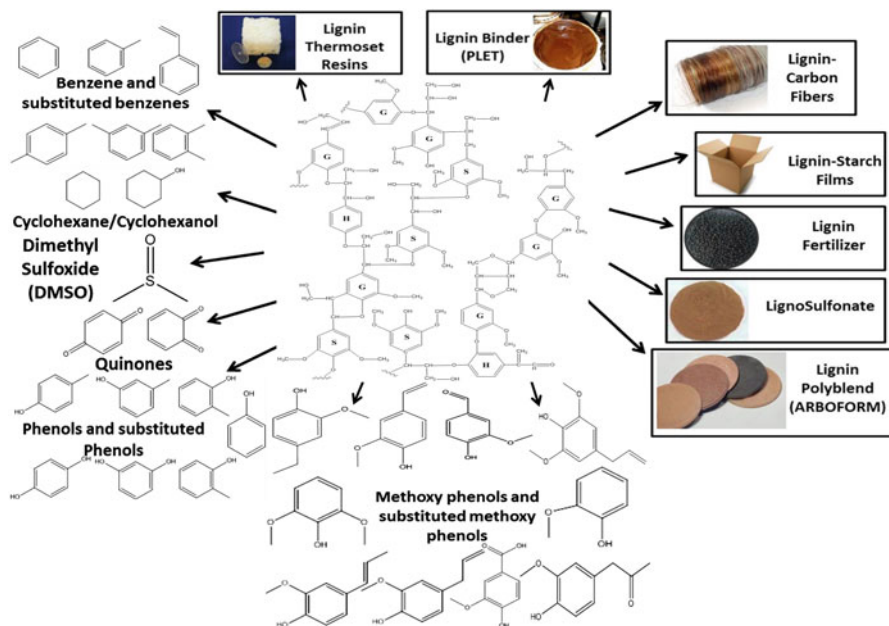
Fig. 1.7 Schematic routes to convert lignin into renewable materials and chemicals (Adapted from Ref. [134], under the terms of the Creative Commons Attribution License http://creativecommons.org/licenses/by/4.0/legalcode)

molecules [149, 150]. Oxygen-blown-pressurized thermal conversion of lignin in black liquor or causticization of lignin solid can produce methanol directly as an important material for biodiesel production [151].

1.3.2.2 Renewable Chemicals

Besides being used as an energy source, lignin is increasingly being applied as a starting material for producing chemicals. Several common technical lignins, i.e., lignosulfonate, Kraft, soda-anthraquinone, enzymatic organosolv and alcoholysis lignin, can act as suitable feedstocks for producing renewable monomeric aromatic compounds that have relatively high value as renewable raw commodity chemicals for direct use or for building specific polymers.

Thermal degradation of lignin for producing chemicals has received much interest. Catalytic thermal-cracking, hydrolysis, reduction or oxidation using temperatures between 250 and 600 °C can lead to low-molecular-weight chemical compounds as commodities or as chemical fragments for further processing [19, 141]. These techniques have been widely employed to obtain phenols or aromatics from lignin, such as guaiacols, syringols, alkyl phenols, catechols [118], C_1-C_2 alkyl-substituted phenols, meth-oxyphenols and C_3-C_4 alkyl-substituted phenols through catalytic or non-catalytic pyrolysis [152]; or 2-methoxyphenol,

4-hydroxy-3-methoxy- benzaldehyde, 2,6-dimethoxyphenol, and 1-(4-hydroxy-3-methoxyphenyl) ethanone through alkaline de-polymerization [153]; or polyols [154] through lignin hydrolysis; or phenols [155, 156] cresols [157], 4-propyl-guaiacol, dihydroconiferyl alcohol [158], alkylphenols, xylenols, guaiacol [156, 159], catechol, syringols [156], phenyl methyl ethers [160], as well as possibly benzene, toluene, and xylene through catalytic hydrogenation or hydrodeoxygenation [161]; or vanillin [162, 163] syringic/vanillic acid [162, 164], syringaldehyde [162] through catalytic oxidation. Generally, lignin-reductive catalytic systems produce bulk chemicals with reduced functionality, whereas lignin-oxidative catalytic systems produce fine chemicals with increased functionality [19].

Chemicals can also be produced from lignin or lignin derivatives through combined catalytic thermo-treating methods. For example, an integrated approach that combines hydrogenation with dihydroxylation catalyzed by zeolites has been applied to efficiently process water-soluble pyrolysis oils for olefins and aromatic hydrocarbons [165]. The hydrogenation produces polyols and alcohols by increasing the intrinsic hydrogen content in the pyrolysis oil. The subsequent conversion of the hydrogenated products with zeolite catalyst leads to a remarkable yield of light olefins and aromatic hydrocarbons (Fig. 1.8).

Alkylbenzenes, which are potential liquid fuels containing C_7–C_{10} components, can be produced from lignin through a two-stage pyrolysis approach [166]. The lignin is firstly decomposed into phenolic compounds and then reformed into the oxygenated products (Fig. 1.9). Moreover, pyrolysis of lignin in fast-fluidized bed with a subsequent catalytic dihydroxylation of the pyrolytic phenolic fraction mainly yields cycloalkanes and alkanes, as well as cyclohexanols that could act as oxygenates in engine fuels [118].

Lignin polymer fragments or bio-oils can be upgraded to more chemically-stable or less-reactive products by using thermo-treating methods, like reductive thermo de-polymerization Kraft lignin with hydrogen or hydrogen donating sources [167]. Nowadays, techniques have been developed for releasing compounds from lignin with alternative reaction media. Through an ionic liquid-based process using 1-ethyl-3-methylimidazolium acetate ([C2mim][OAc]), Kraft lignin and low sulfonate alkali lignin fractions can be depolymerized and converted into a variety of renewable chemicals, including phenols, guaiacols, syringols, eugenol, catechols and their oxidized products, such as vanillin, vanillic acid, syringaldehyde, or derivatized hydrocarbons, such as benzene, toluene, xylene, styrene, biphenyls and cyclohexane [69]. Using protic ionic liquids, e.g. triethylammonium methanesulfonate, the alkali lignin can be depolymerized into low molecular weight compounds through electro-catalytic oxidative cleavage, that include guaiacol, vanillic acid, vanillin, acetovanillone, syringols, syringaldehyde, and syringic acid [168].

Integrating bioprocesses with traditional chemical methods can be an efficient strategy to expand the number of available molecules for lignin upgrading. For example, applying gene-modified bacteria *Pseudomonas putida* Trevisan KT2440 in biochemical separations, and transformation of lignin-derived materials into *cis*, *cis*-muconic acid can be chemically converted to adipic acid and further to the most prevalent dicarboxylic acid with catalytic hydrogenation [169].
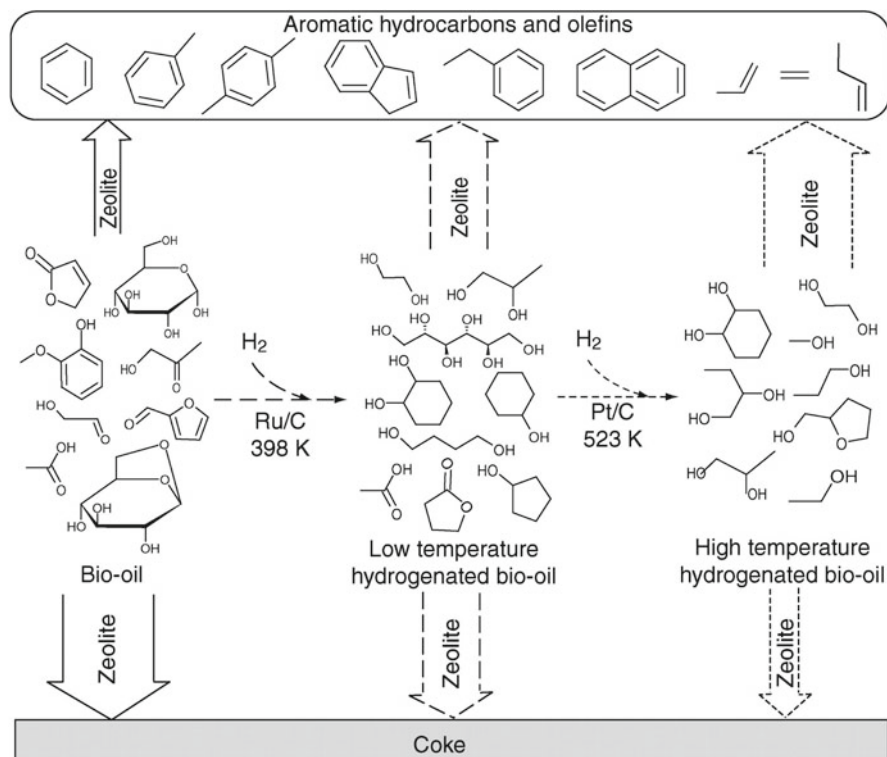
Fig. 1.8 Reaction schematic for integrated hydroprocessing and zeolite upgrading of pyrolysis oil (The width of the vertical arrows represents the product carbon yield from a particular field. Reproduced with copyright permission from Ref. [165]. Copyright © 2010 The American Association for the Advancement of Science)

1.3.2.3 Materials and Additives

Due to the presence of phenolic groups in the lignin structure, the phenolic compound from lignin derivatization can be used for partly replacing petroleum-based phenol substitutes of phenol in preparing bio-based phenol-formaldehyde resol resins. The introduction of lignin in the resin formula decreases the thermal stability of the resin, leading to a lower decomposition temperature and a reduced amount of carbon residue at elevated temperatures. It is applicable if the portion of replaced phenol with lignin is controlled to be below 50 % (*w/w*). The thermal stability can be further improved by using purified lignin with cellulose and hemicellulose contaminants removed [170]. Replacing bisphenol-A with the depolymerized lignin in the epoxy resin synthesis also performs well. Under optimum synthesis conditions, a high product yield (99 %) and high epoxy equivalent of up to 8 can be achieved [171, 172]. The epoxy resin has good dielectric, mechanical and adhesive properties, and can be further used in the electronics industry [173]. Moreover, lignin can

Organosolv lignin

Dissolved polymeric lignin

Stage 1: Base catalyzed depolymerization
Temperature: 300 - 340°C
Media: aqueous solvent
Catalysts: (i) dilute (1-5 %, w/w) aqueous NaOH;
or (ii) solid super base (e.g., CsX zeolite);
or (iii) combination of liquid and solid catalysts.

Depolymerized lignin
(mixture of alkylated phenols, alkoxybenzenes, and alkoxyphenols; and hydrocarbons)

Stage 2: Single-step hydroprocessing, comprising simultaneous exhaustive hydrodeoxy-genation (HDO) and mild hydrocracking (HCR)
Temperature: 350 - 390°C
Media: No solvent
Catalyst: Sulfided co-catalyst systems
(i) MMo/Al₂O₃; or (ii) MMo/SiO₂-Al₂O₃-zeolite.
where M=single metal or multi metals in VI-VIII groups.

C7 - C10 alkylbenzenes
(approx. 80-90%, w/w)

Fig. 1.9 Schematic diagram of selective conversion of lignin through two-stage pyrolysis process for alkylbenzenes as gasoline blending components (Modified from Ref. [166])

be similarly used as an alternative reaction component in synthesis of other polymer composites, such as lignosulfonic acid-doped polyamine [174], ARBOFORM [175] polyesters and polyurethanes [176, 177].

The solid portion of the residue after rapid pyrolysis of Kraft black liquor or lignin mainly contains char, fixed carbon, and inorganic carbonate [178]. Due to the large specific surface area and plenty of microspores, the lignin-char can be applied as activated carbon [138, 179, 180]. Alternatively, the carbonized lignin char is also a promising substitute supporter for preparing the sulphonated solid catalyst used in heterogeneous trans-esterification to produce biodiesel [181, 182].

On the basis of the strong mechanical effect and hydrophobic nature of lignin, the starch-based films incorporated with lignin filler has a high resistance to water with increased elongation. The improved properties have allowed composites to be developed for packaging materials [134, 183]. When used as agriculture additive, technical lignin can slow the release of fertilizers into soil [184]. Moreover, technical lignin powder can be directly blended with synthetic polymers such as polyethylene and polystyrene to improve thermal stability as well as the stabilizer stability against UV radiation [185]. Lignin acts as an antioxidant and reinforcement additive in natural or synthetic rubber [66, 186] PVC [187] and polyolefins polymer [188–191]. As a good water reducing agent, lignin can be evenly applied to the manufacture of wallboards [192, 193]. Through thermal or electrospinning of the blends of fusible lignin or lignin solutions followed by carbonization treatment, lignin based-carbon fibers can be produced for composites with the tensile and thermo stabilization being improved [194–197].

1.4   Conclusions and Future Outlook

Lignin is a complex, but important natural component in biomass. Compared to cellulose or sugars, identifying chemical constituents in lignin and lignin-derived feedstocks faces many challenges because of the nature of lignin as well as its indistinct methods of characterization. In terms of lignin chemistry and structure characterization, fundamentals behind lignin conversion through chemical, thermochemical and biological approaches, have improved as new potential applications are proposed and developed. Advanced use of lignin-based materials as specialty polymers for the paper industry, enzyme protection, biocide neutralization, precious metal recovery aids and wood preservation, have been commercialized in the market [198]. With large quantities of technical lignin originating from industry, there are great opportunities for introducing lignin-derived products into the market. There are multiple questions proposed in the field of scientific and application research on lignin that need to be addressed as listed below:

(i) In characterization of technical lignin and its derivatives, the heterogeneous properties and complexities in the structure of the polymers should be fully considered. Analytical conditions and limitations in the methods of lignin chemistry must be assessed. To confirm the results of the analyses, it is advisable to consider the characterization from multiple perspectives and to use different comparable methods in the study as much as possible.

(ii) It is notable that analysis results of lignin structures are sensitive to changes caused by derivatization, the effect of the severity of the treatment should be evaluated and strictly controlled upon application.

(iii) Although some different methods have been applied or proposed for characterization of lignin, the statistical comparison of analytical methods for the same purpose have been found to be not fully compatible, e.g., for the determination of hydroxyl groups and other functional groups [25]. Investigation of the differences in these results is necessary to reflect inadequacies in the present methods. By doing this, the method can be improved. Moreover, novel technologies capable of solving in-depth analytical problems associated with lignin can be proposed and developed for revealing more detailed structures and activities of the lignin polymers [199].

(iv) In terms of the differences in lignin according to origin and the fractionation techniques employed, dissimilar properties and reactivity of technical lignin and their derivatives offer distinct routes for subsequent end-use of lignin. Clear correlation relationships between lignin physicochemical properties and determined characters, such as lignin polymer purity, molecular weight, or concentrations of functional groups, allow good quantification of the quality of the technical lignin. Fast and reliable determination techniques that provide reliable characterization are essential for model development and for quality control of lignin [43].

(v) The de-polymerization and derivatization towards technical lignin requires multi-disciplinary research as well as much creativity. Green and viable methods that are highly efficient are in great demand. For example, valorization of lignin through conversion of ligninolytic enzymes [200] or through realizing the synergy of enzyme-microbial funneling processes with areas of substrate selection, metabolic engineering and process integration [201] are attractive.

(vi) From the technical point of view, developing or applying currently available methods for making lignin-derived products for a given market should fit within the criteria of purpose of use (product functionality) as well as technical feasibility. Marketing-scale based on scope of market demands, i.e., high volume (thousands tons or up to millions tons/year), medium volume (hundreds to thousands tons/year) or low volume (kgs to tons/year) use, is a key factor to be considered for achieving a balance between market value and product cost in facilities, raw materials, processing and marketing.

References

1. Bruijnincx PCA, Rinaldi R, Weckhuysen BM. Unlocking the potential of a sleeping giant: lignins as sustainable raw materials for renewable fuels, chemicals and materials. Green Chem. 2015;17:4860–1.
2. Campbell MM, Sederoff RR. Variation in lignin content and composition (Mechanisms of control and implications for the genetic improvement of plants). Plant Physiol. 1996;110:3.
3. Heber dos Santos Abreu AMdN, Marcos Antônio Maria. Lignin structure and wood properties. Wood Finer Sci. 1999; 31: 426–33.
4. Higuchi T. Chapter 7 – Biosynthesis of lignin. In: Biosynthesis and biodegradation of wood components. Orlando: Academic; 1985. p. 141–60.
5. Higuchi T. Lignin biochemistry: biosynthesis and biodegradation. Wood Sci Technol. 1990;24:23–63.
6. Freudenberg K, Neish AC. Constitution and biosynthesis of lignin. Berlin/Heidelberg: Springer; 1968. p. 132.
7. Lewis NG, Yamamoto E. Lignin: occurrence, biogenesis and biodegradation. Annu Rev Plant Biol. 1990;41:455–96.
8. Lapierre C. Application of new methods for the investigation of lignin structure. In: Jung HG, Buxton DR, Hatfield RD, Ralph J, editors. Forage cell wall structure and digestibility. Madison: American Society of Agronomy, Crop Science Society of America, Soil Science Society of America; 1993.
9. Adler E. Lignin chemistry—past, present and future. Wood Sci Technol. 1977;11:169–218.
10. Faulon J-L, Hatcher PG. Is there any order in the structure of lignin? Energy Fuels. 1994;8:402–7.
11. Zobel B, Jv B. Wood variation: its causes and control, Springer series in wood science. Berlin: Springer; 1989.
12. Santos RB, Capanema EA, Balakshin MY, H-m C, Jameel H. Lignin structural variation in hardwood species. J Agric Food Chem. 2012;60:4923–30.
13. de Man TJ, de Heus J. Lignin in grass (with special reference to the nitrogen present in the lignin preparations). Recl Trav Chim Pays-Bas. 1950;69:271–6.
14. Mann DG, Labbé N, Sykes RW, Gracom K, Kline L, Swamidoss IM, Burris JN, Davis M, Stewart Jr CN. Rapid assessment of lignin content and structure in switchgrass (Panicum

virgatum L.) grown under different environmental conditions. BioEnergy Res. 2009;2:246–56.

15. Sarkanen K, Chang H-M, Allan G. Species variation in lignins. 2. Conifer lignins. ATPPI J. 1967;50:583–7.

16. Akiyama T, Goto H, Nawawi DS, Syafii W, Matsumoto Y, Meshitsuka G. Erythro/threo ratio of β-O-4-5 structures as an important structural characteristic of lignin. Part 4: Variation in the erythro/threo ratio in softwood and hardwood lignins and its relation to syringyl/guaiacyl ratio. Holzforschung. 2005;59:276–81.

17. Wikberg H, Liisa Maunu S. Characterisation of thermally modified hard- and softwoods by 13C CPMAS NMR. Carbohydr Polym. 2004;58:461–6.

18. Zhao J, Xiuwen W, Hu J, Liu Q, Shen D, Xiao R. Thermal degradation of softwood lignin and hardwood lignin by TG-FTIR and Py-GC/MS. Polym Degrad Stab. 2014;108:133–8.

19. Zakzeski J, Bruijnincx PC, Jongerius AL, Weckhuysen BM. The catalytic valorization of lignin for the production of renewable chemicals. Chem Rev. 2010;110:3552–99.

20. Nimz HH, Robert D, Faix O, Nemr M. Carbon-13 NMR spectra of lignins, 8. Structural differences between lignins of hardwoods, softwoods, grasses and compression wood. Holzforschung. 1981;35:16–26.

21. Chiang VL, Funaoka M. The difference between guaiacyl and guaiacyl-syringyl lignins in their responses to kraft delignification. Holzforschung-Int J Biol Chem Phys Technol Wood. 1990;44:309–13.

22. Holtzapple MT, Lundeen JE, Sturgis R, Lewis JE, Dale BE. Pretreatment of lignocellulosic municipal solid waste by ammonia fiber explosion (AFEX). Appl Biochem Biotechnol. 1992;34:5–21.

23. Galbe M, Zacchi G. A review of the production of ethanol from softwood. Appl Microbiol Biotechnol. 2002;59:618–28.

24. Agarwal U, Atalla R. In-situ Raman microprobe studies of plant cell walls: macromolecular organization and compositional variability in the secondary wall of Picea mariana (Mill.) BSP. Planta. 1986;169:325–32.

25. Ghaffar SH, Fan M. Structural analysis for lignin characteristics in biomass straw. Biomass Bioenergy. 2013;57:264–79.

26. Doherty WOS, Mousavioun P, Fellows CM. Value-adding to cellulosic ethanol: lignin polymers. Ind Crop Prod. 2011;33:259–76.

27. Azuma J-I. Analysis of lignin-carbohydrate complexes of plant cell walls. In: Linskens H-F, Jackson JF, editors. Plant fibers. Berlin: Springer; 1989. p. 100–26.

28. Smook GA. Handbook for pulp & and paper technologists. Vancouver: Angus Wilde Publicaitons; 2002. p. 425.

29. Sun R. Cereal straw as a resource for sustainable biomaterials and biofuels: chemistry, extractives, lignins, hemicelluloses and cellulose. Amsterdam: Elsevier; 2010. p. 292.

30. The Renewable Fuel Standard data. United States Environmental Protection Agency. 2016. https://www.epa.gov/.

31. Mousavioun P, Doherty WO. Chemical and thermal properties of fractionated bagasse soda lignin. Ind Crop Prod. 2010;31:52–8.

32. Wen J-L, Yuan T-Q, Sun S-L, Xu F, Sun R-C. Understanding the chemical transformations of lignin during ionic liquid pretreatment. Green Chem. 2014;16:181–90.

33. Hüttermann A, Mai C, Kharazipour A. Modification of lignin for the production of new compounded materials. Appl Microbiol Biotechnol. 2001;55:387–94.

34. Glasser WG, Hsu OHH, Reed DL, Forte RC, Wu LCF. Lignin-derived polyols, polyisocyanates, and polyurethanes. In: Urethane chemistry and applications. Washington, DC: American Chemical Society; 1981. p. 311–38.

35. Lin S. Ultraviolet spectrophotometry. In: Methods in lignin chemistry. Berlin: Springer; 1992. p. 217–32.

36. Sluiter A, Hames B, Ruiz R, Scarlata C, Sluiter J, Templeton D. Determination of structural carbohydrates and lignin in biomass (NREL/TP-510-42618). Laboratory analytical procedures, National Renewable Energy Laboratory. 2004. p. 15.

37. Dence CW. The determination of lignin. In: Stephen YL, Dence CW, editors. Methods in lignin chemistry. Berlin: Springer; 1992. p. 33–61.

38. Dorris GM, Gray DG. The surface analysis of paper and wood fibers by Esca-electron spectroscopy for chemical analysis-I. Applications to cellulose and lignin. Cellul Chem Technol. 1978;12:9–23.

39. Fardim P, Duran N. Surface chemical composition and mechanical properties of Eucalyptus Kraft pulp investigated by XPS and PCA. In: Proceedings of the 11th international symposium wood pulping chemistry; 2001. p. 305–8.

40. Li K, Reeve DW. Determination of surface lignin of wood pulp fibres by X-ray photoelectron spectroscopy. Cellul Chem Technol. 2004;38:197–210.

41. Johansson L-S, Campbell JM, Koljonen K, Stenius P. Evaluation of surface lignin on cellulose fibers with XPS. Appl Surf Sci. 1999;144–145:92–5.

42. Chen H, Ferrari C, Angiuli M, Yao J, Raspi C, Bramanti E. Qualitative and quantitative analysis of wood samples by Fourier transform infrared spectroscopy and multivariate analysis. Carbohydr Polym. 2010;82:772–8.

43. Boeriu CG, Bravo D, Gosselink RJA, van Dam JEG. Characterisation of structure-dependent functional properties of lignin with infrared spectroscopy. Ind Crop Prod. 2004;20:205–18.

44. Selig MJ, Viamajala S, Decker SR, Tucker MP, Himmel ME, Vinzant TB. Deposition of lignin droplets produced during dilute acid pretreatment of maize stems retards enzymatic hydrolysis of cellulose. Biotechnol Prog. 2007;23:1333–9.

45. Donohoe BS, Decker SR, Tucker MP, Himmel ME, Vinzant TB. Visualizing lignin coalescence and migration through maize cell walls following thermochemical pretreatment. Biotechnol Bioeng. 2008;101:913–25.

46. Kristensen JB, Thygesen LG, Felby C, Jørgensen H, Elder T. Cell-wall structural changes in wheat straw pretreated for bioethanol production. Biotechnol Biofuels. 2008;1:1–9.

47. Kaparaju P, Felby C. Characterization of lignin during oxidative and hydrothermal pretreatment processes of wheat straw and corn stover. Bioresour Technol. 2010;101:3175–81.

48. Košíková B, Zakutna L, Joniak D. Investigation of the lignin-saccharidic complex by electron microscopy. Holzforschung-Int J Biol Chem Phys Technol Wood. 1978;32:15–8.

49. Donaldson LA. Lignification and lignin topochemistry—an ultrastructural view. Phytochemistry. 2001;57:859–73.

50. Maximova N, Österberg M, Koljonen K, Stenius P. Lignin adsorption on cellulose fibre surfaces: effect on surface chemistry, surface morphology and paper strength. Cellulose. 2001;8:113–25.

51. Xu Y, Li K, Zhang M. Lignin precipitation on the pulp fibers in the ethanol-based organosolv pulping. Colloids Surf A Physicochem Eng Asp. 2007;301:255–63.

52. Lei X, Zhao Y, Li K, Pelletier A. Improved surface properties of CTMP fibers with enzymatic pretreatment of wood chips prior to refining. Cellulose. 2012;19:2205–15.

53. Micic M, Radotic K, Jeremic M, Djikanovic D, Kämmer SB. Study of the lignin model compound supramolecular structure by combination of near-field scanning optical microscopy and atomic force microscopy. Colloids Surf B: Biointerfaces. 2004;34:33–40.

54. Wang Y, Hahn TH. AFM characterization of the interfacial properties of carbon fiber reinforced polymer composites subjected to hygrothermal treatments. Compos Sci Technol. 2007;67:92–101.

55. Constantino C, Dhanabalan A, Cotta M, Pereira-da-Silva M, Curvelo A, Oliveira O. Atomic force microscopy (AFM) investigation of Langmuir-Blodgett (LB) films of sugar cane bagasse lignin. Holzforschung. 2000;54:55–60.

56. Pasquini D, Balogh D, Antunes P, Constantino C, Curvelo A, Aroca R, Oliveira O. Surface morphology and molecular organization of lignins in Langmuir-Blodgett films. Langmuir. 2002;18:6593–6.

57. Gustafsson J, Ciovica L, Peltonen J. The ultrastructure of spruce kraft pulps studied by atomic force microscopy (AFM) and X-ray photoelectron spectroscopy (XPS). Polymer. 2003;44:661–70.
58. Mansur HS, Mansur AA, Bicallho SM. Lignin-hydroxyapatite/tricalcium phosphate biocomposites: SEM/EDX and FTIR characterization. In: Key Engineering Materials; 2005. p. 745–8.
59. Liu B, Wang P, Kim JI, Zhang D, Xia Y, Chapple C, Cheng J-X. Vibrational fingerprint mapping reveals spatial distribution of functional groups of lignin in plant cell wall. Anal Chem. 2015;87:9436–42.
60. Dean JF. Lignin analysis. In: Methods in plant biochemistry and molecular biology. Boca Raton: CRC Press; 1997. p. 199–215.
61. Barsberg S, Matousek P, Towrie M. Structural analysis of lignin by resonance Raman spectroscopy. Macromol Biosci. 2005;5:743–52.
62. Yau WW, Kirkland JJ, Bly DD. Modern size-exclusion liquid chromatography: practice of gel permeation and gel filtration chrom atography. Wiley; 1979. p. 494.
63. Glasser WG, Dave V, Frazier CE. Molecular weight distribution of (semi-) commercial lignin derivatives. J Wood Chem Technol. 1993;13:545–59.
64. Scholze B, Hanser C, Meier D. Characterization of the water-insoluble fraction from fast pyrolysis liquids (pyrolytic lignin): Part II. GPC, carbonyl goups, and 13C-NMR. J Anal Appl Pyrolysis. 2001;58:387–400.
65. Sun R, Tomkinson J, Ye J. Physico-chemical and structural characterization of residual lignins isolated with TAED activated peroxide from ultrasound irradiated and alkali pre-treated wheat straw. Polym Degrad Stab. 2003;79:241–51.
66. Gregorová A, Košíková B, Moravčík R. Stabilization effect of lignin in natural rubber. Polym Degrad Stab. 2006;91:229–33.
67. Connors WJ, Sarkanen S, McCarthy JL. Gel chromatography and association complexes of lignin. Holzforschung-Int J Biol Chem Phys Technol Wood. 1980;34:80–5.
68. Walsh A, Campbell A. HPSEC analysis of kraft lignin on a Bondagel column. Holzforschung-Int J Biol Chem Phys Technol Wood. 1986;40:263–6.
69. Mansouri N-EE, Salvadó J. Structural characterization of technical lignins for the production of adhesives: application to lignosulfonate, kraft, soda-anthraquinone, organosolv and ethanol process lignins. Ind Crop Prod. 2006;24:8–16.
70. Sannigrahi P, Ragauskas AJ, Miller SJ. Lignin structural modifications resulting from ethanol organosolv treatment of loblolly pine. Energy Fuels. 2009;24:683–9.
71. Lora JH, Glasser WG. Recent industrial applications of lignin: a sustainable alternative to nonrenewable materials. J Polym Environ. 2002;10:39–48.
72. Lundquist K. Proton (1H) NMR spectroscopy. In: Lin SY, Dence CW, editors. Methods in lignin chemistry. Berlin/Heidelberg: Springer; 1992. p. 242–9.
73. Pan X, Kadla JF, Ehara K, Gilkes N, Saddler JN. Organosolv ethanol lignin from hybrid poplar as a radical scavenger: relationship between lignin structure, extraction conditions, and antioxidant activity. J Agric Food Chem. 2006;54:5806–13.
74. Saito T, Perkins JH, Vautard F, Meyer HM, Messman JM, Tolnai B, Naskar AK. Methanol fractionation of softwood kraft lignin: impact on the lignin properties. ChemSusChem. 2014;7:221–8.
75. Tejado A, Peña C, Labidi J, Echeverria JM, Mondragon I. Physico-chemical characterization of lignins from different sources for use in phenol–formaldehyde resin synthesis. Bioresour Technol. 2007;98:1655–63.
76. Chum LH, Black KS, Johnson KD, Sarkanen VK, Robert D. Organosolv pretreatment for enzymatic hydrolysis of poplars: isolation and quantitative structural studies of lignins. Clean Prod Processes. 1999;1:187–98.
77. Argyropoulos DS. Quantitative phosphorus-31 NMR analysis of lignins, a new tool for the lignin chemist. J Wood Chem Technol. 1994;14:45–63.

78. Granata A, Argyropoulos DS. 2-Chloro-4, 4, 5, 5-tetramethyl-1, 3, 2-dioxaphospholane, a reagent for the accurate determination of the uncondensed and condensed phenolic moieties in lignins. J Agric Food Chem. 1995;43:1538–44.

79. Argyropoulos DS, Jurasek L, Krištofová L, Xia Z, Sun Y, Paluš E. Abundance and reactivity of dibenzodioxocins in softwood lignin. J Agric Food Chem. 2002;50:658–66.

80. Guerra A, Filpponen I, Lucia LA, Saquing C, Baumberger S, Argyropoulos DS. Toward a better understanding of the lignin isolation process from wood. J Agric Food Chem. 2006;54:5939–47.

81. Tiainen E, Drakenberg T, Tamminen T, Kataja K, Hase A. Determination of phenolic hydroxyl groups in lignin by combined use of 1H NMR and UV spectroscopy. Holzforschung. 1999;53:529.

82. Vazquez G, Gonzalez J, Freire S, Antorrena G. Effect of chemical modification of lignin on the gluebond performance of lignin-phenolic resins. Bioresour Technol. 1997;60:191–8.

83. Lai Y-Z, Funaoka M. The distribution of phenolic hydroxyl groups in hardwood lignins. J Wood Chem Technol. 1993;13:43–57.

84. Sonoda T, Ona T, Yokoi H, Ishida Y, Ohtani H, Tsuge S. Quantitative analysis of detailed lignin monomer composition by pyrolysis-gas chromatography combined with preliminary acetylation of the samples. Anal Chem. 2001;73:5429–35.

85. Holtman KM, Hm C, Jameel H, Kadla JF. Quantitative 13C NMR characterization of milled wood lignins isolated by different milling techniques. J Wood Chem Technol. 2006;26:21–34.

86. Pu Y, Chen F, Ziebell A, Davison BH, Ragauskas AJ. NMR characterization of C3H and HCT down-regulated Alfalfa lignin. BioEnergy Res. 2009;2:198–208.

87. Hallac BB, Pu Y, Ragauskas AJ. Chemical transformations of buddleja davidii lignin during ethanol organosolv pretreatment. Energy Fuels. 2010;24:2723–32.

88. Palmer AG, Cavanagh J, Wright PE, Rance M. Sensitivity improvement in proton-detected two-dimensional heteronuclear correlation NMR spectroscopy. J Magn Reson. (1969). 1991; 93: 151–70.

89. Samuel R, Foston M, Jaing N, Cao S, Allison L, Studer M, Wyman C, Ragauskas AJ. HSQC (heteronuclear single quantum coherence) 13C–1H correlation spectra of whole biomass in perdeuterated pyridinium chloride–DMSO system: an effective tool for evaluating pretreatment. Fuel. 2011;90:2836–42.

90. Li H, Pu Y, Kumar R, Ragauskas AJ, Wyman CE. Investigation of lignin deposition on cellulose during hydrothermal pretreatment, its effect on cellulose hydrolysis, and underlying mechanisms. Biotechnol Bioeng. 2014;111:485–92.

91. Pu Y, Cao S, Ragauskas AJ. Application of quantitative 31P NMR in biomass lignin and biofuel precursors characterization. Energy Environ Sci. 2011;4:3154–66.

92. Xu F, Sun J-X, Sun R, Fowler P, Baird MS. Comparative study of organosolv lignins from wheat straw. Ind Crop Prod. 2006;23:180–93.

93. Tian X, Rehmann L, Xu CC, Fang Z. Pretreatment of eastern white pine (Pinus strobes L.) for enzymatic hydrolysis and ethanol production by organic electrolyte solutions. ACS Sustain Chem Eng. 2016;4:2822–9.

94. Sills DL, Gossett JM. Using FTIR to predict saccharification from enzymatic hydrolysis of alkali-pretreated biomasses. Biotechnol Bioeng. 2012;109:353–62.

95. Kubo S, Kadla JF. Hydrogen bonding in lignin: a fourier transform infrared model compound study. Biomacromolecules. 2005;6:2815–21.

96. Klingberg A, Odermatt J, Meier D. Influence of parameters on pyrolysis-GC/MS of lignin in the presence of tetramethylammonium hydroxide. J Anal Appl Pyrolysis. 2005;74:104–9.

97. Hosoya T, Kawamoto H, Saka S. Pyrolysis behaviors of wood and its constituent polymers at gasification temperature. J Anal Appl Pyrolysis. 2007;78:328–36.

98. Patwardhan PR, Brown RC, Shanks BH. Understanding the fast pyrolysis of lignin. ChemSusChem. 2011;4:1629–36.

99. Marques AV, Pereira H. Lignin monomeric composition of corks from the barks of Betula pendula, Quercus suber and Quercus cerris determined by Py–GC–MS/FID. J Anal Appl Pyrolysis. 2013;100:88–94.
100. Adler E, Lundquist K, Miksche GE. The structure and reactivity of lignin. In: Gould RF, editor. Lignin structure and reactions. Washington, DC: American Chemical Society; 1966. p. 22–35.
101. Rolando C, Monties B, Lapierre C. Thioacidolysis. In: Lin SY, Dence CW, editors. Methods in lignin chemistry. Berlin/Heidelberg: Springer; 1992. p. 334–49.
102. Holtman KM, Chang H-M, Jameel H, Kadla JF. Elucidation of lignin structure through degradative methods: comparison of modified DFRC and thioacidolysis. J Agric Food Chem. 2003;51:3535–40.
103. Lu F, Ralph J. Derivatization Followed by Reductive Cleavage (DFRC Method), a new method for lignin analysis: protocol for analysis of DFRC monomers. J Agric Food Chem. 1997;45:2590–2.
104. Lu F, Ralph J. The DFRC method for lignin analysis. 2. Monomers from isolated lignins. J Agric Food Chem. 1998;46:547–52.
105. Lu F, Ralph J. Detection and determination of p-Coumaroylated units in lignins. J Agric Food Chem. 1999;47:1988–92.
106. S-i T, Argyropoulos DS. Determination of arylglycerol-β-aryl ethers and other linkages in lignins using DFRC/31P NMR. J Agric Food Chem. 2001;49:536–42.
107. Brebu M, Vasile C. Thermal degradation of lignin—a review. Cellul Chem Technol. 2010;44:353.
108. Roberts V, Stein V, Reiner T, Lemonidou A, Li X, Lercher JA. Towards quantitative catalytic lignin depolymerization. Chem A Eur J. 2011;17:5939–48.
109. Challinor J. Characterisation of wood by pyrolysis derivatisation—gas chromatography/mass spectrometry. J Anal Appl Pyrolysis. 1995;35:93–107.
110. del Río J, Gutiérrez A, Romero J, Martınez M, Martınez A. Identification of residual lignin markers in eucalypt kraft pulps by Py–GC/MS. J Anal Appl Pyrolysis. 2001;58:425–39.
111. Ibarra D, José C, Gutiérrez A, Rodríguez IM, Romero J, Martínez MJ, Martínez ÁT. Chemical characterization of residual lignins from eucalypt paper pulps. J Anal Appl Pyrolysis. 2005;74:116–22.
112. Meier D, Fortmann I, Odermatt J, Faix O. Discrimination of genetically modified poplar clones by analytical pyrolysis–gas chromatography and principal component analysis. J Anal Appl Pyrolysis. 2005;74:129–37.
113. Meier D, Faix O. State of the art of applied fast pyrolysis of lignocellulosic materials—a review. Bioresour Technol. 1999;68:71–7.
114. Yang H, Yan R, Chen H, Lee DH, Zheng C. Characteristics of hemicellulose, cellulose and lignin pyrolysis. Fuel. 2007;86:1781–8.
115. Pereira H. Chemical composition and variability of cork from Quercus suber L. Wood Sci Technol. 1988;22:211–8.
116. Amen-Chen C, Pakdel H, Roy C. Production of monomeric phenols by thermochemical conversion of biomass: a review. Bioresour Technol. 2001;79:277–99.
117. Lourenço A, Gominho J, Marques AV, Pereira H. Variation of lignin monomeric composition during kraft pulping of Eucalyptus globulus heartwood and sapwood. J Wood Chem Technol. 2013;33:1–18.
118. De Wild P, Van der Laan R, Kloekhorst A, Heeres E. Lignin valorisation for chemicals and (transportation) fuels via (catalytic) pyrolysis and hydrodeoxygenation. Environ Progress Sustain energy. 2009;28:461–9.
119. Challinor J. A pyrolysis-derivatisation-gas chromatography technique for the structural elucidation of some synthetic polymers. J Anal Appl Pyrolysis. 1989;16:323–33.
120. Jackson MG. Review article: the alkali treatment of straws. Anim Feed Sci Technol. 1977;2:105–30.

121. Chakar FS, Ragauskas AJ. Review of current and future softwood kraft lignin process chemistry. Ind Crop Prod. 2004;20:131–41.
122. Heikkila H. Production of pure sugars and lignosulfonate from sulfite spent liquor. US Patent, US4631129 A. 1986.
123. Matsushita Y, Yasuda S. Preparation and evaluation of lignosulfonates as a dispersant for gypsum paste from acid hydrolysis lignin. Bioresour Technol. 2005;96:465–70.
124. Wörmeyer K, Ingram T, Saake B, Brunner G, Smirnova I. Comparison of different pretreatment methods for lignocellulosic materials. Part II: influence of pretreatment on the properties of rye straw lignin. Bioresour Technol. 2011;102:4157–64.
125. Pandey MP, Kim CS. Lignin depolymerization and conversion: a review of thermochemical methods. Chem Eng Technol. 2011;34:29–41.
126. H-m C, Cowling EB, Brown W. Comparative studies on cellulolytic enzyme lignin and milled wood lignin of sweetgum and spruce. Holzforschung-Int J Biol Chem Phys Technol Wood. 1975;29:153–9.
127. Wang K, Bauer S, R-c S. Structural transformation of miscanthus × giganteus lignin fractionated under mild formosolv, basic organosolv, and cellulolytic enzyme conditions. J Agric Food Chem. 2012;60:144–52.
128. Watkins D, Nuruddin M, Hosur M, Tcherbi-Narteh A, Jeelani S. Extraction and characterization of lignin from different biomass resources. J Mater Res Technol. 2015;4:26–32.
129. Hou X-D, Smith TJ, Li N, Zong M-H. Novel renewable ionic liquids as highly effective solvents for pretreatment of rice straw biomass by selective removal of lignin. Biotechnol Bioeng. 2012;109:2484–93.
130. Sun R, Xiao B, Lawther J. Fractional and structural characterization of ball-milled and enzyme lignins from wheat straw. J Appl Polym Sci. 1998;68:1633–41.
131. Samuel R, Pu Y, Raman B, Ragauskas AJ. Structural characterization and comparison of switchgrass ball-milled lignin before and after dilute acid pretreatment. Appl Biochem Biotechnol. 2010;162:62–74.
132. Hammel K. Fungal degradation of lignin. In: Driven by nature: plant litter quality and decomposition. Wallingford: CAB International; 1997. p. 33–45.
133. Xf T, Fang Z, Guo F. Impact and prospective of fungal pre-treatment of lignocellulosic biomass for enzymatic hydrolysis. Biofuels Bioprod Biorefin. 2012;6:335–50.
134. Varanasi P, Singh P, Auer M, Adams PD, Simmons BA, Singh S. Survey of renewable chemicals produced from lignocellulosic biomass during ionic liquid pretreatment. Biotechnol Biofuels. 2013;6:1.
135. Holladay JE, White JF, Bozell JJ, Johnson D. Top value-added chemicals from biomass-volume ii—results of screening for potential candidates from biorefinery lignin (PNNL-16983). Pacific Northwest National Laboratory; 2007. p. 79.
136. Azadi P, Inderwildi OR, Farnood R, King DA. Liquid fuels, hydrogen and chemicals from lignin: a critical review. Renew Sust Energ Rev. 2013;21:506–23.
137. Stewart D. Lignin as a base material for materials applications: chemistry, application and economics. Ind Crop Prod. 2008;27:202–7.
138. Suhas CPJM, Ribeiro Carrott MML. Lignin – from natural adsorbent to activated carbon: a review. Bioresour Technol. 2007;98:2301–12.
139. Thakur VK, Thakur MK, Raghavan P, Kessler MR. Progress in green polymer composites from lignin for multifunctional applications: a review. ACS Sustain Chem Eng. 2014;2:1072–92.
140. Thakur VK, Thakur MK. Recent advances in green hydrogels from lignin: a review. Int J Biol Macromol. 2015;72:834–47.
141. Ragauskas AJ, Williams CK, Davison BH, Britovsek G, Cairney J, Eckert CA, Frederick WJ, Hallett JP, Leak DJ, Liotta CL, Mielenz JR, Murphy R, Templer R, Tschaplinski T. The path forward for biofuels and biomaterials. Science. 2006;311:484–9.
142. Maček A. Research on combustion of black-liquor drops. Prog Energy Combust Sci. 1999;25:275–304.

143. Bridgwater AV. Review of fast pyrolysis of biomass and product upgrading. Biomass Bioenergy. 2012;38:68–94.
144. ArthurL.Kohl, Hills W. Gasification of black liquor. US Patent, US4682985 A. 1987.
145. Backman R, Frederick WJ, Hupa M. Power production from biomass basic studies on black-liquor pyrolysis and char gasification. Bioresour Technol. 1993;46:153–8.
146. Demirbaş A, Karshoğlu S, Ayas A. Hydrogen resources conversion of black liquor to hydrogen rich gaseous products. Fuel Sci Technol Int. 1996;14:451–63.
147. Bach-Oller A, Furusjö E, Umeki K. Fuel conversion characteristics of black liquor and pyrolysis oil mixtures: efficient gasification with inherent catalyst. Biomass Bioenergy. 2015;79:155–65.
148. Nong G, Zhou Z, Wang S. Generation of hydrogen, lignin and sodium hydroxide from pulping black liquor by electrolysis. Energies. 2016;9:13.
149. Tumbalam Gooty A, Li D, Berruti F, Briens C. Kraft-lignin pyrolysis and fractional condensation of its bio-oil vapors. J Anal Appl Pyrolysis. 2014;106:33–40.
150. Huet M, Roubaud A, Chirat C, Lachenal D. Hydrothermal treatment of black liquor for energy and phenolic platform molecules recovery in a pulp mill. Biomass Bioenergy. 2016;89:105–12.
151. Naqvi M, Yan J, Dahlquist E. Bio-refinery system in a pulp mill for methanol production with comparison of pressurized black liquor gasification and dry gasification using direct causticization. Appl Energy. 2012;90:24–31.
152. Shabtai JS, Zmierczak WW, Chornet E. Process for conversion of lignin to reformulated, partially oxygenated gasoline. US Patent, US 6172272 B1. 2001.
153. Nenkova S, Vasileva T, Stanulov K. Production of phenol compounds by alkaline treatment of technical hydrolysis lignin and wood biomass. Chem Nat Compd. 2008;44:182–5.
154. Mahmood N, Yuan Z, Schmidt J, Xu CC. Production of polyols via direct hydrolysis of kraft lignin: effect of process parameters. Bioresour Technol. 2013;139:13–20.
155. Odebunmi EO, Ollis DF. Catalytic hydrodeoxygenation: I. Conversions of o-, p-, and m-cresols. J Catal. 1983;80:56–64.
156. Kallury R, Restivo WM, Tidwell TT, Boocock D, Crimi A, Douglas J. Hydrodeoxygenation of hydroxy, methoxy and methyl phenols with molybdenum oxide/nickel oxide/alumina catalyst. J Catal. 1985;96:535–43.
157. Urban P, Engel DJ. Process for liquefaction of lignin. US Patent, US4731491 A. 1988.
158. Pepper J, Lee Y. Lignin and related compounds. I. A comparative study of catalysts for lignin hydrogenolysis. Can J Chem. 1969;47:723–7.
159. Meier D, Berns J, Faix O, Balfanz U, Baldauf W. Hydrocracking of organocell lignin for phenol production. Biomass Bioenergy. 1994;7:99–105.
160. Ratcliff M, Johnson D, Posey F, Maholland M, Cowley S, Chum H. Hydrodeoxygenation of a lignin model compound. In: Research in thermochemical biomass conversion. London: Springer; 1988. p. 941–55.
161. Jv H, Scott EL, Sanders J. Bulk chemicals from biomass. Biofuels Bioprod Biorefin. 2008;2:41–57.
162. Villar J, Caperos A, Garcia-Ochoa F. Oxidation of hardwood kraft-lignin to phenolic derivatives with oxygen as oxidant. Wood Sci Technol. 2001;35:245–55.
163. Voitl T, Rudolf von Rohr P. Oxidation of lignin using aqueous polyoxometalates in the presence of alcohols. ChemSusChem. 2008;1:763–9.
164. Partenheimer W. The aerobic oxidative cleavage of lignin to produce hydroxyaromatic benzaldehydes and carboxylic acids via metal/bromide catalysts in acetic acid/water mixtures. Adv Synth Catal. 2009;351:456–66.
165. Vispute TP, Zhang H, Sanna A, Xiao R, Huber GW. Renewable chemical commodity feedstocks from integrated catalytic processing of pyrolysis oils. Science. 2010;330:1222–7.
166. Shabtai J, Zmierczak W, Chornet E, Johnson D. Process for converting lignins into a high octane blending component. US Patent, US20030115792. 2003.

167. Huang S, Mahmood N, Tymchyshyn M, Yuan Z, Xu C. Reductive de-polymerization of kraft lignin for chemicals and fuels using formic acid as an in-situ hydrogen source. Bioresour Technol. 2014;171:95–102.
168. Reichert E, Wintringer R, Volmer DA, Hempelmann R. Electro-catalytic oxidative cleavage of lignin in a protic ionic liquid. Phys Chem Chem Phys. 2012;14:5214–21.
169. Vardon DR, Franden MA, Johnson CW, Karp EM, Guarnieri MT, Linger JG, Salm MJ, Strathmann TJ, Beckham GT. Adipic acid production from lignin. Energy Environ Sci. 2015;8:617–28.
170. Wang M, Leitch M, Xu C. Synthesis of phenol–formaldehyde resol resins using organosolv pine lignins. Eur Polym J. 2009;45:3380–8.
171. Koike T. Progress in development of epoxy resin systems based on wood biomass in Japan. Polym Eng Sci. 2012;52:701–17.
172. Ferdosian F, Yuan Z, Anderson M, Xu CC. Synthesis of lignin-based epoxy resins: optimization of reaction parameters using response surface methodology. RSC Adv. 2014;4:31745–53.
173. Simionescu CI, Rusan V, Macoveanu MM, Cazacu G, Lipsa R, Vasile C, Stoleriu A, Ioanid A. Special issue microphenomena in advanced composites lignin/epoxy composites. Compos Sci Technol. 1993;48:317–23.
174. Viswanathan T. Synthesis of lignosulfonic acid-doped polyaniline using transition metal ion catalysts. US Patent, US 6977050 B1. 2005.
175. Nägele H, Pfitzer J, Nägele E, Inone ER, Eisenreich N, Eckl W, Eyerer P. ARBOFORM®-a thermoplastic, processable material from lignin and natural fibers. In: Chemical modification, properties, and usage of lignin. New York: Springer; 2002. p. 101–19.
176. Gandini A, Belgacem MN, Guo Z-X, Montanari S. Lignins as macromonomers for polyesters and polyurethanes. In: Chemical modification, properties, and usage of lignin. New York: Springer; 2002. p. 57–80.
177. Bonini C, D'Auria M, Emanuele L, Ferri R, Pucciariello R, Sabia AR. Polyurethanes and polyesters from lignin. J Appl Polym Sci. 2005;98:1451–6.
178. Sricharoenchaikul V, Hicks AL, Frederick WJ. Carbon and char residue yields from rapid pyrolysis of kraft black liquor. Bioresour Technol. 2001;77:131–8.
179. Gao Y, Yue Q, Gao B, Sun Y, Wang W, Li Q, Wang Y. Preparation of high surface area-activated carbon from lignin of papermaking black liquor by KOH activation for Ni(II) adsorption. Chem Eng J. 2013;217:345–53.
180. Sun Y, Guo F, Zhang L. Optimization of the preparation of activated carbon from steam activated cornstraw black liquor for phenol removal. Asia-Pacific J Chem Eng. 2016.
181. F-l P, Fang Z, Zakaria S, Guo F, C-h C. Direct production of biodiesel from high-acid value Jatrophaoil with solid acid catalyst derived from lignin. Biotechnol Biofuels. 2011;4:1–8.
182. Huang M, Luo J, Fang Z, Li H. Biodiesel production catalyzed by highly acidic carbonaceous catalysts synthesized via carbonizing lignin in sub- and super-critical ethanol. Appl Catal B Environ. 2016;190:103–14.
183. Baumberger S, Lapierre C, Monties B, Della Valle G. Use of kraft lignin as filler for starch films. Polym Degrad Stab. 1998;59:273–7.
184. Palm C, Sanchez P. Nitrogen release from the leaves of some tropical legumes as affected by their lignin and polyphenolic contents. Soil Biol Biochem. 1991;23:83–8.
185. Pucciariello R, Villani V, Bonini C, D'Auria M, Vetere T. Physical properties of straw lignin-based polymer blends. Polymer. 2004;45:4159–69.
186. Lora JH, Trojan MJ, Klingensmith WH. Rubber compositions containing high purity lignin derivatives. US Patent, US5196460 A. 1993.
187. Kubo S, Kadla JF. The formation of strong intermolecular interactions in immiscible blends of poly (vinyl alcohol)(PVA) and lignin. Biomacromolecules. 2003;4:561–7.
188. Kadla JF, Kubo S. Miscibility and hydrogen bonding in blends of poly (ethylene oxide) and kraft lignin. Macromolecules. 2003;36:7803–11.

189. Pouteau C, Dole P, Cathala B, Averous L, Boquillon N. Antioxidant properties of lignin in polypropylene. Polym Degrad Stab. 2003;81:9–18.
190. Kadla JF, Kubo S. Lignin-based polymer blends: analysis of intermolecular interactions in lignin–synthetic polymer blends. Compos A: Appl Sci Manuf. 2004;35:395–400.
191. Kubo S, Kadla JF. Poly (ethylene oxide)/organosolv lignin blends: relationship between thermal properties, chemical structure, and blend behavior. Macromolecules. 2004;37:6904–11.
192. Ladwig RD. Method of wallboard manufacture. US Patent, US4222984 A. 1980.
193. Hu TQ. Chemical modification, properties, and usage of lignin. New York: Springer; 2002. p. 291.
194. Sudo K, Shimizu K. A new carbon fiber from lignin. J Appl Polym Sci. 1992;44:127–34.
195. Kubo S, Uraki Y, Sano Y. Preparation of carbon fibers from softwood lignin by atmospheric acetic acid pulping. Carbon. 1998;36:1119–24.
196. Kadla JF, Kubo S, Venditti RA, Gilbert RD, Compere AL, Griffith W. Lignin-based carbon fibers for composite fiber applications. Carbon. 2002;40:2913–20.
197. Ruiz-Rosas R, Bedia J, Lallave M, Loscertales I, Barrero A, Rodríguez-Mirasol J, Cordero T. The production of submicron diameter carbon fibers by the electrospinning of lignin. Carbon. 2010;48:696–705.
198. Gargulak J, Lebo S. Commercial use of lignin-based materials. In: ACS Symposium Series. Washington, DC: American Chemical Society; 2000. p. 304–20.
199. Lin SY, Dence CW. The determination of lignin. In: Methods in lignin chemistry. Berlin: Springer; 1992. p. 33–61.
200. Hofrichter M. Review: lignin conversion by manganese peroxidase (MnP). Enzyme Microb Technol. 2002;30:454–66.
201. Beckham GT, Johnson CW, Karp EM, Salvachúa D, Vardon DR. Opportunities and challenges in biological lignin valorization. Curr Opin Biotechnol. 2016;42:40–53.

Chapter 2
Extraction of Technical Lignins from Pulping Spent Liquors, Challenges and Opportunities

Pedram Fatehi and Jiachuan Chen

2.1 Introduction

Forest biorefinery is an alternative approach for the pulping industry [1–3] and aims to produce value-added products from lignocelluloses [2]. One biorefinery scenario is to produce value-added products from lignin that is generated, but partially utilized, in pulping processes. To be industrially attractive, processes for producing lignin based chemicals should be able to be integrated into the pulping industry.

Lignin is the second largest renewable source after cellulose and the largest source of aromatic compounds on Earth. However, due to its amorphous and robust structure, the valorisation of lignin is challenging. Lignin can be converted to many products. Kraft lignin is currently used as a fuel in the Kraft pulping process, but it may be used in the production of carbon and composite fibers [4, 5]. Lignosulfonates have been proposed to be used as adhesives [6], plasticisers in concrete [7] and dye dispersants [8]. Moreover, lignin has been used in polymeric applications as stabilizers [9], surfactants [10], epoxy resins [11] and superabsorbent hydrogels [4]. Finally, lignin of prehydrolysis liquor was proposed to be used as a filler modifier [12] and a fuel source in the past [1, 2].

However, lignin needs to be isolated from pulping spent liquors to allow the production of value-added products. Pulping spent liquors have many different

P. Fatehi (✉)
Key laboratory of Pulp and Paper Science and Technology of Ministry of Education, Qilu University of Technology, 250353 Jinan, China

Chemical Engineering Department, Lakehead University,
955 Oliver Road, P7B 5E1 Thunder Bay, ON, Canada
e-mail: pfatehi@lakeheadu.ca

J. Chen
Key laboratory of Pulp and Paper Science and Technology of Ministry of Education, Qilu University of Technology, 250353 Jinan, China
e-mail: chenjc@qlu.edu.cn

characteristics [13], and contain organic compounds (mainly lignin derived compounds, hemicelluloses and acids) and inorganic materials (mainly residual chemicals of pulping processes) [2]. The chemistry of spent liquors significantly impacts the processes by which lignin can be selectively and effectively isolated [14, 15]. To have an economically feasible lignin production process, lignin needs to be extracted from pulping spent liquors effectively and selectively. In this chapter, various methods that have been proposed in the literature, experimentally evaluated at laboratory scales or are commercially practiced for producing lignin are comprehensively reviewed. The challenges and perspectives of each method will be critically discussed. The main objective of this chapter is to familiarize readers to the alternatives for isolating lignin compounds from four industrially produced spent liquors, which are black liquor and prehydrolysis liquor of Kraft pulping process and spent liquors of sulfite pulping and neutral sulfite semichemical (NSSC) pulping processes. This chapter includes the evaluation of only wood based pulping spent liquors. Methods to deal with less commonly practiced pulping methods, e.g. organosolv, are excluded from this chapter.

2.2 Kraft Pulping Process

2.2.1 Properties of Black Liquor

The black liquor of Kraft pulping process contains a significant amount of lignin and residual pulping salts. Table 2.1 shows the properties of black liquor obtained from softwood and hardwood black liquors. It is observable that the solid, lignin and ash contents of black liquors could vary significantly, and this variation is due to the amount of water used in pulping, and the evaporation stage, from which black liquor samples were collected in commercial processes.

In these samples, the amount of sugars in the black liquor samples was not reported, and the pH was higher than 13. Research study has focused on the isolation of Kraft lignin from black liquor, as described in the following sections.

Table 2.1 Properties of black liquors from commercial Kraft pulping processes

Black liquor source	Solid content, wt.%	Lignin content, wt.%	Ash content, wt.%	Sugars, wt.%	pH	Ref.
Softwood	40	30.2	52.5	N/R	13.6	[16]
Softwood	41	29.6	47	N/R	13.3	[16]
Hardwood	49.7	27.9	48.4	N/R	13.5	[16]
Softwood	18.3	6.38	8.43	0.35	13.4	[17]
Softwood	12.7	4	N/R	N/R	N/R	[18]
Softwood/hardwood	21	7.1	N/R	N/R	N/R	[18]

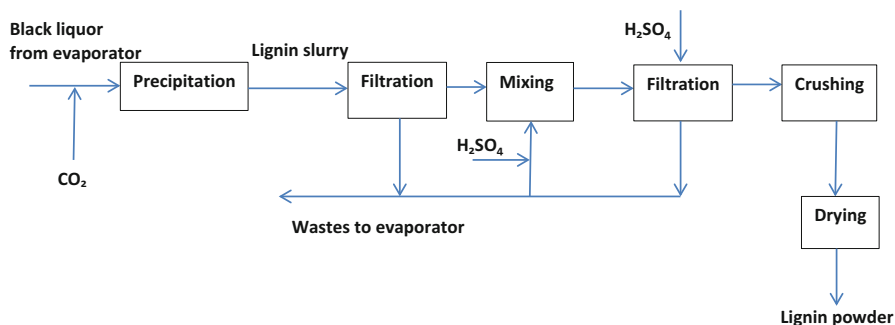*N/R* not reported

2.2.2 Acidification

Acidification has been regarded as an efficient and economical process for isolating lignin from black liquor. In this process, the pH of black liquor is reduced to 9, thus forming lignin particles that can be separated from black liquor via filtration [19, 20]. Table 2.2 shows the properties of precipitated lignin from softwood (weak) black liquor from a Swedish mill [21]. The results in Table 2.2 show the properties of lignin after washing and purification as acidification of black liquor that generally produces lignin with an ash content of more than 1 wt.% prior to purification.

   As shown in Table 2.2, the precipitates consist mainly of Klason lignin and marginal amounts of carbohydrates and ash. As expected, the main element of the precipitates is carbon with a trace of sulfur [21]. It was claimed that increasing temperature during acidification can generate large flocs that might cause filtration problems [21]. The lignin precipitated at pH 9 had between 3000 and 13,000 g/mol molecular weight [21]. Reducing the pH of black liquor is reported to decrease the average molecular weight of both softwood and hardwood lignin, but this also increases the sulfur content of lignin [21, 22]. Kraft pulping degrades lignin into low molecular weight components with a high degree of sulfur substitution. Some elementary sulfur may also be released as a by-product and may contribute to sulfur content of Kraft lignin when the pH of acidification is very low [22].

   However, black liquor filtration at pH 9 is generally challenging because the ionic strength gradients are formed in the lignin precipitates during the washing process [23]. LignoBoost technology was developed and is now commercially used by Domtar Inc. in North Carolina, USA. Figure 2.1 shows the block process

Table 2.2 Properties of lignin precipitated at pH 9 via acidification of a softwood (weak) black liquor [21]

Carbohydrate, wt.%	Klason lignin, wt.%	Acid soluble lignin, wt.%	Precipitated materials, wt.%	Ash, wt.%	S, wt.%	C, wt.%	H, wt.%
2.7	93.7	2	3.3	0.1	1.69	64.88	6.3

Fig. 2.1 Block diagram of LignoBoost Technology [23]

**Black liquor
from evaporator**

	Oxidation	→	Acidification	→	Coagulation	→	Filtration	→

H₂SO₄

Lignin powder

O₂   **CO₂**   **Wastes to evaporator**
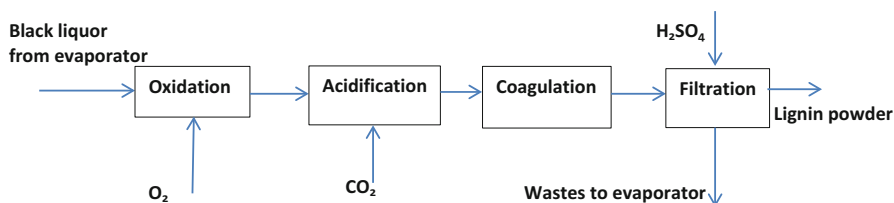
Fig. 2.2 Block diagram of LignoForce technology [24]

diagram of the LignoBoost technology [23]. In this process, black liquor is taken from evaporators of the recovery section of Kraft process, and is acidified with the help of CO_2 to pH 9. Lignin is precipitated at this pH (in a precipitation tank), and filtered. The reduction in pH of black liquor may result in generation of H_2S gas in the process. The precipitated lignin (slurry) is re-dispersed in a subsequent mixing tank with acidic filtrate that is generated in a subsequent filtration stage. In this stage, the pH and temperature of precipitation and mixing tanks are the same, but the concentration gradients of acids in the washing stage (second filtration) are low [23]. It has been reported that the acidification of black liquor in the absence of mixing tank generates large crosslinked lignin macromolecules, but LignoBoost generates small uncrosslinked lignin precipitates [23]. In the LignoBoost process, the change in the pH level, ionic strength and in lignin solubility will take place in the slurry, and not in the precipitates, which helps the properties of precipitated lignin [23]. After the second stage of filtration, precipitated lignin is crushed and dried to form lignin in powder form (Fig. 2.1).

Another process, LignoForce, was developed for isolating Kraft lignin from black liquor by FPInnovations [24]. LignoForce technology was commercialized by West Fraser Inc. in Alberta, Canada in 2016. In this process, black liquor is first oxidized with O_2 and then acidified to pH 9 by CO_2. After the coagulation step, it is washed with acid in a filter press, where lignin precipitates are formed and separated from the system (Fig. 2.2). In this process, the filtrate of coagulation stage is sent to the evaporator of the Kraft process [24].

Both LignoBoost and LignoForce technologies have been commercialized in North America; however, there is no true comparison for the quality of lignin products generated in LignoBoost and LignoForce. Table 2.3 shows the properties of precipitated lignin with and without the oxidation stage conducted in the LignoForce technology. It can be observed that the filtration rate, lignin content and the particle size of the precipitates were increased significantly, but the ash content of the precipitates was reduced. The solid content of the precipitates was similar in both cases. As is well known, the oxidation and acid/base neutralization reactions are exothermic. Therefore, the temperature of black liquor is increased after oxidation and acidification. The charged groups of lignin are more associated at a higher temperature leading to more and larger colloidal lignin particles that are more easily filtered/separated from the suspension [24].

Table 2.3 Properties of lignin precipitated with or without oxidation with LignoForce technology [24]

Property	Without oxidation	With oxidation
Filtration rate, kg/h.m^2	0–80	100–200
Total solids, wt.%	30–58	60–62
Ash content, wt.%	0.2–15	0.1–0.7
UV lignin, wt.%	50–98	97–98
Lignin particle size, μm	0.2–1	5–10
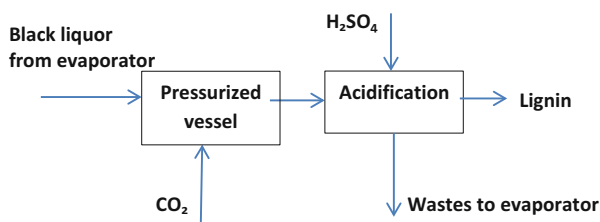
Fig. 2.3 Block diagram of sequential lignin liquid recovery and purification process [16, 25]

However, both LignoForce and LignoBoost are typically operated in batch or semi-batch modes, and they both have a low operating temperature of 70–75 °C. To have a continuous process, sequential liquid lignin recovery and purification (SLRP) was introduced [16, 25, 26]. In this process, black liquor is acidified with CO_2 to pH 9, and heated to 100–150 °C and kept at 4–8 bar (Fig. 2.3). This pretreatment generates a concentrated lignin phase at the bottom of the pressurized vessel that can be pumped in a continuous mode. In the subsequent acidification stage, lignin is separated from black liquor via reducing pH to 2. It has been reported that the temperature changes from 100 to 150 °C increases the molecular weight of precipitated softwood Kraft lignin 4 times [25]. In this process, black liquor with a high ionic strength generates lignin product with a higher molecular weight [16].

2.2.3 Membrane

Membrane filtration has been used to extract lignin from black liquor [17]. In the past, the application of ultrafiltration [27–30] and nanofiltration [31] for isolating lignin from black liquor has been investigated. These studies reported promising results in isolating lignin. Ultrafiltration results in low retention of lignin and a high retention of high molecular weight hemicelluloses, which is larger than that of lignin. In one study, lignin and hemicelluloses were separated from softwood

black liquor by nanofiltration [17]. The introduction of ultrafiltration prior to nano-filtration provided a high flux in the nanofiltration, but the retention of lignin on the nanofilter was reduced [17]. Various membrane types, e.g. polymeric or ceramic, have been used for isolating lignin, and polymeric membranes are found to be more cost effective than ceramic ones [17]. The cost of lignin production for generating 230 g/L lignin solution with nanofiltration was 46 €/t in 2013, while the production of lignin solution with the same concentration using ceramic nanofiltration cost 68 €/t in 2013. The introduction of ultrafiltration increases the cost to 120 €/t (2013) when the same concentration of lignin solution is achieved [17]. Although the application of ultrafilter increases the production cost, it generated lignin with fewer purities (i.e. less of hemicelluloses and other components in the lignin solution). However, the main problem of ultrafiltration/nanofiltration is the adhesion of lignin to the filter surface. As membranes separate lignin components based on their size, they also tend to isolate other components having a similar size (hemicelluloses). Although membranes increase the concentration of lignin in the solutions, they may not necessarily improve the purity of lignin. As lignin possesses functional groups, e.g. phenolic, carboxylic, they may be charged. Therefore, a membrane with a similar charge introduces repulsion force for lignin segments. To increase the purity of linin and improve the filtration performance of membranes, membrane filters can be designed to repel lignin and other compounds in the solution. In this case, membranes with advanced surfaces that repel the black liquor components may improve the separation of lignin from black liquor [18].

2.2.4   Electrolysis

Electrolysis has also been introduced as an alternative to acidification of black liquor. Electrolysis has the advantages of coagulating *in situ* of lignin and generating sodium hydroxide [32, 33]. In the past, electrolysis treatment was carried out on black liquor at different electrode potentials. Figure 2.4 shows a process for separating lignin from black liquor *via* electrolysis technique in a continuous mode. In this process, a membrane separates anode and cathode compartments. In the anode section, oxygen is generated, pH drops and lignin precipitates via oxidation, while sodium hydroxide and hydrogen gas are generated on the cathode section. The production of hydrogen and oxygen gases as well as sodium hydroxide reduce the overall cost of this process, as they are value-added by products of this process.

This process was only conducted at lab scales [34] and feasibility studies were executed to investigate if it is a viable process to be implemented commercially [34, 35]. The main challenges of this process are the electricity requirement, membrane foaling/cleaning and separation of lignin from this system. A study in 1998 reported that, compared to CO_2/acidification process ($ 9.7 M), electrolysis process needed for 6–10 % production increase was $ 12.5 M capital investment for a pulp mill that produced 700 t/day pulp [35].

Fig. 2.4 Process for separating lignin from black liquor via electrolysis [32]
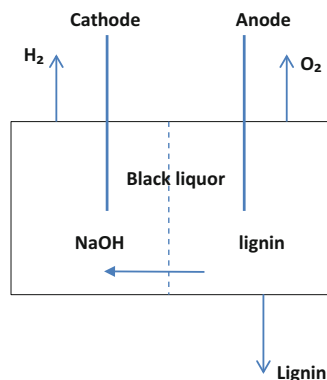
2.2.5 Solvent

Solvents have been applied to extract lignin from black liquor. Water-insoluble organic solvents, e.g. chloroform or dichloromethane, were added to black liquor to precipitate lignin [36], which had an acceptable filtration performance. It was proposed that the creation of hydrogen bonds between lignin and solvent molecules caused the precipitation and improved filtration of black liquor, as lignin was proposed to be surrounded by solvent molecules that made the lignin heavier and hydrophobic, which resulted in lignin agglomeration and precipitation [36].

The precipitation of lignin from black liquor with water-soluble solvents has also been studied. Alcohols were reported to be effective in extracting lignin. For example, the treatment of eucalyptus Kraft black liquor with ethanol at different ratios (0.2–12 L ethanol/L of black liquor) resulted in approximately 40 % of the pentosanes and 22 % of lignin removal [36]. In another study on the use of ethanol, methanol and isopropanol in black liquor, a large amount of alcohol to black liquor (10–1) could be extracted yielding 60 % of the available lignin [37]. Furthermore, lignin recovery of more than 90 % was achieved via having cation-alcohol mixture in black liquor, e.g. calcium (II) or aluminum (III) salt (1.7 g/L of black liquor) and ethanol (0.5 v/v ethanol/black liquor). However, these studies were all conducted at a laboratory scale, and the industrial application of solvent based process requires solvent recovery, which presently is expensive and impractical in Kraft pulping processes.

2.3 Prehydrolysis Based Kraft Process

2.3.1 Properties of PHL

Dissolved pulp is produced via sulfite or Kraft process. Presently, 60 % of dissolving pulp is produced via sulfite process, while 40 % is produced via Kraft process [38]. In the Kraft based dissolving pulp process, prehydrolysis is conducted prior to

Table 2.4 Chemical composition of industrially produced prehydrolysis liquor (PHL)

PHL ID	pH	Dry Solids, wt.%	Ash, wt.%	Acetic acid, wt.%	Furfural, wt.%	lignin, wt.%	Hemicelluloses, wt.%	References
1	3.68	5.39	1.11	1.31	0.18	1.01	1.50	[38]
2	3.80	7.60	1.21	1.41	0.31	1.51	3.16	[14]

Kraft process and is performed *via* treating wood chips with saturated steam (at 443 K for 30 min) or hot water [38]. The prehydrolysis process isolates a part of lignin and hemicelluloses from wood chips. The chemical composition of prehydrolysis liquor (PHL) is shown in Table 2.4.

PHL contains less than 10 wt.% solids, in which approximately 1 wt.% is inorganic material [38, 39]. It contains approximately 1.5–3 % hemicelluloses, 1–1.5 % lignin, 1.4 % acetic acid and less than 0.5 wt.% furfural. Acetic acid is formed *via* liberation of acetyl groups of woody biomass during hydrolysis that reduces the pH of the mixture to 3.6–3.8 (Table 2.4). Although the lignin content of PHL is small, the large production of PHL may provide an incentivise for the producing lignin-based value-added products. The low lignin concentration and the presence of other components in PHL make the direct use of PHL impractical [40]. Various methods have been proposed for isolating lignin from PHL [41–43]. These processes have different efficiencies and selectivities for isolating lignocelluloses.

2.3.2 Acidification of PHL

Similar to the acidification of black liquor, the acidification of PHL may be a viable method to isolate lignin from PHL (i.e. similar to black liquor) [39]. Table 2.5 lists the lignin and hemicelluloses removed from PHL at pH 2. It can be observed that approximately 50 % of lignin can be separated from PHL [40], but it was marginally removed from the PHL in another study [41, 42]. These variations can be related to the properties of lignin in PHL [41]. Lignin removal/precipitation via acidification is significantly affected by the structure/functional groups and molecular weight of the dissolved lignin in the PHL [43]. The variation in the efficiency of acidification can be attributed to the difference in the structures of lignin polymers in PHL. However, the removal of hemicellulose via acidification may contaminate the isolated lignin in PHL. These results imply that acidification process is case dependent, and may be an effective process for lignin removal.

The addition of poly (ethylene oxide) or PEO (0.02 g/g of lignin of PHL) to acidified PHL causes 43 % of lignin to be removed (pH 2) [41]. In another study, 0.03 g/g addition of dodecyltrimethyl ammonium chloride (DTAC) to PHL facilitated lignin removal by 17 % [44]. In these studies, hemicellulose removal was marginal. The separated lignin contained lignin/PEO or lignin/DTAC complexes, which can be used in composites [45, 46]. As the lignin or lignin flocs usually contain

Table 2.5 Performance of acidification of industrially produced prehydrolysis liquor (PHL)

PHL	Lignin removed, %	Hemicelluloses removed, %	Reference
1	47	41	[39]
2	4	NR[a]	[40]
3	5	11.8	[41]

[a]Not Reported

more than 50 % dry solids, their incineration is cost-effective. Alternatively, these flocs can be used in the production of phenolic compounds such as adhesives and carbon fibers [47, 48], as the impurity content of these separated lignin or lignin flocs is not significant [41, 42, 49].

2.3.3   Adsorption

Adsorption can be an alternative to separate lignin from PHL. In this regard, an adsorbent is mixed with PHL in a continuous stirred tank reactor (CSTR) to adsorb lignin. Then, the adsorbent encapsulated with lignin can be used as a value-added filler for composite production or transferred to another stage, in which the desorption of lignin from the adsorbent will take place under desired conditions [14]. The absence of chemical reaction between the adsorbent and lignin promotes the desorption and the recyclability of the adsorbent. In one report, activated carbon was used for adsorbing lignin from industrially produced PHL [50]. It was observed that the maximum adsorption of 400–700 mg/g for lignin was achieved. Furthermore, 200–300 mg/g of hemicelluloses and 100 mg/g of furfural were adsorbed on activated carbon implying that adsorption was not selective. As this process is not selective in lignin isolation, the subsequent desorption and purification of lignin may be complicated and expensive.

2.3.4   Flocculation

Flocculation has been practiced in industry for many years, and recent studies show that it could be used in separating lignin from PHL. In the past, poly diallyldimethylammonium chloride (PDADMAC) and chitosan were added as flocculants to PHL [2, 51]. It has been reported that the separation of lignin is affected by the amount of flocculant applied to the PHL, and the removal of lignin and other PHL components seems to be able to happen simultaneously. However, the concentration of flocculant can control the removal of lignin and other components. A maximum removal of lignin (40 %) was achieved by adding 1.4 mg/g of PDADMAC or 1.6 mg/g of chitosan to the PHL [51]. In this case, the maximum hemicelluloses removal was obtained via 0.5 mg/g of PDADMAC or chitosan addition. As hemicelluloses

can also precipitate in the flocculation, the lignin-based materials with different compositions can be made via controlling the dosage of flocculants in the PHL, and the product can be used in corrugated container (CC) boards or medium density fiber board (MDF) production [51].

2.3.5 In Situ Adsorption/Flocculation System

To increase the adsorption of lignin, flocculation and adsorption has been simultaneously applied to PHL [49, 52]. By adding flocculants, larger flocs are formed in adsorbent/PHL systems, which can be more easily removed from the PHL system [49, 52]. In one report, the addition of 0.5 mg/g PDADMAC to activated carbon/ PHL system (1/40) at room temperature increased the adsorption of lignocelluloses from 200 to 250 mg/g [49], while the application of 0.8 mg/g cationic poly (acryl amide) or CPAM to precipitated calcium carbonate/PHL system (at 40 °C and 120 rpm) enabled the adsorption of 110 mg/g lignin. In addition, 250 mg/g of hemicelluloses and 65 mg/g of furfural were adsorbed on precipitated calcium carbonate (PCC) in the system [53]. When CPAM was replaced with PDADMAC, 203 mg/g of lignin, 530 mg/g of hemicelluloses and 58 mg/g of furfural were adsorbed on PCC under the same experimental conditions [53]. Similar to the adsorption or flocculation processes stated above, the precipitates of in situ systems are impure and thus can only be directly used in composites as stated above.

2.4 Spent Liquor of Sulfite Process

2.4.1 Properties of Spent Liquor

The spent liquor of the sulfite pulping process is generally acidic and contains lignosulfonate, sugars and residual pulping chemicals. In the sulfite pulping process, lignin is sulfonated under acidic conditions to form lignosulfonate. Table 2.6 lists the properties of two spent liquor samples produced from magnesium based sulfite pulping of *Eucalyptus globulus*.

It can be seen that the pH of the spent liquors is approximately 3–4, and they contain 7–8 wt.% lignosulfonate and 4 wt.% sugars. The overall dry solid content of

Table 2.6 Properties of spent liquors of the sulfite pulping process [54]

pH	Conductivity, mS/cm	Lignosulfonate, %	Sugars, %	Total solids, %	Suspended solids, %
3	14	7.9	4	16.9	–
3.7	14	8.3	4.1	16.1	0.21
3.7	15	8.5	5.7	17.1	0.3

the spent liquors is 16–17 wt.%. Presently, the spent liquors are mainly treated in the wastewater system of the sulfite pulping process. In contrast to Kraft lignin, lignosulfonate cannot be precipitated by acidification, which introduces challenges in its separation [55–57]. Membrane, ion exchange, amine extraction and electrodialysis have been used on a laboratory scale for separating lignosulfonate [58].

2.4.2   Membrane

Membrane technology has been studied for separating lignosulfonates from spent liquors for more than 30 years. The possibility for relatively easy scaling up makes ultrafiltration attractive [59]. This process is not very sensitive to pH or temperature, and the molecular weight of the products can be controlled *via* selecting a desired membrane size. Generally, reverse osmosis can separate a solute/solvent of a similar molecular size. The application of reverse osmosis for concentrating sulfite liquors have been studied in the past [60–63]. In one study, the total solid of spent liquors was increased from 6 to 12 % with a flux of about 40 L/m²h by reverse osmosis that had lifetime of more than a year with efficient membrane cleaning two to six times a week [64]. However, reverse osmosis needs a highly selective membrane, and salt rejection may hamper the separation [65]. The most promising ultrafiltration system consists of a Microdyn-Nadir UP010 membrane that can separate high molecular weight lignosulfonates from the low molecular weight ones in the spent liquor [59].

Lignin recovery and fractionation by ultrafiltration have been studied by several researchers [64, 66, 67]. Different membranes from polysulphone, cellulose acetate, fluoropolymer with altered molecular weights cut-off (1 K, 5 K, 10 K, 20 K, 25 K, 50 K and 100 K) have been used for ultrafiltration of spent liquors [68]. In one study, the ultrafiltration of softwood calcium based spent sulfite liquors with cellulose acetate membrane resulted in 40–66 % sugar concentration from 20 to 27 % [68]. The membrane was operated at the pressures of 300–600 psi (20–40 bar) and temperatures of 50–60 °C for 500–1100 h. A lignosulfonate solution of 50–80 wt.% was achieved that contained 80–96 % lignosulfonate on a solid basis [68].

A full-scale ultrafiltration with a membrane area of 1120 m² was installed at Borregaard Industries (Sarpsbog, Norway) in a calcium bisulphate pulp mill in 1981 [64]. A membrane with molecular weight cut-off of 20 k allowed concentrating the spent liquor from 12 to 22 wt.% with a flow rate of 16 m³/h [64]. The lignosulfonate production from the spent liquor of an ammonium based sulfite pulping process was also commercialized in Canada in the 1990s [69]. Figure 2.5 shows the process for producing lignosulfonate from spent liquor of this pulping process. The spent liquor is concentrated from 12 to 22 wt.% prior to the fermentation of sugar present in the spent liquor to ethanol with *S. cerevisiae* [69]. After fermentation, the residual liquor is concentrated to produce liquid lignosulfonate (50 wt.%), which can also be spray-dried and sold as lignosulfonate [69]. However, most membranes are unable to fractionate lignosulfonates or selectively purify them (i.e. they contain sugar contaminants) due to the overlap in the molecular weights of lignosulfonate and sugars.
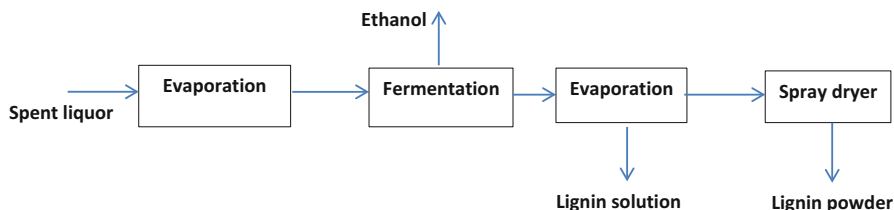
Fig. 2.5 Commercial process for producing lignosulfonate from spent liquor of an ammonium based sulfite pulping process [59]

The membrane technology also requires a special selection of membranes for each spent liquor to reach an optimum yield and degree of purification. In addition, dialysis is a time-consuming process [59].

2.4.3 Amine Extraction

Amine extraction has been proposed for separating lignosulfonate from spent liquors [70]. In this process, lignosulfonate is converted to lignosulfonic acid-amine adducts which are water insoluble [70]. The adducts can be isolated from lignosulfonate via liquid-liquid extraction [70]. In the past, long chain aliphatic amine, tri-n-hexyl-amine, and poly ethyleneimine have been used for extracting lignosulfonates from spent liquors [55, 71–74]. The main challenges of this process are the complete removal of the amine, the formation of salt, foam and emulsion, and the relatively slowness of the process [71]. Moreover, the high consumption of organic solvents limits the application of the process in the industrial scale.

2.4.4 Electrolysis

Similar to Kraft pulping, electrolysis can be applied to isolate lignosulfonate from spent liquor of sulfite pulping process. In the past, spent liquor derived from magnesium bisulfite pulping of beech was electrolyzed in an electrolysis cell [71]. During the electrochemical treatment (125 mA/cm^2; 60 °C; 180 min), anolyte was desalinated and the magnesium concentration was reduced to 60%, which also reduced the pH of the solution from 5 to 1. The results showed that the electrolysis time increased the molar mass of the lignosulfonates from 5700 g/mol at pH 5 to 7400 g/mol at pH 1 and that the phenolic hydroxyl and sulfonic acid groups of separated lignosulfonate were similar. However, lignosulfonates obtained after electrolysis had 1.92 meq/g charge density at pH 1, whereas it was 1.59 meq/g at pH 5 prior to electrolysis [75]. The main challenge of this process is the high cost of electricity and the fouling of the electrodes, which adversely impacts its industrial application.

2.4.5 Ion Exchange Resin

Adsorption processes have been regarded as alternative approaches to separate lignosulfonates from spent liquors, as they are simple and have relatively low operational costs. In the past, the adsorption and desorption of lignosulfonate on minerals such as sandstone, limestone and dolomite have been studied [75, 76]. Polyacryl or polyaromatic based resins, such as Amberlite XAD-4, XAD-7, and XAD-16, have high adsorption capacities that can be used for this purpose [59]. Generally, the adsorption process of phenolic compounds follows either the Freundlich or Langmuir model, and is spontaneous and exothermic. Therefore, conducting the process at ambient temperatures results in a more favourable adsorption and a maximum adsorption of 100–300 mg/g can be achieved [59]. Figure 2.6 shows a process that includes the application of ion exchange resin, filtration and solvent treatment to isolate lignosulfonate from a spent liquor. It is seen that, lignosulfonate is first adsorbed on the resin, then the resin is washed with water to remove the adsorbed sugars from the resin. Then, the resin is treated with ethanol, and this process desorbs and precipitates lignosulfonate in the system, which can be separated from the system with a filter. A series of filtration steps after this treatment can isolate lignosulfonate and ion exchange resin from ethanol. The ion exchange resin is regenerated and recycled, and lignosulfonate is the main product while ethanol is recycled to a previous stage. In the past, the adsorption of lignosulfonate from sulfite pulping spent liquor (250 mg/L lignosulfonate concentration) was studied on resin Amberlite XAD-7 adsorbent. The results showed that mixing the resin with

Fig. 2.6 Process for producing lignosulfonate from spent liquor using ion exchange resin [59]
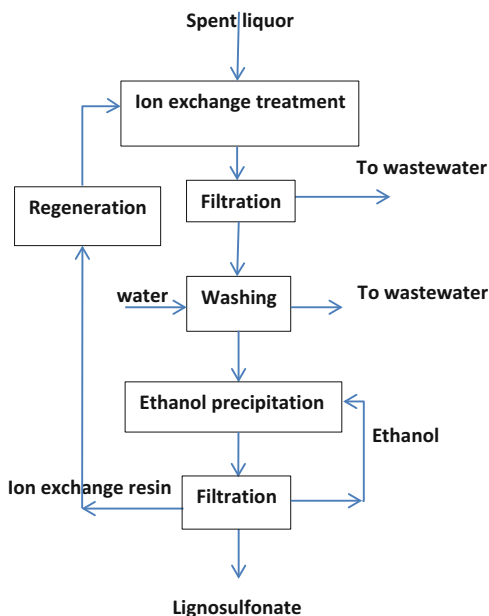
the spent liquor at the weight ratio of 900 mg/g of lignosulfonate/resin (in solution but on a dry basis) led to 300 mg/g of adsorption and thus extraction of lignosulfonate after 10 h at pH 2. The process resulted in lignosulfonates with the molecular weight ranging between 4600 and 398,000 g/mol [59].

2.5   Isolation of Lignosulfonate from Spent Liquor of NSSC Process

2.5.1   Properties of Spent Liquor in NSSC Process

Neutral Sulfite Semi Chemical (NSSC) is a semichemical pulping process that produces pulp with a yield of 60–80 %. In this process, wood chips are first chemically treated with sodium sulfite and sodium bicarbonate, and the treated wood chips are mechanically ground to produce pulp [15]. The chemical treatment of wood chips generates spent liquor that contains organics and inorganics. As an example, the spent liquor, which was produced in a Canadian NSSC process that used mixed hardwood, had a pH of 5.7 and contained 60.22 g/L of lignosulfonate, 22.13 g/L of hemicelluloses, 26.5 g/L acetic acid and a trace of furfural (0.52 g/L) [77]. It also contained about 63.8 g/L of ash, which probably originated from the pulping chemicals used in the pretreatment stage. In another study, the spent liquor of an NSSC process using hybrid poplar contained 59–69 % lignosulfonate, 2–24 % hemicelluloses, 12–29 % acetic acid and 1.6–2.4 % formic acid on ash free basis [78, 79]. The hemicelluloses had two different molecular weights of 8000–19,600 g/mol and 1000 g/mol. The lignosulfonate had average molecular weights of 1030 and 235 g/mol [78, 79]. Based on the molecular weight differences, lignosulfonate and hemicelluloses were separated using an ultrafilter in the same study.

2.5.2   Adsorption/Flocculation/Coagulation

Lignosulfonate has a phenolic structure that is hydrophobic in nature. If a surfactant is added to a spent liquor that contains lignosulfonate, it can interact with lignosulfonate and coagulate it. This may lead to the precipitation of lignosulfonate from the spent liquor. In one report, a pH reduction to 1.8 caused 6 % lignosulfonate and 53 % hemicelluloses removal from a spent liquor [80]. Interestingly, acidification followed by dodecyltrimethylammonium chloride (DTAC) treatment of the spent liquor under the conditions of 22 °C, 1.8 pH and 10 mg/g of DTAC/SL resulted in 40 % lignosulfonate extraction from the spent liquor [81]. In this process, hemicellulose extraction was 78 %.

   Adsorption using activated carbon has also been used for separating lignosulfonate from spent liquors [81]. The results showed that activated carbon adsorbed 0.1 g/g of lignosulfonate and 0.15 g/g of hemicelluloses at the original pH of spent liquor (5.7).

The maximum lignosulfonate adsorption of 0.33 g/g on activated carbon was obtained under the conditions of spent liquor to activated carbon of 30 g/g, 360 min treatment and 30 °C. The hemicellulose adsorption was 0.25 g/g under these conditions [81]. The maximum adsorption of 0.9 g/g lignosulfonate and 0.43 g/g of hemicelluloses on activated carbon was obtained for conditions of 30 °C, 3 h and pH 7 with SL/AC weight ratio of 90 [82]. In another report, the adsorption of lignosulfonate and hemicelluloses was 0.26 g/g and 0.27 g/g on bentonite, respectively, which was achieved under the conditions of 50 °C, 100 rpm and 40 g/g SL/bentonite after 3 h of treatment [13].

Flocculation concept has been also used for extracting lignosulfonate from spent liquors. For example, poly (ethylene imine) or PEI (15 mg/g) treatment of an spent liquor that was produced in an NSSC process of mixed hardwood under the conditions of pH 6, 30 °C resulted in 37 % of lignosulfonate and 37 % hemicelluloses removal from spent liquors. In addition, the simultaneous application of poly (diallyldimethyl ammonium chloride) or PDADMAC and PEI (7.5 mg/g) showed 47 % lignosulfonate and 50 % lignosulfonate removals in the same study [77].

Alternatively, the simultaneous application of adsorption and flocculation can be used for isolating lignosulfonate from spent liquors. In one study, the addition of poly (diallyldimethylammonium chloride) or PDADMAC to the spent liquor and activated carbon system led to 2.5 g/g adsorption of lignosulfonate to 2.5 g/g on AC [82]. In another work, the adsorption of lignosulfonate was increased to 1.8 g/g and that of hemicellulose to 0.45 g/g via adding 15 mg/g of poly (diallyldimethylammonium chloride) or PDADMAC to the system of SL/bentonite stated above (treated under the conditions of 40 g/g of SL/bentonite at 50 °C and 3 h) [13].

However, the precipitates made from the addition of flocculants, surfactants or adsorbents are not pure lignosulfonate, as they contain organic compounds, such as hemicelluloses, flocculants such as PDADMAC, or adsorbents such as bentonite. Therefore, a desorption stage is needed to isolate lignosulfonate from precipitates and to further purify lignosulfonate so that lignosulfonate can be used as a value-added product. However, it is possible to use in packaging paper production as fillers without purification. Although flocculation/adsorption/coagulation process seems to be simple and industrially attractive, they are manly based on laboratory scale experiments. Large scale analyses should be conducted to promote their industrial development.

2.5.3 Solvent Extraction

The application of solvents in removing lignosulfonate from spent liquor of an NSSC process has been assessed by Tarasov et al. [83]. It was reported that lignosulfonate could be removed from the spent liquor via mixing it with ethanol, acetone or isopropyl alcohol. A maximum lignosulfonate removal of 59 % was achieved via mixing isopropyl or acetone with the spent liquor at the weight ratio of 20/80 (solvent/spent liquor) and pH 5.7. A lower removal was obtained via mixing ethanol

with spent liquor under the same experimental conditions. About 30 % of the hemicelluloses was also removed via mixing solvents with spent liquor, regardless of the solvent type. This study also reported a molecular weight and anionic charge density of 5000–70,000 g/mol and 0.2–1.8 meq/g for the precipitates, respectively [83]. As precipitates contain impurities (e.g. hemicelluloses), the product can be used as organic compounds in composites. The recovery of solvent complicates the application of solvents in lignin recovery and makes the practical application of solvent treatment less likely on an industrial scale.

2.6 Conclusions and Future Outlook

Different options have been reviewed and evaluated on the laboratory scale to extract lignin from pulping spent liquors. To extract Kraft lignin from black liquor, acidification is the most industrially reliable process, and LignoBoost and LignoForce technologies were designed based on the acidification concept. Pure lignin can be produced in these processes. To extract lignosulfonate from sulfite spent liquors, ultrafiltration seems to be the most industrially applicable method, but the extracted lignin will have impurities such as hemicelluloses. Laboratory experiments on adsorption and flocculation techniques for isolating lignin derivatives from prehydrolysis liquors (PHL) or spent liquor of the NSSC process show acceptable results. Flocculation seems to be more attractive than adsorption for extracting lignin based compounds from spent liquors as it is easier to be implemented in a large scale. However, the flocculation and adsorption processes cannot generate pure lignin and the product contains either organic impurities such as hemicelluloses or inorganic impurities such as clay (as an adsorbent). There is no clear means for producing pure lignin via the flocculation concept. A desorption process is required to separate lignin from an adsorbent to produce pure lignin via the adsorption concept. Electrolysis and solvent extraction showed promising results on a laboratory scale, but the main barrier for their implementation on the industrial scale is the high usage/cost of electricity and solvent recovery.

References

1. Dansereau LP, El-Halwagi M, Mansoornejad B, Stuart P. Framework for margins-based planning: forest biorefinery case study. Comput Chem Eng. 2014;63:34–50.
2. Saeed A, Fatehi P, Ni Y. Chitosan as a flocculant for pre-hydrolysis liquor of Kraft-based dissolving pulp production process. Carbohydr Polym. 2011;86:1630–6.

3. Van Heiningen A. Converting a kraft pulp mill into an integrated forest biorefinery. Pulp Pap Canada. 2006;107:38–43.
4. El Mansouri NE, Salvadó J. Structural characterization of technical lignins for the production of adhesives: application to lignosulfonate, Kraft, soda-anthraquinone, organosolv and ethanol process lignins. Ind Crop Prod. 2006;24:8–16.
5. Lora JH, Glasser WG. Recent industrial applications of lignin: a sustainable alternative to nonrenewable materials. J Polym Environ. 2002;10:39–48.
6. Yang D, Li H, Qin Y, Zhong R, Bai M, Qiu X. Structure and properties of sodium lignosulfonate with different molecular weight used as dye dispersant. J Dispers Sci Technol. 2014;36:532–9.
7. Kumar S, Mohanty A, Erickson L, Misra M. Lignin and its applications with polymers. J Biobased Mater Bioenergy. 2009;3:1–24.
8. Olsen SN, Bohlin C, Murphy L, Borch K, Mcfarland K, Sweeny M, Westh P. Effects of non-ionic surfactants on the interactions between cellulases and tannic acid: a model system for cellulase–poly-phenol interactions. Enzym Microb Technol. 2011;49:353–9.
9. Sasaki C, Wanaka M, Takagi H, Tamura S, Asada C, Nakamura Y. Evaluation of epoxy resins synthesized from steam exploded bamboo lignin. Ind Crop Prod. 2013;43:757–61.
10. Thakur VK, Thakur MK, Raghavan P, Kessler MR. Progress in green polymer composites from lignin for multifunctional applications: a review. ACS Sustain Chem Eng. 2014;2:1072–92.
11. Kadla J, Kubo S, Venditti R, Gilbert R, Compere A, Griffith W. Lignin-based carbon fibers for composite fiber applications. Carbon. 2002;40:2913–20.
12. Fatehi P, Hamdan FC, Ni Y. Adsorption of lignocelluloses of pre-hydrolysis liquor on calcium carbonate to induce functional filler. Carbohydr Polym. 2013;94:531–8.
13. Oveissi F, Fatehi P. Production of modified bentonite via adsorbing lignocelluloses from spent liquor of NSSC process. Bioresour Technol. 2015;174:152–8.
14. Fatehi P, Ni Y. Integrated forest biorefinery-prehydrolysis/dissolving pulping process. In: Zhu J, Zhang X, Pan X, editors. Sustainable production of fuels, chemicals, and fibers from forest biomass, American chemical society symposium series, NY, 1067. Washington, DC: American Chemical Society; 2011. p. 475–506.
15. Fatehi P, Ni Y. Integrated forest biorefinery-sulfite process. In: Zhu J, Zhang X, Pan X, editors. Sustainable production of fuels, chemicals, and fibers from forest biomass, American chemical society symposium series, NY, 1067. Washington, DC: American Chemical Society; 2011. p. 409–41.
16. Velez J, Thies MC. Liquid lignin from the SLRP process: the effect of process conditions and black liquor properties. J Wood Chem Technol. 2016;36:27–41.
17. Arkall A, Olsson J, Wallberg O. Process performance in lignin separation from softwood black liquor by membrane filtration. Chem Eng Res Des. 2014;92:1792–800.
18. Manttari M, Hatakka JLH, Louhi-Kultanen M, Kallioinen M. Separation phenomena in UF and NF in the recovery of organic acids from Kraft black liquor. J Membr Sci. 2015;490:84–91.
19. Sun RC, Tomkinson J, Bolton J. Effects of precipitation pH on the physicochemical properties of the lignins isolated from the black liquor of oil palm empty fruit bunch fibre pulping. Polym Degrad Stab. 1999;63(2):195–200.
20. Mussatto SI, Fernandes M, Roberto IC. Lignin recovery from brewer's spent grain black liquor. Carbohydr Polym. 2007;70:218–23.
21. Helander M, Theliander H, Lawoko M, Hentiksson G, Zhang L, Lindstrom LE. Fractionation of technical lignin: molecular mass and pH effects. BioRes. 2013;8(2):2270–82.
22. Laurencon TV, Hansel FA, Da Silva TA, Ramos LP, de Muniz GIB, Magalhaes WLE. Hardwood and softwood Kraft lignins fractionation by simple sequential acid precipitation. Sep Purif Technol. 2015;154:82–8.
23. Tomani P. The LignoBoost process. Cell Chem Technol. 2010;44(1–3):53–8.

24. Kouisni L, Holt-Hindle P, Maki K, Paleologou M. The Lignoforce system: a new process for the production of high quality lignin from black liquor. J Sci Technol For Prod. 2012;2(4):6–10.

25. Velez J, Thies MC. Temperature effect on molecular weight properties of liquid lignin recovered from Kraft black liquor. ACS Sustain Chem Eng. 2015;3(6):1032–8.

26. Lake MA, Blackburn JC. Process for recovering lignin. US patent WO2011037967 A2. 2011.

27. Alén R, Sjöström E, Vaskikari P. Ultrafiltration studies on alkaline pulping liquors. Cellul Chem Technol. 1986;20:417–20.

28. Bhattacharjee C, Sarkar P, Datta S, Gupta BB, Bhattacharya PK. Parameter estimation and performance study during ultrafiltration of Kraft black liquor. Sep Purif Technol. 2006;51(3):247–57.

29. Paleologou M, Cloutier JN, Ramamurthy P, Berry RM, Azarniouch MK, Dorica J. Membrane technologies for pulp and paper applications: an outline of Paprican's current work. Pulp Pap Can. 1994;95(10):386–90.

30. Wallberg O, Jönsson AS, Wimmerstedt R. Ultrafiltrationof Kraft black liquor with a ceramic membrane. Desalination. 2003;156:145–53.

31. Keyoumu A, Sjödahl R, Henriksson G, Ek M, Gellerstedt G, Lindström ME. Continuous nano- and ultra-filtration of Kraft pulping black liquor with ceramic filters: a method for lowering the load on the recovery boiler while generating valuable side-products. Ind Crop Prod. 2004;20:143–50.

32. Loutfi H, Blackwell B, Uloth V. Lignin recovery from Kraft black liquor: preliminary process design. Tappi. 1991;74:203–10.

33. Ghatak HR. Electrolysis of black liquor for hydrogen production: some initial findings. Intl J Hydrog Energy. 2006;31:934–8.

34. Cloutier JN, Azarniouch MK, Callender D. Electrolysis of weak black liquor Part I: laboratory study. J Pulp Pap Sci. 1993;19(6):244–8.

35. Davy MF, Uloth VC, Cloutier JN. Economic evaluation of black liquor treatment processes for incremental Kraft pulp production. Pulp Pap Canada. 1998;99(2):35–9.

36. Whalen DM. A simple method for precipitating easily filterable acid lignin from Kraft black liquor. Tappi J. 1975;58(5):110–2.

37. Villar JC. Precipitation of Kraft black liquors by alcohol calcium solutions. Sep Purif Technol. 1996;31(12):1721–39.

38. Saeed A, Jahan MS, Li H, Liu Z, Ni Y, van Heiningen A. Mass balances of components dissolved in the pre-hydrolysis liquor of Kraft-based dissolving pulp production process from Canadian hardwoods. Biomass Bioen. 2012;39:14–9.

39. Sixta H. Hand book of pulp, vol. 1. 1st ed. Weinheim: WILEY-VCH Verlag GmbH & Co. KGaA; 2006.

40. Liu Z, Fatehi P, Jahan MS, Ni Y. Separation of lignocellulosic materials by combined processes of prehydrolysis and ethanol extraction. Bioresour Technol. 2011;102:1264–9.

41. Shi H, Fatehi P, Xiao H, Ni Y. A combined acidification/peo flocculation process to improve the lignin removal from the pre-hydrolysis liquor of Kraft-based dissolving pulp production process. Bioresour Technol. 2011;102:5177–82.

42. Shi H, Fatehi P, Xiao H, Ni Y. Optimizing PEO flocculation process for isolating lignin of pre-hydrolysis liquor of Kraft-based dissolving pulp production process. Ind Eng Chem Res. 2012;51:5330–5.

43. García A, Toledano A, Serrano L, Egüés I, González M, Marín F, Labidi J. Characterization of lignins obtained by selective precipitation. Sep Purif Technol. 2009;68:193–8.

44. Shi H, Fatehi P, Xiao H, Ni Y. A process for isolating lignin of pre-hydrolysis liquor of Kraft pulping process based on surfactant and calcium oxide treatments. Biochem Eng J. 2012;68:19–24.

45. Park Y, Doherty WOS, Halley PJ. Developing lignin based resin coating and composites. Ind Crop Prod. 2008;27:163–7.

46. Kadla JF, Kubo S. Miscibility and hydrogen bonding in blends of poly ethylene oxide and Kraft lignin. Macromolecules. 2003;36:7803–11.
47. Cheng S, Dcruz I, Yuan Z, Wang M, Anderson M, Leitch M, Xu C. Use of biocrude derived from woody biomass to substitute phenol at a high- substitution level for the production of biobased phenolic resol resins. J Appl Polym Sci. 2011;121:2743–51.
48. Cheng S, Yuan Z, Anderson M, Leitch M, Xu C. Synthesis of bio-based phenolic resins/adhesives using methylolated wood-derived bio-oil. J Appl Polym Sci. 2012;126:E430–40.
49. Liu X, Fatehi P, Ni Y. Removing the inhibitors of pre-hydrolysis liquor of Kraft-based dissolving pulp production process using adsorption and flocculation processes. Bioresour Technol. 2012;116:492–6.
50. Liu X, Fatehi P, Ni Y. Adsorption of lignocellulosic materials dissolved in pre-hydrolysis liquor of Kraft-based dissolving pulp process on oxidized activated carbons. Ind Eng Chem Res. 2011;50:11706–11.
51. Saeed A, Fatehi P, Ni Y. An integrated process for removing the inhibitors of the pre-hydrolysis liquor of Kraft-based dissolving pulp process via cationic polymer treatment. Biotechnol Prog. 2012;68:19–24.
52. Shen J, Fatehi P, Soleymani P, Ni Y. A process to utilize the lignocelluloses of pre-hydrolysis liquor in the lime kiln of Kraft-based dissolving pulp production process. Bioresour Technol. 2011;102:10035–9.
53. Fatehi P, Shen J, Hamdan FC, Ni Y. Improving the adsorption of lignocelluloses of prehydrolysis liquor on precipitated calcium carbonate. Carbohydr Polym. 2013;92:2103–10.
54. Restolho JA, Prates A, de Pinho MN, Afonso MD. Sugars and lignosulphonates recovery from eucalyptus spent sulphite liquor by membrane processes. Biomass Bioenergy. 2009;33:1558–66.
55. Ringena O, Saake B, Lehnen R. Isolation and fractionation of lignosulfonates by amine extraction and ultrafiltration: a comparative study. Holzforschung. 2005;59:405–12.
56. Fredheim GE, Braaten SM, Christensen BE. Molecular weight determination of lignosulfonates by size-exclusion chromatography and multi-angle laser light scattering. J Wood Chem Technol. 2003;23(2):197–215.
57. Ekeberg D, Gretland KS, Gustafsson J, Braten SM, Fredheim GE. Characterization of lignosulfonate and Kraft lignin by hydrophobic interaction chromatography. Anal Chim Acta. 2006;565:121–8.
58. Chakrabarty K, Krishna KV, Prabirkumar S, Ghoshal AK. Extraction and recovery of lignosulfonate from its aqueous solution using bulk liquid membrane. J Membr Sci. 2009;330:135–44.
59. Sumerskii I, Korntner P, Zinovyev G, Rosenau T, Potthast A. Fast track for quantitative isolation of lignosulfonates from spent sulfite liquors. RSC Adv. 2015;5:92732–42.
60. Tsapiuk EA, Byrk MT, Medvedev MI, Kochkodan VM. Fractionation and concentration of lignosulphonates by ultrafiltration. J Membr Sci. 1989;47:107–30.
61. Wiley AJ, Ammerlaan ACF, Dubey GA. Application of reverse osmosis to processing of spent liquors from the pulp and paper industry. Tappi J. 1967;50:455–60.
62. Wiley AJ, Dubey GA, Holderby JM, Ammerlaan ACF. Concentration of dilute pulping wastes by reverse osmosis and ultrafiltration. J Water Pollut Control Fed. 1970;42:R279–89.
63. Ammerlaan ACF, Lueek BF, Wiley AJ. Membrane processing of dilute pulping wastes by reverse osmosis. Tappi J. 1969;52:118–22.
64. Bhattacharya A, Todi RK, Tiwari M, Bhattacharjee C, Bhattacharjee S, Datta S. Studies on ultrafiltration of spent sulfite liquor using various membranes for the recovery of lignosulphonates. Desalination. 2005;174:287–97.
65. Basal IK, Wiley AJ. Fractionation of spent sulfite liquors using ultrafiltration cellulose acetate membrane. Environ Sci Technol. 1974;8(13):1085–90.
66. Nystrom M, Lindstrom M. Optimal removal of chlorolignin by ultrafiltration achieved by pH control. Desalination. 1988;70:145–56.

67. Wilde FG. Recovery of lignosulphonate from a calcium bisulphite pulp mill effluent by ultra-filtration. Desalination. 1988;67:495–505.
68. Bansal IK, Wiley AJ. Membrane processes for fractionation and concentration of spent sulphite liquors. Tappi. 1975;58(1):125–30.
69. Magdzinski L. Tembec Temiscaming integrated biorefinery. Pulp Pap Canada. 2006;107(6):44–6.
70. Lin SY. Commercial spent pulping liquor. In: Lin SY, Dence CW, editors. Methods in lignin chemistry. Berlin: Springer; 1992. p. 75–80.
71. Ringena O, Saake B, Lehnen R. Characterization of electrolyzed magnesium spent-sulfite liquor. Holzforschung. 2005;59(6):604–11.
72. Eisenbraun EW. The separation and fractionation of lignosulfonic acid from spent sulfite liquor with tri-n-hexylamine in organic solvents. Tappi. 1963;2:104–7.
73. Haars A, Lohner S, Huttermann A. Quantitative determination of lignosulfonates from sulfite spend liquors using precipitation with polyethyleneimine. Holzforschung. 1981;3:59–65.
74. Kontturi AK, Sundholm G. The extraction and fractionation of lignosulfonates with long chain aliphatic amine. Acta Chem Scand. 1986;40:121–5.
75. Grigg RB, Bai BJ. Calcium lignosulfonate adsorption and desorption on Berea sandstone. J Colloid Interface Sci. 2004;279:36–45.
76. Pranovich AV, Reunanen M, Sjoholm R, Holmbom B. Dissolved lignin and other aromatic substances in thermomechanical pulp waters. J Wood Chem Technol. 2005;25:109–32.
77. Sitter T, Oveissi F, Fatehi P. A process for producing lignocellulosic flocs from NSSC spent liquor. J Biotechnol. 2014;173:19–23.
78. Area MC, Felissia FE, Nunez CE, Venica A, Valade JL. Upgrading spent liquors from NSSC process: III separation of spent liquors components by ultrafiltration. Cellul Chem Technol. 2000;34:173–82.
79. Area MC, Felissia FE, Nunez CE, Venica A, Valade JL. Upgrading spent liquors from NSSC process: quality and quantity of organic components. Cellul Chem Technol. 2000;34:525–35.
80. Cave G, Fatehi P. Separation of lignosulfonate from spent liquor of neutral sulphite semichemical pulping process via surfactant treatment. Sep Purif Technol. 2015;151:39–46.
81. Dashtban M, Gilbert A, Fatehi P. Separation of lignocelluloses from spent liquor of NSSC pulping process via adsorption. J Environ Manag. 2014;136:62–7.
82. Dashtban M, Gilbert A, Fatehi P. A combined adsorption and flocculation process for producing lignocellulosic complexes from spent liquors of neutral sulfite semichemical pulping process. Bioresour Technol. 2014;159:373–9.
83. Tarasov D, Leitch M, Fatehi P. Production of lignosulfonate in NSSC-based biorefinery. Biotechnol Prog. 2015;31(6):1508–14.

Chapter 3
Recovery of Low-Ash and Ultrapure Lignins from Alkaline Liquor By-Product Streams

Mark C. Thies and Adam S. Klett

3.1   Introduction and Background

Lignin is one of the most abundant organic compounds on the planet, second only to cellulose. About 30 % of all organic carbon and 30 % of wood occurs in nature in the form of the biopolymer lignin. Although lignin is plentiful, it has been far more difficult to find uses for lignin than has been the case for its compatriot in woody biomass, namely, cellulose. In fact, probably the most common expression that one hears when lignin is mentioned is that "You can make anything that you want with lignin – except money!" In general, lignin is readily available, albeit in a raw, unpurified form, whenever cellulose is being recovered from biomass. For example, in the nascent lignocellulosic biofuels industry, cellulose and hemicellulose (the two major constituents in biomass besides lignin) are converted by hydrolysis to sugars, which can then be biologically or catalytically converted to biofuels. However, the remaining lignin is a fuel at best if it can be adequately concentrated – and a waste stream at worst. But the largest source of lignin today is not derived from cellulosic ethanol, but instead is generated as a by-product in the manufacture of cellulosic pulp in the pulp-and-paper industry. For example, in the dominant (95 % of the market) Kraft (sulfate) process, an alkaline liquor of sodium hydroxide and sodium sulfide at elevated temperatures is used to dissolve the lignin components of wood, freeing the cellulosic fibers in the form of pulp, which is then used to make paper [1]. The spent alkaline liquor by-product stream contains most of the lignin and is known as "black liquor". Typically, this lignin-rich stream is burned at the pulp mill for its fuel value (as lignin has the same heating value as coal), with only about 0.2 % being recovered for nonfuel uses [2, 3]. However, because lignin is the only abundant biopolymer with aromaticity (see Fig. 3.1), it should have far more value

M.C. Thies (✉) • A.S. Klett
Department of Chemical and Biomolecular Engineering, Clemson University,
Earle Hall, Clemson, SC 29634-0909, USA
e-mail: mcths@clemson.edu
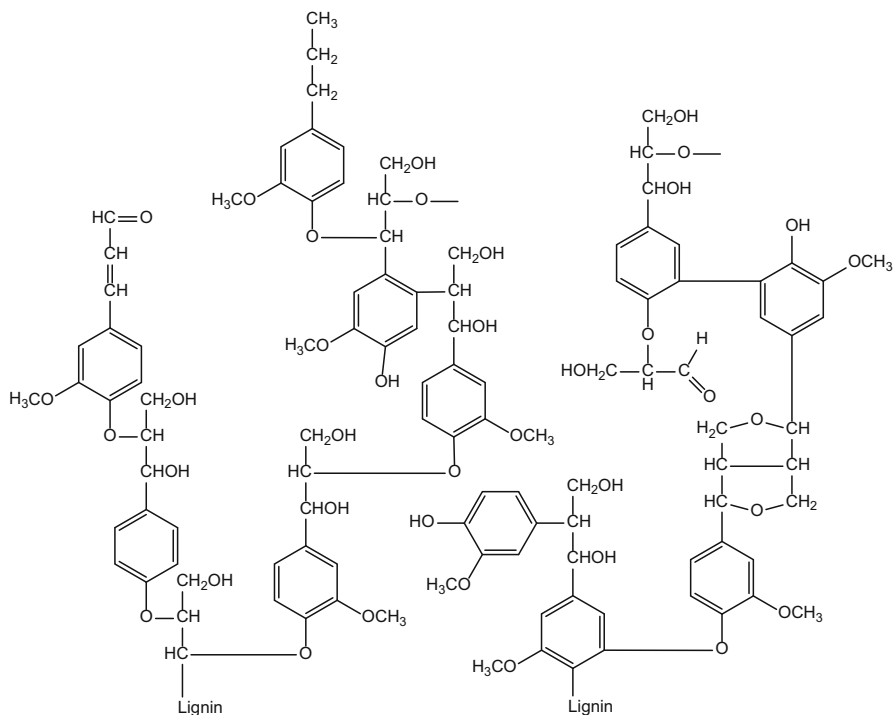
Fig. 3.1 A portion of a structural model for spruce lignin, representing the types of linkages and structural units (Reprinted with permission from Ref. [5]. Copyright © 1977, Springer-Verlag)

as a renewable biopolymer [3, 4]. As seen in the next section, evidence is increasing that this indeed is the case.

3.1.1 Low-Ash Lignins from Alkaline Liquors

Three processes have been developed in recent years for the recovery of lignin from Kraft black liquor: LignoBoost™ (LB), LignoForce™ (LF), and Sequential Liquid-Lignin Recovery and Purification (SLRP™) [6–8]. Although these processes are conceptually similar, they also differ in significant ways. For example, all three use carbon dioxide (CO_2) to lower the pH of the highly alkaline black liquor from about 13.5 to 9 in order to effect the precipitation of the lignin from solution. However, with LB and LF the lignin is precipitated as a solid phase at temperatures up to 70–75 °C, whereas with SLRP the lignin separation is carried out at higher temperatures and pressures (e.g., 90–130 °C and 4–8 bar) such that a liquid, and not a solid lignin phase is formed [8]. The liquid-lignin phase forms only at elevated temperatures and pressures. One advantage of creating this "liquid-lignin" phase in SLRP is that it can be pumped, so SLRP can be carried out in a continuous fashion. All three

processes then carry out a final acidification step with 1–2 N sulfuric acid and recover a solid, low-ash (1–4 %) lignin that typically contains 1500–7500 ppm sodium, the dominant metal impurity.

As far as commercialization of the above technologies is concerned, the LB process has been used by Domtar to recover lignin from their pulp mill in Plymouth, NC since 2014 [9]. West Fraser started up a lignin-recovery facility based on LF technology in April 2016 at its mill in Hinton, Alberta [10]. SLRP is completing the pilot-plant stage and is planning commercial start-up at a U.S. pulp mill by 2017. Total world capacity of low-ash lignin is estimated to be over 100,000 ton/a, so the commercialization of lignin recovery is still in its infancy.

According to insiders (unpublished work), producers of low-ash Kraft lignin anticipate that two of the largest markets for their products will be (1) the partial replacement of phenol for phenol-formaldehyde (PF) resins and (2) the partial replacement of polyols for making rigid polyurethane foams. With the total market for phenols and polyols estimated at 10–15 million ton/a, the anticipated replacement of even 10–40 % of these petroleum-derived materials with lignin would represent a huge market. Other potential applications reported in the literature include the use of lignin as a precursor or substitute in thermosetting and thermoplastic composites [11, 12], or even as a clean-burning biofuel, with the latter being feasible in countries with "green fuel" regulations [13].

3.1.2 From Low-Ash to Ultrapure Lignins

Although ash contents of <5 % and metals contents of <10,000 ppm in lignin are acceptable for the above-mentioned uses, for other, higher-value applications the lignin must be "ultrapure", with overall metals content not exceeding 100–200 ppm and sodium levels <100 ppm. Control of the molecular weight of the lignin would also be expected to be important for higher-value applications. For example, metals in carbon fibers create critical flaws as the metals burn off during the carbonization step, severely impacting final fiber properties such as strength [14]. The market for an ultrapure lignin of a molecular weight that could be spun into a high-performance carbon fiber would be significant, as the selling price of the fiber would be much lower than those derived from polyacrylonitrile polymer, which has the dominant share of the market. Current demand for high-performance carbon fiber is already significant at 67,000 ton/yr, but is expected to triple to 200,000 ton/yr by 2025, primarily due to stringent Corporate Average Fuel Economy (CAFE) standards that will require drastic light-weighting of cars and trucks [15]. A large fraction of the increase in demand for carbon fibers is anticipated in the industrial and automotive sectors, which are cost-sensitive, so an inexpensive precursor such as lignin of acceptable quality would be welcomed by industry, leading to further increases in market share. Another potential high-value application for ultrapure lignin is in coatings, as the metals in a low-ash lignin would generate flaws in the final product, especially when deposited electrolytically. Experts estimate an initial market of

pKa1 = 1.60   pKa1 = 8.80   pKa1 = 4.9
pKa2 = 7.54   pKa2 = 11.0   pKa2 = 9.2
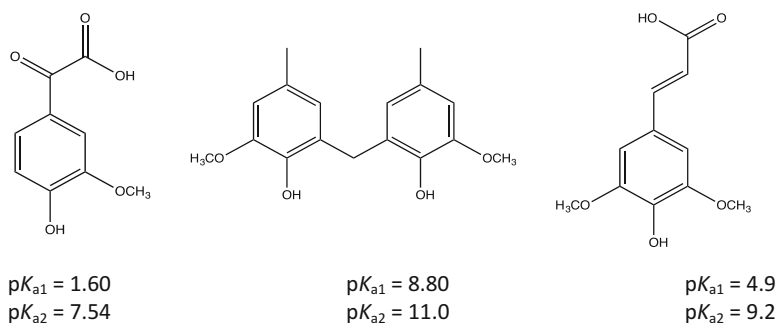
Fig. 3.2 The p*K*a values of many acidic functional groups of lignin are lower than the pH of the feed alkaline liquor; thus they are present in their salt form in the liquor (only acid forms shown)

10,000 ton/yr for ultrapure lignin with a molecular weight appropriate for coatings applications.

One of the disadvantages of lignin recovery processes in which sodium hydroxide (NaOH) is used as a key pulping chemical, such as the Kraft process and classic soda-ash processes, is that the NaOH converts the lignin groups from the acid to the salt form (e.g., see Fig. 3.2) in the alkaline (or black) liquor stream that dissolves the lignin, thus, in effect, making the lignin "dirty". Thus, so-called "organosolv" processes have been proposed, where one starts directly with the original woody biomass and then uses organic solvents mixed with water to separate the constituents of wood (cellulose, hemicellulose, and lignin) from each other. The classic organosolv solvent is ethanol–water solutions at elevated temperatures and pressures (e.g., ~180–195 °C) [16]; other aqueous organic solvents have also been used [17, 18]. Because no inorganic pulping chemicals are used, the final lignin product is ultrapure with a low metals/ash content. However, even after decades of research in the area [19, 20], no viable commercial manufacturer of organosolv lignins exists in the world, as the processes proposed to date have been too expensive [21].

Recently, Clemson researchers have discovered [22] a promising technique for producing ultrapure lignin from low-ash Kraft lignins. The method, known as Aqueous Lignin Purification using Hot Acids, or ALPHA for short, allows one to simultaneous purify, fractionate, and solvate lignins. The essence of the invention is that when a solid, low-ash Kraft lignin is combined with mixtures of acetic acid (AcOH) and water at elevated temperatures under autogenous pressure, the lignin melts in the presence of the solvent (i.e., the AcOH–H_2O mixture) to form not one – but two liquid phases: (1) a more viscous lignin-rich phase containing the higher molecular weight portion of the lignin solvated in about 50 % solvent and (2) a solvent-rich phase of water-like viscosity into which is extracted not only the lower molecular weight portion of the lignin, but also the metal salts [23]. The salts are extracted surprisingly well (i.e., with selectivities as high as 150) out of the lignin-rich phase and into the solvent-rich phase; thus, a lignin-rich phase containing less than 50 ppm sodium can be recovered from a low-ash lignin feed having sodium

levels of several thousand ppm. Finally, because the lignin-rich phase is solvated, it can be directly processed into useful articles (e.g., spun into fibers) if so desired.

In this chapter, the starting point is assumed to be a biomass feedstock (e.g., woody, herbaceous biomass, sorghum) previously subjected to an alkaline pretreatment process (e.g., the Kraft or soda-ash process), such that the cellulose and hemicellulose have been precipitated out and recovered as solids, and the lignin has been dissolved in the alkaline (pretreatment) liquor phase, where it is available for processing via one or more of the lignin-recovery processes described above. Here the discussion will be on the use of SLRP to recover a low-ash lignin from the alkaline liquor, followed by the use of ALPHA to generate an ultrapure, essentially metals-free lignin of well-defined molecular weight. To this date, neither of these processes has been previously discussed in detail in the literature. Another rationale for the focus on SLRP and ALPHA is that both can be carried out continuously, so they are uniquely suited for integration into a single unit.

3.2 Low-Ash Lignins via the SLRP Process

3.2.1 Procedure

A detailed description of the SLRP process being operated in the continuous mode is given below, and a photograph of the research facility is given in Fig. 3.3. Here it is assumed that the alkaline liquor feed is Kraft black liquor from a pulp-and-paper mill, but essentially the same procedure would apply regardless of the feedstock or type of alkaline-liquor pretreatment being used (i.e., whether Kraft, soda-ash, or soda-ash/anthraquinone [24–27]). As depicted in the process schematic in Fig. 3.4, SLRP can be considered to consist of four sections: carbonation, acidification, filtration, and vent-gas capture. Each is described below.

3.2.1.1 Carbonation

For a given experimental run, the alkaline-liquor feed is delivered to the top of the carbonation column, and carbon dioxide (CO_2) gas is delivered to the bottom. The flow of CO_2 gas from a Dewar reservoir is controlled via a metering valve, and the alkaline (black) liquor is delivered from a reservoir to the column with a positive displacement pump. As the black liquor cascades down the column, it reacts with the upward flowing CO_2, partially neutralizing the black liquor down to a pH of ~9.5, as measured by a pH probe in the carbonation settler. As a result of this pH change, a portion (roughly half) of the phenolic and carboxylic acid groups on the lignin are converted from the salt to the acid form (see Fig. 3.2). Thus, most of the lignin becomes less soluble in the caustic black liquor and precipitates out in the form of a separate phase in the carbonation settler located at the base of the carbonation column (see Fig. 3.4).

Fig. 3.3 The continuous-operation Sequential Liquid-Lignin Recovery and Purification (SLRP) unit at Clemson University, USA

It is at this point that the SLRP process deviates significantly from the other lignin recovery processes (i.e., LignoBoost (LB) and LignoForce (LF)), because with SLRP the lignin separates out in the carbonation settler in the form of a "liquid-lignin" phase (vs. the solid-lignin phase that precipitates when using either LB or LF). Clemson and Lignin Enterprises Co., LLC researchers discovered the existence of this phase during laboratory experiments at elevated temperatures. Analyses have shown that the liquid-lignin phase contains about half the metal salts (mostly Na) and half the water of the starting black-liquor phase; thus, this lignin is considerably more lipophilic than it was before the carbonation step, inducing the formation of a new liquid phase. During typical SLRP operation, the column and settler are maintained at 90–150 °C so that the lignin that separates out during the carbonation process is recovered as the desired liquid-lignin phase. Note that the process must be operated under some positive pressure (e.g., 4–8 bar) to prevent both the black-liquor and liquid-lignin phases from losing water by boiling, as they contain significant quantities (50–60 % and 30–40 %, respectively) of water.

Next, the liquid-lignin phase is continuously pumped from the settler to the acidification reactor via a positive displacement pump, see Fig. 3.4. Note how the continuous nature of SLRP is made possible because the lignin is in the form of a pumpable liquid instead of a solid. The lignin-depleted black liquor (also called
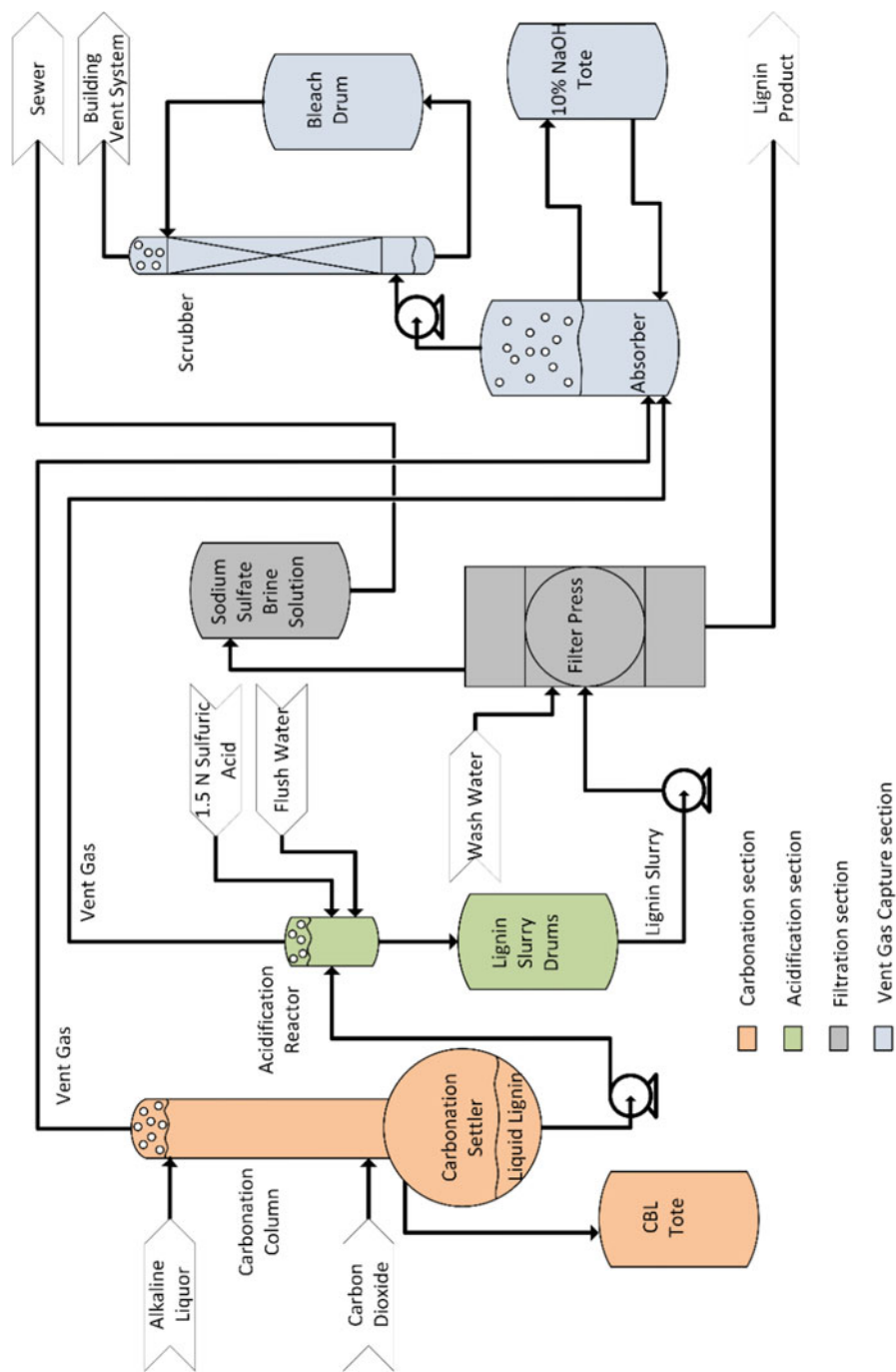
Fig. 3.4 Process flow diagram of the continuous Sequential Liquid-Lignin Recovery and Purification (SLRP) unit at Clemson University, USA

carbonated black liquor, CBL) is removed from the top of the settler via a control valve and collected in a tote. The vent gas/black-liquor level in the top of the carbonation column is controlled by the rate of removal of CBL from the settler, and the liquid-lignin level in the settler is controlled by the rate of removal of liquid lignin via the positive displacement pump.

3.2.1.2   Acidification

Reaction of the liquid-lignin phase with 1.5 N sulfuric acid is then carried out in the acidification reactor in order to convert most of the remaining phenolic and carboxylic acid salt groups to their acid forms. The dominant metal salt in lignin is sodium (derived from the pulping chemicals of NaOH and Na_2S used in the Kraft process), so in essence this step converts most of the remaining O^- Na^+ groups in lignin to OH. The acidification reactor is agitated and made of Hastelloy C to inhibit corrosion, and the sulfuric acid is delivered to the reactor via a diaphragm pump. The pH of the reactor is controlled to 2–3, as measured by a pH probe in the acidification reactor, by controlling the acid flow rate at temperatures and pressures similar to those used in the carbonation section, with pressures again being sufficient to prevent any boiling from occurring. Within this reactor, the liquid lignin is converted to the solid state, forming large particles that resemble brown beach sand and that are easy to filter. The interface level in the reactor between the lignin slurry and the vent gas is monitored via a differential pressure (DP) cell, and lignin slurry is let out through a control valve so as to maintain a constant level in the reactor.

3.2.1.3   Filtration

The lignin slurry (i.e., solid lignin particles plus brine, which consists of sodium sulfate plus water) exiting the acidification reactor is collected in the lignin slurry drums during the course of a run, with the lignin slurry subsequently being delivered to the plate-and-frame filter press with a diaphragm pump (see Fig. 3.4). As the final filter cake contains 50 % brine by weight, this brine is then removed from the filter cake with wash water equivalent to 1–2 times the volume of the original brine in the filter cake. For a typical 24-h run, about 50 kg of lignin product are produced with an ash content of 1–2 %.

3.2.1.4   Vent-Gas Capture

One of the most attractive features of SLRP versus other lignin-recovery technologies is that the entire system is pressurized, because the liquid-lignin phase forms only at elevated temperatures and pressures. Thus, the vent gases to be recovered contain only process gases undiluted by air, minimizing their volumetric flow rate and the quantity of material that has to be treated. Referring to Fig. 3.4, the vent

gases from the carbonation column and acidification reactor are delivered to the vent-gas capture system, which consists of a 10 % NaOH-solution absorber and tote for converting sulfur gases to sodium salts, followed by a bleach-solution (NaOCl) scrubber and drum for similarly converting any possible residual sulfur gases not treated in the NaOH absorber. Back-pressure regulators set at the carbonation column and acidification reactor pressures are located in the vent-gas lines to the absorber and serve to control the flow rate of vent gases to the vent-gas capture system. Analysis has shown that the vent gas consists almost exclusively of CO_2 and H_2S, along with trace levels of other sulfur gases, including methyl mercaptan, dimethyl sulfide, and dimethyl disulfide. Because there is no air to inhibit mass transfer, the CO_2 and H_2S gases absorb rapidly into the solutions. In the NaOH absorber, they are converted to sodium carbonate (Na_2CO_3) and sodium hydrogen sulfide (NaHS), respectively. The pH of this solution is monitored, and NaOH is added to always maintain the pH >12.

The vapor phase escaping the (NaOH) absorber is then delivered to the (bleach) scrubber. The scrubber consists of a packed column that uses an absorbent liquid consisting of a solution of 1–3 % NaOCl and 1–3 % NaOH in water. The absorbent irreversibly converts any residual H_2S that still might be in the system into sodium sulfite (Na_2SO_3) or sulfate (Na_2SO_4). NaOCl and NaOH are added as required to always keep the pH in the drum >12. Air is drawn from the top of the scrubber by the building vent system, so that the absorber and scrubber always operate under a slightly negative pressure. The fact that the bleach drum has had to be changed only once every 30 SLRP runs attests to the very low levels of H_2S and CO_2 vent gas that are generated, along with the outstanding effectiveness of the vent-capture system. H_2S levels are essentially always below the minimum detectable level of 0.3 ppm and no H_2S odor has ever been detected during a SLRP run, indicating virtually zero emissions.

3.2.2 Properties of Liquid-Lignin Phase

To elucidate the properties of the liquid-lignin phase generated in the SLRP process, experiments were also performed on the batch scale. As shown in Fig. 3.5, the batch apparatus consisted of a 2-L pressure reactor with a conical bottom to facilitate collection of the denser liquid-lignin phase. For a typical run, the reactor was charged with 2200 g of alkaline (black) liquor (pH ~13.5), purged and pressurized with nitrogen, heated up to the desired temperature of 100–150 °C, and agitated. Carbon dioxide was then sparged into the black liquor in the reactor at ~250 mL/min until the acidification process with CO_2 was complete, which occurred at a pH of 9.3 ± 0.3. After the reactor vessel was allowed to cool, the spent alkaline (black) liquor (top) phase was decanted off, and the cooled, now solidified liquid-lignin phase was removed from the vessel for analysis. Alternatively, the liquid-lignin phase was removed while hot via the valve in the bottom of the reactor. A more detailed description of the liquid-lignin collection process is given elsewhere [28, 29].
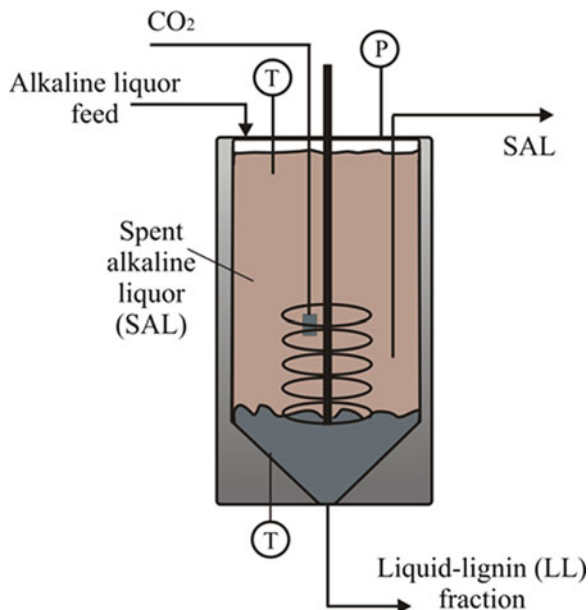
Representative properties of the liquid-lignin phase formed by SLRP at 125 °C from a feed alkaline (black) liquor derived from softwood are given in Fig. 3.6. Here liquid-lignin properties are plotted vs. the solids content of the alkaline black liquor (ABL) feed. Solids content varies depending on the extent to which the alkaline liquor feed is concentrated beforehand by the removal of water using, for example, evaporation or membrane filtration. Because the solids content of the alkaline liquor feed was changed only by the addition of water or its removal via evaporation, it is directly proportional to the ionic strength. Figure 3.6a gives the liquid-lignin yields obtained via SLRP; these results are in-line with those obtained with other lignin-recovery processes [30] for a given solids content. Figure 3.6b shows that the liquid-lignin phase is highly hydrated, containing 30–40 wt % water over the range of feed liquors evaluated. As can be seen in Fig. 3.6c, d, at even the highest solids content in the feed liquor, the ash and sodium content in the liquid-lignin phase are less than half of their original levels. With a good percentage of the metals being excluded from the liquid-lignin phase, the potential exists with SLRP for obtaining a lower ash level in the final lignin product obtained after the sulfuric acid acidification step (see Fig. 3.4). Figure 3.7 shows how the molecular weight decreases and the aromatic OH content of the liquid-lignin phase increases as the ionic strength (solids content) of the alkaline liquor increases.

The effect of solids content on both the bulk (Fig. 3.6) and molecular (Fig. 3.7) properties of the liquid-lignin phase can be explained in terms of molecular interactions, providing useful insight into the phase behavior of this unusual system. Referring to Fig. 3.6a, at the lowest ionic strengths (e.g., 20 % solids) the more lipophilic lignin species, where (attractive) dispersion forces between the lignin
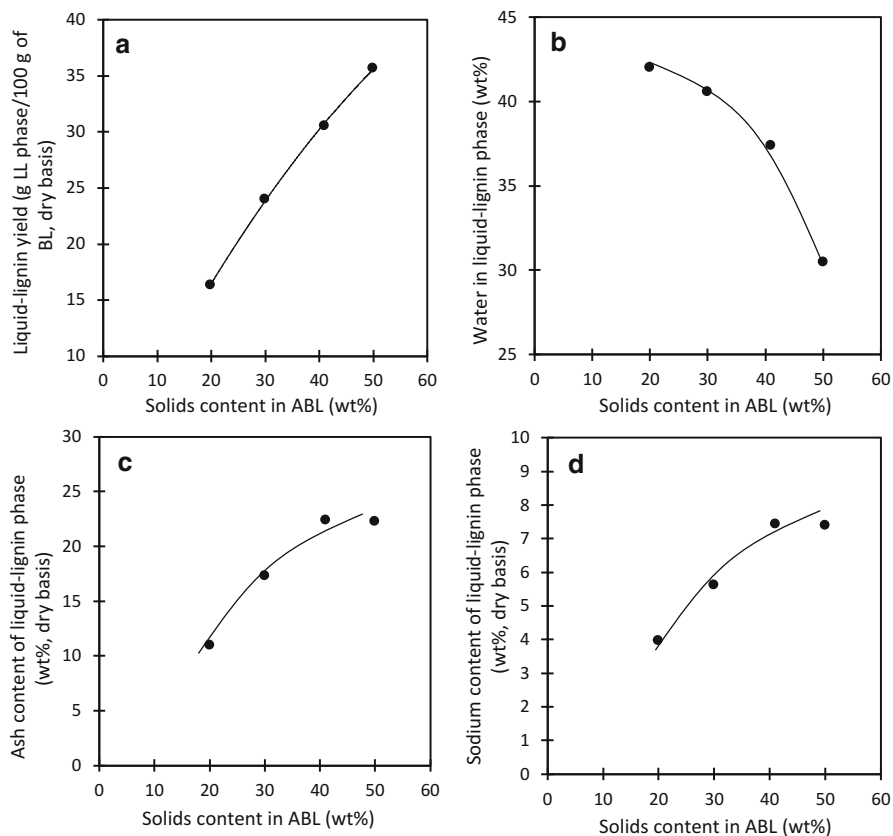
Fig. 3.6 Sequential Liquid-Lignin Recovery and Purification (SLRP) processing of a softwood Kraft black liquor with starting pH of 13.3 and Kappa number of 25, total lignin content of 29.6 %, and ash content of 47.0 %: (**a**) Liquid-lignin yields, (**b**) water content, (**c**) ash content, and (**d**) sodium content of the liquid-lignin phase as a function of solids content of the alkaline black liquor (ABL) phase. Curves are regressions of the data

species dominate, are the first to separate out and form the liquid-lignin phase. Such behavior is analogous to that observed by others for dilute solutions of lignin in alkaline solutions [31]. As seen in Fig. 3.7a, b, these are also the lignins with the highest molecular weights and lowest phenolic content. This latter fact is consistent with how alkaline pulping works, as it tends to depolymerize lignin and add OH groups [32]. As sodium is largely present in lignin as O^-Na^+, the more lipophilic species are also the lowest in ash and metals content (Fig. 3.6c, d). Note also in Fig. 3.6b that at 20 % solids, the liquid lignin is at a maximum in water hydration, so the amount of water available in the liquid lignin for ionizable and polarizable groups is adequate. However, as the alkaline liquor is evaporated and its solids content (ionic strength) increases, the more ionized and polarizable species in lignin (i.e., those for which (repulsive) electrostatic forces dominate) are increasingly screened
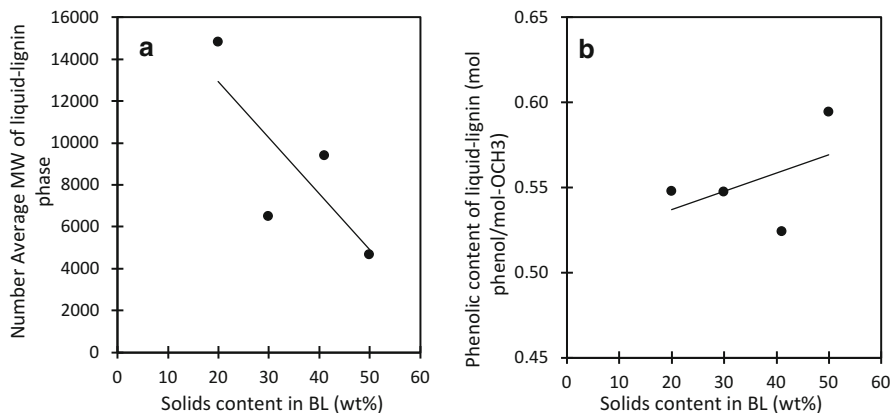
Fig. 3.7 Sequential Liquid-Lignin Recovery and Purification (SLRP) processing of a softwood Kraft black liquor with starting pH of 13.3 and Kappa number of 25, total lignin content of 29.6 %, and ash content of 47.0 %: (**a**) No. avg. molecular weight and (**b**) phenolic content of the liquid-lignin phase vs. solids content of the alkaline (*black*) liquor phase. Lines are regressions of the data

out by the added salts, reducing their stability in the alkaline-liquor solution and causing them to precipitate out, increasing the yield of the liquid-lignin phase (Fig. 3.6a). As seen in Fig. 3.7a, b, these species are of lower molecular weight with more phenolic groups. Finally, at the highest solids content, the ionic strength is at a maximum, as is the driving force for lignin separation. Thus, as shown in the figures above, the highest yield for liquid lignin is obtained, the average molecular weight of the lignin is at a minimum, and the phenolic content is at a maximum. However, far less water is available for hydration of the lignin (Fig. 3.6b), as more water is tied up for solvation of the high level of salt ions in the alkaline-liquor solution. The observed increase in liquid-lignin yield with ionic strength because of decreased water availability is consistent with the well-known "salting-out" effect that occurs with proteins [33, 34].

3.2.3 Fractionating the Liquid-Lignin Phase via SLRP for Control of the Bulk and Molecular Properties of Lignin

One of the attractive features of SLRP vs. other lignin-recovery processes is that the presence of a liquid (vs. a solid) lignin phase facilitates separation of the lignin into fractions. Referring to the continuous version of SLRP in Fig. 3.4, instead of taking the alkaline feed liquor down from a pH of ~13.5–9.5 in a single step in the carbonation column, the pH drop can be decremented. For example, the alkaline (black) liquor feed could be reduced in pH via CO_2 acidification down to a pH of 12.0, and a 1st liquid-lignin fraction recovered. The carbonated black liquor (CBL) generated

Table 3.1 Recovery and selected bulk properties of liquid-lignin fractions generated via Sequential Liquid-Lignin Recovery and Purification (SLRP) at 115 °C and 6.2 bar from a softwood alkaline Kraft liquor

Liquid-lignin fraction	Final pH of fraction[a]	Mass percent of lignin recovered		Water content (wt%)	Ash (wt%)
		Per fraction (%)	Cumulative (%)		
Feed	13.6	0	0	58	47.7
F1	12.8	0.8	0.8	37.9	31.5
F2	12.1	0.6	1.4	32.3	28.1
F3	11.6	3.4	4.8	37.9	22.1
F4	11.1	31.8	36.6	48.2	22.2
F5	10.6	36.2	72.8	42.9	27.8
F6	10	22.6	95.4	39.2	25
F7	9.5	4.6	100	41.9	27.6

[a]pH measurements were made at ambient temperatures

would then be stored in the CBL tank until the desired quantity of that 1st lignin fraction had been (continuously) processed via SLRP to a low-ash lignin product. Then a second SLRP run would commence, with the CBL tank contents now serving as the feed to the Carbonation Column and the pH being decremented to, for example, 11.0 by CO_2 acidification. The 2nd liquid-lignin fraction obtained at a pH of 11.0 would be processed by SLRP until the desired quantity of that low-ash lignin had been obtained, with a second batch of CBL being collected during that time. This second CBL batch could then be processed at a pH of 10.0, for example, in a manner analogous to that described above, to generate a 3rd low-ash lignin product. Finally, the steps could be repeated once again to obtain the last, low-ash lignin fraction at a pH of 9.3. Such a pH-based fractionation process could be carried out to generate as few as two and as many as (practically speaking) 5–6 fractions.

Of course there is little point in such a fractionation process if the fractions generated have no significant property differences! Thus Hodge, Thies, and co-workers [28, 35] carried out SLRP experiments on the batch scale in which a softwood alkaline Kraft (black) liquor was decremented from its initial pH of 13.6 down to 9.5 by ~0.5 units, in order to determine the differences, if any, in the properties of the various fractions. The batch apparatus shown in Fig. 3.5 was used, with the spent (carbonated) black liquor from the preceding CO_2 acidification step serving as the alkaline (black) liquor feed for generation of the next liquid-lignin fraction.

Seven liquid-lignin fractions were obtained via SLRP with incremental pH reduction. Table 3.1 gives the final pH reached for each fraction (measured at room temperature after the samples had cooled), the mass and cumulative mass percentages of lignin recovered per fraction, and selected bulk properties for each liquid-lignin fraction, including water and ash content. Fractions F1 and F2 were reported by Stoklosa et al. [35] to contain a high level of impurities, including aliphatic extractives and by implication polysaccharides (i.e., hemicellulose). Note, then, that the purity of the lignin product could be improved by discarding the part that

precipitates from 13.6 to 12.1 (which represents only 1.4 % of the lignin) and recovering only the portion that precipitates from a pH of 12.1 and down (i.e., F3–F7).

As shown in Fig. 3.8a, b, both the molecular weight and the phenolic content of fractions F3–F7 follow a well-behaved trend with pH, consistent with our understanding of the phenomenon of lignin precipitation from solution [24, 30]. As would be expected, the highest molecular weight fractions (F3–F4) precipitate out first, as they contain the most lipophilic molecules, which have the fewest number of ionizable functional groups (phenolic and other ionizable groups participate in the condensation reactions that form larger lignin polymers) [36]. When they are converted from the salt to acid form (see Fig. 3.2), these ionizable groups no longer tend to keep the lignin species in solution, resulting in lignin aggregation and precipitation [31, 32]. As shown in Fig. 3.8a, b, lower pH's are required to precipitate the lower molecular weight lignin species from solution, as they have more ionizable groups; also, with more groups the probability increases that some have lower pK_a values (see Fig. 3.2). Because the highest molecular weight lignin polymers have a lower number of ionizable groups, they also have a lower sodium content, see Fig. 3.9b. As would be expected, the ash content (see Table 3.1) also correlates well with sodium levels and inversely with molecular weight. Finally, the softening (melting) points of the liquid-lignin fractions were measured [28] under slight positive pressure in a water–saturated air environment so that no water solvated in the liquid-lignin phase would evaporate away and thus influence the measured softening points. The goodness of the correlation of softening point with molecular weight (Fig. 3.9a) is somewhat surprising but also encouraging, as it provides evidence that the GPC method used for relative molecular weight determination is reliable.

In summary, SLRP can be used not only to obtain a generic, low-ash lignin product, but also as a continuous fractionation process to produce low-ash lignin fractions with specified molecular weights, phenolic contents, and purity levels. Such an improved control of both the bulk and molecular properties of low-ash lignin, as
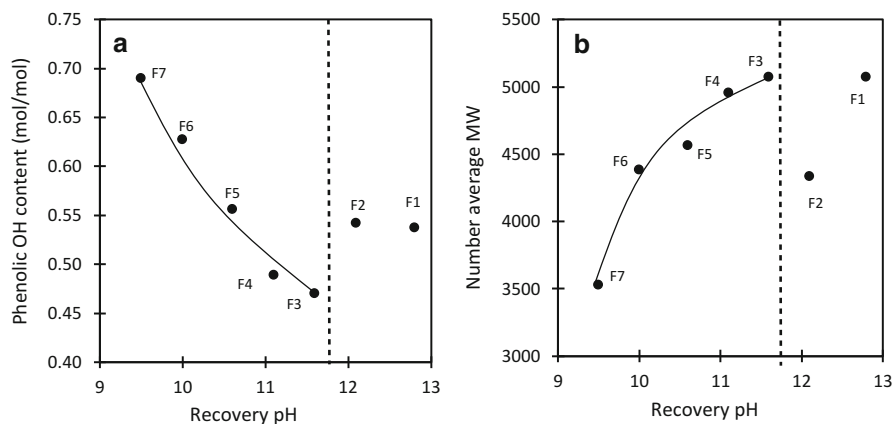
Fig. 3.8 The lignin fractions shown in Table 3.1 exhibit significant differences in molecular structure (e.g., phenolic content) and molecular weight
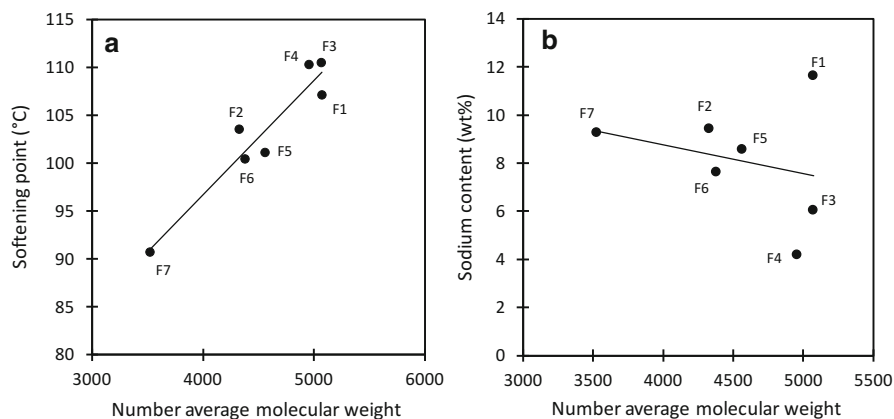
Fig. 3.9 (**a**) Correlation of softening points of the liquid-lignin fractions in Table 3.1 with number average molecular weight; (**b**) sodium content of lignin fractions vs. molecular weight

provided by the SLRP process, would be expected to expand the range of potential product applications for lignin in the future.

3.3 Ultrapure Lignins via the ALPHA Process

3.3.1 Liquid–Liquid Equilibrium Phase Behavior for the Acetic Acid–Water–Lignin System

In order for the Aqueous Lignin Purification with Hot Acids (ALPHA) process to be successfully applied, one must operate in the region of liquid–liquid equilibrium (LLE) previously mentioned in Sect. 3.1.2, which consist of (1) a solvent-rich phase into which the low molecular weight lignin and the metals are extracted and (2) a lignin-rich phase containing lignin species of higher molecular weight from which the metal salts and other impurities have been efficiently removed. Thus, the first task is to locate this region of liquid–liquid equilibrium, which generally exists at above-ambient temperatures for lignin dissolved in mixtures of acetic acid and water. Roberts, Thies, and co-workers [23, 37] used both visual observation and electrochemical impedance spectroscopy (EIS) to locate the desired transition from solid–liquid equilibrium (SLE) to LLE for a low-ash lignin recovered from an alkaline (Kraft black) liquor via the SLRP process (see Fig. 3.4). The results of this work are summarized with the phase diagram shown in Fig. 3.10, which can be used as a guide for selecting the appropriate operating temperatures for the ALPHA process. For example, if one wishes to carry out ALPHA with a solvent mixture of 40/60 wt/wt acetic acid/water, operation above the SLE–LLE phase transition temperature of ~60 °C is required in order to be in the desired LLE region.
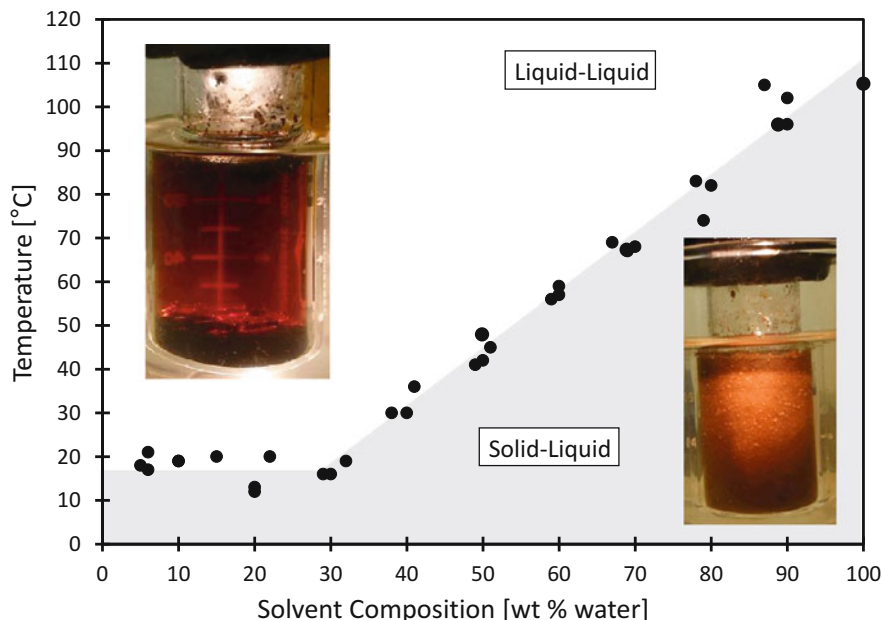
Fig. 3.10 Phase diagram of the lignin–acetic acid–water system. The feed lignin was a low-ash, softwood Kraft lignin obtained via the Sequential Liquid-Lignin Recovery and Purification (SLRP) process. Points represent both electrochemical impedance spectroscopy (EIS) and visual data. Below the points, solid lignin is in equilibrium with the solvent phase, and above the data, a second lignin-rich liquid phase is in equilibrium with the solvent-rich phase

3.3.2 ALPHA as a Single-Stage, Batch Process

The first step was to carry ALPHA out as a batch, single-stage extraction, so that important characteristics of the process could be determined. To determine the distribution of both the lignin and the metal (salts) between the solvent-rich and lignin-rich phases, specified mixtures of acetic acid, water, and (solid) lignin were added to 20 mL GC headspace vials, which were then sealed and heated above the phase-transition temperatures shown in Fig. 3.10 so as to be in the desired LLE region. In particular, the vials were inserted into an oil bath that was maintained at the desired temperature, the vial contents were stirred and their temperature monitored, and the phase transition from SLE to LLE (see Fig. 3.11) was observed to occur within 5–10 min. After the phases were allowed to come to temperature and equilibrate in the LLE region for 15–20 min, the solvent-rich phase was drawn off with a syringe, and the remaining, lignin-rich liquid phase was collected from the vial. Both phases were dried in a vacuum oven at ambient temperatures, and the amount of lignin in each phase was determined gravimetrically. The metals content of the dried lignin from each phase was determined via ICP–AES and the molecular weight was determined by GPC. Additional details of the technique are given elsewhere [23].
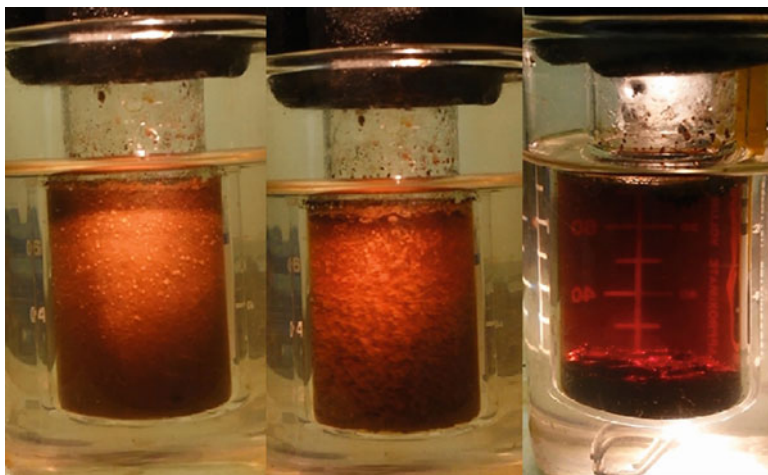
Fig. 3.11 Observed phase transition for the lignin–acetic acid–water system shown in Fig. 3.10, using a solvent mixture of 40/60 acetic acid/water and a solvent:lignin ratio of 9:1. The left-most picture is at room temperature where solid particles are seen suspended in the solution by the action of the stir bar. The middle picture was taken at the phase transition where particle swelling and agglomeration is observed. The third picture on the right is taken above the phase transition; here a clear interface is observed between the two liquid phases

Figure 3.12 illustrates the general characteristics of how the lignin distributes between each phase in the LLE region above the SLE–LLE phase transition temperature. Note the versatility of the ALPHA process: depending on the solvent composition, most of the lignin can be distributed into either the solvent-rich or the lignin-rich phase. For example, at 75/25 acetic acid/water, only a small percentage of the lignin is present in the lignin-rich phase; most is dissolved in the solvent-rich phase, which is a powerful solvent at these conditions. However, less than 10 % of the lignin dissolves in the solvent-rich phase of a 25/75 acetic acid/water solvent system, as this is a relatively weak solvent for lignin. Generally speaking, the above acetic acid/water composition ranges encompass the region of practical interest for carrying out the SLRP process. Within this range, we can dramatically change the amount of lignin dissolved in either the solvent-rich or lignin-rich phase. Two final comments about Fig. 3.12 are needed here.

First, it should be noted that the lignin distribution shown in Fig. 3.12 is not a strong function of temperature for a given solvent mixture (as long as you are above the SLE–LLE line in Fig. 3.10). Second, the solvent compositions given here are for the overall solvent compositions that were put into the vial; experiments to determine the solvent composition *in each phase* are in progress (e.g., the lignin-rich phase is highly solvated and contains a surprisingly large amount of solvent (i.e., typically 50–60 wt % of that phase is solvent). The usefulness of the LLE region for fractionating the lignin is illustrated in Fig. 3.13. Here it can be seen that the lignin species distribute between the two phases according to molecular weight, with the
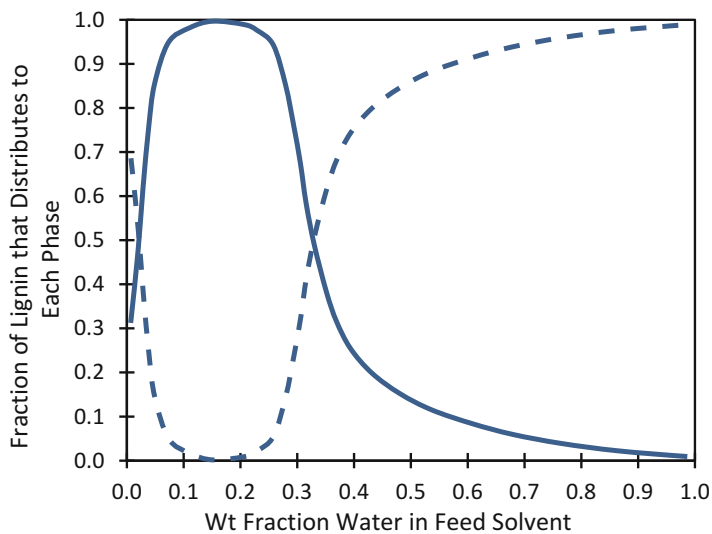
Fig. 3.12 Distribution of the lignin (described in Fig. 3.10) between the solvent-rich and the lignin-rich phase as a function of solvent composition at a temperature of 70 °C and a solvent:lignin ratio of 9:1. The solid line represents the lignin dissolved in the solvent-rich phase, and the dashed line represents the lignin in the lignin-rich phase
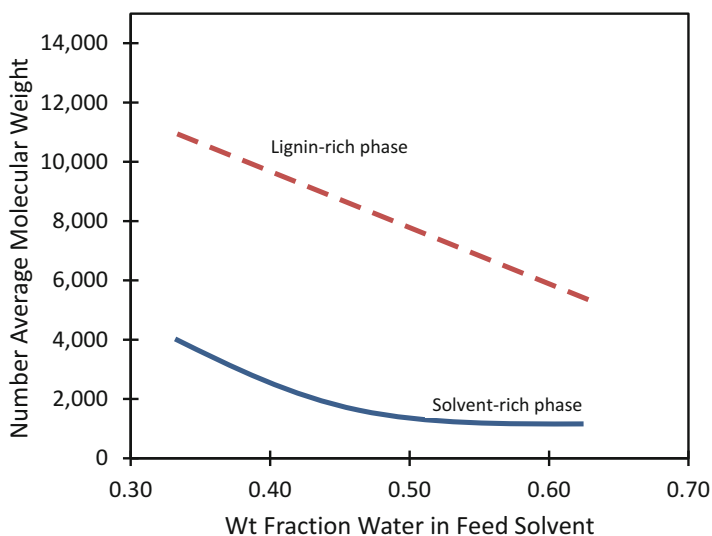
Fig. 3.13 Molecular weight data for the lignin dissolved in the solvent-rich and lignin-rich phases of Fig. 3.12 as a function of the feed solvent composition

solvent-rich phase containing the lower molecular weight species and the lignin-rich phase the higher molecular weights. In addition, as the water content of the solvent-rich phase increases from the "powerful solvent" region of 10–20 % water, the molecular weight of the lignin recovered in the solvent-rich phase decreases even more. The specific trends for molecular weight changes in the lignin-rich phase with changing solvent composition are less clear, partly because lignin condensation reactions, which have been observed in other types of lignin-rich phases [36], can occur and increase the molecular weight beyond the original equilibrium composition unless residence times are kept under 30 min.

Probably the most surprising feature of the ALPHA process is the ability to generate clean lignin fractions of higher molecular weight without a washing step. As shown in Fig. 3.14, a low-ash lignin feed with a sodium content of 1400 ppm can be cleaned to <200 ppm in a single ALPHA processing step. The cleaned lignin comprises the lignin-rich phase, which is more than 70 % by weight of the original lignin at all tested solvent compositions (60/40 to 40/60), so good lignin yields are obtained. Furthermore, the cleaned, lignin-rich phase requires no washing step; <200 ppm is the sodium composition of the final lignin after drying. Figure 3.14 also shows (right axis) that excellent selectivities are obtained for sodium (and the other metals) being extracted into the solvent-rich phase.

3.3.3 Two-Stage Batch ALPHA for Generating Ultrapure Lignins

As stated in Sect. 3.1.2, lower levels of sodium (<100 ppm) and total metals (100–200 ppm) are required for high-value applications of lignin. Thus, the addition of a 2nd step of ALPHA extraction to the single step discussed above was investigated to see how much lower the sodium levels could be reduced in the lignin-rich phase.

Fig. 3.14 Sodium content of the lignin in the lignin-rich phase of Fig. 3.12 and selectivities for the extraction of sodium into the solvent-rich phase of Fig. 3.12 as a function of the feed solvent composition. Circles are sodium content and triangles are selectivities
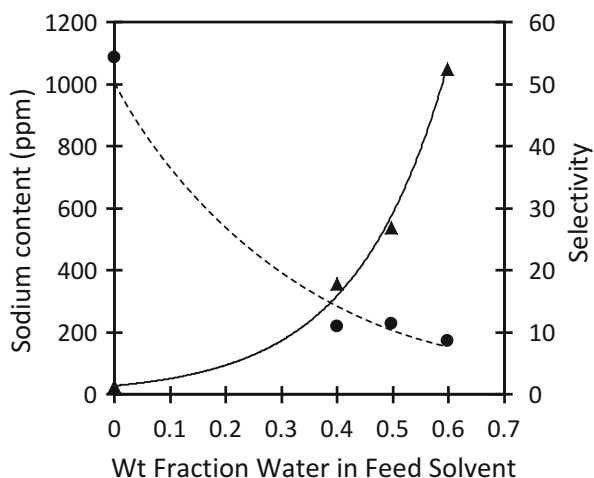
The setup used is shown schematically in Fig. 3.15. A Parr reactor system was used for this work, and a temperature of 95 °C was used so that the system would always be in the LLE region, regardless of the solvent composition employed. For the 1st extraction stage, a solvent composition of 50/50 wt/wt acetic acid/water was combined with the low-ash lignin feed (containing 1400 ppm sodium) to produce solvent-rich and lignin-rich phases. The resultant lignin-rich phase was then contacted in a 2nd stage with a 70/30 acetic acid–water solution (a more powerful solvent system was needed because the lignin-rich phase is now of a higher molecular weight than the feed lignin), and that mixture also created a system of LLE comprised of a solvent-rich and a lignin-rich phase. The final lignin-rich phase from Stage 2 was found to contain only 25 ppm sodium and less than 100 ppm total metals, a most encouraging result. This phase was also found to consist of ~60 wt % solvent, so in principle it was ready for direct processing into a fiber or film, for example. Each solvent-rich phase generated from the 1st and 2nd stages was then contacted with water at ambient temperatures to precipitate out a solid lignin phase
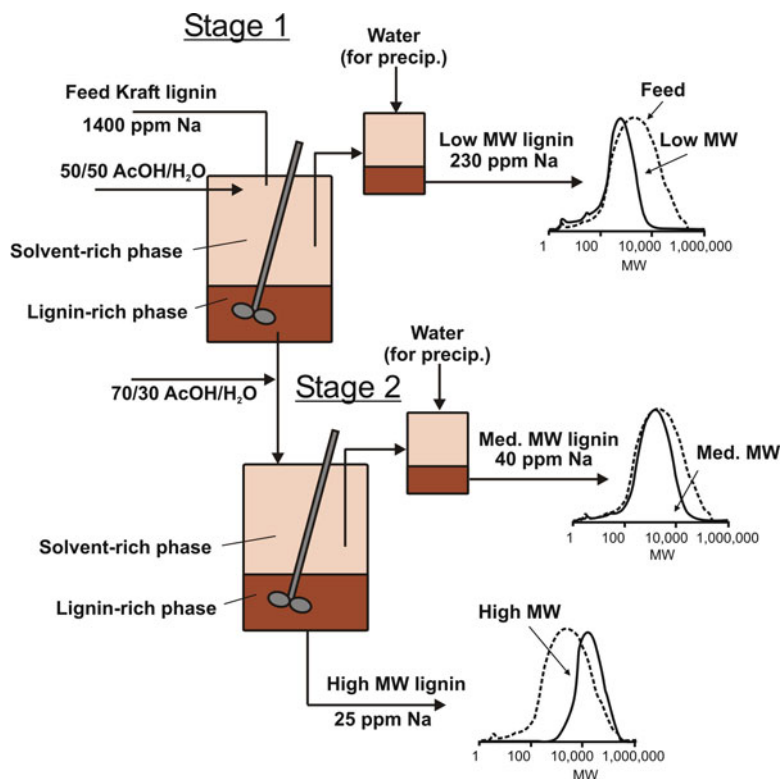
Fig. 3.15 Two-stage batch Aqueous Lignin Purification with Hot Acids (ALPHA) process [22, 23] for producing ultrapure lignin fractions encompassing a range of molecular weights. For each stage, the solvent:lignin ratio was 9:1. The lignin source was the low-ash Kraft lignin described in Fig. 3.10

with the sodium contents shown in the figure. A hot but weaker acetic acid–water mixture could have been used instead to form a lignin-rich lignin phase of similar or better purity. Thus, a simple, 2-stage batch version of the ALPHA process can be used to generate three lignin fractions of low, medium, and high molecular weight, with two of them being ultrapure [23]. Finally, note that one can envision multiple options of this two-stage setup, depending on the solvent compositions needed to obtain the desired product purities. For example, if an ultrapure low molecular weight lignin was the objective, the 1st stage could use a 60/40 acetic acid/water mixture to distribute less of the salts into the solvent-rich phase. Then the solvent-rich phase could be contacted with a 40/60 acetic acid/water mixture, for example, to obtain an ultrapure, lignin-rich phase of low molecular weight.

3.3.4   ALPHA as a Continuous Process: Minimizing Residence Times and Maximizing Throughputs for Ultrapure Lignins

With larger portions of ultrapure lignin being needed for evaluation in product applications, we have recently developed a continuous version of the ALPHA process. Further motivation for this work was to minimize residence times, as the results described above indicate that condensation (polymerization) reactions in the lignin-rich phase can occur during batch processing. A schematic of our process is given in Fig. 3.16 for a one-stage, continuous version of ALPHA. For a typical experiment, the lignin is mixed with water in approximately equal weight ratios to create a slurry with a batter-like consistency. This slurry is input via a feed hopper into a progressive cavity pump; the slurry leaving the pump is then combined with a preheated mixture of acetic acid and water in a tee. The amounts of lignin–water slurry and acetic acid–water mixture are both calculated a priori so that the overall composition of each component has been set to its desired value (e.g., 10 g lignin/100 g overall mixture and a 50/50 acetic acid/water ratio). The resultant mixture of acetic acid, water, and lignin, which is now at the desired temperature for the formation of LLE (e.g, 70–80 °C), is then fed to a static mixer, where intensive mixing of the components occurs, and solvent-rich and lignin-rich liquid phases are formed. After a residence time in the static mixer of about 30 s, the phases are separated in a settler and are collected.

This work is in its preliminary stages, but initial results are encouraging. Two kinds of Kraft lignin, SLRP and BioChoice™ (Domtar Corp.), were processed in the continuous ALPHA setup described above. Reductions of an order of magnitude and more were achieved in the levels of sodium and other metals in both lignins tested. For example, the sodium level in SLRP lignin was reduced from 1400 to <75 ppm sodium when contacted with a 30/70 acetic acid/water mixture. Furthermore, GPC of this lignin-rich phase indicated no change in the molecular weight distribution, indicating that the reduced residence time was successful in eliminating the polymerization condensation reactions that occurred with batch processing.

Fig. 3.16 Process flow
diagram of continuous,
one-stage Aqueous Lignin
Purification with Hot Acids
(ALPHA) process [22, 23]
for producing ultrapure
lignin
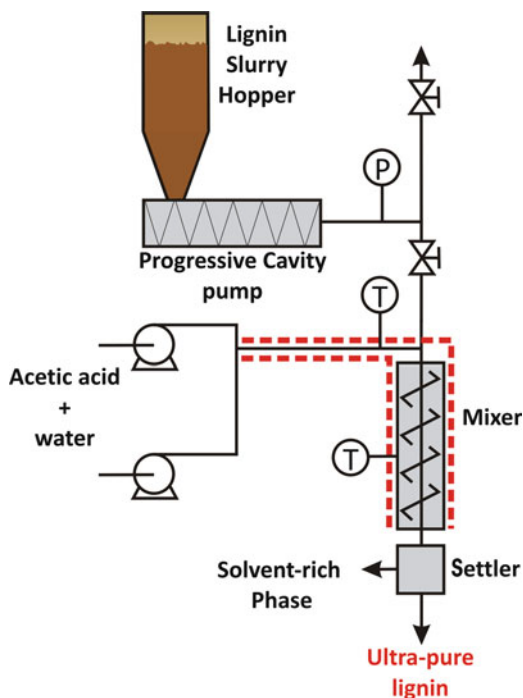
3.4 Conclusions and Future Outlook

Continuous-processing technologies for recovering clean and ultrapure lignins from
alkaline black liquors and other alkaline liquor biomass streams have been developed. These technologies were enabled by the discovery of a novel phase-partitioning
phenomenon involving liquid–liquid equilibrium, which allows for the fractionation, solvation, and purification of lignin. The ability to generate lignin fractions
with controllable bulk and molecular properties of high purity, using technologies
such as SLRP and ALPHA, should enable advances in the nascent industry that is
arising and is dedicated to the generation of lignin-based biomaterials.

The results presented herein were for an alkaline (black) liquor generated as a
by-product of the Kraft processing of softwood; hardwoods have also been investigated and similar results were obtained [29]. From a conceptual standpoint, the
technologies described herein should also be directly applicable to the alkaline
liquors generated as a by-product of the soda-ash processing of other biomass
streams, such as hybrid poplar and switchgrass, in which cellulose and hemicellulose are recovered and converted to biofuels. However, experimental data analogous
to what is presented herein will be needed to quantify systems using alternative
biomass feedstocks and alkaline processing techniques that are similar to, but nonetheless different from, the Kraft process.

References

1. Patt R, Kordsachia O, and Süttinger R. Pulp. In: Ullmann's encyclopedia of industrial chemistry. Weinheim: Wiley-VCH; 2011. P. 487–491.
2. Biermann CJ. Handbook of pulping and papermaking. 2nd ed. San Diego: Elsevier; 1996.
3. Gosselink RJA, et al. Co-ordination network for lignin-standardisation, production and applications adapted to market requirements (EUROLIGNIN). Ind Crop Prod. 2004;20:121–9.
4. Doherty WOS, Mousavioun P, Fellows CM. Value-adding to cellulosic ethanol: lignin polymers. Ind Crop Prod. 2011;33:259–76.
5. Adler E. Lignin chemistry – past, present and future. Wood Sci Technol. 1977;11:169–218.
6. Tomani P. The lignoboost process. Cellul Chem Technol. 2010;44:53–8.
7. Kouisni L, et al. The LignoForce system: a new process for the production of high-quality lignin from black liquor. J Sci Technol For Prod Processes. 2012;2:6–10.
8. Lake MA, Blackburn JC. 2009. Process for recovering lignin. US Patent 9,260,464, FEb. 16, 2016.
9. LignoBoost plant at Domtar's Plymouth mill in North Carolina. 2016. http://www.valmet.com/industries-we-serve/references/pulping-and-fiber/lignoboost-plant-at-domtars-plymouth-mill-in-north-carolina/. Accessed 10 May 2016.
10. Pulp and Paper Canada. West Fraser lignin project gets $6 million from SDTC. 2015. http://www.pulpandpapercanada.com/news/west-fraser-lignin-project-gets-6-million-from-sdtc-1003550314. Accessed 10 May 2016.
11. Gordobil O, et al. Kraft lignin as filler in PLA to improve ductility and thermal properties. Ind Crops Prod. 2015;72:46–53.
12. Hilburg SL, et al. A universal route towards thermoplastic lignin composites with improved mechanical properties. Polymer. 2013;55:995–1003.
13. The National Archives, Department of Transport, United Kingdom. Renewable Transport Fuels Obligation (RTFO) order. 2013. Accessed 10 May 2016.
14. Gellerstedt G, Sjöholm E, Brodin I. The wood-based biorefinary: a source of carbon fiber? The Open Agric J. 2010;3:119–24.
15. Compare AL et al. Low cost carbon fibers from renewable resources. Adv Affordable Mat Technol. 2001. http://web.ornl.gov/~webworks/cppr/y2001/pres/111380.pdf. Accessed 12 May 2016.
16. Arato C, Pye EK, Gjennestad G. The lignol approach to biorefining of woody biomass to produce ethanol and chemicals. Appl Biochem Biotechnol. 2005;121:871–82.
17. Pan X, Sano Y. Acetic acid pulping of wheat straw under atmospheric pressure. J Wood Sci. 1999;45:319–25.
18. Hasegawa I, et al. New pretreatment methods combining a hot water treatment and water/acetone extraction for thermo-chemical conversion of biomass. Energy Fuels. 2004;18:755–60.
19. Kleinert TN. Organosolv pulping and recovery process. US Patent US3585104. 1968.
20. Iakovlev M, You X, van Heiningen A, Sixta H. SO2–ethanol–water (SEW) fractionation of spruce: kinetics and conditions for paper and viscose-grade dissolving pulps. RSC Adv. 2014;4:1938–50.
21. Holladay JE, et al. Top value-added chemicals from biomass – volume II-results of screening for potential candidates from biorefinery lignin. Richland: Pacific Northwest National Laboratory; 2007.

22. Thies MC, Klett AS, Bruce DA. Solvent and recovery process for lignin. U.S. Patent Application No. 2016/0137680 A1, May 19, 2016.
23. Klett AS, Chappell PV, Thies MC. Recovering ultraclean lignins of controlled molecular weight from Kraft black-liquor lignins. Chem Commun. 2015;51:12855–8.
24. Sixta H. Handbook of pulp. Weinheim: Wiley-VCH Verlag GmbH; 2008.
25. Farrington A, Nelson P, Vanderhoek N. New alkaline pulping process. APPITA J. 1977;31(2):119–20.
26. Francis RC, et al. Positive and negative aspects of soda/anthraquinone pulping of hardwoods. Biores Technol. 2008;99(17):8453–7.
27. Springer EL, Atalla RH, Reiner RS. Potential sulfur-free pulping methods. TAPPI fall technical conference and trade fair. Atlanta, GA; 2002.
28. Velez J, Thies MC. Solvated liquid-lignin fractions from a Kraft black liquor. Bioresour Technol. 2013;148:586–90.
29. Velez J, Thies MC. Liquid lignin from the SLRP process: the effect of processing conditions and black-liquor properties. J Wood Chem and Technol. 2016;36:27–41.
30. Zhu W, Westman G, Theliander H. Investigation and characterization of lignin precipitation in the Lignoboost process. J Wood Chem Technol. 2014;34:77–97.
31. Norgren M, et al. Aggregation of kraft lignin derivatives under conditions relevant to the process, part I: phase behavior. Colloids Surf. 2001;194:85–96.
32. Koda K, et al. Molecular weight-functional group relations in softwood residual kraft lignins. Holzforschung. 2005;59:612–9.
33. Coen CJ, Blanch HW, Prausnitz JM. Salting out of aqueous proteins: phase equilibria and intermolecular potentials. AIChE J. 1995;41(4):996–1004.
34. Bailey JE, Ollis DF. Biochemical engineering fundamentals. New York: McGraw-Hill; 1986.
35. Stoklosa RJ, et al. Correlating lignin structural features to phase partitioning behavior in a novel aqueous fractionation of softwood Kraft black liquor. Green Chem. 2013;15:2904–12.
36. Velez J, Thies MC. Temperature effects on the molecular properties of liquid lignin recovered from Kraft black liquor. ACS Sustain Chem Eng. 2015;3(6):1032–8.
37. Klett AS, Gamble JA, Thies MC, Roberts ME. Identifying thermal phase transitions of lignin-solvent mixtures using electrochemical impedance spectroscopy. Green Chem. 2016;18:1892–7.

Part II
Biological Conversion

Chapter 4
Lignin Degrading Fungal Enzymes

Ayyappa Kumar Sista Kameshwar and Wensheng Qin

4.1   Introduction

Lignin is the most complex and abundant naturally occurring biopolymer present in plant cell walls. It forms a tight matrix around the carbohydrates, and it is closely associated with cellulose, hemicellulose and pectin, forming an intricate structure. Lignin provides several advantages to the plant cell wall such as mechanical strength supporting large plant structures, protection against microbial infections as it is hard to degrade, impermeability and stability against chemical and mechanical attacks [1]. Lignin is an aromatic polymer made up of three basic units: p-coumaryl alcohol (4-hydroxycinnamyl alcohol), coniferyl alcohol and sinapyl alcohol which are collectively called monolignols that are derived from phenylalanine (aromatic amino acid) [2]. Monolignols produce three phenylproponoid units, p-hydroxyphenyl (H), syringyl alcohol (S), guaiacyl (G) later these units are collectively joined to form the lignin polymer [3]. The percentage of the different phenylproponoids present in lignin varies based on the type of cell, taxa, wood, environment and developmental conditions. Lignin present in dicotyledonous angiosperms contains mainly G and S, with traces of H units. Gymnosperms, contain high G and low H and, grasses (Monocots) contain high H units with, comparable G and S units [3]. Lignin contains several interionic bonds such as alkyl-alkyl, aryl-alkyl and aryl-aryl, lignin also associates with plant cell wall polysaccharides which makes the breakdown and separation of lignin very difficult [4]. Separation of lignin from lignocellulosic materials is not possible without partial disruption of the lignocellulosic network. During plant cell wall polymerization several intermediates are produced and, these intermediates react with oligolignols, carboxyl and hydroxyl groups of glucuronic acids in hemicellulose units resulting in ethers and esters [5–7]. Research groups

A.K.S. Kameshwar • W. Qin (✉)
Department of Biology, Lakehead University,
955 Oliver Road, P7B 5E1 Thunder Bay, ON, Canada
e-mail: wqin@lakeheadu.ca

have tried to efficiently separate lignin from lignocellulosic biomass (cellulose, hemicellulose) for production of cellulosic ethanol (biofuels). Biofuel and paper pulp industries make use of cellulose for the production of paper and cellulosic ethanol, leaving behind hemicellulose and lignin as industrial effluents. The depolymerization of the polyphenolic chemical structure of lignin offers many opportunities for producing conventional phenolic compounds [8].

Several studies have showed that lignin is resistant to the microbial attack however a few groups of microorganisms belonging to bacteria and fungi are able to efficiently degrade lignin [9]. It has been reported that anaerobic processes fail to attack aromatic rings while aerobic processes tend to degrade lignin [7, 9]. Fungi are the most studied organisms for lignin degradation. Basidiomycota phylum consists of a wide range of wood degrading fungi, thus it is the largest wood degrading fungal group [10, 11]. Wood degrading fungi belonging to Basidiomycota phylum can be further divided into white, brown and soft rotting fungi based on their wood decaying patterns. In the Basidiomycota phylum, most of the wood degrading fungi belong to the Agaricales and Aphyllophorales orders [12]. White rot fungi are considered to be the most efficient lignin degraders, but their degradation rates for lignin and cellulose in wood tissue vary considerably [13]. Some white rot fungi are able to selectively degrade lignin without degrading much cellulose while other white rot fungi are able to attack both lignin and carbohydrates. However, fungi which are able to selectively degrade lignin are of higher significance due to their commercial applications (e.g. paper and pulp industries) [10, 13]. White rot fungi secrete a wide range of wood degrading enzymes that are involved in the breakdown of carbohydrate components (cellulose and hemicellulose) and lignin. White rot fungi secrete different lignin degrading enzymes such as lignin peroxidase, manganese dependent peroxidase, laccase, horse radish peroxidase, and dioxygenases such as protocatechuate 3,4 dioxygenase, 1,2,4-trihydroxybenzene 1,2-dioxygenase, catechol 1,2-dioxygenase, superoxide dismutase, glyoxal oxidase, glucose 1-oxidase, aryl alcohol oxidase, veratryl alcohol oxidase, pyranose oxidase and, quinone oxidoreductase [13, 14]. When compared to white rot fungi, brown rot fungi are more efficient in degrading cellulose and hemicellulose than lignin, however these fungi potentially modify lignin [10]. Wood affected by brown rot fungi generally appears shrunken and dark in color with brick and cubical shaped fragments, these fragments can be easily broken down further to a brown color powder (modified lignin). Wood decaying fungi belonging to the phyla Ascomycota and Deuteromycota are mostly soft rot fungi, these fungi usually decay wood, causing a light brown color. Based on the patterns they form on the wood these fungi can be further classified into type I (form biconical or cylindrical cavities in secondary walls) and type II (this type of fungi cause erosion). When compared to white rot fungi, type II soft rot fungi do not attack the middle lamella (Table 4.1) [10]. Some basidiomycete fungi form unique symbiotic associations with wood degrading termites belonging to Termitomyces, Bacteroidetes and Firmicutes classes. Some bacteria and flagellated protists also resides in the termite hind gut [7]. Both lower and higher termites maintain a remarkable microbial diversity in their guts and, some

Table 4.1 Illustrates potential wood degrading fungal phylum and their properties

Type of wood degradation	Phyla and order	Wood degradation property	Decaying wood	Fungal strain
White Rot	Basidiomycota:	Causes cell wall erosion in cell lumina by occupying large spaces with its mycelium.	Moist, spongy appearance white or yellow	*Phanerochaete chrysosporium, Ceriporiopsus subvermispora,*
	Agaricales Aphyllophorales	Efficiently degrade lignin.		
Brown Rot	Basidiomycota:	Penetrates through cell wall pores, by effecting the S2 layer of cell wall in lumen.	Dry, shrunken, cracked, in brown colored fragments	*Gleophylum trabeum, Postia placenta,*
	Agaricales Aphyllophorales	Efficiently degrades cellulose and hemicellulose.		*Serpula lacrymans,*
Soft Rot	Ascomycota:	Type I fungi forms cylindrical, biconical cavities in secondary cell walls.	Decayed wood is brown in color with soft look which further cracks and becomes dry.	*Fusarium solani, Penicillium chrysogenum, Daldinia concentrica*
	Deuteromycota	Type II fungi are erosive wood degraders.		

bacteria were found to colonize in hindgut, fore and midgut. Termites depend on their gut microbiota for their nutrition, as most of their nutrition is derived from the downstream products of microbial metabolism [7]. The underlying mechanisms behind the utilization and degradation of lignocellulose biomass by termites was only revealed recently. Genome sequencing and metagenome sequencing (termite gut microbiome) studies conducted on different lignocellulose degrading fungi have revealed several interesting facts about lignin degradation [15].

4.2   Carbohydrate Active Enzyme Database (CAZy)

CAZy is a sequence based classification of the enzymes which are involved in the formation, modification and breakdown of poly and oligosaccharides [16]. There are three major defining features underlying CAZyme classification, (a) Classification is based on significant similarity of amino acid sequences with a

minimum of one biochemically characterized founding member (b) CAZymes generally are modular proteins with a catalytic module containing different discrete units, thus it is classified module by module [17]. Third important feature CAZyme classification is based on systematical protein sequences upon daily GenBank releases which avoids analyzing unfinished protein sequences with changing accession numbers. The CAZy database is currently divided into two main classes as Carbohydrate active enzymes and Carbohydrate binding modules (CBMs). Carbohydrate active enzymes are further divided into five classes they are (a) Glycoside hydrolases (GH) (b) Glycosyl Transferases (GT) (c) Polysaccharide Lyases (PL) (d) Auxiliary Activity enzymes (AA) (e) Carbohydrate Esterases [16]. Carbohydrate binding modules (CBMs) earlier known as Cellulose binding modules, recent discovery of several new binding modules which bind to carbohydrates other than cellulose was the main reason behind the name change to carbohydrate binding modules. The occurrence of lignin in close associations with other polysaccharides (cellulose and hemicellulose) in plant cell walls led to, lignin degrading enzymes and lytic polysaccharide monoxygenases (LPMO) to be classified into "Auxiliary activity enzymes" among the large class of enzymes involved in the modification and breakdown of lignocellulose. Auxiliary activity enzymes are currently classified into three subfamilies of polysaccharide monoxygenases and eight classes of lignolytic enzymes, a total of 1045 enzymes were classified into 13 subfamilies and 304 non classified enzymes [16]. CAZy database can be used to analyze the genomes (Carbohydrate active enzymes encoded in the genome of an organism CAZome), and also to study the molecular details of substrate recognition. CAZome can provide significant insights about the nature and amount of metabolism of complex carbohydrates by a species. At present the CAZy database covers 4623 genomes in the following kingdoms they are: bacteria (3946), archaea (220), eukaryota (180) and viruses (277) [16].

4.3   Fungal Oxidative Lignin Enzymes (FOLy)

When compared to other microorganisms, fungi are the most efficient lignin degraders. Fungi secrete a wide range of extra and intracellular enzymes for the degradation of lignin. Lignin degradation by fungi is a significant step during carbon recycling and for maintaining terrestrial ecosystems. Thus, understanding the fungal enzymes involved in the breakdown of lignin is important. FOLy database was developed to classify the enzymes involved in the breakdown of lignin, by retrieving publicly available information from GenBank, Uniprot PDB, EMP PMD, and Pubmed [18]. The structure of FOLy is similar to that of Carbohydrate Active Enzyme (CAZy) [16]. Degradation of carbohydrates by enzymes is dependent on cocktails of highly specific extracellular enzymes for breaking glycosidic bonds. While lignin depolymerization makes use of various extracellular oxidative enzymes, which are responsible for generating highly reactive free radicals that cause cleavage of carbon-carbon, and inter unit ether bonds. FOLy has classified

lignin breaking enzymes into two major classes as (a) Lignin Oxidizing (LO) enzymes and (b) Lignin degrading auxiliary enzymes (LDA's), based on their potential involvement in lignin breakdown [18].

4.4   Lignin Oxidizing Enzymes (LO)

Non-specificity and high oxidation potential are the main attributes of lignin oxidizing enzymes. Lignin oxidizing enzymes are categorized into three classes LO1 (Laccases), LO2 (Lignin peroxidases, Manganese peroxidases, Versatile peroxidases and Chloroperoxidases) and LO3 (Cellobiose dehydrogenase) (Fig. 4.1). The most thoroughly studied fungal enzymes involved in lignin attack are described below:

4.4.1   Laccases (EC 1.10.3.2, Benzenediol: Oxygen Oxidoreductase)

Laccases represents the largest sub group of blue multicopper oxidases (MCO) and are widely distributed among eukaryotes (fungi, plants) prokaryotes (bacteria) [22] They perform varied functions based on the source organism [22]. Laccase was first discovered in the sap of the Japanese lacquer tree *Rhus vernicifera* [23] and then it was also demonstrated in fungi [24]. Although laccases were discovered during early nineteenth century they have received much attention during the last five
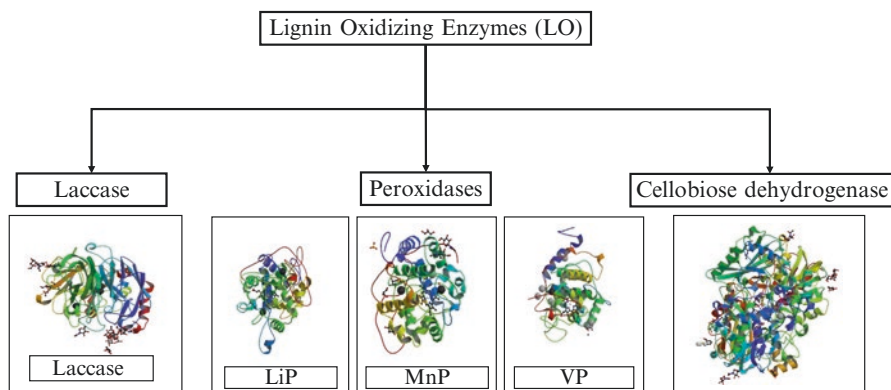
Fig. 4.1 Schematic representation of different lignin oxidizing enzymes namely, laccases (PDB ID: 3FPX), lignin peroxidase (LiP) (PDB ID: 1B85) [19], manganese peroxidase (MnP) (PDB ID: 1YYD) [20], versatile peroxidase (VP) (PDB ID: 3FKG), cellobiose dehydrogenase (PDB ID: 1KDG) [21]. All the enzyme structures were obtained from the PDB RCSB repository

decades for their application to biofuel and biorefinery fields. The involvement of laccase in the degradation of wood by fungal groups such as basidiomycetes, ascomycetes has attracted scientific communities to study the structure, function and mechanisms of laccases [25]. Many fungal species belonging to the basidiomycetes phylum such as *Abortiporus biennis, Agaricus bisporus, Agaricus brunnescens, Armillaria mellea, Aspergillus nidulans, Botrytis cinerea, Ceriporiopsis subvermispora, Ganoderma lucidum, Lentinus edodes, Myceliophthora thermophile, Neurospora crassa, Penicillium crysogenum, Phanerochaete chrysosporium, Phlebia brevispora, Phlebia radiata, Pleurotus erygii, Pleurotus ostreatus, Pleurotus sojar-caju Polyporus species, Rhizoctonia Solani, Trametes hirsuta, Trametes versicolor and Trichoderma* were reported to secrete laccase [26]. Laccases are widely studied for two major functions (a) there role in lignin polymerization (lignification) in plants, (b) lignin depolymerization by fungi [27]. The contrasting role of laccases on lignin depolymerization was proved in vitro by Hatakka 1994 and Youn et al. 1995, showing the oxidative reaction of laccases on lignin, resulting in loss of an electron from phenolic hydroxyl groups of lignin resulting in phenoxy radicals [28, 29]. These studies have also showed that these radicals can spontaneously reorganize leading to the cleavage of alkyl side chains of polymer. At the same time, the polymerizing activity of the laccase might result in the polymerization of low molecular weight compounds [26]. These studies suggested that lignin degradation by fungi in nature occurs by the synergistic effect of other lignin degrading enzymes and non-enzymatic components which establishes a balanced environment between lignin depolymerization and enzymatic polymerization [26]. Although studies have reported the involvement of laccases in both lignin polymerization and depolymerization, the exact role of laccases and other partnering enzymes in the degradation and modification of lignin were still under investigation [26, 27]. Apart from wood decay, laccases play important role in fungal physiological processes such as morphogenesis, fungal plant pathogen/host interactions, stress defense and lignin degradation [26, 30]. In fungi, laccases are expressed during different stages of fungal development (morphogenesis, growth of rhizomorphs, sporulation, pathogenesis and virulence). According to Leatham and Stahmann 1981, increased laccase activity was observed in the developing fruiting bodies of *Lentinus edodes* (a commercially cultivable mushroom) [31]. The role of laccases on mushroom development was proved by Ikegaya et al. (1993), in this study the developing fruiting bodies of *L. edodes* were treated with diethyldithiocarbamate (a potential inhibitor of laccase) which resulted in the decreased growth of *L. edodes* fruiting bodies, thus proving the role of laccase in fungal development [32]. A similar study was conducted on *Armillaria mellea* by Worrall et al. (1986) which showed the requirement of laccase for the development and growth of rhizomorphs [33]. Laccases are also involved in imparting specific virulence properties to the fungi, *Botrytis cinerea* (common plant infecting fungi) secretes laccases which causes infection in some plants especially carrot and cucumber by triggering plant toxins such as cucurbitacins and tetracyclic triterpenoids. However, the virulence of these laccases was inhibited in EDTA pretreated plant tissues [34]. Thus fungal laccases play three major functions: lignin degradation, detoxification and pigment formation. Industrially laccases are important in paper and pulp, bio bleaching, textile industries etc.

Structure Several X-ray crystallography studies were conducted to determine the structural properties of laccases (Table 4.2), however in this chapter we are focusing on *Trametes versicolor* laccase. The structural analysis of laccase isolated from *Trametes versicolor* was first done by Klaus Pointek et al. (2002) [35]. Laccase is a monomeric protein ordered in three sequentially arranged domains with dimensions ranging $65 \times 55 \times 45$ Å^3, each domain consists of a β-barrel shaped architecture which is similar to other blue copper proteins such as azurin or plastocyanin [35]. With each domain different from the other domains in their structural composition. First domain comprises two four-stranded β-sheets and four 3_{10}-helices, of which three acts as a connecting peptide between β-strands and one helix forms the segments between first and second domains. The second domain consists of one six stranded and one five stranded β-sheets, with three 3_{10}-helices peptides connecting the individual β-strands and domains 1 and 3. A 3_{10}-helix forms a 40 amino acid long extended loop region between domains 2 and 3. The third domain contains two five stranded and a two stranded β-sheet, which together form a β-barrel. The β-barrel together with an α-helix and a β-turn, forms a cavity for a type-I copper. Compared to the other two domains, the third domain has the highest helical content with one 3_{10}-helix and two α-helices situated in between the connecting regions of different β-sheets. The completion of the protein fold involves the C-terminal end of domain 3 and three sequentially arranged α-helices. Two disulfide bridges (Cys85-Cys488 and Cys117-Cys205) were reported which connects domain 1 and 2 and stabilizes a 13 amino acid residue α-helix. An oxygen reducing site is present at the T2/T3 cluster which accesses the solvent through two channels, leading to type-III copper and to type-II copper sites. The type-II copper site is more exposed and easily altered, when compared to the other two copper sites present near the T3 site. Actually T2 copper site is deficient in copper in the copper depleted forms of both laccase and ascorbate oxidase [36, 62]. Electrostatic potential studies of *Trametes versicolor* laccase shows that it possess a high negative charge, which suggests the specific binding of the substrate to the negatively charged cavity near the T1 copper site. Negative charge occurring at binding site imparts functional significance to the enzyme by imparting stability to the radical cation products formed during catalytic cycle. The two channels near the copper sites provide access to molecular oxygen and allow water release from the T2/T3 cluster. At the same time a conserved His-Cys-His tripeptide is associated with the electron transfer pathway between the T1 copper and the trinuclear cluster. A two site ping pong bi-bi reaction mechanism was proposed for the catalytic mechanism of laccase enzyme [63], which means that products are released before binding of new substrates.

Mechanism of Action Laccases use their distinctive redox ability of copper ions for catalyzing the oxidation of various aromatic substrates concurrently reducing the molecular oxygen to water [64]. Laccases are able to catalyze direct oxidation of ortho, para-diphenols, aminophenols, polyphenols, polyamines, aryl diamines and also some inorganic ion [26, 65–69]. Laccases depends on copper (Cu) for their catalytic action, based on the number of copper ions laccases can be classified as dimeric or tetrameric glycoproteins. In addition, based on the types of copper ion centers they are classified as: (a) Type-I (blue copper center) (b) Type-II (normal

Table 4.2 Lists the catalytic mechanism and structural studies of different lignin oxidizing enzymes

Enzyme, FOLy Class	Catalytic mechanism	Structural studies, references
Laccase (LO1) (EC 1.10.3.2)	4 benzendiol $+ H_2O_2 \rightarrow 4$ benzosemiquinone $+ 2H_2O$	*Trametes versicolor* [35], *Coprinus cinereus* [36], *Melanocarpus albomyces* [37], *Cerrena maxima* [38], *Thielavia arenaria* [39], *Lentinus tigrinus* [40]
Lignin Peroxidase ((LO2) (EC 1.11.1.14)	LiP oxidizes alkyl side chains and benzyl alcohol, It is involved in breakdown of C–C side chains and aromatic rings of lignin	*Trametes cervina* [41], *Phanerochaete chrysosporium* [42, 43] [44–48]
Manganese Peroxidase (LO2) (EC 1.11.1.13)	MnP's catalytic mechanism is dependent on hydrogen peroxide and Mn^{2+} ions.	*Phanerochaete chrysosporium* [20, 49–52]
Versatile Peroxidase (LO2) (EC 1.11.1.16)	VP has substrate specificity features similar to that of MnP and LiP	*Pleurotus eryngii* [53–57]
Cellobiose Dehydrogenase (LO2) (EC 1.1.99.18)	CDH catalyzed reactions [58] Cellobiose $+ 2 Fe^{3+} \rightarrow$ Cellobionolactone $+ 2 Fe^{2+}$ Cellobiose $+ + O_2 \rightarrow$ Cellobionolactone $+ H_2O_2$ $Fe^{2+} + H_2O_2 \xrightarrow{\text{(Spontaneous reaction)}} Fe^{3+} + OH^- + OH*$	*Phanerochaete chrysosporium* [21, 59–61]
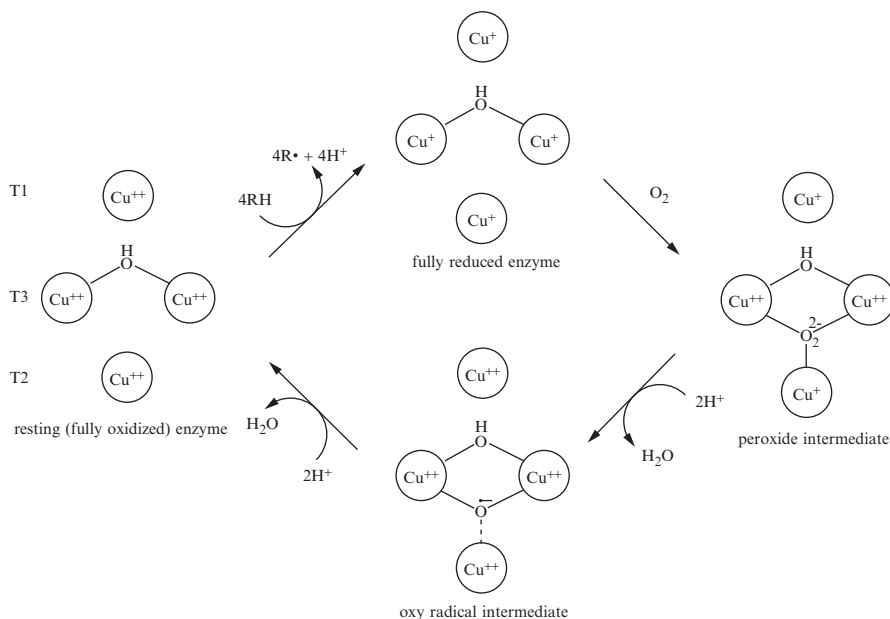
Fig. 4.2 Catalytic cycle of laccase (Reprinted with permission from Ref [9], Copyright © 2008 Springer Science + Business Media B.V)

copper center) (c) Type-III (coupled binuclear copper center) that differ in their characteristic electronic paramagnetic resonance (EPR) signals [70, 71]. Type-I copper coordinates with four amino acids as ligands: two histidines, one cysteine and one methionine. Type-I copper containing laccases are generally a deep blue color, which can be detected by its absorbance at 600 nm wavelength. However, laccases which fail to absorb at 600 nm were reported in *Pleurotus ostreatus* (called white laccase) [72] *Panus tirinus* (called yellow laccases) [73]. Type-II copper coordinates with two histidine and water as ligands, Type-III copper coordinates with three histidines and a hydroxyl bridge which imparts strong anti-ferromagnetic coupling between the type-III copper atoms [35]. Type-II copper atoms do not absorb in the visible spectrum, while type-III copper atoms have an electron absorption at a wavelength of 330 nm. Based on the structural properties of type of copper ions laccases are divided into high and low redox potential enzymes. Bacteria and plants secrete low redox potential laccases, whereas white rot fungi and some basidiomycetes secrete high-redox potential laccases [74, 75].

Different copper centers present in the laccase participate and complete the enzymatic reaction. Unlike peroxidases laccases does not require hydrogen peroxide for the oxidation of monolignols. Enzyme catalysis can be divided into three main stages: the copper ion of type-I is reduced by the reducing substrate followed by internal electron transfer between the type-I, type-II and type-III Cu clusters [22]. Finally the reduction of oxygen takes place at the type-II and III Cu's resulting in water formation (Fig. 4.2). *In vitro* lignin degradation by laccase primarily oxidizes

phenolic hydroxyl groups of lignin to form phenoxy radicals which further reorganize to cleave the alkyl side chains. Laccase can degrade β-1 and β-O-4 dimer linkages between Cα-Cβ and cause Cα oxidation and aryl-alkyl cleavages [22]. Thus the generated reactive radicals further release monomers by breaking down covalent bonds [76]. Due to the steric hindrance of laccase it cannot directly contact large polymers, thus small organic compounds or metals such as veratryl alcohol, manganese and 3-hydroxy anthranilic acid are oxidized and further activated to mediate radical catalyzed depolymerization of lignin [9, 76].

4.4.2 Peroxidases (EC:1.11.1.x)

Peroxidases are large group of enzymes widely distributed among plants, animals and microbes. Peroxidases play a wide variety of activities based on the source of the organism. Peroxidases are involved in several physiological processes such as plants defense mechanisms (response to pathogens), wound healing, auxin catabolism, lignification and suberization [77]. Microbes such as fungi and bacteria are well known for their ability of delignification which is efficiently fulfilled by the different types of peroxidases such as (LiP, MnP and VP). Peroxidases can also efficiently decolorize synthetic dyes and bioremediation of waste water and degradation of several toxic chemicals such as phenolic contaminants, polychlorinated biphenyls, chlorinated alkanes and alkenes, chlorinated dioxins, chlorinated insecticides and removal of endocrine disruptive chemicals etc, thus playing variety of roles in the environment [78]. Molecular structures of lignin degrading peroxidases share several common characteristics such as [79], Ligninolytic peroxidases generally contain a haem cofactor located internally in a cavity (haem pocket), which is connected to the protein by two small access channels [79–83]. Larger channel are common among all haem peroxidases, they are required for the hydrogen peroxide to reach the haem and react with (Fe^{+3}) forming an activated two electron enzyme form called compound I [79–83]. The entrance of this channel forms the substrate binding site in some peroxidases. A second channel extends to the heme propionate substrate where some specific lignolytic enzymes oxidize Mn^{2+} and Mn^{3+} which acts a diffusible oxidizers of phenolic lignin and other organic molecules [79–83]. In this section we will be focusing on the delignification mechanisms of lignin peroxidases, manganese peroxidases, and versatile peroxidase.

4.4.3 Lignin Peroxidases (E.C. 1.11.1.14)

Lignin peroxidases (LiP) the most studied lignin depolymerizing enzymes, LiP was first discovered in the extracellular medium of *P. chrysosporium* under nitrogen limited conditions [84]. Similar to classic peroxidases, LiP are dependent on

hydrogen peroxide. The overall reaction mechanism of LiP is 1,2-bis(3,4-dimethoxyphenyl) propane-1,3-diol + H_2O_2 $\rightleftharpoons$ 3,4-dimethoxybenzaldehyde + 1-(3,4-dimethoxyphenyl)ethane- 1,2-diol + H_2O [9]. LiP can oxidize a wide range of phenolic compounds, organic compounds and also different lignin model non-phenolic compounds by using hydrogen peroxide with a redox potential up to 1.4 V, thus showing its non-specificity towards substrates [85].

Structure Structure of *P. chrysosporium* lignin peroxidase (LiP) was determined using protein crystallography by Edward, et al. (1992). These studies revealed that fungal LiPs are globular and mostly helical glycoproteins with a molecular size of 38-46 kDa with 343–344 amino acids depending on the isozyme with a reduction potential exceeding 1.4 V [9, 42]. Compared to other lignolytic peroxidases it has a characteristic low optimum pH 3 with pI values ranging between 3.2 and 4.0 [9]. LiP contains several *N*- and *O*- glycosylation sites, it was reported that *N*-glycosylated sites (Asn257) and *O*-glycosylated site (Ser334 and Thr320) were clustered at the end of the proximal domain [43]. LiP is a globular protein with proximal C-terminal and distal N-terminal domains, the C-terminal segment of about 50 amino acids is extended to pass through the surface with less contact to the protein core [9]. LiP consists of eight major and eight minor α-helices and limited β structure in the proximal domains, it also has eight Cys residues forming disulfide bonds. The calcium binding site present in each domain is involved in maintaining the topology of the active site. The peroxide binding site is located on the distal end of the heme with an extended channel towards the exterior of the protein. The negative charge developed as a result of peroxide cleavage is stabilized by the Arg43 residue, it also stabilizes the ferryl oxygen of compound I. At the same time His47 with Asn82 present on the distal end of the enzyme acts as a proton acceptor for the bound peroxide substrate [9]. The overall protein fold of LiP is similar to other typical haem peroxidases such as cytochrome c peroxidase, manganese peroxidase, horseradish peroxidase [42]. The haem moiety divides the protein structure of LiP into a proximal and a distal domain. The haem moiety is hidden inside the protein with limited access to the outer medium by a small channel [43]. Thus the crystal structure of LiP shows that the haem access channel is not sufficient to allow entry to large polymers like lignin, however this is the only channel to form a suitable binding site for the attachment of small molecule substrates [43]. Protein modeling studies have confirmed its suitability for binding of veratryl alcohol, however the exact binding site of veratryl alcohol was not determined. LiP possess two substrate binding sites for veratryl alcohol (VA), the first one is Trp 171 and the second one is the anionic substrate oxidation site [43]. To find the binding site of the VA on LiP, the molecular docking study was conducted by chemically modifying the surface of LiP enzyme with 1-ethyl-3-(3-dimethylaminopropyl) carbodiimide (EDC) in the presence and absence of 2-aminoethanesulfonic acid for the introduction of N-acyl-urea groups in place of carboxyl groups. LiP was also modified by N-bromosuccinimide (NBS) to yield a Trp modified enzyme [86]. From these studies it was shown that VA probably binds to Trp171 or its surrounding area as a reducing substrate and enzyme bound mediator. At the same time it has been suggested that VA binds at different
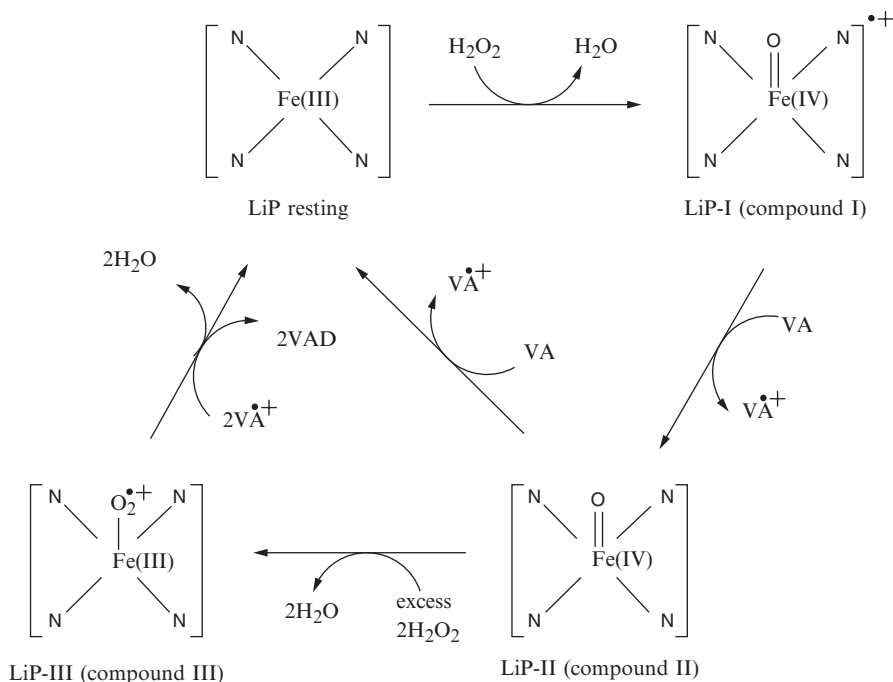
Fig. 4.3 Catalytic cycle of lignin peroxidase (Reprinted with permission from Ref [9], Copyright © 2008 Springer Science + Business Media B.V)

locations when it reacts with LiP compound III* for the reverse reaction. The major difficulty in determination of the VA binding site is the lack of inhibitors causing classical inhibition patterns like competitive or non-competitive inhibitions. Thus, studies should be conducted by using X-ray crystallography and NMR methods for the determination of the LiP binding site for VA [9, 86].

Mechanism Lignin peroxidase resembles horse radish peroxidase (a classical peroxidase highly studied) by containing Fe (III) as a cofactor which is pentacoordinated to four heme tetrapyrrole nitrogens and to a histidine residue [87]. Lignin peroxidases are dependent on H_2O_2 for their reaction. H_2O_2 oxidize LiP resulting a two electron-oxidized intermediate (Compound I) in which iron is present as Fe (IV) leaving a free radical on the tetrapyrrole ring or on a nearby amino acid. Compound I then oxidizes a donor substrate to form a second intermediate (Compound II) and a substrate free radical (Fig. 4.3) [87]. Later reduction of the enzyme to its resting state can be accomplished either by the same substrate molecule or with a second substrate molecule by giving off substrate-free radical [87]. An important functional difference between LiP and other classical peroxidases is that lignin peroxidases can oxidize aromatic rings that are moderately activated by electron donating substituents, at the same time classical peroxidases act only on strongly activated aromatic substrates. Therefore, LiP and horseradish peroxidase can oxidize 1, 2, 4, 5-tetra-
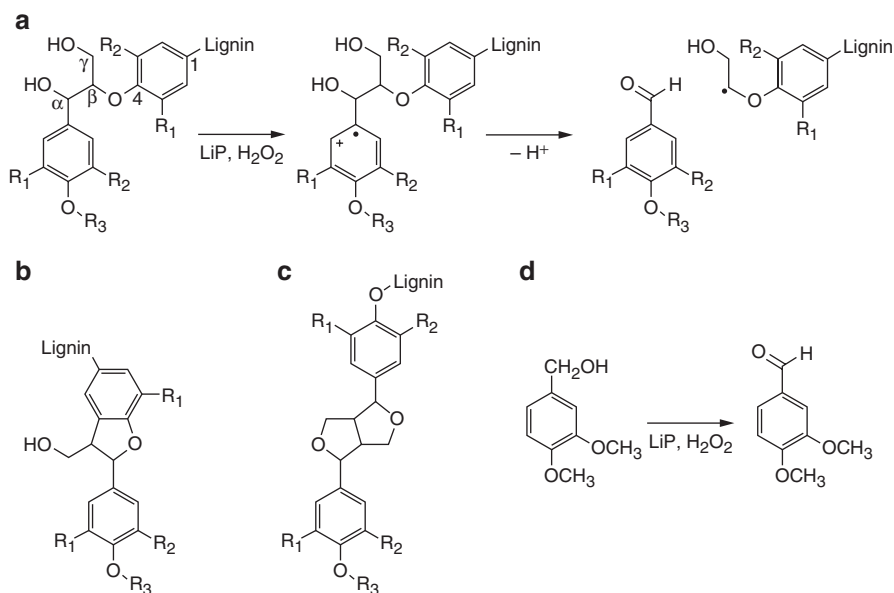
Fig. 4.4 Chemical structures and reactions discussed in the text. (**a**) The principal β-O-4 structure of lignin and pathway for its C_α–C_β cleavage by LiP. (**b**) A phenylcoumaran lignin structure. (**c**) A resinol lignin structure. (**d**) LiP-catalyzed oxidation of the fungal metabolite veratryl alcohol. Gymnosperms contain lignin's in which most subunits have $R_1 = OCH_3$ and $R_2 = H$. Angiosperm lignin's also contain these structures, but have in addition subunits in which $R_1 = OCH_3$ and $R_2 = OCH_3$. Grass lignin's contain both types of structures but have in addition some subunits in which $R_1 = H$ and $R_2 = H$. These nonmethoxylated lignin structures are more difficult to oxidize than those that contain one or two methoxyl groups. In the predominating nonphenolic structures of lignin, $R_3 = $ lignin, whereas $R_3 = H$ in the minor phenolic structures (Reprinted with permission from Ref [87], Copyright © 2008, Elsevier)

methoxybenzene, phenols and anilines, at the same time LiP are capable of abstracting an electron from aromatics that carry only two or three ether like the major nonphenolic structures of lignin [88]. Primary products of this oxidation are temporary cation radical intermediates which certainly breakdown. Majorly Cα-Cβ bonds of propyl side chains are broken down to give benzaldehydes which are the precursors of benzoic acid molecules, these benzoic acid molecules are mainly observed in lignin decaying white rot fungi (Fig. 4.4) [89]. The unusual activity of lignin peroxidases is due to two structural differences, an electron-deficient iron atom in the porphyrin compared to classical peroxidases which makes LiP a stronger oxidant [90] and an invariant Trp171 in the isozyme of LiPA. This residue is present on the enzyme surface and is known to participate in a wide range electron transfers from aromatic substrates since they cannot contact the oxidized haem directly [91]. This important feature of LiP is responsible for oxidizing complex lignin and its related substrates directly. This function of Trp171 in LiPA was proved by a site directed mutagenesis in which the Trp171 was replaced by serine, which resulted in the loss of activity [92]. It was shown that the efficiency of LiP catalyzed oxidation of lignin

molecules markedly decreases with an increase in size of the lignin molecule. LiP catalyzed oxidation of lignin trimers was found to be only 4 % of the rate of oxidation of a monomer model [93]. Oxidation of lignin molecules by LiP takes place in the presence of veratryl alcohol, and the role of VA in oxidation by LiP are given below [87]. Studies have showed that the VA cation radical oxidizes has a long half-life of 40 ms even at acidic conditions [94, 95]. VA is the substrate of LiP. It was suggested that the VA cation radical oxidizes lignin molecules at remote locations [96]. VA acts as an efficient electron donor to protect LiP from oxidative inactivation by hydrogen peroxide. As LiP oxidizes large and complex lignin substrates, which is a slow reaction, VA prevents oxidization of LiP [97]. VA is also essential for the reduction of LiP compound II. Compound I is reduced by non-methoxylated lignin structures. As these lignin structures are difficult to oxidize since they carry only one electron donating ether group. Compound II of LiP is a comparatively weaker oxidant than compound I [98].

4.4.4   Manganese Peroxidases (EC 1.11.1.13)

Wood decaying white rot fungus and other litter decomposing fungi efficiently degrade lignin in wood. These fungi secrete several non-specific oxidoreductases, among them manganese peroxidase plays an important role [99]. Manganese peroxidase (MnP) was first discovered in *P. chrysosporium* two decades ago [100, 101], however it received less attention then lignin peroxidase in beginning. Later it was found that LiP is not produced by all white rot fungi [28, 102, 103]. Production of MnP is limited only to basidiomycetes. Mainly two ecophysiological groups of fungi i.e. wood degrading fungi causing white rot and soil litter decomposing fungi secrete manganese peroxidase [103]. Wood decaying fungi belonging to families such as *Meruliaceae, Coriolaceae, Polyporaceae* and soil litter decomposing fungi such as *Strophoriaceae, Tricholomataceae* are known fungal families, which secrete MnP. Some prominent MnP producing fungi are *Abortiporus biennis, Agaricus bisporus, Armillaria mellea, Auricularia sp. M37, Bjerkandera adusta, Ceriporiopsis subvermispora, Coriolopsis polyzona, Dichomitus squalens, Ganoderma lucidum, Heterobasidion annosum, Hypholoma fasciculare, Lentinula (Lentinus) edodes, Panus tigrinus, Phaeolus schweinitzii, Phallus impudicus*, *Phanerochaete chrysosporium, Phanerochaete sordida, Phlebia brevispora, Phlebia radiata, Pleurotus enryngii, Pleurotus sajor-caju, Stropharia aeruginosa, Stropharia coronilla, Trametes hirsuta, Trametes versicolor* [99].

Structure   The enzyme mechanism of MnP is similar to that of classical haem containing peroxidases, but this enzyme is unique by having Mn^{+2} as a reducing substrate [49]. Crystal structure of *P. chrysosporium* MnP was demonstrated by Sundaramoorthy et al. (1994). MnP is an acidic glycoprotein with pI near to 4.5, it is often produced as a sequence of isozymes which are differentially regulated by different genes [104]. It contains one molecule of heme in iron protoporhyrin IX, showing a maximal activity at Mn (II) with concentrations above 100 μM [100]. The

enzyme oxidizes Mn from Mn^{+2} to Mn^{+3}, it forms complexes with oxalate and acts as a diffusible redox mediator for the oxidization of lignin and other phenolic compounds. MnP is a haem containing glycoprotein with a molecular weight ranging between 38 and 62.5 kDa, however most of the purified enzymes have molecular weights around 45 kDa. About 43 % of the amino acid sequence of MnP is identical to LiP, overall protein folding of MnP is similar to that of other plant and fungal peroxidases [49, 50]. MnP consists of two domains and haem submerged between these domains, similar to that of LiP. MnP enzyme consists of ten major and one minor helix similar to that of LiP. Eight minor helices are present in MnP of which two minor helices are similar to that of LiP all are in the 3_{10} helical confirmation. It contains five disulfide bonds of which Cys^3-Cys^{15}, Cys^{33}-Cys^{117}, Cys^{14}-Cys^{289}, Cys^{253}-Cys^{319} are similar to that of LiP and only one disulfide bond is unique to MnP [49, 50]. The unique disulfide bond Cys^{341}-Cys^{348} is part of the long C-terminal tail in MnP which is partially responsible for forcing C-terminus away from the main body of the protein, which might be involved in manganese binding site formation. Arg^{42} and His^{46} on the distal domain of MnP form the peroxide binding pocket, and histidine in the distal domain is required for the formation of compound I by acting as acid base catalyst [20, 49]. Superposition studies conducted on LiP and MnP have shown few significant facts such as differences occurring at the insertion sites of these enzymes. In LiP, the C-terminus lies between two heme propionate groups while in MnP the C-terminus is separated from the heme by the combined effects of a 7-residue insertion (Leu^{228}-Thr^{234}) in the loop between the G and H helices, Arg^{177}, Glu^{35}, and the Cys^{341}-Cys^{348} disulfide bond [20, 50]. It was also reported that the His46 and Asn80 residues present in the distal end are hydrogen bonded, which is required for $N\varepsilon_2$ of His46 to accept proton from the peroxide during acid-base catalysis. Similarly the hydrogen bond between His173 and Asp242 involved in increasing the anionic character of the ligand and further stabilizing the oxyferric iron in MnP-I. The cation binding site present on the surface of the protein is formed by several interactions of Mn (II) with the carboxylate oxygen groups of Glu35, Glu39, and Asp179, the heme propionate oxygen and two water. The oxygens impart flexibility and facilitate the binding of a wide range of metal ions. MnP also contains of two calcium ions bound tightly on the proximal and distal side chains of the heme that are involved in maintaining the thermal stability of the active site of MnP [9, 20, 49, 50].

Mechanism MnP is different from other peroxidases as it uses Mn (II) as the reducing substrate. MnP oxidizes Mn (II) to Mn (III), which then catalyzes the oxidation of a wide range of monomeric phenols, lignin model phenolic compounds and dyes [100, 105, 106]. The reaction mechanism of MnP proceeds as: first oxidation of Mn (II) by compound I (MnP-I), followed by oxidation of compound II (MnP-II) yielding Mn (III). MnP is a strong oxidizing agent like LiP, it cannot oxidize nonphenolic lignin related compounds because it lacks the invariant Trp171 residue which is required for electron transfer to aromatic substrates [87]. MnP has a manganese binding site which contains many acidic amino acids and also a heme propionate group. Thus one electron transfers to compound I of MnP takes place from bound Mn^{+2}. Further Mn^{+3} is released from the active site in presence of the
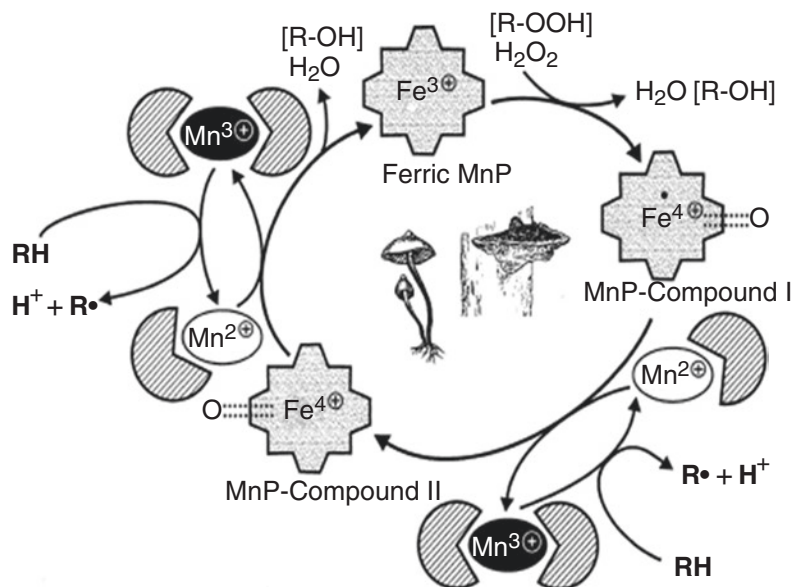
Fig. 4.5 Catalytic cycle of manganese peroxidase (Reprinted with permission from Ref [99], Copyright © 2002, Elsevier)

bidentate chelators such as oxalate, which helps prevent the disproportionation to Mn^{+2} and insoluble Mn^{+4}. This reaction is required for the transfer of oxidizing power of MnP to Mn^{3+}, which diffuses into the lignified cell wall thus attacking it from inside [87]. An important feature of MnP is to oxidize the low permeable lignocellulose network making it different from other peroxidases [9]. Chelators such as oxalate increase the electron density on Mn^{+3} which makes it a weak oxidant, thus Mn^{+3} organic acid chelates produced by MnP cannot oxidize the nonphenolic substrates of lignin. Mn^{+3} chelates cannot cause extensive lignolysis as they can only attack rare phenolic structures of lignin, which often are the end groups of lignin. The catalytic cycle of MnP begins with the binding of hydrogen peroxide or an organic peroxide to the native ferric enzyme resulting in the formation of an iron-peroxide complex (Fig. 4.5). Further the breakdown of the oxygen-oxygen peroxide bond depends on a 2-electron transfer reaction from the heme resulting in the formation of MnP compound I (i.e. a Fe^{4+}-oxo-porphyrin radical complex). The dioxygen bond is cleaved resulting in removal of water and further reduction proceeds via MnP compound II. The Mn^{2+} ion (monochelated) donates one electron to the porphyrin intermediate and is oxidized to Mn^{3+}. Similarly compound II is reduced by releasing another Mn^{3+} and a second water molecule, thus leading to the resting state of the enzyme (Fig. 4.5) [107–109].

The oxidation of phenolic compounds by MnP occurs by Mn (III) chelator complexes, which diffuses and catalyzes one electron oxidation of phenolic compounds producing a phenoxy radical intermediate. The phenoxy radical intermediate under-

goes bond cleavages, rearrangements and degradation of compounds non-enzymatically to produce different breakdown products [106, 110, 111]. In contrast unchelated Mn (III) causes the formation of reactive radicals as second mediators for the oxidation of non-phenolic compounds. Oxidation of non-phenolic compounds by MnP is different from LiP, as LiP oxidizes by abstracting electrons from the aromatic ring resulting in a radical cation. In presence of thiols like glutathione, Mn (III) causes the oxidation of benzyl alcohol and diarylpropane structures to their corresponding aldehydes [112, 113].

4.4.5 Versatile Peroxidases

Versatile peroxidases a new family of lignolytic peroxidases were reported for the first time in *P. chrysosporium* along with other lignolytic enzymes such as LiP and MnP [79]. Several fungi belonging to genera such as *Pleurotus, Bjerkandera, Lepista, Panus* and *Trametes* species were reported to produce versatile peroxidase (VP). Versatile peroxidase have important properties which combines the substrate specificity characteristics of the three fungal peroxidases such as manganese peroxidase, lignin peroxidase and Coprinus cinereus peroxidase [79]. Two well-known studies have revealed the occurrence of versatile peroxidases in nature, in the first study a Mn^{2+} binding site was introduced into the LiP of *P. chrysosporium* by site directed mutagenesis, the resulting enzyme had MnP activity [114]. In the second study a tryptophan residue similar to that in LiP was introduced into the MnP of *P. chrysosporium* and the enzyme acquired LiP activity [115]. Versatile peroxidase coding genes were first cloned and sequenced from *Pleurotus eryngii*. Studies of the catalytic properties of VP suggested that they were due to its hybrid molecular construction combining different oxidation and substrate binding sites [116, 117].

Structure Crystallographic studies conducted by Boada et al. (2005) showed that the structures of VP and its variant W164S are very similar. A total of 319 (VP) and 320 (W164S) amino acid residues along with heme and other cations were shown in the structural studies [53, 79]. The VP structure includes 11 α-helices (Ala12-Asn27, Glu36-Ala49, Ser64-Glu72, Ile81-Lys94, Ala99-Ser112, Val145-Ala155, Pro159-Ile171, Gln196-Glu200, Gln229-Arg236, Ala241-Ser246 and Gln251-Ala266), four disulphide bridges (Cys3- Cys15, Cys14-Cys278, Cys34-Cys114 and Cys242- Cys307) and two structural Ca^{2+} ions [79]. The Mn^{2+} binding site of VP contains three amino acid residues: Glu36, Glu40 and Asp175, The binding site is formed by the carboxylate groups of these amino acids and also the carboxylate group of the heme propionate. It is known that oxidation of compounds by VP occurs through LRET (Long Range Electron Transfer) pathways, structural studies reveal that three putative LRET pathways were present in the VPL isoenzyme for the oxidation of aromatic compounds. They are (i) His232-Asp231 via backbone atoms and H-bond from the carboxylate of Asp231 to the side chains of the proximal His169, (ii) backbone atoms between Trp164 and Leu165 and a van der Waals

contact between C^β of Leu165 to the methyl group C of the heme, and (iii) Pro/ His76-Ala77– Asn78 via backbone atoms and a H-bond from the side-chain oxygen atom of Asn78 to the distal His47 [79]. From site directed mutagenesis studies of the LRET pathways clearly show that the Trp164 pathway of VP is involved in the oxidation of high redox potential compounds such as veratryl alcohol and reactive black 5. Studies also showed that oxidation of veratryl alcohol and reactive black 5 and other high redox potential compounds by VP involves electron transfer from activated VP* through the Trp164 side chain to the backbone and then to the side chain of Leu165, whose $C\beta$ is 3.66 A ° from the carbon of the methyl-C of heme (2.37 A° hydrogen distance) [79]. A comparison with LiP isoenzymes shows either Met (LiPH8) or Leu (LiPH2) are homologous with VP Leu165. Eight neighboring residues with three conserved regions are shown to illustrate the differences between the structures, as well as the position of the proximal histidine residues, whose Nε atoms act as ligand of heme iron at 2.11 A° in VP and 2.15 A° in LiP [53–56, 79].

Mechanism Basic features of versatile peroxidase are similar to those of all other classical peroxidases, however it is unique as far as the substrates that it is able to oxidize. A complete catalytic cycle combining those of other fungal peroxidases such as LiP and MnP was proposed by Ruiz-Duenas et al. Similar to LiP, versatile peroxidase also initiates the LRET pathway (Long range electron transfer) at an exposed tryptophan residue [79, 118]. Studies have examined the catalytic mechanism of VP using veratryl alcohol (reducing substrate) and its transitory states in the catalytic cycle. On reaction with one molecule of hydrogen peroxide the ferric group of VP (resting state) was converted to Compound I (Fe^{4+}-oxo-porphyrin$^+$ complex) causing spectral changes (Fig. 4.6) [54, 55, 79]. Compound I oxidizes a molecule of veratryl alcohol resulting in Compound II (Fe^{4+}-oxo), which will further oxidize another molecule of veratryl alcohol further reducing the enzyme back to its resting state [54, 79]. VP can oxidize high redox potential dyes like reactive black 5 (RB5) and also can oxidize low redox potential compounds such as phenolic monomers, simple amines, Mn^{2+} etc [118]. Compared to LiP and MnP the oxidization capacity of VP is higher for phenolic compounds, this ability might be due to its relatively more accessible distal main solvent channel allowing a third lower redox potential substrate oxidation site as in CiP. A research study conducted by Parez-Boada et al. reported that the spectral changes occurring during the oxidation of phenolic compounds by VP shows that VP in its resting state has a higher absorbance at 407 nm. Similarly during charge transfer, the transient states such as Compound I and II have an absorbance at 505 nm and 637 nm respectively [54, 79]. Two major enzymes MnP and VP are known for their ability to oxidize Mn^{2+} to Mn^{3+}, the Mn^{2+} oxidation site of *P. eryngii* VP is similar to that of *P. chrysosporium* MnP. In VP, the Mn^{2+} binding site is formed by the side chains of Glu36, Glu40 and Asp175 located in front of the internal propionate of heme. Carboxylate groups of the amino acids and heme propionate are responsible for Mn^{2+} binding and for succeeding electron transfer to the activated heme of VP compounds I and II. Studies of the VP crystal structure showed a variable orientation of the Glu36, and Glu40 sidechains by interaction with Asp175 [118]. The position of these amino acids in
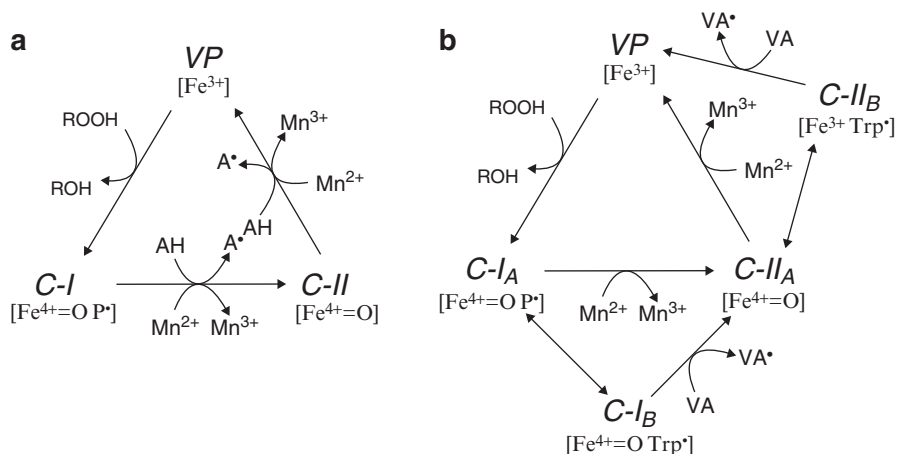
Fig. 4.6 Schemes of VP catalytic cycle. (**a**) Basic cycle described by [116] including two-electron oxidation of the resting peroxidase (VP, containing Fe^{3+}) by hydroperoxide to yield compound I (C-I, containing Fe^{4+}-oxo and porphyrin cation radical), whose reduction in two one-electron reactions results in the intermediate compound II (C-II, containing Fe^{4+}-oxo after porphyrin reduction) and then the resting form of the enzyme. As shown in the cycle, VP can oxidize both: (i) aromatic substrates (AH) to the corresponding radicals (A·); and (ii) Mn^{2+} to Mn^{3+}, the latter acting as a diffusible oxidizer. (**b**) Extended cycle including also compounds I_B (C-I_B, containing Fe^{4+}-oxo and Trp radical) and II_B (C-II_B, containing Fe^{3+} and Trp radical) involved in oxidation of veratryl alcohol (VA) and other high redox potential aromatic compounds (C-I_B and C-II_B are in equilibrium with C-I_A and C-II_A respectively, which correspond to C-I and C-II in (**a**) (other low redox potential aromatic compounds are probably oxidized by both the A and B forms but they are not included for simplicity). The active Trp in C-I_B and C-II_B would be Trp164 (the part of the cycle showing aromatic substrate oxidation would be also applicable to LiP, being Trp171 the active amino acid) (Reprinted with permission from ref [79], Copyright © 2005, Elsevier)

recombinant VP shows an open gate conformation before exposure to Mn^{2+}, thus enabling the oxidation of the Mn^{2+}. At the same time native *P. eryngii* VP shows that the two glutamate side chains are pointed towards the Mn^{2+} corresponding to a closed gate conformation. In this conformation the carboxylate groups of Glu36, Glu40, Asp 175 and the propionate heme groups are at a distance from Mn^{2+}. VP also oxidizes high redox potential substrates similar to LiP (a classic ligninolytic enzyme) through the LRET pathway. This pathway occurs in several redox proteins like cytochrome-c-peroxidase, which oxidizes cytochrome-c on its surface by transferring electrons to tryptophan residues [54, 55, 118]. The LRET pathway was known earlier for its involvement in lignin degradation by different ligninolytic enzymes, thus overcoming steric hindrance which prevent the direct interaction of the heme group and the lignin polymer. Structural studies of VP show that three possible LRET pathways are involved during the oxidation of aromatic substrates by VP [118]. Oxidation of aromatic substrates starts at Trp 164 or His232 of VPL and at His82 or Trp170 of VPS1. VP can also efficiently oxidize low reduction potential compounds like ABTS, p-hydroquinone and 2, 6 dimethoxy phenol. Enzyme kinetics studies have showed that VP has two independent oxidation sites

characterized by high and low specificities. Site directed mutagenesis of VP Trp164 performed by Ruiz-Duenas et al. showed that in Trp164 mutants the high specificity active site was removed while the low specificity site remained intact [55, 118]. Studies have confirmed a similar effect of a W164S mutation on VP oxidation of phenols. Based on these studies we conclude that the catalytic features of VP are due to its hybrid molecular architecture which includes different oxidation sites for Mn2+, high redox potential substrates (aromatic compounds) and low redox potential substrates (phenols and dyes) [55, 118].

4.5   Cellobiose Dehydrogenase

Cellobiose dehydrogenase is an extracellular enzyme involved in carbohydrate metabolism that was shown to be involved in lignin degradation [119, 120]. It was first isolated from an imperfect form of *P. chrysosporium* (*Sporotrichum pulverulentum*) [121]. Cellobiose dehydrogenase is a flavocytochrome enzyme which can oxidize various carbohydrates such as cellobiose (major product of cellulose degradation) and mannobiose (product of mannose degradation) [58]. Several fungi were reported to produce cellobiose dehydrogenase, mostly white rot fungi such as *P. chrysosporium* (*Sporotrichum pulverulentum*), *Trametes versicolor, Pycnoporus cinnabarinus, Polyporus dichrous, Merulius tremellosus, Phlebia radiata, Pleurotus ostreatus* and *Fomes annosus. Coniophora puteana (brown rot fungi)* soft rot fungi, such as *Sporitrichum thermophile (Myceliophthore thermophile), Schizophyllum commune, Humicola insolens, Sclerotium Rolfsii, Chaetomium cellulolyticum*, imperfect soft rot fungi such as *Monilla sitophila, Agaricus bisporus (Mushroom, Stachybotrys (Mold), Cladodporium(Mold)* [121]. CDH degrades cellobiose and mannobiose to lactones by removing two electrons, which can be further transported to electron acceptors such as quinones, phenoxyradicals and dioxygen [58]. In CDH two prosthetic groups, FAD and heme, makes the enzyme suitable for the reduction of one electron acceptors such as radicals and metal ions. CDH has a high specificity for amorphous cellulose and less towards microcrystalline cellulose a unique property among non-hydrolytic enzymes [58]. CDH can produce hydroxyl radicals by reducing Fe^{3+} to Fe^{2+} and O_2 to H_2O_2, These reactive species depolymerize cellulose, xylan and to some extent lignin polymers [58].

Structure   A crystallographic study of cellobiose dehydrogenase was performed by Hallberg et al. (2002) [21]. Cellobiose dehydrogenase is a 90 kDa protein consisting of 752 amino acid residues, with a MW of 80 kDa and 10 kDa due to mannose glycosylation [121]. CDH is a monomeric enzyme with a flavin domain containing FAD (60 kDa) and a heme domain (30 kDa) containing a cytochrome b type heme. These two domains are connected by a fifteen amino acid residue linker. The FAD-binding subdomain consists of 205 amino acids, in an α/β type fold containing a six stranded parallel β-pleated sheet which is between three anti parallel β-sheets (β meander) and three α-helices [21]. Its sequence and structural predictions suggests that the ADP binding moiety of the cofactor consists of a βαβ motif, which is usually seen in NAD or FAD dependent enzymes [21]. The F-subdomain also consists of three α-helices

which together form the substructure on one side of the F-subdomain [21]. The substrate binding domain (S-subdomain) consists of 335 amino acid residues forming a central twisted seven stranded β-sheet (Sheet B), also containing three α-helices on one side of the sheet with the active site on the other side. The S-subdomain consists of a relatively long 3_{10} helix and two α-helical regions, finally sheet B forms the bottom of the active site. The beginning of the S-subdomain forms a loop and lid structure that outlines the entrance of the active site and the outer wall of the FAD binding pocket [21]. The heme unit of CDH is highly glycosylated relative to the flavin domain. The isoelectric point of the flavin domain is 5.45, that of the heme domain is 3.42 and that of CDH is 4.2 [21, 121]. CDH is thermostable and pH stable and it has maximum activity at room temperature for 24 h in a pH range of 3–10. CDH is highly stable between pH 3–5 and its stability decreases with an increase or decrease from this range. CDH has highest specificity for sugars mainly disaccharides and oligosaccharides and the k_{cat} (enzyme turnover number) for cellobiose reduction by CDH is ten times higher than glucose [21, 121]. Cellobiose is the most effective electron donor for CDH but many other reducing sugars can be used for electron transfer. CDH can reduce a wide range of electron acceptors, which include oxidative radicals, transition metals and two electron acceptors (quinones). Studies have reported that one electron acceptors are reduced preferentially at the heme domain [121]. CDH has a strong binding specificity for microcrystalline cellulose, once bound it cannot be easily eluted even at high pH, high salt concentrations, detergents or by cellobiose. It was reported that CDH inhibits LiP (lignin peroxidases) by reducing the veratryl alcohol and also can reduce compound II (intermediate formed during the catalytic cycle of LiP). CDH also reduces Mn^{3+} (redox mediator used by MnP) and also compound II of MnP similar to LiP [21, 121].

Mechanism   CDH has the properties of a typical dehydrogenase with both oxidative and reductive reactions. CDH oxidizes the C1 position of a saccharide to a lactone which is spontaneously hydrolyzed to a carboxylic acid. The electrons taken up by the enzyme are later transferred to one or two electron acceptors [122, 123]. Substrate specificity of CDH is higher for cellobiose, cellodextrins, lactose, mannobiose and galactosylmannose. However, the later substrates have higher Km-values, the true substrates for CDH are di or oligosaccharides with reducing ends containing glucose or mannose residues. Monosaccharides such as glucose, mannose and maltose have very high Km values suggesting that there is binding of two glucose residues to the active site in separate subsites, at the same time monosaccharides have lower *Kcat* values then the di or oligo saccharides which suggests that binding of the β-dihexosides to the active site stimulates the catalysis creating an induced fit [124]. CDH also generates highly reactive hydroxyl radicals by a Fenton type reaction in the presence of an electron donor. Several studies were conducted to study the individual roles of the two prosthetic groups (flavin and heme domains) in the oxidation of compounds, which showed that oxidation of cellobiose (electron donor) is carried out by the FAD group which is further converted to $FADH_2$ and later transfers the electrons to the heme group (Fig. 4.7) [122, 123, 127]. Several groups have proposed a role for CDH in lignin depolymerization by reduc-
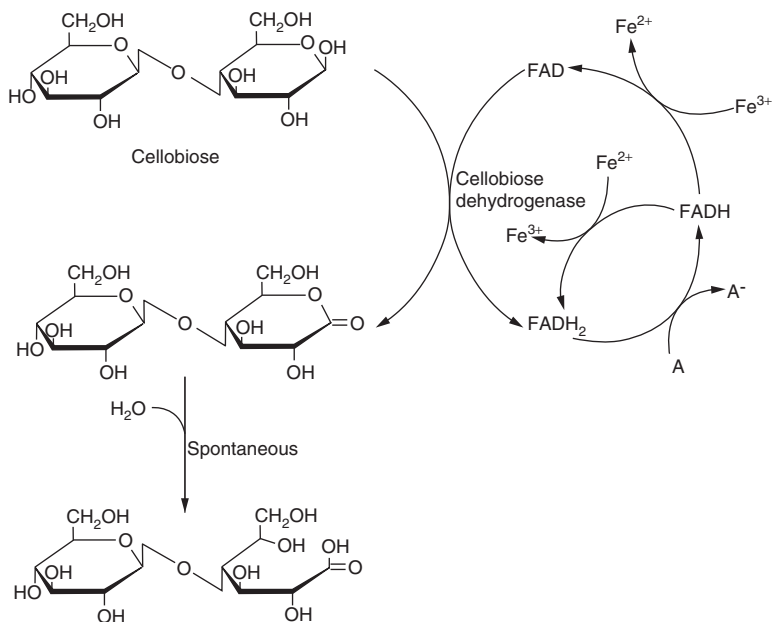
Fig. 4.7 Reactions of cellobiose dehydrogenase based on [125]. '*Fe*' represents the heme iron, '*A*' represents the one-electron acceptor (Reprinted with permission from Ref [126], Copyright ©2008, Oxford University Press)

ing phenoxy radicals thus preventing repolymerization of the radicals. Studies conducted by Henriksson et al. (1995) have showed that the CDH could stop the repolymerization of lignin model compounds, this was showed by incubating CDH with cellobiose, ferric ions, hydrogen peroxide and lignin model compounds. CDH generates highly reactive hydroxyl molecules that depolymerized the polymers showing that CDH does not depolymerize lignin or its subunits directly but hydroxyl radical groups are involved in the degradation of lignin related compounds [119, 128–130].

4.6 Lignin Degrading Auxiliary Enzymes (LDA)

Lignin degrading auxiliary enzymes are mostly H_2O_2 producers, as lignin degrading enzymes such as lacccase, LiP, MnP, VP require the presence of extracellular H_2O_2. Currently there are 7 enzymes classified as lignin degrading auxiliary enzymes (LDA): aryl alcohol oxidase (LDA1), vanillyl alcohol oxidase (LDA2), glyoxal oxidase (LDA3), pyranose oxidase (LDA4), galactose oxidase (LDA5), glucose oxidase (LDA6) and benzoquinone reductase (LDA7) (Fig. 4.8) [18]. Among these 7 different enzymes aryl alcohol oxidase, glyoxal oxidase are the most active hydrogen peroxide (H_2O_2) generating enzymes [120, 136].
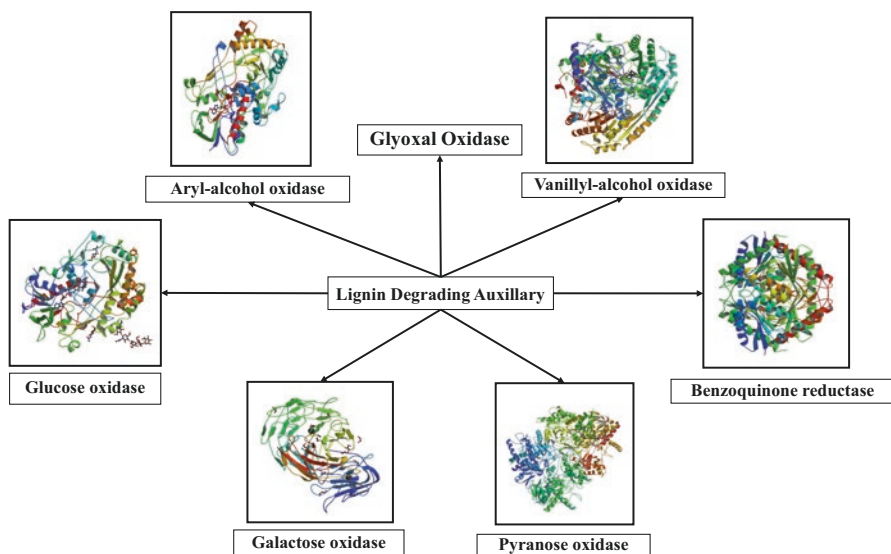
Fig. 4.8 Schematic representation of lignin degrading auxiliary enzymes namely, aryl alcohol oxidase (PDB ID: 3FIM) [131], vanillyl alcohol oxidase (PDB ID:1W1J) [132], glucose oxidase (PDB ID: 1CF3) [133], galactose oxidase (PDB ID: 2WQ8) [134], pyranose oxidase (PDB ID: 4MIF) [135]. benzoquinone reductase (PDB ID: 4LA4). All the above enzyme structures were obtained from PDB RCSB repository

4.6.1   Aryl Alcohol Oxidase

Aryl alcohol oxidase (AAO) (EC.1.1.3.7) was first observed in *Polystictus versi-color* or (*Trametes versicolor*) during the 1960s. Aryl alcohol oxidase was detected and characterized in white rot basidiomycetes such as *Pleurotus* species (*P. eryngii*), *Bjerkandera adusta* and a few ascomycetous fungi [137–141]. White rot fungi were found to be involved in efficient degradation of lignin, aryl alcohol oxidase was found to be involved in lignin depolymerization process by generating H_2O_2 and fueling ligninolytic peroxidases [137]. AAO is an FAD containing enzyme belong-ing to the glucose-methanol-choline oxidase (GMC) family of oxidoreductases. It was reported that AAO of Pleurotus eryngii was found to be involved in generation of peroxide by redox cycling of *p*-anisaldehyde (a fungal extracellular metabolite), in addition AAO also was found to be involved in oxidation of polyunsaturated primary alcohols [142]. Redox cycling of *p*-methoxylated benzylic metabolites by *P. eryngii* takes places through an oxygen activation reaction by AAO. Amino acid sequence comparisons of AAO revealed homology with glucose oxidase. AAO genes from *P. eryngii* and *Pleurotus pulmonarius* were cloned and sequenced [143]. For several years only the AAO sequence from *P.eryngii* was available, however recent advancements in genome sequencing and the sequencing of basidiomycetes genomes has revealed the sequence of around 40 AAO sequences and 112 GMC (glucose-methanol-choline oxidases) superfamily sequences were reported [144].

Kinetic isotope studies have showed that alcohol oxidation by AAO occurred by hydride transfer to the flavin domain and then hydroxyl proton transfer to the base [144]. At the same time site directed mutagenesis studies of AAO have showed that His502 is involved in activation of alcohol substrates by proton abstraction, this mechanism was later extended to other GMC oxidoreductases [144].

Structure Sequence comparison and structural analysis studies of AAO were conducted by Fernandez et al. (2009) and Varela et al. (2000). Aryl alcohol oxidase is a monomeric glycoflavoprotein with a molecular weight of 69.1 kDa with flavin adenine dinucleotide (FAD) as a cofactor. Primary structure analysis of AAO revealed that it belongs to the glucose-methanol-choline oxidoreductase family, the presence of consensus sequences such as N-terminal conserved βαβ dinucleotide binding motif (DBM) which are involved in FAD binding. According to Varela et al. (2000) AAO is composed of 593 amino acids of which 27 residues form a signal peptide, structural prediction analysis shows that it contains 13 putative α-helices and two major β-sheets where each major β-sheet contains six β-strands [145]. AAO showed 33 % sequence similarity with *Aspergillus niger* glucose oxidase and has a similar predicted secondary structure, at the same time it showed less homology with other oxidoreductases. The shape of AAO looks like an "elongated cylinder crowned by a cap, with dimensions of 75 Å 40 Å and 60 Å, respectively. Based on function, the protein can be divided into two domains: a substrate binding domain (cap region) and FAD binding domain (cylinder region). The FAD binding domain contains five stranded parallel β-sheets surrounding three α-helices and three stranded antiparallel β-sheets which is crosslinked to the other domains [131]. The additional crosslinked three stranded β-sheets are in return connected to another β-sheet motif of two antiparallel β-strands. The core substrate binding domain consisted of six stranded antiparallel β-sheets edged by two long α-helices (similar to the substrate binding domain of vanillyl alcohol oxidase) finally the central core of the substrate binding domain is covered by two pairs of two α-helices forming the widest portion of the cap [131]. The substrate binding domain and FAD binding domain are connected by three long nonstructured segments which spreads from one domain to the other domain, a second connection involves two extended two stranded parallel β-sheets which are present at the junction of the two domains [131]. The non-covalently bound FAD in AAO when compared to GO shows that the principle sites of FAD binding are on the ADP part of the molecule with βαβ protein interactions proving the role of flavin ring in substrate oxidation [146, 147]. Conserved amino acid residues between GO and AAO around the FAD group are G9, E33, G81, G86, S87, V231, A272, H502, D535, G536 and H546. Closer comparisons of the GO and AAO sequences show that the conserved amino acid residue N107 of GO involved in binding of the oxygen of ribityl moiety of FAD is replaced by H91 in AAO. At the same time the conserved amino acid residue E33 of AAO takes part in ADP-binding by hydrogen bonding with the O2' of ribose moiety [148].

Mechanism Structural and functional studies of AAO isolated from *P. eryngii* show that it has a variety of substrates, catalyzing the oxidation of primary and polyunsaturated alcohols [142]. The overall reaction mechanism of AAO can be

divided into an oxidative and a reductive reaction, first AAO catalyzes the oxidative dehydrogenation of the substrate (reductive reaction) later the flavin adenine dinucleotide is reoxidized by molecular oxygen, generating H_2O_2 (Fig. 4.9) [137]. Comprehensive studies of the substrate specificities of AAO revealed that it catalyses the oxidation of aromatic alcohols such as p-anisyl alcohol and aliphatic polyunsaturated primary alcohols to their corresponding aldehydes [142]. It was reported that phenolic hydroxyls strongly inhibits the enzymatic activity of AAO. The redox cycling of p-Anisaldehyde (important extracellular metabolite of *P. eryngii*) involves intracellular aryl-alcohol dehydrogenase along with AAO which results in hydrogen peroxide generation (Fig. 4.9) [149]. AAO seems to have a similar catalytic mechanism to choline oxidase (GMC oxidoreductase family) which catalyzes the oxidization of alcohol substrates resulting in the production of aldehydes. Earlier studies on AAO of *P. eryngii* shows that it catalyzes the conversion of primary alcohols of varied structural properties. AAO exhibits a wide range of electron donor substrate specificity by catalyzing the oxidation of aromatic and π-system containing primary alcohols such as benzylic alcohol, napthylic alcohol and aliphatic polyunsaturated alcohols [137, 142, 150]. The π-systems cause an increase in electron availability at the benzylic position causing hydride abstraction by the flavin N5 atom. The structural of the AAO active site prevents the oxidation of secondary alcohols as they cannot be accommodated at the appropriate distance from the catalytic histidine and flavin N5 atom due to the presence of Phe501 [151]. Bisubstrate kinetic analysis with different benzylic alcohols shows the overall AAO catalytic cycle is highly influenced by the nature of substituents on the benzene ring. AAO catalysis is divided into a reductive and oxidative reactions, when it is treated with electron
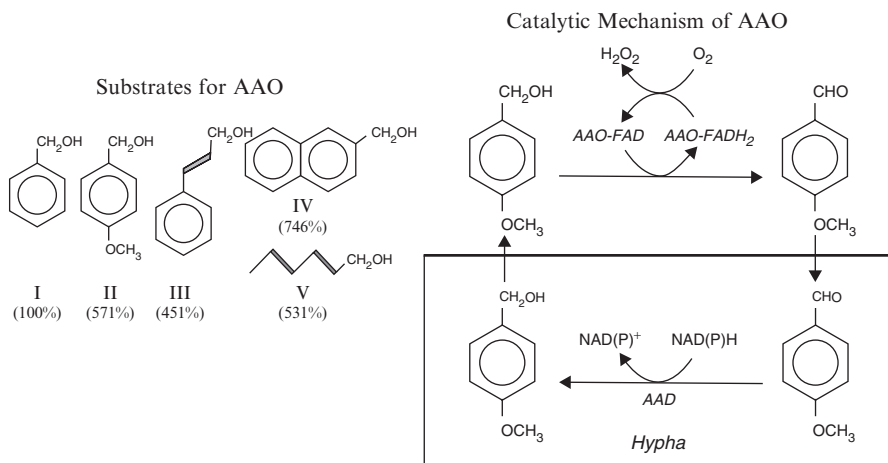
Fig. 4.9 Chemical structure of various substrates of *Pleurotus* AAO (I, benzyl alcohol; II, p-anisyl alcohol; III, cinnamyl alcohol; IV, 2-naphthalenemethanol; and V, 2,4-hexadien-1-ol) and relative activity estimated as O_2 consumption [142]. Scheme for H_2O_2 production by anisaldehyde redox-cycling involving extracellular AAO and intracellular AAD (Reprinted with permission from Ref [145], Copyright © 2000, Elsevier)

withdrawing substrates such as 3-chloro and 3-fluorobenzyl alcohols both t half reactions become independent resulting in aldehyde product dissociation before the oxygen reaction by a ping-pong steady state mechanism [152]. In electron donor substituents such as methoxylated benzyl alcohols, oxygen reacts with the reduced AAO-aldehyde complex resulting in a ternary complex prior to aldehyde product release [152]. The catalytic cycle of AAO depends on the stacking and stabilizing interactions of aromatic substrate and product at the active site Tyr92 residue (involved in stabilization of alcohol substrate) which occur by switching between ternary and ping-pong mechanisms [152].

4.6.2 Vanillyl Alcohol Oxidase

Vanillyl alcohol oxidase (EC.1.1.3.38) is a flavin containing protein which was first isolated from *Penicillium simplicissimum* based on its ability to oxidize vanillyl alcohol to vanillin, 4(methoxymethyl) phenol to 4-hydroxybenzaldehyde [153]. It was also studied for its ability to degrade lignin. Vanillyl alcohol oxidase (VAO) can convert phenolic compounds by different catalytic processes such as oxidation, deamination, demethylation, hydroxylation and dehydrogenation [154]. The reaction mechanism of VAO for oxidation of 4(methoxy methyl) phenol involves a primary transfer of hydride from the substrate to the flavin leading to the formation of a two electron reduced enzyme complex with a *p*-quinone methide compound as an intermediate. Further the reduced flavin is reoxidized by oxygen associated with hydration of *p*-quinone methide [155] VAO is an industrially important enzyme for the production of the compounds: vanillin, 4-hydroxybenzaldehyde, coniferyl alcohol and pure phenolic derivatives [154].

Structure Crystallographic studies of VAO were first reported by Mattevi et al. (1997). The VAO protein structure consists of 560 amino acid residues with a covalently bound FAD cofactor. VAO has two major subunits: a larger domain (FAD-binding domain, smaller cap domain (FAD isoalloxazine ring). The larger FAD-binding site consists of amino acids ranging between 6–270 and 500–560 which form one antiparallel sheet with six α-helices surrounding one mixed β-sheet [154, 156]. Smaller domain (FAD-isoalloxazine ring) consists of amino acids271–499 constituting large seven stranded antiparallel β-sheets bordered on both sides by seven α-helical regions. The structure of VAO resembles that of PCMH (both enzymes are FAD-dependent oxidoreductases) with an rms deviation of 1.2 Å for about 470 Cα atom pairs showing about 31 % of amino acid sequence similarity. In solution, vanillyl alcohol oxidase is an octamer of eight identical subunits. The crystal packing of VAO reveals an oligomer with tetragonal crystals[157]. The VAO octamer has 42 symmetry with a fourfold axis and a similar crystallographic axis The oligomer consists of tetramers of dimers and each dimer is stabilized by extensive intersubunit contacts, burying 18 % of the monomer surface area upon dimer formation [154]. However, upon octamer formation only 5 % of the monomer surface area is buried [156]. The flavin ring in VAO is covalently bound to His-422 and

the flavin is planar, not distorted by the covalent attachment. The crystal structures of four VAO ligand complexes reveal the remarkable architecture of the VAO active site, comprising an elongated cavity which is not accessible by solvent. Amino acid residues Tyr108, Tyr503 and Arg 504 form an anion binding site (activates the substrates by stabilization of its phenolate form),. The binding of ligands within the catalytic cavity is well matched with substrate oxidation, commencing via direct hydride transfer from Cα atom to the N5 atom of flavin domain [154, 156, 157]. Earlier structural studies showed that Asp-170, situated near the N5 atom of the flavin was an active site base. Site directed mutagenesis conducted by Van den Heuvel et al. (2000) reported on the catalytic role of Asp-170 in VAO. It was showed that active site amino acid residue Asp-170 is involved in catalysis and covalent flavinylation [153]. Van den Heuvel et al. (2000) carried out kinetic characterization studies of VAO variants and reported that Asp-170 mutants are 50 % less active than the wild type enzyme. The Asp-170 variants also showed that the reduced catalysis was due to the flavin reduction. Mutant proteins lost the ability to form a stable complex between the reduced enzyme and a *p*-quinone methide intermediate. Thus, supporting the role of Asp-170 in the process of autocatalytic flavinylation and efficient redox catalysis [153]. A structural study conducted by van den Heuvel et al. (2000), showed changing the stereospecificity of the active site by relocating an active site amino acid to the opposite side by site directed mutagenesis effected the catalysis of VAO [158]. This study confirms the role of Asp-170 in VAO for efficient redox catalysis and also the stereospecificity of VAO, showing that VAO is highly stereospecific for the production of alcohols [158].

Mechanism Based on spectroscopic and kinetic studies it was shown that substrate oxidation commences via direct hydride transfer from the Cα atom to N5 of flavin adenine dinucleotide. As a result a *p*-quinone methide (intermediate) is formed which is further activated by the preferential binding of the phenolate form of the substrate, this is supported by the three dimensional structure of the VAO [156]. Studies of VAO binding with VAO-isoeugenol, VAO-2-nitro-*p*-cresol complexes shows that VAO achieves hydride transfer from the Cα atom 3.5 Å from N5 atom. The hydroxyl oxygen is bound to three residues: Arg504, Tyr503 and Tyr108 through hydrogen bonds which stabilize the negative charge of the phenolate ion [156]. Under anaerobic conditions, VAO reaction with 4-methoxymethyl phenol results in a stable reduced enzyme-*p*-quinone methide complex, however the final product is synthesized and released immediately after exposure to oxygen, following FAD reoxidation. From three dimensional structures of VAO, it is suggested that charge stabilizations between the flavin, quinone intermediate and Arg-504 regulate the catalytic cycle. Besides its role in interacting with the phenolate oxygen, Arg-504 is involved in balancing the negative charge on the N1-C2=O2 locus of the anionic reduced cofactor. The C2 atom of flavin deviates from its expected position due to the oxygen atom of *p*-quinonemethide molecule binding to the reduced enzyme [156]. Thus in the reduced enzyme, the negative charge of the flavin C2 atom causes electrostatic repulsion which prevents the formation of a phenolate ion resulting in the stabilization of the quinone intermediate form. Upon reoxidation of
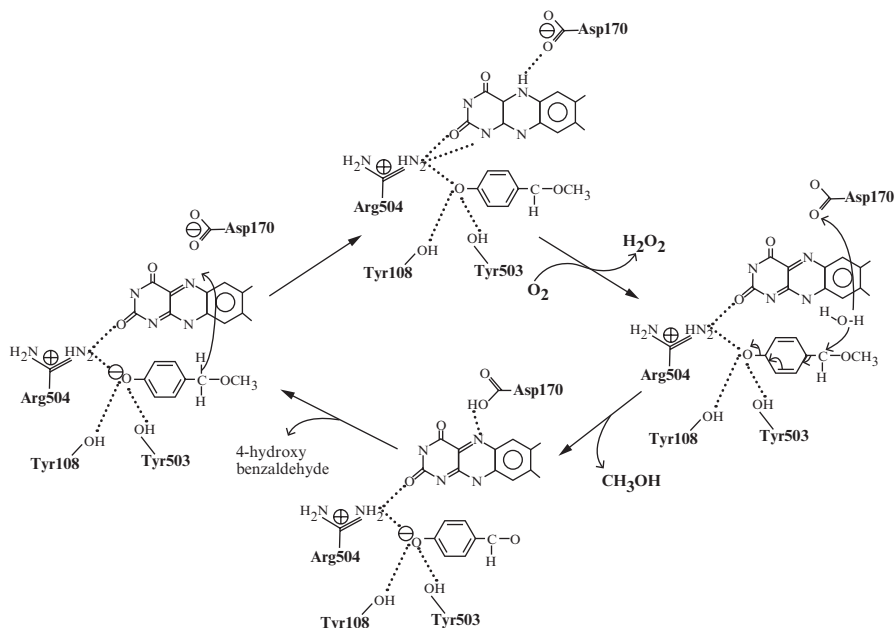
Fig. 4.10 The reaction mechanism for the oxidation of 4-(methoxymethyl) phenol. In the first step, the substrate is oxidised via a direct hydride transfer from the substrate Cα atom to the N5 of flavin. The reduced cofactor is then reoxidised by molecular oxygen with the production of a hydrogen peroxide molecule. In the next step, the p-quinone-methoxymethide intermediate is hydroxylated by a water molecule, possibly activated by Asp170. The resulting 4-hydroxy-benzaldehyde and methanol products are released (Reprinted with permission from Ref [156], Copyright © 1997, Elsevier)

flavin, Arg-504 lacks an anionic partner which triggers the development of negative charge on the oxygen atom of the quinone group. The electrophilicity of the methide carbon is increased enabling hydroxylation of 4-methoxymethyl phenol or deprotonation of the intermediate (vanillyl-alcohol) thus generating the final product (Fig. 4.10) [156, 157].

4.6.3   Glyoxal Oxidase

Glyoxal oxidase an extracellular hydrogen peroxide producing enzyme secreted by lignolytic cultures of *P. chrysosporium* [159]. Glyoxal oxidases catalyzes the oxidation of wide range of aldehydes and α-hydroxyl carbonyl compounds by reducing O_2 to H_2O_2, thus glyoxal oxidase fuels the process of lignin degradation by generating H_2O_2 which is used by ligninolytic peroxidases (such as lignin peroxidase, manganese peroxidase) [159, 160]. Glyoxal (OHCCHO) and methylglyoxal (CH_3COCHO) are two well known substrates for glyoxal oxidase in the extracellular fluids of lignolytic cultures [161].

Structure Glyoxal oxidase was isolated and characterized from the supernatants of lignolytic cultures of *P. chrysosporium*. Little was known about the structure and function of glyoxal oxidase until recently.. Studies have shown that glyoxal oxidase is a monomeric acidic glycoprotein with a molecular mass of 57 kDa [161]. It is a copper metalloenzyme with a free radical coupled copper active site similar to that of galactose oxidase. Both glyoxal oxidase and galactose oxidase have a conserved mononuclear copper radical active site coordinated by two histidine residues (His-496–His581) and two tyrosine residues, one unmodified (Tyr-495) and the covalently modified tyrosine (Tyr272), which is crosslinked to (Cys-228) thus forming a new dimeric (cysteine-tyrosine) bond. Sequence comparison of glyoxal and galactose oxidase show they have a homology of only 20 % [162, 163]. Spectrographic studies have shown a remarkable degree of similarity between them at their active site, both in structure and chemistry. These studies suggested that glyoxal oxidase and galactose oxidase are functional variants catalyzing distinct reactions at their identical active sites [159]. Glyoxal oxidase has a broad pH optimum with maximum enzyme activity at pH6. A wide range of simple aldehydes, α-hydroxycarbonyl and α-dicarbonyl compounds were found to act as substrates however highest activity was observed with methylglyoxal and it has no activity on glucose, xylose, cellobiose, galactose or other sugars [161].

Mechanism Studies have revealed that *P. chrysosporium* secretes three extracellular enzymes: lignin peroxidase, manganese peroxidase and glyoxal oxidase. Glyoxal oxidase fuels the complete ligninolytic mechanism by generating extracellular H_2O_2, which is required for the functioning of lignolytic peroxidases [164]. Pure glyoxal oxidase is inactive, however it is activated by peroxidases and peroxidase substrates) [164]. Though glyoxal and methylglyoxal (substrates) of glyoxal oxidase were observed in ligninolytic cultures, there are other substrates such as formaldehyde, acetaldehyde, glycolaldehyde, glyoxylic acid, dihydroxyacetone, glyceraldehyde. In addition, downstream lignin degradation products act as substrates for glyoxal oxidase [164]. Glyoxal oxidase has an efficient sequential oxidation process by converting glycolaldehyde to oxalate (glycolaldehyde → glyoxal → glyoxalate → oxalate) The catalytic mechanism behind oxidation of aldehydes by glyoxal oxidase is not known, however it was suggested that it oxidizes substrates similarly to galactose oxidase.

4.6.4 Pyranose Oxidase

Pyranose oxidase (EC.1.1.3.10; oxygen 2-oxidoreductase) is a hydrogen peroxide producing enzyme. Pyranose oxidase catalyzes the oxidation of the C-2 of several aldopyranoses, D-glucose is a ideal substrate for the enzyme [165–167]. Several fungi belonging to basidiomycetes and particularly members of the order *Aphyllophorales* secrete extracellular pyranose oxidase[168]. The structure and catalytic mechanism of pyranose oxidase were extensively studied in *Trametes*

multicolor fungi,. Its amino acid sequence suggests that it belongs to the glucose-methanol-choline (GMC) family of flavin adenine dinucleotide (FAD) dependent oxidoreductases [169]. Pyranose oxidase is a large flavoproteins which can oxidize a number of monosaccharides at their carbon-2 position in the presence of molecular oxygen, producing 2-keto sugars and hydrogen peroxide [168].

Structure Structural studies of pyranose oxidase protein were carried out by Hallberg, BM et al. (2004). Pyranose oxidase is a homotetramer localized in the hyphal periplasmic space of ligninolytic cultures of fungi with a molecular mass of 270 kDa [170]. Its amino acid sequence and protein structure show that it belongs to the glucose-methanol-choline (GMC) family of long chain oxidoreductases with a large FAD domain. Its structure consists of a six stranded central β-sheet and three α-helices [170]. The large homodimer contains a large internal cavity of 15,000 Å, which has four active sites [170]. Pyranose oxidase from *Trametes multicolor* is a homotetramer and its cavity serves as a storage site for quinones generated during lignin degradation [170]. The cavity prevents diffusal of toxic quinines until they are reduced by pyranose oxidase. The enzyme oxidizes polymeric carbohydrates substrates, when compared to other FAD-dependent enzymes such as GMC-enzymes. The FAD is linked covalently by its α-methyl group to the N^{e2} atom of His-167 [170]. The active sit of the enzyme retains the typical amino acid residues of catalytic GMC-type enzymes such as a His-Asn pair below the isoallaxazine ring of the FAD domain [170]. Docking studies of D-glucose in the pyranose oxidase active site suggests that the active site loop under goes dynamic changes during the reductive half reaction allowing the binding of carbohydrates [170]. These studies also suggest that the active site loop is involved in the regioselective catalysis of aldopyranoses at their C2 and C3 positions by pyranose oxidase [170].

Mechanism Pyranose oxidase is an hydrogen peroxide generating enzyme which catalyzes the oxidation of D-glucose and other aldopyranoses at the C-2 position resulting in the production of 2-keto sugars it was also found to be involved in lignin depolymerization. It catalyses the regioselective oxidation of different aldopyranoses at their C-2 position using molecular oxygen resulting in 2-keto aldoses and H_2O_2. The whole reaction can be divided into an oxidative and a reductive reaction, in the reductive half reaction the sugar is oxidized to a keto sugar followed by reduction of FAD. The oxidative reaction involves the reduction of O_2 to H_2O_2 and reoxidization of the FAD [168, 171]. Pyranose oxidase also oxidizes certain compounds at the C-3 position such as 2-deoxy-D-glucose, 2-keto-D-glucose and methyl-β-D-glucosides [172, 173]. The (k_{cat}/K_m) is highest for β-D-glucose. Studies have reported that pyranose oxidase also oxidizes monosaccharides such as D-xylose, D-galactose and L-arabinose (constituents of hemicellulose) with lower catalytic efficiencies, which may extend the enzymes ability to generate hydrogen peroxide from the lignincellulose derived sugars. The optimum pH of the enzyme varies based on the type of electron acceptors used ie oxygen, various quinones and radicals. Quinones and radicals are the best substrates of pyranose oxidase, suggesting its role in lignin depolymerization is as a hydrogen peroxide generating and

quinone reducing enzyme. It was reported that pyranose oxidase from *Phlebiopsis gigantea* has the ability to hydrolyze β 1→4 linked disaccharides (cellobiose and lactose) and α 1→4 linked disaccharides (such as maltose) to the corresponding monosaccharides at their C2 position [174]. β glycosides of higher alcohols such as hexyl, phenyl, o-nitrophenyl and p-nitrophenyl) are converted to disaccharides by pyranose oxidase through a glycosyl transferase reaction [174].

4.6.5   Galactose Oxidase

Galactose oxidase (EC 1.1.3.9) an extracellular enzyme secreted by *Fusarium spp.* Galactose oxidase is a monomeric enzyme containing a single copper ion, catalyzing the oxidation of primary alcohol substrates (D-isomers) such as D-galactose and other polysaccharides containing D-galactose on their reducing ends resulting in the production of aldehydes and hydrogen peroxide [175, 176]. Galactose oxidase belongs to the alcohol oxidoreductase family (also known as alcohol oxidase), enzymes belonging to this generally use molecular oxygen as electron acceptors for generating hydrogen peroxide [177]. Most alcohol oxidoreductases are flavoproteins that use FAD+ as primary electron acceptors, however some of these enzymes are copper radical containing oxidases (CROs) such as galactose oxidase, glyoxal oxidase and hexose-1-oxidase [177].

Structure   The structure and catalytic mechanism of galactose oxidase were extensively studied by biochemical and spectroscopic methods. Galactose oxidase has a mass of 68 kDa consisting of three major β structure domains and single α-helix (amino acid residues 327–332) [178]. The presence of three β structures in the protein imparts structural stability, The first domain has a β sandwich structure (amino acid residues 1–155) that is linked to the second domain by polypeptide chains. The second domain is the largest domain residues 156–532, it has pseudo sevenfold symmetry. The third domain (residues 533–639) is on the opposite side of the second domain from the copper [178]. The structure of galactose oxidase is similar to that of glyoxal oxidase, containing a mononuclear copper radical with a crosslinked cysteine-tyrosine residue along with one unmodified axial tyrosine and a histidine side chain as coordinating residues [177]. The active site of the galactose oxidase contains a copper complex with two tyrosine (Tyr 272 and Tyr495) and two histidine (His496 and His581) amino acid side chains [178]. One of the tyrosine residue (Tyr272) was found to be crystallographically crosslinked to the carbon atom (Cε) of a phenolic side chain and the sulfur (Sγ) of Cys228, forming a thioether Tyr-Cys bond. The thioether bond formed between Tyr-Cys affects both the structure and function of the protein, structurally this crosslinking also affects the active site by making it more rigid similar to a disulfide bond [178].

Mechanism   Galactose oxidizes primary alcohols resulting in the production of aldehydes and hydrogen peroxide. This is a two electron reaction with only one copper ion at the active site and a second redox active center, a tyrosine residue. Tyr-272 also acts as ligand to the copper ion [178]. The catalytic mechanism of galactose

oxidase can be divided into two reactions (a) proton transfer from the O-6 position of galactose to the axial tyrosine anion (hydrogen atom transfer) then from the C6 of galactose to the Tyr-Cys radical cofactor followed by electron transfer from the carbohydrate, generating an aldehyde and Cu^+ [177]. In the second half of the reaction electron transfer continues from Cu+ to oxygen by producing superoxide then through hydrogen transfer, a proton is transferred from the phenolic hydroxyl group of the Tyr-Cys cofactor to superoxide, producing a metal bound hydroperoxide. The final proton transfer from the axial tyrosine to hydroperoxide generates hydrogen peroxide and Cu^{2+} (resting state of the enzyme) [177].

4.6.6 Glucose Oxidase

Glucose oxidase (E.C.1.1.3.4) is an important H_2O_2 generating oxidoreductase produced by ligninolytic cultures of *P. chrysosporium*. Glucose oxidase catalyzes the oxidation of β-D-glucose to gluconic acid, using molecular oxygen (as electron acceptor) thus producing H_2O_2 [179, 180]. Glucose oxidase has several commercial applications such as increasing the quality of food materials (color, flavor and shelf life), oxygen removal from fruit juices and canned food etc [180]. Apart from these applications, glucose oxidase also inhibits different food-borne pathogens such as *Salmonella infantis, Staphylococcus aureus, Clostridium perfringens, Bacillus cereus, Campylobacter jejuni* and *Listeria monocytogens* [181].

Structure Glucose oxidase (GOD) is a homodimeric glycoprotein containing two identical polypeptide chains that are covalently linked together by disulfide bonds. The molecular mass of glucose oxidase ranges from 130 to 175 kDa [182], containing two molecules of FAD which bind tightly to the protein thus maintaining its three dimensional structure. The structure of glucose oxidase from *P. amagasakiense* shows that each of the protein subunit contains one mole of tightly bound FAD. GOD has a very high specificity for β-D-glucose as α-D-glucose is not a suitable substrate for GOD. Very low activity was observed when 2-deoxy –D-glucose, D-Mannose or D-Galactose were used as substrates. Metals such as Ag+, Hg 2+, Cu2+ and chemicals such as hydroxylamine, hydrazine, *p*-chloromercuribenzoate, phenylhydrazine, dimedone and sodium bisulphate inhibit the activity of GOD [183, 184]. GOD from *P. amagasakiense* was found to be glycosylated predominantly with mannose residues, with a total carbohydrated content of 11–13 % [183, 184]. Structural studies of GOD from *A. niger* and *P. amagasakiense* were found to contain similar carbohydrate residues such as glucose, mannose and hexosamine. *A. niger* GOD showed higher mannose and hexosamine and less glucose then *P. amagasakiense* GOD, resulting in total carbohydrate contents of 16 % (*A. niger*) and 11 % (*P. amagasakiense)* respectively. The active site of *P. amagasakiense* GOD contains: Tyr-73, Phe-418, Trp-430, Arg-516, Asn-518, His-520 and His-563. Arg-516 and Asn-518 (lesser extent) were found to be required for the efficient binding of β-D-glucose by GOD [185]. Aromatic amino acids such as Tyr-73, Phe-418 and Trp-430 were required for the correct orientation of the substrate and also for speeding up the

oxidation of glucose molecules. His-520 and His-563 are involved in hydrogen bond formation to the hydroxyl group (1-OH) of glucose during the reaction. *A. niger* GOD contained more histidine, arginine, tyrosine and less lysine, phenylalanine then *P. amagasakiense* GOD [184, 185].

Mechanism The reaction of GOD can be divided into an oxidative step and a reductive step. The reductive step of GOD oxidizes β-D-glucose to D-glucano-δ-lactone which is further hydrolyzed to gluconic acid (non-enzymatically). In *A. niger* a lactonase catalyzes the hydrolysis of D-glucano-δ-lactone to gluconic acid. It also reduces the FAD domain of GOD to $FADH_2$ [185]. Reduced GOD is re-oxidized by molecular oxygen to H_2O_2 in the oxidative reaction, H_2O_2 from the above reaction is cleaved by catalase producing water and oxygen [186]. The flavin domains of GOD are involved in the redox reaction, during the oxidative reaction of GOD and electrons from electron donors are transferred to the isoalloxazine nucleus of flavin domain (FMN) and then to the electron acceptor [187]. GOD catalyzes the reaction by transferring the electrons from glucose to oxygen, producing H_2O_2, thus placing GOD in the oxidoreductase class of enzymes. Overall enzyme catalysis of GOD depends on oxidation and reduction reaction steps of its flavin group (FAD) primarily glucose reduces the FAD to $FADH_2$ by producing gluconic acid (product) without forming free radical containing semiquinone (intermediate). At the same molecular oxygen (electron acceptor) reduces the $FADH_2$ back to FAD generating H_2O_2 as a product (Fig. 4.11) [187].

4.6.7 Benzoquinone Reductase

The 1,4-Benzoquinone reductase (EC.1.6.5.6) is an intracellular enzyme which was purified and characterized from the agitated cultures of *P. chrysosporium*. 1,4-Benzoquinone reductase was expressed in both nitrogen sufficient and limited conditions [188, 189]. *P. chrysosporium*, one of the highly studied lignin degrading
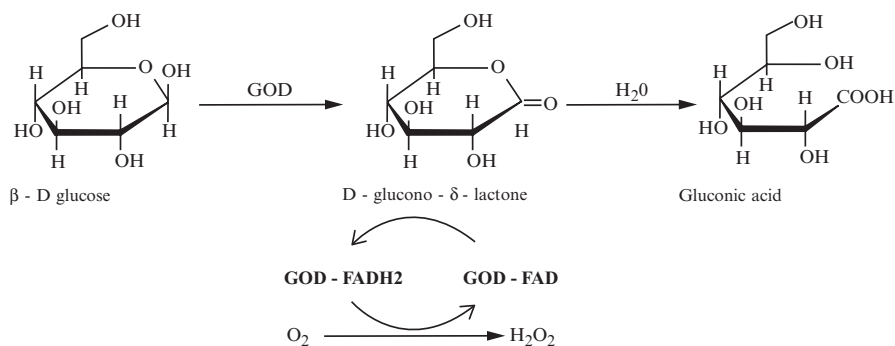
Fig. 4.11 Reaction mechanism of glucose oxidase (GOD) [185] (Reprinted with permission from Ref [179], Copyright © 2009, Elsevier)

fungi, secretes two classes of ligninolytic peroxides: lignin peroxidase(LiP)and manganese peroxidase(MnP) along with several H_2O_2 generating enzymes. These enzymes catalyze the primary steps of lignin depolymerization resulting in a wide variety of intermediate products such as substituted quinones, hydroquinones, benzaldehydes and other ring opened fragments. Methoxylated lignin derived quinones are reduced by intracellular quinone reductases [188, 189].

Structure The 1,4-Benzoquinone reductases from *P. chrysosporium* was purified and characterized. These studies showed that it is a NADPH dependent 1,4-benzoquinone reductase with a molecular mass of 44 kDa containing two similar 22 kDa subunits which contain flavin mononucleotide [189]. Purified 1,4-benzoquinone reductase shows a typical oxidized flavin spectrum from 375 to 450 nm [188]. Upon reduction of the enzyme with sodium dithionate a drop in absorbance of the flavin was observed. The presence of flavin was proved by two methods, the released flavin from the boiled enzyme was isolated using ultrafiltration., HPLC analysis of the ultrafiltrate had same retention time as standard flavin mononucleotide (FMN), secondly fluorescence of the flavin isolated from the enzyme showed a pH dependence identical to FMN [188, 189]. Purified quinone reductase uses either NADH or NADPH as its electron donor with Km for NADH (55 μM) and NADPH (48 μM) respectively. 2-MBQ and 2-DMBQ were two substituted paraquinones identified as fungal metabolites of lignin model compounds, quinone reductases are capable of reducing both paraquinones and ortho quinones. 2-DMBQ is one of the best substrate for quinone reductases because of its stability and being a downstream product produced during oxidation of lignin model compounds. Quinone reductase showed a high turnover for 2-MBQ and 2-DMBQ which suggests a role for this enzyme in the degradation of lignin and related compounds [188, 189].

Mechanism Benzoquinone or quinone reductases are significant enzymes secreted by several fungi especially *P. chrysosporium.* 1,4-Benzoquinone reductase is a NADPH dependent intracellular enzyme, it contains flavin mononucleotide (FMN). 1,4-Benzoquinone reductase was active during both primary and secondary metabolism but the enzyme inducers are stronger during the primary metabolic processes [188–190]. Studies showed that when vanillate or methoxy-*p*-quinone are added to cells, carrying out primary metabolism, enzyme expression was increased. However, the effect was small when the same compounds were added to secondary metabolic cells, which suggests that quinone reductase is regulated independently of lignin and manganese peroxidase [188]. LiP and MnP are expressed only during the secondary metabolic stage of the growth and the there expression is not induced by aromatic substrates. The regulation of quinone reductases is similar to that of vanillate hydroxylase, which suggests its involvement in vanillate metabolism [188–190]. Quinone reductase was expressed during the lignolytic phase of *P. chrysosporium*, suggesting a role in the reduction of quinones generated during lignin degradation. It was reported that quinone reductases are induced upon quinone addition, suggesting the involvement of quinone reductase in lignin and quinone degradation [188–190]. Besides degrading of quinone and lignin derived compounds, it is also reported that quinone reductases protects *P. chrysosporium*

from oxidative stress by acting as redox active toxins. Quinones obtained by metabolic conversion are reduced by one electron generating semiquinone radicals, which are then oxidized by oxygen generated super oxide anion, this superoxide anion is further converted to H_2O_2 through superoxide dismutase and later in the presence of suitable electron donors it results in production of highly reactive hydroxyl radicals from H_2O_2 [188–190]. The detailed mechanisms of the regulation and catalytic mechanism of quinone reductase need to be explored (Table 4.3).

4.7   A Short Note on Genome Sequencing Studies of Lignin Degrading Fungi

In 2004, Martinez et al., had sequenced the whole genome sequence of *Phanerochaete chrysosporium* [206]. As it was the first wood decaying fungus to be sequenced from the phylum Basidiomycota there were few difficulties in annotating the whole genome. In the year 2006, Vanden Wymelenberg et al. have improved the genome assembly and reannotated the *P. chrysosporium* genome [207]. *P. chrysosporium* genome has revealed a wide array of hydrolytic and oxidative enzymes mainly class-II peroxidases apparently supporting its lignocellulose degrading ability. Later in the year 2009, complete genome sequencing of *Postia placenta* was performed by Martinez et al, genome of *P. placenta* has revealed several interesting facts about its wood decaying patterns. *P. placenta* genome lacks genes coding for peroxidases, few genes coding for enzymes involved in degradation of crystalline cellulose (GH6, GH7 and GH61) [208]. However, these studies have reported that *P. placenta* genome codes for enzymes involved in generating Fenton reagents (reactive oxygen species). Whole genome sequences of prominent brown rot fungus such as *Serpula lacrymans* [209], *Fibroporia radiculosa* [210] have shown similar results such as lacking the genes coding for peroxidases, reduced expression of genes coding for CAZymes and possessing oxidoreductases involved in Fenton reactions. The genome sequence of the *Schizophyllum commune* was first wood decaying fungus to be sequenced from order Agaricales [211]. Though it was reported to degrade lignin, *S. commune* lacked the genes coding for peroxidases. While whole genome sequencing of several white rot fungus such as *Ceriporiopsis subvermispora* [212], *Phanerochaete carnosa* [213], *Heterobasidion irregulare* [214], *Laccaria bicolor* [215], *Volvariella volvacea* [216], *Agaricus bisporus* [217], *Armillaria mellea* [218] etc., have revealed several significant facts about lignocellulose degrading enzymes and their corresponding mechanisms [219]. Large scale genome comparison studies showed that whiterot fungi has wide range of genes coding for lignocellulolytic enzymes compared to brown rot fungi [220]. Especially enzymes involved in breakdown of crystalline cellulose such as GH6, GH7, GH61 and CBM1 are predominant in white rot fungi. Similarly whiterot fungi possess several genes coding for peroxidases, whereas in most of the brown rot fungi genes coding for peroxidases are mostly absent or reduced [220, 221].

These sequencing studies has dramatically raised the interest in sequencing projects of wood decaying fungi. The large scale sequencing projects like 1000 Fungal Genome Project, Joint Genome Institute (JGI) are playing a critical role in revealing

Table 4.3 Catalytic mechanisms and structural studies of different lignin degrading auxiliary enzymes (LDA)

Enzyme and FOLy class	Catalytic mechanism	Structural studies and reference
Aryl alcohol oxidase (LDA1) EC 1.1.3.7	Aromatic primary alcohol $+ O_2 \rightarrow$ Aromatic aldehyde $+ H_2O_2$	*Pleurotus eryngii* [131, 191–193]
Vanillyl alcohol oxidase (LDA2) EC 1.1.3.38	Vanillyl alcohol $+ O_2 \rightarrow$ vanillin $+ H_2O_2$	*Penicillium simplicissimum* [153, 156, 158, 194, 195]
Glyoxal oxidase (LDA3) EC 1.1.3.-.	Glyoxal oxidase catalyzes oxidation of wide range of simple aldehydes, α-hydroxy carbonyl compounds by producing hydrogen peroxide	*Aspergillus nidulans, Pichia pastoris, Phanerochaete chrysosporium* [160, 196, 197]
Pyranose oxidase (LDA4) EC 1.1.3.10	$FAD_{(Oxidized)} + D$ Glucose $\rightarrow FAD_{(Reduced)} + 2$ keto D glucose $FAD_{(Oxidized)} + O_2 \rightarrow FAD_{(Reduced)} + H_2O_2$	*Trametes multicolor* [170, 198–200], *Peniophora* sp. [201, 202] *Phanerochaete chrysosporium* [135]
Galactose oxidase (LDA5) EC 1.1.3.9	D Galactose $+ O_2 \rightarrow D$ Galacto hexodialdose $+ H_2O_2$	*Aspergillus nidulans, Pichia pastoris* [175–178, 203, 204]
Glucose oxidase (LDA6) EC 1.1.3.4	β D glucose $+ O_2 \rightarrow D$ glucono 1,5 lactone $+ H_2O_2$	*Aspergillus niger* [146, 205]
Benzoquinone reductase (LDA7) EC 1.6.5.6	$NADPH + H^+ + p$ benzoquinone $\rightarrow NADP^+ +$ hydroquinone	*Phanerochaete chrysosporium* [188–190]
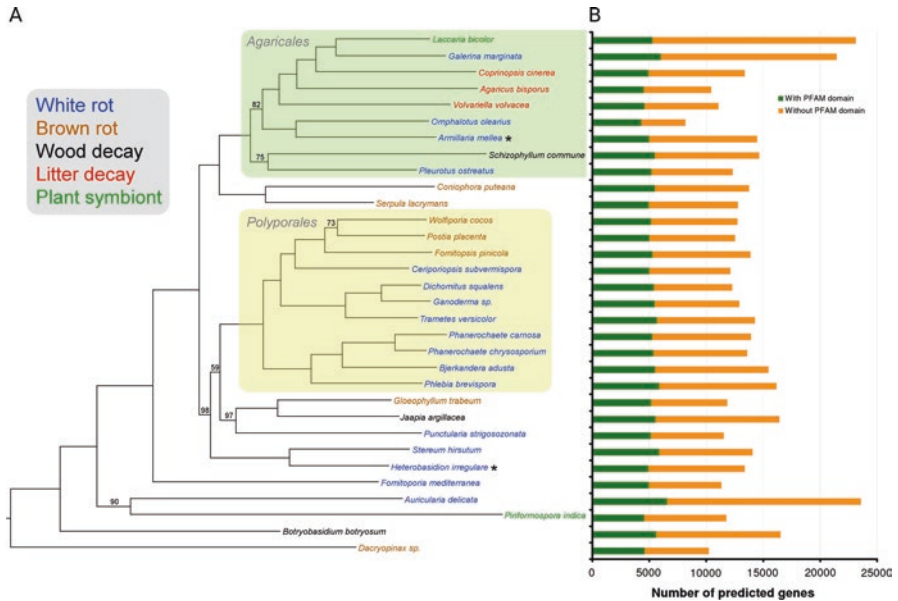
Fig. 4.12 (**a**) Phylogeny and main lifestyles of Agaricomycetes with a published genome sequence. The major orders Agaricales and Polyporales are indicated. The majority of these species are wood decayers and can be further classified as either white rot fungi (which degrade all components of the plant cell wall) or brown rot fungi (which modify lignin, but do not break it down to a large extent). *Schizophyllum commune*, *Jaapia argillacea* and *Botryobasidium botryosum* are also wood decayers, but cannot be easily classified as either white or brown rot fungi. *Coprinopsis cinerea*, *Agaricus bisporus* and *Volvariella volvacea* are saprotrophs growing on non-woody substrates. The ectomycorrhizal fungus Laccaria bicolor and the endophyte Piriformospora indica both form interactions with plant roots. Species with an asterisk (*) are predominantly plant pathogens. The genomes of *G. marginata*, *P. ostreatus*, *J. argillacea* and *B. botryosum* have been submitted for publication. (**b**) Number of predicted genes for each genome. Each bar lines up with a species from the tree in (**a**). The total number of genes varies per genome, but the number of genes with at least one PFAM domain is more constant. Genes without a PFAM domain outnumber those with a PFAM domain, showing that much remains to be learned about these organisms (Reprinted with performance from Ref [219], Copyright © 2014 Elsevier)

and understanding the whole genome of sequences of several fungi (Figs. 4.12 and 4.13). The JGI have also developed a strong web based interactive and integrated genome analysis portal called MycoCosm [222]. As of 2016 JGI MycoCosm offers over 563 sequenced and annotated fungal whole genome sequences. As most of the wood decaying fungi were reported from the phylum Basidiomycota out of which 202 fungal genome sequences belongs to the phylum Basidiomycota. Among Basidiomycetes fungi 159 fungal genome sequences reported belongs to subphylum Agaricomycotina, 16 and 27 fungal genome sequences belong to Ustilaginomycotina and Pucciniomycotina respectively. Thus, the recent advancements in genomics field in the past decade has prominently improved our understanding the genes involved in coding for the lignocellulose degrading enzymes and their pathways [219].
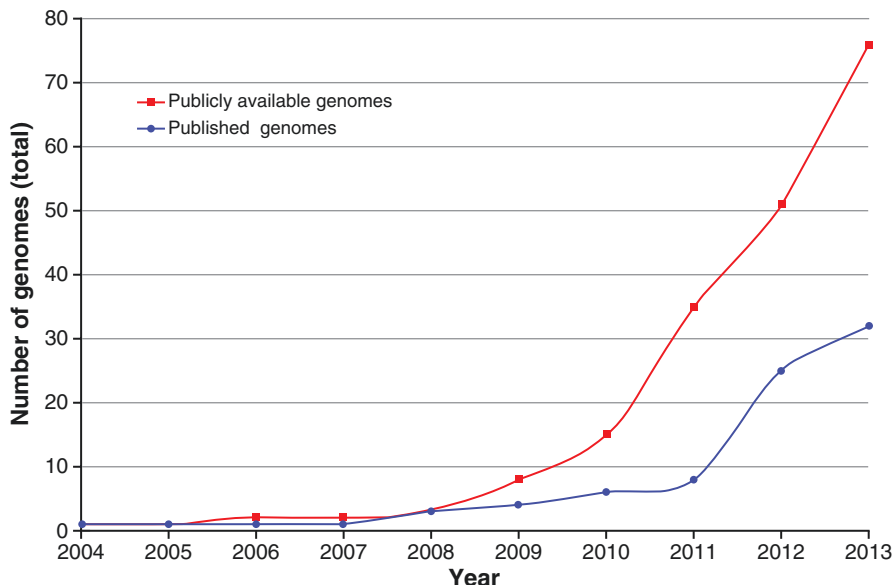
Fig. 4.13 The number of available genome sequences of the Agaricomycetes has dramatically increased over the past decade. For each year, the total number of published and publicly available genomes are given. The number of publicly available genomes (*red line*) is higher than the number of published genomes (*blue line*), since in the case of genomes sequenced by the Joint Genome Institute those genomes are publicly available in MycoCosm well before being published (Reprinted with performance from Ref [219], Copyright © 2014 Elsevier)

4.8   Conclusion and Future Outlook

Depletion of fossil fuels in the world is one of the major reasons for increased bio-fuel research. Lignocellulose is one of the major alternative resource fulfill the current requirement for fuels and chemicals. The biofuel and paper pulp industries efficiently use cellulose in the production of paper and cellulosic ethanol, however lignin is left as a major industrial byproduct. Fungi are the most efficient lignin degrading microorganisms, producing several extra and intra cellular enzymes for breakdown of lignin. Understanding the lignin degrading mechanisms employed by white rot fungi is very important. Recent advances in the field of genomics and proteomics have revealed significant information about genes related to lignocellulose degradation and detoxification mechanisms. Whole genome sequences of *Phanerochaete chrysosporium, Postia placenta, Gloeophyllum trabeum* and *Dichomitus squalens* prove the occurrence of lignocellulolytic enzymes. Integrated computational analyses of proteome and secretome show that fungi undergo severe oxidative stress during the process of wood degradation, for which it employs various antioxidative and detoxification mechanisms. Application of advanced sequencing methodologies integrated with HPLC, GC and mass spectrometry techniques can help to elucidate the pathways involved in wood degradation.

References

1. Fengel D, Wegener G. Wood: chemistry, ultrastructure, reactions. Berlin: Walter de Gruyter; 1984. 613:1960–1982.
2. Whetten R, Sederoff R. Lignin biosynthesis. Plant Cell. 1995;7(7):1001.
3. Boerjan W, Ralph J, Baucher M. Lignin biosynthesis. Annu Rev Plant Biol. 2003;54(1):519–46.
4. Ten E, Ling C, Wang Y, Srivastava A, Dempere LA, Vermerris W. Lignin nanotubes as vehicles for gene delivery into human cells. Biomacromolecules. 2013;15(1):327–38.
5. Freudenberg K, Neish AC. Constitution and biosynthesis of lignin. Berlin/Heidelberg: Springer; 1968.
6. Higuchi T. Lignin biochemistry: biosynthesis and biodegradation. Wood Sci Technol. 1990;24(1):23–63.
7. Breznak JA, Brune A. Role of microorganisms in the digestion of lignocellulose by termites. Annu Rev Entomol. 1994;39(1):453–87.
8. Pandey MP, Kim CS. Lignin depolymerization and conversion: a review of thermochemical methods. Chem Eng Technol. 2011;34(1):29–41.
9. Wong DW. Structure and action mechanism of ligninolytic enzymes. Appl Biochem Biotechnol. 2009;157(2):174–209.
10. Hatakka A. Biodegradation of lignin. Biopolymers Online. 2005.
11. Arantes V, Goodell B. Current understanding of brown-rot fungal biodegradation mechanisms a review. In: Deterioration and protection of sustainable biomaterials, American chemical society symposium series. Washington, DC: American Chemical Society; 2014. p. 1–21.
12. Alexopoulos C, Mims C, Blackwell M. Introductory mycology. 4th ed. New York: Wiley; 1996, 869pp.
13. Leonowicz A, Matuszewska A, Luterek J, Ziegenhagen D, Wojtaś-Wasilewska M, Cho N-S, Hofrichter M, Rogalski J. Biodegradation of lignin by white rot fungi. Fungal Genet Biol. 1999;27(2):175–85.
14. Manavalan T, Manavalan A, Heese K. Characterization of lignocellulolytic enzymes from white-rot fungi. Curr Microbiol. 2015;70(4):485–98.
15. Kameshwar AKS, Qin W. Recent developments in using advanced sequencing technologies for the genomic studies of lignin and cellulose degrading microorganisms. Int J Biol Sci. 2016;12(2):156–71.
16. Cantarel BL, Coutinho PM, Rancurel C, Bernard T, Lombard V, Henrissat B. The Carbohydrate-Active EnZymes database (CAZy): an expert resource for glycogenomics. Nucleic Acids Res. 2009;37 suppl 1:D233–8.
17. Henrissat B. A classification of glycosyl hydrolases based on amino acid sequence similarities. Biochem J. 1991;280:309–16.
18. Levasseur A, Piumi F, Coutinho PM, Rancurel C, Asther M, Delattre M, Henrissat B, Pontarotti P, Asther M, Record E. FOLy: an integrated database for the classification and functional annotation of fungal oxidoreductases potentially involved in the degradation of lignin and related aromatic compounds. Fungal Genet Biol. 2008;45(5):638–45.
19. Blodig W, Smith AT, Doyle WA, Piontek K. Crystal structures of pristine and oxidatively processed lignin peroxidase expressed in Escherichia coli and of the W171F variant that eliminates the redox active tryptophan 171. Implications for the reaction mechanism. J Mol Biol. 2001;305(4):851–61.
20. Sundaramoorthy M, Youngs HL, Gold MH, Poulos TL. High-resolution crystal structure of manganese peroxidase: substrate and inhibitor complexes. Biochemistry. 2005;44(17):6463–70.
21. Hallberg BM, Henriksson G, Pettersson G, Divne C. Crystal structure of the flavoprotein domain of the extracellular flavocytochrome cellobiose dehydrogenase. J Mol Biol. 2002;315(3):421–34.

22. Dwivedi UN, Singh P, Pandey VP, Kumar A. Structure–function relationship among bacterial, fungal and plant laccases. J Mol Catal B Enzym. 2011;68(2):117–28.

23. Yoshida H. LXIII.-chemistry of lacquer (Urushi). Part I. Communication from the chemical society of Tokio. J Chem Soc Trans. 1883;43(0):472–86. doi:10.1039/CT8834300472.

24. Bertrand G. Sur la presence simultanee de la laccase et de la tyrosinase dans le suc de quelques champignons. CR Hebd Seances Acad Sci. 1896;123:463–5.

25. Heinzkill M, Messner K. The ligninolytic system of fungi. Fungal Biotechnol. 1997; 213–227.

26. Gianfreda L, Xu F, Bollag J-M. Laccases: a useful group of oxidoreductive enzymes. Bioremediation J. 1999;3(1):1–26.

27. O'Malley DM, Whetten R, Bao W, Chen CL, Sederoff RR. The role of laccase in lignification. Plant J. 1993;4(5):751–7.

28. Hatakka A. Lignin-modifying enzymes fungi: production and role. FEMS Microbiol Rev. 1994;13:125–35.

29. Youn H-D, Hah YC, Kang S-O. Role of laccase in lignin degradation by white-rot fungi. FEMS Microbiol Lett. 1995;132(3):183–8.

30. Thurston CF. The structure and function of fungal laccases. Microbiology. 1994;140(1):19–26.

31. Leatham GF, Stahmann MA. Studies on the laccase of Lentinus edodes: specificity, localization and association with the development of fruiting bodies. J Gen Microbiol. 1981;125(1):147–57.

32. Ikegaya N, Goto M, Hayashi Y. Effect of phenolic compounds and urovides on the activities of extracellular enzyme during vegetative growth and fruit-body formation of Lentinus edodes. Transactions of the Mycological Society of Japan (Japan). 1993.

33. Worrall J, Chet I, Hüttermann A. Association of rhizomorph formation with laccase activity in Armillaria spp. J Gen Microbiol. 1986;132(9):2527–33.

34. Viterbo A, Staples RC, Yagen B, Mayer AM. Selective mode of action of cucurbitacin in the inhibition of laccase formation in Botrytis cinerea. Phytochemistry. 1994;35(5):1137–42.

35. Piontek K, Antorini M, Choinowski T. Crystal structure of a laccase from the fungus Trametes versicolor at 1.90-Å resolution containing a full complement of coppers. J Biol Chem. 2002;277(40):37663–9.

36. Ducros V, Brzozowski AM, Wilson KS, Brown SH, Østergaard P, Schneider P, Yaver DS, Pedersen AH, Davies GJ. Crystal structure of the type-2 Cu depleted laccase from Coprinus cinereus at 2.2 Å resolution. Nat Struct Mol Biol. 1998;5(4):310–6.

37. Hakulinen N, Kiiskinen L-L, Kruus K, Saloheimo M, Paananen A, Koivula A, Rouvinen J. Crystal structure of a laccase from Melanocarpus albomyces with an intact trinuclear copper site. Nat Struct Mol Biol. 2002;9(8):601–5.

38. Lyashenko AV, Zhukhlistova NE, Gabdoulkhakov AG, Zhukova YN, Voelter W, Zaitsev VN, Bento I, Stepanova EV, Kachalova GS, Koroleva OV. Purification, crystallization and preliminary X-ray study of the fungal laccase from Cerrena maxima. Acta Crystallogr Sect F: Struct Biol Cryst Commun. 2006;62(10):954–7.

39. Kallio JP, Gasparetti C, Andberg M, Boer H, Koivula A, Kruus K, Rouvinen J, Hakulinen N. Crystal structure of an ascomycete fungal laccase from Thielavia arenaria–common structural features of asco-laccases. FEBS J. 2011;278(13):2283–95.

40. Ferraroni M, Myasoedova N, Schmatchenko V, Leontievsky A, Golovleva L, Scozzafava A, Briganti F. Crystal structure of a blue laccase from Lentinus tigrinus: evidences for intermediates in the molecular oxygen reductive splitting by multicopper oxidases. BMC Struct Biol. 2007;7(1):60.

41. Miki Y, Calviño FR, Pogni R, Giansanti S, Ruiz-Dueñas FJ, Martínez MJ, Basosi R, Romero A, Martínez AT. Crystallographic, kinetic, and spectroscopic study of the first ligninolytic peroxidase presenting a catalytic tyrosine. J Biol Chem. 2011;286(17):15525–34.

42. Edwards SL, Raag R, Wariishi H, Gold MH, Poulos TL. Crystal structure of lignin peroxidase. Proc Natl Acad Sci. 1993;90(2):750–4.

43. Piontek K, Smith A, Blodig W. Lignin peroxidase structure and function. Biochem Soc Trans. 2001;29(Pt 2):111–6.
44. Johjima T, Itoh N, Kabuto M, Tokimura F, Nakagawa T, Wariishi H, Tanaka H. Direct interaction of lignin and lignin peroxidase from Phanerochaete chrysosporium. Proc Natl Acad Sci. 1999;96(5):1989–94.
45. Blodig W, Smith AT, Winterhalter K, Piontek K. Evidence from spin-trapping for a transient radical on tryptophan residue 171 of lignin peroxidase. Arch Biochem Biophys. 1999;370(1):86–92.
46. Choinowski T, Blodig W, Winterhalter KH, Piontek K. The crystal structure of lignin peroxidase at 1.70 Å resolution reveals a hydroxy group on the C β of tryptophan 171: a novel radical site formed during the redox cycle. J Mol Biol. 1999;286(3):809–27.
47. Poulos T, Edwards S, Wariishi H, Gold M. Crystallographic refinement of lignin peroxidase at 2 A. J Biol Chem. 1993;268(6):4429–40.
48. Piontek K, Glumoff T, Winterhalter K. Low pH crystal structure of glycosylated lignin peroxidase from Phanerochaete chrysosporium at 2.5 Å resolution. FEBS Lett. 1993;315(2):119–24.
49. Sundaramoorthy M, Kishi K, Gold MH, Poulos TL. The crystal structure of manganese peroxidase from Phanerochaete chrysosporium at 2.06-A resolution. J Biol Chem. 1994;269(52):32759–67.
50. Sundaramoorthy M, Kishi K, Gold MH, Poulos TL. Crystal structures of substrate binding site mutants of manganese peroxidase. J Biol Chem. 1997;272(28):17574–80.
51. Sundaramoorthy M, Gold MH, Poulos TL. Ultrahigh (0.93 Å) resolution structure of manganese peroxidase from Phanerochaete chrysosporium: implications for the catalytic mechanism. J Inorg Biochem. 2010;104(6):683–90.
52. Pfister TD, Mirarefi AY, Gengenbach AJ, Zhao X, Danstrom C, Conatser N, Gao Y-G, Robinson H, Zukoski CF, Wang AH-J. Kinetic and crystallographic studies of a redesigned manganese-binding site in cytochrome c peroxidase. J Biol Inorg Chem. 2007;12(1):126–37.
53. Pogni R, Baratto MC, Teutloff C, Giansanti S, Ruiz-Dueñas FJ, Choinowski T, Piontek K, Martínez AT, Lendzian F, Basosi R. A Tryptophan Neutral Radical in the Oxidized State of Versatile Peroxidase from Pleurotus eryngii a combined multifrequency EPR and density functional theory study. J Biol Chem. 2006;281(14):9517–26.
54. Camarero S, Sarkar S, Ruiz-Dueñas FJ, Martınez MJ, Martınez ÁT. Description of a versatile peroxidase involved in the natural degradation of lignin that has both manganese peroxidase and lignin peroxidase substrate interaction sites. J Biol Chem. 1999;274(15):10324–30.
55. Ruiz-Dueñas FJ, Pogni R, Morales M, Giansanti S, Mate MJ, Romero A, Martínez MJ, Basosi R, Martínez AT. Protein radicals in fungal versatile peroxidase catalytic tryptophan radical in both compound I and compound II and studies on W164Y, W164H and W164S variants. J Biol Chem. 2009;284(12):7986–94.
56. Moreira PR, Duez C, Dehareng D, Antunes A, Almeida-Vara E, Frère J-M, Malcata FX, Duarte J. Molecular characterisation of a versatile peroxidase from a Bjerkandera strain. J Biotechnol. 2005;118(4):339–52.
57. Ruiz-Duenas FJ, Morales M, Mate MJ, Romero A, Martínez MJ, Smith AT, Martínez ÁT. Site-directed mutagenesis of the catalytic tryptophan environment in Pleurotus eryngii versatile peroxidase. Biochemistry. 2008;47(6):1685–95.
58. Henriksson G, Zhang L, Li J, Ljungquist P, Reitberger T, Pettersson G, Johansson G. Is cellobiose dehydrogenase from Phanerochaete chrysosporium a lignin degrading enzyme? Biochim Biophys Acta Protein Struct Mol Enzymol. 2000;1480(1):83–91.
59. Ferri S, Sode K. Amino acid substitution at the substrate-binding subsite alters the specificity of the Phanerochaete chrysosporium cellobiose dehydrogenase. Biochem Biophys Res Commun. 2010;391(2):1246–50.
60. Hallberg BM, Henriksson G, Pettersson G, Vasella A, Divne C. Mechanism of the reductive half-reaction in cellobiose dehydrogenase. J Biol Chem. 2003;278(9):7160–6.

61. Hallberg BM, Bergfors T, Bäckbro K, Pettersson G, Henriksson G, Divne C. A new scaffold for binding haem in the cytochrome domain of the extracellular flavocytochrome cellobiose dehydrogenase. Structure. 2000;8(1):79–88.

62. Albrecht Messerschmidt WS, Huber R, Lang G, Kroneck PM. X-ray crystallographic characterisation of type-2-depleted ascorbate oxidase from zucchini. Eur J Biochem. 1992;209:597–602.

63. Petersen LC, Degn H. Steady-state kinetics of laccase from Rhus vernicifera. Biochimica et Biophysica Acta (BBA)-Enzymology. 1978;526(1):85–92.

64. Giardina P, Faraco V, Pezzella C, Piscitelli A, Vanhulle S, Sannia G. Laccases: a never-ending story. Cell Mol Life Sci. 2010;67(3):369–85.

65. Solomon EI, Sundaram UM, Machonkin TE. Multicopper oxidases and oxygenases. Chem Rev. 1996;96(7):2563–606.

66. Yaropolov A, Skorobogat'Ko O, Vartanov S, Varfolomeyev S. Laccase. Appl Biochem Biotechnol. 1994;49(3):257–80.

67. Sakurai T. Anaerobic reactions of Rhus vernicifera laccase and its type-2 copper-depleted derivatives with hexacyanoferrate (II). Biochem J. 1992;284:681–5.

68. Höfer C, Schlosser D. Novel enzymatic oxidation of Mn 2+ to Mn 3+ catalyzed by a fungal laccase. FEBS Lett. 1999;451(2):186–90.

69. Schlosser D, Höfer C. Laccase-catalyzed oxidation of Mn2+ in the presence of natural Mn3+ chelators as a novel source of extracellular H_2O_2 production and its impact on manganese peroxidase. Appl Environ Microbiol. 2002;68(7):3514–21.

70. Bento I, Carrondo MA, Lindley PF. Reduction of dioxygen by enzymes containing copper. J Biol Inorg Chem. 2006;11(5):539–47.

71. Solomon EI, Baldwin MJ, Lowery MD. Electronic structures of active sites in copper proteins: contributions to reactivity. Chem Rev. 1992;92(4):521–42.

72. Palmieri G, Cennamo G, Faraco V, Amoresano A, Sannia G, Giardina P. Atypical laccase isoenzymes from copper supplemented Pleurotus ostreatus cultures. Enzym Microb Technol. 2003;33(2):220–30.

73. Leontievsky AA, Vares T, Lankinen P, Shergill JK, Pozdnyakova NN, Myasoedova NM, Kalkkinen N, Golovleva LA, Cammack R, Thurston CF. Blue and yellow laccases of ligninolytic fungi. FEMS Microbiol Lett. 1997;156(1):9–14.

74. Gutiérrez A, del Río JC, Ibarra D, Rencoret J, Romero J, Speranza M, Camarero S, Martínez MJ, Martínez ÁT. Enzymatic removal of free and conjugated sterols forming pitch deposits in environmentally sound bleaching of eucalypt paper pulp. Environ Sci Technol. 2006;40(10):3416–22.

75. Mikolasch A, Schauer F. Fungal laccases as tools for the synthesis of new hybrid molecules and biomaterials. Appl Microbiol Biotechnol. 2009;82(4):605–24.

76. Claus H. Laccases: structure, reactions, distribution. Micron. 2004;35(1):93–6.

77. Kawano T. Roles of the reactive oxygen species-generating peroxidase reactions in plant defense and growth induction. Plant Cell Rep. 2003;21(9):829–37.

78. Bansal N, Kanwar SS. Peroxidase (s) in environment protection. Sci World J. 2013;2013:1–9.

79. Perez-Boada M, Ruiz-Duenas FJ, Pogni R, Basosi R, Choinowski T, Martínez MJ, Piontek K, Martínez AT. Versatile peroxidase oxidation of high redox potential aromatic compounds: site-directed mutagenesis, spectroscopic and crystallographic investigation of three long-range electron transfer pathways. J Mol Biol. 2005;354(2):385–402.

80. Martınez AT. Molecular biology and structure-function of lignin-degrading heme peroxidases. Enzym Microb Technol. 2002;30(4):425–44.

81. Smith AT, Veitch NC. Substrate binding and catalysis in heme peroxidases. Curr Opin Chem Biol. 1998;2(2):269–78.

82. Banci L. Structural properties of peroxidases. J Biotechnol. 1997;53(2):253–63.

83. Gold M, Youngs H, Gelpke M. Manganese peroxidase. Met Ions Biol Syst. 2000;37:559.

84. Orth A, Denny M, Tien M. Overproduction of lignin-degrading enzymes by an isolate of Phanerochaete chrysosporium. Appl Environ Microbiol. 1991;57(9):2591–6.
85. Valli K, Wariishi H, Gold MH. Oxidation of monomethoxylated aromatic compounds by lignin peroxidase: role of veratryl alcohol in lignin biodegradation. Biochemistry. 1990;29(37):8535–9.
86. Johjima T, Wariishi H, Tanaka H. Veratryl alcohol binding sites of lignin peroxidase from Phanerochaete chrysosporium. J Mol Catal B Enzym. 2002;17(2):49–57.
87. Hammel KE, Cullen D. Role of fungal peroxidases in biological ligninolysis. Curr Opin Plant Biol. 2008;11(3):349–55.
88. Kersten PJ, Kalyanaraman B, Hammel KE, Reinhammar B, Kirk TK. Comparison of lignin peroxidase, horseradish peroxidase and laccase in the oxidation of methoxybenzenes. Biochem J. 1990;268:475–80.
89. Hammel KE, Kalyanaraman B, Kirk TK. Substrate free radicals are intermediates in ligninase catalysis. Proc Natl Acad Sci. 1986;83(11):3708–12.
90. Millis CD, Cai D, Stankovich MT, Tien M. Oxidation-reduction potentials and ionization states of extracellular peroxidases from the lignin-degrading fungus Phanerochaete chrysosporium. Biochemistry. 1989;28(21):8484–9.
91. Doyle WA, Blodig W, Veitch NC, Piontek K, Smith AT. Two substrate interaction sites in lignin peroxidase revealed by site-directed mutagenesis. Biochemistry. 1998;37(43):15097–105.
92. Mester T, Ambert-Balay K, Ciofi-Baffoni S, Banci L, Jones AD, Tien M. Oxidation of a tetrameric nonphenolic lignin model compound by lignin peroxidase. J Biol Chem. 2001;276(25):22985–90.
93. Baciocchi E, Fabbri C, Lanzalunga O. Lignin peroxidase-catalyzed oxidation of nonphenolic trimeric lignin model compounds: fragmentation reactions in the intermediate radical cations. J Org Chem. 2003;68(23):9061–9.
94. Bietti M, Baciocchi E, Steenken S. Lifetime, reduction potential and base-induced fragmentation of the veratryl alcohol radical cation in aqueous solution. Pulse radiolysis studies on a ligninase "mediator". J Phys Chem A. 1998;102(38):7337–42.
95. Candeias LP, Harvey PJ. Lifetime and reactivity of the veratryl alcohol radical cation. Implications for lignin peroxidase catalysis. J Biol Chem. 1995;270(28):16745–8.
96. Gilardi G, Harvey PJ, Cass AE, Palmer JM. Radical intermediates in veratryl alcohol oxidation by ligninase. NMR evidence. Biochim Biophys Acta Protein Struct Mol Enzymol. 1990;1041(2):129–32.
97. Cai D, Tien M. Kinetic studies on the formation and decomposition of compounds II and III. Reactions of lignin peroxidase with H_2O_2. J Biol Chem. 1992;267(16):11149–55.
98. Koduri RS, Tien M. Kinetic analysis of lignin peroxidase: explanation for the mediation phenomenon by veratryl alcohol. Biochemistry. 1994;33(14):4225–30.
99. Hofrichter M. Review: lignin conversion by manganese peroxidase (MnP). Enzym Microb Technol. 2002;30(4):454–66.
100. Glenn JK, Gold MH. Purification and characterization of an extracellular Mn (II)-dependent peroxidase from the lignin-degrading basidiomycete, Phanerochaete chrysosporium. Arch Biochem Biophys. 1985;242(2):329–41.
101. Paszczyński A, Huynh V-B, Crawford R. Enzymatic activities of an extracellular, manganese-dependent peroxidase from Phanerochaete chrysosporium. FEMS Microbiol Lett. 1985;29(1-2):37–41.
102. Tien M, Kirk TK. Lignin-degrading enzyme from the hymenomycete Phanerochaete chrysosporium Burds. Science (Washington). 1983;221(4611):661–2.
103. Glenn JK, Morgan MA, Mayfield MB, Kuwahara M, Gold MH. An extracellular H_2O_2-requiring enzyme preparation involved in lignin biodegradation by the white rot basidiomycete Phanerochaete chrysosporium. Biochem Biophys Res Commun. 1983;114(3):1077–83.
104. Pease EA, Tien M. Heterogeneity and regulation of manganese peroxidases from Phanerochaete chrysosporium. J Bacteriol. 1992;174(11):3532–40.

105. Glenn JK, Akileswaran L, Gold MH. Mn (II) oxidation is the principal function of the extracellular Mn-peroxidase from Phanerochaete chrysosporium. Arch Biochem Biophys. 1986;251(2):688–96.

106. Paszczyński A, Huynh V-B, Crawford R. Comparison of ligninase-I and peroxidase-M2 from the white-rot fungus Phanerochaete chrysosporium. Arch Biochem Biophys. 1986;244(2):750–65.

107. Wariishi H, Akileswaran L, Gold MH. Manganese peroxidase from the basidiomycete Phanerochaete chrysosporium: spectral characterization of the oxidized states and the catalytic cycle. Biochemistry. 1988;27(14):5365–70.

108. Wariishi H, Dunford HB, MacDonald I, Gold MH. Manganese peroxidase from the lignin-degrading basidiomycete Phanerochaete chrysosporium. Transient state kinetics and reaction mechanism. J Biol Chem. 1989;264(6):3335–40.

109. Wariishi H, Valli K, Gold MH. Manganese (II) oxidation by manganese peroxidase from the basidiomycete Phanerochaete chrysosporium. Kinetic mechanism and role of chelators. J Biol Chem. 1992;267(33):23688–95.

110. Wariishi H, Valli K, Gold MH. Oxidative cleavage of a phenolic diarylpropane lignin model dimer by manganese peroxidase from Phanerochaete chrysosporium. Biochemistry. 1989;28(14):6017–23.

111. Tuor U, Wariishi H, Schoemaker HE, Gold MH. Oxidation of phenolic arylglycerol. beta.-aryl ether lignin model compounds by manganese peroxidase from Phanerochaete chrysosporium: oxidative cleavage of an. alpha.-carbonyl model compound. Biochemistry. 1992;31(21):4986–95.

112. Reddy GVB, Sridhar M, Gold MH. Cleavage of nonphenolic β-1 diarylpropane lignin model dimers by manganese peroxidase from Phanerochaete chrysosporium. Eur J Biochem. 2003;270(2):284–92.

113. Wariishi H, Valli K, Renganathan V, Gold MH. Thiol-mediated oxidation of nonphenolic lignin model compounds by manganese peroxidase of Phanerochaete chrysosporium. J Biol Chem. 1989;264(24):14185–91.

114. Mester T, Tien M. Engineering of a manganese-binding site in lignin peroxidase isozyme H8 from Phanerochaete chrysosporium. Biochem Biophys Res Commun. 2001;284(3):723–8.

115. Timofeevski SL, Nie G, Reading NS, Aust SD. Addition of veratryl alcohol oxidase activity to manganese peroxidase by site-directed mutagenesis. Biochem Biophys Res Commun. 1999;256(3):500–4.

116. Ruiz-Dueñas FJ, Martínez MJ, Martínez AT. Molecular characterization of a novel peroxidase isolated from the ligninolytic fungus Pleurotus eryngii. Mol Microbiol. 1999;31(1):223–35.

117. Camarero S, Ruiz-Dueñas FJ, Sarkar S, Martínez MJ, Martínez AT. The cloning of a new peroxidase found in lignocellulose cultures of Pleurotus eryngii and sequence comparison with other fungal peroxidases. FEMS Microbiol Lett. 2000;191(1):37–43.

118. Ruiz-Dueñas FJ, Morales M, García E, Miki Y, Martínez MJ, Martínez AT. Substrate oxidation sites in versatile peroxidase and other basidiomycete peroxidases. J Exp Bot. 2009;60(2):441–52.

119. Henriksson G, Ander P, Pettersson B, Pettersson G. Cellobiose dehydrogenase (cellobiose oxidase) from Phanerochaete chrysosporium as a wood-degrading enzyme. Studies on cellulose, xylan and synthetic lignin. Appl Microbiol Biotechnol. 1995;42(5):790–6.

120. Kersten P, Cullen D. Extracellular oxidative systems of the lignin-degrading Basidiomycete Phanerochaete chrysosporium. Fungal Genet Biol. 2007;44(2):77–87.

121. Cameron MD, Aust SD. Cellobiose dehydrogenase–an extracellular fungal flavocytochrome. Enzym Microb Technol. 2001;28(2):129–38.

122. Henriksson G, Johansson G, Pettersson G. Is cellobiose oxidase from Phanerochaete chrysosporium a one-electron reductase? Biochim Biophys Acta Protein Struct Mol Enzymol. 1993;1144(2):184–90.

123. Morpeth FF. Some properties of cellobiose oxidase from the white-rot fungus Sporotrichum pulverulentum. Biochem J. 1985;228:557–64.
124. Henriksson G, Sild V, Szabó IJ, Pettersson G, Johansson G. Substrate specificity of cellobiose dehydrogenase from Phanerochaete chrysosporium. Biochim Biophys Acta Protein Struct Mol Enzymol. 1998;1383(1):48–54.
125. Henriksson G, Johansson G, Pettersson G. A critical review of cellobiose dehydrogenases. J Biotechnol. 2000;78(2):93–113.
126. Baldrian P, Valášková V. Degradation of cellulose by basidiomycetous fungi. FEMS Microbiol Rev. 2008;32(3):501–21.
127. Henriksson G, Pettersson G, Johansson G, Ruiz A, Uzcategui E. Cellobiose oxidase from Phanerochaete chrysosporium can be cleaved by papain into two domains. Eur J Biochem. 1991;196(1):101–6.
128. Ander P. The cellobiose-oxidizing enzymes CBQ and CbO as related to lignin and cellulose degradation– a review. FEMS Microbiol Rev. 1994;13(2):297–312.
129. Archibald F, Bourbonnais R, Jurasek L, Paice M, Reid I. Kraft pulp bleaching and delignification by Trametes versicolor. J Biotechnol. 1997;53(2):215–36.
130. Cameron MD, Aust SD. Degradation of chemicals by reactive radicals produced by cellobiose dehydrogenase from Phanerochaete chrysosporium. Arch Biochem Biophys. 1999;367(1):115–21.
131. Fernández IS, Ruiz-Duenas FJ, Santillana E, Ferreira P, Martínez MJ, Martínez ÁT, Romero A. Novel structural features in the GMC family of oxidoreductases revealed by the crystal structure of fungal aryl-alcohol oxidase. Acta Crystallogr D Biol Crystallogr. 2009;65(11):1196–205.
132. van den Heuvel RH, van den Berg WA, Rovida S, van Berkel WJ. Laboratory-evolved vanillyl-alcohol oxidase produces natural vanillin. J Biol Chem. 2004;279(32):33492–500.
133. Wohlfahrt G, Witt S, Hendle J, Schomburg D, Kalisz HM, Hecht H-J. 1.8 and 1.9 Å resolution structures of the Penicillium amagasakiense and Aspergillus niger glucose oxidases as a basis for modelling substrate complexes. Acta Crystallogr D Biol Crystallogr. 1999;55(5):969–77.
134. Rannes JB, Ioannou A, Willies SC, Grogan G, Behrens C, Flitsch SL, Turner NJ. Glycoprotein labeling using engineered variants of galactose oxidase obtained by directed evolution. J Am Chem Soc. 2011;133(22):8436–9.
135. Hassan N, Tan T-C, Spadiut O, Pisanelli I, Fusco L, Haltrich D, Peterbauer CK, Divne C. Crystal structures of Phanerochaete chrysosporium pyranose 2-oxidase suggest that the N-terminus acts as a propeptide that assists in homotetramer assembly. FEBS Open Bio. 2013;3:496–504.
136. Shah V, Nerud F. Lignin degrading system of white-rot fungi and its exploitation for dye decolorization. Can J Microbiol. 2002;48(10):857–70.
137. Ferreira P, Medina M, Guillén F, Martinez M, Van Berkel W, Martinez A. Spectral and catalytic properties of aryl-alcohol oxidase, a fungal flavoenzyme acting on polyunsaturated alcohols. Biochem J. 2005;389:731–8.
138. Farmer V, Henderson ME, Russell J. Aromatic-alcohol-oxidase activity in the growth medium of Polystictus versicolor. Biochem J. 1960;74(2):257.
139. Guillén F, Martinez AT, Martínez MJ. Production of hydrogen peroxide by aryl-alcohol oxidase from the ligninolytic fungus Pleurotus eryngii. Appl Microbiol Biotechnol. 1990;32(4):465–9.
140. Muheim A, Waldner R, Leisola MS, Fiechter A. An extracellular aryl-alcohol oxidase from the white-rot fungus Bjerkandera adusta. Enzym Microb Technol. 1990;12(3):204–9.
141. Kim SJ, Suzuki N, Uematsu Y, Shoda M. Characterization of aryl alcohol oxidase produced by dye-decolorizing fungus, geotrichum candidum decl. J Biosci Bioeng. 2001;91(2):166–72.

142. Guillen F, Martinez AT, Martinez MJ. Substrate specificity and properties of the aryl-alcohol oxidase from the ligninolytic fungus Pleurotus eryngii. Eur J Biochem. 1992;209(2):603–11.

143. Varela E, Martinez A, Martinez M. Molecular cloning of aryl-alcohol oxidase from the fungus Pleurotus eryngii, an enzyme involved in lignin degradation. Biochem J. 1999;341:113–7.

144. Hernández-Ortega A, Ferreira P, Martínez AT. Fungal aryl-alcohol oxidase: a peroxide-producing flavoenzyme involved in lignin degradation. Appl Microbiol Biotechnol. 2012;93(4):1395–410.

145. Varela E, Martınez MJ, Martınez AT. Aryl-alcohol oxidase protein sequence: a comparison with glucose oxidase and other FAD oxidoreductases. Biochim Biophys Acta Protein Struct Mol Enzymol. 2000;1481(1):202–8.

146. Hecht H, Kalisz H, Hendle J, Schmid R, Schomburg D. Crystal structure of glucose oxidase from Aspergillus niger refined at 2·3 Å reslution. J Mol Biol. 1993;229(1):153–72.

147. Pazur JH, Kleppe K. The oxidation of glucose and related compounds by glucose oxidase from Aspergillus niger*. Biochemistry. 1964;3(4):578–83.

148. Wierenga RK, Terpstra P, Hol WG. Prediction of the occurrence of the ADP-binding βαβ-fold in proteins, using an amino acid sequence fingerprint. J Mol Biol. 1986;187(1):101–7.

149. Gutierrez A, Caramelo L, Prieto A, Martínez MJ, Martinez AT. Anisaldehyde production and aryl-alcohol oxidase and dehydrogenase activities in ligninolytic fungi of the genus Pleurotus. Appl Environ Microbiol. 1994;60(6):1783–8.

150. Romero E, Ferreira P, Martínez ÁT, Martínez MJ. New oxidase from Bjerkandera arthroconidial anamorph that oxidizes both phenolic and nonphenolic benzyl alcohols. Biochim Biophys Acta Protein Struct Mol Enzymol. 2009;1794(4):689–97.

151. Hernández-Ortega A, Ferreira P, Merino P, Medina M, Guallar V, Martínez AT. Stereoselective hydride transfer by aryl-alcohol oxidase, a member of the GMC superfamily. ChemBioChem. 2012;13(3):427–35.

152. Ferreira P, Hernández-Ortega A, Lucas F, Carro J, Herguedas B, Borrelli KW, Guallar V, Martínez AT, Medina M. Aromatic stacking interactions govern catalysis in aryl-alcohol oxidase. FEBS J. 2015;282:3091–106.

153. van den Heuvel RH, Fraaije MW, Mattevi A, van Berkel WJ. Asp-170 is crucial for the redox properties of vanillyl-alcohol oxidase. J Biol Chem. 2000;275(20):14799–808.

154. van den Heuvel RH, Fraaije MW, Mattevi A, Laane C, van Berkel WJ. Vanillyl-alcohol oxidase, a tasteful biocatalyst. J Mol Catal B Enzym. 2001;11(4):185–8.

155. Fraaije MW, van Berkel WJ. Catalytic mechanism of the oxidative demethylation of 4-(Methoxymethyl) phenol by vanillyl-alcohol oxidase evidence for formation of a p-quinone methide intermediate. J Biol Chem. 1997;272(29):18111–6.

156. Mattevi A, Fraaije MW, Mozzarelli A, Olivi L, Coda A, van Berkel WJ. Crystal structures and inhibitor binding in the octameric flavoenzyme vanillyl-alcohol oxidase: the shape of the active-site cavity controls substrate specificity. Structure. 1997;5(7):907–20.

157. van den Heuvel RH, Fraaije MW, Mattevi A, van Berkel WJ Structure, function and redesign of vanillyl-alcohol oxidase. In: International Congress Series, 2002. Elsevier, p. 13–24

158. van den Heuvel RH, Fraaije MW, Ferrer M, Mattevi A, van Berkel WJ. Inversion of stereospecificity of vanillyl-alcohol oxidase. Proc Natl Acad Sci. 2000;97(17):9455–60.

159. Whittaker MM, Kersten PJ, Nakamura N, Sanders-Loehr J, Schweizer ES, Whittaker JW. Glyoxal oxidase from Phanerochaete chrysosporium is a new radical-copper oxidase. J Biol Chem. 1996;271(2):681–7.

160. Whittaker MM, Kersten PJ, Cullen D, Whittaker JW. Identification of catalytic residues in glyoxal oxidase by targeted mutagenesis. J Biol Chem. 1999;274(51):36226–32.

161. Kersten PJ, Kirk TK. Involvement of a new enzyme, glyoxal oxidase, in extracellular H_2O_2 production by Phanerochaete chrysosporium. J Bacteriol. 1987;169(5):2195–201.

162. Kersten PJ, Cullen D. Cloning and characterization of cDNA encoding glyoxal oxidase, a H_2O_2-producing enzyme from the lignin-degrading basidiomycete Phanerochaete chrysosporium. Proc Natl Acad Sci. 1993;90(15):7411–3.

163. Itoh S, Hirano K, Furuta A, Komatsu M, Ohshiro Y, Ishida A, Takamuku S, Kohzuma T, Nakamura N, Suzuki S. Physicochemical properties of 2-Methylthio-4-methylphenol, a model compound of the novel cofactor of galactose oxidase. Chem Lett. 1993;12:2099–102.

164. Kersten PJ, Witek C, Vanden Wymelenberg A, Cullen D. Phanerochaete chrysosporium glyoxal oxidase is encoded by two allelic variants: structure, genomic organization, and heterologous expression of glx1 and glx2. J Bacteriol. 1995;177(21):6106–10.

165. Danneel HJ, Rossner E, Zeeck A, Giffhorn F. Purification and characterization of a pyranose oxidase from the basidiomycete Peniophora gigantea and chemical analyses of its reaction products. Eur J Biochem. 1993;214(3):795–802.

166. Izumi Y, Furuya Y, Yamada H. Purification and properties of pyranose oxidase from basidiomycetous fungus no. 52. Agric Biol Chem. 1990;54(6):1393–9.

167. Machida Y, Nakanishi T. Purification and properties of pyranose oxidase from Coriolus versicolor. Agric Biol Chem. 1984;48(10):2463–70.

168. Daniel G, Volc J, Kubatova E. Pyranose oxidase, a major source of H_2O_2 during wood degradation by Phanerochaete chrysosporium, Trametes versicolor, and Oudemansiella mucida. Appl Environ Microbiol. 1994;60(7):2524–32.

169. Cavener DR. GMC oxidoreductases: a newly defined family of homologous proteins with diverse catalytic activities. J Mol Biol. 1992;223(3):811–4.

170. Hallberg BM, Leitner C, Haltrich D, Divne C. Crystal structure of the 270 kDa homotetrameric lignin-degrading enzyme pyranose 2-oxidase. J Mol Biol. 2004;341(3):781–96.

171. Giffhorn F. Fungal pyranose oxidases: occurrence, properties and biotechnical applications in carbohydrate chemistry. Appl Microbiol Biotechnol. 2000;54(6):727–40.

172. Volc J, Sedmera P, Havlíček V, Přikrylová V, Daniel G. Conversion of D-glucose to D-erythrohexos-2, 3-diulose (2, 3-diketo-D-glucose) by enzyme preparations from the basidiomycete Oudemansiella mucida. Carbohydr Res. 1995;278(1):59–70.

173. Freimund S, Huwig A, Giffhorn F, Köpper S. Rare keto-aldoses from enzymatic oxidation: substrates and oxidation products of pyranose 2-oxidase. Chem Eur J. 1998;4(12):2442–55.

174. Giffhorn F, Köpper S, Huwig A, Freimund S. Rare sugars and sugar-based synthons by chemo-enzymatic synthesis. Enzym Microb Technol. 2000;27(10):734–42.

175. Baron AJ, Stevens C, Wilmot C, Seneviratne KD, Blakeley V, Dooley DM, Phillips S, Knowles PF, McPherson MJ. Structure and mechanism of galactose oxidase. The free radical site. J Biol Chem. 1994;269(40):25095–105.

176. Firbank S, Rogers M, Wilmot C, Dooley D, Halcrow M, Knowles P, McPherson M, Phillips S. Crystal structure of the precursor of galactose oxidase: an unusual self-processing enzyme. Proc Natl Acad Sci. 2001;98(23):12932–7.

177. Yin D, Urresti S, Lafond M, Johnston EM, Derikvand F, Ciano L, Berrin J-G, Henrissat B, Walton PH, Davies GJ, Brumer H. Structure-function characterization reveals new catalytic diversity in the galactose oxidase and glyoxal oxidase family. Nat Commun. 2015;6:10197. doi:10.1038/ncomms10197.

178. Ito N, Phillips SE, Stevens C, Ogel ZB, McPherson MJ, Keen JN, Yadav KD, Knowles PF. Novel thioether bond revealed by a 1.7 Å crystal structure of galactose oxidase. Nature. 1991;350:87–90.

179. Bankar SB, Bule MV, Singhal RS, Ananthanarayan L. Glucose oxidase—an overview. Biotechnol Adv. 2009;27(4):489–501.

180. Hatzinikolaou D, Macris B. Factors regulating production of glucose oxidase by Aspergillus niger. Enzym Microb Technol. 1995;17(6):530–4.

181. Kapat A, Jung J, Park Y. Enhancement of glucose oxidase production in batch cultivation of recombinant Saccharomyces cerevisiae: optimization of oxygen transfer condition. J Appl Microbiol. 2001;90(2):216–22.

182. Kalisz H, Hendle J, Schmid R. Structural and biochemical properties of glycosylated and deglycosylated glucose oxidase from Penicillium amagasakiense. Appl Microbiol Biotechnol. 1997;47(5):502–7.

183. Kusai K, Sekuzu I, Hagihara B, Okunuki K, Yamauchi S, Nakai M. Crystallization of glucose oxidase from Penicillium amagasakiense. Biochim Biophys Acta. 1960;40:555–7.

184. Nakamura S, FUJIKI S. Comparative studies on the glucose oxidases of Aspergillus niger and Penicillium amagasakiense. J Biochem. 1968;63(1):51–8.

185. Witt S, Wohlfahrt G, Schomburg D, Hecht H, Kalisz H. Conserved arginine-516 of Penicillium amagasakiense glucose oxidase is essential for the efficient binding of β-D-glucose. Biochem J. 2000;347:553–9.

186. Witteveen CF, Veenhuis M, Visser J. Localization of glucose oxidase and catalase activities in Aspergillus niger. Appl Environ Microbiol. 1992;58(4):1190–4.

187. Raba J, Mottola HA. Glucose oxidase as an analytical reagent. Crit Rev Anal Chem. 1995;25(1):1–42.

188. Brock BJ, Rieble S, Gold MH. Purification and Characterization of a 1, 4-Benzoquinone Reductase from the Basidiomycete Phanerochaete chrysosporium. Appl Environ Microbiol. 1995;61(8):3076–81.

189. Akileswaran L, Brock BJ, Cereghino JL, Gold MH. 1, 4-Benzoquinone reductase from Phanerochaete chrysosporium: cDNA cloning and regulation of expression. Appl Environ Microbiol. 1999;65(2):415–21.

190. Brock BJ, Gold MH. 1, 4-Benzoquinone reductase from the basidiomycetePhanerochaete chrysosporium: spectral and kinetic analysis. Arch Biochem Biophys. 1996;331(1):31–40.

191. Aitor H-O, Kenneth B, Patricia F, Milagros M, Angel TM, Victor G. Substrate diffusion and oxidation in GMC oxidoreductases: an experimental and computational study on fungal aryl-alcohol oxidase. Biochem J. 2011;436(2):341–50.

192. Hernández-Ortega A, Lucas F, Ferreira P, Medina M, Guallar V, Martínez AT. Modulating O_2 reactivity in a fungal flavoenzyme involvement of aryl-alcohol oxidase PHE-501 contiguous to catalytic histidine. J Biol Chem. 2011;286(47):41105–14.

193. Hernández-Ortega A, Lucas F, Ferreira P, Medina M, Guallar V, Martínez AT. Role of active site histidines in the two half-reactions of the aryl-alcohol oxidase catalytic cycle. Biochemistry. 2012;51(33):6595–608.

194. Fraaije MW, van den Heuvel RH, van Berkel WJ, Mattevi A. Covalent flavinylation is essential for efficient redox catalysis in vanillyl-alcohol oxidase. J Biol Chem. 1999;274(50):35514–20.

195. Fraaije MW, van den Heuvel RH, van Berkel WJ, Mattevi A. Structural analysis of flavinylation in vanillyl-alcohol oxidase. J Biol Chem. 2000;275(49):38654–8.

196. Vaidyanathan M, Palaniandavar M, Gopalan RS. Copper (II) complexes of sterically hindered phenolate ligands as structural models for the active site in galactose oxidase and glyoxal oxidase: x-ray crystal structure and spectral and redox properties. Inorg Chim Acta. 2001;324(1):241–51.

197. Halfen JA, Jazdzewski BA, Mahapatra S, Berreau LM, Wilkinson EC, Que L, Tolman WB. Synthetic models of the inactive copper (II)-tyrosinate and active copper (II)-tyrosyl radical forms of galactose and glyoxal oxidases. J Am Chem Soc. 1997;119(35):8217–27.

198. Kujawa M, Ebner H, Leitner C, Hallberg BM, Prongjit M, Sucharitakul J, Ludwig R, Rudsander U, Peterbauer C, Chaiyen P. Structural basis for substrate binding and regioselective oxidation of monosaccharides at C3 by pyranose 2-oxidase. J Biol Chem. 2006;281(46):35104–15.

199. Pitsawong W, Sucharitakul J, Prongjit M, Tan T-C, Spadiut O, Haltrich D, Divne C, Chaiyen P. A conserved active-site threonine is important for both sugar and flavin oxidations of pyranose 2-oxidase. J Biol Chem. 2010;285(13):9697–705.

200. Spadiut O, Tan TC, Pisanelli I, Haltrich D, Divne C. Importance of the gating segment in the substrate-recognition loop of pyranose 2-oxidase. FEBS J. 2010;277(13):2892–909.

201. Heckmann-Pohl DM, Bastian S, Altmeier S, Antes I. Improvement of the fungal enzyme pyranose 2-oxidase using protein engineering. J Biotechnol. 2006;124(1):26–40.
202. Bannwarth M, Heckmann-Pohl D, Bastian S, Giffhorn F, Schulz GE. Reaction geometry and thermostable variant of pyranose 2-oxidase from the white-rot fungus Peniophora sp. Biochemistry. 2006;45(21):6587–95.
203. Rogers MS, Tyler EM, Akyumani N, Kurtis CR, Spooner RK, Deacon SE, Tamber S, Firbank SJ, Mahmoud K, Knowles PF. The stacking tryptophan of galactose oxidase: a second-coordination sphere residue that has profound effects on tyrosyl radical behavior and enzyme catalysis. Biochemistry. 2007;46(15):4606–18.
204. Ito N, Phillips SE, Yadav KD, Knowles PF. Crystal structure of a free radical enzyme, galactose oxidase. J Mol Biol. 1994;238(5):704–814.
205. Hecht H, Schomburg D, Kalisz H, Schmid R. The 3D structure of glucose oxidase from Aspergillus niger. Implications for the use of GOD as a biosensor enzyme. Biosens Bioelectron. 1993;8(3):197–203.
206. Martinez D, Larrondo LF, Putnam N, Gelpke MDS, Huang K, Chapman J, Helfenbein KG, Ramaiya P, Detter JC, Larimer F. Genome sequence of the lignocellulose degrading fungus Phanerochaete chrysosporium strain RP78. Nat Biotechnol. 2004;22(6):695–700.
207. Wymelenberg AV, Minges P, Sabat G, Martinez D, Aerts A, Salamov A, Grigoriev I, Shapiro H, Putnam N, Belinky P. Computational analysis of the Phanerochaete chrysosporium v2. 0 genome database and mass spectrometry identification of peptides in ligninolytic cultures reveal complex mixtures of secreted proteins. Fungal Genet Biol. 2006;43(5):343–56.
208. Martinez D, Challacombe J, Morgenstern I, Hibbett D, Schmoll M, Kubicek CP, Ferreira P, Ruiz-Duenas FJ, Martinez AT, Kersten P. Genome, transcriptome, and secretome analysis of wood decay fungus Postia placenta supports unique mechanisms of lignocellulose conversion. Proc Natl Acad Sci. 2009;106(6):1954–9.
209. Eastwood DC, Floudas D, Binder M, Majcherczyk A, Schneider P, Aerts A, Asiegbu FO, Baker SE, Barry K, Bendiksby M. The plant cell wall–decomposing machinery underlies the functional diversity of forest fungi. Science. 2011;333(6043):762–5.
210. Tang JD, Perkins AD, Sonstegard TS, Schroeder SG, Burgess SC, Diehl SV. Short-read sequencing for genomic analysis of the brown rot fungus Fibroporia radiculosa. Appl Environ Microbiol. 2012;78(7):2272–81.
211. Ohm RA, De Jong JF, Lugones LG, Aerts A, Kothe E, Stajich JE, De Vries RP, Record E, Levasseur A, Baker SE. Genome sequence of the model mushroom Schizophyllum commune. Nat Biotechnol. 2010;28(9):957–63.
212. Fernandez-Fueyo E, Ruiz-Dueñas FJ, Ferreira P, Floudas D, Hibbett DS, Canessa P, Larrondo LF, James TY, Seelenfreund D, Lobos S. Comparative genomics of Ceriporiopsis subvermispora and Phanerochaete chrysosporium provide insight into selective ligninolysis. Proc Natl Acad Sci. 2012;109(14):5458–63.
213. Suzuki H, MacDonald J, Syed K, Salamov A, Hori C, Aerts A, Henrissat B, Wiebenga A, Barry K, Lindquist E. Comparative genomics of the white-rot fungi, Phanerochaete carnosa and P. chrysosporium, to elucidate the genetic basis of the distinct wood types they colonize. BMC Genomics. 2012;13(1):444.
214. Olson Å, Aerts A, Asiegbu F, Belbahri L, Bouzid O, Broberg A, Canbäck B, Coutinho PM, Cullen D, Dalman K. Insight into trade-off between wood decay and parasitism from the genome of a fungal forest pathogen. New Phytol. 2012;194(4):1001–13.
215. Martin F, Aerts A, Ahrén D, Brun A, Danchin E, Duchaussoy F, Gibon J, Kohler A, Lindquist E, Pereda V. The genome of Laccaria bicolor provides insights into mycorrhizal symbiosis. Nature. 2008;452(7183):88–92.
216. Bao D, Gong M, Zheng H, Chen M, Zhang L, Wang H, Jiang J, Wu L, Zhu Y, Zhu G. Sequencing and comparative analysis of the straw mushroom (Volvariella volvacea) genome. PLoS One. 2013;8(3), e58294.
217. Morin E, Kohler A, Baker AR, Foulongne-Oriol M, Lombard V, Nagye LG, Ohm RA, Patyshakuliyeva A, Brun A, Aerts AL. Genome sequence of the button mushroom Agaricus

bisporus reveals mechanisms governing adaptation to a humic-rich ecological niche. Proc Natl Acad Sci. 2012;109(43):17501–6.
218. Collins C, Keane TM, Turner DJ, O'Keeffe G, Fitzpatrick DA, Doyle S. Genomic and proteomic dissection of the ubiquitous plant pathogen, Armillaria mellea: toward a new infection model system. J Proteome Res. 2013;12(6):2552–70.
219. Ohm RA, Riley R, Salamov A, Min B, Choi I-G, Grigoriev IV. Genomics of wood-degrading fungi. Fungal Genet Biol. 2014;72:82–90.
220. Floudas D, Binder M, Riley R, Barry K, Blanchette RA, Henrissat B, Martínez AT, Otillar R, Spatafora JW, Yadav JS. The Paleozoic origin of enzymatic lignin decomposition reconstructed from 31 fungal genomes. Science. 2012;336(6089):1715–9.
221. Hofrichter M, Ullrich R, Pecyna MJ, Liers C, Lundell T. New and classic families of secreted fungal heme peroxidases. Appl Microbiol Biotechnol. 2010;87(3):871–97.
222. Grigoriev IV, Nikitin R, Haridas S, Kuo A, Ohm R, Otillar R, Riley R, Salamov A, Zhao X, Korzeniewski F. MycoCosm portal: gearing up for 1000 fungal genomes. Nucleic Acids Res. 2013;42:D699–704.

Chapter 5
Bacterial Enzymes for Lignin Oxidation and Conversion to Renewable Chemicals

Timothy D.H. Bugg, Rahman Rahmanpour, and Goran M.M. Rashid

5.1 Discovery of Lignin-Metabolising Bacteria

Lignin modification and degradation have been studied extensively in basidiomycetes, which produce several extracellular lignin-oxidising enzymes, that have been characterised [1, 2]. Although literature studies on microbial degradation of lignin have focused primarily on white-rot and brown-rot fungi, there were a number of reports from the 1980s and 1990s that bacteria that can break down polymeric lignin preparations [3, 4]. Several streptomycetes have been reported to break down polymeric lignin such as ^{14}C-labelled milled wood lignin or DHP lignin [3], of which *Streptomyces viridosporus* T7A has been studied in most detail [5]. This strain produces several extracellular peroxidases, which show activity for oxidative cleavage of β-aryl ether lignin model compounds [5]. Using a radiochemical assay for breakdown of ^{14}C-labelled milled wood lignin, activity has been shown in strains of *Nocardia* and *Rhodococcus*, which are actinobacteria [4]. Amongst Gram-negative bacteria, *Sphingomonas paucimobilis* SYK-6 is able to degrade several different dimeric lignin model compounds, for which the gene clusters and biochemical pathways have been elucidated [6].

In 2010, Ahmad et al. reported two spectrophotometric assays for lignin breakdown, involving either fluorescently-labelled industrial Kraft lignin, or chemically nitrated ball-milled dioxane lignin prepared from wheat straw, miscanthus and pine, the latter assay generating a small increase in absorbance at 430 nm versus time [7]. Several bacterial strains known to be aromatic degraders showed activity in the latter assay, including *Pseudomonas putida* mt-2 and *Rhodococcus jostii* RHA1 [7]. The lignin degradation ability of *P. putida* and *R. jostii* RHA1 was confirmed by the release of two low molecular weight phenolic products after treatment of miscanthus

T.D.H. Bugg (✉) • R. Rahmanpour • G.M.M. Rashid
Department of Chemistry, University of Warwick, CV4 7AL Coventry, UK
e-mail: T.D.Bugg@warwick.ac.uk

lignocellulose in small-scale incubations [7]. The activities of these bacterial strains were compared with that of basidiomycetes using this assay, and white-rot fungus *Phanerochaete chrysosporium* was highest of all strains tested, but the activities of these bacterial lignin degraders were comparable to other lignin-degrading fungi [7].

This assay was subsequently used as a screening method for isolating lignin-degrading bacteria from environmental samples [8]. Eight mesophilic strains were isolated from samples of woodland soil enriched with wheat straw lignocellulose, including three *Microbacterium* strains, two *Micrococcus* strains, and a *Rhodococcus* isolate (all actinobacteria), and two *Ochrobactrum* strains (α-proteobacteria). Screening of composted wheat straw at 45 °C also led to the isolation of two further strains, of which a *Sphingobacterium* (Bacteroidetes) isolate showed very high activity in the nitrated lignin assay [8]. Treatment of size-fractioned industrial Kraft lignin with these bacterial isolates resulted in depolymerisation of high molecular weight lignin fractions as observed by gel filtration HPLC [8].

The majority of bacterial lignin degraders identified in the literature fall into three phyla: the actinomycetes, α-proteobacteria, and γ-proteobacteria, members of which phyla have also been found in the intestines of wood-infesting termites and insects [9]. A recent review of lignin-degrading phenotypes and genotypes lists 22 actinobacteria, 10 α-proteobacteria and 11 γ-proteobacterial strains with lignin degradation phenotypes, but also 7 firmicutes, 4 β-proteobacteria, 1 δ-proteobacterium, 1 bacteroides and 1 archaeal strain [10]. Metagenomic DNA sequencing of lignin-amended tropical forest soils have revealed enrichment of Acidobacteria, Actinobacteria, Proteobacteria and Verrucomicrobia [11]. Genome sequences have been reported for an *Enterobacter lignolyticus* strain which shows activity for lignin degradation under anaerobic conditions [12], and a *Cupriavidus basilensis* B-8 strain which oxidises industrial Kraft lignin [13]. Strains of *Bacillus* and *Paenibacillus* [14], *Comamonas* sp. [15], and *Citrobacter freundii* [16] have also been reported as degraders of industrial Kraft lignin (Table 5.1).

Salvachua et al. have recently studied the breakdown of alkaline-pretreated liquor (APL) containing polymeric lignin by a set of 14 bacteria, using several different methods [17]. The extent of delignification was measured using the gravimetric Klason assay, which revealed optimal delignification of 26–32 % over 7 days by *Amycolatopsis* sp., *P. putida* mt-2 and its derivative *P. putida* KT2440, and *R. jostii* RHA1 [17]. Analysis by gel permeation chromatography revealed >80 % removal of low molecular weight (<1 kDa) components by these four strains, but only *P. putida* mt-2, *P. putida* KT2440 and *P. fluorescens* appeared to significantly consume higher molecular weight lignin components [17].

Table 5.1 Bacteria reported to degrade/metabolise lignin

Phylum	Species and isolate	Evidence for polymeric lignin breakdown[a]	Refs.
Gram-positive bacteria			
Actinobacteria	*Streptomyces viridosporus*	Mineralisation of ^{14}C-labelled milled wood lignin	[5]
	Streptomyces coelicolor	Colorimetric assay	[7]
	Amycolatopsis sp. 75iv2	Delignification of APL via Klason assay, depolymerisation via GPC	[17]
	Rhododoccus jostii RHA1	Colorimetric assay, aromatic metabolites observed from miscanthus lignocellulose	[7]
		Delignification of APL via Klason assay, depolymerisation via GPC	[17]
	Rhodococcus erythropolis	Colorimetric assay, depolymerisation of industrial Kraft lignin via GPC	[8]
	Nocardia autotrophica	Mineralisation of ^{14}C-labelled milled wood lignin	[4]
	Microbacterium phyllosphaerae	Colorimetric assay, depolymerisation of industrial Kraft lignin via GPC	[8]
	Micrococcus sp.	Colorimetric assay, depolymerisation of industrial Kraft lignin via GPC	[8]
	Arthrobacter globiformis	Colorimetric assay	[7]
Firmicutes	*Bacillus* sp.	Use of Kraft lignin as carbon source for growth	[14]
	Paenibacillus sp.	Use of Kraft lignin as carbon source for growth	[14]
Gram-negative bacteria			
α-Proteobacteria	*Sphingobium* SYK-6	Degradation of lignin model compounds	[6]
	Ochrobactrum sp.	Colorimetric assay, depolymerisation of industrial Kraft lignin via GPC	[8]
β-Proteobacteria	*Cupriavidus basiliensis*	Use of Kraft lignin as carbon source for growth	[13]
	Comamonas sp. *B-9*	Use of Kraft lignin as carbon source for growth, observation of aromatic metabolites from Kraft lignin	[15]

Table 5.1 (continued)

Phylum	Species and isolate	Evidence for polymeric lignin breakdown[a]	Refs.
γ-Proteobacteria	*Pseudomonas putida* mt-2, *Pseudomonas putida* KT2440	Colorimetric assay, aromatic metabolites observed from miscanthus lignocellulose	[7]
		Delignification of APL via Klason assay, depolymerisation via GPC	[17]
	Acinetobacter sp.	Colorimetric assay	[7]
	Enterobacter lignolyticus	Degrades alkali lignin preparation under anaerobic conditions	[12]
	Citrobacter freundii	Use of Kraft lignin as carbon source for growth	[16]
Bacteroidetes	*Sphingobacterium* sp. T2	Colorimetric assay, depolymerisation of industrial Kraft lignin via GPC	[8]

[a]Describes evidence for depolymerisation (conversion of polymeric lignin to lower molecular weight species), mineralisation (metabolism to CO_2) or delignification (via Klason assay) of polymeric lignin substrate, or utilisation as carbon source for growth. APL, alkaline pretreated liquor; GPC, gel permeation chromatography

5.2   Bacterial Enzymes for Lignin Biotransformation

Although there were a number of reports of bacterial lignin degradation in the 1980s [3, 4], and evidence for the presence of lignin-oxidising peroxidase enzymes in *S. viridosporus* [5], until recently, no bacterial genes responsible for lignin oxidation had been identified. Since 2011, there have been several bacterial lignin-oxidising enzymes identified and characterised, which will be described in turn.

5.2.1   Dye-Decolorizing Peroxidases

The discovery of lignin oxidation in *Rhodococcus jostii* RHA1, a degrader of polychlorinated biphenyls, prompted a search for unannotated peroxidase genes in the genome of this bacterium, that were also present in other lignin-degrading bacteria. Two dye-decolorising peroxidases, named *dypA* and *dypB*,, were found, for which homologues were present in other lignin-degrading bacteria. The dye-decolorizing peroxidases (DyPs) form a distinct superfamily of peroxidases, found in bacteria and fungi, since their specific primary and tertiary structure is unrelated to other peroxidase families, and they show a specific ability to decolorise a range of synthetic dyes [18]. Phylogenetic analyses have led to the classification of DyPs into four subfamilies (A–D), bacterial DyPs belonging to the A, B and C subfamilies, whereas fungal enzymes are found in the D subfamily [19].

Gene deletion in *R. jostii* RHA1 revealed that a Δ*dypB* mutant showed decreased lignin degradation activity using the nitrated lignin assay, and recombinant DypB was found to catalyse oxidative C_α-C_β cleavage of a β-aryl ether lignin model compound, and Mn^{2+}-dependent oxidation of Kraft lignin and wheat straw lignocellulose [20]. Stopped-flow kinetic analysis revealed the existence of a compound I intermediate formed upon reaction of the heme cofactor with hydrogen peroxide, that reacted at similar rates with Mn(II) and the β-aryl ether lignin model compound [20]. The structure of *R. jostii* DypB contained a ferredoxin-like fold, similar to other DyP structures, and a Mn^{2+} binding site close to the heme cofactor, as shown in Fig. 5.1 [21]. The active site Asp-158 found in all DyPs is thought to act as proton donor for the formation of the intermediate compound I, and Arg-244 is thought to stabilise compound I [18, 21]. Replacement of active site Asn-246 in *R. jostii* DypB by Ala was found to increase the k_{cat} for Mn^{2+} oxidation by 80-fold [22]. Adjacent to the *R. jostii dypB* gene is an encapsulin gene that encodes a protein nanocompartment, into which the DypB protein is packaged *in vivo*, and encapsulation of DypB has been shown to increase its lignin oxidation activity [23].

Three DyPs from Gram-negative *Pseudomonas fluorescens* Pf-5 have been characterised kinetically, and enzyme Dyp1B was found to show activity for oxidation of Kraft lignin and Mn^{2+}, and releases an oxidised lignin dimer from wheat straw lignocellulose in the presence of Mn^{2+} [24]. A heme-dependent lignin-oxidising enzyme has also been identified in actinobacterium *Amycolatopsis* sp. 75iv2 ATCC 39116 which shows activity towards a β-aryl ether lignin model compound [25]. A DypC class peroxidase enzyme has also been identified from the same strain, which shows much higher catalytic efficiency Mn^{2+} oxidation activity than *R. jostii* DypB [26].

Fig. 5.1 Structure of *R. jostii* DypB, showing active site heme cofactor (*red*), active site residues Asp-158 and Arg-244, and the Mn(II) binding site (*magenta*) formed by Asp-141, Glu-156, Glu-215 and Glu-239. Figure drawn using Pymol software
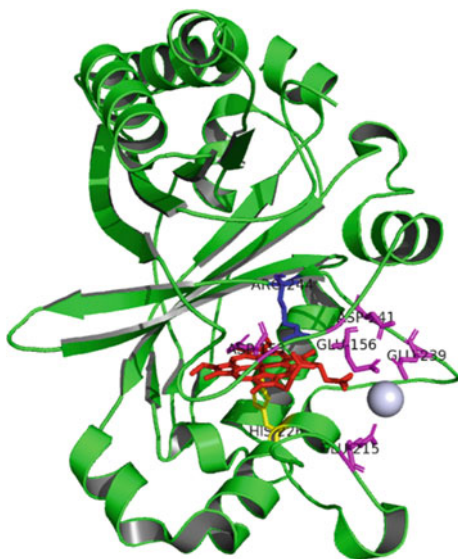
5.2.2 Bacterial Laccases

Laccases are multi-copper dependent enzymes that utilise dioxygen as substrate to catalyse oxidation of a range of phenolic and aromatic compounds. A number of laccase enzymes have been identified in wood-degrading fungi that have activity for lignin oxidation [1, 2], but few prokaryotic laccases have been characterised. Bacterial laccase genes have been identified in genomes of many soil bacteria [27], especially in actinobacteria [28], but also found in α-,β- and γ-proteobacteria [10].

Recombinant laccase enzymes from *Streptomyces coelicolor* A3(2), *S. lividans* TK24, *S. viridosporus* T7A, and *Amycolatopsis* sp. 75iv2 have been characterised kinetically, and were found to catalyse C_α oxidation of lignin model compounds [29]. The crystal structure of *S. coelicolor* A3 laccase was determined [29], showing the typical trinuclear Cu_A cluster and Cu_B centre, as shown in Fig. 5.2. Deletion of the laccase gene from *S. coelicolor* A3(2) was found to diminish the ability of this strain to form acid-precipitable lignin (APPL), supporting a role in lignin oxidation *in vivo* [29]. Treatment of ethanosolv lignin *in vitro* gave a higher molecular weight product, due to competing repolymerisation of lignin fragments, a phenomenon also observed for peroxidase enzymes [29]. A bacterial multicopper oxidase has also been identified from a novel screen of metagenomic DNA libraries using an *ermR* reporter gene that is activated by aromatic lignin degradation products [30]. This multicopper oxidase, related in sequence to *Pseudomonas stutzeri* CopA, was found to oxidise an industrial high-performance lignin substrate to generate several products including 2,6-dimethoxybenzene-1,4-diol [30]. Fungal laccase enzymes have been used for delignification of wood and biomass, using a suitable laccase mediator [31], hence bacterial laccases might be interesting biocatalysts for industrial biotechnology applications.
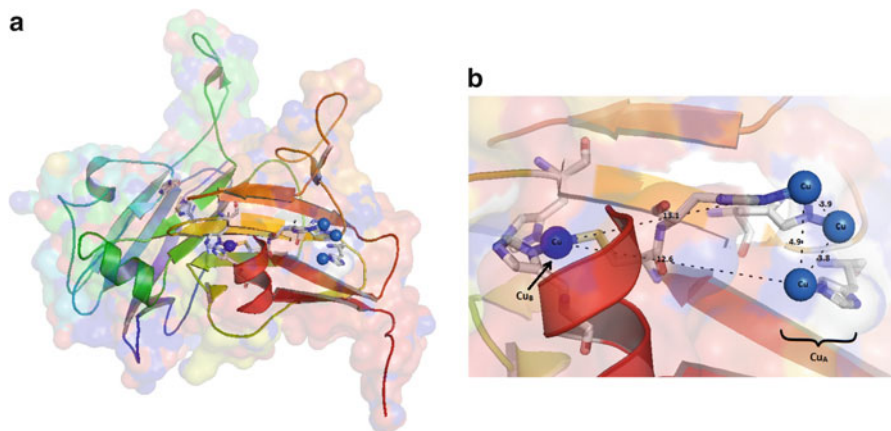
Fig. 5.2 Structure of *S. coelicolor* laccase (PDB 3kw8) (**a**), showing trinuclear Cu_A and mononuclear Cu_B centres (**b**). Copper atoms labelled in *blue*. Figure drawn using Pymol software

5.2.3   Glutathione-Dependent β-Etherase Enzymes

A novel type of glutathione-dependent β-etherase enzyme was first discovered in *Sphingobium* SYK-6, a bacterial strain capable of breakdown of a number of lignin model compounds [6]. The nucleophilic thiol sidechain of glutathione was used to cleave the ether linkage of β-aryl ether model compounds [6], as shown in Fig. 5.3. Stereospecific LigDEF enzymes were discovered in *Sphingobium* SYK-6 that catalysed the cleavage of *R* and *S* enantiomers of β-aryl ether lignin model compounds [32].

Picart et al. have recently identified four β-etherase enzymes in strains of *Novosphingobium*, which catalyse glutathione-dependent cleavage of β-aryl ether lignin model compounds, and also show activity towards a fluorescently labelled polymeric lignin substrate [33]. Gall et al. have also characterised β-etherase enzymes from *Sphingobium* SYK-6 [34] and from two *Novosphingobium* strains [35], showing that LigE-type enzymes are selective for the *R*-enantiomer of β-aryl ether substrates, while LigF-type enzymes are selective for the *S*-enantiomer of β-aryl ether substrates [34, 35]. The genome of an *Enterobacter lignolyticus* strain which shows activity for alkali lignin degradation under anaerobic conditions contains many annotated glutathione S-transferase genes, which might encode enzymes of similar function to the LigEF β-etherases [12].

5.2.4   Other Lignin-Metabolising Enzymes

To metabolise such a complex and heterogeneous substrate, it seems likely that bacteria will require a group of extracellular oxidative enzymes, together with protein transporters for uptake of lignin fragments, and gene regulators, which remain unknown at present. One novel lignin-oxidising enzyme has been identified in lignin-oxidising *Sphingobacterium* sp. T2 [36]. Genome sequencing of this organism revealed an absence of DyP-type peroxidases and laccases. Proteomic studies indicated the presence of two extracellular manganese superoxide dismutase enzymes, which were expressed and characterised in recombinant form, and both enzymes were found to be highly active for oxidation of polymeric organosolv and industrial Kraft lignin [36]. A range of aromatic products were characterised from
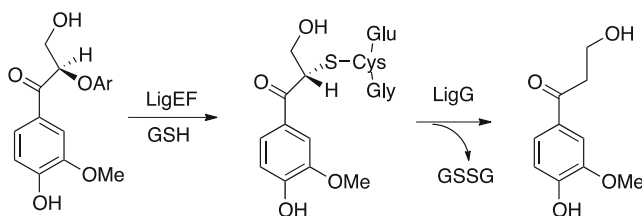
Fig. 5.3 Reaction catalysed by β-etherase enzymes on phenolic lignin model compounds
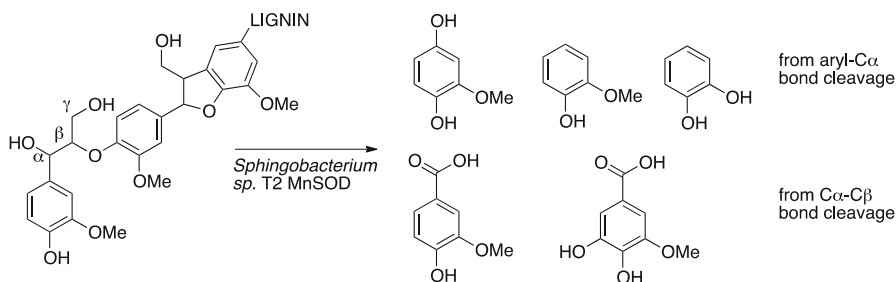
Fig. 5.4 Aromatic products from oxidation of polymeric organosolv lignin by *Sphingobacterium* sp. manganese superoxide dismutase

oxidation of organosolv lignin, including 2-methoxyhydroquinone, arising from aryl-C_α oxidative cleavage, and 5-hydroxyvanillic acid, arising from phenolic hydroxylation, as shown in Fig. 5.4 [36]. The reactive oxidant in this enzyme is hypothesised to be hydroxyl radical, generated via further one-electron reduction of hydrogen peroxide, based upon the presence of metabolites containing additional hydroxyl groups, characteristic of hydroxyl radical oxidation [36]. Hydroxyl radical is known to be generated by brown-rot fungi via Fenton oxidation, and is used for oxidation of lignocellulose [37].

5.3   Metabolic Pathways for Lignin Metabolism in Bacteria

Bacterial lignin degraders such as *Rhodococcus jostii* RHA1 and *Pseudomonas putida* are known to be active degraders of low molecular weight aromatic compounds. The pathways used for degradation of aromatic compounds by soil bacteria are well-studied, and proceed via oxidative cleavage of catechol substrates by non-heme iron-dependent catechol dioxygenases [38]. Therefore, it seems very likely that the pathways for degradation of lignin are connected to these aromatic degradation pathways. At present, the pathways by which polymeric lignin is broken down to monocyclic intermediates are not fully understood, but the existing knowledge has been reviewed elsewhere [39].

Extensive studies on the pathways for metabolism of lignin model compounds by *Sphingobium* SYK-6 has led to the elucidation of several biochemical pathways in this organism, including a β-etherase pathway for β-aryl ether cleavage, and an oxidative cleavage pathway for biphenyl di-acid DDVA metabolism [6]. *Rhodococcus jostii* RHA1 DypB is known to cleave a β-aryl ether lignin model compound via oxidative C_α-C_β cleavage [20], generating vanillin, which is known to be oxidised in this organism to vanillic acid, then demethylated to form protocatechuic acid [40], a key intermediate in bacterial aromatic degradation pathways. Vanillic acid has also been detected as a metabolite from lignin degradation in bacterial lignin degraders [39], and bacterial lignin degraders isolated from

environmental sources utilise vanillic acid as a growth substrate on minimal media [8], hence it seems likely that vanillic acid is one central metabolite in bacterial lignin degradation. It therefore seems likely that polymeric lignin attached to ligno-cellulose is oxidised (Stage 1) by extracellular peroxidases and laccases to yield fragments containing the different sub-structures found in polymeric lignin, as illustrated in Fig. 5.5. These fragments are then taken up into bacterial cells (Stage 2) and metabolised (Stage 3) to give central intermediates such as vanillic acid, which can be converted via oxidative cleavage pathways to primary metabolic pathways such as the citric acid cycle.

Protocatechuic acid is then commonly metabolised via the β-keto-adipate pathway, via intradiol oxidative cleavage, catalysed by protocatechuate 3,4-dioxygenase, as shown in Fig. 5.6a [41]. A bioinformatic survey of actinobacteria, α- and γ-proteobacteria revealed that the majority of such bacteria utilise the β-ketoadipate pathway [39]. However, some bacteria such as *Sphingobium* SYK-6 utilise proto-catechuate 4,5-dioxygenase to catalyse extradiol cleavage of protocatechuic acid, followed by a meta-cleavage pathway, shown in Fig. 5.6b [6].

5.4 Use of Metabolic Engineering for Generation of Renewable Chemicals from Lignin

Metabolic (or pathway) engineering has been used in *Escherichia coli* to engineer the production of primary metabolites such as amino acids [42], and practically useful metabolites such as alkanol biofuels [43] and fatty acid ester biofuels [44]. Alternative hosts such as *Saccharomyces cerevisiae* have been used to engineer the production of artemisinic acid, a precursor to anti-malarial drug artemisinin [45]. In all of the above cases, biosynthetic machinery has been used to produce novel metabolic products. A topical question is therefore whether metabolic engineering could be used in lignin-degrading bacteria to generate target metabolites from lignin degradation?

As noted above, vanillic acid appears to be one central metabolite in bacterial lignin degradation, and its metabolic precursor, vanillin, is a high value chemical used in the food/flavour industry [46]. Sainsbury et al. have shown that deletion of the vanillin dehydrogenase gene in *Rhodococcus jostii* RHA1 gave a gene deletion strain which accumulated vanillin at up to 96 mg/L yield after 6 days when grown on minimal media containing 2.5 % wheat straw lignocellulose [47]. Other bioproducts were 4-hydroxybenzaldehyde, from the H units present in grass lignin, and ferulic acid, which is linked to grass lignin via ester and α-ether linkages [47]. Vanillin can be generated via chemocatalysis from lignosulfonates [48], so this is unlikely to be a commercial route for vanillin production, but it demonstrates the feasibility of generating aromatic metabolites from lignin via metabolic engineering. Mycroft et al. have recently shown that insertion of genes encoding protocatechuate 4,5-dioxygenase or protocatechuate 2,3-dioxygenase into *Rhodococcus*
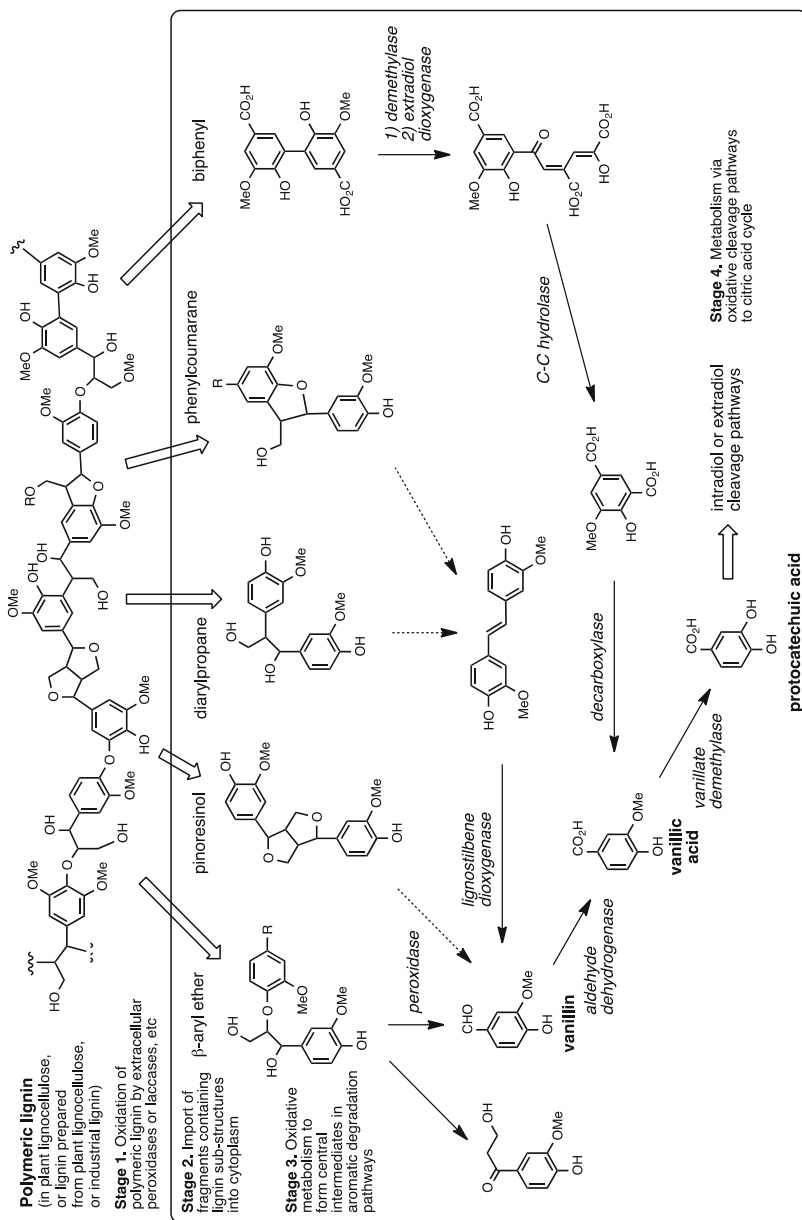
Fig. 5.5 Schematic representation of the different stages involved in metabolism of polymeric lignin to vanillic acid
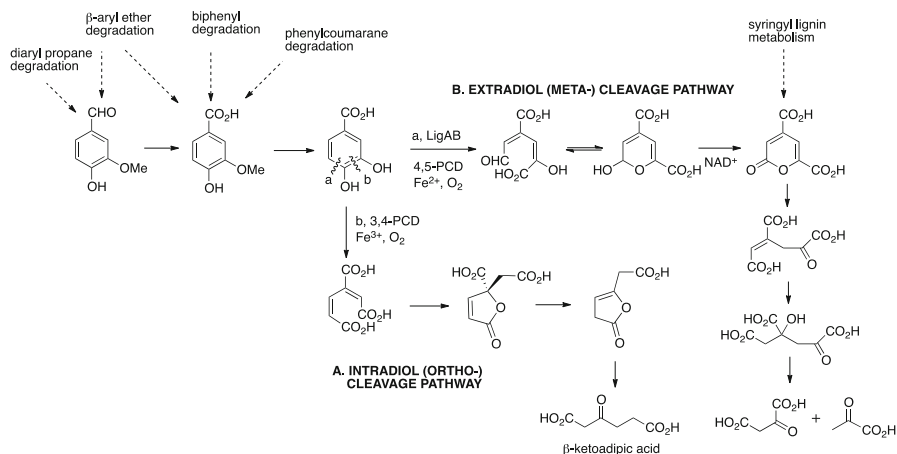
Fig. 5.6 Pathways for bacterial degradation of protocatechuic acid via (**a**) intradiol cleavage (**b**) extradiol cleavage

jostii, followed by ammonia cyclisation of the extradiol ring cleavage products, allows the formation of 2,4- or 2,5-pyridinedicarboxylic acid bioproducts (see Fig. 5.7) from bacterial fermentation, using minimal media containing wheat straw lignocellulose, in yields of 100–150 mg/L after 6–9 days [49]. These compounds are potential replacements for terephthalic acid used to make oil-based plastics [49].

Rhodococcus has also been used as a host to generate bioproducts via primary metabolism. *Rhodococcus opacus* DSM1069 and PD630 are known to accumulate triglyceride lipids from primary metabolism under nitrogen-limiting conditions, and both strains can grow on minimal media containing ultrasonicated ethanol organosolv lignin as carbon source [50]. Under these conditions, triglyceride lipids can be generated as fermentation bioproducts in yields of 4 mg/g lignin (or 20 mg/L media) after a 9 day fermentation [50]. The triglyceride lipid products are potential precursors for production of biodiesel.

Pseudomonas putida is a well-characterised aromatic degrader that has activity for lignin breakdown [7], for which genetic tools are also available, and metabolic engineering has also been reported in this host. *P. putida* can accumulate polyhydroxyalkanoate (PHA) biopolyesters under nitrogen-limiting conditions, and Linger et al. have shown that *P. putida* can convert lignin from alkaline pretreated liquor (APL) into PHAs in a 48 h fermentation in a yield of 252 mg/L [51]. Metabolic engineering has also been used in *P. putida* to accumulate ring cleavage product *cis*-muconic acid from aromatic degradation, via gene disruption of the protocatechuate cleavage pathway, and re-routing of metabolic flux to catechol cleavage [52]. Using *p*-coumaric acid as a carbon source, a yield of 13.5 g/L was obtained in a fed-batch bioreactor after 78 h fermentation, whereas using alkali-pretreated lignin, a yield of 0.7 g/L was obtained after 24 h fermentation [52]. *Cis,cis*-muconic acid can then be converted via catalytic hydrogenation into adipic acid, a feedstock chemical for plastics manufacture, thereby providing a renewable route to adipic acid from lignin
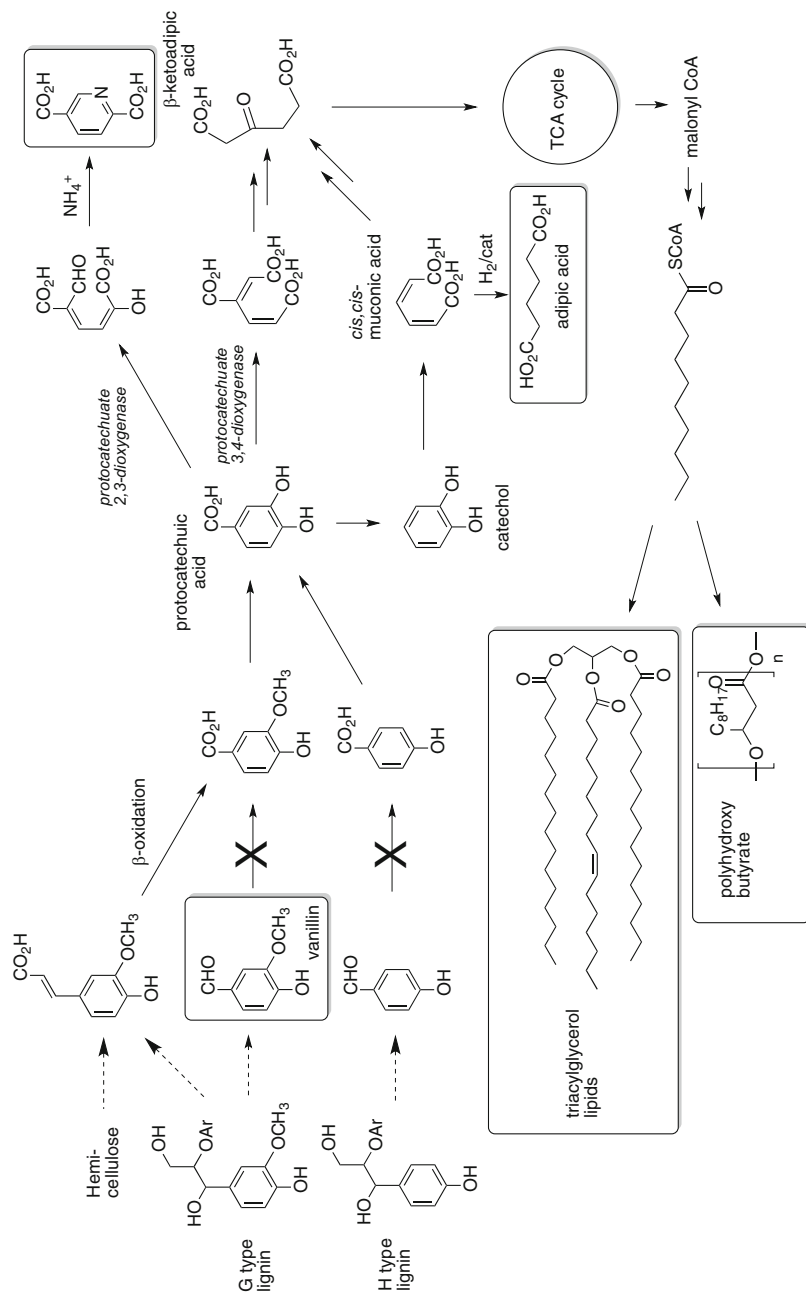
Fig. 5.7 Bioproducts generated from polymeric lignin via metabolic engineering. Only partial structures of G type and H type polymeric lignin are shown (*Ar* indicates aromatic ring, connected to lignin polymer)

[52]. Johnson and Beckham have also shown that replacement of the genes encoding the catechol intradiol pathway in *Pseudomonas putida* by genes encoding a corresponding extradiol pathway leads to an increase in yield of pyruvate from aromatic substrates [53].

5.5 Conclusions and Future Outlook

Several bacterial enzymes for lignin oxidation have been discovered since 2011, and pathway engineering strategies are emerging for the conversion of polymeric lignin or lignocellulose into valuable bio-products using bacterial fermentation. As our understanding of bacterial lignin degradation pathways and their regulation improves, metabolic engineering of lignin degradation should allow increases in product yield and generation of other useful co-products. Other tools such as selective inhibitors of oxidative cleavage pathways may provide alternative approaches to manipulating bacterial lignin degradation [54]. The use of bacterial fermentation makes use of the host's ability to deconvolute a complex mixture of lignin breakdown products via convergent pathways to a finite number of aromatic degradation pathways, and hence the production of unique products, but the toxicity of bioproducts (observed with vanillin accumulation [47]), and transport in and out of bacterial cells, are potential limitations of this approach. Lignin valorisation remains a very challenging but important area for industrial biotechnology.

References

1. Wong DWS. Structure and action mechanism of lignolytic enzymes. Appl Biochem Biotechnol. 2009;157:174–209.
2. Hofrichter M, Ullrich R, Pecyna MJ, Liers C, Lundell T. New and classic families of secreted fungal heme peroxidases. Appl Microbiol Biotechnol. 2010;87:871–97.
3. Vicuna R. Bacterial degradation of lignin. Enzyme Microb Technol. 1988;10:646–55.
4. Zimmermann W. Degradation of lignin by bacteria. J Biotechnol. 1990;13:119–30.
5. Ramachandra M, Crawford DL, Hertel D. Characterization of an extracellular lignin peroxidase of the lignocellulolytic actinomycete *Streptomyces viridosporus*. Appl Environ Microbiol. 1988;54:3057–63.
6. Masai E, Katayama Y, Fukuda M. Genetic and biochemical investigations on bacterial catabolic pathways for lignin-derived aromatic compounds. Biosci Biotechnol Biochem. 2007;71:1–15.
7. Ahmad M, Taylor CR, Pink D, Burton K, Eastwood D, Bending GR, Bugg TDH. Development of novel assays for lignin degradation: comparative analysis of bacterial and fungal lignin degraders. Mol Biosyst. 2010;6:815–21.

8. Taylor CR, Hardiman EM, Ahmad M, Sainsbury PD, Norris PR, Bugg TDH. Isolation of bacterial strains able to metabolize lignin from screening of environmental samples. J Appl Microbiol. 2012;113:521–30.

9. Bugg TDH, Ahmad M, Hardiman EM, Singh R. The emerging role for bacteria in lignin degradation and bio-product formation. Curr Opin Biotechnol. 2011;22:394–400.

10. Tian J-H, Pourcher A-M, Bouchez T, Gelhaye E, Peu P. Occurrence of lignin degradation genotypes and phenotypes among prokaryotes. Appl Microbiol Biotechnol. 2014;98:9527–44.

11. De Angelis KM, Allgaier M, Chavarria Y, Fortney JL, Hugenholtz P, Simmons B, et al. Characterization of trapped lignin-degrading microbes in tropical forest soil. PLoS One. 2011;6, e19306.

12. De Angelis KM, D'Haeseleer P, Chivian D, Fortney JL, Khudyakov J, Simmons B, Woo H, Arkin AP, Davenport KW, Goodwin L, et al. Complete genome sequence of *Enterobacter lignolyticus* SCF1. Stand Genomic Sci. 2011;5:69–85.

13. Shi Y, Chai L, Tang C, Yang Z, Zhang H, Chen R, Chen Y, Zheng Y. Characterization and genomic analysis of kraft lignin biodegradation by the beta-proteobacterium *Cupriavidus basilensis* B-8. Biotechnol Biofuels. 2013;6:1–14.

14. Chandra R, Singh S, Krishna Reddy MM, Patel DK, Purohit AJ, Kapley A. Isolation and characterisation bacterial strains *Paenibacillus* sp. and *Bacillus* sp. for kraft lignin decolorization from pulp paper mill waste. J Gen Appl Microbiol. 2008;54:399–407.

15. Chen YH, Chai LY, Zhu YH, Yang ZH, Zheng Y, Zhang H. Biodegradation of kraft lignin by a bacterial strain *Comamonas* sp. B-9 isolation from eroded bamboo slips. J Appl Microbiol. 2012;112:900–6.

16. Chandra R, Bharagava RN. Bacterial degradation of synthetic and Kraft lignin by axenic and mixed culture and their metabolic products. J Environ Biol. 2013;34:991–9.

17. Salvachua D, Karp EM, Nimlos CT, Vardon DR, Beckham GT. Towards consolidated lignin bioprocessing: simultaneous lignin depolymerisation and product generation by bacteria. Green Chem. 2015;17:4951–67.

18. Yoshida T, Sugano Y. A structural and functional perspective of DyP-type peroxidase family. Arch Biochem Biophys. 2015;574:49–55.

19. Ogola HJO, Kamiike T, Hashimoto N, Ashida H, Ishikawa T, Shibata H, Sawa Y. Molecular characterization of a novel peroxidase from the cyanobacterium *Anabaena* sp. strain PCC7120. Appl Environ Microbiol. 2009;75:7509–18.

20. Ahmad M, Roberts JN, Hardiman EM, Singh R, Eltis LD, Bugg TDH. Identification of DypB from *Rhodococcus jostii* RHA1 as a lignin peroxidase. Biochemistry. 2011;50:5096–107.

21. Roberts JN, Singh R, Grigg JC, Murphy MEP, Bugg TDH, Eltis LD. Characterization of dye-decolorizing peroxidases from *Rhodococcus jostii* RHA1. Biochemistry. 2011;50:5108–19.

22. Singh R, Grigg JC, Qin W, Kadla JF, Murphy MEP, Eltis LD. Improved manganese-oxidizing activity of DypB, a peroxidase from a lignolytic bacterium. ACS Chem Biol. 2013;8:700–6.

23. Rahmanpour R, Bugg TDH. Assembly *in vitro* of *Rhodococcus jostii* RHA1 encapsulin and peroxidase DypB to form a nanocompartment. FEBS J. 2013;280:2097–104.

24. Rahmanpour R, Bugg TDH. Characterisation of Dyp-type peroxidases from *Pseudomonas fluorescens* Pf-5: oxidation of Mn(II) and polymeric lignin by Dyp1B. Arch Biochem Biophys. 2015;574:93–8.

25. Brown ME, Walker MC, Nakashige TG, Iavarone AT, Chang MCY. Discovery and characterization of heme enzymes from unsequenced bacteria: application to microbial lignin degradation. J Am Chem Soc. 2011;133:18006–9.

26. Brown ME, Barros T, Chang MCY. Identification and characterization of a multifunctional dye peroxidase from a lignin-reactive bacterium. ACS Chem Biol. 2012;7:2074–81.

27. Ausec L, Zakrzewski M, Goesmann A, Schlüter A, Mandic-Mulec I. Bioinformatic analysis reveals high diversity of bacterial genes for laccase-like enzymes. PLoS One. 2011;10:25724–32.

28. Fernandes TAR, da Silveira WB, Passos FML, Zucchi TD. Laccases from actinobacteria – what we have and what to expect. Adv Microbiol. 2014;4:285–96.

29. Majumdar S, Lukk T, Solbiati JO, Bauer S, Nair SK, Cronan JE, Gerlt JA. Roles of small laccases from *Streptomyces* in lignin degradation. Biochemistry. 2014;53:4047–58.
30. Strachan CR, Singh R, VanInsberghe D, Ievdokymenko K, Budwill K, Mohn WW, Eltis LD, Hallam SJ. Metagenomic scaffolds enable combinatorial lignin transformation. Proc Natl Acad Sci U S A. 2014;111:10143–8.
31. Gutierrez A, Rencoret J, Cadena EM, Rico A, Barth D, del Rio JC, Martinez AT. Demonstration of laccase-based removal of lignin from wood and non-wood plant feedstocks. Bioresour Technol. 2012;119:114–22.
32. Masai E, Ichimura A, Sato Y, Miyauchi K, Katayama Y, Fukuda M. Roles of enantioselective glutathione S-transferases in cleavage of β-aryl ether. J Bacteriol. 2003;185:1768–75.
33. Picart P, Müller C, Mottweiler J, Wiermans L, Bolm C, Dominguez de Maria P, Schallmey A. From gene towards selective biomass valorization: bacterial β-etherases with catalytic activity on lignin-like polymers. ChemSusChem. 2014;7:3164–71.
34. Gall DL, Kim H, Lu F, Donohoe TJ, Noguera DR, Ralph J. Stereochemical features of glutathione-dependent enzymes in the *Sphingobium* sp. strain SYK-6 β-aryl etherase pathway. J Biol Chem. 2014;289:8656–67.
35. Gall DL, Ralph J, Donohoe TJ, Noguera DR. A group of sequence-related sphingomonad enzymes catalyzes cleavage of β-aryl ether linkages in lignin β-guaiacyl and β-syringyl ether dimers. Environ Sci Technol. 2014;48:12454–63.
36. Rashid GMM, Taylor CR, Liu Y, Zhang X, Rea D, Fülöp V, Bugg TDH. Identification of manganese superoxide dismutase from *Sphingobacterium* sp. T2 as a novel bacterial enzyme for lignin oxidation. ACS Chem Biol. 2015;10:2286–94.
37. Hyde SM, Wood PM. A mechanism for production of hydroxyl radicals by the brown-rot fungus *Coniophora puteana*: Fe(III) reduction by cellulose dehydrogenase and Fe(II) oxidation at a distance from the hyphae. Microbiology. 1997;143:259–66.
38. Bugg TDH, Winfield CJ. Enzymatic cleavage of aromatic rings: mechanistic aspects of the catechol dioxygenases and later enzymes of bacterial aromatic degradation pathways. Nat Prod Rep. 1998;15:513–30.
39. Bugg TDH, Ahmad M, Hardiman EM, Rahmanpour R. Pathways for degradation of lignin in bacteria and fungi. Nat Prod Rep. 2011;28:1883–96.
40. Chen H-P, Chow M, Liu CC, Lau A, Liu J, Eltis LD. Vanillin catabolism in Rhodococcus jostii RHA1. Appl Environ Microbiol. 2012;113:521–30.
41. Harwood CS, Parales RE. The beta-ketoadipate pathway and the biology of self-identity. Annu Rev Microbiol. 1996;50:553–90.
42. Park JH, Lee KH, Kim TY, Lee SY. Metabolic engineering of *Escherichia coli* for the production of L-valine based on transcriptome analysis and *in silico* gene knockout simulation. Proc Natl Acad Sci U S A. 2007;104:7797–802.
43. Atsumi S, Hanai T, Liao JC. Non-fermentative pathways for synthesis of branched-chain higher alcohols as biofuels. Nature. 2008;451:86–90.
44. Steen EJ, Kang Y, Bokinsky G, Hu Z, Schirmer A, McClure A, Del Cardayre SB, Keasling JD. Microbial production of fatty-acid-derived fuels and chemicals from plant biomass. Nature. 2010;463:559–62.
45. Ro D-K, Paradise EM, Ouellet M, Fisher KJ, Newman KL, Ndungu JM, Ho KA, Eachus RA, Ham TS, Kirby J, Chang MCY, Keaslin JD. Production of the antimalarial drug precursor artemisinic acid in engineered yeast. Nature. 2006;440:940–3.
46. Priefert H, Rabenhorst J, Steinbüchel A. Biotechnological production of vanillin. Appl Microbiol Biotechnol. 2001;56:296–314.
47. Sainsbury PD, Hardiman EM, Ahmad M, Otani H, Seghezzi N, Eltis LD, Bugg TDH. Breaking down lignin to high-value chemicals: the conversion of lignocellulose to vanillin in a gene deletion mutant of *Rhodococcus jostii* RHA1. ACS Chem Biol. 2013;8:2151–6.
48. Bjørsvik HR, Minisci F. Fine chemicals from lignosulfonates. 1. Synthesis of vanillin by oxidation of lignosulfonates. Org Process Dev. 1999;3:330–40.

49. Mycroft Z, Gomis M, Mines P, Law P, Bugg TDH. Biocatalytic conversion of lignin to aromatic dicarboxylic acids in *Rhodococcus jostii* RHA1 by re-routing aromatic degradation pathways. Green Chem. 2015;17:4974–9.
50. Kosa M, Ragauskas AJ. Lignin to lipid bioconversion by oleaginous *Rhodococci*. Green Chem. 2013;15:2070–4.
51. Linger JG, Vardon DR, Guarneri MT, Karp EM, Hunsinger GB, Franden MA, Johnson CW, Chupka G, Strathmann TJ, Pienkos PT, Beckham GT. Lignin valorization through integrated biological funnelling and chemical catalysis. Proc Natl Acad Sci U S A. 2014;111:12013–8.
52. Vardon DR, Franden MA, Johnson CW, Karp EM, Guarneri MT, Linger JG, Salm MJ, Strathman TJ, Beckham GT. Adipic acid production from lignin. Energy Environ Sci. 2015;8:617–28.
53. Johnson CW, Beckham GT. Aromatic catabolic pathway selection for optimal production of pyruvate and lactate from lignin. Metab Eng. 2015;28:240–7.
54. Sainsbury PD, Mineyeva Y, Mycroft Z, Bugg TDH. Chemical intervention in bacterial lignin degradation pathways: development of selective inhibitors for intradiol and extradiol catechol dioxygenases. Bioorg Chem. 2015;60:102–9.

Chapter 6
Lignin Biodegradation with Fungi, Bacteria and Enzymes for Producing Chemicals and Increasing Process Efficiency

Lionel Longe, Gil Garnier, and Kei Saito

List of Abbreviation

ABTS	2,2′-azino-bis(3-ethylbenzothiazoline-6-sulphonic acid)
Acetyl COA	Acetyl coenzyme A
Aff.	"affinis", Latin form of "related"
CTMP	Chemithermomechanical Pulping
DPM	Diphenyl Methane bond
EC	Enzyme Commission number
GFC	Gel Filtration Chromatography
1-HBT	1-Hydroxybenzotriazole
Lac	Laccase
LC-MS	Liquid Chromatograph-Mass Spectrometry
LiP	Lignin Peroxidase
mcl-PHA	Medium Chain Length Polyhydroxyalkanoate
MnP	Manganese Peroxidase
NMR	Nuclear Magnetic Resonance
Sp.	Species (sing.)
Spp.	Species (plur.)

L. Longe
School of Chemistry, Bioresource Processing Research Institute of Australia (BioPRIA), Monash University, Clayton, VIC 3800, Australia
e-mail: lionel.longe@monash.edu

G. Garnier (✉)
Department of Chemical Engineering, Bioresource Processing Research Institute of Australia (BioPRIA), Monash University, Clayton, VIC 3800, Australia
e-mail: gil.garnier@monash.edu

K. Saito (✉)
School of Chemistry, Monash University, Clayton, VIC 3800, Australia
e-mail: kei.saito@monash.edu

TCA cycle	Tricarboxylic Acid cycle
TEMPO	2,2,6,6-Tetramethyl-1-piperidinyloxy
VLA	Violuric acid
VP	Versatile peroxidase

6.1 Introduction

The word "Lignin" comes from Latin, "lignum", that can be literally translated as tree, timber or even firewood. Evolving from this, the word "lignin" was specifically used in 1813 by A.P. de Candolle, a Swiss botanist, to denote the product obtained after wood treatment with solvents and mild acid. Twenty-five years later, Anselme Payen reported on two products in wood: cellulose, and what would be later called "lignin" [1]. During the following decades, scientists investigated this peculiar product to identify its structure. The NMR studies [2] of Ludwig [3] and Nimz [4] have led to the commonly admitted representation of the lignin structure: a 3D polymer network, highly cross-linked, and resulting from the co-polymerisation of three different phenol derivative monomers (Fig. 6.1a, b). The reaction of these three monomers leads to the creation of a wide variety of linkages, among which six common bonds: the β-O-4, 5–5, β-5, 4-O-5, β-1 and β-β (Fig. 6.1b and Table 6.1). This large range of bonds and the high cross-linking density render lignin extremely recalcitrant to degradation [5]. It is this high degree of bonding and chemical heterogeneity that has prevented science from upgrading lignin into fine chemicals or bio-based polymers on industrial scale. As a result, 98 % of the lignin world production at present is currently simply burned for energy [6].

Numerous studies have described approaches to depolymerise lignin. Many approaches apply pretreatment and rely on chemical methods to depolymerise lignin. However, results are often difficult to compare as a consequence of the complicated 3D structure of lignin and the lack of standard analytical methods. In nature, organisms naturally degrade wood by different catabolic pathways involving enzymes.

The present chapter primarily focuses on how these organisms have been investigated and utilised to break down lignin into valuable chemicals and by-products. This review first analyses fungi as catalyst to synthesise fine chemicals from lignin. Second, the application of bacteria and the mechanism by which they operate is studied; last, the role of enzymes is analysed. It is the objective of this chapter to review the biodegradation approaches for selectively breaking down and converting lignin into fine chemicals, to provide a perspective on the promising strategies and to map the current scientific frontiers.

6.2 Fungal Degradation

When considering decaying wood, the first organisms to come to mind are fungi. Wood degrading fungi are mostly divided into three broad categories: white-rot, brown-rot and soft-rot fungi [10] (Table 6.2). Biomass degrading fungi described in
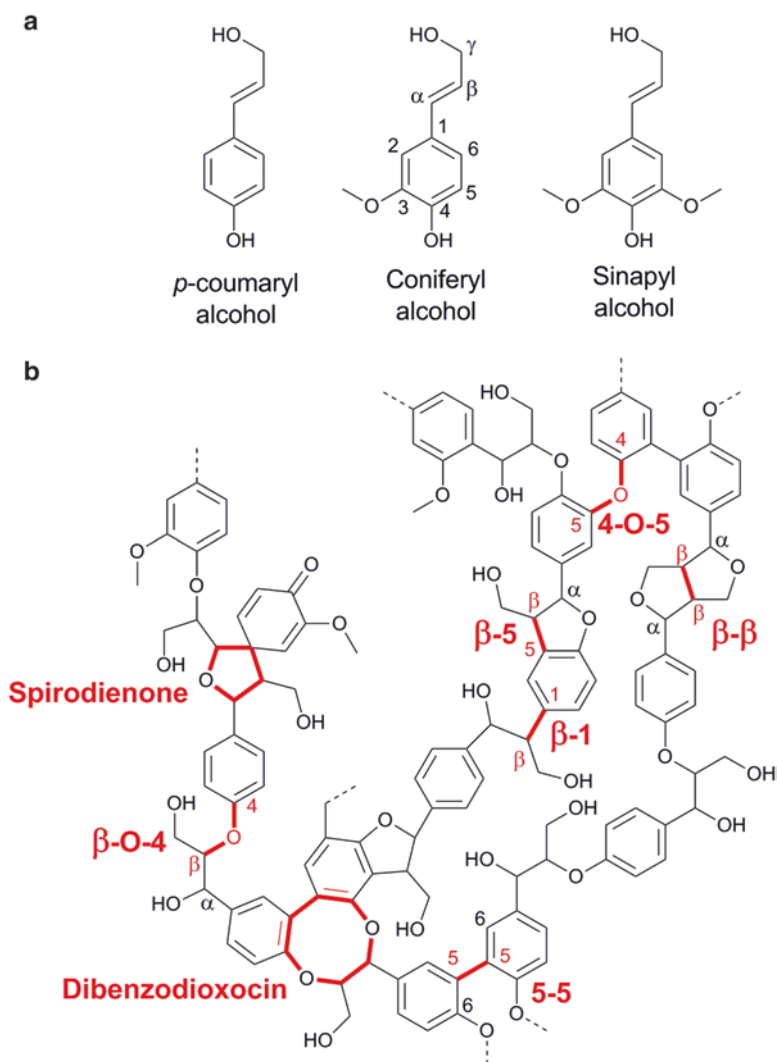
Fig. 6.1 (**a**) Three constitutive monomers of lignin: *p*-coumaryl alcohol, coniferyl alcohol and sinapyl alcohol (**b**) Structure illustrating the principal bonds in lignin, a three dimensional highly cross-linked biopolymer

the literature are mostly from two phyla (subdivision in biological classification): Basidiomycota and Ascomycota, both from the subkingdom of fungi Dikarya [11]. Although, other phyla are sometimes considered, these two are the most commonly reported for biomass degradation. In the literature, basidiomycetous white-rot fungi are the most studied, since they can selectively degrade lignin, leaving the cellulose and hemicellulose fraction rather intact. However, lignin degradation can also result from the action of other strains and even marine-derived fungi [12]. The term

Table 6.1 Repartition of the different bonds found in lignin from two different woods. *Spruce*, a softwood, has more 5-positions available, enabling more 5–5 and β-5 linkages, than *Eucalyptus grandis*, a hardwood [1]

Abundance per 100 C9-units	*Spruce* [7, 8]	*Eucalyptus grandis* [9]
β-O-4	45–50	61
5-5	19–22	3
β-5	9–12	3
4-O-5	4–7	9
β-1	7–9	2
β-β	2–4	3
Spirodienone	ND	5
Dibenzodioxocin	ND	ND

ND not determined

Table 6.2 Different categories of wood degrading fungi and their action on lignin [10]

Fungi (Subdivision)	Main examples	Action	Preferred substrate
White-rot fungi (Basidiomycota)	*Phanerochaete, Pleurotus, Trametes, Phlebia spp.*	Active degradation of lignin and possibly cellulose	Hardwood
Soft-rot fungi (Ascomycota)	*Chaetomium, Ceratocystis, Kretzschmaria deusta spp.*	Lignin modification	Hardwood
			Softwood
Brown-rot fungi (Basidiomycota)	*Serpula lacrymans, Piptoporus betulinus, Gloeophyllum trabeum, Postia Placenta, Fomitopsis cajanderi*	Slight lignin modification	Softwood

white-rot fungi results from the colour of the degraded wood; as lignin is being digested by the organism, the only remains are the white cellulose and hemicellulose. This selectivity is particularly important for applications that upgrade cellulose, such as pulp or bioethanol production.

White-rot fungi represent a large group of species, each featuring a different mechanism to attack the lignin barrier directly with a cocktail of enzymes [13, 14]. Fungi produces various enzymes, some to degrade lignocellulose, and others with different roles but with essential role for the fungi to prosper on complex biomass. It has been shown that inhibition of the production of these enzymes can highly hinder or even prevent any growth of the fungi on ligneous and cellulosic mediums [15–17].

For the last 50 years, lignin degrading fungi have been studied from a microbiological perspective, focussing on the mechanisms of lignin degradation and identifying the enzymes involved. Three different types of fungi application have emerged [18]: (a) conversion of lignocellulosic biomass into animal feed and food [19–21] (b) pretreatment agent for delignification (c) biodegradation agent for some phenolic contaminants or various wastes. Transformation of woody biomass into edible mushrooms falls beyond the scope of this study. This review focuses on the two latter applications.

It is worthwhile to clarify some of the nomenclature that can be confusing. There is a clear distinction between delignification, which is the actual removal of lignin from biomass, and lignin degradation/depolymerisation, which represents the cleavage of C-C bonds or ether bonds within the lignin structure, yielding lignin oligomers [22]. Delignification, characterised, for example, by a smaller kappa number,[1] is often due to increased solubility of lignin, either by modification or by radical grafting [24, 25]. Consequently, it is possible that lignin degradation also contributes to increased solubility through decreased molecular weight; however delignification does not imply lignin depolymerisation. Both delignification and lignin bio-degradation are reviewed in this chapter. These two phenomena are critical for unlocking economically feasible bio-refineries capable of producing a full range of marketable chemicals and materials.

6.2.1 Delignification

The delignification process has two main domains of application: pulp and paper industry, and biofuel production. The pulp and paper industry converts wood into fibres for paper. There are two main pulping processes: mechanical and chemical pulping. In mechanical pulping, lignocellulosic fibres are separated from the wood structure by applying stress. An example is Thermo-Mechanical Pulping (TMP) which relies on steam to plasticise and heat wood above the glass transition temperature (T_g) of lignin while applying defibrillating shear, thus reducing fibre damage and energy consumption. Chemical pulping relies on chemical agents and heat to dissolve the ligning-rich fraction of the lumen lamella binding fibres. There are two main chemical processes: Kraft pulping (alkaline) and sulphite pulping (acidic). Kraft pulping is the most important pulping process producing 70 % of all pulp. Pulping aims at developing good quality fibres; full delignification is not always required as it decreases pulp yield. Full fibre delignification or whitening requires bleaching, increasing cost and environmental impact [27–31]. White-rot fungi, with their mild reaction condition, have been investigated as low energy and environment-friendly treatment to reduce lignin content or to replace an existing step of the chemical/thermomechanical pretreatment; this process is referred to as biopulping. In biofuel production processes, sugars from diverse lignocellulosic resources are fermented by microorganisms to yield targeted products. Hence, the first step of biomass processing is its conversion into simple sugars (glucose, xylose), usually by an enzymatic pathway. Although this process is easy for starch (glucose units linked by α-1,4 and α-1,6 glycosidic bonds) compounds, it is much more complicated for cellulose due to its regular structure (glucose unit linked by β-1,4 glycosidic bonds) which makes it highly crystalline and compact leading to a high

---

[1] Kappa number is a titration process representative of the pulp colour and approximatively proportional to lignin content at low concentration [23]; it can be used to assess delignification efficiency.

resistance to biological degradation [26]. Moreover, the intertwining between cellulose, hemicellulose and lignin results in recalcitrance which hinders the action of the microorganisms [5]. Fungi represent a promising pretreatment agent to reduce this intertwining considering its mild reaction conditions [27, 28]. White-rot strains are of special consideration because of their low uptake of cellulose sugars.

It is estimated that enzymes account (sing.) for 4.5 % of the cost for biofuel production from corn starch and up to 20 % when the whole plant is involved [29–31]. Reviews note that mechanical and chemical pretreatment of biomass for biofuel production can become costly [5, 32–37]. Therefore pretreatment is a critical step for the economics of a process. Different approaches with fungi have been considered to promote delignification by pretreatment combinations.

Single Fungus Treatment Physical and chemical pretreatment of biomass are notorious for the harsh reaction conditions required. On the contrary, biological pretreatment involves much milder conditions, representing a perfect substitute or complementary degrading agent for delignification [38]. Ge and co-workers have reported on the use of *Ceriporiopsis subvermispora*, a white-rot fungus, as treatment for *Albizia moluccana* (Albizia), a widespread invasive tree species in tropical and subtropical regions [39]. The white-rot fungus efficiently decreased the lignin content by 24 % while degrading cellulose and hemicellulose only by half this value. As a consequence, pretreatment with *Ceriporiopsis subvermispora* allowed a jump in cumulative methane yields from 33.9 L/kg of volatile solid for raw albizia to 123.9 L/kg for pretreated wood chips.

For biofuel applications, fungi could serve not only as delignification agents, but also as production vectors for various products. Indeed, some fungi can degrade lignin along with cellulose which can be useful for production of sugars (Table 6.2) White-rot fungus *Phlebia* sp. were shown by Kamei et al. to exhibit such combined behaviour for the direct production of bioethanol from cellulosic materials [40]. The same group later reported on the direct conversion of lignocellulosic biomass to bioethanol using this same fungus [41], then proving *Phlebia* sp. MG-60 to have the combined abilities of lignin degradation, cellulose saccharification, and ethanol fermentation.

Sugar cane bagasse was treated to improve bioethanol yield. Biomass and process variables such as moisture content, additives and presence of metallic cations were shown to greatly affect delignification efficacy [42]. Growth medium addition improved both delignification and ethanol production. Addition of Fe^{2+}, Mn^{2+} or Cu^{2+} slightly decreased delignification but bioethanol production was improved by reducing bagasse carbohydrate degradation.

Following the same strategy, Xie et al. reported on the use of an oleaginous fungus strain as lignin degrading microorganism [43]. *Cunninghamella echinulate FR3* was determined to be able to degrade cell wall lignin as efficiently as most Basidomycetes fungi. Two strains of sorghum, the wild-type and reduced-lignin-content type (genetically modified to feature improved saccharification efficiency), were submitted to enzymatic hydrolysis followed by fungal biodegradation. Lignin

loss reached 31 % for the wild-type sorghum, while toping up to 46 % for the mutant strain. However, up to 35 % wt of cellulose was degraded during the process. This oleaginous fungus was not targeted as pretreatment to increase sugar production, but was used for lipid bioaccumulation, potentially leading to a new way to provide feedstock for biodiesel refineries [43].

Fungus as Co-treatment Even though the current chemical and thermomechanical pulping pretreatments are efficient, an additional bio-treatment stage could further increase delignification yield, decrease energy consumption, increase selectivity or fibre quality while decreasing environmental impact. With those benefits in mind, Baker et al. reported on the synergistic effect combining pressure refining, a common process for the pulp and paper industry, with three different white-rot fungi [44]. *Ceriporiopsis subvermispora*, *Phlebiopsis gigantea* and *Phlebia radiata* were fed with pressure refined Miscanthus wood chips. In this strategy, pressure refining concentrates lignin in pellets on the surface of the cellulose fibres [45]. This configuration was tested to increase delignification efficiency by improving the lignin accessibility to the degrading enzymes. After 28 days, the three strains reached their white-rot fungi expectation by decreasing the relative amount of lignin in Miscanthus medium by 10–20 %. However, it is the *Ceriporiopsis subvermispora* strain that exhibited the best lignin degrading properties by decreasing lignin by 70–75 % of the original content. Un-pressure refined Miscanthus could only reach 10 % of lignin content reduction, highlighting the cooperative action of physical and biological pretreatments.

Kamei et al. reported on the decrease of lignin content and increase in ethanol production when *Phlebia* sp. MG-60 was fed with alkaline-pretreated sugarcane bagasse compared to untreated sugarcane bagasse [46]. The final results depended on the initial alkaline concentration. After 10 days, the total production of ethanol was 210 mg/g of treated bagasse, providing an ethanol yield (production of ethanol compared to theoretical maximum) of 66 % for the bagasse pretreated with 0.8 % NaOH. Untreated bagasse only reached ca. 2 % of ethanol yield these demonstrating the synergistic effect of the two pretreatments.

Fungi Co-culture Fungi co-cultures have been investigated to improve lignocellulosic ethanol production efficiency. The cumulative effects of pretreating biomass with two fungi can either improve delignification in the case of two lignolytic fungi [47], or significantly improve the release of reducing sugars by incubating white-rot and brown-rot fungi together [48]. Co-culture of white-rot *Ceriporiopsis subvermispora* and brown-rot *Postia placenta* fungi on *Liriodendron tulipifera* wood chips was reported by Parrow et al. [49]. Although each species increased reducing sugar production during the post saccharification process compared to sterile conditions, rising from 75 to 250 mg/g, the co-culture showed no benefits. Evaluation of interspecific growth interactions showed that an "inhibition" zone was created at the intersection of each taxon growth domain. The two fungi can coexist in the same medium, but did not feature interspecific stimulatory (or inhibitory) interactions. Better understanding of how different species can cooperate in the same biomass is required to improve delignification and saccharification efficiency.

Ma and Ruan reported that *Coprinus comatus* (producing lignolytic enzymes) and *Trichoderma reesei* (producing hemi and cellulolytic enzymes) have synergistic interaction on corn stover [50]. No inhibition was observed at the intersection of the two growth domains, even with intertwining. The co-culture improved delignification by 10 % compared with the lignolytic fungus alone, giving a maximum of 66.5 % delignification after 72 h at optimum temperature conditions. Weight loss, glucan and xylan degradation were also synergistically improved by the co-cultivation of the two strains. A total reducing sugar yield of 82 % was achieved.

Table 6.3 summarises the current critical studies on fungal delignification. Comparison of results remains a challenge because of the different methods used to measure delignification; methods used range from lignin content measurement to IR spectroscopy [51] and even include wettability testing [52].

6.2.2 Waste Treatment

Lignin degrading fungi have been investigated for their waste degrading properties. Indeed, many fungi have phenol degrading properties suitable to treat a wide range of phenolic pollutants [69, 70]. This field is investigated not only for the treatment of oil -or paper-mill waste water for lignin removal, but also for the textile industry waste water which has a high content of toxic aromatic dyes [71, 72]. Martin and Manzanares reported on the delignification of straw alkaline-pulping liquors by *Trametes versicolor* [73]. The white-rot fungus was able to remove 75 % of the lignin in the effluent, bringing it from 2 g/L to 0.5 g/L. An important simultaneous decolourisation of the effluent resulted from the delignification.

6.2.3 Chemical Production

Some studies have considered fungi for lignin chemical modification to change its properties and also to produce chemicals from lignin derivatives. Falconnier et al. reported on the production of vanillin from ferulic acid by white-rot fungus *Pycnoporus cinnabarinus* I-937 [74]. Vanillin concentration up to 64 mg/L was achieved for a molar yield of 27.5 % w/w. However, recovering vanillin from this mixture proved to be challenging as the fungus produces laccase that repolymerises ferulic acid into a lignin-like polymer.

Work from Zou and co-workers detail lignin demethylation by two fungal strains, *Cylindrocladium* sp. and *Aspergillus* sp. [75]. Demethylation of lignin is of high interest for functionalising lignin by liberating reactive groups. The new hydroxyl groups can serve for grafting new functionalities, dangling chains, or even for resins [76, 77]. After 3 weeks in culture, 40 % of the methoxy groups were removed from lignin without causing significant degradation (10 % decrease in content). This work

Table 6.3 Overview of lignin degradation process by fungi and their performance

Measurement method	Fungi	Substrate	Delignification amount	Ref.
Klason lignin weight loss: TAPPI [53], NREL [54] or Kirk and Obst [55]	*Arthrinium. phaeospermum* and *Phanerochaete chrysosporium*	*Miscanthus* leaves and sugarcane	11 % and 15 %	[31]
	Coprinus comatus and *Trichoderma reesi* (synergistic interaction)	Corn stover	66.5 %	[50]
	Ceriporiopsis subvermispora	*Albizia moluccana*	24 %	[39]
	Ceriporiopsis subvermispora	Pressure refined *Miscanthus sacchariflorus* and *giganteus*	25–30 %	[44]
	Coriolopsis caperata RCK 2011, *Ganoderma* sp. rckk-02 and *Pleurotus florida*	Sugarcane bagasse	5.5 %, 5.6 % and 7.9 %	[56]
	Cunninghamella echinulate FR3	Wild-type and mutant lines of *Sorghum bicolor*	46 % and 31 %	[43]
	Dichomytus squalens, Formitopsis pinicola, Ganoderma lucidum, Lenzites betulinus, Pleurotus ostreatus, Pleurotus eryngii, Trametes versicolor	Wheat straw	34 %, 32 %, 20 %, 28 %, 7 %, 14 % and 21 %	[57]
	Phlebia sp.	Oak wood	40.7 %	[41]
	Phlebia sp.	Sugarcane bagasse	44 %	[42]
	Pleurotus ostreatus	Sugarcane bagasse	34.8 % (compared to 19.6 % for CTMP)	[58]
	Trametes multicolor and *Trametes pubescens*	Wheat straw and oak sawdust	6 % and 50 %	[59]
Lignin weight loss, Van Soest method [60]	*Phanerochaete flavido-alba*	Wood fibre, corn stover and wheat straw	20 %	[61]
	Phanerochaete chrysosporium	Corn stover and corn stover silage	60 % and 20 %	[62]

Table 6.3 (continued)

Measurement method	Fungi	Substrate	Delignification amount	Ref.
Kappa number (TAPPI [63])	*Pleurotus ostreatus*	Sugarcane bagasse	70 % (dat)	[58]
	Trametes versicolor	Oil palm trunk chips	35 % (dat)	[64]
Acetyl bromide soluble lignin loss by quantitative spectrophotometry [65]	*Trichoderma viride* and surfactant	Rice straw	74 %	[66]
Reducing sugars released from enzymatic degradation of cellulose (saccharification efficacy)	*Ceriporiopsis subvermispora* and *Postia placenta*	*Liriodendron tulipifera* wood chips	330 % (isr)	[49]
	Ceriporiopsis subvermispora	Wheat straw	60 % (acs)	[67]
	Coriolopsis caperata RCK 2011, *Ganoderma* sp. rckk-02 and *Pleurotus. Florida*	Sugarcane bagasse	150–240 % (isr)	[56]
	Pleurotus ostreatus and *Pleurotus pulmonarius*	*Eucalyptus grandis* sawdust	17 % and 15 % (acs) (3 % for blank)	[38]
	Myrothecium roridum	Rice straw	37 % better than chemical pretreatment (dilute acid)	[68]
Ethanol released during fermentation of free sugars (ethanol yield)	*Phlebia* sp.	Sugarcane bagasse	39 % (mey)	[42]
		Oak wood	43.9 % (mey)	[41]
		Alkaline-pretreated sugarcane bagasse	66 % (mey)	[46]

CTMP Chemithermomechanical Pulping, *dat* decrease after treatment, *isr* increase in sugar release, *acs* available cellulose saccharified, *mey* maximum ethanol yield

represents a promising start for using fungi as biological modifiers in industrial applications.

6.2.4 Perspectives

Even though engineering fungi is in its infancy, the current trend to engineer fungi as reactant or catalyst to convert lignin into valued products is very promising. Fungus can be genetically modified as has been proven in the past [15–17, 78], but there are presently only a small number of applications compared with those for bacteria.

White-rot fungi in general, and the *Pleurotus ostreatus* strain in particular, are of interest for their high delignification rate. However, most of the previous studies have been limited either to basic pretreatment process for lignocellulosic biomass or to waste biodegradation. Using fungi as individual species, co-culture or even combined with chemical reactions has tremendous potential, including the synthesis of fine chemicals and functionalisation of lignin into value added polymers. A clear understanding of the fungi reaction mechanisms is needed, along with their kinetics and the adoption of standard lignin analytical (for yield and content) methods for enabling unbiased comparisons among processes and studies.

6.3 Bacterial Degradation

In contrast to fungal lignin degradation, enzymology of bacterial lignin breakdown is currently not well understood [79]; extracellular peroxidase and laccase enzymes also appear to be involved. These bacteria can be found in soils, where decaying wood is present, but also in the digestive systems of herbivores, like cows rumens, or in xylophage insects guts, like termites [80]. These bacteria belong to three phyla, actinomycetes, α-proteobacteria and γ-proteobacteria [79]. One review reports on some lignin-degrading prokaryotes in the following phyla: firmicutes, β-proteobacteria, δ-proteobacteria, bacteroidetes and archaea [81].

As a lignin degrading organism, bacteria have been studied for delignification or bioremediation, just as fungi, but to a smaller extent, which is probably because bacterial enzymes have shown to have a lower redox potential [82, 83]. However bacteria have some interesting properties over those of fungi: they are stable over a wide range of pH [84], they can feed on lignin as the sole source of carbon and energy [85], and they are easy to genetically modify [86].

6.3.1 Delignification

Although considered less effective than fungi, lignin degrading bacteria are also able to utilise lignocellulosic biomass. They are used in delignification processes, either for biopulping or for the biofuel production to increase accessibility of cellulose, but also for bioremediation and waste management. Hacq et al. reported that

Serratia liquefaciens could detoxify pulp and paper mill effluent by removing contaminants and lignin by up to 58 % [87]. Agricultural residues can also create environmental pollution, and as a lignin degrading organism, bacteria have received wide interest for treatment [88, 89].

Bacteria delignification research has focused onto Kraft pulp applications because of its high annual production [90]. Shi and co-workers showed that different bacteria strains could successfully degrade Kraft lignin with good yields [91–93]. *Cupriavidus basilensis* B-8 and *Pandaroea* sp. B6, two protobacteria, expressed high lignolytic enzymes (manganese peroxidase and laccase) activity when reacted with Kraft lignin. After 7 days in optimum concentration and pH, a total lignin removal of ca. 45 % was achieved. By degrading Kraft lignin with no other source of carbon required, these two bacteria strains showed good potential for industrial delignification.

Priyadarshinee et al. reported improvement of eucalyptus Kraft pulping by bacterial treatment, resulting in a decrease in kappa number [23]. The raw eucalyptus Kraft pulp was inoculated with two different bacteria strains, *Pseudomonas fluorescens* NITDPY and *Planococcus* sp.TRC1. The two bacteria decreased the kappa number by 32 and 37 % in 7 days, respectively. The total amount of phenolic compounds was also reduced. The two different strains react differently to their new carbon source, with *P. fluorescens* NITDPY degrading lignin faster in the early stage of the experiment through phenolic compound release. Both strains released reducing sugar, but only in a small amount: 0.32 mg/g and 0.15 mg/g for *Planococcus* sp.TRC1 and *P. fluorescens* NITDPY, respectively. This indicates that cellulose is not much affected much by the bacteria which is important for pulp and paper applications. The *Pseudomonas fluorescens* NITDPY and *Planococcus* sp.TRC1 bacteria show good industrial potential, more than some fungi and they provide non-negligible cellulose degradation. Example of lignin degrading bacteria studied for delignification can be found in Table 6.4.

6.3.2   Chemical Production

Bacteria are considered to be merely as effective as fungi for delignification; however, they are much easier to genetically modify than fungi [86]. The ability of bacteria to accumulate some of the lignin degradation products as carbon source or energy is an interesting property for chemical production [98]. In the last few years, applications for lignin degrading bacteria have changed. Initially, microorganisms were mostly investigated to degrade and remove lignin from biomass to facilitate recovery of other compounds. Now some research groups are reporting their use for lignin valorisation. While procedures can be complex, the principles are simple. By genetically modifying some bacteria strains, disruption in the metabolic pathway is created, leading to the accumulation of a compound of interest in the medium.

Sainsbury and co-workers reported on the conversion of lignocellulose to vanillin by deleting one enzyme coding gene in *Rhodococcus jostii* RHA1 [99]. *R. jostii*

Table 6.4 Overview of lignin degradation process by bacteria and their performance

Measurement method	Bacteria	Substrate	Delignification amount	Ref.
Klason lignin weight loss: TAPPI [53]	*Pandoraea* sp. *ISTKB*	Sugarcane bagasse	10.4% after 20 days	[94]
Lignin weight loss	*Cupriavidus basilensis* B-8	Kraft lignin	44.4%	[92]
	Pandoraea sp. B-6		45.5%	[91]
Lignin loss by quantitative GFC	*Bacillus pumilus* and *Bacillus atrophaeus*		50% and 70% for high molecular lignin	[95]
Lignin weight loss, Van Soest [60]	*Escherichia coli* from beef cattle rumen	Maize stover	36.8% after 4 days	[96]
Measurement of lignin loss by quantitative UV spectroscopy	*Bacillus* sp. extracted from soil	Alkali lignin	40% after 24 h, 80% after 48 h	[86]
Kappa number (TAPPI method [63])	*Cryptococcus albidus*	Bagasse	22% smaller than control, still 4.5% smaller when further Kraft pulping is applied	[97]
	Planococcus sp. *TRC1* and *Pseudomonas fluorescens NITDPY*	Raw eucalyptus Kraft pulp	37% and 32% decrease	[23]

GFC Gel Filtration Chromatography

degrades lignin derivatives using a biological funnelling process, creating a few intermediates from multiple substrates. The genetic material coding the mechanism responsible for the degradation of vanillin and vanillic acid intermediates were removed from the bacterium DNA. The resulting suppression of *vanillin dehydrogenase* production causes vanillin to accumulate along with by-products in the reaction medium (Fig. 6.2). After 144 h in a medium containing 2.5% wheat straw lignocellulose and 0.05% glucose, the genetically modified bacterium accumulated vanillin up to 96 mg/L. An important amount of ferulic acid could also be observed after 168 h of reaction. When the substrate was changed to Kraft lignin, which is a major industrial by-product of the pulp and paper, an amount of 13 mg/L of vanillin could still be obtained, indicating, however, that lignocellulose remains a better substrate than Kraft lignin. With a similar objective, Graf et al. reported the identification of the gene coding *vanillin dehydrogenase* in *Bacillus subtilis* 3NA [100], proving the versatility of this technique.

Linger et al. reported on the biological funnelling behaviour of a bacteria, *Pseudomonas putida* KT2440. This organism converts a heterogeneous substrate, such as lignin derivatives, into a sole product, in this case a medium chain length polyhydroxyacid (mcl-PHA). The process was tested on alkaline pretreated liquor (APL), a highly concentrated depolymerised lignin mixture: 32% lignin made mostly of monomers, dimers and trimers. The result was an accumulation of mcl-
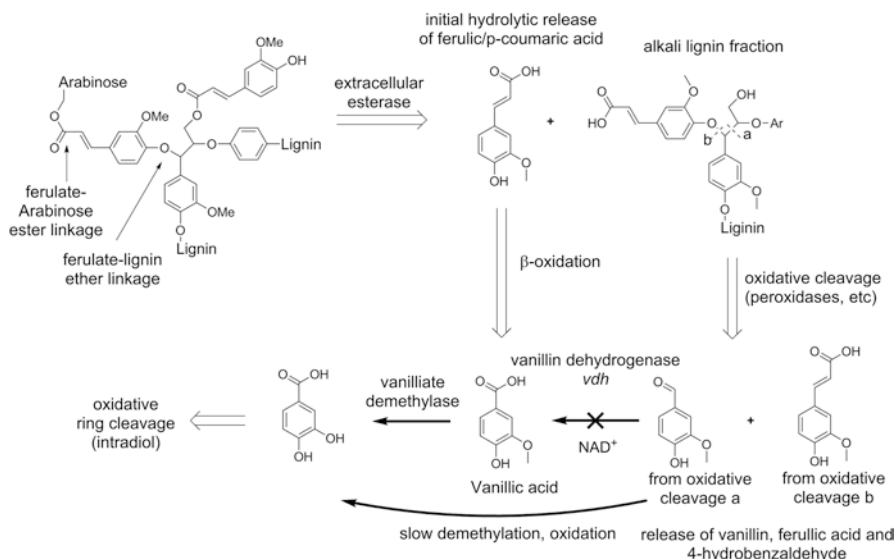
Fig. 6.2 Catabolic pathways of *R. jostii* RHA1 used for lignin depolymerisation. Italicised names are gene coding the elementary reaction involved. Vanillin accumulation is due to the aldehyde dehydrogenase gene *vdh* deletion (Adapted with permission from Sainsbury et al. [99]. Copyright 2013 American Chemical Society. NAD: Nicotinamide adenine dinucleotide)

PHA into *P. putida* at high concentration (0.252 g/L at 32 % cell dry weight). Mcl-PHA has a wide range of possible use, from depolymerisation to alkenoic acids, via the thermal pathway, to alkane productions; these reactions were reported in the article [101].

Vardon et al. highlighted an innovative pathway to produce fine chemicals from lignin [102]. Through genetic modification, the natural degradation pathway of bacterium *Pseudomonas putida* KT2440 was reshaped to yield the production of muconate. *P. putida* was engineered to transform lignin derived aromatics into catechol and to prevent muconate degradation (Fig. 6.3). Basically, the *pcaHG* gene that encodes the degradation of protocatechuate is replaced by *aroY*, a gene from another bacterium, *Enterobacter cloacae*, which allows decarboxylation instead. The genomic portion that promotes degradation of muconate is then deleted and the transformation of phenol to catechol is allowed through the addition of genomic material *dmpKLMNOP* from *Pseudomonas* sp. *CF600*. The overall production of muconate was reported to reach 0.70 g/L after 24 h [102].

Similarly, Johnson and Beckham reported on the genetic modification of *P. putida* to create pyruvate from lignin derivatives [103]. This was achieved by removing the undesired endogenous reactions in *P. putida*, the ortho (intradiol) degradation pathway of catechol and protocatechuate and replacing it with the meta (extradiol) cleavage, from another bacterium, *Sphingobium* sp.*,* to increase the production of pyruvate which is ultimately converted into L-lactate. To avoid the pyruvate from undergoing side reactions, the gene encoding pyruvate dehydrogenase
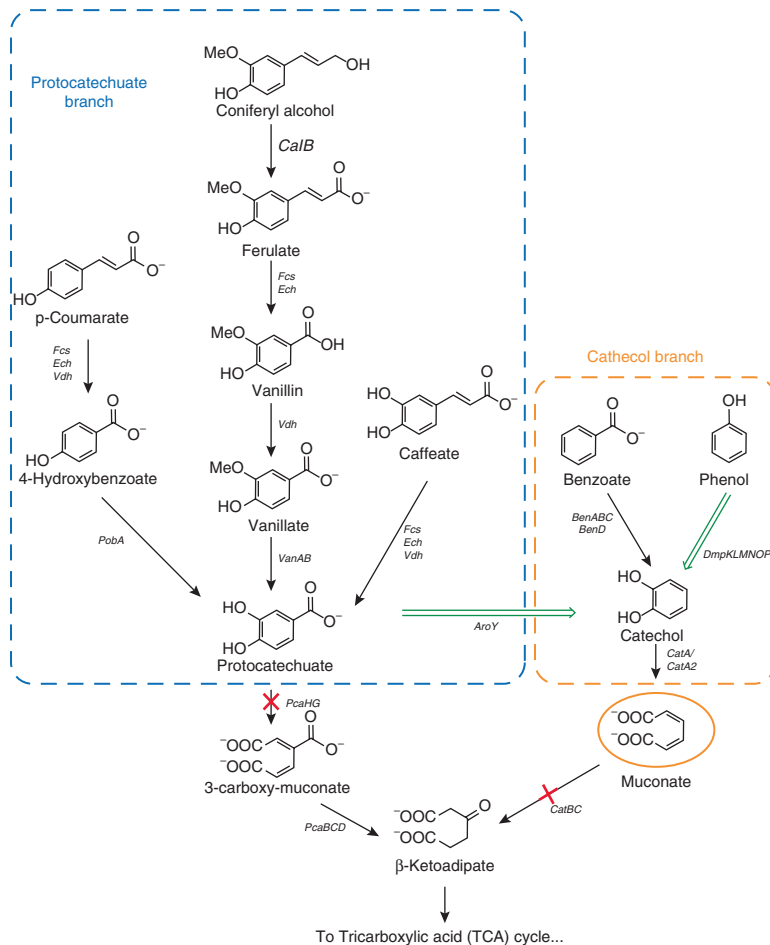
Fig. 6.3 Protocatechuate and catechol branch of the β-ketoadipate pathway in *P. putida* KT2440 disrupted by deletion of the genes encoding *PcaHG* and *CatBC* (*crossed arrow*). Italicised names are genes coding the elementary reaction involved. Insertion of genes encoding *AroY* and *DmpKLMNOP* (*double line arrow*) yielded muconate accumulation (Adapted from Vardon et al. 2015 [102] with permission of The Royal Society of Chemistry)

was deleted, preventing any reaction into acetyl-CoA. Moreover, the addition of an external genetic material coding bovine lactate dehydrogenase into *Pseudomonas putida* was part of a strategy to provide greater competition for pyruvate that might otherwise react within the TCA cycle. However, the efficiency of this method was only tested with lignin model compounds such as benzoate or *p*–coumarate. No experiments have been performed with lignin.

6.3.3   Perspectives

Delignification by bacteria is still very poorly understood and less studied than fungal degradation. An attractive strategy currently being explored is to rely on microbial consortia consisting of mixtures of bacteria and fungi to synergistically further lignin biodegradation [104, 105]. Another promising avenue to explore is the bacteria's bio-funnelling behaviour for chemical production. Through advances in genetic engineering, the synthesis of valuable products from lignin is now achievable; reactions rates, control of competitive reaction and selectivity will determine the economics.

6.4   Enzymatic Degradation

Both fungi and bacteria involve complex mechanisms of enzymes and intermediates to degrade lignin [13]. However, there is a major drawback for their deployment toward bio-refineries. The control over the inner process is poor and often non-existent, making it difficult to recover the intermediate species of interest. Using enzymes directly and individually in a controlled way is an attractive alternative to deconstructing the degradation process into elementary reactions, allowing a better understanding of the depolymerisation mechanisms and control, which can improve the isolation of the selected chemicals [106].

Enzymes are macro-proteins which can be described as biological catalysts of high selectivity. Each enzyme accepts a very defined range of substrates. Hence, to degrade the different lignin bonds, organisms require multiple types of enzymes classified into two families: peroxidases and laccases. Peroxidases represent a large group of enzymes involving hydrogen peroxide as the electron acceptor for the specific oxidative reaction they catalyse, such as lignin peroxidases (LiP, EC 1.11.1.14), manganese peroxidase (MnP, EC 1.11.1.13), versatile peroxidase (VP, EC 1.11.1.16), and horseradish peroxidase (HRP, EC 1.11.1.7). Peroxidases belong to the super family of heme-dependent peroxidases. Laccases represents the other major enzyme family for lignin degradation. (Lac, EC 1.10.3.2) Laccase forms its own group by itself belonging to the family of multidomain cupredoxin, and the superfamily of cupredoxins. Laccases use oxygen as electron acceptor. That process avoids any deactivation by hydrogen peroxide that sometimes happens with peroxide enzymes.

Lignolytic enzymes have complex mechanisms. Their origin, structure of substrate (type of lignin) and exterior condition play a major role in their actions. Laccase native from plants, for example, tend to polymerise lignin while fungal or bacterial laccase rather catalyse lignin degradation [107]. Laccases by themselves tend to polymerise low phenolic lignin [108–111] while depolymerisation is favoured with the presence of mediator molecules or with high phenolic ratio lignin [110–114]. Versatile peroxidase from *Pleurotus eryngii* have been demonstrated to polymerise low molecular weight compounds by inducing cross-linking [115].

Lignolytic enzymes can be produced by bacteria or fungi in a stimulating medium, then extracted, purified and concentrated. The optimisation of this costly

production influences industrial viability of enzyme processes. It has been well investigated along with improving enzymes performance (temperature stability, pH sensitivity, etc.) [116–121].
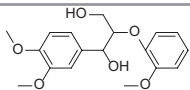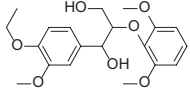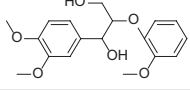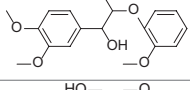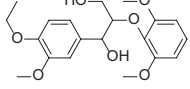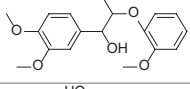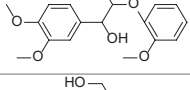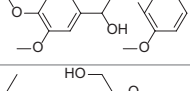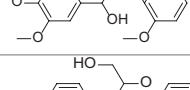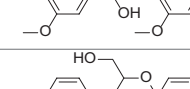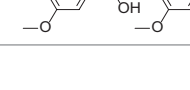
Enzymes can be considered for similar application as those of fungi or bacteria, such as delignification or waste treatment [122–127], but they also have been widely used to better understand the mechanism of lignin degradation by organisms. A series of model lignin molecules, each representing a specific bond in lignin (Fig. 6.1) have been investigated [128, 129].

6.4.1 Laccases

Laccase represents one of the most reported lignolytic enzymes in the literature [22, 130, 131]. For a long time, laccase was ignored for lignin degradation for two reasons: (i) *Phanerochaete chrysosporium*, considered a model lignin degrading organism was thought to be unable to produce laccase (ii) its low redox potential (0.5–0.8 V versus normal hydrogen electrode [6]) only allows it to oxidise a small portion of lignin components (the phenolic parts). The role of laccase in lignin degradation is now well demonstrated [17, 22, 128, 132, 133]. The laccase reaction happens around four different copper ions explaining its blue colour [6]. The indirect mechanism of degradation was highlighted in 1990 by Bourbonnais and Paice [132] which who showed the importance of small intermediate molecules, called mediators. Laccase uses molecular oxygen to oxidise the mediator, which then acts as chemical oxidant for lignin. This process allows enzymes to overcome their steric limitation that otherwise eliminates bulky molecules, such as lignin, as potential substrates. These intermediates allow laccases to overcome their phenolic-substrate restriction, thus expanding the range of potential oxidation of the enzyme. Laccase mediators are usually small phenolic compounds such as lignin phenolic components, vanillin, syringaldehyde, veratryl alcohol, or even synthetic mediators, 1-hydroxybenzotriazole (1-HBT), 2,2′-azinobis(3-ethylbenzthiazoline-6-sulphonate) (ABTS), 2,2,6,6-tetramethylpiperidine 1-oxyl (TEMPO), violuric acid (VLA) [134]. The choice of mediator can influence the oxidative potential of laccase and also induce stereo-preference in the substrate. Bohlin et al. showed laccase to exhibit different behaviours with a mixture of diastereoisomers of a β-O-4 model bond molecule [135]. The oxidation is maximum with HBT and shows no preferential isomer, while it is slightly lower with ABTS which exhibits the threo diastereoisomer to be less reactive than the erythro isomer.
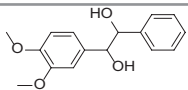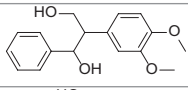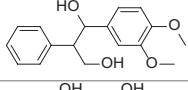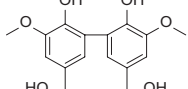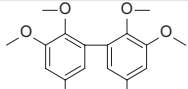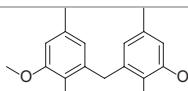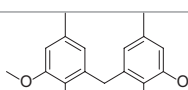
The source of laccase, the mediator and the substrate significantly influence the products and reaction rate. Heap et al. reported on the reaction between laccase from *Trametes versicolor* (white-rot fungus) and various model compounds of β-O-4 bonds with and without mediator [136]. For phenolics, dimerisation can happen with or without the mediator 1-HBT, while Cα oxidation (oxidation of the hydroxyl group on the α position to ketone, see Fig. 6.1b) proceeded with the two non-phenolic compounds (Table 6.5). Bond degradation can happen through ring cleavage for the most electron-rich aromatic ring dimer due to the addition of a

Table 6.5 Lignin model bond degradation conversion by enzymes

Bond	Molecule	Enzymes and conditions	Results	Ref.
Non phenolic β-O-4	*(structure)* diastereomer erythro and threo	Laccase with 1-HBT, TEMPO, ABSTS and VLA as mediators	HBT 55 % (o)	[135]
			TEMPO 41 % (o)	
			VLA 51 % (o)	
			ABTS 43 % (o) preferentially erythro	
	(structure)	Laccase 1-HBT as mediator	Aromatic ring (c), β-ether (c), Cα-Cβ (c), Cα (o)	[129]
	(structure)	Laccase 1-HBT as mediator	50 % (o).	[169]
	(structure)	Laccase with or without 1-HBT as mediator	Cα (o) with 1-HBT	[136]
	(structure)		Cα (o) and (c) with 1-HBT	
	(structure)	Lignin peroxidase H_2O_2	27 % (o).	[143]
	(structure)	Versatile peroxidase H_2O_2 and Mn^{2+}	19 % (c) & (o)	[148]
	(structure)	Versatile peroxidase	3 % Cα (o)	[170]
		Manganese peroxidase	4.5 % Cα (o)	
	(structure)	Manganese *meso*-tetra(*N*-methylpyridino) porphyrin pentaacetate	81 % (c). & (o).	[160]
Phenolic β-O-4	*(structure)*	Laccase with or without 1-HBT as mediator	(d) w/and w/o 1-HBT	[136]
	(structure)	Versatile peroxidase H_2O_2 and Mn^{2+}	65 % (c) & (o)	[148]

(continued)

Table 6.5 (continued)

Bond	Molecule	Enzymes and conditions	Results	Ref.
β-1		Laccase ABTS as mediator	60 % (o)	[169]
		Lignin peroxidase H$_2$O$_2$	46 % (c)	[141]
			39 % (c)	
5-5		Manganese *meso*-tetra(*N*-methylpyridino) porphyrin pentaacetate	93 % (c) & (o)	[160]
			73 % (c) & (o)	[165]
DPM			48 % (c) & (o)	[160]
			15 % (c) & (o)	[165]

ABTS 2,2′-azino-bis(3-ethylbenzothiazoline-6-sulphonic acid), *1-HBT* 1-Hydroxybenzotriazole, *TEMPO* 2,2,6,6-Tetramethyl-1-piperidinyloxy, *VLA* Violuric Acid, *DPM* Diphenyl Methane bond
(c): cleavage, (d): dimerisation, (o): oxidation

methoxy group; for both these non-phenolic molecules, the suppression of mediator prevents any reaction and yields unreacted dimers. The same couple laccase-HBT improved the saccharification of wheat straw. Combining 150 U/g of laccase with 5 % w/w 1-HBT as mediator increased the dilute acid pretreated wheat straw saccharification process by increasing the glucose concentration by 35 % (6.6–8.9 g/L) [136].

The degradation of the β-O-4 bonds were extensively studied as it is the most prevalent lignin bond. Kawai et al. reviewed the mechanism of a non-phenolic β-O-4 model bond, 1,3-dihydroxy-2-(2,6-dimethoxyphenoxy)-1-(4-ethoxy-3-methoxyphenyl)propane, to identify the resulting products [129, 137, 138]. After characterisation of the products, multiple reactions were identified. From 1000 nmol of initial β-O-4 model bond molecule, 120 nmol of products from Cα-Cβ cleavage (cleavage of the bond between carbon α and carbon β, see Fig. 6.1) were collected, along with 99 nmol from β-ether cleavage, 64 nmol from aromatic ring degradation and 43 nmol from Cα oxidation highlighting the complexity of enzymatic lignin degradation.

6.4.2   Peroxidases

Peroxidases represent the second main category of lignolytic enzymes. Lignin peroxidase (LiP), manganese peroxidase (MnP), versatile peroxidase (VP) and horseradish peroxidase (HRP) belong to this group, with a respective redox potential of 1.2 V, 0.8 V, 1.4 V and 0.95 V versus standard hydrogen electrode [6]. Their reaction mechanism are extensively described in two reviews [6, 139].

The high redox potential of lignin peroxidase allows it to oxidise both the phenolic and non-phenolic moieties of lignin. Its heme ion is a ferric one contained inside a ferric protoporphyrin [6]. In the past, lignin peroxidase was shown able to cleave the C-C bond in synthetic lignin[2] [140]. Lim and co-workers presented the C-C cleavage in different β-1 model bonds [141]. The different model bonds had various substituent groups on the two aromatic rings, and showed different reactivity towards lignin peroxidase, with a conversion ranging from 46 % for the less substituted dimer to 14 % for the dimer with two methoxy groups on each ring. A slight stereo-preference was also highlighted with erythro dimers preferred for degradation. Product analysis suggests a single electron transfer on one of the aromatic rings, followed by a Cα-Cβ cleavage.

Lignin peroxidase can degrade ether model bonds [142]. Lim et al. studied the action of lignin peroxidase of β-O-4 dimers and tetramers with different amounts of methoxy substituent on aromatic rings [143]. Similar to the β-1 bond models, the less substituted model underwent faster bond cleavage. The mechanism combines single electron transfer from dimer or trimer followed by bond cleavage. These two studies highlight different lignin degradation for the two different structures of lignin.

Manganese peroxidase is one of the most common lignolytic enzymes in organisms. It uses hydrogen peroxide just as LiP. Although it can function without [144], MnP requires manganese ions Mn^{2+} in solution to be fully efficient. In acidic medium, Mn(II) is oxidised by hydrogen peroxide, creating free Mn^{3+} ions which diffuse and oxidise the lignin phenolic moieties (Eq. 6.1). MnP structure is very similar to LiP, both having ferric ions in their heme group [6].

$$2Mn(II) + 2H^+ + H_2O_2 \rightleftharpoons 2Mn(III) + 2H_2O \qquad (6.1)$$
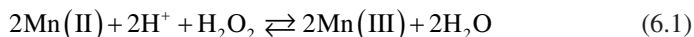
After reporting biobleaching abilities of *Bjerkandera* sp. strain BOS55 with a high concentration of MnP, Moreira et al. isolated this enzyme and tested it for delignification properties [145]. After 6 h, and under optimal conditions of pH, H_2O_2 and Mn^{2+}, a maximum reduction of kappa number of 13 % was obtained for eucalyptus

---

[2] Synthetic polymer is a polymer with structure similar to lignin. It can vary from simple polyphenol to more elaborate structure.

unbleached Kraft pulp. This work highlights the potential application of manganese peroxidase as a bio-bleaching additive.

Versatile peroxidase (VP) is another lignolytic enzyme that can be found in some lignin degrading fungi such as *Pleurotus eryngii* or *Bjerkandera* spp. [146]. Its high redox potential ($E^0 > +1.4$ V versus standard hydrogen electrode) allows it to accept a wide range of potential substrate compared to other lignolytic enzymes [6]. VP can degrade β-O-4 model bonds and synthetic lignin [147, 148]. Fernández-Fueyo and co-workers successfully isolated versatile peroxidase from *Pleurotus ostreatus* [147]. It was shown that this fungus lacked any lignin peroxidase activity; VP assumed this role instead. A phenolic β-O-4 model bond was exposed to VP and both Cα-Cβ cleavage and Cα oxidation occurred. A few products from Cβ-O-C$_4$ were detected. A significant depolymerisation was measured by gel permeation chromatography when the same enzyme was fed to synthetic lignin (dehydrogenation polymer).

Horseradish peroxidase (HRP) is considered to be part of the phenoloxidase responsible for lignin degradation [13]. However, it is also an important lignin and aromatic compounds polymerisation promoter [149, 150]. For that reason, HRP is usually considered as a polymerisation biocatalyst or as a lignin modifier agent [151, 152]. Xia et al. reported horseradish peroxidase to depolymerise two synthetic highly phenolic lignin-based polymers (lignophenols) [153]. Upon continuous addition of hydrogen peroxide, HRP degraded products at a yield of 17 % for lignocatechol and 33 % for lignocresol. Average molecular weight was significantly decreased by about 4–8 fold. For comparison laccase was able to degrade the two lignophenols but at lower conversions, probably due to a low activity of laccase on the lignin moieties in lignophenols.

6.4.3   Cocktails

From the research perspective, using only one type of enzyme with one well-defined substrate is ideal to elucidate the fundamental mechanism behind delignification and lignin degradation. However, it is a costly operation since it requires production and isolation of the enzyme. Millions of years of natural evolution have lead microorganisms to use not a single enzyme but a cocktail of enzymes to degrade lignin. Mixture of lignolytic enzymes might represent a cheaper and more effective alternative to achieve lignin degradation.

Schroyen and co-workers investigated peroxide enzyme VP from Bjerk*andera adusta* and laccase from *Trametes versicolor* to improve production of phenolic compounds and biomethane potential from various lignocellulosic substrates [154]. The two enzymes created a significant increase in phenolic compounds and showed potential as enzymatic pretreatment.

Afrida et al. studied extracellular enzymes from two fungi, *Irpex lacteus* KB-1.1 and *Lentinus tigrinus* LP-7 for biobleaching [155]. No separation, isolation or purification of those enzymes mixture was performed, allowing the full enzyme broth to

participate to biobleaching. After 4 days, the kappa number was reduced by 4.4% and 6.7%, respectively, while the combination of the two enzymes reduced the kappa number by up to 7.4%. This small improvement demonstrates a synergistic interaction between the extracellular enzymes and has applicability on the industrial scale to significantly decrease chlorine dioxide for bleaching. A similar study showed the use of xylanase and laccase to save 15% and 25% of ClO_2 respectively, even reaching 35% when used one after the other (xylanase then laccase) [127]. However, the co-operation of the two enzymes has not been investigated.

6.4.4 Bioinspired Enzyme-Like Synthetic Compounds

Enzyme production is often complex and costly, thus limiting industrial applications. After identification of lignin degrading enzymes in early 1980s in *Phanerochaete chrysosporium*, numerous research groups tried to biomimic these "ligninases", by synthesising competitive enzyme-like complexes. Zucca et al. brought these compounds back to the front scene with an extensive review [156]. Natural metalloporphines, such as hemin or heme group in hemoglobin, are well known to exhibit peroxidase or catalase-like activity and inspired research on new oxidation catalyst. The ferriheme in lignolytic peroxidases was shown to degrade high-potential lignin structure [156]. After several generations of synthetic heme groups, the stability became higher than enzymes with higher catalytic activity [156–159]. Immobilisation on clay or other substrate can significantly increase its stability [160, 161]. Metalloporphines quickly proved similar efficiency than enzymes at degrading common lignin model bond molecules [162–164], and even more. Compared to enzymes, the absence of protein scaffold reduced hindrance, allowing a wider range of substrate. Some lignin model bonds usually not considered for enzymatic degradation (e.g. 5–5, β-5, or diphenyl methane DPM bond) can be cleaved, oxidised or undergo ring cleavage reaction with metalloporphines [160, 165, 166].

Farell and Skerker analysed four metalloporphines/metalloporphyrin (Fig. 6.4) and their catalytic degradation of different model bonds [166]. Similar to natural enzymes, these biomimic catalysts were deactivated by high H_2O_2 concentration, and their activity was pH dependent. Veratryl alcohol, a typical substrate for lignolytic enzymes, could be readily oxidised by the two catalysts. Metalloporphine compound with iron metallic ion can oxidise β-1 and β-O-4 model bonds, but also induce C-C cleavage in β-5 model bond and aromatic ring cleavage in 5–5 model bonds, which has never been observed with enzyme of fungal systems. For metalloporphyrin with manganese for active centre, clear delignification was identified, with a reduction of 40% in the kappa number in just 15 min.

Crestini and co-workers highlighted the catalytic activity between manganese and iron porphyrin [165]. As Kraft lignin contains a significant amount of DPM and 5–5 substructure, two model molecules representing these bonds were studied for degradation. The manganese porphines exhibited higher conversions than the iron one, with a particular high activity for manganese *meso*-tetra(*N*-
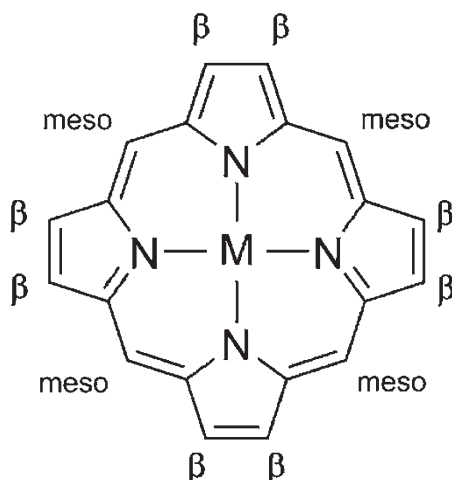
Fig. 6.4 Structure of a metalloporphine, M being the metallic ion, with the eight β positions and four meso one. IUPAC nomenclature [168] defines porphyrins as porphine derivatives where organic side chains are substituted for all the eight hydrogen atoms in the porphine pyrrole rings (the β positions). Although most of the synthetic heme catalysts are porphines by definition, they are nevertheless they are usually misleadingly referred as porhyrins [156]

methylpyridinio)porphine pentaacetate. Higher activity of Mn porphines was attributed to higher stability of these complexes. When residual Kraft lignin was submitted to the different catalysts, results indicated that manganese and iron porphines oxidised the lignin, but the latter induced a high amount of coupling reactions probably yielding higher molecular weight lignin. In general, manganese porphines proved superior to iron porphines for delignification and model bond cleavage.

A delignification of wood sawdust by metalled phthalocyanine or porphyrin was reported by Barbat and co-workers [167]. This pretreatment is considered for replacement of chemical process, sodium chlorite solution followed by alkaline extraction, for holocellulose recovery. Although this is a promising technique, with 1 % w/w phenolic compounds release from biomass, quantitative delignification amount has not been measured.

6.4.5 Perspectives

An emerging pathway for enzymes (natural or synthetic) is the catabolic treatment of biomass for delignification. To this end, enzymes represent a more manageable alternative to fungi or bacteria as their degradation mechanism is much simpler. Despite significant progress, there is still no commercial application of lignolytic enzymes for lignin degradation. The lack of efficient production systems and the poor understanding of the degradation pathways have prevented the development of efficient systems implementable on the industry industrial scale. A good

comprehension of the interaction mechanism between enzymes and the role of the different mediators (natural and synthetic) is needed for critical breakthrough in lignin bio-treatment. This knowledge can enable engineering microorganisms with high efficient lignin degradation properties tailored for specific industrial application, including fine chemical production.

6.5 Conclusion and Future Outlook

Lignin is the second most abundant polymer on earth, just behind cellulose. It represents a widely available, low cost and sustainable feedstock offering tremendous opportunities for the production of phenolic bio-based fine chemicals and monomers. Despite numerous studies devoted to its degradation, lignin still remains a most recalcitrant polymer to break down into oligomers and reproducible monomers. This is because of the multitude of chemical bonds involved and the variability of lignin chemical composition which is a function of the lignocellulosic source and the extraction process. This chapter has highlighted many of the shortcomings in fundamental knowledge restricting development; a methodical and comprehensive study on the principles and mechanism of biodegradation is required to unleash lignin as a controlled source for conversion into fine chemicals. Alternatives mimicking nature are of special interest. Many fungi and bacteria can degrade lignin, inspiring a plethora of schemes and processes for delignification and production of fine chemicals. Of those currently studied, white-rot fungi appear as the most promising delignification microorganism. The choice to genetic engineer – or not – has to be considered as it offers new routes for increased yields and selectivities needed for fine chemical production. Enzymatic degradation of lignin still faces high costs, low reaction rates, and poorly known bond selectivity. The inhibition mechanisms typical to enzymatic degradation are not well understood for "ligninases", as well as the effect of temperature resistant enzymes and reactions in a solvent. A promising avenue is to rely on enzyme cocktails or sequential enzymatic reaction schemes, because purification is typically an important cost of the process, and a wide array of products can be expected from lignin biodegradation into monomers/short oligomer due to the multitude of bonds. As lignin represents the best and most renewal natural source of phenol, it is well worth investing into the fundamental biodegradation studies that will lead to breakthroughs for process commercialization.

References

1. Zakzeski J, Bruijnincx PC, Jongerius AL, Weckhuysen BM. The catalytic valorization of lignin for the production of renewable chemicals. Chem Rev. 2010;110(6):3552–99.
2. Laurichesse S, Avérous L. Chemical modification of lignins: towards biobased polymers. Prog Polym Sci. 2014;39(7):1266–90.
3. Ludwig CH, Nist BJ, McCarthy JL. Lignin. XII. 1 the high resolution nuclear magnetic resonance spectroscopy of protons in compounds related to lignin. J Am Chem Soc. 1964;86(6):1186–96.
4. Nimz H. Beech lignin—proposal of a constitutional scheme. Angew Chem Int Ed Engl. 1974;13(5):313–21.
5. Himmel ME, Ding S-Y, Johnson DK, Adney WS, Nimlos MR, Brady JW, Foust TD. Biomass recalcitrance: engineering plants and enzymes for biofuels production. Science. 2007;315(5813):804–7.
6. Pollegioni L, Tonin F, Rosini E. Lignin‐degrading enzymes. FEBS J. 2015;282(7):1190–213.
7. Adler E. Lignin chemistry—past, present and future. Wood Sci Technol. 1977;11(3):169–218.
8. Hon DN-S, Shiraishi N. Wood and cellulosic chemistry, revised, and expanded. CRC Press; 2000.
9. Capanema EA, Balakshin MY, Kadla JF. Quantitative characterization of a hardwood milled wood lignin by nuclear magnetic resonance spectroscopy. J Agric Food Chem. 2005;53(25):9639–49.
10. Arora DK. Fungal biotechnology in agricultural, food, and environmental applications. New York: CRC Press; 2003.
11. Hibbett DS, Binder M, Bischoff JF, Blackwell M, Cannon PF, Eriksson OE, Huhndorf S, James T, Kirk PM, Lücking R, Thorsten Lumbsch H, Lutzoni F, Matheny PB, McLaughlin DJ, Powell MJ, Redhead S, Schoch CL, Spatafora JW, Stalpers JA, Vilgalys R, Aime MC, Aptroot A, Bauer R, Begerow D, Benny GL, Castlebury LA, Crous OW, Dai Y-C, Gams W, Geiser DM, Griffith GW, Gueidan C, Hawksworth DL, Hestmark G, Hosaka K, Humber RA, Hyde KD, Ironside JE, Kõljalg U, Kurtzman CP, Larsson K-H, Lichtwardt R, Longcore J, Miadlikowska J, Miller A, Moncalvo J-M, Mozley-Standridge S, Oberwinkler F, Parmasto E, Reeb V, Rogers JD, Roux C, Ryvarden L, Sampaio JP, Schüßler A, Sugiyama J, Thorn RG, Tibell L, Untereiner WA, Walker C, Wang Z, Weir A, Weiss M, White MM, Winka K, Yao Y-J, Zhang N. A higher-level phylogenetic classification of the Fungi. Mycol Res. 2007;111(5):509–47.
12. Atalla MM, Zeinab HK, Eman RH, Amani AY, Abeer A. Screening of some marine-derived fungal isolates for lignin degrading enzymes (LDEs) production. Agric Biol J N Am. 2010;1(4):591–9.
13. Leonowicz A, Matuszewska A, Luterek J, Ziegenhagen D, Wojtaś-Wasilewska M, Cho N-S, Hofrichter M, Rogalski J. Biodegradation of lignin by white-rot fungi. Fungal Genet Biol. 1999;27(2–3):175–85.
14. Salame TM, Knop D, Levinson D, Mabjeesh SJ, Yarden O, Hadar Y. Inactivation of a *Pleurotus ostreatus* versatile peroxidase‐encoding gene (mnp2) results in reduced lignin degradation. Environ Microbiol. 2014;16(1):265–77.
15. Bourdais A, Bidard F, Zickler D, Berteaux-Lecellier V, Silar P, Espagne E. Wood utilization is dependent on catalase activities in the filamentous fungus *Podospora anserina*. PLoS One. 2012;7(4):e29820.
16. Xie N, Ruprich‐Robert G, Silar P, Chapeland‐Leclerc F. Bilirubin oxidase‐like proteins from *Podospora anserina*: promising thermostable enzymes for application in transformation of plant biomass. Environ Microbiol. 2015;17(3):866–75.
17. Xie N, Chapeland‐Leclerc F, Silar P, Ruprich‐Robert G. Systematic gene deletions evidences that laccases are involved in several stages of wood degradation in the filamentous fungus *Podospora anserina*. Environ Microbiol. 2014;16(1):141–61.

18. Kirk TK, Chang H-M. Potential applications of bio-ligninolytic systems. Enzym Microb Technol. 1981;3(3):189–96.

19. van Kuijk SJA, Sonnenberg ASM, Baars JJP, Hendriks WH, Cone JW. Fungal treated ligno-cellulosic biomass as ruminant feed ingredient: a review. Biotechnol Adv. 2015;33(1):191–202.

20. Khan NA, Hussain S, Ahmad N, Alam S, Bezabhi M, Hendriks WH, Yu P, Cone JW. Improving the feeding value of straws with *Pleurotus ostreatus*. Anim Prod Sci. 2015;55(2):241–5.

21. Colavolpe MB, Albertó E. Cultivation requirements and substrate degradation of the edible mushroom *Gymnopilus pampeanus*-A novel species for mushroom cultivation. Sci Hortic. 2014;180:161–6.

22. Munk L, Sitarz AK, Kalyani DC, Mikkelsen JD, Meyer AS. Can laccases catalyze bond cleavage in lignin? Biotechnol Adv. 2015;33(1):13–24.

23. Priyadarshinee R, Kumar A, Mandal T, Dasguptamandal D. Improving the perspective of raw eucalyptus Kraft pulp for industrial applications through autochthonous bacterial mediated delignification. Ind Crop Prod. 2015;74:293–303.

24. Lund M, Ragauskas AJ. Enzymatic modification of Kraft lignin through oxidative coupling with water-soluble phenols. Appl Microbiol Biotechnol. 2001;55(6):699–703.

25. Moldes D, Vidal T. New possibilities of Kraft pulp biobleaching with laccase and sulfonated mediators. Process Biochem. 2011;46(3):656–60.

26. Gray KA, Zhao L, Emptage M. Bioethanol. Curr Opin Chem Biol. 2006;10(2):141–6.

27. Palli L, Gullotto A, Tilli S, Gori R, Lubello C, Scozzafava A. Effect of carbon source on the degradation of 2-naphthalenesulfonic acid polymers mixture by *Pleurotus ostreatus* in petro-chemical wastewater. Process Biochem. 2014;49(12):2272–8.

28. Shrestha P, Szaro TM, Bruns TD, Taylor JW. Systematic search for cultivatable fungi that best deconstruct cell walls of Miscanthus and sugarcane in the field. Appl Environ Microbiol. 2011;77(15):5490–504.

29. Kazi FK, Fortman J, Anex R, Kothandaraman G, Hsu D, Aden A, Dutta A. Techno-economic analysis of biochemical scenarios for production of cellulosic ethanol. NREL/TP-6A2-46588, National Renewable Energy Laboratory; June 2010; 2010

30. Klein‐Marcuschamer D, Oleskowicz‐Popiel P, Simmons BA, Blanch HW. The challenge of enzyme cost in the production of lignocellulosic biofuels. Biotechnol Bioeng. 2012;109(4):1083–7.

31. Shrestha P, Ibáñez AB, Bauer S, Glassman SI, Szaro TM, Bruns TD, Taylor JW. Fungi isolated from Miscanthus and sugarcane: biomass conversion, fungal enzymes, and hydrolysis of plant cell wall polymers. Biotechnol Biofuels. 2015;8(1):38.

32. Harmsen P, Huijgen W, Bermudez L, Bakker R. Literature review of physical and chemical pretreatment processes for lignocellulosic. Biomass. 2010; 1–49.

33. Donohoe BS, Decker SR, Tucker MP, Himmel ME, Vinzant TB. Visualizing lignin coalescence and migration through maize cell walls following thermochemical pretreatment. Biotechnol Bioeng. 2008;101(5):913–25.

34. Kumar P, Barrett DM, Delwiche MJ, Stroeve P. Methods for pretreatment of lignocellulosic biomass for efficient hydrolysis and biofuel production. Ind Eng Chem Res. 2009;48(8):3713–29.

35. McMillan JD. Pretreatment of lignocellulosic biomass. In: ACS symposium series (USA), 1994.

36. Agbor VB, Cicek N, Sparling R, Berlin A, Levin DB. Biomass pretreatment: fundamentals toward application. Biotechnol Adv. 2011;29(6):675–85.

37. Alvira P, Tomás-Pejó E, Ballesteros M, Negro MJ. Pretreatment technologies for an efficient bioethanol production process based on enzymatic hydrolysis: a review. Bioresour Technol. 2010;101(13):4851–61.

38. Castoldi R, Bracht A, de Morais GR, Baesso ML, Correa RCG, Peralta RA, Moreira RDFPM, Polizeli MDLTDM, de Souza CGM, Peralta RM. Biological pretreatment of *Eucalyptus grandis* sawdust with white-rot fungi: study of degradation patterns and saccharification kinetics. Chem Eng J. 2014;258:240–6.

39. Ge X, Matsumoto T, Keith L, Li Y. Fungal pretreatment of albizia chips for enhanced biogas production by solid-state anaerobic digestion. Energy Fuels. 2015;29(1):200–4.

40. Kamei I, Hirota Y, Mori T, Hirai H, Meguro S, Kondo R. Direct ethanol production from cellulosic materials by the hypersaline-tolerant white-rot fungus *Phlebia* sp. MG-60. Bioresour Technol. 2012;112:137–42.

41. Kamei I, Hirota Y, Meguro S. Integrated delignification and simultaneous saccharification and fermentation of hard wood by a white-rot fungus, *Phlebia* sp. MG-60. Bioresour Technol. 2012;126:137–41.

42. Khuong LD, Kondo R, De Leon R, Anh TK, Meguro S, Shimizu K, Kamei I. Effect of chemical factors on integrated fungal fermentation of sugarcane bagasse for ethanol production by a white-rot fungus, *Phlebia* sp. MG-60. Bioresour Technol. 2014;167:33–40.

43. Xie S, Qin X, Cheng Y, Laskar D, Qiao W, Sun S, Reyes LH, Wang X, Dai SY, Sattler SE, Kao K, Yang B, Zhang X, Yuan J. Simultaneous conversion of all cell wall components by an oleaginous fungus without chemi-physical pretreatment. Green Chem. 2015;17(3):1657–67.

44. Baker PW, Charlton A, Hale MD. Increased delignification by white-rot fungi after pressure refining Miscanthus. Bioresour Technol. 2015;189:81–6.

45. Gustafsson J, Lehto JH, Tienvieri T, Ciovica L, Peltonen J. Surface characteristics of thermo-mechanical pulps; the influence of defibration temperature and refining. Colloids Surf A Physicochem Eng Asp. 2003;225(1–3):95–104.

46. Khuong LD, Kondo R, De Leon R, Anh TK, Shimizu K, Kamei I. Bioethanol production from alkaline-pretreated sugarcane bagasse by consolidated bioprocessing using *Phlebia* sp. MG-60. Int Biodeterior Biodegrad. 2014;88:62–8.

47. Cook C, Francocci F, Cervone F, Bellincampi D, Bolwell PG, Ferrari S, Devoto A. Combination of pretreatment with white-rot fungi and modification of primary and secondary cell walls improves saccharification. Bioenergy Res. 2015;8(1):175–86.

48. Giles RL, Galloway ER, Zackeru JC, Naithani V, Parrow MW. Two stage fungal biopulping solubilizes lignocellulosic carbohydrates without supplemental enzymatic hydrolysis. Int Biodeterior Biodegrad. 2014;86:265–71.

49. Giles RL, Zackeru JC, Galloway ER, Elliott GD, Parrow MW. Single versus simultaneous species treatment of wood with *Ceriporiopsis subvermispora* and *Postia placenta* for ethanol applications, with observations on interspecific growth inhibition. Int Biodeterior Biodegrad. 2015;99:66–72.

50. Ma K, Ruan Z. Production of a lignocellulolytic enzyme system for simultaneous biodelignification and saccharification of corn stover employing co-culture of fungi. Bioresour Technol. 2015;175:586–93.

51. Gai YP, Zhang WT, Mu ZM, Ji XL. Involvement of ligninolytic enzymes in degradation of wheat straw by *Trametes trogii*. J Appl Microbiol. 2014;117(1):85–95.

52. Liu L, Qian C, Jiang L, Yu H-Q. Direct three-dimensional characterization and multiscale visualization of wheat straw deconstruction by white-rot fungus. Environ Sci Technol. 2014;48(16):9819–25.

53. TAPPI. Acid-insoluble lignin in wood and pulp. T222 om-88. Atlanta: TAPPI Press; 1988.

54. Sluiter A, Hames B, Ruiz R, Scarlata C, Sluiter J, Templeton D, Crocker D. Determination of structural carbohydrates and lignin in biomass. Version 2010. National Renewable Energy Laboratory, USA; 2008.

55. Kirk TK, Obst JR. Lignin determination. In: Methods in enzymology-biomass, part b, lignin, pectin, and chitin. vol 161. Academic Press. Inc.;1988. p. 87–101.

56. Deswal D, Gupta R, Nandal P, Kuhad RC. Fungal pretreatment improves amenability of lignocellulosic material for its saccharification to sugars. Carbohydr Polym. 2014;99:264–9.

57. Knežević A, Milovanović I, Stajić M, Lončar N, Brčeski I, Vukojević J, Ćilerdžić J. Lignin degradation by selected fungal species. Bioresour Technol. 2013;138:117–23.

58. Karp SG, Faraco V, Amore A, Letti LAJ, Soccol VT, Soccol CR. Statistical optimization of laccase production and delignification of sugarcane bagasse by *Pleurotus ostreatus* in solid-state fermentation. BioMed Res Int. 2015;12(16):19.

59. Knežević A, Milovanović I, Stajić M, Vukojević J. Potential of *Trametes* species to degrade lignin. Int Biodeterior Biodegrad. 2013;85:52–6.
60. Van Soest PJ, Robertson JB, Lewis BA. Methods for dietary fiber, neutral detergent fiber, and nonstarch polysaccharides in relation to animal nutrition. J Dairy Sci. 1991;74(10):3583–97.
61. López MJ, Suárez-Estrella F, Vargas-García MC, López-González JA, Verstichel S, Debeer L, Wierinck I, Moreno J. Biodelignification of agricultural and forest wastes: effect on anaerobic digestion. Biomass Bioenergy. 2013;58:343–9.
62. Liu S, Wu S, Pang C, Li W, Dong R. Microbial pretreatment of corn stovers by solid-state cultivation of *Phanerochaete chrysosporium* for biogas production. Appl Biochem Biotechnol. 2014;172(3):1365–76.
63. TAPPI. Kappa number of pulp. T236 cm-85. Atlanta: TAPPI Press; 1985.
64. Singh P, Sulaiman O, Hashim R, Peng LC, Singh RP. Evaluating biopulping as an alternative application on oil palm trunk using the white-rot fungus *Trametes versicolor*. Int Biodeterior Biodegrad. 2013;82:96–103.
65. Fukushima RS, Hatfield RD. Extraction and isolation of lignin for utilization as a standard to determine lignin concentration using the acetyl bromide spectrophotometric method. J Agric Food Chem. 2001;49(7):3133–9.
66. Ghorbani F, Karimi M, Biria D, Kariminia H, Jeihanipour A. Enhancement of fungal delignification of rice straw by *Trichoderma viride* sp. to improve its saccharification. Biochem Eng J. 2015;101:77–84.
67. Cianchetta S, Di Maggio B, Burzi PL, Galletti S. Evaluation of selected white-rot fungal isolates for improving the sugar yield from wheat straw. Appl Biochem Biotechnol. 2014;173(2):609–23.
68. Mohanram S, Rajan K, Carrier DJ, Nain L, Arora A. Insights into biological delignification of rice straw by *Trametes hirsuta* and *Myrothecium roridum* and comparison of saccharification yields with dilute acid pretreatment. Biomass Bioenergy. 2015;76:54–60.
69. Haroune L, Saibi S, Bellenger J-P, Cabana H. Evaluation of the efficiency of *Trametes hirsuta* for the removal of multiple pharmaceutical compounds under low concentrations relevant to the environment. Bioresour Technol. 2014;171:199–202.
70. García-Delgado C, Alfaro-Barta I, Eymar E. Combination of biochar amendment and mycoremediation for polycyclic aromatic hydrocarbons immobilization and biodegradation in creosote-contaminated soil. J Hazard Mater. 2015;285:259–66.
71. Namhyun C, Lee I-S, Song H-S, Bang W-G. Mechanisms used by white-rot fungus to degrade lignin and toxic chemicals. J Microbiol Biotechnol. 2000;10(6):737–52.
72. Han Y, Shi L, Meng J, Yu H, Zhang X. Azo dye biodecolorization enhanced by *Echinodontium taxodii* cultured with lignin. PLoS ONE. 2014;9(10):7185–8.
73. Martin C, Manzanares P. A study of the decolourization of straw soda-pulping effluents by *Trametes versicolor*. Bioresour Technol. 1994;47(3):209–14.
74. Falconnier B, Lapierre C, Lesage-Meessen L, Yonnet G, Brunerie P, Colonna-Ceccaldi B, Corrieu G, Asther M. Vanillin as a product of ferulic acid biotransformation by the white-rot fungus *Pycnoporus cinnabarinus* I-937: identification of metabolic pathways. J Biotechnol. 1994;37(2):123–32.
75. Zou L, Ross BM, Hutchison LJ, Christopher LP, Dekker RF, Malek L. Fungal demethylation of Kraft lignin. Enzym Microb Technol. 2015;73:44–50.
76. Qin J, Woloctt M, Zhang J. Use of polycarboxylic acid derived from partially depolymerized lignin as a curing agent for epoxy application. ACS Sustain Chem Eng. 2014;2(2):188–93.
77. Hilburg SL, Elder AN, Chung H, Ferebee RL, Bockstaller MR, Washburn NR. A universal route towards thermoplastic lignin composites with improved mechanical properties. Polymer (United Kingdom). 2014;55(4):995–1003.
78. Brun S, Malagnac F, Bidard F, Lalucque H, Silar P. Functions and regulation of the Nox family in the filamentous fungus *Podospora anserina*: a new role in cellulose degradation. Mol Microbiol. 2009;74(2):480–96.

79. Bugg TDH, Ahmad M, Hardiman EM, Singh R. The emerging role for bacteria in lignin degradation and bio-product formation. Curr Opin Biotechnol. 2011;22(3):394–400.

80. Singh A, Singh DP, Tiwari R, Kumar K, Singh RV, Singh S, Prasanna R, Saxena AK, Nain L. Taxonomic and functional annotation of gut bacterial communities of *Eisenia foetida* and *Perionyx excavatus*. Microbiol Res. 2015;175:48–56.

81. Tian J-H, Pourcher A-M, Bouchez T, Gelhaye E, Peu P. Occurrence of lignin degradation genotypes and phenotypes among prokaryotes. Appl Microbiol Biotechnol. 2014;98(23):9527–44.

82. Brown ME, Chang MCY. Exploring bacterial lignin degradation. Curr Opin Chem Biol. 2014;19(1):1–7.

83. Ahmad M, Taylor CR, Pink D, Burton K, Eastwood D, Bending GD, Bugg TDH. Development of novel assays for lignin degradation: comparative analysis of bacterial and fungal lignin degraders. Mol Biosys. 2010;6(5):815–21.

84. Mathews SL, Pawlak J, Grunden AM. Bacterial biodegradation and bioconversion of industrial lignocellulosic streams. Appl Microbiol Biotechnol. 2015;99(7):2939–54.

85. L-y C, Y-h C, C-j T, Yang Z-h, Zheng Y, Shi Y. Depolymerization and decolorization of Kraft lignin by bacterium *Comamonas* sp. B-9. Appl Microbiol Biotechnol. 2014;98(4):1907–12.

86. Chang Y-C, Choi D, Takamizawa K, Kikuchi S. Isolation of *Bacillus* sp. strains capable of decomposing alkali lignin and their application in combination with lactic acid bacteria for enhancing cellulase performance. Bioresour Technol. 2014;152:429–36.

87. Haq I, Kumar S, Kumari V, Singh SK, Raj A. Evaluation of bioremediation potentiality of ligninolytic *Serratia liquefaciens* for detoxification of pulp and paper mill effluent. J Hazard Mater. 2016;305:190–9.

88. Buraimoh OM, Ilori MO, Amund OO, Michel FC, Grewal SK. Assessment of bacterial degradation of lignocellulosic residues (sawdust) in a tropical estuarine microcosm using improvised floating raft equipment. Int Biodeterior Biodegrad. 2015;104:186–93.

89. Liang J, Peng X, Yin D, Li B, Wang D, Lin Y. Screening of a microbial consortium for highly simultaneous degradation of lignocellulose and chlorophenols. Bioresour Technol. 2015;190:381–7.

90. Gellerstedt G. Softwood Kraft lignin: raw material for the future. Ind Crop Prod. 2015;77:845–54.

91. Shi Y, Chai L, Tang C, Yang Z, Zheng Y, Chen Y, Jing Q. Biochemical investigation of Kraft lignin degradation by *Pandoraea* sp. B-6 isolated from bamboo slips. Bioprocess Biosyst Eng. 2013;36(12):1957–65.

92. Shi Y, Chai L, Tang C, Yang Z, Zhang H, Chen R, Chen Y, Zheng Y. Characterization and genomic analysis of Kraft lignin biodegradation by the beta-proteobacterium *Cupriavidus basilensis* B-8. Biotechnol Biofuels. 2013;6(1):1.

93. Chen Y, Chai L, Tang C, Yang Z, Zheng Y, Shi Y, Zhang H. Kraft lignin biodegradation by *Novosphingobium* sp. B-7 and analysis of the degradation process. Bioresour Technol. 2012;123:682–5.

94. Kumar M, Singhal A, Thakur IS. Comparison of submerged and solid state pretreatment of sugarcane bagasse by *Pandoraea* sp. ISTKB: enzymatic and structural analysis. Bioresour Technol. 2016;203:18–25.

95. Huang XF, Santhanam N, Badri DV, Hunter WJ, Manter DK, Decker SR, Vivanco JM, Reardon KF. Isolation and characterization of lignin‐degrading bacteria from rainforest soils. Biotechnol Bioeng. 2013;110(6):1616–26.

96. Chen J, Xu L, Wu Y, Tong J, Chen Y. Production, characterization of acetyl esterase from a rumen bacteria strain RB3, and application potential of the strain in biodegradation of crop residues. Renew Energy. 2014;68:134–9.

97. Singhal A, Jaiswal PK, Thakur IS. Biopulping of bagasse by *Cryptococcus albidus* under partially sterilized conditions. Int Biodeterior Biodegrad. 2015;97:143–50.

98. Salvachúa D, Karp EM, Nimlos CT, Vardon DR, Beckham GT. Towards lignin consolidated bioprocessing: simultaneous lignin depolymerization and product generation by bacteria. Green Chem. 2015;17(11):4951–67.

99. Sainsbury PD, Hardiman EM, Ahmad M, Otani H, Seghezzi N, Eltis LD, Bugg TDH. Breaking down lignin to high-value chemicals: the conversion of lignocellulose to vanillin in a gene deletion mutant of *Rhodococcus jostii* RHA1. ACS Chem Biol. 2013;8(10):2151–6.

100. Graf N, Wenzel M, Altenbuchner J. Identification and characterization of the vanillin dehydrogenase YfmT in *Bacillus subtilis* 3NA. Appl Microbiol Biotechnol. 2016;100(8):3511–21.

101. Linger JG, Vardon DR, Guarnieri MT, Karp EM, Hunsinger GB, Franden MA, Johnson CW, Chupka G, Strathmann TJ, Pienkos PT. Lignin valorization through integrated biological funneling and chemical catalysis. Proc Natl Acad Sci U S A. 2014;111(33):12013–8.

102. Vardon DR, Franden MA, Johnson CW, Karp EM, Guarnieri MT, Linger JG, Salm MJ, Strathmann TJ, Beckham GT. Adipic acid production from lignin. Energy Environ Sci. 2015;8(2):617–28.

103. Johnson CW, Beckham GT. Aromatic catabolic pathway selection for optimal production of pyruvate and lactate from lignin. Metab Eng. 2015;28:240–7.

104. Jiménez DJ, Dini-Andreote F, Van Elsas JD. Metataxonomic profiling and prediction of functional behaviour of wheat straw degrading microbial consortia. Biotechnol Biofuels. 2014;7(1):1–18.

105. Brzonova I, Kozliak E, Kubátová A, Chebeir M, Qin W, Christopher L, Ji Y. Kenaf biomass biodecomposition by basidiomycetes and actinobacteria in submerged fermentation for production of carbohydrates and phenolic compounds. Bioresour Technol. 2014;173:352–60.

106. Bugg TDH, Rahmanpour R. Enzymatic conversion of lignin into renewable chemicals. Curr Opin Chem Biol. 2015;29:10–7.

107. Awasthi M, Jaiswal N, Singh S, Pandey VP, Dwivedi UN. Molecular docking and dynamics simulation analyses unraveling the differential enzymatic catalysis by plant and fungal laccases with respect to lignin biosynthesis and degradation. J Biomol Struct Dyn. 2015;33(9):1835–49.

108. Grönqvist S, Viikari L, Niku-Paavola M-L, Orlandi M, Canevali C, Buchert J. Oxidation of milled wood lignin with laccase, tyrosinase and horseradish peroxidase. Appl Microbiol Biotechnol. 2005;67(4):489–94.

109. Areskogh D, Li J, Gr G, Henriksson G. Investigation of the molecular weight increase of commercial lignosulfonates by laccase catalysis. Biomacromolecules. 2010;11(4):904–10.

110. Shleev S, Persson P, Shumakovich G, Mazhugo Y, Yaropolov A, Ruzgas T, Gorton L. Interaction of fungal laccases and laccase-mediator systems with lignin. Enzym Microb Technol. 2006;39(4):841–7.

111. Kondo R, Iimori T, Imamura H, Nishida T. Polymerization of DHP and depolymerization of DHP-glucoside by lignin oxidizing enzymes. J Biotechnol. 1990;13(2–3):181–8.

112. Xia Z, Yoshida T, Funaoka M. Enzymatic synthesis of polyphenols from highly phenolic lignin-based polymers (lignophenols). Biotechnol Lett. 2003;25(1):9–12.

113. Fernaud JRH, Carnicero A, Perestelo F, Cutuli MH, Arias E, Falcón MA. Upgrading of an industrial lignin by using laccase produced by *Fusarium proliferatum* and different laccase-mediator systems. Enzym Microb Technol. 2006;38(1–2):40–8.

114. Eggert C, Temp U, Dean JFD, Eriksson K-EL. A fungal metabolite mediates degradation of non-phenolic lignin structures and synthetic lignin by laccase. Febs Lett. 1996;391(1–2):144–8.

115. Salvachúa D, Prieto A, Mattinen M-L, Tamminen T, Liitiä T, Lille M, Willför S, Martínez AT, Martínez MJ, Faulds CB. Versatile peroxidase as a valuable tool for generating new biomolecules by homogeneous and heterogeneous cross-linking. Enzym Microb Technol. 2013;52(6–7):303–11.

116. Yamasaki Y, Yamaguchi M, Yamagishi K, Hirai H, Kondo R, Kamei I, Meguro S. Expression of a manganese peroxidase isozyme 2 transgene in the ethanologenic white-rot fungus *Phlebia* sp. *strain* MG-60. SpringerPlus. 2014;3(1):699.

117. Vaithanomsat P, Sangnam A, Boonpratuang T, Choeyklin R, Promkiam-on P, Chuntranuluck S, Kreetachat T. Wood degradation and optimized laccase production by *Resupinate* white-rot fungi in Northern Thailand. BioResources. 2013;8(4):6342–60.

118. Feng H, Zhang D, Sun Y, Zhi Y, Mao L, Luo Y, Xu L, Wang L, Zhou P. Expression and characterization of a recombinant laccase with alkalistable and thermostable properties from *Streptomyces griseorubens* JSD-1. Appl Biochem Biotechnol. 2015;176(2):547–62.

119. Kannaiyan R, Mahinpey N, Kostenko V, Martinuzzi RJ. Nutrient media optimization for simultaneous enhancement of the laccase and peroxidases production by coculture of *Dichomitus squalens* and *Ceriporiopsis subvermispora*. Biotechnol Appl Biochem. 2015;62(2):173–85.

120. Lim S-J, Jeon S-J. Optimal conditions for laccase production from the white-rot fungus *Marasmius scorodonius*. Korean J Microbiol Biotechnol. 2014;42(3):225–31.

121. Gorska EB, Jankiewicz U, Dobrzynski J, Galazka A, Sitarek M, Gozdowski D, Russel S, Kowalczyk P. Production of ligninolytic enzymes by cultures of white-rot fungi. Pol J Microbiol. 2014;63(4):461–5.

122. Yadav M, Yadav HS. Applications of ligninolytic enzymes to pollutants, wastewater, dyes, soil, coal, paper and polymers. Environ Chem Lett. 2015;13(3):309–18.

123. Chandrasekaran G, Choi S-K, Lee Y-C, Kim G-J, Shin H-J. Oxidative biodegradation of single-walled carbon nanotubes by partially purified lignin peroxidase from *Sparassis latifolia* mushroom. J Ind Eng Chem. 2014;20(5):3367–74.

124. Moreira S, Milagres AMF, Mussatto SI. Reactive dyes and textile effluent decolorization by a mediator system of salt-tolerant laccase from *Peniophora cinerea*. Sep Purif Technol. 2014;135:183–9.

125. Kuhar F, Castiglia V, Levin L. Enhancement of laccase production and malachite green decolorization by co-culturing Ganoderma lucidum and *Trametes versicolor* in solid-state fermentation. Int Biodeterior Biodegrad. 2015;104:238–43.

126. Inoue S, Igarashi Y, Yoneda Y, Kawai S, Okamura H, Nishida T. Elimination and detoxification of fungicide miconazole and antidepressant sertraline by manganese peroxidase-dependent lipid peroxidation system. Int Biodeterior Biodegrad. 2015;100:79–84.

127. Sharma A, Thakur VV, Shrivastava A, Jain RK, Mathur RM, Gupta R, Kuhad RC. Xylanase and laccase based enzymatic Kraft pulp bleaching reduces adsorbable organic halogen (AOX) in bleach effluents: a pilot scale study. Bioresour Technol. 2014;169:96–102.

128. Kawai S, Umezawa T, Higuchi T. Degradation mechanisms of phenolic β-1 lignin substructure model compounds by laccase of *Coriolus versicolor*. Arch Biochem Biophys. 1988;262(1):99–110.

129. Kawai S, Nakagawa M, Ohashi H. Degradation mechanisms of a nonphenolic β-O-4 lignin model dimer by *Trametes versicolor* laccase in the presence of 1-hydroxybenzotriazole. Enzym Microb Technol. 2002;30(4):482–9.

130. Youn H-D, Hah YC, Kang S-O. Role of laccase in lignin degradation by white-rot fungi. FEMS Microbiol Lett. 1995;132(3):183–8.

131. Mayer AM, Staples RC. Laccase: new functions for an old enzyme. Phytochemistry. 2002;60(6):551–65.

132. Bourbonnais R, Paice MG. Oxidation of non-phenolic substrates: an expanded role for laccase in lignin biodegradation. FEBS Lett. 1990;267(1):99–102.

133. Ander P, Eriksson K-E. The importance of phenol oxidase activity in lignin degradation by the white-rot fungus *Sporotrichum pulverulentum*. Arch Microbiol. 1976;109(1–2):1–8.

134. Moldes D, Díaz M, Tzanov T, Vidal T. Comparative study of the efficiency of synthetic and natural mediators in laccase-assisted bleaching of eucalyptus Kraft pulp. Bioresour Technol. 2008;99(17):7959–65.

135. Bohlin C, Andersson P-O, Lundquist K, Jönsson LJ. Differences in stereo-preference in the oxidative degradation of diastereomers of the lignin model compound 1-(3, 4-dimethoxyphenyl)-2-(2-methoxyphenoxy)-1, 3-propanediol with enzymic and non-enzymic oxidants. J Mol Catal B Enzym. 2007;45(1–2):21–6.

136. Heap L, Green A, Brown D, Van Dongen B, Turner N. Role of laccase as an enzymatic pretreatment method to improve lignocellulosic saccharification. Catal Sci Technol. 2014;4(8):2251–9.

137. Kawai S, Asukai M, Ohya N, Okita K, Ito T, Ohashi H. Degradation of a non-phenolic β-O-4 substructure and of polymeric lignin model compounds by laccase of *Coriolus versicolor* in the presence of 1-hydroxybenzotriazole. FEMS Microbiol Lett. 1999;170(1):51–7.

138. Kawai S, Nakagawa M, Ohashi H. Aromatic ring cleavage of a non-phenolic β-O-4 lignin model dimer by laccase of *Trametes versicolor* in the presence of 1-hydroxybenzotriazole. FEBS Lett. 1999;446(2–3):355–8.

139. Wong DWS. Structure and action mechanism of ligninolytic enzymes. Appl Biochem Biotechnol. 2009;157(2):174–209.

140. Hammel KE, Jensen K, Mozuch MD, Landucci LL, Tien M, Pease EA. Ligninolysis by a purified lignin peroxidase. J Biol Chem. 1993;268(17):12274–81.

141. Lim SH, Lee WS, Kim Y-I, Sohn Y, Cho DW, Kim C, Kim E, Latham JA, Dunaway-Mariano D, Mariano PS. Photochemical and enzymatic SET promoted C–C bond cleavage reactions of lignin β-1 model compounds containing varying number of methoxy substituents on their arene rings. Tetrahedron. 2015;71(24):4236–47.

142. Baciocchi E, Fabbri C, Lanzalunga O. Lignin peroxidase-catalyzed oxidation of nonphenolic trimeric lignin model compounds: fragmentation reactions in the intermediate radical cations. J Org Chem. 2003;68(23):9061–9.

143. Lim SH, Nahm K, Ra CS, Cho DW, Yoon UC, Latham JA, Dunaway-Mariano D, Mariano PS. Effects of alkoxy groups on arene rings of lignin β-O-4 model compounds on the efficiencies of single electron transfer-promoted photochemical and enzymatic C–C bond cleavage reactions. J Org Chem. 2013;78(18):9431–43.

144. Moreira MT, Feijoo G, Mester T, Mayorga P, Sierra-Alvarez R, Field JA. Role of organic acids in the manganese-independent biobleaching system of *Bjerkandera* sp. strain BOS55. Appl Environ Microbiol. 1998;64(7):2409–17.

145. Moreira MT, Sierra-Alvarez R, Lema JM, Feijoo G, Field J. Oxidation of lignin in eucalyptus Kraft pulp by manganese peroxidase from *Bjerkandera* sp. strain BOS55. Bioresour Technol. 2001;78(1):71–9.

146. Hofrichter M, Ullrich R, Pecyna MJ, Liers C, Lundell T. New and classic families of secreted fungal heme peroxidases. Appl Microbiol Biotechnol. 2010;87(3):871–97.

147. Fernández-Fueyo E, Ruiz-Dueñas FJ, Martínez MJ, Romero A, Hammel KE, Medrano FJ, Martínez AT. Ligninolytic peroxidase genes in the oyster mushroom genome: heterologous expression, molecular structure, catalytic and stability properties, and lignin-degrading ability. Biotechnol Biofuels. 2014; 7(3).

148. Caramelo L, Martínez MJ, Martínez ÁT. A search for ligninolytic peroxidases in the fungus *Pleurotus eryngii* involving α-Keto-γ-thiomethylbutyric acid and lignin model dimers. Appl Environ Microbiol. 1999;65(3):916–22.

149. Guerra A, Ferraz A, Cotrim AR, Da Silva FT. Polymerization of lignin fragments contained in a model effluent by polyphenoloxidases and horseradish peroxidase/hydrogen peroxide system. Enzym Microb Technol. 2000;26(5–6):315–23.

150. SCtälä H, Pajunen A, Rummakko P, Sipilä J, Brunow G. A novel type of spiro compound formed by oxidative cross coupling of methyl sinapate with a syringyl lignin model compound. A model system for the β-1 pathway in lignin biosynthesis. J Chem Soc Perkin Trans. 1999;1(4):461–4.

151. Liu R, Dong A, Fan X, Wang Q, Yu Y, Cavaco-Paulo A. HRP-mediated polyacrylamide graft modification of raw jute fabric. J Mol Catal B Enzym. 2015;116:29–38.

152. Zhou H, Chang Y, Wu X, Yang D, Qiu X. Horseradish peroxidase modification of sulfomethylated wheat straw alkali lignin to improve its dispersion performance. ACS Sustain Chem Eng. 2015;3(3):518–23.

153. Xia Z, Yoshida T, Funaoka M. Enzymatic degradation of highly phenolic lignin-based polymers (lignophenols). Eur Polym J. 2003;39(5):909–14.

154. Schroyen M, Vervaeren H, Vandepitte H, Van Hulle SWH, Raes K. Effect of enzymatic pretreatment of various lignocellulosic substrates on production of phenolic compounds and biomethane potential. Bioresour Technol. 2015;192:696–702.

155. Afrida S, Tamai Y, Watanabe T, Osaki M. Biobleaching of Acacia Kraft pulp with extracellular enzymes secreted by *Irpex lacteus* KB-1.1 and *Lentinus tigrinus* LP-7 using low-cost media. World J Microbiol Biotechnol. 2014;30(8):2263–71.
156. Zucca P, Rescigno A, Rinaldi AC, Sanjust E. Biomimetic metalloporphines and metalloporphyrins as potential tools for delignification: molecular mechanisms and application perspectives. J Mol Catal A Chem. 2014;388–389:2–34.
157. Meunier B. Metalloporphyrins as versatile catalysts for oxidation reactions and oxidative DNA cleavage. Chem Rev. 1992;92(6):1411–56.
158. Zakavi S, Mojarrad AG, Rayati S. Substituent effects on the catalytic activity of a series of manganese meso-tetra (aryl) porphyrins:(2-, 3-, 4)-Pyridyl, 4-sulfonatophenyl and 3-sulfonato-4-methoxyphenyl groups compared to phenyl and 4-methoxyphenyl ones. J Mol Catal A Chem. 2012;363–364:153–8.
159. Tsuchiya S, Seno M. Novel synthetic method of phenol from benzene catalysed by perfluorinated hemin. Chem Lett. 1989;2:263–6.
160. Crestini C, Pastorini A, Tagliatesta P. Metalloporphyrins immobilized on motmorillonite as biomimetic catalysts in the oxidation of lignin model compounds. J Mol Catal A Chem. 2004;208(1–2):195–202.
161. Crestini C, Pastorini A, Tagliatesta P. The immobilized porphyrin‐mediator system Mn (TMePyP)/clay/HBT (clay‐PMS): a lignin peroxidase biomimetic catalyst in the of lignin and lignin model compounds. Eur J Inorg Chem. 2004;2004(22):4477–83.
162. Cui F, Dolphin D. Metallophthalocyanines as possible lignin peroxidase models. Bioorg Med Chem. 1995;3(5):471–7.
163. Artaud I, Ben-Aziza K, Mansuy D. Iron porphyrin-catalyzed oxidation of 1, 2-dimethoxyarenes: a discussion of the different reactions involved and the competition between the formation of methoxyquinones or muconic dimethyl esters. J Org Chem. 1993;58(12):3373–80.
164. Labat G, Meunier B. Factors controlling the reactivity of a ligninase model based on the association of potassium monopersulfate to manganese and iron porphyrin complexes. J Org Chem. 1989;54(21):5008–11.
165. Crestini C, Saladino R, Tagliatesta P, Boschi T. Biomimetic degradation of lignin and lignin model compounds by synthetic anionic and cationic water soluble manganese and iron porphyrins. Bioorg Med Chem. 1999;7(9):1897–905.
166. Cui F, Wijesekera T, Dolphin D, Farrell R, Skerker P. Biomimetic degradation of lignin. J Biotechnol. 1993;30(1):15–26.
167. Barbat A, Gloaguen V, Sol V, Krausz P. Aqueous extraction of glucuronoxylans from chestnut wood: new strategy for lignin oxidation using phthalocyanine or porphyrin/H 2 O 2 system. Bioresour Technol. 2010;101(16):6538–44.
168. The Merck index. 12th ed. Whitehouse Station: Merck and Co. Inc; 1996.
169. Rochefort D, Bourbonnais R, Leech D, Paice MG. Oxidation of lignin model compounds by organic and transition metal-based electron transfer mediators. Chem Commun. 2002;11:1182–3.
170. Nousiainen P, Kontro J, Manner H, Hatakka A, Sipilä J. Phenolic mediators enhance the manganese peroxidase catalyzed oxidation of recalcitrant lignin model compounds and synthetic lignin. Fungal Genet Biol. 2014;72:137–49.

Part III
Chemical Conversion

Chapter 7
Chemical Modification of Lignin for Renewable Polymers or Chemicals

Nicholas J. Westwood, Isabella Panovic, and Christopher S. Lancefield

7.1 Introduction

7.1.1 Lignin: An Important Renewable Resource

Arguably, one of the greatest challenges society faces in the twenty-first century is reducing our over-dependence on fossil fuels. With the possibility that peak production from easily accessible oil reserves has already passed [1], how will society survive in an oil restricted world? Lignin, the most abundant natural source of aromatic compounds, may offer part of the solution. Lignin is a complex, amorphous biopolymer which is a major constituent of lignocellulosic biomass. It is biosynthesized in plant cell walls by enzyme-catalysed radical polymerization reactions. Further details on the biosynthesis and structure of lignin can be found in Chap. 1. Lignin is liberated from biomass as a significant by-product from the pulp and paper industries. Additional details on these industrial lignins, and other sources of lignin, can be found in Chap. 2.

7.1.2 Possible Uses of Lignin

So how could the use of this resource be maximised? When considering the use of lignin, three of the many factors to consider are:

1. *Lignin can be burnt as a low-value fuel.* At present about 2 % of lignin-based resources are converted into commercially viable chemical products, with the

N.J. Westwood (✉) • I. Panovic • C.S. Lancefield
Department of Chemistry and Biomedical Sciences Research Complex,
University of St. Andrews and EaStCHEM, St. Andrews, Fife KY16 9ST, UK
e-mail: njw3@st-andrews.ac.uk

rest being burnt to provide energy [2]. This valid approach is entirely consistent with the fact that present biomass fractionation processes take little notice of lignin integrity and purity. This results in industrial lignins being heavily modified compared to lignin in its native state, with many of the most recognizable linkages in lignin being absent. The modified nature of the currently available lignins complicates plans to add value to them by forming designer materials or depolymerizing lignin to create usable aromatic monomers. For more elaboration on the challenges faced in releasing lignin from biomass, see the Chapter in this book authored by P. Fatehi. Ideally, however, industry would not burn so much of this complex and important natural resource without first recycling as many of the useable chemical units as possible.

2. *Lignins that retain much of their native chemical structure can be selectively depolymerized and serve as a source of renewable, possibly high value, aromatic chemicals.* Depolymerization can be achieved, however, much current research is developed on lignin model compounds with the protocols having variable success on lignin itself. The "chemicals from lignin" approach has been limited to date, with the notable exception of the oxidative cleavage processes used for the industrial production of syringaldehyde and vanillin [3]. A process yielding vanillin from the oxidation of waste sulfite process liquor was patented in 1979 by Borregaard Industries Ltd and is now applied on a major scale [4]. A recent review describes the various routes for vanillin production, and some of its current applications as a renewable chemical [5]. Section 7.2. of this chapter discusses chemical modifications that facilitate lignin's selective depolymerization. For further details on direct (one-step) depolymerization of lignin to give mixtures of aromatic compounds see Chap. 10 in this book for chemical and Chaps. 3, 4, and 5 for biological approaches.

3. *Lignin can be maintained in its polymeric state and be used in materials applications.* This can be done using lignin in the state it has been liberated in or it can be chemically modified to add value. The use of lignin in this context, that is as a component of a more complex material, is discussed in detail in Sect. 7.3.

The aim of this Chapter is to provide a summary of the main types of chemical modifications applied to lignin, highlighting the most recent examples (excluding the patent literature). Only studies that have used lignin itself, excluding most studies on lignin model compounds and model polymers, will be discussed.

For other relevant reviews please refer to Elsevier's book 'Monomers, Polymers and Composites from Renewable Resources' [6] and the review by Glasser and Lora [7]. Other reviews also cover various aspects of the use of lignin in the formation of novel polymeric materials [8–15], including an excellent review by Lawoko [8]. Other reviews that have inspired this Chapter include reviews and books by Weckhuysen, Bruijnincx et al. [2], Ralph et al. [16], Dumesic et al. [17], Leitner et al. [18] and Barta, de Vries et al. [19].

7.1.3   The Types of Chemical Modifications Carried Out on Lignin

Lignin has been the subject of intense scientific investigation for well over 100 years. For much of this time researchers have been treating lignin with chemicals predominantly to try and learn more about its very complex structure. Our coverage of the early literature in this area is unfortunately brief but this should in no way detract from the quality of the work which was well ahead of its time.

Figure 7.1 highlights general classes of chemical reactions that have been carried out on lignin. An excellent review by Avérous et al. discusses these reactions in much greater detail [9]. This Section will briefly update Avérous' review providing recent specific examples that fall into the various categories highlighted in Fig. 7.1.

7.1.3.1   Alkylation and Oxidation

Lignin researchers have identified many ways to determine the structure of lignin and this has led them to attempt its chemical modification and depolymerization into simpler units via increasingly ingenious methods. Much of this outstanding work was done before the recent advances in analytical methods but it nevertheless underpins all of the thought processes of the modern day lignin scientist. Increasingly, this type of work has benefited from the use of high level NMR methods. One early example of the chemical modification of lignin was the work of Freudenberg who developed the potassium permanganate oxidation of lignin for structural assignment purposes in 1936 [20]. This technique was further developed by Miksche et al. in
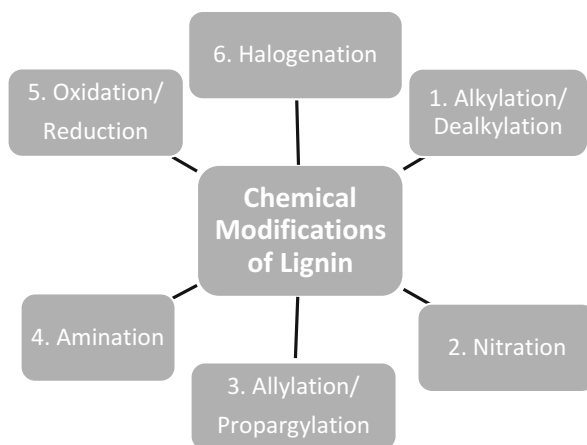
Fig. 7.1 Chemical modifications of lignin. Examples of the chemical derivatization of lignin and their applications are depicted. Figure based on that of Avérous et al. [9]

1973 [21]. The protocol proceeds via initial alkylation of phenolic hydroxyls in the lignin at alkaline pH with diethyl or dimethyl sulfate to give an alkylated lignin. Once alkylated, the lignin undergoes two oxidation steps with potassium permanganate and hydrogen peroxide to give a variety of aromatic di- and monocarboxylic acids (Scheme 7.1A). These acids are then methylated with diazomethane and analyzed by gas chromatography [21–23].

7.1.3.2 Alkylation and Thioacidolysis

A technique known as thioacidolysis has been developed as a standard method of identifying lignin components. This is achieved by the analysis of the monomers that are produced on treatment of lignin with a dioxane/ethanethiol solvent system
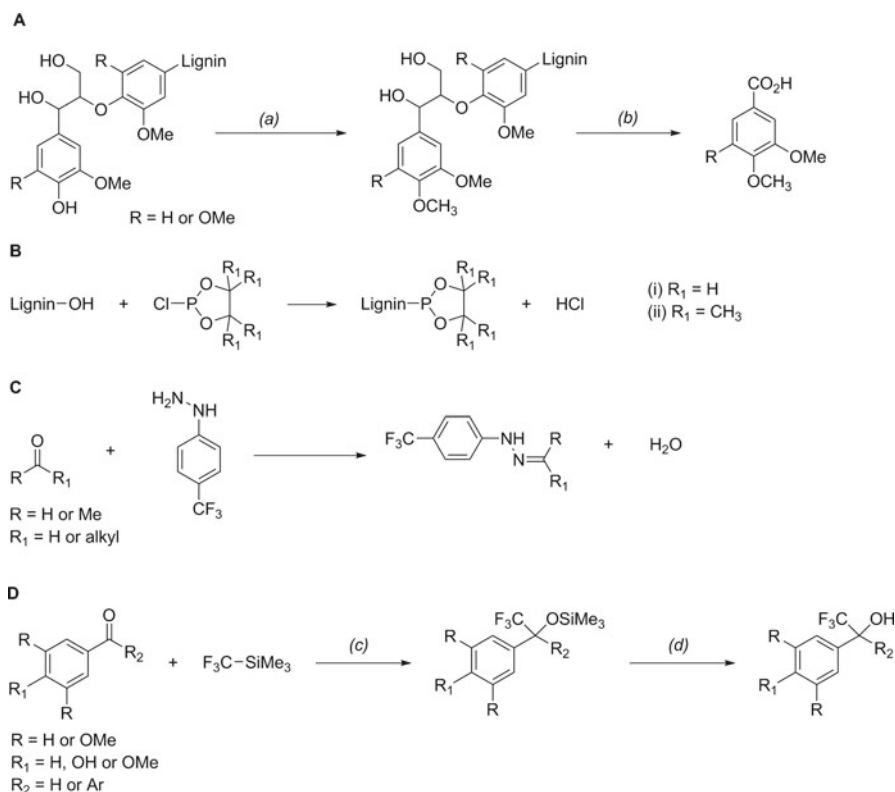
Scheme 7.1 (**A**) Lignin is alkylated in a separate step prior to permanganate oxidation to provide information on phenolic content using conditions (*a*) $(CH_3)_2SO_4$ to give an alkylated lignin. Once alkylated, lignin undergoes oxidation with conditions (*b*) H_2O_2, $KMnO_4$. This produces a variety of aromatic di- and monocarboxylic acids detected and analysed by GC. (**B**) Lignin is phosphitylated through its many hydroxyl groups using derivatizing reagent 2-chloro-1,3,2-dioxaphospholane (i) where $R_1 = H$ or 2-chloro-4,4,5,5-tetra-methyl-1,3,2-dioxaphospholane (ii) where $R_1 = CH_3$. (**C**) Carbonyl compounds in bio-oil were reacted with 4-(trifluoromethyl)phenylhydrazine to allow direct ^{19}F NMR analysis of the modified lignin [29]. (**D**) A series of model carbonyl compounds were trifluoromethylated using conditions (*c*) TMAF (catalytic), followed by hydrolysis with conditions (*d*) CH_3CN, HF [30]

and BF$_3$ etherate as a Lewis acid catalyst [24, 25]. Alkylation of lignin in a separate step prior to thioacidolysis has been used to provide information on the lignin's phenolic content [26]. Additional examples of the alkylation of phenolic oxygen atoms are given in Sect. 7.3.4.

7.1.3.3 Halogenation

The modification of lignin by introducing fluorine-containing groups has been established as a labelling technique for ^{19}F NMR experiments. Sevillano et al. demonstrated the use of trifluoromethyl and trifluoromethoxyphenylhydrazine for the quantification of carbonyl groups in lignin [27, 28]. Other studies on pyrolysis oil built on this approach using 4-(trifluoromethyl)phenylhydrazine (Scheme 7.1C) [29]. Another method developed by Argyropoulos used trifluoromethylation of carbonyl groups within a number of different industrial lignins (Scheme 7.1D) and compared the subsequently modified material with model studies in order to assign the carbonyl environments [30, 31].

7.1.3.4 Nitration

Lignin derivatization by nitration is a modification that has not attracted significant attention, apart from notable examples in which nitrolignin is used in the synthesis of graft interpenetrating networks from polyurethane. In one example, milled wood lignins were nitrated for use in fluorescence-based enzymatic assays [32]. Further discussion of this modification is provided in Sect. 7.3.2.2. In 1931, Kurschner et al. described nitrolignin, prepared from spruce wood via extraction with ethanol and nitric acid [33]. Since this initial investigation on lignin nitration, the standard procedure for preparing nitrolignin has not been significantly altered. The procedure generally involves the use of a nitrating agent such as nitric acid with acetic anhydride or acetic acid [34–36]. A more recent investigation suggests that upon treatment with nitric acid, several chemical processes, including nitration, oxidation, demethoxylation and partial depolymerization all occur. This study also demonstrated that nitrolignin has potential applications as an adsorbent for heavy metal ions [37].

7.1.3.5 Amination

Studies into the modification of lignin by amination have been more extensive due to its successful use in both high surface activity cationic surfactant materials and in the preparation of lignin composites to reinforce interfacial mechanical performance [38–40]. The modification is generally achieved through a Mannich reaction with amines and formaldehyde [41]. In particular, aminated lignin surfactants have been prepared through reaction with diethylamine and formaldehyde [42].

Amination of Kraft lignin has been assisted by the use of ultrasound to produce a cationic surfactant for the removal of anionic azo-dyes, with an optimal removal of 96 % [43]. Another route to aminated alkali lignin was its synthesis through reaction with chlorinated epoxide, epichlorohydrin, followed by amination, though this resulted in cross-linking within the lignin as well. The incorporation of amino groups on the polymer enables its use in engineering materials, this synthesis in particular showed high levels of primary and secondary groups which can be used as curing agents for epoxy resins, as a bio-based reactive additive [44].

7.1.3.6 Phosphitylation

Lignin hydroxyl groups have been derivatized with phosphorus-containing reagents, known as phosphitylation, for ^{31}P NMR analysis. This procedure provides valuable structural information and allows the distinction between the many hydroxyl chemical environments found within lignin. Phosphitylation was first reported on lignin by Argyropoulos using 1,3,2-dioxaphospolanyl chloride in the early 1990s [45]. In later publications both 2-chloro-1,3,2-dioxaphospholane and 2-chloro-4,4,5,5-tetramethyl-1,3,2-dioxaphospholane (see Scheme 7.1B for structures) were used as derivatizing agents. However the use of the first of these two was largely discontinued due to signal overlap between syringyl and condensed phenolics [46, 47].

7.1.3.7 Other Chemical Modifications of Lignin

Many additional chemical reactions that have been carried out on lignin, including several that are shown in Fig. 7.1, occur in the remainder of this review. The next Sections will discuss two major applications of lignin chemical modification: Section 7.2 covers lignin depolymerization to aromatic monomers and Sect. 7.3 covers chemical modifications that enable the preparation of novel materials.

7.2 Depolymerization of Modified Lignin

The one-pot depolymerization of lignin to mono-aromatics frequently results in the formation of complex mixtures of products as a result of non-selective depolymerization pathways (for a recent example of controlling this type of reaction see Deuss et al. [48].) This may not be a problem if the target is lower value bulk chemicals such as phenol substitutes, but for the production of higher value single chemicals this can pose a major purification challenge. One potential solution is to introduce functional handles into lignin which allow for the controlled and selective depolymerization of specific linkages by a defined pathway, hence giving simpler product mixtures. This section will cover selected examples of this approach in detail.

7.2.1 Sequential Lignin Modification Applied to Lignin Structural Analysis

DFRC (derivatization followed by reductive cleavage) was developed by Ralph and co-workers as a degradation method that produced monomers, the analysis of which provided important structural information [49]. DFRC has been widely adopted in the lignin community due to its selectivity and employment of mild reaction conditions. The process involves derivatization and solubilization of the lignin with acetyl bromide in acetic acid, causing bromination at the benzylic position of the β-O-4 unit and acetylation of the remaining free hydroxyls (Scheme 7.2a) [50]. The resulting α-bromo β-aryl ethers are reductively cleaved with zinc under acidic conditions. The newly formed free phenolic groups on the cleaved monomers are then acetylated, detected and quantified using gas chromatography [49]. Although DFRC typically produces hydroxycinnamyl acetate monomers from β-aryl functionalities, it has also been shown to yield monomers from phenolic end groups and oxidised α-ketone units. In addition to monomeric units, dimeric and trimeric units have been recovered via DRFC that are diagnostic not only of the abundant β-O-4 unit, but also the β-β, β-5, β-1 and 4-O-5 linkages [51]. Interestingly, the analysis of grass lignins, in particular, benefited from the use of DFRC modification because, whilst β-O-4 linkages are cleaved, esters remain intact. This enabled the quantification of *p*-coumarate side chains that are abundant in grass lignins [52].

Since its introduction, the technique has been adapted and modified for various additional purposes. For instance, a DFRC' technique was introduced that allowed detection of naturally occurring acetates in non-wood plants, through substitution of the acetylating reagent (typically acetyl bromide, Scheme 7.2a) with the corresponding propionylating reagent. This allowed the identification of the natural γ-acetates in the released monomers from plants such as kenaf and aspen [53]. Furthermore, the technique can be modified through the use of deuterated solvents, or the combination of DFRC with a subsequent ^{31}P NMR derivatization. This provided new quantitative structural information on β-aryl ethers linked to condensed and non-condensed aromatics, such as dibenzodioxocins [54–58]. When compared to thioacidolysis, DFRC gives relatively low monomer yields by GC analysis, however when a combined DFRC-^{31}P protocol is used, more similar values are recorded. Using DFRC analysis, several key insights into lignin's natural structure have been elucidated, such as the identification of tetrahydrofuran β-β cross-coupled dehydrodimers in naturally acetylated lignins, or new aryl isochroman lignin trimers isolated from loblolly pine [59, 60]. However, DFRC has some disadvantages compared to thioacidolysis, such as reproducibility and a multi-step nature that prevents its use on any significant scale or as a monomer production technique.

An alternative multi-step protocol for cleavage of the β-O-4 unit is based on the selective tosylation of the γ-hydroxyl of this linkage. With this in mind Matsumoto et al. impressively developed a four-step γ-tosylation, iodine substitution, sulfinyl-
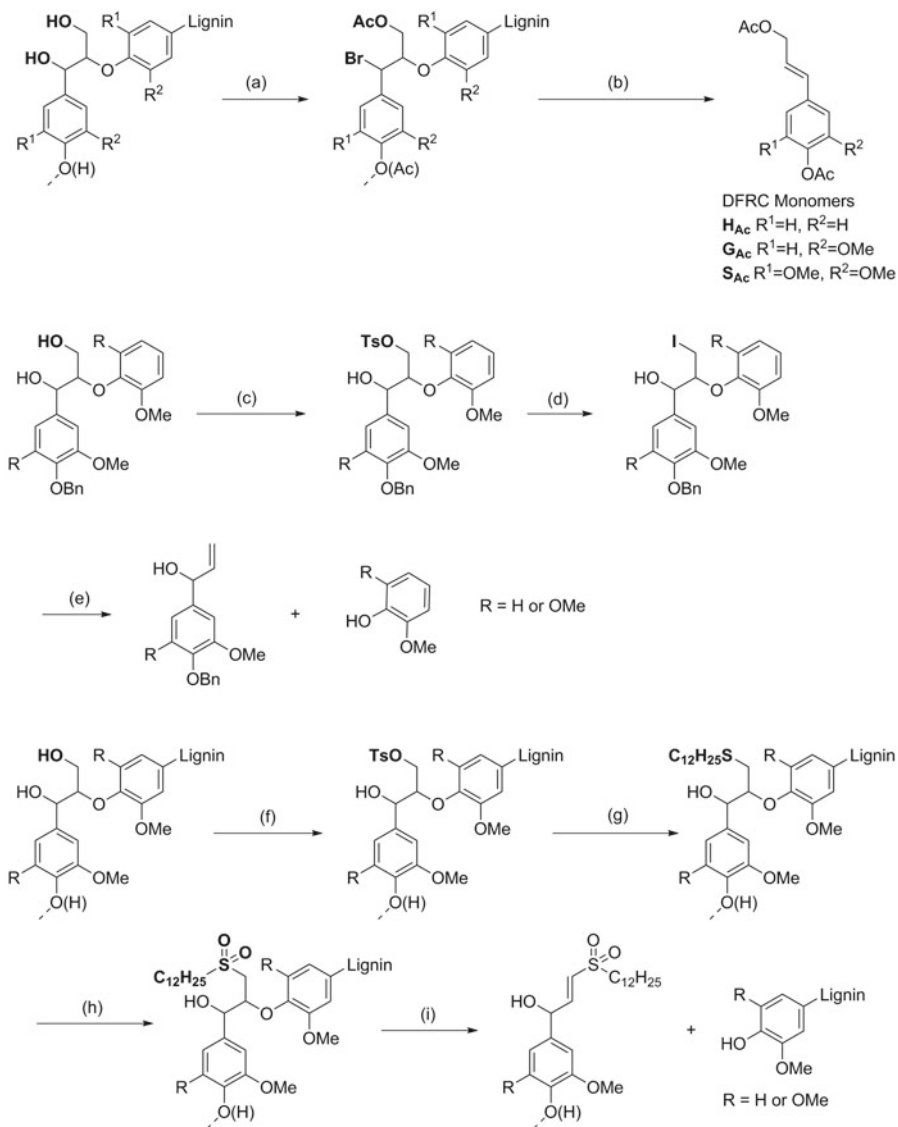
Scheme 7.2 (**a**) DFRC (derivatization followed by reductive cleavage): monomers H_{Ac}, G_{Ac} and S_{Ac} are cleavaged from β-O-4 linkages by derivatization with acetyl bromide in acetic acid, followed by reductive cleavage with zinc, using the following conditions; (*a*) AcBr, AcOH; (*b*) 1. Zn, dioxane/AcOH/H₂O 2. Ac₂O, pyridine; (**b**) TIZ (tosylations, iodination, zinc reductive cleavage): guaiacyl and syringyl non-phenolic model compounds are γ-tosylated, iodinated and reductively cleavage with the following conditions; (*c*) TsCl, pyridine; (*d*) KI; (*e*) Zn. [61]. (**c**) TTSA (tosylations, thioetherification, sulfonylation, alkali degradation): using the following conditions; (*f*) TsCl, pyridine; (*g*) C₁₂H₂₅SH, K₂CO₃ (*h*) oxone; (*i*) NaOH [62]

ation and alkali degradation protocol in the 1980s [63]. Several similar γ-tosylation multi-step procedures have been reported. In 2003 Nakatsubo and co-workers established a three-step TIZ (γ-tosylation, iodination and zinc reductive cleavage) method and applied it to guaiacyl and syringyl non-phenolic model compounds (Scheme 7.2b). They recovered quantitative monomer yields [61]. Later the same group contributed towards a series of publications investigating a four-step γ-TTSA procedure (γ-tosylation, thioetherification, sulfonylation, alkali degradation) (Scheme 7.2c). This procedure was applied to a series of model systems, including a model lignin DHP polymer, with its eventual application on *Eucalyptus Globulus* milled wood lignin (MWL). They reported the selective cleavage of the β-O-4 unit to give a selection of olefinic degradation products, similar to those they observed in their model studies [62, 64, 65].

7.2.2 Benzylic Oxidations Followed by Cleavage as a Route to Chemicals

To improve the likelihood that the process of lignin modification prior to depolymerization to aromatic chemicals will be used in industry, it is important that the modification step can be achieved catalytically and so economically. One way to do this is the selective catalytic oxidation of the benzyl alcohols in the β-O-4 linkages to ketones in lignin (Fig. 7.2). DFT calculations have indicated that this
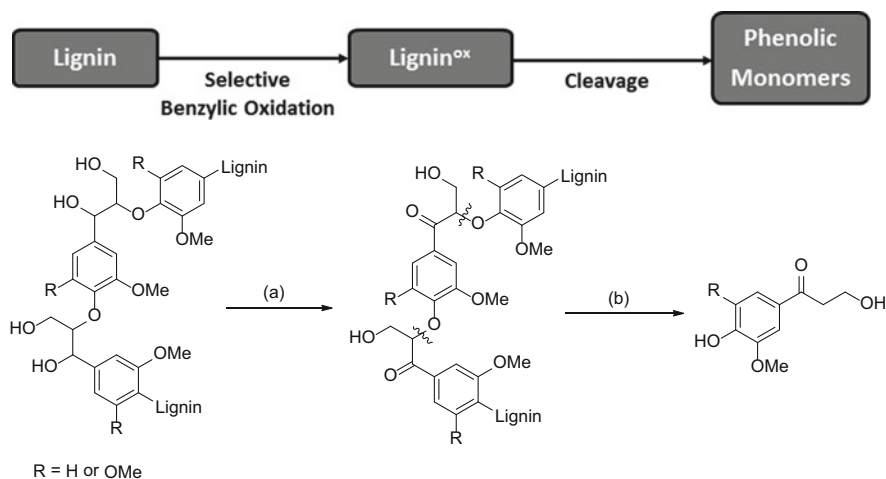
Fig. 7.2 Lignin undergoes selective benzylic oxidation with conditions (**a**) to produce lignin^ox [66] This material can then be selectively cleaved with conditions (**b**) to give phenolic monomers. The monomer shown is produced using the procedure developed by Westwood et al. with the following conditions shown; (a) DDQ, ^tBuONO, O_2, 2-methoxyethanol/DME (2:3), 80 °C, 14 h; (b) Zn/NH_4Cl, H_2O, 80 °C, 1 h [67]

modification results in a significant weakening of the C-O aryl bond and hence a more easily cleaved linkage [68, 69]. However, this strategy depends on the abundance of β-O-4 units within a given lignin sample, which in turn varies greatly between biomass sources and pretreatments used.

Stahl et al. reported a method for achieving this oxidation [66]. Using a catalytic oxidation system consisting of AcNH-TEMPO, HNO_3 and HCl under an O_2 atmosphere the β-O-4 linkages in an aspen cellulytic enzyme lignin were selectively oxidized, with good conversion, to the corresponding α-keto linkages. This reaction took 24 h at 65 °C as revealed by 2D HSQC analysis. Under these conditions inorganic nitrogen oxide is generated *in situ* from HNO_3 and HCl which acts as a co-oxidant mediating the regeneration of the active TEMPO oxoammonium species by O_2. Following this work, the same authors reported on the ability of aqueous formic acid to depolymerize the oxidized lignin under redox neutral conditions giving a 60 wt% yield of low molecular weight products, of which 52 wt% could be assigned to known monomers [70]. Interestingly, 5.5 wt% of the original lignin was isolated as nitrated monomers indicating probable consumption of the co-oxidant during the oxidation reaction. Detailed DFT mechanistic studies of the formic acid induced depolymerization suggest that the rate limiting elimination step proceeds via an unusual E1H-3c4e elimination rather than the expected E2 pathway [69].

At the same time, an alternative depolymerization method was reported by Westwood, Lancefield et al. employing a chemoselective catalytic aerobic oxidation system consisting of 2,3-dichloro-5,6-dicyano-1,4-benzoquinone (DDQ) with ᵗBu-ONO as a co-oxidant. This system was shown to oxidise selectively the β-O-4 benzylic alcohols in a range of model systems in excellent yields (86–98 %) and when applied to a dioxasolv birch lignin showed similar reactivity. Detailed 2D HSQC analysis of the original and oxidized birch lignins revealed that the α-keto-β-O-4 structure was formed with good apparent conversion and selectivity, together with the complete disappearance of the signals characteristic of the unoxidised β-O-4 linkages. A subsequent one-pot treatment with zinc and NH_4Cl as a promoter resulted in cleavage of the C-O aryl bond and formation of phenolic monomers which could be readily isolated and purified in a combined isolated 6 wt% yield (Fig. 7.3) [67]. The functionality retained in these monomers allowed the authors to demonstrate their potential as building blocks for the synthesis of a range of compounds.

Alternative methods for the selective oxidation of the benzylic position in β-O-4 linkages have also been successfully developed. Zhu et al. reported the use of Cp*Ir complexes for the chemoselective dehydrogenation of this unit in lignin models and a birch dioxasolv lignin [71]. In the model studies moderate to good yields of the expected α-keto products were obtained after treatment with the catalyst at 150 °C in 1,4-dioxane for 20 h. When this was applied to lignin a significant decrease in molecular weight was observed by GPC following oxidation and then treatment with Zn/NH_4Cl, suggesting benzylic oxidation of the β-O-4 linkage had taken place. Unfortunately, no other structural analysis of the lignin was carried out to confirm this oxidation.
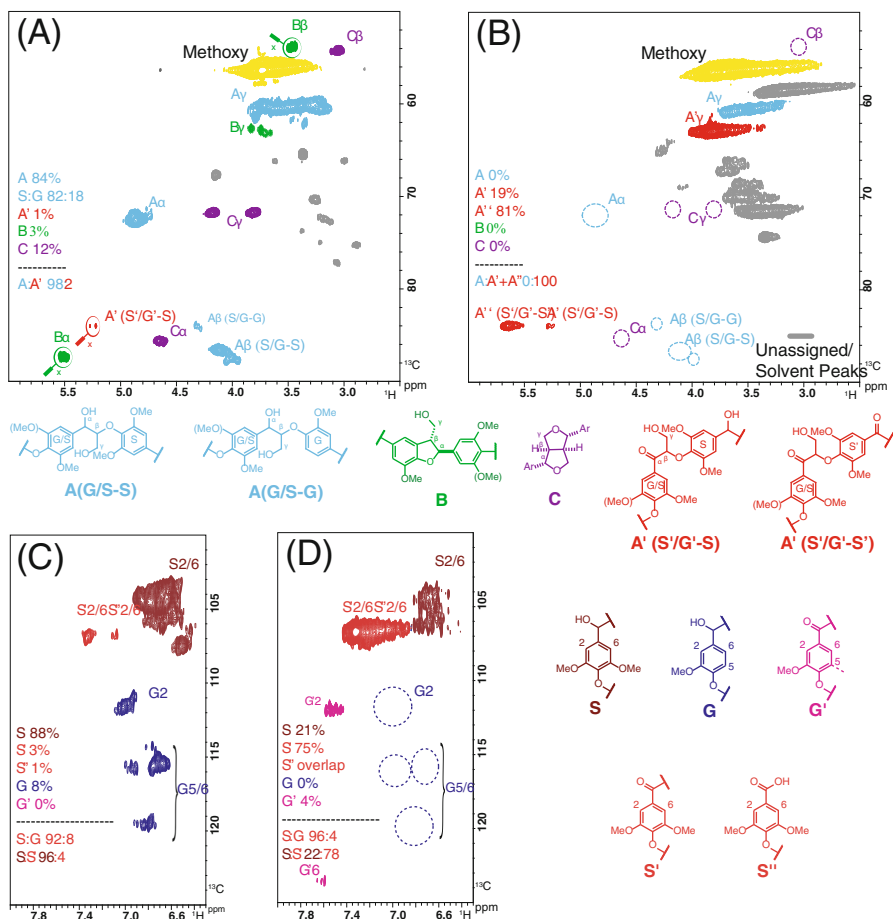
Fig. 7.3 2D HSQC NMR spectra of dioxasolv birch lignin before and after oxidation with a catalytic aerobic DDQ oxidation system (2.40 g scale, 10 wt% DDQ, 4.4 wt% ᵗBuONO) [67]. (**a**). The oxygenated alkyl region in native birch lignin. (**b**). The oxygenated alkyl region in oxidized birch lignin. (**c**). The aromatic region of native birch lignin. (**d**). The aromatic region of oxidized birch lignin. Cross peaks for the β-5 (B) and oxidized β-O-4 (A′) structures in native birch lignin have been magnified to make them visible

Within nature, lignin degradation is most commonly mediated by white rot fungi, however some brown rot fungi and bacteria possess this capability. Such organisms typically degrade lignin via a selection of oxidising enzymes, mostly comprised of laccases and peroxidases. When these enzymes are used *in vitro*, one of the challenges that must be overcome is the strong tendency for lignin and any low molecular weight phenolic degradation products to undergo repolymerization reactions. With this in mind, the use of mediators with laccase and peroxidase enzymes for the

degradation of lignin has been explored. Hammel and Srebotnik showed that recombinant *Trametes villosa* laccase together with 1-hydroxybenzotriazole as a mediator could depolymerize both phenolic and non-phenolic synthetic lignins [72]. They employed both phenolic and nonphenolic (permethylated) synthetic [^{14}C]lignins, and compared these to several model dimers. In the absence of a mediator, laccase treatment had no detectable effect on the non-phenolic substrate whilst the phenolic synthetic lignin was further polymerized. They observed with both the phenolic and nonphenolic lignins, depolymerization occurred only in the presence of both the laccase and the mediator. Studies with a non-phenolic β-O-4 model compound revealed the major reaction occurring in the laccase-mediator system was oxidation of the benzylic position to the α-keto-β-O-4 unit. In addition, minor amounts of bond cleavage products were also identified, consistent with the observed depolymerization of synthetic lignins. Similar reactivity has been observed in the pretreatment of whole eucalyptus feedstocks with a *Myceliophthora thermophila* laccase and methyl syringate mediator followed by alkaline hydrogen peroxide extraction. Gel state 2D HSQC NMR analysis after pretreatment showed that the laccase-mediator system led to significantly higher levels of *in situ* benzylic oxidation of the β-O-4 linkages than either laccase alone or with no enzyme [73]. It has also been shown that this oxidation can be incorporated into the actual biosynthesis of lignin. Tsuji et al. demonstrated that by incorporating the gene for a Cα-dehydrogenase (LigD) enzyme from a *Sphingobium* sp. SYK-6 bacterium into *Arabidopsis thaliana* the levels of α-keto-β-O-4 linkages in isolated cellulytic lignin samples increased 2.1–2.8-fold over the wild type plants [74]. For more information on the modification of lignin by enzymatic methods see the Chapter in this book authored by Bugg et al. and a series of earlier reviews on the use of enzymes for the depolymerization of lignin [75–77].

In summary, there is increasing interest in the selective depolymerization of suitable lignins and this section has provided an overview of the current thinking in this area. The use of the most abundant β-O-4 unit is very tempting and at present it seems that lignin[ox] [70] is a key intermediate for this. Has the best way to oxidize the benzylic position in lignin been found yet – perhaps not. In the end this reaction will have to be the subject of process intensification which may well provide some major chemical engineering challenges. [78] There is also the interesting question of the physical characteristics of lignin[ox]. Does this vary with lignin source? What is the optimum conversion for the oxidation reaction? There remain many important questions. At this stage this concludes this Section's discussion of the modification/depolymerization challenges and we will now focus on the modification of lignin to produce novel materials.

7.3   Lignin Modification Leading to Novel Polymeric Materials

7.3.1   Overview

Lignin in its unmodified state is a non-uniform polar macromolecule due to the presence of the many hydroxyl groups. It also has a relatively high molecular weight with the weight distribution depending on the source of lignin and the extraction technique employed [79]. As a result of these factors and its abundance and low cost, there is considerable interest in the use of lignin as a polymeric material without further modification. For example, it has potential as a precursor for carbon-fibers and materials due to its high carbon content [80]. Unmodified lignin has also been shown to absorb heavy metal ions [81, 82] and it can be used directly in lignin polymer blends [83]. However, the use of unmodified lignin as a polymeric material is often restricted by some of its other properties, such as its poor thermal stability and poor mechanical behavior. These restraints prevent it from competing with more commonly used polymers. Therefore, attempts have been made to blend lignin with other synthetic polymers or biopolymers [13]. However, even this approach is limited by the unmodified lignin's poor blend compatibility with some blending partners. For instance, lignin has been shown to be largely immiscible with poly(vinyl acetate) and poly(vinyl alcohol) [84–86]. In addition, blends with poly(ethylene) and poly(propylene) have poorer mechanical properties, such as reduced tensile strength and increased melt flow index. If too high, this index correlates with reduced mechanical strength, as the lignin content increases [87, 88]. Consequently, one of the main reasons for modifying lignin as a polymer is to assist either its ability to blend with other polymers or to be incorporated in other materials. Many chemical modifications have been tried. However, for these modifications to be of use to industry it is important that they fit the following criteria:

1. The processes and chemicals used to modify the original lignin must be low in cost, otherwise lignin loses its main incentive for use.
2. The modifications should be applicable to a variety of lignin feedstocks, regardless of source or extraction procedure to allow for economic feasibility on an industrial scale.

Many derivatization strategies are directed at two key reactive sites in lignin: (i) the available C5-positions on the guaiacyl and coumaryl phenolic units and (ii) the many phenolic and aliphatic hydroxyl groups. These sites are in all lignins although their relative abundance does change. It is important to note that although aliphatic hydroxyls are available for derivatization, many industrial lignins are substituted at these positions. For instance, in lignosulfonates sulfonic acid groups are often located on alkyl side-chains, meaning these lignins will respond differently to modifications intended for these positions [89].

Having argued that it is necessary to modify the structure of lignin in polymer applications, the question of how to achieve this arises. The overall macrostructure

of the lignin-based material produced on chemical modification depends on whether the coupling partner (the reagent the lignin is reacted with) is mono- or multifunctional. If a mono-functional monomer is used as a coupling partner, a star-like structure based on a lignin-core is produced (Fig. 7.4a, b). This approach can be broadly categorized into two strategies:

- **Grafting from**: where lignin acts as the initiator for a following polymerization reaction in which a monomer reacts with one of lignin's many reactive hydroxyl sites and polymerization builds from the lignin core outwards to create a star-like macromolecule. It is important to note that while polymerization reactions can occur off the growing polymer chain, the monomers only react with other monomers (Fig. 7.4a),
- **Grafting onto**: where an intended polymer chain is preformed by conventional means, followed by functionalization at one end, culminating in a grafting reaction with one of lignin's many hydroxyl groups per polymer chain (Fig. 7.4b),

In cases where the monomer has two functional groups that can react with the lignin functionalities then it is referred to as a 'multi-functional' monomer and networks of polymers or chains are formed (Fig. 7.4c, d respectively). This approach is often applied in the preparation of polyurethanes, polyesters and phenol-formaldehyde thermoset resins (Sect. 7.3.3).

Recent selected examples of the modification of lignin for materials applications are provided in Sects. 7.3.2, 7.3.3, and 7.3.4.

7.3.2 Reaction with Mono-functional Monomers

7.3.2.1 'Grafting Onto' Approach

This strategy (Fig. 7.4b) has the advantage of simplifying the characterization of the new polymer chains, as they are pre-prepared in full prior to grafting. The molecular weight dispersity of chain lengths in this pre-grafted polymer are often narrower compared to the alternative, 'grafting from', variety. However, 'grafting to' is used less often compared to 'grafting from' due to the multi-step procedure required.

A notable example from Iovine and co-workers links the preformed polymer chains to lignin through boronic ester linkages incorporating the β-O-4 unit (Scheme 7.3a). This was shown to work with lignin model polymers [90], with an additional report in 2012 that used analogous conditions enabling grafting onto an organosolv lignin [91]. Interestingly, when attempting to incorporate higher loadings of the boronic acid functionalized polymer, the boronic ester linkage was formed but considerable amounts of unreacted polymer remained. The authors hypothesized that this may be to the increased steric bulk of the lignin copolymer core as it became increasingly modified. It was also suggested that there are a number of inaccessible hydroxyl groups, possibly deep within lignin's complex three-dimensional arrangement [91]. However, this may not be the case as relatively little is known of lignin's three-dimensional spatial structure.
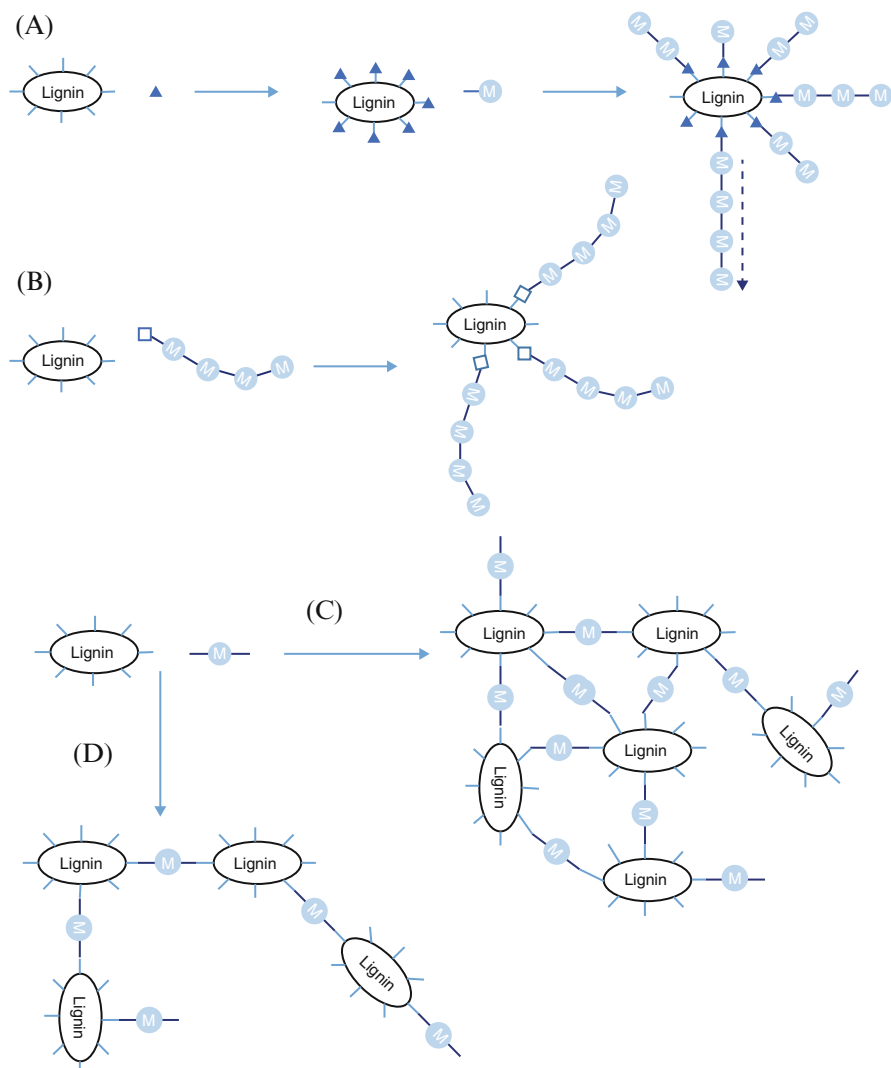
Fig. 7.4 (**a**) Lignin reacts with a mono-functional monomer a star-like polymer is produced with lignin at its core through a 'grafting' process in which the polymerization occurs outwards from modified lignin. (**b**) Grafting is performed onto lignin with a preformed polymer that is functionalized and attached to lignin. (**c**) When lignin reacts with a bifunctional or multi-functional monomer it effectively acts as a 'macro-monomer', resulting in a cross-linked three-dimensional network. (**d**) If lignin reacts sequentially in a copolymerization fashion a multi-functional monomer a chain-like copolymer forms

7.3.2.2 'Grafting From' Approach

In the case of the 'grafting from' approach (Fig. 7.4a) for the copolymerization of lignin, either (i) an initiator is added to the lignin hydroxyls or (ii) a functional group with the lignin itself acts as the initiator. The generation of a radical on the initiator facilitates coupling onto the next monomer resulting in a new radical from which the polymerization with additional monomers continues outwards from the lignin core. Most often, these polymerizations are either ring opening polymerizations (ROPs) or atom transfer radical polymerizations (ATRPs).

ROPs most often occur when cyclic ethers are used. For example, Scheme 7.3b shows the use of propylene oxide to achieve oxypropylation with the lignin phenolic group acting as the initiator unit [8]. Lignin modified with alkylene oxides, such as ethylene, propylene or butylene oxide, have often proved a more soluble component when incorporated into blends. This was demonstrated by an observable decrease in T_g and better solubility [95]. The use of this approach has been hindered by the high pressures and temperatures required for the reaction due to the volatile nature of the alkylene oxides being used. *Furthermore, the procedure with alkylene oxides was not considered safe, preventing its use on an industrial scale. A violent explosion destroyed a lab when large quantities of propylene oxide was used* [7].

Derivatizing lignin with one alkylene oxide unit provides an alternative approach, leading in this case to ROP being considered as an unwanted side-reaction. To solve this problem, Argyropoulos et al. developed a milder route for the oxypropylation of lignin that did not lead to unwanted ROP reactions [96]. *They were able to show that approximately 99 % of the phenolic hydroxyl groups were successfully oxypropylated using 2.5 eq of propylene oxide at 40 °C for 18 h (Scheme 7.3b)* [96]. In addition, if the modification is carried out in aqueous media the oxypropylated lignin precipitates as the reaction progresses and is easily analyzed by NMR spectroscopy [97].

The phenolic oxygen of lignin has also been used as an initiator for the ROP of ε-caprolactone to form lignin-polycaprolactone copolymers [98–100] and with propylene oxide or with lactide to form lignin-polylactic acid copolymers [101, 102]. An early publication by Glasser and de Oliveira reported the preparation of polycaprolactone-lignin star-like copolymers using both 'grafting onto' and 'grafting from' approaches to compare the degree of polymerization of the two products. For the 'grafting onto' approach they used oxypropylated lignin so that the lignin contained only aliphatic hydroxyls and was therefore (more) uniform in functionality. Pre-formed mono-functional isocyanate-terminated polycaprolactone arms were then added. They compared this polymer to one prepared by a copolymerization with a ROP with ε-caprolactone. They found that the synthesis method had a significant influence on the intrinsic viscosity, though the thermal behavior and degree of crystallinity of the resulting copolymers were more affected by copolymer arm length. With the 'grafting onto' approach a higher intrinsic viscosity was observed due to the urethane linkage, present as a result of the reaction of the isocyanate end-group on the preformed poly(caprolactone) arms with the lignin derived alcohols [103].

Another approach to grafting from lignin is the generation of a radical on lignin, usually generated through irradiation or with a chemical initiator, which then proceeds to react with a vinylic monomer through a free radical polymerization reaction. An example of this is the synthesis of lignin-polyacrylate copolymers chemically initiated by peroxide ions [104, 105]. A more controlled alternative to this type of approach is known as ATRP. This allows greater manipulation over living radical polymerizations, resulting in the formation of long polymer chains with lower polydispersity. In this process lignin is initially modified to form what is known as the lignin-macroinitiator that the ATRP process will branch from (Scheme 7.3c). In most cases this is formed by the esterification of both the phenolic and aliphatic hydroxyls using bromo *iso*-butyryl bromide, followed by polymerization with a vinylic monomer in the presence of an ATRP ligand such as HMTETA or PMDETA, and usually CuBr as a catalyst [106–108]. Using this technique graft copolymers of lignin-poly(N-*iso*-propyl-acrylamide) (PNIPAM), lignin-poly(methyl methacrylate) (PMMA) and lignin-polystyrene (PS) have been prepared [93, 106, 107, 109].

An innovative self-polymerization approach that used lignin itself as a multi-functional monomer was developed by Argyropoulos et al. who achieved selective modification of the phenols in Kraft lignin using propargyl bromide (Scheme 7.3d) and then demonstrated chain-extension chemistries using two approaches. In the first, copper-mediated oxidative coupling was used and in the second a thermally-mediated Claisen rearrangement polymerization lead to a polymer that was significantly more cross-linked than the original material. The derivatization chemistry used offers a route to a higher molecular weight material formed under selective conditions with a high degree of molecular control [94].

7.3.3 Reaction with Multi-functional Monomers

With multiple reactive sites for coupling to monomers, lignin is often considered a 'macro-monomer'. Upon reaction with a multi-functional monomeric coupling partner a two-dimensional linear or branched assembly, or a three-dimensional lignin network can be formed (Fig. 7.4c, d). Industry has shown particular interest in the use of lignin as a replacement for phenols in phenol formaldehyde thermoset resins and the use of lignin's aliphatic hydroxyls in the preparation of polyesters or polyurethanes. These approaches are discussed in more detail here.

7.3.3.1 Phenol Formaldehyde Thermoset Materials

Conventional polymers are often classified by their responses to heat stimuli. Thermoplastic materials respond to increased temperatures by becoming more malleable, allowing them to be 'moulded' and set upon subsequent cooling. They are also capable of being reheated and remoulded. In contrast, thermoset materials and
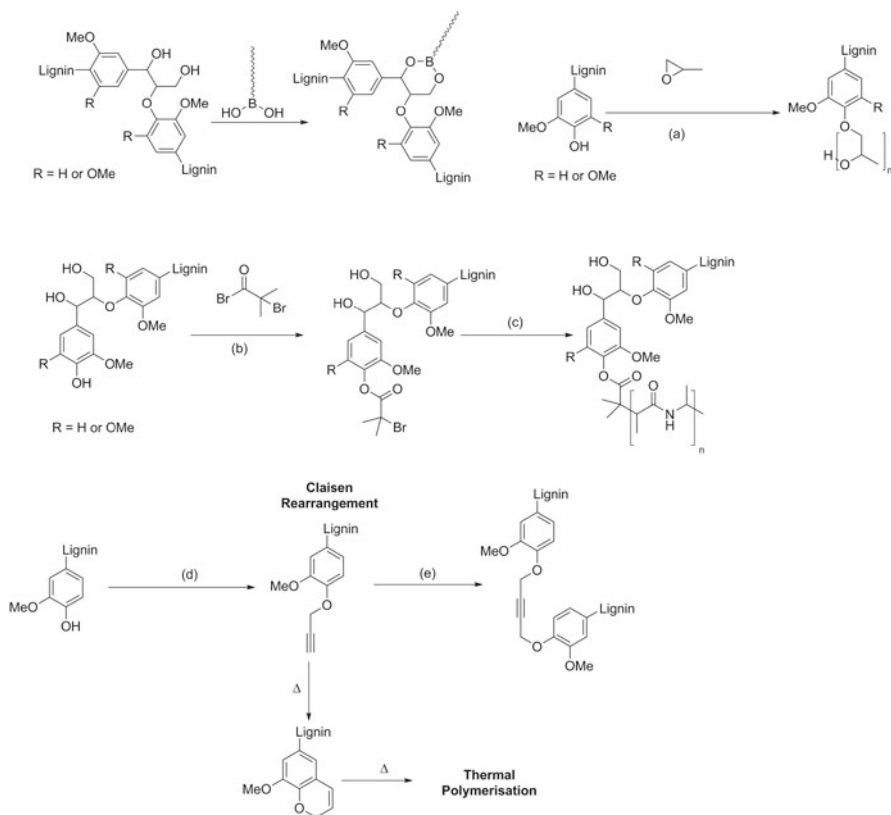
Scheme 7.3 (**a**). Polymer with boronic acid end-group reacts with α- and γ-aliphatic hydroxyls on a β-O-4 unit to form a boron-ester linked grafted co-polymer [91]. (**b**). Lignin undergoes oxypropylation with conditions; (*a*) propylene oxide, NaOH, 40 °C, 18 h. Subsequent additions of alkylene oxides lead to chain extension [92]. (**c**). Phenolic hydroxyls are derivatized with conditions; (*b*) bromoisobutyryl bromide, triethylamine, EtOAc. Lignin then undergoes atom transfer radical polymerization (ATRP) with conditions; (*c*) n-isopropylacrylamide (NIPAM), CuBr, N,N,N′,N′,N′′-pentamethyldiethylenetriamine (PMDTA) [93]. (**d**). Kraft lignin is propargylated with conditions; (*d*) aq. NaOH, propargyl bromide, 80 °C, 2 h. Propargylated lignin either undergoes a thermally mediated Claisen rearrangement, followed by polymerization, or a copper-mediated oxidative coupling reaction with conditions; (*e*) CuCl, O₂, Tetramethylethylenediamine (TMEDA) [94]

resins are formed from flexible prepolymers, becoming irreversibly set and insoluble following curing that is induced by increased temperatures [110]. Phenol formaldehyde (PF) resins are synthetic polymers formed via the reaction of phenols and formaldehyde and are widely used as binders and laminates by industry. Conventional formaldehyde-resins are environmentally hazardous and toxic to humans. The synthesis of a renewable alternative with reduced toxicity could be achieved through the incorporation of lignocellulose biomass. Due to the number of phenolic functionalities in lignin, industry has significant interest in its use as a replacement for the phenol component of the polymer [111]. However, this potential is limited by

the considerable steric bulk of the methoxy groups present on one or both sides of the lignin phenolic oxygen nucleophile. The quality of lignin PF is generally considered inferior to conventional PF products due to the disruptive influence of lignin's many ether linkages [112]. However, differential scanning calorimetry (DSC) studies have indicated that industrial soda bagasse samples are more reactive towards formaldehyde [113].

A strategy to reduce lignin's steric bulk would ideally involve the demethylation of phenolic methoxy-substituents. However, phenolation or hydroxymethylation, known as metholylation, have been more closely studied as a strategy to lead to increase accessibility for incoming coupling partners due to the lower costs associated [111, 112]. Phenolation is a well-established modification which involves the introduction of phenolic groups at aliphatic hydroxyl positions within lignin (Scheme 7.4a). The reaction proceeds in acidic media, however side reactions can result in fragmentation and a reduced molecular weight. The resulting phenolated lignin is useful for incorporation in lignin-based thermoset resins because there are more phenolic hydroxyls for subsequent co-polymerization processes [8, 111, 114]. The phenolation procedure was most effective for hardwood organosolv and softwood sulfite lignins when using ion-exchanged material. In the sulfite case the reaction was proposed to proceed autocatalytically due to the presence of sulfonic acids, removing the need for the addition of a sulfuric acid catalyst [115]. A thorough study into the characterization and 2D HSQC analysis on phenolated technical lignins has also recently been published [116].

Demethylation of lignin is most often performed enzymatically, with a postulated route that proceeds via partial depolymerization and demethylation, followed
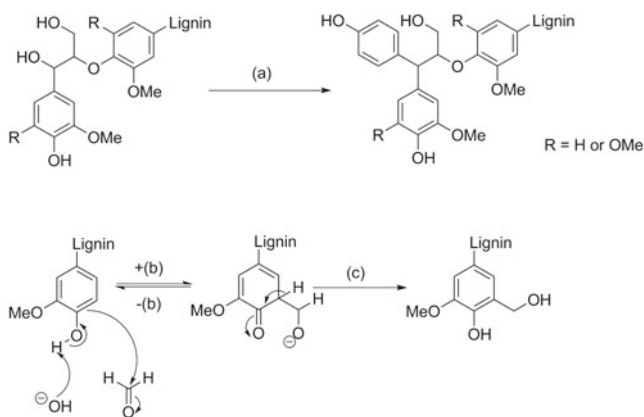
Scheme 7.4 (**a**) Proposed reaction between lignin hydroxyls and phenol during phenolation reaction using conditions (*a*) PhOH, H⁺ (**b**) Proposed Lederer-Manasse type-reaction on lignin phenols with conditions; (*b*) formaldehyde, followed by (*c*) H⁺. This results in methylolation on aromatic C5 positions

by repolymerization to a higher molecular weight lignin [117, 118]. In 2013 it was reported that reaction with iodocyclohexane in DMF at reflux yielded 87 % demethylated Kraft lignin. The basicity of the solvent used was crucial as the production of HI was required for the demethylation reaction. The total number of hydroxyls group present were confirmed by phthalation, (a procedure developed by Kurimoto et al. involving esterification with phthalic anhydride and dioxane/imidazole, followed by NaOH titration [119, 120]), and ^{31}P NMR analysis [121].) Sulfur-mediated demethylation processes are also widely used and well-understood within industry. Wu et al. and An and coworkers both independently studied sulfur dioxide-mediated lignin demethylation processes on lignin, though there have been relatively few advances in this area since [122, 123].

Methylolation involves the incorporation of hydroxymethyl groups at the C_5 position on guaicyl units. The modification increases the amount of reactive hydroxyl positions for co-polymerization processes. The reaction is most often carried out in alkali media with formaldehyde, with a mechanism that likely proceeds via a Lederer-Manasse type reaction (Scheme 7.4b) [124]. However, this modification is also prone to undesirable side reactions such as the Canizzaro reaction, where formaldehyde reacts with itself or a reaction in which lignin side chains are also substituted by aliphatic methylol functionalities [125]. However, Mu et al. were able to demonstrate that methylolated lignin could substitute 40 % phenol in PF resin synthesis and produce a material that met industrial standards [126].

7.3.3.2 Polyurethanes

As previously described (Sect. 7.3.2.2), oxypropylation of lignin can result in a modified material with more reactive hydroxyls. This strategy has been used to allow increased lignin incorporation into polyurethane foams [127, 128]. Lewis acid catalyzed demethylation has been used as a chemical modification strategy to increase the number of phenolic hydroxyls present and facilitate lignin's coupling with diisocyanate, to produce a lignin-based polyurethane material (Scheme 7.5). In this case, hydrobromic acid and hexadecyltributyl- phosphonium bromide were used catalytically in DMF for 20 h at 115 °C to produce a 28 % increase in hydroxyl content, as shown by ^{1}H NMR integration. Other demethylation systems, including BBr$_3$ and TMSI, were attempted with less success. Following preparation of a prepolymer system with toluene-2,4-diisocyanate (TDI) and samples of unmodified or modified lignin, polymerization was carried out with polyethylene glycol (PEG). The modified lignin polyurethane displayed a 6.5-fold improvement in modulus, a quantification of polymer elasticity, compared to the unmodified lignin, likely due to the higher concentration of hydroxyl groups facilitating polymerization [129].

Lignin nitration, as mentioned previously, is often used to prepare 'nitrolignin' for use in graft-interpenetrating polymer networks for polyurethanes [12]. This has been useful in enhancing the tensile strength and mechanical properties of the resulting material [130]. In one publication [131] a conventional polyurethane was compared with the corresponding nitrolignin-polyurethane. A beneficial lower breaking elon-
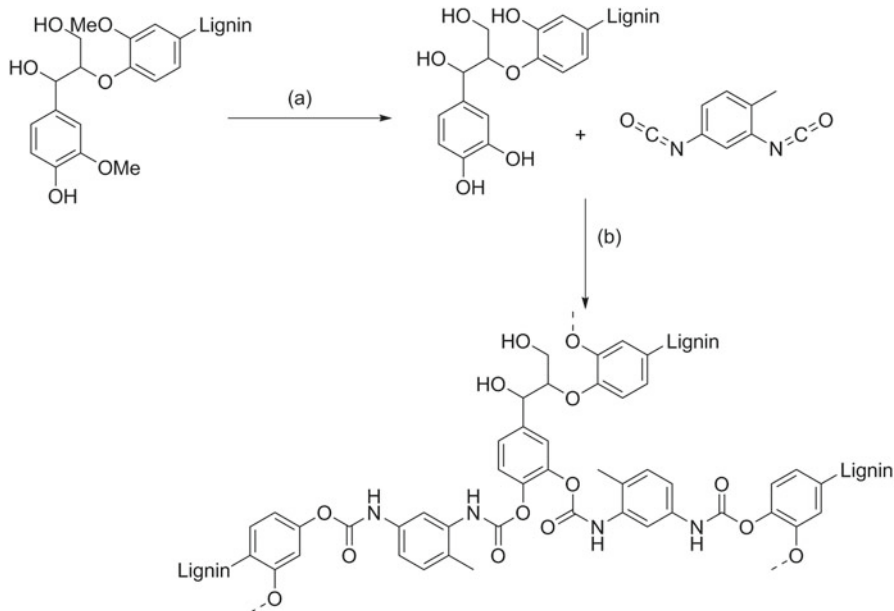
Scheme 7.5 Lignin treated with the following conditions; (**a**) HBr, tributylhexadecylphospho-nium bromide (TBHDPB), H$_2$O/DMF, heat. This resulting in demethylation then co-polymerization was performed with conditions (**b**) toluene diisocyanate, PEG [129]

gation or fracture strain (which represents the difference in chain length observed after elongation or strain of the polymer) was also seen in lignin-polyurethane films that contained nitrolignin. This indicates that the introduction of nitrolignin increases the interaction between hard (glassy) segments by crosslinking [131].

Oxypropylated lignin has also been used as a macro-monomer with isocyanates in polyurethane synthesis. This approach has the advantage of transforming lignin's phenolic hydroxyls into aliphatic hydroxyls, making them more reactive towards isocyanate. [132] Oxypropylated lignin has also been shown to be more viscous, leading to a reduction in the brittleness often seen in lignin-derived copolymers, and exhibiting improved viscoelastic properties [128, 133, 134].

7.3.4 Polymer Blending

Polymer blending is a technique that allows the combination of two distinct poly-mers to create a novel polymer system with modified thermal and physical proper-ties. Blends can either be categorized as immiscible, with two distinct glass transition temperatures (T$_g$), or miscible, exhibiting uniform macroscopic properties and a singular T$_g$. The preparation of miscible blends generally requires strong

intermolecular forces and good blend compatibility. It is also well established that a decrease in T_g generally leads to a distinct increase in blend compatibility. As previously mentioned, in its unmodified state lignin does not show miscibility with commercial polyolefins, leading to complications in creating miscible blends. To overcome this, alkylation and acetylation in particular have been shown to result in a reduced lignin T_g and increased solubility [7]. This type of modification also has the advantage of removing the possibility of further radical polymerizations within lignin initiated by the formation of phenolic radicals [92, 100, 135, 136]. Initially, early research suggested that copolymer blends would only tolerate lignin loadings of less than 40 % [137]. However, Sarkanen et al. demonstrated that loadings of 95–100 % Kraft lignin were possible and that, upon alkylation, thermoplastic blends with aliphatic polyesters could be formed [137, 138]. The modification of lignin by an initial reaction with maleic anhydride has been shown to result in a miscible blend with polypropylene, achieving lignin loadings of up to 25 %. The blend's properties also displayed an increase in mechanical stability and greater process stability compared to unmodified material [92, 136].

Another use of alkylation has been the selective masking of phenolic hydroxyl groups through methylation, leading to a lignin 'protected' at the phenolic hydroxyls. This modification was shown to lead to an increase in thermal stability and a subsequent decrease in the extent of unwanted thermal crosslinking side-reactions, as well as an overall lowering of the glass transition properties of lignin. Both dimethyl carbonate and dimethyl sulfate have been used to achieve phenolic methylation, though methyl iodide as a methylating agent was shown to be unselective and ineffective [96, 139]. It was observed that the modification allowed an increase in thermal stability, reduced thermally induced crosslinking and resulted in an overall decrease in T_g, which would allow for higher solubility in modified blends [139]. Studies on the methylation of lignosulfonate material have also been conducted, allowing the production of an 85 % w/w lignosulfonate polymer blend with poly(ethylene glycol), capable of matching the tensile strength of polyethylene [140].

A novel approach to lignin solubilisation has been the use of a liquid ammonia solvent system [141]. This has been shown to work on a variety of technical and industrial lignins. Interestingly, elemental analysis also demonstrated the incorporation of nitrogen into the lignin structure, benefiting its solubilisation and leading to lignin rearrangement into higher molecular weight fractions. 2D HSQC analysis displayed the loss of peaks corresponding to the β-β linkages, and the gain of several new signals, suggesting some amination reactions may occur that involve this linkage [141]. This method could be of use to enhance the solubility of lignin, to facilitate its incorporation into novel polymer blends in future.

7.3.5 Smart Lignin Materials

Smart lignin materials, such as self-healing polymers, shape-memory polymers or other stimuli-responsive materials incorporating lignin, are a relatively new field. Progress on the use and attachment of reactive handles within lignin has led to early advances in the use of lignin as a smart polymer. For a lignin-based polymer to be considered 'smart' it must exhibit a response to an external stimulus, such as temperature or pH.

For instance, Crestini and co-workers used the many available hydroxyl groups in lignin to prepare furan and maleimide functionalized lignins (Scheme 7.6a). Upon mixing the two functionalized varieties of modified lignin, a coupling reaction occurred via a [4 + 2] Diels-Alder reaction to form a cross-linked gel. The material showed apparent self-healing properties as upon heating to 120 °C the retro-Diels Alder allowed recovery of both modified lignins, which could presumably then react with each other again at lower temperatures [142]. A reversible cross-linking strategy is useful in several lignin applications, such as in the production of adhesives, which would allow a reversible curing process to occur.

The same group has also reported the selective modification of the phenolic groups in Kraft lignin with styrene oxide, followed by reaction of diazonium cations to yield a pH-responsive diazobenzene group (Scheme 7.6b). The material exhibited a colour change depending on the pH environment, facilitated by the *cis-trans* photo-isomerization of the lignin handle [143]. Kadla et al. also developed a pH responsive lignin-based polymer, however this was formed via a copolymerization of lignin with poly[2-(dimethylamino)ethyl methacrylate] (PDMAEMA) [144]. The 2-(4-nitrophenyl azo) and 2-(4-methoxyphenyl azo) phenol modified lignin polymers have been prepared from an alkali lignin. This involved an initial alkaline hydrogen peroxide oxidation of the lignin to give "oxidated lignin" which was then reacted with pre-prepared diazonium salts to give the chemically modified lignin-based azopolymers. The 2-(4-methoxyphenyl azo) phenol lignin-modified polymer did not exhibit an obvious photo-response, unlike the 2-(4-nitrophenyl azo) derived lignin-material displayed a significant photochromic effect. The photo-response of the new lignin-based azo-polymers was found to be slower than conventional polymers containing the same azo end groups. It was suggested that this is the result of the strong steric hindrance of lignin backbone inhibiting isomerization of the azo-chromophores [145].

In 2014 a novel lignin-based smart material was prepared through diisocyanate modification to produce a self-cleaning, super-hydrophobic aerogel. Aerogels are low density porous solids that can facilitate mass transfer of gas or liquid substrates, therefore they are widely used as catalyst supports, absorbents and insulators by industry. The aerogel was shown to be absorbent towards organic solvents, but highly hydrophobic. Experiments with gasoline absorption demonstrated that upon heating, the absorbed material was released as gasoline vapor and the aerogel retained almost 100 % absorption capacity and was highly recyclable. This lignin-based
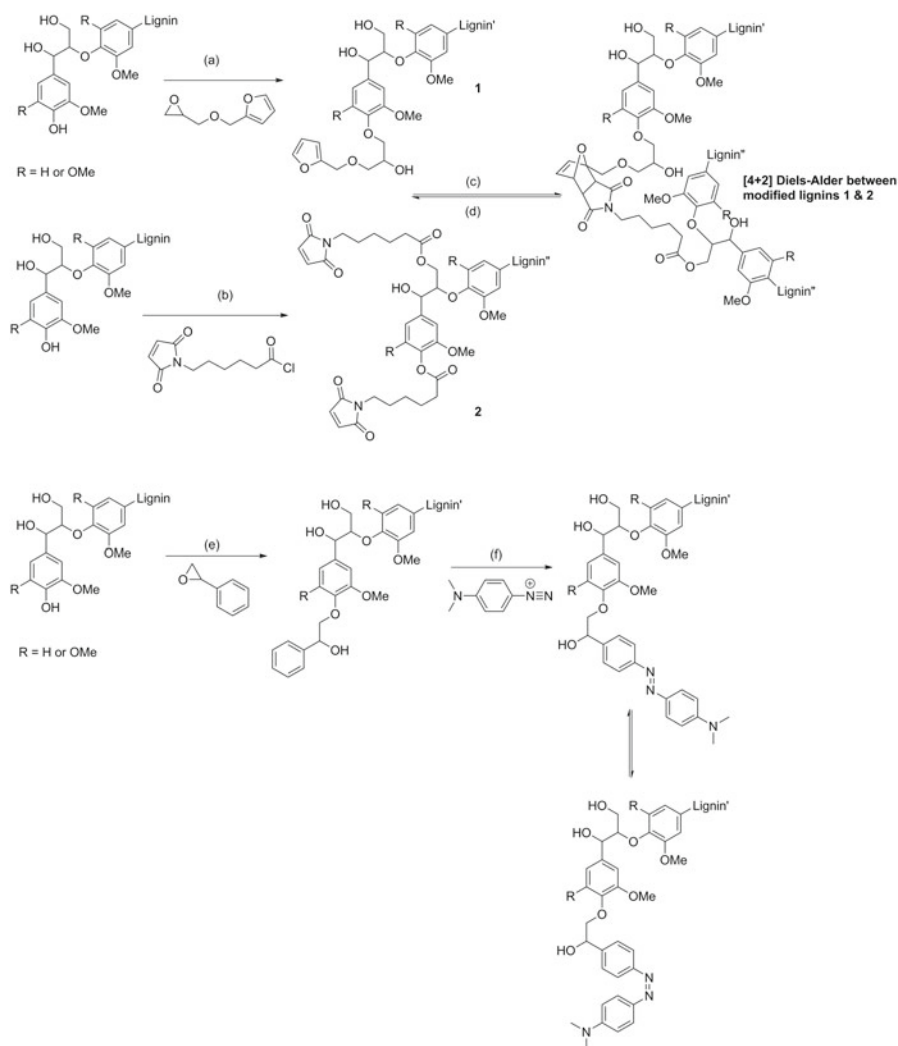
Scheme 7.6 (**a**) One lignin reacts with furfuryl glycidyl ether at phenolic positions to form lignin 1 using the following conditions; (*a*) NaOH, furfuryl glycidyl ether. Lignin 2 is functionalized with conditions; (*b*) 6-maleimidohexanoic acyl chloride. Reversible [4+2] Diels-Alder reaction occurs between functionalized lignin 1 and 2 with the forward reaction occurring with conditions; (*b*) 70 °C, and the reverse reaction occurring with conditions; (*c*) 120 °C [146]. (**b**) Phenols react with styrene under the following conditions; (*d*) NaOH, heat, styrene oxide. Oxypropylated lignin is coupled to a diazo linker under conditions; (*e*) NaOH, 0 °C, 4-dimethylamino-benzenediazonium [143]
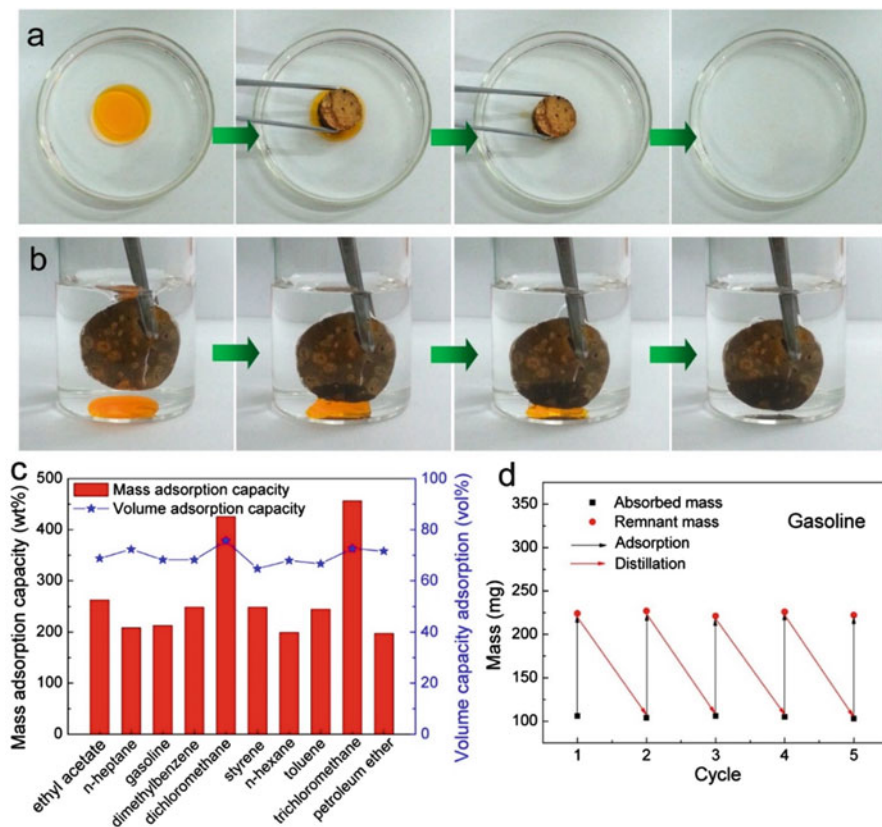
Fig. 7.5 (**a**) dyed n-hexane separated from water and adsorbed by lignin xerogel material (**b**) dyed dichloromethane separated from water and adsorbed by lignin xerogel material (**c**) mass and volume adsorption capacity of the lignin xerogel material for a variety of solvents (**d**) the reusability of lignin xerogel material following subsequent adsorptions of gasoline and distillation of gasoline to regenerate the material, capacity is retained after many cycles (Reprinted with permission from Ref. [147]. Copyright 2014 American Chemical Society)

smart material exhibits ideal properties for the removal of oil contaminants from water (Fig. 7.5) [147].

Lignin has also been used to prepare shape memory materials: materials capable of retaining the ability to return to their original states after deformation into a temporary state on exposure to an external stimulus, such as temperature change. In one example lignin was used in the preparation of a triple shape memory polymer, which is able to switch from a temporary state at an initial transition temperature, followed by transformation to a permanent state at an even higher activation temperature. In this case a hyperbranched poly(ester-amine-amide) prepolymer network of adipic acid, triethanolamine and tris(hydroxymethyl) aminomethane (THAM) was prepared and then mixed with a fractionated methanol-soluble lignin.

The polymerization was then carried out at 120 °C at 650 mmHg for 20 h to give a tough and flexible lignin copolymer. The triple shape memory properties arose from the combined effect of the microtransitions between the two poly(ester-amine) and poly(ester-amine-amide) phases, which were linked by lignin, shown by the broadening of a single T_g. The triple shape memory response in the lignin copolymer might suggest that lignin has a highly adaptable architecture to allow development of adjustable smart memory materials [148]. The synthesis of a similar lignin-based shape memory material from a hyperbranched prepolymer blend of adipic acid, glycerol, THAM and diisopropylamine has also been reported; however, the material did not exhibit triple shape memory properties [149]. In this case, the shape transition temperature was shown to be tunable according to the composition of DIPA, THAM and glycerol, allowing for applications requiring different shape transition temperatures to be accommodated for. Whilst this is still an emerging field in lignin-chemistry several other reports of lignin-based shape responsive materials highlight the potential in this area [150–152].

In summary, the use of lignin in polymers and materials is becoming increasingly attractive as a renewable alternative to petrochemical feedstocks. The wealth of recent innovative literature in this area, some of which has been highlighted in this section, certainly points towards this. The potential to use lignin in low volume, high value performance and smart materials, as well as in higher volume, lower value products such as phenol formaldehyde resins is significant. How many of these research findings make their way into industrial applications and, crucially, whether consumers embrace them remains to be seen. However, given the abundance of this low value material many more novel and commercial applications will appear in the coming years.

7.4   Concluding Remarks & Future Outlook

This chapter has highlighted important examples of the chemical modifications of lignin either for the production of aromatic chemicals or in the use of lignin as a material. In doing so the growing importance of lignin as a renewable resource with diverse potential applications has been established.

Whilst the word 'lignin' is often used as a catch all term, it is important to bear in mind that the structures of no two lignins are the same. For example, a hardwood Kraft lignin is different in structure to a softwood Kraft lignin and both are very different compared to a sulfite lignin. As such different lignins are better suited to different applications. For the selective modification leading to the production of aromatic chemicals approach, lignins with high β-O-4 contents and hence low phenolic content, high molecular weight and poor solubility are desirable. Conversely, for polymer and material applications high phenolic content and good solubility are often desirable. Clearly one 'lignin' will not fit all applications and so effective valorization will also require a detailed understanding of the molecular structure of different lignins. In the future, it is likely that further advances in the structural

elucidation of lignins will be made, aided by additional developments in lignin's NMR characterization. This will aid our understanding of the structural changes lignin undergoes upon chemical modification.

References

1. Miller RG, Sorrell SR, Lane H, et al. The future of oil supply. Philos Trans R Soc A. 2013; 20130179. doi: 10.1098/rsta.2013.0179.
2. Zakzeski J, Bruijnincx PCA, Jongerius AL, Weckhuysen BM. The catalytic valorization of lignin for the production of renewable chemicals. Chem Rev. 2010;110:3552–99. doi:10.1021/cr900354u.
3. Sandborn LT, Richter SJ, Clemens HG. Process for making vanillin (US2057117). 1936;205: 7117.
4. Evju H. 1979. Process for preparation of 3-methoxy-4-hydroxybenzaldehyde.
5. Fache M, Boutevin B, Caillol S. Vanillin production from lignin and its use as a renewable chemical. ACS Sustain Chem Eng. 2015;4:35–46. doi:10.1021/acssuschemeng.5b01344.
6. Belgacem MN, Gandini A. Monomers, polymers and composites from renewable resources. 1st ed. Oxford: Elsevier; 2008.
7. Lora JH, Glasser WG. Recent industrial applications of lignin: a sustainable alternative to nonrenewable materials. J Polym Environ. 2002;10:39–48. doi:10.1023/a:1021070006895.
8. Duval A, Lawoko M. Reactive & functional polymers a review on lignin-based polymeric, micro- and nano-structured materials. React Funct Polym. 2014;85:78–96.
9. Laurichesse S, Avérous L. Chemical modification of lignins: towards biobased polymers. Prog Polym Sci. 2014;39:1266–90. doi:10.1016/j.progpolymsci.2013.11.004.
10. Liu W-J, Jiang H, Yu H-Q. Thermochemical conversion of lignin to functional materials: a review and future directions. Green Chem. 2015;17:4888–907. doi:10.1039/C5GC01054C.
11. Argyropoulos DS, Sen S, Patil S. Thermal properties of lignin in copolymers, blends, and composites; a review. Green Chem. 2015; doi: 10.1039/C5GC01066G.
12. Zhang Q, Zhang G, Xu J, et al. Recent advances on lignin-derived polyurethane polymers. Rev Adv Mater Sci. 2015;40:146–54.
13. Thakur VK, Thakur MK, Raghavan P, Kessler MR. Progress in green polymer composites from lignin for multifunctional applications: a review. ACS Sustain Chem Eng. 2014;2:1072–92.
14. Upton BM, Kasko AM Strategies for the conversion of lignin to high-value polymeric materials: review and perspective. Chem Rev acs.chemrev.5b00345. 2015; doi: 10.1021/acs.chemrev.5b00345.
15. Lange H, Decina S, Crestini C. Oxidative upgrade of lignin – recent routes reviewed. Eur Polym J. 2013;49:1151–73. doi:10.1016/j.eurpolymj.2013.03.002.
16. Lu F, Ralph J. Chapter 6: Lignin. 1st ed. Cereal Straw as a Resour Sustain Biomater Biofuels. 2010; doi: 10.1016/B978-0-444-53234-3.00006-7.
17. Luterbacher JS, Martin Alonso D, Dumesic JA. Targeted chemical upgrading of lignocellulosic biomass to platform molecules. Green Chem. 2014;16:4816–38. doi:10.1039/C4GC01160K.
18. de María PD, Grande PM, Leitner W. Current trends in pretreatment and fractionation of lignocellulose as reflected in industrial patent activities. Chemie Ing Tech. 2015;87:1686–95. doi:10.1002/cite.201500122.
19. Deuss PJ, Barta K. From models to lignin: transition metal catalysis for selective bond cleavage reactions. Coord Chem Rev. 2015;306:510–32.
20. Freudenberg K. Constitution and biosynthesis of lignin. 1968.
21. Erikson E, Larsson S, Miksche G. Gaschromatographische Analyse von Ligninoxydationsprodukten: VIII. Zur Struktur des Lignins von Fichte. Acta Chem Scand. 1973;27:903–14.

22. Dimmel D, Lapierre C, Schmidt J, et al. Lignins & lignans: advances in chemistry. 2010; doi: 10.1007/s13398-014-0173-7.2.

23. Gellerstedt G. Chemical degradation methods: permanganate oxidation. In: Lin S, Dence C, editors. Methods in lignin chemistry, SE – 22. Berlin/Heidelberg: Springer; 1992. p. 322–33.

24. Lapierre C, Monties B, Rolando C, de Chirale L. Thioacidolysis of lignin: comparison with acidolysis. J Wood Chem Technol. 1985;5:277–92. doi:10.1080/02773818508085193.

25. Lapierre C, Bernard M, Christian R. Preparative thioacidolysis of spruce lignin: isolation and identification of main monomeric products. Holzforsch – Int J Biol Chem Phys Technol Wood. 1986;40:47. doi:10.1515/hfsg.1986.40.1.47.

26. Lapierre C, Rolando C. Thioacidolyses of pre-methylated lignin samples from pine compression and poplar woods. Holzforschung. 1988;42:1–4. doi:10.1515/hfsg.1988.42.1.1.

27. Sevillano RM, Mortha G, Froment P, et al. 19 F NMR spectroscopy for the quantitative analysis of carbonyl groups in lignin. In: 4th Eur. Work. Lignocellul. Pulp, Stresa, Italy; 1996. p. 292.

28. Sevillano RM, Mortha G, Barrelle M, Lachenal D. 19 F NMR spectroscopy for the quantitative analysis of carbonyl groups in lignins. Holzforschung. 2001;55:286. doi:10.1515/HF.2001.048.

29. Huang F, Pan S, Pu Y, et al. 19 F NMR spectroscopy for the quantitative analysis of carbonyl groups in bio-oils. RSC Adv. 2014;4:17743. doi:10.1039/c4ra01293c.

30. Ahvazi BC, Crestini C, Argyropoulos DS. 19 F nuclear magnetic resonance spectroscopy for the quantitative detection and classification of carbonyl groups in lignins. J Agric Food Chem. 1999;47:190–201.

31. Ahvazi BC, Argyropoulos DS. 19 F nuclear magnetic resonance spectroscopy for the elucidation of carbonyl groups in lignins. 1. Model compounds. J Agric Food Chem. 1996;44:2167–75.

32. Ahmad M, Taylor CR, Pink D, et al. Development of novel assays for lignin degradation: comparative analysis of bacterial and fungal lignin degraders. Mol Biosyst. 2010;6:815–21. doi:10.1039/b908966g.

33. Kurschner K. Separation of wood into cellulose and nitrolignin. Cellul Chemie. 1931; 281–286.

34. Ivanov VI, Chuksanova AA, Sergeeva LL. Nitration of saccharification lignin. Bull Acad Sci USSR Div Chem Sci. 1958;6:513–18. doi:10.1007/BF01171974.

35. Grushnikov OP, Shorygina NN, Mikhailov NP. Nitration of some isolated lignins by an alcoholic solution of nitric acid. Bull Acad Sci USSR Div Chem Sci. 1968;17:1991–6. doi:10.1007/BF00905000.

36. Grushnikov OP, Shorygina NN. The nitration of spruce wood lignin by Kurschner's method. Bull Acad Sci USSR Div Chem Sci. 1967;16:1703–8. doi:10.1007/BF00906816.

37. Khvan AM, Abduazimov BB. Nitration of lignin and sorptive properties of the resulting products. Chem Nat Compd. 2002;38:471–2.

38. Yue X, Chen F, Zhou X. Improved interfacial bonding of PVC/wood-flour composites by lignin amine modification. Bioresources. 2011;6:2022–34.

39. Liu X, Zhu H, Qin C, et al. Adsorption of heavy metal ion from aqueous single metal solution by aminated epoxy-lignin. Bioresources. 2013;8:2257–69.

40. Dizhbite T, Zakis G, Kizima A, et al. Lignin — a useful bioresource for the production of sorption-active materials. Bioresour Technol. 1999;67:221–8. doi:10.1016/S0960-8524(98)80004-7.

41. Forostyan YN. Modification of lignin by phosphorylation and amination. Chem Nat Compd. 1977;13:474–6. doi:10.1007/BF00565843.

42. Matsushita Y, Yasuda S. Reactivity of a condensed–type lignin model compound in the Mannich reaction and preparation of cationic surfactant from sulfuric acid lignin. J Wood Sci. 2003;49:166–71. doi:10.1007/s100860300026.

43. Wang X, Zhang Y, Hao C, et al. Ultrasonic-assisted synthesis of aminated lignin by a Mannich reaction and its decolorizing properties for anionic azo-dyes. RSC Adv. 2014;4:28156. doi:10.1039/c4ra03133d.

44. Pan H, Sun G, Zhao T. Synthesis and characterization of aminated lignin. Int J Biol Macromol. 2013;59:221–6. doi:10.1016/j.ijbiomac.2013.04.049.

45. Argyropoulos DS. Quantitative phosphorus-31 NMR analysis of lignins, a new tool for the lignin chemist. J Wood Chem Technol. 1994;14:45–63. doi:10.1080/02773819408003085.

46. Granata A, Argyropoulos DS. 2-Chloro-4,4,5,5-tetramethyl-1,3,2-dioxaphospholane, a reagent for the accurate determination of the uncondensed and condensed phenolic moieties in lignins. J Agric Food Chem. 1995;43:1538–44. doi:10.1021/jf00054a023.

47. Argyropoulos DS. 31P NMR in wood chemistry: a review of recent progress. Res Chem Intermed. 1995;21:373–95. doi:10.1007/BF03052265.

48. Deuss PJ, Scott M, Tran F, et al. Aromatic monomers by in situ conversion of reactive intermediates in the acid-catalyzed depolymerization of lignin. J Am Chem Soc. 2015; 137:150522131446003. doi: 10.1021/jacs.5b03693.

49. Lu F, Ralph J. Derivatization followed by reductive cleavage (DFRC Method), a new method for lignin analysis: protocol for analysis of DFRC monomers. J Agric Food Chem. 1997;45:2590–2. doi:10.1021/jf970258h.

50. Lu F, Ralph J. The "DFRC" method: a new method for structural characterization of lignins. US Dairy Forage Res Center, Res Summ. 1997;62–65.

51. Lu F, Ralph J, Guerra A, et al. Structural characterization of lignin during Pinus taeda wood treatment with Ceriporiopsis subvermispora. Appl Environ Microbiol. 2004;70:4073–8. doi:10.1128/AEM.70.7.4073.

52. Lu F, Ralph J. Detection and determination of p-coumaroylated units in lignins. J Agric Food Chem. 1999;47:1988–92. doi:10.1021/jf981140j.

53. Ralph J, Lu F. The DFRC method for lignin analysis. 6. A simple modification for identifying natural acetates on lignins. J Agric Food Chem. 1998;46:4616–19. doi:10.1021/jf980680d.

54. Guerra A, Filpponen I, Lucia LA, Argyropoulos DS. Comparative evaluation of three lignin isolation protocols for various wood species. J Agric Food Chem. 2006;54:9696–705. doi:10.1021/jf062433c.

55. Wu S, Argyropoulos D. An improved method for isolating lignin in high yield and purity. J Pulp Pap Sci. 2003;29:235–40.

56. Tohmura S, Argyropoulos DS. Determination of Arylglycerol-β-aryl ethers and other linkages in lignins using DFRC/31P NMR. J Agric Food Chem. 2001;49:536–42.

57. Martone PT, Estevez JMJM, Lu F, et al. Discovery of lignin in seaweed reveals convergent evolution of cell-wall architecture. Curr Biol. 2009;19:169–75. doi:10.1016/j.cub.2008.12.031.

58. Guerra A, Norambuena M, Freer J, Argyropoulos DS. Determination of arylglycerol-beta-aryl ether linkages in enzymatic mild acidolysis lignins (EMAL): comparison of DFRC/(31) P NMR with thioacidolysis. J Nat Prod. 2008;71:836–41. doi:10.1021/np800080s.

59. Lu F, Ralph J. Novel tetrahydrofuran structures derived from β–β-coupling reactions involving sinapyl acetate in Kenaf lignins. Org Biomol Chem. 2008;6:3681. doi:10.1039/b809464k.

60. Peng J, Lu F, Ralph J. Isochroman lignin trimers from DFRC-degraded Pinus taeda. Phytochemistry. 1999;50:659–66. doi:10.1016/S0031-9422(98)00572-X.

61. Ujihara M, Nakatsubo F, Katahira R. A novel selective cleavage method for β-O-4 substructure in lignins named TIZ method. I. Degradation of guaiacyl and syringyl models. J Wood Chem Technol. 2003;23:71–87. doi:10.1081/WCT-120018616.

62. Ando D, Nakatsubo F, Takano T, et al. Multi-step degradation method for β-O-4 linkages in lignins: γ-TTSA method. Part 3. Degradation of milled wood lignin (MWL) from Eucalyptus globulus. Holzforschung. 2013;67:835–41. doi:10.1515/hf-2013-0008.

63. Matsumoto Y, Ishizu A, Iiyama K, Nakano J. Selective cleavage of arylglycerol-β-aryl ether type structures in lignin. II. Determination of the arylglycerol-β-aryl ether type structure in milled wood lignin of spruce. Mokuzai Gakkaishi. 1982;28:249–54.

64. Ando D, Nakatsubo F, Takano T, et al. Multistep degradation method for β-O-4 linkage in lignins: γ-TTSA method. Part 2: Reaction of lignin model polymer (DHP). Holzforschung. 2013;67:249–56. doi:10.1515/hf-2012-0082.

65. Ando D, Takano T, Nakatsubo F. Multi-step degradation method for β-O-4 linkages in lignins: α-TSA method. Part 1: Reaction of non-phenolic dimeric β-O-4 model compound. Holzforschung. 2014;68:369–75. doi:10.1515/hf-2013-0126.

66. Rahimi A, Azarpira A, Kim H, et al. Chemoselective metal-free aerobic alcohol oxidation in lignin. J Am Chem Soc. 2013;135:6415–18. doi:10.1021/ja401793n.

67. Lancefield CS, Ojo OS, Tran F, Westwood NJ. Isolation of functionalized phenolic monomers through selective oxidation and C-O bond cleavage of the β-O-4 linkages in lignin. Angew Chemie Int Ed. 2015;54:258–62. doi:10.1002/anie.201409408.

68. Kim S, Chmely SC, Nimlos MR, et al. Computational study of bond dissociation enthalpies for a large range of native and modified Lignins. J Phys Chem Lett. 2011;2:2846–52. doi:10.1021/jz201182w.

69. Qu S, Dang Y, Song C, et al. Depolymerization of oxidized lignin catalyzed by formic acid exploits an unconventional elimination mechanism involving 3c–4e bonding: A DFT mechanistic study. ACS Catal. 2015;5:6386–96. doi:10.1021/acscatal.5b01095.

70. Rahimi A, Ulbrich A, Coon JJ, Stahl SS. Formic-acid-induced depolymerization of oxidized lignin to aromatics. Nature. 2014;515:249–52. doi:10.1038/nature13867.

71. Zhu R, Wang B, Cui M-S, et al. Chemoselective oxidant-free dehydrogenation of alcohols in lignin using Cp*Ir catalysts. Green Chem. 2015; doi: 10.1039/C5GC02347E.

72. Srebotnik E, Hammel KE. Degradation of nonphenolic lignin by the laccase/1-hydroxybenzotriazole system. J Biotechnol. 2000;81:179–88. doi:10.1016/S0168-1656(00)00303-5.

73. Rico A, Rencoret J, Del Río JC, et al. Pretreatment with laccase and a phenolic mediator degrades lignin and enhances saccharification of Eucalyptus feedstock. Biotechnol Biofuels. 2014;7:6. doi:10.1186/1754-6834-7-6.

74. Tsuji Y, Vanholme R, Tobimatsu Y, et al. Introduction of chemically labile substructures into Arabidopsis lignin through the use of LigD, the Cα-dehydrogenase from Sphingobium sp. strain SYK-6. Plant Biotechnol J. 2015;6:1–12. doi:10.1111/pbi.12316.

75. Ruiz-Dueñas FJ, Martínez ÁT. Microbial degradation of lignin: how a bulky recalcitrant polymer is efficiently recycled in nature and how we can take advantage of this. Rev Microb Biotechnol. 2009;2:164–77. doi:10.1111/j.1751-7915.2008.00078.x.

76. Tuomela M, Vikman M, Hatakka A, It M. Biodegradation of lignin in a compost environment: a review. Bioresour Technol. 2000;72:169–83.

77. Bugg TDH, Bugg TDH, Ahmad M, et al. Pathways for degradation of lignin in bacteria and fungi. Nat Prod Rep. 2011;28:1883–96. doi:10.1039/c1np00042j.

78. Sanders JPM, Clark JH, Harmsen GJ, et al. Process intensification in the future production of base chemicals from biomass. Chem Eng Process Process Intensif. 2012;51:117–36. doi:10.1016/j.cep.2011.08.007.

79. Tolbert A, Akinosho H, Khunsupat R, et al. Characterization and analysis of the molecular weight of lignin for biorefining studies. Biofuels, Bioprod Biorefining. 2014;836–856. doi: 10.1002/bbb.

80. Suhas K, Carrott PJM, Ribeiro Carrott MML. Lignin – from natural adsorbent to activated carbon: a review. Bioresour Technol. 2007;98:2301–12. doi:10.1016/j.biortech.2006.08.008.

81. Guo X, Zhang S, Shan X. Adsorption of metal ions on lignin. J Hazard Mater. 2008;151:134–42. doi:10.1016/j.jhazmat.2007.05.065.

82. Ahluwalia SS, Goyal D. Microbial and plant derived biomass for removal of heavy metals from wastewater. Bioresour Technol. 2007;98:2243–57. doi:10.1016/j.biortech.2005.12.006.

83. Doherty WOS, Mousavioun P, Fellows CM. Value-adding to cellulosic ethanol: lignin polymers. Ind Crops Prod. 2011;33:259–76. doi:10.1016/j.indcrop.2010.10.022.

84. Yu LY, Shen HM, Xu ZL. PVDF–TiO2 composite hollow fiber ultrafiltration membranes prepared by TiO2 Sol–Gel method and blending method. J Appl Phys. 2009;113:1763–72. doi:10.1002/app.

85. Yue X, Chen F, Zhou X, He G. Preparation and characterization of poly (vinyl chloride) polyblends with fractionated lignin. Int J Polym Mater. 2012;61:214–28. doi:10.1080/00914037.2011.574659.

86. Kubo S, Kadla JF. The formation of strong intermolecular interactions in immiscible blends of poly(vinyl alcohol) (PVA) and lignin. Biomacromolecules. 2003;4:561–7. doi:10.1021/bm025727p.

87. Alexy P, Košíková B, Crkonová G, et al. Modification of lignin-polyethylene blends with high lignin content using ethylene-vinylacetate copolymer as modifier. J Appl Polym Sci. 2004;94:1855–60. doi:10.1002/app.20716.

88. Alexy P, Košíková B, Podstránska G. The effect of blending lignin with polyethylene and polypropylene on physical properties. Polymer (Guildf). 2000;41:4901–8. doi:10.1016/S0032-3861(99)00714-4.

89. Berlin A, Balakshin M. Industrial lignins. Bioenergy Res Adv Appl. 2014; doi: 10.1016/B978-0-444-59561-4.00018-8.

90. Korich AL, Clarke KM, Wallace D, Iovine PM. Chemical modification of a lignin model polymer via arylboronate ester formation under mild reaction conditions. Macromolecules. 2009;42:5906–8. doi:10.1021/ma901146b.

91. Korich AL, Fleming AB, Walker AR, et al. Chemical modification of organosolv lignin using boronic acid-containing reagents. Polymer (Guildf). 2012;53:87–93. doi:10.1016/j.polymer.2011.10.062.

92. Thielemans W, Wool RP. Lignin esters for use in unsaturated thermosets: Lignin modification and solubility modeling. Biomacromolecules. 2005;6:1895–905. doi:10.1021/bm0500345.

93. Kim YS, Kadla JF. Preparation of a thermoresponsive lignin-based biomaterial through atom transfer radical polymerization. Biomacromolecules. 2010;11:981–8. doi:10.1021/bm901455p.

94. Sen S, Sadeghifar H, Argyropoulos DS. Kraft lignin chain extension chemistry via propargylation, oxidative coupling, and Claisen rearrangement. Biomacromolecules. 2013;14:3399–408. doi:10.1021/bm4010172.

95. Mbotchak L, Le Morvan C, Duong KL, et al. Purification, structural characterization and modification of organosolv wheat straw lignin. J Agric Food Chem. 2015;63:5178–88. doi:10.1021/acs.jafc.5b02071.

96. Sadeghifar H, Cui C, Argyropoulos DS. Toward thermoplastic lignin polymers. Part 1. Selective masking of phenolic hydroxyl groups in kraft lignins via methylation and oxypropylation chemistries. Ind Eng Chem Res. 2012;51:16713–20. doi:10.1021/ie301848j.

97. Glasser WG, Barnett CA, Rials TG, Saraf VP. Engineering plastics from lignin II. Characterization of hydroxyalkyl lignin derivatives. J Appl Polym Sci. 1984;29:1815–30. doi:10.1002/app.1984.070290533.

98. Laurichesse S, Avérous L. Synthesis, thermal properties, rheological and mechanical behaviors of lignins-grafted-poly(ε-caprolactone). Polymer (Guildf). 2013;54:3882–90. doi:10.1016/j.polymer.2013.05.054.

99. Liu X, Zong E, Jiang J, et al. Preparation and characterization of Lignin-graft-poly (ε-caprolactone) copolymers based on lignocellulosic butanol residue. Int J Biol Macromol. 2015;81:521–9. doi:10.1016/j.ijbiomac.2015.08.046.

100. Teramoto Y, Lee S-H, Endo T. Phase structure and mechanical property of blends of organosolv lignin alkyl esters with poly(ε-caprolactone). Polym J. 2009;41:219–27. doi:10.1295/polymj.PJ2008301.

101. Maharana T, Pattanaik S, Routaray A, et al. Synthesis and characterization of poly(lactic acid) based graft copolymers. React Funct Polym. 2015;93:47–67. doi:10.1016/j.reactfunctpolym.2015.05.006.

102. Sun Y, Yang L, Lu X, He C. Biodegradable and renewable poly(lactide)–lignin composites: synthesis, interface and toughening mechanism. J Mater Chem A Mater Energy Sustain. 2015;3:3699–709. doi:10.1039/c4ta05991c.

103. de Oliveira W, Glasser W. Multiphase materials with lignin. XIV. Star-like copolymers with caprolactone. J Wood Chem Technol. 1994;14:119–26. doi:10.1080/02773819408003089.

104. Chen R, Kokta BV. Graft copolymerization of lignocellulosic fibers. 1982; doi: 10.1021/bk-1982-0187.
105. Chen R, Kokta BV, Valade JL. Study on the graft copolymerization of lignosulfonate and acrylic monomers. J Appl Polym Sci. 1980;25:2211–20. doi:10.1002/app.1980.070251008.
106. Liu X, Yin H, Zhang Z, et al. Functionalization of lignin through ATRP grafting of poly(2-dimethylaminoethyl methacrylate) for gene delivery. Colloids Surf B: Biointerfaces. 2015;125:230–7. doi:10.1016/j.colsurfb.2014.11.018.
107. Hilburg SL, Elder AN, Chung H, et al. A universal route towards thermoplastic lignin composites with improved mechanical properties. Polymer (Guildf). 2014;55:995–1003. doi:10.1016/j.polymer.2013.12.070.
108. Qian Y, Zhang Q, Qiu X, Zhu S. CO 2 -responsive diethylaminoethyl-modified lignin nanoparticles and their application as surfactants for CO 2/N 2 -switchable Pickering emulsions. Green Chem. 2014;16:4963–8. doi:10.1039/c4gc01242a.
109. Kim YS, Youe W-J, Kim SJ, et al. Preparation of a thermoplastic lignin-based biomaterial through atom transfer radical polymerization. J Wood Chem Technol. 2015;35:251–9. doi:10.1080/02773813.2014.937006.
110. Raquez JM, Deléglise M, Lacrampe MF, Krawczak P. Thermosetting (bio)materials derived from renewable resources: a critical review. Prog Polym Sci. 2010;35:487–509. doi:10.1016/j.progpolymsci.2010.01.001.
111. Fan M. Lignin in straw and its applications as an adhesive. Int J Adhes Adhes. 2014;48:92–101.
112. Hemmilä V, Trischler J, Sandberg D. Lignin – an adhesive raw materials of the future or a waste of research energy? Northern European Network for wood science and engineering proceedings 9th meetings. 2013:98–103.
113. Ysbrandy RE, Gerischer RD, Sanderson GFR. Adhesives from autohydrolysis bagasse lignin, a renewable resource - Part II. DSC thermal analysis of novolac resins. Holzforschung. 2009;46:253–6.
114. Podschun J, Saake B, Lehnen R. Reactivity enhancement of organosolv lignin by phenolation for improved bio-based thermosets. Eur Polym J. 2015;67:1–11. doi:10.1016/j.eurpolymj.2015.03.029.
115. Podschun J, Stücker A, Saake B, Lehnen R. Structure–function relationships in the phenolation of lignins from different sources. ACS Sustain Chem Eng. 2015;3:2526–32. doi:10.1021/acssuschemeng.5b00705.
116. Yang S, Wen J, Yuan T, Sun R. Characterization and phenolation of biorefinery technical lignins for lignin–phenol–formaldehyde resin adhesive synthesis. RSC Adv. 2014;4:57996–8004. doi:10.1039/C4RA09595B.
117. Zou L, Ross BM, Hutchison LJ, et al. Enzyme and microbial technology fungal demethylation of Kraft lignin. Enzym Microb Technol. 2015;73–74:44–50. doi:10.1016/j.enzmictec.2015.04.001.
118. Nieto L, Jiménez-Barbero J, Martínez AT, et al. White and brown rot decay as two models for biotechnological processing of wood: structural analysis by 2D NMR and analytical pyrolysis. Oxid Enzym Sustain Ind Biocatal. 2010;1–6.
119. Kurimoto Y, Doi S, Tamura Y. Species effects on wood-liquefaction in polyhydric alcohols. Holzforschung. 1999; doi: 10.1515/HF.1999.102.
120. Kurimoto Y, Takeda M, Doi S, et al. Network structures and thermal properties of polyurethane films prepared from liquefied wood. Bioresour Technol. 2001;77:33–40. doi:10.1016/S0960-8524(00)00136-X.
121. Sain NYM. A new method for demethylation of lignin from woody biomass using biophysical methods. J Chem Eng Process Technol. 2013;4:1–6. doi:10.4172/2157-7048.1000160.
122. An XN, Schroeder HA, Thompson GE. Demethylated kraft lignin as a substitute for phenol in wood adhesive. Chem Ind For Prod. 1995;15:36–42.
123. Wu SB, Zhan HY. Characteristics of demethylated wheat straw soda lignin and its utilization in lignin-based phenolic formaldehyde resins. Cellul Chem Technol. 2001;35:253–62.

124. Malutan T, Nicu R, Popa VI. Contribution to the study of hydroxymethylation. Bioresources. 2008;3:13–20.
125. Hu L, Pan H, Zhou Y, Zhang M. Methods to improve lignin's reactivity as a phenol substitute and as replacement for other phenolic compounds: a brief review. Bioresources. 2011;6:3515–25. doi:10.15376/biores.6.3.3515-3525.
126. YouBing M, ChunPeng W, LinWu Z, FuXiang C. Study on composite adhesive of hydroxy-methylated lignosulfonate/phenol-formaldehyde resin with low free formaldehyde. Chem Ind For Prod. 2009;29:38–42.
127. Li Y, Ragauskas AJ. Kraft lignin-based rigid polyurethane foam. J Wood Chem Technol. 2012;32:210–24. doi:10.1080/02773813.2011.652795.
128. Yang L, Wang X, Cui Y, et al. Modification of renewable resources-lignin-by three chemical methods and its applications to polyurethane foams. Polym Adv Technol. 2014;25:1089–98. doi:10.1002/pat.3356.
129. Chung H, Washburn NR. Improved lignin polyurethane properties with lewis acid treatment. Appl Mater Interfaces. 2012;4:2840–6.
130. Huang J. Effects of NCO/OH molar ratio on structure and properties of graft-interpenetrating polymer networks from polyurethane and nitrolignin. Polymer (Guildf). 2002;43:2287–94. doi:10.1016/S0032-3861(02)00028-9.
131. Zhang L, Huang J. Effects of hard-segment compositions on properties of polyurethane-nitrolignin films. J Appl Polym Sci. 2001;81:3251–9. doi:10.1002/app.1780.
132. Pan X, Saddler JN. Effect of replacing polyol by organosolv and kraft lignin on the property and structure of rigid polyurethane foam. Biotechnol Biofuels. 2013;6:12. doi:10.1186/1754-6834-6-12.
133. Bernardini J, Cinelli P, Anguillesi I, et al. Flexible polyurethane foams green production employing lignin or oxypropylated lignin. Eur Polym J. 2015;64:147–56. doi:10.1016/j.eurpolymj.2014.11.039.
134. Cateto CA, Barreiro MF, Rodrigues AE, Belgacem MN. Optimization study of lignin oxypropylation in view of the preparation of polyurethane rigid foams. Ind Eng Chem Res. 2009;48:2583–9. doi:10.1021/ie801251r.
135. Tserki V, Zafeiropoulos NE, Simon F, Panayiotou C. A study of the effect of acetylation and propionylation surface treatments on natural fibres. Compos Part A Appl Sci Manuf. 2005;36:1110–18. doi:10.1016/j.compositesa.2005.01.004.
136. Maldhure AV, Ekhe JD, Deenadayalan E. Mechanical properties of polypropylene blended with esterified and alkylated lignin. J Appl Polym Sci. 2012;125:1701–12. doi:10.1002/app.
137. Li Y, Sarkanen S. First alkylated 95–100% kraft lignin based plastics. 1997. In: Int. Symp. Wood Pulping Chem. Proceedings, ISWPC. Canadian Pulp & Paper Association, p. 63–1/63.
138. Li Y, Sarkanen S. Alkylated kraft lignin-based thermoplastic blends with aliphatic polyesters. Macromolecules. 2002;35:9707–15. doi:10.1021/ma021124u.
139. Sen S, Patil S, Argyropoulos DS. Methylation of softwood kraft lignin with dimethyl carbonate. Green Chem. 2015;17:1077–87. doi:10.1039/C4GC01759E.
140. Wang Y-Y, Chen Y, Sarkanen S. Path to plastics composed of ligninsulphonates (lignosulfonates). Green Chem. 2015;17:5069–78. doi:10.1039/C5GC01865J.
141. Strassberger Z, Prinsen P, van der Klis F, et al. Lignin solubilisation and gentle fractionation in liquid ammonia. Green Chem. 2015;17:325–34. doi:10.1039/C4GC01143K.
142. Duval A, Lange H, Lawoko M, Crestini C. Reversible crosslinking of lignin via the furan-maleimide Diels-Alder reaction. Green Chem. 2015; doi: 10.1039/C5GC01319D.
143. Duval A, Lange H, Lawoko M, Crestini C. Modification of Kraft lignin to expose diazobenzene groups: toward pH- and light-responsive biobased polymers. Biomacromolecules. 2015;16:2979–89. doi:10.1021/acs.biomac.5b00882.
144. Gao G, Xu WZ, Kadla JF. Reversible pH-responsive hydrogels of softwood Kraft lignin and poly [(2-dimethylamino) ethyl Methacrylate] -based polymers. J Wood Chem Technol. 2014;35:73–90. doi:10.1080/02773813.2014.909656.

145. Deng Y, Liu Y, Qian Y, et al. Preparation of photoresponsive azo polymers based on lignin, a renewable biomass resource. ACS Sustain Chem Eng. 2015;3:1111–16. doi:10.1021/acssuschemeng.5b00261.

146. Duval A, Lange H, Lawoko M, Crestini C. Reversible crosslinking of lignin via the furan–maleimide Diels–Alder reaction. Green Chem. 2015;17:4991–5000. doi:10.1039/C5GC01319D.

147. Yang Y, Deng Y, Tong Z, Wang C. Renewable lignin-based xerogels with self-cleaning properties and superhydrophobicity. ACS Sustain Chem Eng. 2014;2:1729–33. doi:10.1021/sc500250b.

148. Sivasankarapillai G, Li H, McDonald AG. Lignin-based triple shape memory polymers. Biomacromolecules. 2015;16:2735–42. doi:10.1021/acs.biomac.5b00655.

149. Li H, Sivasankarapillai G, McDonald AG. Highly biobased thermally-stimulated shape memory copolymeric elastomers derived from lignin and glycerol-adipic acid based hyperbranched prepolymer. Ind Crops Prod. 2015;67:143–154. doi: http://dx.doi.org/10.1016/j.indcrop.2015.01.031.

150. Li H, Sivasankarapillai G, McDonald AG. Lignin valorization by forming thermally stimulated shape memory copolymeric elastomers—partially crystalline hyperbranched polymer as crosslinks. J Appl Polym Sci. 2015; doi: 10.1002/app.41389.

151. Li H, Sivasankarapillai G, McDonald AG. Lignin valorization by forming toughened thermally stimulated shape memory copolymeric elastomers: evaluation of different fractionated industrial lignins. J Appl Polym Sci. 2015;132:41389–402. doi:10.1002/app.41389.

152. Dallmeyer I, Chowdhury S, Kadla JF. Preparation and characterization of kraft lignin-based moisture-responsive films with reversible shape-change capability. Biomacromolecules. 2013;14:2354–63. doi:10.1021/bm400465p.

Chapter 8
Carbon Materials from Lignin and Their Applications

Juan J. Rodríguez, Tomás Cordero, and José Rodríguez-Mirasol

8.1   Introduction

Lignin is a naturally-occurring polymer widely available since it is one of the three major components of wood and lignocellulosics. Nevertheless, lignin has not been exploited so far as a raw material itself but as a waste or at most, a byproduct from chemical and pulp cellulose production. As a rough estimate, the pulping processes give rise to about 60 Mt/year of lignin in black liquors that are mostly used as fuel. Among other considerations, alternative ways for diversifying the valorization of those black liquors would provide industry the chance of eventually increasing the production rate without the expensive revamping of the evaporation unit. Moreover, new concepts of biorefineries based on lignocellulosic resources will contribute in the future to increase the availability of lignin, thus reinforcing the need of developing technical solutions allowing its commercial valorization.

Industrial processes involving the separation of the cellulosic and lignin fractions leave different types of modified or so-called technical lignins going from hydrolytic (i.e., organosolv) to more deeply transformed ones, like Kraft lignin and lignosufonates. In all the cases, the polymeric structure of lignin is degraded to varying extents implying strong chemical conversion such as in Kraft and sulfite processes and some foreign elements are introduced. Kraft lignin, derived from the most important pulping process commonly contains more than 1 % S on a dry ash-free (d.a.f.) basis and ash contents that can exceed 10 % on a dry basis (d.b.) depending on its method of isolation from the black liquors. However, in spite of those

J.J. Rodríguez (✉)
Sección de Ingeniería Química, Universidad Autónoma de Madrid, Madrid, Spain
e-mail: juanjo.rodriguez@uam.es

T. Cordero (✉) • J. Rodríguez-Mirasol
Andalucía Tech, Departamento de Ingeniería Química, Universidad de Málaga, Málaga, Spain
e-mail: cordero@uma.es; mirasol@uma.es

modifications, the so-called technical lignins maintain two important features regarding their potential applications. Firstly, a fairly high C content compared with the other most abundant non-fossil carbonaceous material (cellulose, including hemicelluloses) and on the other hand an aromatic-rich chemical structure. Both issues favor conversion into carbon materials as a promising way of valorization. This can be achieved upon well-known thermal or, more generally, so-called thermochemical processes, like pyrolysis and gasification. These kinds of solutions appear in principle to be more feasible for full-scale implementation in the short term than those addressed to the conversion of lignin into chemicals that require extensive research and development. Although heterogeneous chemical composition of lignin offers the opportunity of obtaining a wide diversity of potentially useful compounds at low individual yields, expensive separation and purification steps would be required thus representing a serious drawback for industrial development. Therefore, thermochemical conversion provides a number of promising solutions for lignin valorization scarcely investigated up to the last three decades when a growing interest has been emerging in the literature.

The most basic carbon material obtainable from lignin, as from any carbonaceous precursor, is char, namely the solid resulting from devolatilization upon thermal treatment in inert (or oxygen-poor) atmosphere. That process is a form of pyrolysis, commonly called carbonization or charring, whose extent depends on the operating temperature, holding time and the own nature of the precursor, which determine the C content of the final product as well as its basic structural and textural characteristics. Activated carbons with a well-developed porosity are value-added materials allowing applications in adsorption and catalysis. More advanced carbon materials have also been prepared from lignin, including carbon fibers, nanostructured carbons with hierarchical porous structure and highly ordered carbons showing in some cases well developed graphitic domains although without the regular tri-dimensional order of graphite. All of these materials, which have been prepared so far only on the lab-scale, will be reviewed in the following sections. Figure 8.1 shows a picture of the possibilities investigated for the synthesis of carbon materials from so-called technical lignins, namely more or less modified lignins derived from pulping processes, most commonly kraft and organosolv. A review on those possibilities has been published by our group [1].

8.2   Activated Carbons from Lignin

Activated carbons (AC) are C-rich solids with high surface area associated to a well-developed porosity predominantly within the micropore range (up to 2 nm width) but with varying contributions of mesopores (2–50 nm) and macropores (>50 nm). In principle, they can be obtained from almost any carbonaceous precursor but in practice the nature of the starting material is an important issue regarding the porous texture and the mechanical resistance of the final product, both affecting their potential applications. A large number of materials have been tested as activated carbon precursors, going from peat, lignite and coals of different ranges to a heterogeneous
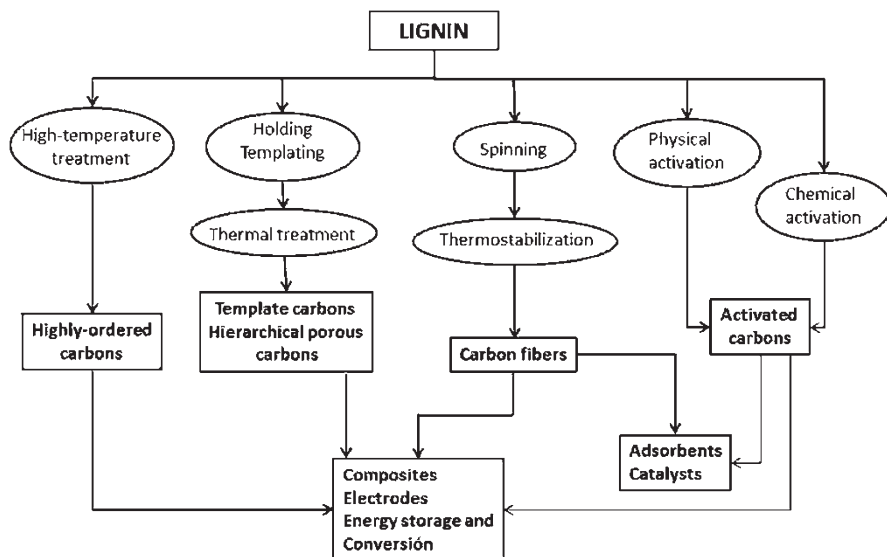
Fig. 8.1 Synthesis of carbon materials from lignin and their potential applications

universe of agricultural and woody residues as well as synthetic polymers. However, many of them have been used only in lab-scale research-oriented studies and the most commonly used as industrial raw materials include peat, lignite, coals, wood and coconut shell [2–4].

Lignin has not been used thus far for full-scale manufacture of activated carbon in spite of the existence of some patents already in the 1970s and 1980s [5, 6] and the renewed interest in the recent patent literature [7, 8]. However, in the last three decades a growing number of papers have been published in the scientific literature devoted to the preparation and characterization of lignin-derived activated carbons. Different types of lignins have been used, proceeding mainly from pulping and hydrolytic processes of wood and other lignocellulosic materials. In this chapter, the focus will be on that scientific literature since it contains more comprehensive information in terms of the porous texture and the surface chemistry, the main features of the activated carbons regarding their potential applications. ACs can be obtained upon partial gasification of chars from previous carbonization, the so-called physical activation, or by heat-treatment of the raw precursor with the addition of some chemicals, namely chemical activation. Both ways have been used with lignin, giving rise to the diversity of activated carbons so far reported in the literature.

8.2.1   Physical Activation

Physical activation proceeds most commonly in two steps consisting in a previous carbonization of the starting precursor followed by partial gasification of the resulting char with steam, carbon dioxide or eventually air. The former is more frequently

used at industrial scale whereas in experimental lab-studies carbon dioxide has been usually preferred since it allows easier control of the porosity development due to its lower reactivity.

Scientific studies on physical activation of lignin have mainly used carbon dioxide as activating agent and Kraft lignin as precursor, although steam and other types of lignin have also been employed, always in the above mentioned two-step approach of carbonization followed by partial gasification. Del Bagno et al. [9] presented a technical report in 1978 on pilot plant manufacture of char and activated carbon but using directly black liquors rather than lignin as starting material. More than one-decade later, Li and Van Heiningen [10, 11] reported on the CO_2-gasification of kraft black liquors focusing on the kinetics. Pioneer work in the scientific literature on the preparation and in-depth characterization of activated carbons from lignin was accomplished by the authors of this chapter [12, 13]. We studied the CO_2-activation of chars from eucalyptus kraft lignin isolated from black liquors by precipitation with H_2SO_4 followed by centrifugation and fluidized bed drying. The resulting lignin yielded around 12 % (d.b.) ash content and a representative elemental composition of around 65 % C, 5 % H and 1.2 % S (d.a.f.). To avoid the undesirable swelling observed upon carbonization at low ash content, the starting lignin was pre-devolatilized under N_2 atmosphere at low temperature (350 °C) before deashing and the resulting solid was then washed up to a low ash percentage (≈ 2 %) with 1 % aqueous H_2SO_4. Further carbonization was performed in a static horizontal tube furnace under continuous nitrogen flow at different final temperatures (450–900 °C) reached at low heating rate (10 °C/min) and maintained for 2 h. The activation of the resulting chars was carried out in the same device by partial gasification under continuous flow of CO_2 at 800 and 850 °C and holding times between 4 and 40 h in order to cover a wide range of burn-off (b.o., namely the percentage weight-loss of the char on d.a.f. basis upon gasification).

Although the partial gasification step, namely activation, gives rise to the well-developed porous texture demanded as a main feature of activated carbons, the previous carbonization is in general quite important for the sake of creating, upon devolatilization, the starting frame of pores facilitating further activation. Thus, it also deserves attention as in fact demonstrates the existing literature. Otani et al. [14] reported results on the carbonization of hydrolytic lignin byproduct of ethanol production from eucalyptus wood. These authors followed the structural changes of the carbonized material at increasing temperature up to 2400 °C by means of infrared spectroscopy (IR), X-ray diffraction (XRD) and small-angle X-ray scattering (SAXS). From this, they detected the presence of micropores above 700 °C. Between that temperature and 1700 °C the size of micropores increased slowly and their number remained about constant. At higher temperatures the microporosity was disappearing. However, the authors did not provide values of surface area neither of pore volume. Cordero et al. [15] studied the thermal decomposition of eucalyptus Kraft lignin from thermogravimetric experiments in N_2 atmosphere at low heating rate (5 °C/min). It extended over a wider temperature range than that of cellulose, covering approximately from 200 to 550 °C, with most of the weight loss occurring within 300–500 °C. Several peaks were clearly detected by DTG, the most important

being centered around 400 °C but extending upon the 300–450 °C region. Since it is a complex process involving multiple reactions, the authors obtained a distribution function of activation energy showing at least three peaks, the main one spreading over a relatively broad region ($\approx$80–105 kJ/mol). Orfao et al. [16] reported on the thermal decomposition of a commercial lignin from pine wood. At the same heating rate of 5 °C/min they obtained a broad DTG curve with a single recognizable maximum around 360–370 °C. They did not found significant differences in inert and air atmosphere up to about 300 °C, indicative of the resistance of lignin to combustion below that temperature.

The results of the carbonization step in terms of carbon yield and porous texture of the char is dependent of the nature of the precursor but is affected also by the final temperature and holding time as well as the heating rate, this last being in general a crucial issue. In the carbonization step of the above described Kraft lignin we [12] observed an increase of BET surface area at increasing temperature followed by further decrease, consistently with a pore constriction effect, commonly found with other precursors, associated to the increased severity of thermal treatment. The micropore volumes measured with CO_2 at 0 °C were higher than the obtained with N_2 at −196 °C, being the difference more pronounced as the charring temperature was increased. That indicates a narrow microporosity of the chars and supports the above mentioned effect of the thermal treatment temperature. The maximum BET surface area achieved for the 550 °C char was almost 500 m^2/g which decreased somewhat at 800 °C ($\approx$460 m^2/g) and much more significantly at the highest carbonization temperature tested ($\approx$280 m^2/g at 900 °C). A similar trend on the evolution of BET surface area with the heat treatment temperature was observed by Baklanova et al. [17] in the carbonization of hydrolytic lignin at a very low heating rate (0.1–4 °C/min). Xie et al. [18] obtained chars with BET surface area also close to 450 m^2/g, but at higher temperature (700 °C), upon carbonization of an organosolv lignin previously air-treated at 240 °C. This previous treatment must have a relevant effect on the behavior during the following pyrolysis step since no significant development of BET surface area was observed up to 500 °C while a sharp increase up to the above mentioned value occurred at 700 °C without further significant variation at 1000 °C. Kijima et al. [19] reported on the carbonization of kraft lignin up to 900 °C at different heating rates. They found a dramatic effect of that variable so that the resulting chars yielded BET surface area values as different as 30 and 530 m^2/g at 10 and 1 °C/min, respectively. The highest surface area char can be considered in fact as a true activated carbon since after water washing yielded 740 m^2/g. It was an essentially microporous solid but the authors obtained carbons with much higher surface area and a very important contribution of mesoporosity upon carbonization under the same conditions of micellar and polymeric gelled lignins prepared from the starting kraft lignin. They achieved as much as 1340 and 1420 m^2/g BET surface area, respectively, with close to 40 and more than 60 % of the total pore volume corresponding to mesopores. As one conclusion, carbonization of lignin allows formation of chars with fairly high surface area values compared with many other of different origins in spite of the significantly higher mass yield obtained upon lignin carbonization (up to 40–45 % vs less than 20–25 % for

most non-fossil carbonaceous precursors). In fact, that 20–25 % yield can be achieved in the case of woody and other lignocellulosic precursors thanks to the lignin component since the cellulosic fractions give much lower relative amounts of char upon carbonization [15, 18]. However, while the carbon yield is not significantly affected by the heating rate this variable seems to be very important regarding the porosity of the resulting chars. Sharma et al. [20], working at heating rates in the order of 100–150 °C/min, reported maximum BET surface area values as low as 5 m^2/g at 350–400 °C, decaying sharply beyond that range whereas the carbon yield was maintained within the above mentioned commonly found values for lignin (40 % at 750 °C). Kuznetsov and Shchipko [21] obtained chars with up to almost 150 m^2/g upon carbonization of an industrial hydrolytic lignin from wood hydrolysis in a fluidized bed pilot plant, thus at a very high heating rate which might be in the range of flash pyrolysis. However, their results serve only to partially assess the effect of very high heating rates on the textural properties of chars from lignin pyrolysis, since those authors used substoichiometric air as fluidizing gas and a γ-alumina-supported Cu-Cr catalyst. In fact, comparatively low yields (15–28 %) and a wide range of BET surface area values (12–144 m^2/g) were obtained.

Upon CO_2-activation at 800 °C of our aforementioned Kraft lignin chars of high surface area (≈500 m^2/g) activated carbons were obtained with differently developed porous texture depending on the burn-off [12]. Up to around 30 % b.o. essentially microporous carbons were obtained with a very low contribution of mesoporosity so that the so-called external area (namely, the non-microporous area) was only 6 % of the 760 m^2/g BET surface area obtained at 28 % b.o. Within that b.o. range close values of micropore volumes were measured with N_2 and CO_2, indicative of narrow and homogeneous microporosity. Beyond that b.o. a progressive widening of the microporosity and growing mesoporosity were observed. After 20 h of activation somewhat more than 50 % b.o. was achieved. The resulting AC was a frankly mesoporous carbon with more than 30 % of its 1100 m^2/g BET surface area corresponding to external area. Upon 40 h of activation the burn-off exceeded 75 %, giving rise to a carbon with around 1350 m^2/g BET surface area and a highly developed mesoporosity (≈500 m^2/g external area). We also investigated the CO_2-activation of the aforementioned low-temperature char (350 °C) [13]. Now 800 and 850 °C were tested as activation temperatures, covering a similarly wide b.o. range than before. The evolution of the porous texture was analogous to the above described but now higher surface area values were achieved, reaching more than 1850 m^2/g at the highest b.o. (77 %), with 480 m^2/g being external area. The activation temperature did not show significant effect on the final porous texture which was essentially determined by the degree of burn-off. Table 8.1 summarizes a representative picture on the porous texture of the resulting carbons. In addition to the b.o. values, those of the overall yield of lignin to activated carbon are included. These results indicate a fairly regular development of porosity as activation proceeds consisting on continuous creation of micropores as well as widening of existing micro and mesopores.

Figure 8.2 helps to follow the evolution of the porous texture upon physical activation of Kraft lignin with CO_2. The N_2 adsorption-desorption isotherms (−196 °C)

Table 8.1 Characterization of the porous texture of representative activated carbons obtained by CO_2-activation of a low temperature char (350 °C) from Kraft lignin

Burn-off (% d.a.f.)	Overall yield (% d.a.f.)	BET surface area (m^2/g)	External area (m^2/g)	Micropore volume (cm^3/g)	Mesopore volume (cm^3/g)	Macropore volume (cm^3/g)
11.5	35.4	747	24	0.29	0.02	0.02
21.3	31.5	822	62	0.31	0.06	0.02
34.3	26.3	947	183	0.34	0.31	0.03
51.2	19.5	1223	327	0.36	0.63	0.06
63.5	14.6	1348	409	0.42	0.78	0.15
76.8	9.3	1853	480	0.57	0.86	0.53
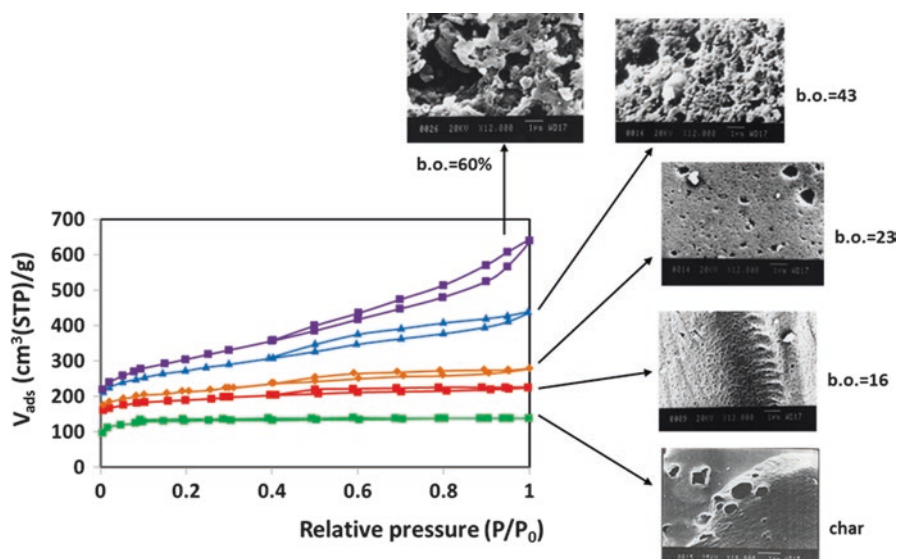
Fig. 8.2 N_2 adsorption–desorption isotherms (−196 °C) of activated carbons from Kraft lignin at different burn-off (b.o.)

of the activated carbons obtained at different b.o. show the progressive shift towards more open porosity with higher contribution of mesopores as activation proceeds. A char has been also included confirming its essentially microporous character.

In addition to the development of the porous texture upon activation, it is important to understand the kinetics of the process for design purposes. In that sense, we have investigated the kinetics of CO_2-gasification of chars derived from conventional pyrolysis of eucalyptus kraft lignin at different charring temperatures within a wide range (550–1400 °C). The experiments were carried out in a temperature-programmed reaction system based on a modified thermogravimetric device [22]. Our conclusion is that the gasification process was a combined result of uncatalysed and Na-catalysed reaction, both well represented by similar values of apparent

activation energy ($\approx$200–250 kJ/mol, depending on the charring temperature) within the range of gasification temperatures investigated (800–950 °C). Almost similar values of apparent activation energy were obtained for the low-temperature (350 °C) chars under similar gasification conditions [13]. Both, the magnitude of the apparent activation energy and the fact that the Arrhenius plots showed essentially parallel straight lines at different conversion values within a wide range (X = 0.2–0.8) support the conclusion that CO_2-gasification in those experiments proceeded under chemical control and thus the values of activation energy could be extrapolated to a full-scale process without mass-transfer limitations. The values of reactivity were about threefold lower that the obtained for CO_2-gasification of eucalyptus wood [23] but the temperature-dependence was quite similar according to the activation energy (230–260 kJ/mol). All these values are in the vicinity of the 250 kJ/mol reported by Li and Van Heiningen for the aforementioned CO_2-gasification of Kraft black liquors chars [10, 11].

Steam-activation of lignin chars has been also investigated by some authors. Steam is more reactive than CO_2 as gasifying agent, thus making it more difficult to control the development of porosity along the process since diffusion limitations are more likely. Therefore, lower temperatures are commonly used to obtain carbons with a well-developed microporosity providing high surface areas. Steam-activation is expected to create pores with a wider size distribution from the early stages of burn-off. Carrott et al. [24] compared steam- and CO_2-activation of chars from spruce Kraft lignin and a hydrolytic lignin from sugar can bagasse. They found up to fivefold higher gasification rates with steam. Although the activation was carried out at a relatively low temperature (750 °C), the Kraft lignin-derived carbons showed a poorly developed porous texture which can be explained by the high content of inorganic matter of the precursor, close to 24 %, consisting mainly in sodium carbonate and sulfate. First of all, that inorganic matter represents an inert fraction for the sake of pore creation but moreover it catalyzes the gasification reactions so that, even at that low temperature, activation proceeds under diffusion control, more pronounced in the case of steam. The highest BET surface area values were 79 and 460 m²/g by steam- and CO_2-activation, respectively. Meanwhile, with the hydrolytic lignin ($\approx$2 % ash content) somewhat more than 1000 and almost 1650 m²/g were achieved, with a higher relative contribution of mesoporosity in the case of steam-activation.

Earlier work on steam-activation of lignin was carried out by Gergova et al. [25]. The authors provided some data on the porous texture of chars obtained by steam pyrolysis of hydrolytic lignin at 700 °C and 2 h, but without any additional information on the extent of activation. They reported a total pore volume around 1.5 cm³/g. This value was much higher than the obtained from microcrystalline cellulose but corresponded mostly to macropores, while the micropore volumes were quite similar with both precursors ($\approx$0.35 cm³/g). Kuznetsov and Shchipko [21] obtained activated carbons by steam-activation of chars from an industrial wood hydrolysis-derived lignin in a fluidized bed pilot plant. The authors reported a high BET surface area of almost 770 m²/g, at 780 °C and 53 % burn-off, equivalent to 15 % overall yield. Perezdrienko et al. [26] analyzed the creation of surface oxygen groups upon

steam-activation of lignin chars from cotton hydrolytic lignin at 800 °C but did not include information on the development of porosity. Baklanova et al. [17] prepared activated carbons by steam-activation at higher temperature (800 °C) using as precursor an industrial hydrolytic lignin with 13 % of cellulose and slightly more than 3 % ash content. The authors found a continuous increase of BET surface area with burn-off, reaching 860 m^2/g at 82 % b.o. Nevertheless, they did not report data within the 57–82 % range, where it cannot be discarded the existence of a maximum value of surface area. Beyond 40 % b.o. the resulting activated carbons showed quite similar values of micropore and mesopore volume, being the last increasingly higher at b.o. above 50 % (0.30 vs 0.36 cm^3/g at 57 % b.o. and 0.36 vs 0.46 cm^3/g at 82 % b.o.). However, even at intermediate burn-offs the average micropore size remained fairly small (0.6–0.7 nm) although the authors do not provide information on the size distribution. Fu et al. [27] prepared activated carbons by steam-activation of chars obtained from dewatered black liquors. The starting material had more than 40 % ash content hindering seriously the development of porosity along the carbonization and the subsequent steam-activation. The chars from the first step had less than 60 m^2/g BET surface area, half of it corresponding to external or no-microporous area. Upon steam-activation at 700–850 °C the resulting carbons yielded 310 m^2/g at the most, being one-half external area so that most of the pore volume felt within the mesopore range, allowing methylene blue adsorption capacities in the vicinity of 90 mg/g, a fairly nice value in terms of per unit surface area.

In comparison with wood and other lignocellulosic precursors [28–34], physical activation of lignin, such as CO_2-activation, yields activated carbons of higher surface area and wider pore size distribution, with a more developed mesoporosity which is an important feature for liquid-phase applications in adsorption and catalysis. Therefore, lignin can be considered as a key component regarding the activation of those materials. Another important difference for the sake of the potential application of lignin as activated carbon precursor comes from the significantly higher mass yield compared with wood and other lignocellulosic materials at similar extent of activation (measured as burn-off).

8.2.2   Chemical Activation

So-called chemical activation proceeds upon carbonization with the addition of some agents that promote the thermal decomposition of the precursor with a reduced formation of tarry matter so that a high porosity is created without needing the further gasification step of physical activation. Moreover, some activating agents used favor dehydration and dehydrogenation pathways so that porosity can be developed with a lower loss of C, thus allowing significantly higher carbon yields with equivalent and even higher surface area values. The most common activating agents are zinc chloride, phosphoric acid and sodium and potassium hydroxides and carbonates. All of them have been used in chemical activation studies of lignin. The use of zinc chloride, which was the preferred agent in the past, has been progressively restricted due to the stringent regulations derived from environmental concerns.

Our group [35] reported earlier results on the chemical activation of lignin. A wide spectrum of activated carbons were obtained upon activation with $ZnCl_2$ of our already described kraft lignin by varying the temperature (350–600 °C) and the impregnation ratio (IR = $ZnCl_2$/lignin weight ratio, 0.4–2.3). The holding time at the final temperature (reached at 10 °C/min) was always 1 h. At low temperature (≈400 °C) and impregnation ratios up to 1 the resulting carbons showed a predominantly narrow microporous texture with fairly low contribution of mesopores, being the highest BET surface area achieved close to 1250 m^2/g. Increasing the activation temperature and the impregnation ratio allowed obtaining activated carbons still essentially microporous but with an increasingly wider distribution of micropore size while the mesopore volume and the corresponding external area were also progressively increased although remaining always the mesopore size distribution predominantly within the lower range (≤5 nm diameter). The nature of this porous texture suggests a quite uniform distribution of $ZnCl_2$ throughout the carbonizing lignin matrix, favored by the softening of Kraft lignin within a low temperature range (≈180–280 °C). BET and external area values in the vicinity of 1800 and 200 m^2/g, respectively, were obtained at 500 °C and IR = 2.3. Above that temperature a decrease of surface area was observed. The highest value of BET surface area is equivalent to the previously given for CO_2-activation of the same precursor, but the relative contribution of mesoporosity is now much lower. A very important difference is the much higher yield associated to $ZnCl_2$-activation (more than 40 % vs around 10 % for the highly activated carbons with CO_2). Regarding to other precursors, the activation of Kraft lignin with $ZnCl_2$ yielded carbons with lower mesoporosity than the obtained by other authors from coconut shell [34] but the opposite can also be found compared with some other lignocellulosic materials [29, 36].

Chemical activation of the aforementioned Kraft lignin was also accomplished with H_3PO_4 [37] within the same temperature range and at impregnation ratios of 1–3. Some significant differences were observed respect to $ZnCl_2$-activation. Now, significantly higher BET surface area was achieved at lower temperature (almost 1050 m^2/g vs less than 750 m^2/g at 350 °C). The activation temperature for maximum surface area was also lower (425 vs 500 °C) but the highest BET surface area (≈1450 m^2/g) was now about 20 % below the obtained with $ZnCl_2$. The most relevant feature was the remarkable effect of the impregnation ratio on the development of mesoporosity, so that increasing IR led to significantly higher mesopore volume and correspondingly external area values. Table 8.2 summarizes the results obtained with H_3PO_4 activation at 425 °C and different impregnation ratios.

Table 8.2 Characterization of the porous texture of the activated carbons from H_3PO_4-activation of Kraft lignin at 425 °C and different impregnation ratios (IR)

IR	BET surface area (m^2/g)	External area (m^2/g)	Micropore volume (cm^3/g)	Mesopore volume (cm^3/g)
1	1336	18	0.62	0.16
2	1459	281	0.82	0.53
3	1363	662	0.36	0.72
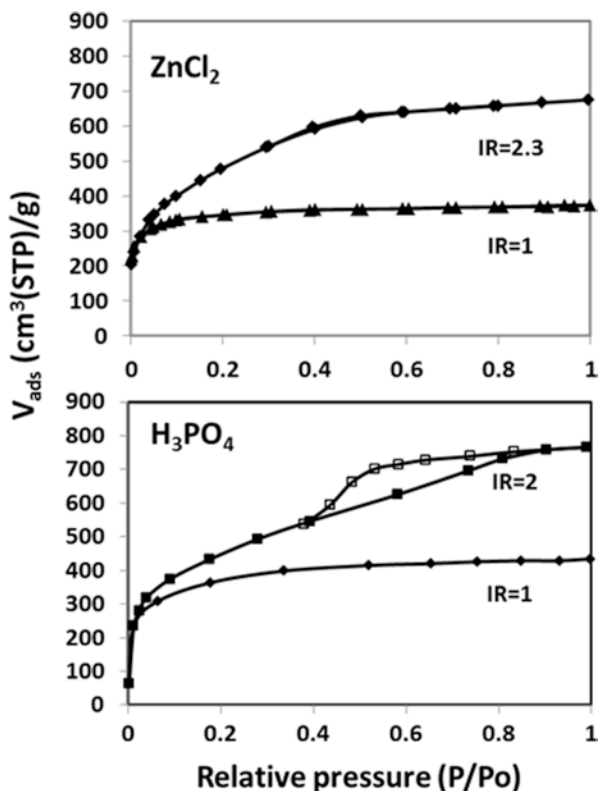
Fig. 8.3 N_2 adsorption–desorption isothems (-196 °C) of chemically-activated carbons from kraft lignin with $ZnCl_2$ and H_3PO_4 at different impregnation ratios. Adapted with permission from reference [35] (Copyright 1997, American Chemical Society) and from Ref. [37] (Copyright 2004, Elsevier)

Figure 8.3 depicts representative N_2 adsorption–desorption isotherms of activated carbons prepared from kraft lignin with $ZnCl_2$ and H_3PO_4 as activating agents at the respective optimum temperature and different impregnation ratios. The already described effect of this variable can be clearly seen from the evolution of the shape of the isotherms. Activation with H_3PO_4 gives rise to a significantly more pronounced development of mesoporosity at increasing IR compared to $ZnCl_2$.

The results of Table 8.2 clearly show a dramatic increase of the external surface area (basically that of mesopores) with the IR. At the highest IR tested (IR = 3) the contribution of mesoporosity represents close to one-half the total or BET surface area whereas at IR = 1 that contribution becomes of a very low relevance. Up to IR ≈ 2, significant creation of micropores coexists with conversion into mesopores whereas at IR = 3 this last seems by far the prevailing phenomenon through widening and coalescence of existing micropores. Guo and Rockstraw [38] observed a similar trend on the effect of the impregnation ratio in H_3PO_4-activation of Kraft

lignin at 400 °C, although with significantly lower values of micropore volume within the whole range of IR tested (0.5–2.5). They found also a dramatic increase of the mesopore volume beyond an impregnation ratio of 2. The highest BET surface area occurred at 450 °C, close to the above mentioned temperature, and the value was also quite similar ($\approx$1500 m^2/g). They reported a higher value for cellulose-derived activated carbon under the same conditions, but with a highly microporous texture.

Hayashi et al. [39] covered a range of higher activation temperatures in the H_3PO_4- and $ZnCl_2$-activation (IR = 1 in both cases) of a CO_2-precipitated lignin from spruce Kraft black liquors. The highest BET surface area occurred at 600 °C, with around 1050 and 1300 m^2/g, respectively, both quite similar to our previous values under the same conditions. Further decrease of surface area was observed at increased temperatures, falling to $\approx$700 m^2/g at 900 °C with both activating agents. That decrease was attributed to thermal shrinkage after analyzing the fractal dimension of the carbons [40]. Sun et al. [41] obtained microporous-mesoporous carbons from corn straw lignin acid-precipitated from black liquors upon H_3PO_4-activation at IR = 2 and temperatures between 300 and 600 °C. The highest BET surface area ($\approx$800 m^2/g) and total pore volume ($\approx$0.8 cm^3/g) occurred at 500 °C. The pore size distribution from the DFT method showed two peaks around 1 and 3 nm and a modest contribution of mesoporosity except at the above mentioned activation temperature. Myglovets et al. [42] reported on the H_3PO_4-activation of softwood sodium lignosulfonate within a wide range of temperature (400–1000 °C) and using the same impregnation ratio. The BET surface area of the resulting carbons decreased monotonically from 400 to 700 °C where a value as low as 180 m^2/g was obtained, much lower than the above indicated from Hayashi et al. under the same conditions. However, opposite to these authors, beyond 800 °C a sharp increase of surface area was observed, leading to a highest value around 1370 m^2/g at 1000 °C with almost 60 % of the pore volume corresponding to mesopores. The authors explain that increased porosity at high activation temperatures as the result of thermal decomposition of phosphorus-carbon complexes gives rise to P_2O_5 and elemental P evolution.

Fierro et al. [43] analyzed the effect of H_3PO_4 on the thermal decomposition of Kraft lignin from thermogravimetric experiments. Whereas the bare lignin decomposed along a wide range of temperature starting around 150 °C and extending up to about 650 °C the addition of H_3PO_4 initiates some kind of reaction already at room temperature during impregnation. Then that activating agent promotes dehydration as the main pathway of thermal decomposition which ends at a lower temperature decreasing as the impregnation ratio increases. At IR $\approx$ 1 the final weight-loss temperature was around 400 °C. The carbon yield was significantly higher than that from pyrolytic decomposition of the bare Kraft lignin. The DTG curves showed maximum weight-loss rates within the range of 180–185 °C, substantially lower and narrower than that for the raw lignin (300–370 °C) and the TG curves under air atmosphere were similar to those in N_2 up to 450 °C, indicative of a protecting effect of P_2O_5 to burn-off which disappeared at increasing temperature because of evaporation. Researchers of this same group [44] developed a

phenomenological model to describe the kinetics of the process based on a set of pseudo-first order rate equations for each of the five steps identified form TG and DTG experiments. They obtained 48 and 106 kJ/mol as activation energy values for the main activation path (carbonization) and the final devolatilization of the activated carbon, respectively. They also reported [45] on the textural characteristics of the activated carbons prepared at different temperatures (400–650 °C) and impregnation ratios (IR=0.7–1.75). The carbon yield increased significantly with IR (21–32 % at IR=0.7 and 1.4, respectively) and the resulting carbons were essentially microporous solids with around 80 % of the total pore volume corresponding to micropores in all the activation conditions tested. Increasing the temperature decreased the contribution of the narrower micropores Maximum values of BET surface area ($\approx$1300 m^2/g) and pore volume ($\approx$0.7 cm^3/g) were achieved at 600 °C while beyond that temperature a significant decrease of both was observed which was attributed to shrinkage of the structure because of the destruction of phosphorus groups acting as bridges as well as to carbon combustion consequent to the loss of P_2O_5 that plays a protecting role. IR values above 1.4 caused a decrease of surface area and pore volume that the authors attributed to partial destruction of the carbon matrix by the excess of H_3PO_4. Working with the as received and demineralized Kraft lignin (11 and 0.2 % ash content, respectively) those authors found some significant differences between the resulting carbons [46]. Firstly, the carbon yield (on a daf basis) was lower with the demineralized lignin which the authors attributed to the loss of hydroxyl groups upon demineralization thus reducing cross-linking. The surface area of the activated carbons obtained from the as received Kraft lignin increased with the activation temperature while the opposite was observed for those derived from the demineralized lignin. The maximum value achieved was higher for the former (close to 1200 vs around 1000 m^2/g, at 600 and 400 °C, respectively). However both carbons showed fairly similar porous texture corresponding to essentially microporous solids. From the FT-IR spectra the authors concluded that the former showed a more developed aromatic structure. They yielded also higher methylene blue adsorption capacities, attributed by the authors to the higher ash and sulphur contents.

The mechanisms involved in the H_3PO_4 activation of Kraft and organosolv Alcell lignin as well as some lignocellulosic materials together with in-depth characterization of the surface chemistry of the resulting carbons have been comprehensively studied by our research group [47, 48]. As one main feature, the oxygen-phosphorus groups provide a highly acid character to the carbon surface which is maintained at temperatures high enough for some useful catalytic applications as will be described in Sect. 8.3.2 of this chapter. Phosphorus-containing groups as CPO_3 and $COPO_3$ make the carbon surface resistant to oxidation up to substantially higher temperatures allowing also interesting applications in catalysis. Air-gasification of the H_3PO_4-activated carbons proceeds quite differently than that of the corresponding chars obtained without that agent. While the oxidation of these last occurs in the entire available surface of the particle, the former are gasified following an unreacted shrinking core model [48]. The nature of the precursor whether it was lignin or the lignocellulosic materials tested (hemp stem and olive stones) did not give

significant differences in oxidation resistance of the resulting H_3PO_4-activated carbons or in the kinetics of air-gasification, thus confirming the key role of the phosphorus-containing surface complexes.

Compared to other precursors, Kraft lignin yielded in general H_3PO_4-activated carbons with equivalent surface area than the obtained with lignocellulosic materials, like wood [49], peach stones [50] and coconut shell [51].

For the sake of comparison Fig. 8.4 collects representative N_2 adsorption-desorption isotherms of Kraft lignin-derived activated carbons obtained by physical and chemical activation. The different shapes of those isotherms confirm the possibility of achieving a wide diversity of porous texture. The curves correspond to highly activated carbons in all the cases and, of course, they can be modulated varying the operating conditions. However, they serve to show some features of each activation procedure. As discussed before, physical activation with CO_2 allows obtaining carbons with a high relative contribution of mesoporosity more easily than steam-activation. In the case of Fig. 8.4 the partial gasification with steam was performed at lower temperature in order to achieve a high surface area corresponding mostly to microporosity with a moderate creation of mesopores. Transition towards diffusion-control regime occurs at lower temperature than with CO_2. Under that regime particle burn-out prevails and thus the temperature is more critical in steam-activation. With regard to chemical activation, $ZnCl_2$ yields carbons with predominantly microporous texture even at high activation degrees whereas with H_3PO_4 much more significant mesoporosity is developed at the expenses of micropores as activation proceeds.

Carbonization in the presence of alkaline hydroxides and carbonates provides another way of chemical activation that allows achieving significantly higher surface areas that the methods described so far. It has been widely investigated with different biomass and coal precursors. This activation procedure appeared in the patent literature almost four decades ago [52] reporting the preparation of carbons with very high BET surface area (≈ 2000–4000 m^2/g) from coal and petroleum coke.

Fig. 8.4 Typical N_2 isotherms (-196 °C) of lignin-derived carbons from physical and chemical activation
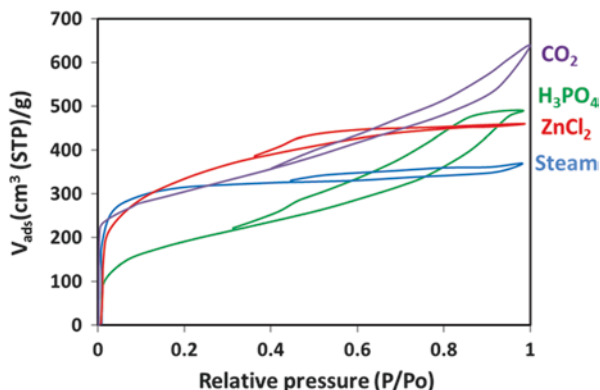
An interesting extended revision of this method has been published by Linares-Solano et al. [53]. It works in general at higher temperatures than the previously described chemical activation methods and allows development of significantly higher porosity, in particular with the potassium compounds. An important advantage of this procedure is the small or even no effect of the precursor ash content on activation, which besides can be reduced to very low values in the resulting carbon by simple water washing. The activating agent is most commonly added to the raw precursor in the case of coal, although previous carbonization has been also considered for biomass precursors and the addition can be performed via impregnation with an aqueous solution or by physically mixing the starting material with the solid hydroxide since the low melting point of KOH and NaOH allows their effective distribution in the reaction mixture.

Potassium hydroxide has been the most frequently used agent in this way of activation. It reacts with carbon according to:

$$6KOH + 2C \rightarrow 2K + 3H_2 + 2K_2CO_3 \tag{8.1}$$

The equivalent reaction can be written for NaOH whereas the carbonates react also with C, but in this case giving rise to the corresponding metal and CO:

$$K_2CO_3 + 2C \rightarrow 2K + 3CO \tag{8.2}$$

The carbonates also decompose into the corresponding metal oxides and CO_2 and at the same time this gas can react with the metal hydroxide to give the carbonate. The metal oxide reacts also with C:

$$2K_2O + C \rightarrow 4K + CO_2 \tag{8.3}$$

Of course, previous to these reactions specific of this way of activation, the pyrolytic decomposition of the precursor gives rise to the evolution, among others, of important amounts of H_2O and CO_2 which, depending of the temperature, can act in more or less extension as gasifying agents thus contributing to the development of porosity. The significance of that contribution will depend not only of the chemical composition of the precursor (more or less volatile matter) but also on the technical characteristics and operating conditions of the activation system which will determine whether those gases acquire more or less concentration in the reactor atmosphere at sufficiently high temperatures to be reactive. In lab-scale devices most commonly used so far thermal decomposition occurs at a low heating rate and under continuous flow of nitrogen so that H_2O and CO_2 are in practice evacuated from the system before significant gasification can take place. This is important to understand the development of porosity occurring as reported in the literature on the topic.

Earlier work on the activation of lignin with alkaline hydroxides and carbonates was reported by Hayashi et al. [39, 40] working with Kraft lignin precipitated with CO_2 from spruce pulping black liquors, whose ash content was reduced to 4 % after

acid washing. A wide range of temperature (500–900 °C) was covered, always at IR=1, and the activating agent was added by impregnation with aqueous solution. The optimum temperature in terms of BET surface area development was 800 °C and K_2CO_3 was the agent leading to the highest value, close to 2000 m^2/g. Activation with KOH yielded up to 1500 m^2/g, a somewhat higher value than the maximum obtained with NaOH, whereas Na_2CO_3 rendered the lowest surface area ($\approx$750 m^2/g at the most). Essentially microporous carbons were obtained although with a growing contribution of mesoporosity as the activation temperature was increased beyond 800 °C. In particular, with NaOH at 900 °C the micro- and mesopore volumes were almost equivalent. The potassium agents allowed obtaining carbons with significantly higher surface area and pore volume (both, micro- and mesopores) than the obtained by the authors upon $ZnCl_2$- and H_3PO_4-activation of the same precursor. Khezami et al. [54] investigated the activation of indulin C (a Kraft lignin from Westvaco, now WestRock) with KOH in a two-step procedure consisting in a previous carbonization at low temperature (300 °C) followed by impregnation of the resulting char with a concentrated boiling solution of KOH at a fairly low impregnation ratio (IR=0.25) and heat treatment under N_2 atmosphere for 1 h at 700 °C reached at 3 °C/min heating rate. Under these conditions the resulting carbon showed a low BET surface area only somewhat above 500 m^2/g. That value was significantly lower than the obtained by the same procedure from wood and its cellulosic components, α-cellulose and xylan.

Activation of kraft lignin with KOH and NaOH has been studied in depth by Fierro et al. [55, 56] and researchers of the same group [57]. They reported on the KOH-activation of their aforementioned demineralised kraft lignin (0.2 % ash content) within a wide range of temperature (500–900 °C) and KOH/lignin impregnation ratio (IR=1–5) varying also the holding time (0.5–2 h) and the N_2 flow in a lab-scale static horizontal tube furnace. The BET surface area increased dramatically with temperature up to a maximum of about 3100 m^2/g at 750 °C and IR=3, being the resulting carbons highly microporous with a pore volume close to 1.5 cm^3/g. Beyond that temperature the surface area decreased somewhat while the pore volume was still growing (up to $\approx$2 cm^3/g) since the mesopore volume increased at the expenses of micropores so that at 900 °C both pore volumes were almost equivalent. The carbon yield decreased monotonically at increasing temperature and impregnation ratio within the ranges tested. At the above mentioned optimum values of both variables the carbon yield was around 30 %. At high impregnation ratios KOH causes a progressive deleterious effect on the carbon structure enhanced at increasing temperature. Beyond IR$\approx$3 the micropore volume decreases but without creation of mesopores according to the evolution of the total pore volume. Two issues have to be considered before comparing these results with the previously reported by Hayashi et al. [39]. First, the de-ashing procedure provokes some small physicochemical and structural changes in the original Kraft lignin and, more important, the addition of the activating agent now was made by physically mixing it in solid state with the precursor. KOH melts at 360 °C, well below the experimental activation temperatures, thus allowing an effective mixing of the reactants, probably better than the achieved by impregnation with an aqueous solution of the

activating agent. Torne-Fernandez et al. [57] performed an optimization study on the activation of the same precursor with NaOH using a response surface method. They established 755 °C and IR ≈ 3.5 as optimum conditions, leading to a highly microporous carbon with 2610 m^2/g BET surface area and close to 95 g/100 g methylene blue adsorption. In a later paper Gao et al. [58] obtained quite similar conclusions in the KOH-activation of a lignin from pulping black liquors with much higher ash content ($\approx 40\%$) previously carbonized (500 °C, 1 h). The char was impregnated with KOH solution and the resulting activated carbons were washed with HCl. The authors reported a fairly close value for the maximum BET surface area (≈ 2950 m^2/g) which was obtained at the same temperature and impregnation ratio (750 °C and 3, respectively). Li et al. [59] analyzed the effect of acid (aqueous H_2SO_4 at pH=1) and basic (5 M NaOH followed by H_2SO_4-precipitation) de-ashing pretreatments of Kraft lignin on the yield and the porous texture of the carbons obtained upon KOH-activation. Both pretreatments led to comparable ash contents (2.1 vs 2.7 %, respectively) and almost equal elemental composition ($\approx 62\%$ C) of the resulting lignin but the acid one was more effective for further development of porosity. Again, the highest BET area (≈ 2760 m^2/g) was obtained at 750 °C but now at a somewhat higher impregnation ratio (IR=4). However, an important difference was observed with respect to the results of previous authors. Now, all the carbons obtained within 650–850 °C and a wide range of impregnation ratios (IR=1–5) showed an important contribution of mesoporosity only reported by other authors at higher temperature (≈ 900 °C) and lower IR (≈ 3). Under the above mentioned optimum conditions the external area represented 45 % of the total BET surface area and the pore volume (1.3 cm^3/g) was almost equally shared by the micro- and mesopores. Jin et al. [60] reported much lower BET surface area values for activated carbons prepared from straw pulping-derived lignin with K_2CO_3 and KOH as activating agents. With the former they achieved under the optimum conditions around 1100 m^2/g but corresponding almost 40 % to mesopore area. With KOH the maximum surface area was only somewhat above 900 m^2/g. The carbon yield was below 20 % with both agents.

Compared to other precursors, in particular of lignocellulosic nature, lignin has rendered by this way activated carbons with higher [61] or similar [62] pore volume and BET surface area under equivalent activation conditions, using coconut shell and wood of different species, respectively. In this last case, opposite to the observed with lignin a continuous increase of both textural parameters took place by increasing the activating agent to precursor weight ratio up to 5.

8.2.3   Applications of Lignin-Derived Activated Carbons

Activated carbons in general are used in applications associated to their highly developed porous texture as well as to their surface chemistry. In that sense, they are well known as adsorbents both in gas and liquid phase, most in particular although not only, for environmental applications in gas and water cleaning operations. Their textural and surface characteristics make them also useful materials in

heterogeneous catalysis, mostly as supports of the active phases but also as catalysts themselves. Within this common picture for activated carbons, those derived from lignin have been tested in the aforementioned applications, although, there is so far a limited inventory of scientific references and commercial applications.

8.2.3.1   Applications in Adsorption

Lignin itself without further activation has been tested as adsorbent by several authors. In fact, the number of works in that respect is equivalent, if not larger, than the relative to adsorption with lignin-derived activated carbons. The most widely tested species in lignin adsorption studies have been metal ions, in particular heavy metals, well known as highly concerning water pollutants. Suhas et al. [63] have summarized the results from different authors showing remarkable discrepancies between the adsorption capacities reported for same species. As representative example, for Cu(II), values from 3.4 to 137 mg/g have been given, both with Kraft lignin. Srivastava et al. [64] reported an extraordinarily high uptake of 1865 mg/g that they attributed to phenolic and other functional groups on the surface of the black liquor-extracted lignin used. They also found a high, although more discrete, value of 95 mg/g for Zn(II). Lignin has been also tested as adsorbent for different organic molecules including phenols, surfactants and dyes, as collected by Suhas et al. [63].

   With the exceptions noted above, the adsorption capacity of lignin is much lower than that of activated carbons, as expected from the dramatic differences in surface area. However, lignin commonly yields uptake values well above what should correspond to its non-porous character. The functional groups of non-activated lignin must play an important role on that respect, so that specific chemical interactions may be involved in many cases [65]. Nevertheless, despite the more or less ability of lignin as adsorbent an important question needs to be clarified relative to its stability in aqueous solutions. In that sense, the solubility of virgin and modified forms of lignins depends on their own nature as well as on some environmental conditions like pH. Huang et al. [66] reported highly selective adsorption of Pb(II) and Cu(II) with maximum values of 123 and 64 mg/g, respectively, by a composite material prepared from a sulfonated lignin intercalated in the interlayer space of a Mg_2Al-double hydroxide structure. By crosslinking organosolv lignin with formaldehyde dimethyl acetal Meng and Weber [67] prepared a polymeric material with a very narrow microporous texture indicative of potential interest as molecular sieve adsorbent.

   The potential application of Kraft lignin-derived activated carbons for the removal of a diversity of target pollutants from water has been extensively studied by our group. The CO_2-activated carbons were tested as adsorbents in a series of papers. Cotoruelo et al. studied the equilibrium [68] and kinetics [69] of adsorption of several aromatic compounds, including benzene, toluene, nitrobenzene, p-nitrotoluene, aniline and p-nitroaniline and also reported on the adsorption of p-nitrophenol [70]. As expected, the equilibrium uptake and the adsorption rate

increased with the b.o. consistently with the more developed porosity. The nitro group improves adsorption whereas the amine group presents the opposite effect, which can be explained by activation and deactivation of the aromatic ring, respectively. In the case of p-nitrophenol the uptake, which reached up to 4.5 mmol/g with the highest surface area carbon ($\approx$1850 m^2/g), decreased dramatically beyond neutral pH, this being related with its pK value ($\approx$7.2). The process was always exothermic with enthalpy values ranging between -10 and -35 kJ/mol, typical of physical adsorption. With regard to the kinetics, internal diffusion was the controlling step and the values of the effective diffusivity were calculated, decaying as surface coverage increased. For the sake of potential applications it is important that the adsorption was fairly rapid in all the cases with the activated carbons of intermediate and high b.o. given the relative contribution of mesoporosity. Sodium dodecylbenzene sulfonate was tested as a representative example of anionic surfactants [71], yielding Langmuir capacities around 1.5 and 2 mmol/g at 20 and 5 °C, respectively, with a 60 % b.o. activated carbon. The adsorption of dyes on these CO_2-activated carbons was also studied. The Langmuir saturation capacity for methylene blue [72] increased significantly with the temperature within the range tested (5–40 °C) so that the process was endothermic, with the adsorption enthalpy approaching 50 kJ/mol, although negative values around 10–20 kJ/mol were obtained for the free energy. The uptake increased also with the pH consistently with the character of cationic dye of methylene blue. Other cationic dyes, fuchsine and malachite green, were also tested, with the adsorption being again endothermic [73]. The isotherms were indicative of multilayer adsorption. Congo red [74] and crystal violet [75] were also tested. Paracetamol, salicylic and benzoic acids were studied as representative of pharmaceuticals [76]. The adsorption of the two last was strongly dependent of pH and exothermic whereas that of paracetamol was slightly endothermic with negative values of free energy in the three cases.

In an earlier paper [37] our H_3PO_4-activated carbons from Kraft lignin were tested as adsorbents of phenol, 2,4,5-trichlorophenol (TCP) and chromate. The micropore volume and the surface concentration of non-acidic oxygen groups determined the adsorption of phenol rather than the BET surface area. Langmuir monolayer capacity for phenol reached up to 2.4 mmol/g. A similar highest value was achieved also for TCP. In the case of Cr(VI), the adsorption capacity increased significantly at frankly acid pH ($\approx$3) reaching 1.8 mmol/g, almost twofold the achieved at neutral pH.

The potential application of lignin-derived activated carbons as liquid-phase adsorbents has also been studied by other authors. Fierro et al. [77] reported Langmuir adsorption capacities for phenol up to around 2.5 mmol/g with high-surface area carbons ($\approx$2900 m^2/g) obtained from kraft lignin upon activation with NaOH and KOH. Mussatto et al. [78] used H_3PO_4-activated carbons from brewer's spent grain lignin for the detoxification of the hemicellulosic hydrolysates containing a complex mixture of sugars, phenolic compounds and metallic ions like Ni, Cr, and Fe, among other species. In spite of the relatively low BET surface area (around 700 m^2/g at the most), the carbons showed a fairly good behavior, especially for the uptake of the metal ions. Huang et al. [79] reported interesting results on the adsorp-

tion of two pharmaceuticals, tetracycline and ciprofloxacin, onto a 930 m^2/g carbon from H$_3$PO$_4$-activation of lignin. The Langmuir adsorption capacities were 475 and 418 mg/g, respectively. Myglovets et al. [42] tested their activated carbons prepared from a high-molecular-weight softwood sodium lignosulfonate upon H$_3$PO$_4$ activation as adsorbents of copper ions. The highest surface area was 1370 m^2/g and the authors found a fairly good adsorption capacity even at highly acidic pH, well below the PZC (point of zero charge) were, in principle, the positively charged carbon surface and the copper cations should be subjected to repulsive electrostatic forces. The uptake of the metal ions was attributed to ion-exchange with the protons adsorbed into the delocalized π-electrons cloud of the graphene layers.

In general, activated carbons derived from lignin are comparable as adsorbents to similar carbon materials prepared from other precursors of equivalent porous texture and surface chemistry, which are the main issues determining the adsorption capacity and rate. A complete overview on the application of activated carbons in liquid-phase adsorption, although not including specifically lignin-derived carbons can be seen in reference [80].

We tested also the CO$_2$-activated carbons from Kraft lignin in gas-phase adsorption [81] for the removal of volatile organic compounds (VOCs). Three target molecules of different polarity, benzene, methyl ethyl ketone (MEK) and methanol, were used. The adsorption capacity of the adsorbents reached around 500 mg/g for benzene at 20 °C and 50 % relative pressure with a 1850 m^2/g carbon. That capacity, as well as the adsorption rate, followed the order benzene>MEK>methanol, inverse to that of polarity, although methanol was completely desorbed opposite to the two other compounds. The adsorption process was barely affected by the presence of water vapor, which was reversibly adsorbed. The potential use of those carbons as desiccants was analyzed in a later paper [82], where the presence of well dispersed sodium on the carbon surface was found to play a key role.

8.2.3.2 Applications in Catalysis

The porous texture and the surface chemistry of activated carbons (ACs) make them useful materials in heterogeneous catalysis. Furthermore, those features can be tailored to a certain extent so that carbon materials can be designed as active phase-supports and as catalysts by themselves for specific reactions. The use of activated carbons in catalysis has been widely reported in the scientific and technical literature and a number of industrial applications have been implemented. So far, many references on the use of lignin-derived activated carbons in this field have appeared [47, 83–86].

Bedia et al. [47] reported on the 2-propanol dehydration with an activated carbon prepared from Alcell lignin with H$_3$PO$_4$ at IR=3 and 500 °C. The carbon had a BET surface area of 1100 m^2/g, corresponding almost 30 % to mesopores. The main feature of the AC was the acidic nature of its surface that had a fairly high concentration of hydroxyl groups associated with phosphates and polyphosphate esters that can act as strong Brönsted acid sites. That promoted the conversion of 2-propanol
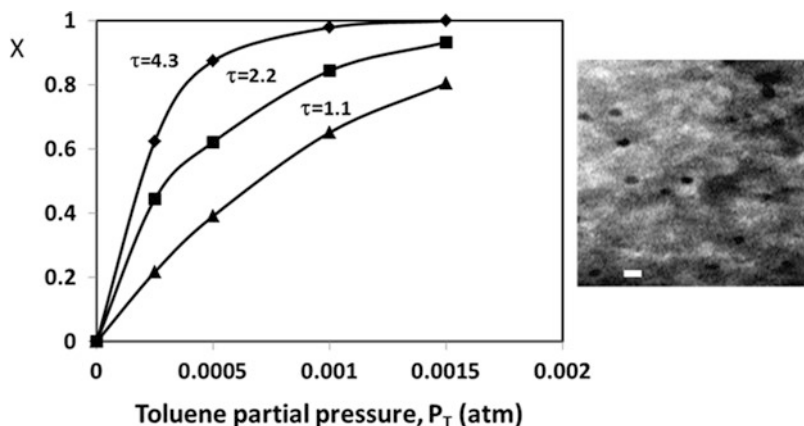
Fig. 8.5 Oxidation of toluene catalyzed with Pd (0.5 %) on H_3PO_4-activated carbon from kraft lignin at different space-times (τ, g cat s/μmol). Bar length of the SEM micrograph of the catalyst is 10 nm

via dehydration rather than dehydrogenation. The reaction proceeded through intramolecular dehydration giving rise to propylene with almost 100 % selectivity at complete 2-propanol conversion working at atmospheric pressure, somewhat above 300 °C and 5 h^{-1} space velocity. The catalyst showed a high stability under these conditions and the presence of water vapor up to 10 % in the feed stream (2-propanol at saturation in N_2) did not show any significant effect. The same authors [83] used a highly mesoporous carbon (1250 m^2/g BET surface area, corresponding 65 % to mesopores) from H_3PO_4-activation of Kraft lignin as support for a low-load palladium catalyst (0.5 % Pd) which was tested for the destruction of BTX via catalytic oxidation into CO_2 and H_2O. Complete oxidation of toluene and xylenes was achieved at 400 and 350 °C, respectively, under atmospheric pressure. Figure 8.5 shows the conversion of toluene vs its partial pressure in the feed stream at different space times. In the case of benzene, conversion was no more than 50 % at 425 °C but it must be considered the high space velocity used in the experiments (19000 h^{-1}). The catalyst showed an excellent stability due to the phosphorus groups created during the activation process, which improve significantly the oxidation resistance of the carbon support, impeding its burn-off. The TG curve of the catalyst showed no weight-loss up to about 500 °C. This same catalyst was used by Guillen et al. [84] in hydrogenation and Suzuki reactions, showing very good performance with regard to both activity and selectivity. In the Suzuki-Miyaura reactions triphenylphosphine was no needed as ligand mainly because of the C_3P groups on the surface of the carbon support.

Zazo et al. [85] prepared a highly stable catalyst upon activation of lignin from alkaline pulping black liquors with $FeCl_3$ at 800 °C. The resulting material had a relatively low Fe content (<1 %) but with a homogeneous distribution onto the carbon particles. It was tested for heterogeneous Fenton oxidation, the so-called catalytic wet peroxide oxidation (CWPO), showing lower activity than a previous Fe on

activated carbon catalyst prepared by incipient wet impregnation of a commercial activated carbon with ferric nitrate. However, the new catalyst was highly stable, avoiding the main drawback of the previous one derived from its rapid loss of activity due to strong iron leaching. That is the important challenge regarding the development of catalysts for CWPO which has hindered so far the implementation of this promising modification of the conventional Fenton process.

Although from a different approach, Chieffi et al. [86] investigated the valorization of a lignin waste for potential application in heterogeneous catalysis. The authors reported in a recent paper on the preparation of a catalyst based on Fe and Ni nanoparticles supported on a moderately porous carbon ($\approx$540 m^2/g BET surface area) with a well-developed mesoporosity. The precursor was a lignin-like precipitate from hydrothermal treatment of rye straw using $Ba(OH)_2$. It was carbonized at 800 °C for 2 h so that the accompanying $BaCO_3$ acted as activating agent. The metallic active phase, Fe and Ni, was then incorporated by impregnation and further heating at 800 °C under N_2. The resulting material was a carbon-metal composite with as much as 14 % Fe and 22 % Ni. It was tested in the hydrogenation of nitrobenzene and phenylacetylene. From the former, complete conversion was achieved at 125 °C and 20 bar with 95 % selectivity to aniline. Under the same conditions, the bare carbon support yielded less than 10 % conversion but with 99 % selectivity. Phenylacetylene was completely converted with the Fe-Ni catalyst at 150 °C and 50 bar giving 95 % selectivity to ethylbenzene.

8.3 Lignin-Based Carbon Fibers

One of the most interesting and promising valorization routes of lignin, from both the economic and environmental points of view, is the preparation of low-cost carbon fibers (CFs) with high added-value, given their industrial and technological importance and the price of the conventional petroleum- or coal-derived precursors, mainly poly(acrylonitrile) (PAN) and pitches [87–92]. The fields of interest for carbon fibers include: (i) CFs for functional applications (energy storage, adsorption and catalysis), based on properties such as electrical conductivity, porosity, surface area and chemistry and oxidation resistance and (ii) CFs for structural applications (advanced composite materials, aerospace, military, sporting and luxury goods, etc.) where the determining properties are mechanical.

The use of lignin as a source of CFs has, besides its availability and low cost, other important advantages that have been mentioned before, such as high carbon content ($\geq$60 %) and high yields upon heat-treatment (carbonization). Compared with conventional PAN and pitch precursors the use of lignin also avoids the evolution of toxic products, as HCN or nitrous gases, during carbonization. Moreover the higher oxygen content of lignin facilitates a faster oxidative thermostabilization and a better conversion into CFs.

The preparation of CFs from lignin involves commonly five successive steps: (i) conditioning, including purification and/or some kind of modification; (ii) spinning

into lignin fibers; (iii) thermostabilization under oxidative atmosphere (air, 200–250 °C) to avoid further melting or softening; (iv) carbonization in inert atmosphere at 500–1000 °C and (v) post-treatment to tailor the properties of the resulting CFs for structural or functional applications.

In spite of the advantages of using lignin as precursor it should be recognized that the fibers prepared so far have shown lower quality than those obtained from PAN or pitch. On the other hand, the morphology and final properties as well as the production cost of lignin-based CFs depend not only on the characteristics of the lignin used, associated to its origin and the extraction procedure, but also on the spinning technique employed for the conformation of the fiber. Consequently, most research efforts regarding the development of lignin-based CFs have been addressed to optimize the spinning method (wet-, dry-, melt- and electro-spinning) adapted to the type of lignin.

Otani et al. [93] described in a patent the preparation of lignin-derived CFs, including graphitized and activated CFs, using three different spinning methods (wet-, dry- and melt-) with different types of lignins and the inclusion of additives and/or post-treatments. After this pioneer work, lignin-based CFs were prepared during the following decade by wet- and dry-spinning processes using soluble lignins. Nippon Kayaku Co. manufactured CFs from lignin that were commercialized as Kayacarbon, although on a small scale [94, 95]. The precursor of those CFs was an alkaline lignosulfonate/poly(vinyl alcohol) (PVA) solution and dry-spinning was used for fiber conformation. The use of an infusible ligninic material did not require thermostabilization and produced higher yields in a more cost-efficient process. However, research on lignin-derived CFs by these methods declined considerably and almost ceased in the 1980s. The British patent of Mansmann [96] represents an interesting example on the preparation of stable lignin fibers by dry-spinning. In this case, lignin sulfonates were used as precursors with low amounts (less than 5 wt%) of poly-ethylene oxide (PEO) or poly-acrylamide. Several references to the manufacture of CFs by wet-spinning from lignin-PAN blends can be seen in the US patent literature [97]. Maradur et al. [98] prepared CFs from a copolymer of lignin and poly-acrylonitrile, the process including the synthesis of the co-polymer followed by wet-spinning and the subsequent carbonization of the spun fiber. Seydibeyoglu [99] also studied the possibility of obtaining CFs from a PAN-lignin blend.

8.3.1 Lignin-Based CFs by Melt-Spinning Methods

The most investigated technique for the production of lignin-based CFs has been so far melt-spinning. In this process molten (fusible) lignin is extruded in an inert atmosphere; no solvents are needed and more homogeneous fibers are obtained. Nevertheless, the partially-oxidized nature of lignin and its character of non-regular polymer demand a rigorous control of the melt-spinning operation and in this sense lignin usually needs to be purified, chemically-modified and/or plasticized with additives for a suitable spinnability. The main objective of those pretreatments is

achieving a low softening temperature (Ts) to avoid polymerization and cross-linking reactions during the extrusion process, but at the same time maintaining a high glass transition temperature (Tg), which facilitates stabilization of the fibers. That means a narrow temperatures range for preparing lignin-stabilized fibers by melt-extrusion.

Sudo and Shimizu [100] described the preparation of lignin-based CFs from lignin isolated upon steam-treatment of wood at high pressure. However, the preferred strategy was to adapt the pulping processes, like Kraft and organosolv, to obtain spinnable lignin. Uraki et al. [101] reported on the preparation of CFs from organosolv lignin obtained by aqueous acetic acid pulping. They concluded that direct melt-spinning was enabled due to the partial acetylation of some of the lignin hydroxyl groups during pulping. In two latter papers the same authors reported on the preparation of activated carbon fibers (ACFs) based in lignin derived from hardwood [102] and softwood [103] acetic acid-pulping. They compared the fusibility of both lignins and concluded that the former showed adequate fusibility whereas the second needed further removal of the infusible high-molecular fraction and even after that could not be converted into a fusible material [104]. Kraft lignin was not useful for melt-spinning because of its low content in fusible fraction ($\approx 13\%$). Lignins from other isolation procedures have been studied more recently as precursors for melt-spun CFs [105, 106].

Thermal and purification treatments can be used for the sake of controlling the fusibility of lignin for CFs. Kadla et al. [107] used a heat-treatment at 145 °C for 1 h under vacuum to make melt-spinnable two hardwood lignins (Alcell and Kraft). CFs of around 30 μm diameter were obtained from the resulting lignins alone as well as in physical blends with PEO. On the other hand, purification by extraction with organic solvents has been proposed by Baker et al. [108] as a way to reduce the melting temperature of lignins and improve their spinnability. The same authors proposed combined thermal and purification pre-treatments addressed to obtain lignins for multifilament melt-spinning [109] or to make melt-spinnable Kraft lignin from softwood [110]. Membrane ultrafiltration has been also tested as purification treatment previous to melt-spinning [111].

Several groups have reported on the use of Kraft or organosolv lignin with synthetic polymers to prepare suitable melt-extrusion blends. Kadla and co-workers [112, 113] analyzed the intermolecular interactions in those blends. Poly(ethylene) (PE), poly(propylene) (PP), poly(ethylene terephthalate) (PET), PEO and PVA were investigated and the authors concluded that the best additives regarding the spinnability were PEO and PET, due to their high miscibility with lignin. Also, non-spinnable lignin form softwood was successfully melt-spun into fibers after blending with 50 wt% PEO [114, 115]. The use of lignin as plasticizer of PVA has been described by these authors [116], who found strong intermolecular interactions in immiscible blends of both components. An interesting approach, in this sense, is the use of fusible hardwood lignins (low Tg) as plasticizer of infusible softwood lignins (high Tg) [111, 117, 118].

Sevastyanova et al. [119] prepared lignin composite fibers by the addition of montmorillonite organoclays to an organosolv lignin with the result of improved

spinnability. Also, the diameter of melt-spun fibers was increased [120]. Carbon nanotubes have been also used as additives in the preparation of composite fibers. The introduction of multiwall carbon nanotubes (MWCNTs) in different lignins improved the spinning process and increased the heat capacity. However, beyond 15 wt % MWCNTs, the resulting composites could not be melt-spun [121].

Chemical modification represents another way of lignin conditioning for CFs preparation. Hydrogenolysis, phenolysis, acetylation, derivatization and copolymerization have been investigated among other solutions in that respect. Sudo and Shimizu [122] hydrogenated a steam-exploded lignin with a Raney Ni catalyst. This allowed partial removal of aliphatic groups upon alkyl–aryl ether bonds cleavage and the formation of ethylene bridges between aromatic rings, giving rise to the decrease of the softening temperature of lignin which favored melt-spinning. The authors also tested phenolated lignins produced by different processes, in the preparation of melt-spun CFs [123, 124]. Demethoxylation [125] and acetylation [126] were used in two US patents. Wohlmann et al. [127] introduced ester, ether and urethane functionalities in the lignin structure through its free hydroxyl groups. That provided plasticity to the resulting lignins improving their fusibility and spinnability. Co-polymerization of lignins with other monomers and polymers has been patented by Shen et al. [128] who described the reaction of the guaiacyl groups of lignin with formaldehyde to produce lignin–phenol–formaldehyde (LPF) resins. Thunga et al. [129] reported on the preparation of CFs from lignin functionalized by butyration with poly(lactic acid) (PLA). Finally the extension of the lignin chains by different reactions provides another interesting approach. Propargyl derivatization of the low-molecular-weight lignin fraction followed by oxidative coupling or thermal polymerization via Claisen rearrangement has been reported by Sen et al. [130].

8.3.2   Electrospinning

Electrospinning has emerged in recent years as a promising technique for the preparation of lignin-derived fibers. Compared with the most conventional spinning methods electrospinning shows remarkable advantages: (i) simplicity and low cost; (ii) commercialization is expected to be feasible since it is a rapid and efficient technique; (iii) high versatility to prepare pure and composite fibrous materials with different morphologies (linear, curly, interconnected), structures (solid, hollow, coaxial) or arrangements (preferentially- or randomly-orientated woven and nonwoven fibers), by adjusting different experimental conditions, like spinneret configuration, flow rates, voltage and tip-to-collector distance; (iv) so far it is the only technique (top-down approach) that enables the manufacture of CFs and other fibrous structures within a wide range of diameters from the few microns to the nanometer scale. In that sense, the more conventional melt-spinning produces fibers typically ranging between 80 and 30 μm while smaller diameters desirable for some purposes are difficult to obtain by this technique from lignin. Nevertheless, in spite

of these benefits of electrospinning and the low cost of lignin as precursor, there is still scarce literature on the preparation of electro-spun lignin-derived fibers.

Our group published pioneering work on the preparation of CFs from pure lignin using the electro-spinning technique [131]. That paper presented a novel and simple method for preparing micro- and nanofibers, both solid and hollow, from lignin solutions at room temperature without any added polymer or chemical modifications. As-received Alcell lignin was used in highly concentrated ethanol solutions that were electro-spun in coaxial and triaxial configurations to obtain solid and hollow fibers, respectively. Figure 8.6 depicts a schematic picture of both approaches, including representative SEM images of the solid and hollow final carbon fibers. These fibers were obtained after thermostabilization in air at low temperature (<200 °C) and further carbonization. CFs within 200 nm–1.5 μm were prepared and their properties were evaluated. The addition of a Pt-acetyl acetonate to the lignin/ethanol solution for electrospinning allowed preparing Pt-doped lignin fibers [132]. Thus, lignin fibers with and without platinum nanoparticles could be synthesized in a single step by electrospinning the corresponding solutions. After thermostabilization and carbonization, the resulting carbon fibers yielded BET surface areas of 1178 and 1195 m^2/g, respectively.

Berenguer et al. [131] prepared binderless fibrous carbon electrodes for ultrafast energy storage by electrospinning of Alcell lignin. The approach involves the synthesis of interconnected porous carbon fibers (CFs), with submicron diameter and high surface area and conductivity. This provides a promising way of lignin valorization into high added-value products. Some of the electrodes prepared yielded power and energy densities up to 61 kW kg^{-1} and 10 Wh kg^{-1}, respectively, in aqueous electrolyte.
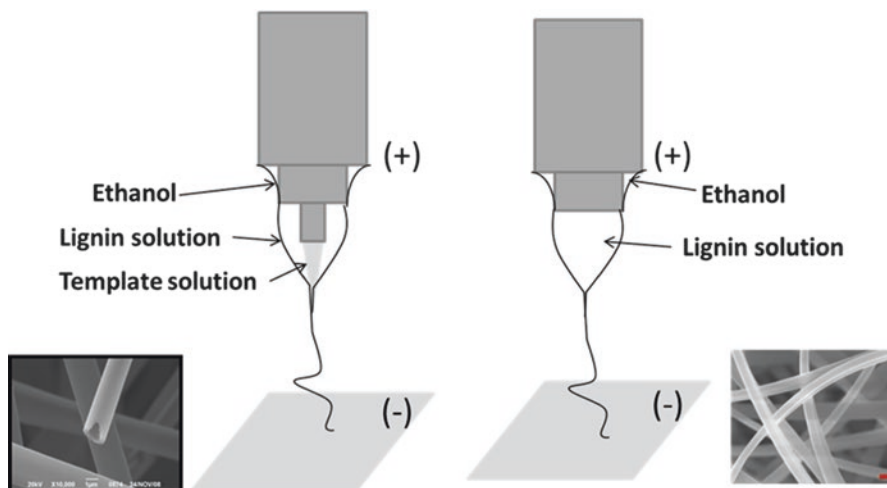
Fig. 8.6 Electrospinning in triaxial and coaxial configurations (Bar length: 1 μm)

Some other authors have used also the electro-spinning technique with pure lignins but in most cases, some plasticizing agents or functionalized lignins have been employed. Dallmeyer et al. [132] found poor electrospinnability working with solutions of different types of lignin (organosolv, Kraft and pyrolytic). Hosseinaei and Baker [133] used a solution of purified softwood Kraft lignin in dimethylformamide (DMF) and methanol to obtain fibers with 300–500 nm of average diameter and different morphologies.

With regard to plasticizing agents, Montero et al. [134] used blends of softwood kraft lignin (SKL) and PEO to obtain electrospun CFs of ~4 μm diameter. Dallmeyer et al. [132] observed, in their above mentioned work, that the addition of PEO provoked a clear transition from electrospray or beaded fibers to uniform lignin fibers. These authors [135] have presented a correlation between the diameter of the fibers and the elongational fluid properties in electrospinning of SKL solutions. Kang and co-workers reported the electrospinning of PAN/alkali lignin blends (from 100:0 to 20:80 w/w) and prepared sub-micron-fiber mats of different morphologies. Uniform sub-microfibers were produced with lignin loads up to 50 wt.% while above that a remarkably shift to a beaded morphology was observed. These changes were attributed to a decrease of the solution conductivity [136, 137]. By electrospinning alkali-lignin/PVA aqueous mixtures Lai et al. [138] prepared CFs with diameters between 140 and 300 nm. The difference in diameter was attributed to an increase in the conductivity of the blends and a decrease of viscosity.

Some authors studied the electrospinning of solutions of different SKL fractions with various concentrations of suspended MWCNTs [139, 140]. Hu et al. [141, 142] have reported that 10 wt% of PEO in lignin blends enables the efficient electrospinning of aqueous NaOH or KOH/Alcali lignin solutions into fibers. Lin et al. [139] proposed emulsion electrospinning as a method to obtain advanced fine lignin fibers.

8.3.3 Oxidative Thermostabilization of Lignin Fibers

Lignins have glass transition temperatures (T_g) much lower than the required for carbonization (T_c). Thus, prior to this last step it is necessary to stabilize the lignin fibers to prevent softening. This is accomplished most commonly upon air-oxidation at a temperature below T_g to induce cross-linking of the lignin structure [143]. Lignin needs low heating rates to avoid melting or softening and its relatively high oxygen content enables faster stabilizations than PAN or pitches, the commonly used materials for CFs manufacture. Some other stabilization treatments have been proposed in the literature (UV radiation, electron irradiation, plasma treatment) but so far cannot compete with the simple oxidative thermostabilization in air. It has been investigated by different authors for lignin-derived fibers. Braun et al. [143] used several techniques to characterize the changes of hard wood Kraft lignin (HKL) during air thermostabilization. They observed that at low temperatures oxidation reactions produce carbonyl and carboxyl functionalities, whereas at higher

temperatures, oxygen groups are incorporated as ester and anhydride linkages giving rise to cross-linking of the lignin polymer. The optimum heating rate for thermostabilization of hardwood Kraft lignin keeping its T_g below the operating temperature was as low as 0.06 °C/min. Foston et al. [144] with NMR concluded that during thermostabilization of hardwood Alcell lignin an important reduction of methoxyl groups (demetoxylation) takes place. The presence of carbonyl and carboxyl-related structures was also detected by these authors in the same work. Brodin et al. [145, 146] found that in the oxidative thermostabilization of Kraft lignin slower heating rates, higher temperatures and longer holding times improve the final yield to carbon fiber. In contrast, Baker and Gallego [109] found an optimum heating rate for thermostabilization to improve the final carbon yield. Below that heating rate lignin degradation became more important than the oxidative cross-linking reactions, thus reducing the carbon yield whereas at higher heating rates lignin devolatilization was more intense. A shift of the T_g towards higher temperatures could be observed upon thermostabilization of HKL, whereas in the case of SKL no T_g could be measured after a short period of time because it became no longer fusible due to cross-linking [146]. Therefore, softwood lignin-derived fibers exhibited more rapid oxidative cross-linking than those from hardwood lignin. Furthermore, it was found that air diffusion during the stabilization treatment was less affected by the fiber diameter in the case of lignin because of its already highly-oxidized nature compared to other precursors [145]. Besides, Dallmeyer et al. [145] found that the intrinsic differences in thermal softening behavior among kraft lignin fractions allows obtaining different morphologies, from linear to (partly-fused) interconnected.

In general, different lignins have been subjected to thermal pre-treatments and/or purification processes with solvents or membranes to increase their T_g and T_s and in consequence their thermostabilization rates [133, 148]. Additives for co-extrusion such as PEO and PET favor a faster stabilization [149] or even avoid in part the need of that step [141, 142]. Finally, it is worth to mention the so-called "chemical thermostabilization", with aqueous solution of hexamethylenetetramine (HMTA) and HCl, it has been successfully used with poly(ethylene glycol) (PEG)-lignin fibers [106].

8.3.4 Potential Applications of Lignin-Based Carbon Fibers

As described so far, different approaches have been used for the preparation of lignin-derived carbon fibers, which affect to the technical characteristics of the process as well as to the starting materials. Consequently, a diversity of products has been obtained showing different properties and therefore potential uses. Two main fields can be recognized in that respect: structural and functional applications.

8.3.4.1 CFs for Structural Applications

The first-reported lignin-based CFs prepared by dry- and wet-spinning methods with additives such as PVA, PAN or viscose, showed tensile strengths up to 0.8 GPa [93]. Since the 1990s important research efforts have been devoted to the development of fibers with improved mechanical properties mainly by melt-spinning. Tensile strength values up to 0.66 GPa and Young's modulus of 40.7 GPa were reported for fibers prepared from a lignin pitch extracted by hydrothermal treatment [123]. Heat-treated and melt-spun lignins from acetic acid pulping gave rise to CFs with strengths up to 0.36 GPa and 39.1 GPa of Young's modulus [101]. These values are in good agreement with the reported by Kadla et al. using a commercial hardwood organosolv lignin (HOL) or a HKL [107]. The addition of 5 % PEO [112] or the application of an optimized thermal pre-treatment [148] improved significantly the mechanical properties of HKL- and HHOL-derived carbon fibers.

Thanks to the continuous research work carried out by the groups of Kadla and Baker, the mechanical properties of lignin-derived CFs were greatly enhanced by co-extrusion of lignin–polymer blends or the combination of organic purification with optimized thermal pretreatment, respectively. The thermal pretreatment of a purified Alcell lignin (AP86) yielded various lignins with selected T_g and T_s values, that in the best case produced CFs with an average tensile strength of 1.07 GPa and Young's modulus of 82.7 GPa as well as 55 % carbon yield [109], much better than those obtained from the original Alcell lignin [108]. On the other hand, based on previous results of Kubo and Kadla with lignin–PET blends [115], Compere evaluated the mechanical properties of soda hardwood lignin–PET fibers carbonized at 1200 °C, obtaining tensile strengths up to 1.03 GPa and Young's modulus up to 109 GPa [150]. These are the best mechanical properties reported so far for lignin-based CFs.

Earlier work on the structure of lignin-based CFs by Johnson and Tomizuka [151] revealed a high degree of cross-linking, an important porosity and heterogeneities and consequently a low degree of orientation in the fine structure of the CFs. In addition, the presence of inorganic impurities in the starting lignin could act as graphitization catalysts promoting structural ordering. This provokes density fluctuations and local inhomogeneous melting which reduces the tensile strength and mechanical properties of the final CFs. Baker and Gallego [109], studied the carbonization of lignin-derived fibers and found highly ordered graphite-like structures in the CFs obtained at high temperatures. Similar results were obtained by Rodríguez-Mirasol et al. [152] on the heat treatment of powdered kraft lignin.

An important barrier for preparing lignin-derived CFs with enhanced mechanical performance derives from the heterogeneous nature of the precursor [153, 154]. Moreover, impurities such ashes and/or infusible/insoluble components have a significant effect on the homogeneity and uniformity of the resulting CFs [63, 155]. Consequently, some strategies like heat-treatment, purification and modification of the starting lignin as well as the addition of solvents have been used to enhance the mechanical properties of the lignin-fibers CFs.

The spinning procedure can have a relevant influence on the mechanical properties of the final lignin-based CFs. In this sense, electrospinning represents a novel promising method to strengthen those fibers, because the reduced diameter and the alignment of the lignin molecules achievable by that technique.

The operating conditions (temperature, heating rate, and atmosphere composition) during thermostabilization and further carbonization of the lignin fibers determine not only the time and energy consumption of the overall process, but also the properties of the final CFs. Thus, during stabilization, a higher extent of crosslinking reduces swelling and softening of the fibers and leads to the formation of rigid oxidized segments [145], but can be negative for the structural ordering upon carbonization [156]. Dallmeyer et al. [147] have recently reported that the interconnection in fused CFs enhances the mechanical properties of both the thermostabilized and carbonized fibers. Berenguer et al. [133] reached similar conclusions with CFs prepared by electrospinning of Alcell lignin.

The structural performance of lignin-based CFs may be improved by the incorporation of reinforcement fillers, like carbon nanotubes [121, 139, 140] and organoclays [119, 120]. However, once again the literature shows controversial results and future research is needed for a comprehensive knowledge on the action of those fillers and their effect on the mechanical properties of the fiber.

8.3.4.2   CFs for Functional Applications

Carbon fibers have potential applications in different fields, most in particular dealing with adsorption, heterogeneous catalysis and energy conversion and storage, depending on some useful properties other than mechanics, such as porosity, surface area and chemistry, electrical conductivity and oxidation resistance. Activated carbon fibers (ACFs) are interesting and versatile materials and thus have been widely studied. Different approaches have been proposed in the literature to prepare ACFs (chemical, physical or inherently-driven activation). Otani's early patent in 1969 [93] described the production of ACFs by the addition of chemical activating agents to the molten lignin (sulphur, $ZnCl_2$) or to lignin solutions (NaOH, KOH, H_2SO_4) as well as by physical activation with air, oxygen or steam after carbonization.

Hu and Hsieh [141] prepared submicron fibers by electrospinning blends of alkali lignin (ALs) and PEO (9/1 w/w) together with NaOH or KOH. The ACFs produced after carbonization and chemical activation of the spun fibers showed high BET surface area (up to 1400 m^2/g). Upon steam-activation, Uraki et al. [102] prepared ACFs using as precursor acetic acid lignins from hardwood and softwood. Those fibers yielded up to 1930 m^2/g BET surface area and pore volumes above 0.5 cm^3/g. Activated carbon fibers with very high surface area ($\approx$3000 m^2/g) have been reported by Lin et al. [106] from softwood lignin.

During carbonization inherently-driven activation can occur due to the composition of the starting material. In this sense, Kubo et al. [157] studied the porosity generated during the complete thermal treatment (thermostabilization and carbonization) of blends of hardwood lignin and polypropylene. BET areas around 500 m^2/
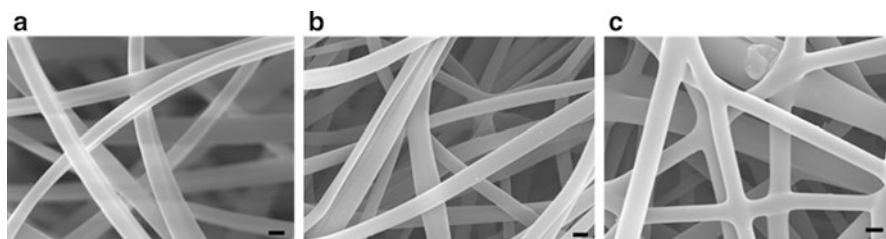
Fig. 8.7 SEM images of (**a**) as-electrospun Alcell lignin fibers; (**b**) lineal CFs and (**c**) interconnected CFs (Bar length: 1 μm)

were found. Similar results were obtained in the carbonization of electrospun lignin/PVA fibers [138]. Ruiz-Rosas et al. [132], reported frankly interesting results upon carbonization of electrospun Alcell lignin to CFs (BET area of 1200 m^2/g and pore volume of 0.52 cm^3/g). This development of porosity was attributed the to the inherent activation process occurred during carbonization promoted by the high oxygen content of the thermostabilized fibers (~33 wt%).

The application of carbon materials with fibrous structures as electrodes in energy conversion and storage devices has received a growing interest in the last years. The lower inter-particle resistance of the CFs and the possibility of using them without binders and conductivity promoters make CFs very interesting materials for that purpose.

Dallmeyer et al. [147] prepared interconnected Kraft lignin-based submicrometer CFs by electrospinning and found that their conductivity was much higher than that of the non-interconnected fibers. Similar results have been obtained for CFs from Alcell lignin [133] that were used to prepare flexible carbon fibers binderless electrodes. The potential use of lignin-derived CFs in energy storage systems like lithium-ion batteries (LIBs), supercapacitors or fuel cells has been studied in some recent papers. Fairly good performance has been demonstrated by ACFs for supercapacitors and fuel cells [142]. Regarding lignin-based carbon fibers for LIBs, Wang et al. [158] reported that intercalation and N-doping improve the electrical conductivity and LIB specific capacity. SEM images of as electrospun Alcell lignin and the resulting interconnected linear CFs can be seen in Fig. 8.7.

8.4   Templated Carbons from Lignin

Nanostructured carbon materials with hierarchical pore frame are receiving a growing interest given their versatile potential applications derived from the possibility of preparing tailored structures showing interconnected pores within highly ordered size ranges. The synthesis of these materials has been usually accomplished by nanocasting techniques based on the use of a porous material as sacrifice template. Different carbon precursors have been used for that purpose that can be incorporated to the porous templating material by liquid-phase impregnation [159] or chemical vapor deposition from a light hydrocarbon [160].

Work on template carbons from lignin was reported by Fierro et al. [161]. The authors obtained microporous-mesoporous carbons from a microwave-pretreated Kraft lignin. Colloidal silica with two different particle sizes ($\approx$13–20 nm) was used as hard template which was dispersed in bicarbonate/lignin aqueous solution. After slow evaporation the resulting solid was carbonized at low heating rate up to 850 °C, maintaining that final temperature for 2 h. That allowed obtaining carbon materials with tunable mesopores after dissolving the colloidal silica with 3 % NaOH at 70 °C. Upon further CO_2-activation microporosity was created, giving rise to final BET surface areas up to 2000 m^2/g and pores volumes exceeding 2 cm^3/g. In a latter work Saha et al. [162] prepared ordered mesoporous carbons from Alcell lignin using a surfactant as soft template (surfactant templating synthesis). The resulting carbons, with around 200 m^2/g BET surface area and 0.2 cm^3/g, were used for controlled drugs delivery. Valero-Romero et al. [163] obtained carbons with hierarchical pore structures using also Alcell as precursor, which was incorporated from ethanol solutions to three different zeolites and a mordenite used as templating materials. The resulting carbons showed varying mesopore sizes within 3 and 10 nm, depending on the type of zeolite template. Upon electro-oxidation under positive polarization a large amount of CO-evolving oxygen groups were created on the surface of the carbons giving rise to a significant improvement of the pseudocapacitance by up to 30 % maintaining the rate performance. The interconnected porous frame allowed achieving specific capacitance values up to 250 F/g at 50 mA/g with 50 % capacitance retention. The volumetric capacitance reached 75 F/cm^3 at more than 20 A/g [164].

Wang et al. [165] synthesized porous carbon-CeO_2 composites using sodium lignosulphonate as template, that was dry-mixed with cerium nitrate and carbonized at different temperatures (400–600 °C) reached at 5 °C/min. The resulting material was used as catalyst for SO_2 at room temperature under sunlight irradiation with significantly better results than CeO_2 alone. Zhang et al. [166] reported in a recent paper the preparation of hierarchical porous carbons from steam-explosion lignin using KOH as template and activating agent at 700 °C. These carbons, showing a 3-D macroporous network with coexisting meso- and micropores with $\approx$900 m^2/g BET surface area, were successfully tested as active material for lithium ion-battery anodes. Capacity values as high as 470 mA·h/g were measured after 400 cycles working at 200 mA/g. The same lignin was used by that group as precursor for KOH-activated carbons with hierarchical porous structure yielding almost 3800 m^2/g surface area. They were used as electrode material for supercapacitors. It was reported an specific capacitance of 287 F/g at 200 mA/g in 6 M KOH [167].

8.5   Lignin Graphitization

Graphite is a well-known allotropic form of carbon integrated by parallel layers of C atoms with covalent bonding in sp^2 hybridization forming a condensed-hexagons net known as graphene. These graphene layers are bonded to each other by weaker

van der Waals-type interactions due to delocalized electronic π-orbitals, maintaining an interlayer distance of 0.3354 nm. This crystalline structure gives graphite its anisotropic character with different properties in the basal planes and the perpendicular directions. Graphite behaves as a good conductor (both thermal and electric) along the former direction and as an insulating material along the second. Its high thermal and chemical stability as well as its good mechanical resistance together with other interesting properties make graphite a versatile high-value material with a diversity of potential applications. The manufacture of synthetic graphite from highly available low-cost precursors, like lignin from pulping and biorefinery processes, represents an encouraging challenge.

Lignin is so far recognized as non-graphitizable due to its highly crosslinked structure with a relative abundance of heteroatoms, in particular oxygen. In fact, a carbon material with evidenced graphite structure has not been obtained yet. Wood and other lignocellulosic materials are also believed as non-graphitizable. However, Hata et al. [168] presented TEM imaging evidence on the formation of wide regions of highly ordered graphite-like carbon upon heat-treatment of a sugi wood char by spark plasma sintering at high temperature and pressure ($\approx$2500 °C and 500 atm) for a short time (5 min).

As indicated before, Otani et al. [14] reported pioneer work on the structural changes occurring upon heat-treatment of a hydrolytic lignin under inert atmosphere up to 2400 °C. Beyond 1700 °C increased structural ordering was evidenced by XRD accompanied by a decrease of the electrical resistivity and increase of real density, this attributed to closer stacking of graphene layers. However, even at the highest temperature only small graphitic crystals appear to be formed in a predominantly turbostratic carbon matrix. A detailed study on the preparation of highly ordered carbons from Kraft lignin was reported two decades ago by the authors of this chapter [169]. The kraft lignin, already described in Sect. 8.2.1, was predevolatilized for 2 h at 350 °C under N_2 atmosphere and the resulting char was washed with 1 % aqueous H_2SO_4 up to 2 % ash content and heat-treated for 2 h at 1100 °C (reached at 50 °C/min) giving rise to a carbon with 2.9 % ash content and more than 98.5 % C. This intermediate treatment has been recognized to influence the onset of structural ordering of other carbon materials upon subsequent heating at higher temperatures. Further heat-treatment was carried out in a graphite tubular induction furnace under Ar atmosphere at different temperatures up to 2800 °C, reached at 100 °C/min and maintained for 1 h.

The heat-treatment led to progressive loss of the inorganic matter. The analysis of the carbon obtained at 2400 °C yielded no ash content and 99.7 % C. The BET surface area decayed severely from 275 to 25 m²/g at 1100 and 2200 °C, respectively, and then slowly up to 21 m²/g at 2800 °C, with more than 55 % corresponding to external area. The X-ray diffraction profiles, using 10 % Si as internal standard, revealed a progressive evolution towards graphitization. That of the 2800 °C carbon is shown in Fig. 8.8. Increasing the temperature the 002 diffraction peak gained intensity and its width at half maximum decreased substantially, being centered closer to the 2θ value of graphite (26.53°). Consequently, the interlayer spacing (d_{002}) approached that of graphite (0.3354 nm). Beyond 2400 °C, a modulation of
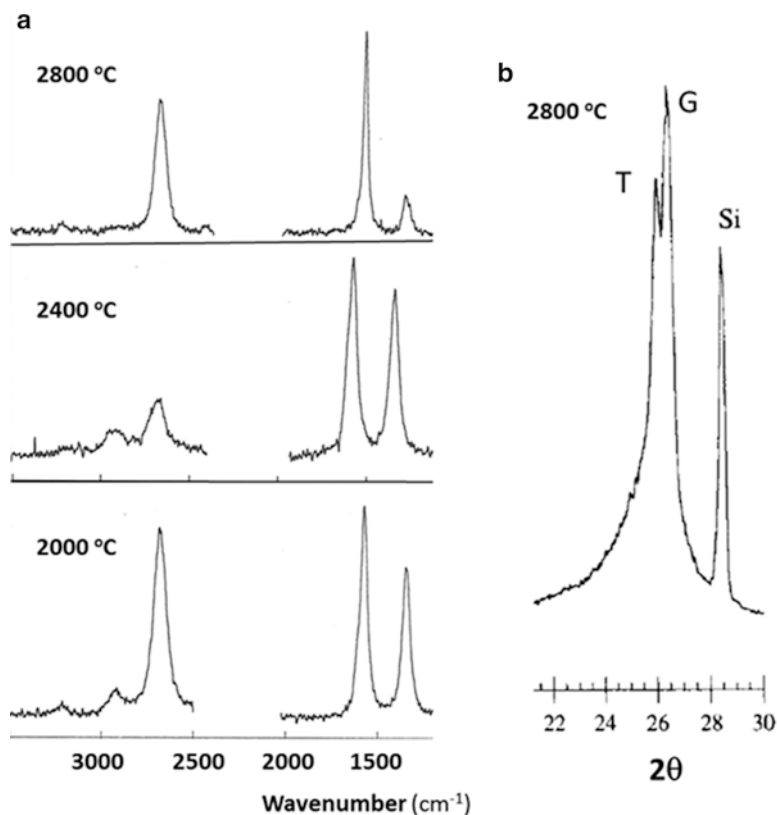
Fig. 8.8 Raman (**a**) and XRD (**b**) spectra of carbons from high-temperature treatment of Kraft lignin (Adapted with permission from Ref. [169] (Copyright (1995) Elsevier))

the 002 reflection was observed, more evident in the 2800 °C carbon (see Fig. 8.8). This has been reported for other high-temperature carbon materials and explained by the coexistence of graphitic and turbostratic structures [170]. Upon deconvolution of the modulated 002 reflection, the values of the crystallite parameters were determined for the graphitic (or highly ordered, G) and the turbostratic (less ordered, T) fractions, summarized in Table 8.3. As can be seen, the interlayer spacing for the G fraction of the 2800 °C carbon is fairly close to that of graphite. The calculated average thickness of the stacks (L_c) is significantly higher for that fraction indicating a larger development of the graphitic versus the turbostratic domains. The Raman spectra of the carbons confirmed the structural ordering towards graphitization at increasing temperature. The profiles of selected samples are included in Fig. 8.8. The decreasing width of the E_{2g} line and its progressive displacement towards the frequency value for graphite (1582 cm^{-1}) are some main features. The intensity of the band in the 1350 cm^{-1} region, characteristic of turbostratic carbon decayed significantly at increasing the heat-treatment temperature and the evolution of the

Table 8.3 XRD- and Raman-derived structural parameters of the high-temperature carbons from kraft lignin

Heat-treatment temperature (°C)	d_{002} (nm)	L_c (nm)	L_a (nm)
1100	0.382		
2000	0.346	1.71	20.2
2400	0.3416 (T)	10.34	24.3
2800	0.3418 (T)	8.16	93.3
2800	0.3361 (G)	23.32	
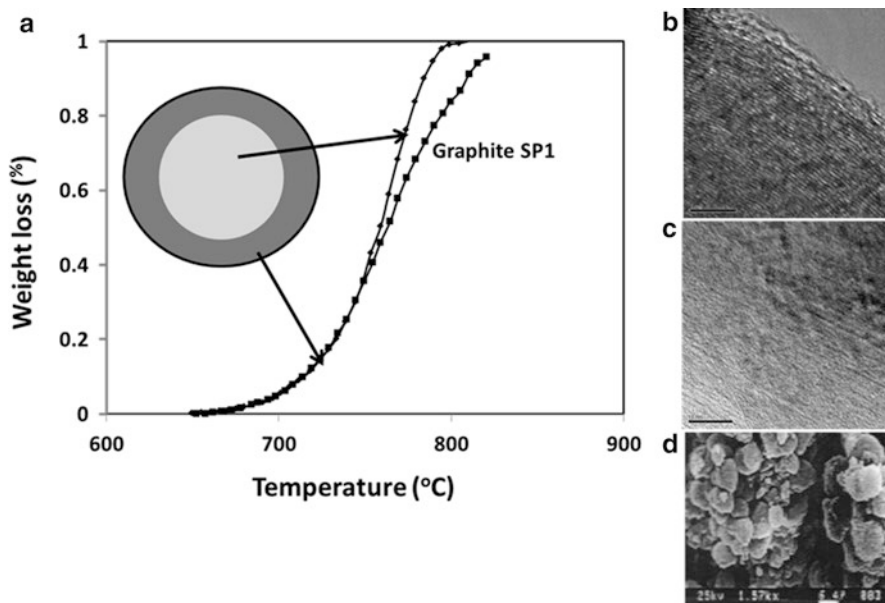
Fig. 8.9 Oxidation resistance (**a**), SEM (**b**) and TEM (**c**, **d**) micrographs of the 2800 °C carbon from Kraft lignin (bar length for TEM micrograph: (**c**) 5 nm; (**d**) 10 nm)

2700 cm^{-1} band supports the development of tridimensional order associated to progress in the graphitization path. Table 8.3 includes the values of the average apparent crystallite dimension (L_a) calculated from the equation developed by Pimenta et al. [171] where it can be seen the substantial increase of that dimension at 2800 °C.

Further evidence on the onset of graphitization was obtained from the oxidation behavior of the carbons, evaluated from dynamic TG experiments under oxygen flow at 5 °C/min up to 1100 °C. The 2800 °C carbon exhibited the same behavior as a commercial graphite (SP-1) up to about 40 % burn-off and beyond that a lower oxidation resistance was observed (Fig. 8.9). These results support the existence of graphitic and turbostratic carbon domains, with a significant contribution of the former in the highest temperature carbon. The oxidation behavior suggests a

core-shell structure with graphitic carbon prevailing in the outer part of the sphere-like particles surrounding a predominantly turbostratic internal structure. Figure 8.9 includes SEM and TEM images of the 2800 °C carbon supporting the sphere-like morphology and the proposed core-shell structure. The effect of the inorganic matter of the starting Kraft lignin was also investigated since it can affect to the structural evolution of lignin-derived carbons [172]. As indicated before, the ash content of the as-precipitated lignin was somewhat above 12 %, being Na by far the main metallic component (≈95 % as determined from the LTA residue). That ash content was 24 % after the heat-treatment at the intermediate temperature of 1100 °C. The XRD profiles and the oxidation curves of the resulting 2800 °C carbon confirmed the favorable effect of the inorganic matter on the extent of graphitization. In particular, the oxidation resistance was frankly improved, being now similar to that of the SP-1 graphite up to about 70 % burn-off.

Kubo et al. [173] investigated the catalytic graphitization of lignin from birch pulping with acetic acid. The authors worked at relatively low temperatures (850–1000 °C) reached at a low heating rate (3 °C/min) and maintained for 1 h. They used nickel acetate as catalyst at 0.1 to 10 % of the lignin weight. The structure of the resulting carbons was analyzed by X-ray diffraction and according to the results remained essentially turbostratic with small domains of less than 10 nm height and a interlayer spacing of 0.339 nm as the closest value to that of graphite. Popova et al. [174, 175] claimed in two recent papers the attainment of a carbon material with around 95 % graphitization degree from hydrolysis lignin by heat-treatment at 2500–2800 °C after previous charring at 600 °C. The lignin was obtained from different lignocellulosic precursors by so-called percolation hydrolysis, carried out with H_2SO_4 solution at 200 °C and 6–7 atm. It is believed that this process causes important modifications of the virgin lignin giving rise to incipient condensed aromatic units which may favor further evolution towards more ordered carbon structures. Although their conclusions seem to be in principle interesting, the authors did not provide solid evidence on the above mentioned graphitization. They presented some XRD profile without direct contrast with that of any recognized graphite. Information on the parameters derived from XRD was limited as well as details on the experimental procedure. TEM images that could support graphitization were not included. Similar comments can be made on the paper of Demir et al. [176]. The authors conclude that lignin (Norlig A from Lignotech) was converted into "graphitic porous carbon" after hydrothermal carbonization at 300 °C and more than 100 atm followed by heat-treatment at 900 and 1100 °C catalyzed by manganese and cobalt nitrate, respectively. However, the XRD and Raman profiles provided in the paper cannot be taken as typical graphite patterns. In fact the existence of amorphous together with graphitic carbon is recognized. On the other hand, the carbons show a fairly important porosity with BET surface area values within as much as ≈130–270 m^2/g and again TEM image evidences are not supplied.

8.6   Conclusions and Future Outlook

The C-rich polymeric structure of lignin mostly based on functionalized aromatic units makes it a useful precursor for carbon materials. A diversity of such materials has been already prepared from lignins and lignosulfonates of different sources, most in particular Kraft and organosolv lignins. Carbonization upon heating in inert atmosphere provides the most direct way of lignin conversion into carbon materials, biochars in this case. Further partial gasification with CO_2, steam or air (physical activation) yields carbons with highly developed porous texture, showing high surface area (up to $\approx$ 1800 m²/g has been reported) and variable contributions of micro and mesoporosity. Carbonization with added activating agents, like $ZnCl_2$, H_3PO_4 or KOH, also allows obtaining activated carbons within a wide range of porous texture. In particular, with KOH, surface area values above 3000 m²/g have been described in the literature. Lignin-derived activated carbons have been successfully tested as adsorbents for a wide diversity of organic compounds as well as for heavy metals in water. Gas-phase adsorption of VOCs has been also demonstrated. Application in heterogeneous catalysis has been also explored and provides the most interesting field of future research and development with those activated carbons, most in particular for the H_3PO_4-activated ones, given their surface chemical characteristics.

Lignin-based carbons with hierarchical pore structure and a variety of surface oxygen and nitrogen groups that confer them interesting surface feature as electrodes in electrochemical capacitors have been obtained using nanocasting techniques with sacrificial hard templates. The interconnected porous frame and surface chemistry, associated to the hard template used, allows these materials achieving a high capacitance enhancement compared to that of petroleum-pitch-based carbons.

Lignin presents also highly promising potential as precursor of carbon fibers. The origin (hardwood, softwood) and extraction procedure (Kraft, organosolv) of the lignin determine their physical and chemical characteristics and the spinning technique (wet, dry, melting) used for the conformation of the fiber governs not only the morphology and properties but also the production cost of the final CFs. Physical blends with synthetic polymers, chemical modification and thermal and purification treatments with solvents or membrane have been studied for conditioning and controlling the fusibility of lignin in order to reduce the time of the long oxidative thermostabilization step, needed to avoid lignin fiber melting or softening during the CFs production process, and to improve their mechanical properties. However, the high degree of cross-linking, porosity and heterogeneities occurring during the preparation process reduce the tensile strength and mechanical properties of the final lignin-based CFs, limiting their possibilities for structural applications. Interconnection in the partial fused lignin fibers or the incorporation of reinforcement filler, like carbon nanotubes, seem to enhance those mechanical properties, although future research is needed for a more comprehensive knowledge on their action and effect. Porosity, high surface area and a rich surface chemistry, the main drawback of the lignin-derived CFs for structural applications, along with electrical conductivity and oxidation resistance are important and useful properties for

functional applications in the fields of adsorption, heterogeneous catalysis and energy conversion and storage. In this sense, electrospinning, a novel promising technology, has been used for the preparation of lignin-derived activated carbon fibers of different conformation, with very low diameters (submicron) and high surface area. These materials have interesting potential application in energy storage systems like lithium-ion batteries, supercapacitors or fuel cells. Future work should be focused to learn on the influence of the electrospinning conditions and lignin solution characteristics on the properties of the resulting fibers in order to control the preparation of binderless carbon fiber electrodes with tailored pore structure and high conductivity. The high versatility of this technology should be also explored toward direct (one-pot) production of surface functionalized lignin fibers that allows high thermostabilization rates and production of CFs with improved surface properties (chemistry) of different character (acid, basic, metallic), of great interest in heterogeneous catalysis, adsorption and energy storage applications.

Obtaining graphite from lignin is a challenge which has not been accomplished thus far. In fact, lignin is considered as non-graphitizable material because of its cross-linked structure and the relative abundance of oxygen in its chemical composition. Highly ordered carbons have been obtained upon thermal treatment of Kraft lignin at temperature up to 2800 °C. A core-shell particle structure has been proposed for those carbons, with extended graphitic domains in the external shell surrounding the turbostratic carbon core. That encourages future research addressed to graphitize lignin by using higher heat-treatment temperatures and/or appropriate catalysts.

Growing availability of lignin is expected in the near future associated with lignocellulosic-based biorefineries. Therefore, lignin valorization must be a key factor in the development of those industrial projects. In that overall strategy, conversion of lignin into different value-added carbon materials provides a fairly promising way as has been experimentally demonstrated through the research efforts thus far accomplished in this field.

References

1. Rosas JM, Berenguer R, Valero-Romero MJ, Rodriguez-Mirasol J, Cordero T. Preparation of different carbon materials by thermochemical conversion of lignin. Front Mater. 2014;1:1–17.
2. Mattson JS, Mark HB. Activated carbon. Surface chemistry and adsorption from solution. New York: Marcel Dekker; 1971.
3. Bansal RC, Donnet JP, Stoeckli F. Active carbon. New York: Marcel Dekker; 1988.
4. Marsh H, Rodríguez-Reinoso F. Activated carbon. New York: Elsevier Science; 2006.
5. Suzuki H. Jap Patent 73–50989. 1973.
6. Ivanchenko AV, Simkin YY, Voropaev YM. USSR Patent 1328288. 1987.
7. Chevykin VV, Gostev VS, Karev VA, Mukihin VM, Nagornaya GA, Solorev SN. RU Patent RU2362734-C1. 2009.
8. Jiang J, Deng X, Wang Z. CN Patent CN1425607-A. 2005.

9. Del Bagno VD, Miller RL, Watkins JJ. On-site production of activated carbon from kraft black liquor. USEPA Report 600/2-78-191. 1978.

10. Li J, Van Heinigen ARP. Reaction kinetic of gasification of black liquor char. Can J Chem Eng. 1989;67:693–7.

11. Li J, Van Heinigen ARP. Kinetics of carbon dioxide gasification of fast pyrolysis black liquor char. Ind Eng Chem Res. 1990;29:1776–85.

12. Rodríguez-Mirasol J, Cordero T, Rodríguez JJ. Preparation and characterization of activated carbons from eucalyptus kraft-lignin. Carbon. 1993;31:87–95.

13. Rodríguez-Mirasol J, Cordero T, Rodríguez JJ. Activated carbons from CO_2 partial gasification of eucalyptus kraft lignin. Energy Fuel. 1993;7:133–8.

14. Otani C, Polidoro HA, Otani S, Craievich AF. Structure variations of carbonizing lignin. J Chim Phys Phys Chim Biol. 1984;81:887–91.

15. Cordero T, Rodriguez-Maroto JM, Rodríguez-Mirasol J, Rodríguez JJ. On the kinetics of thermal decomposition of wood and wood components. Thermochim Acta. 1990;164:135–44.

16. Órfão JJM, Antunes FJA, Figueiredo JL. Pyrolysis kinetics of lignocellulosic materials-three independent reactions model. Fuel. 1999;78:349–58.

17. Baklanova ON, Plaksin GV, Drozdov VA, Duplyakin VK, Chesnokov NV, Kuznetsov BN. Preparation of microporous sorbents from cedar nutshells and hydrolytic lignin. Carbon. 2003;41:1793–800.

18. Xie X, Goodell B, Zhang D, Nagle DC, Qian Y, Peterson ML, Jellison J. Characterization of carbons derived from cellulose and lignin and their oxidative behavior. Bioresour Technol. 2009;100:1797–802.

19. Kijima M, Hirukawa T, Hanawa F, Hata T. Thermal conversion of alkaline lignin and its structured derivatives to porous carbonized materials. Bioresour Technol. 2011;102:6279–85.

20. Sharma RK, Wooten JB, Baliga VL, Lin X, Chan WG, Hajaligol MR. Characterisation of chars from pyrolysis of lignin. Fuel. 2004;83:1469–82.

21. Kuznetsov BN, Shchipko ML. The conversion of wood lignin to char materials in a fluidized bed of Al-Cu-Cr oxide catalysts. Bioresour Technol. 1995;52:13–9.

22. Rodríguez-Mirasol J, Cordero T, Rodríguez JJ. CO_2-reactivity of eucalyptus kraft-lignin. Carbon. 1993;31:53–61.

23. Tancredi N, Cordero T, Rodriguez-Mirasol J, Rodriguez JJ. CO_2-gasification of eucalyptus wood chars. Fuel. 1996;75:1505–8.

24. Carrott PJM, Suhas, Ribeiro-Carrott MML, Guerrero CI, Delgado LA. Reactivity and porosity development during pyrolysis and physical activation in CO_2 or steam of kraft and hydrolytic lignins. J Anal Appl Pyrolysis. 2008;82:264–71.

25. Gergova K, Petrov N, Eser S. Adsorption properties and microstructure of activated carbons produced from agricultural by-products by steam pyrolysis. Carbon. 1994;32:693–702.

26. Perezdrienko IV, Molodozhenyuk TB, Shermatov BE, Yunusov MP. Effect of carbonization temperature and activation on structural formation of active lignin carbons. Russian J Appl Chem. 2001;74:1650–2.

27. Fu K, Yue Q, Gao B, Sun Y, Zhu L. Preparation, characterization and application of lignin-based activated carbon from black liquor lignin by steam activation. Chem Eng J. 2013;228:1074–82.

28. Rodriguez-Reinoso F, Martin-Martinez JM, Molina-Sabio M, Perez-Lledo I, Prado-Berruguete C. A comparison of the porous texture of two CO_2-activated botanic materials. Carbon. 1985;23:19–24.

29. Rodriguez-Reinoso F, Molina-Sabio M. Activated carbons from lignocellulosic materials by chemical and/or physical activation: an overview. Carbon. 1992;30:1111–8.

30. Tancredi N, Cordero T, Rodriguez-Mirasol J, Rodriguez JJ. Activated carbons from Uruguayan eucalyptus wood. Fuel. 1996;75:1701–6.

31. Tancredi N, Cordero T, Rodriguez-Mirasol J, Rodriguez JJ. Activated carbons from eucalyptus wood. Influence of the carbonization temperature. Sep Sci Technol. 1997;32:1115–26.

32. Arriagada R, Garcia R, Molina-Sabio M, Rodriguez-Reinoso F. Effect of steam activation on the porosity and chemical nature of activated carbons from *Eucalytus globulus* and peach stones. Microporous Mater. 1997;8:123–30.

33. Marquez-Montesinos F, Cordero T, Rodriguez-Mirasol J, Rodriguez JJ. Powdered activated carbons from *Pinus caribaea* sawdust. Sep Sci Technol. 2001;36:3191–206.

34. Prauchner MJ, Rodriguez-Reinoso F. Chemical versus physical activation of coconut shell: a comparative study. Microporous Mesoporous Mater. 2012;152:163–71.

35. Gonzalez-Serrano E, Cordero T, Rodriguez-Mirasol J, Rodrıguez JJ. Development of porosity upon chemical activation of kraft lignin with $ZnCl_2$. Ind Eng Chem Res. 1997;36:4832–8.

36. Torregrosa R, Martin-Martinez JM. Activation of lignocellulosic materials: a comparison between chemical, physical and combined activation in terms of porous texture. Fuel. 1991;70:1173–80.

37. Gonzalez-Serrano E, Cordero T, Rodriguez-Mirasol J, Cotoruelo LM, Rodrıguez JJ. Removal of water pollutants with activated carbons prepared from H_3PO_4 activation of lignin from kraft black liquors. Water Res. 2004;38:3043–50.

38. Guo Y, Rockstraw DA. Physical and chemical properties of carbons synthesized from xylan, cellulose, and kraft lignin by H_3PO_4 activation. Carbon. 2006;44:1464–75.

39. Hayashi J, Kazehaya A, Muroyama K, Watkinson AO. Preparation of activated carbon from lignin by chemical activation. Carbon. 2000;38:1873–8.

40. Hayashi J, Muroyama K, Gomes VG, Watkinson AO. Fractal dimensions of activated carbons prepared from lignin by chemical activation. Carbon. 2002;40:617–36.

41. Sun Y, Yang G, J-p Z, Wang Y, Yao MS. Activated carbon preparation from lignin by H_3PO_4 activation and its application to gas separation. Chem Eng Technol. 2012;35:309–16.

42. Myglovets M, Poddubnaya OI, Sevastyanova O, Lindström ME, Gawdzik B, Sobiesiak M, Tsyba MM, Sapsay VI, Klymchuk DO, Puzuy AM. Preparation of carbon adsorbents form lignosulfonate by phosphoric acid activation for the adsorption of metal ions. Carbon. 2014;80:771–83.

43. Fierro V, Torne-Fernandez V, Montane D, Celzard A. Study of the decomposition of kraft lignin impregnated with orthophosphoric acid. Thermochem Acta. 2005;433:142–8.

44. Montane D, Torne-Fernandez V, Fierro V. Activated carbons from lignin: kinetic modeling of the pyrolysis of kraft lignin activated with phosphoric acid. Chem Eng J. 2005;106:1–12.

45. Fierro V, Torne-Fernandez V, Celzard A. Kraft lignin as a precursor for microporous activated carbons prepared by impregnation with ortho-phosphoric acid: synthesis and textural characterisation. Microporous Mesoporous Mater. 2006;92:243–50.

46. Fierro V, Torne-Fernandez V, Celzard A, Montane D. Influence of the demineralisation on the chemical activation of kraft lignin with orthophosphoric acid. J Hazard Mater. 2007;149:126–33.

47. Bedia J, Rosas JM, Marquez J, Rodriguez-Mirasol J, Cordero T. Preparation and characterization of carbon based acid catalysts for the dehydration of 2-propanol. Carbon. 2009;47:286–94.

48. Rosas JM, Ruiz-Rosas R, Rodriguez-Mirasol J, Cordero T. Kinetic study of the oxidation resistance of phosphorus-containing activated carbons. Carbon. 2012;50:1523–37.

49. Jagtoyen M, Derbyshire F. Some considerations of the origins of porosity in carbons from chemically activated wood. Carbon. 1993;31:1185–92.

50. Molina-Sabio M, Rodriguez-Reinoso F, Caturla F, Selles MJ. Porosity in granular carbons activated with phosphoric acid. Carbon. 1995;33:1105–13.

51. Laine J, Calafat A, Labady M. Preparation and characterization of activated carbons from coconut shell impregnated with phosphoric acid. Carbon. 1989;27:191–5.

52. Wennenberg AN, O'Grady TM. US Patent 4082694. 1978.

53. Linares-Solano A, Lozano-Castello D, Lillo-Rodenas MA, Cazorla Amoros D. Carbon activation by alkaline hydroxides: preparation and reactions, porosity and performances. In: Radovic LR, editor. Chemistry and physics of carbon, vol. 30. Boca Raton: CRC Press; 2008.

54. Khezami L, Chetouani A, Taouk B, Capart R. Production and characterization of activated carbon from wood components in powder: cellulose, lignin, xylan. Powder Technol. 2005;157:48–56.

55. Fierro V, Torne-Fernandez V, Celzard A. Highly microporous carbons prepared by activation of kraft lignin with KOH. Stud Surf Sci Catal. 2007;160:607–14.

56. Fierro V, Torne-Fernandez V, Celzard A. Methodical study of the chemical activation of kraft lignin with KOH and NaOH. Microporous Mesoporous Mater. 2007;101:419–31.

57. Torne-Fernandez V, Mateo- Sanz JM, Montane D, Fierro V. Statistical optimization of the synthesis of highly microporous carbons by chemical activation of kraft lignin with NaOH. J Chem Eng Data. 2009;54:2216–21.

58. Gao Y, Yue Q, Gao B, Sun Y, Wang W, Li Q, Wang Y. Preparation of high surface area-activated carbon from lignin of papermaking liquor by KOH activation for Ni(II) adsorption. Chem Eng J. 2013;217:345–53.

59. Li X-F, Xu Q, Fu Y, Guo Q-X. Preparation and characterization of activated carbon from kraft lignin via KOH activation. Environ Prog Sustain Energy. 2014;33:519–25.

60. Jin XJ, Yu ZM, Wu Y. Preparation of activated carbon from lignin obtained by straw pulping by KOH and K$_2$CO$_3$ chemical activation. Cellul Chem Technol. 2012;46:79–85.

61. Hu Z, Srinivasan MP. Preparation of high-surface-area activated carbons from coconut shell. Microporous Mesoporous Mater. 1999;27:11–8.

62. Marco-Lozar JP, Linares-Solano A, Cazorla-Amoros D. Effect of the porous texture and surface chemistry of activated carbons on the adsorption of a germanium complex from dilute aqueous solutions. Carbon. 2011;49:3325–31.

63. Suhas CPJM, Ribeiro Carrott MML. Lignin-from natural adsorbent to activated carbon: a review. Bioresour Technol. 2007;98:2301–12.

64. Srivastava SK, Singh AK, Sharma A. Studies on the uptake of lead and zinc by lignin obtained from black liquor-a paper-industry waste material. Environ Technol. 1994;15:353–61.

65. Toles CA, Marshall WE, Mitchell MJ. Surface functional groups on acid-activated nutshells carbons. Carbon. 1999;37:1207–14.

66. Huang G, Wang D, Ma S, Chen J, Jiang L, Wang P. A new low-cost adsorbent: preparation, Characterization and adsorption behavior of Pb(II) and Cu(II). J Colloid Interface Sci. 2015;445:294–302.

67. Meng CB, Weber J. Lignin-based microporous materials as selective adsorbents for carbon dioxide separation. ChemSusChem. 2014;7:3312–8.

68. Cotoruelo LM, Marques MD, Rodriguez-Mirasol J, Cordero T, Rodriguez JJ. Adsorption of aromatic compounds on activated carbons from lignin: equilibrium and thermodynamic study. Ind Eng Chem Res. 2007;46:4982–90.

69. Cotoruelo LM, Marques MD, Rodriguez-Mirasol J, Cordero T, Rodriguez JJ. Adsorption of aromatic compounds on activated carbons from lignin: kinetic study. Ind Eng Chem Res. 2007;46:2853–60.

70. Cotoruelo LM, Marques MD, Díaz FJ, Rodriguez-Mirasol J, Rodriguez JJ, Cordero T. Adsorbent ability of lignin-based activated carbons for the removal of p-nitrophenol from aqueous solutions. Chem Eng J. 2012;184:176–83.

71. Cotoruelo LM, Marques MD, Diaz FJ, Rodriguez-Mirasol J, Rodriguez JJ, Cordero T. Lignin-based activated carbons for adsorption of sodium dodecylbenzene sulfonate: equilibrium and kinetic studies. J Colloid Interface Sci. 2009;332:39–45.

72. Cotoruelo LM, Marques MD, Diaz FJ, Rodriguez-Mirasol J, Cordero T, Rodriguez JJ. Activated carbons from lignin: their application in liquid phase adsorption. Sep Sci Technol. 2007;42:3363–89.

73. Cotoruelo LM, Marques MD, Rodriguez-Mirasol J, Rodriguez JJ, Cordero T. Cationic dyes removal by multilayer adsorption on activated carbons from lignin. J Porous Mater. 2011;18:693–702.

74. Cotoruelo LM, Marques MD, Diaz FJ, Rodriguez-Mirasol J, Rodriguez JJ, Cordero T. Equilibrium and kinetic study of congo red adsorption onto lignin-based activated carbons. Transp Porous Media. 2010;83:573–90.

75. Cotoruelo LM, Marques MD, Diaz FJ, Rodriguez-Mirasol J, Rodriguez JJ, Cordero T. Lignin-based activated carbons as adsorbents for crystal violet removal from aqueous solutions. Environ Prog Sustainable Energy. 2012;31:386–96.

76. Cotoruelo LM, Marques MD, Leiva A, Rodriguez-Mirasol J, Cordero T. Adsorption of oxygen-containing aromatics used in petrochemical, pharmaceutical and food industries by means of lignin-based active carbons. Adsorption. 2011;17:539–50.

77. Fierro V, Torne-Fernandez V, Montane D, Celzard A. Adsorption of phenol onto activated carbons having different textural and surface properties. Microporous Mesoporous Mater. 2008;111:276–84.

78. Mussatto SI, Fernandes M, Rocha GJM, Orfao JJM, Teixeira JA, Roberto IC. Production, characterization and application of activated carbon from brewer's spent grain lignin. Bioresour Technol. 2010;101:2450–7.

79. Huang LH, Wang M, Shi CX, Huang J, Zhang B. Adsorption of tetracycline and ciprofloxacin on activated carbon prepared from lignin with H3PO4 activation. Desalin Water Treat. 2014;52:2678–87.

80. Radovic LR, Moreno-Castilla C, Rivera-Utrilla J. Carbon materials as adsorbents in aqueous solutions. In: Radovic LR, editor. Chemistry and physics of carbon, vol 27. New York: Marcel Dekker; 2000. p. 228–405.

81. Rodriguez-Mirasol J, Bedia J, Cordero T, Rodríguez JJ. Influence of water vapor on the adsorption of VOCs on lignin-based activated carbons. Sep Sci Technol. 2005;40:3113–35.

82. Bedia J, Rodriguez-Mirasol J, Cordero T. Water vapour adsorption on lignin-based activated carbons. J Chem Technol Biotechnol. 2007;82:548–57.

83. Bedia J, Rosas JM, Rodriguez-Mirasol J, Cordero T. Pd supported on mesoporous activated carbons with high oxidation resistance as catalysts for toluene oxidation. Appl Catal B Environ. 2010;94:8–18.

84. Guillen E, Rico R, Lopez-Romero JM, Bedia J, Rosas JM, Rodriguez-Mirasol J, Cordero T. Pd-activated carbon catalysts for hydrogenation and Suzuki reactions. Appl Catal A Gen. 2009;368:113–20.

85. Zazo JA, Bedia J, Fierro CM, Pliego G, Casas JA, Rodriguez JJ. Highly stable Fe on activated carbon catalyst for CWPO upon FeCl3 activation of lignin from black liquors. Catal Today. 2012;187:115–21.

86. Chieffi G, Fechler N, Esposito D. Valorization of lignin waste from hydrothermal treatment of biomass: towards porous carbonaceous composites for continuous hydrogenation. RCS Adv. 2015;5:63691–6.

87. Leitten C, Griffith W, Compere A, Shaffer J. High-volume, low-cost precursors for carbon iber roduction. SAE Technical Paper 2002-01-1907. 2002.

88. Lallave M, Bedia J, Ruiz-Rosas R, Rodriguez-Mirasol J, Cordero T, Otero JC, Marquez A, Barrero A, Loscertales IG. Filled and hollow carbon nanofibers by coaxial electrospinning of Alcell lignin without binder polymers. Adv Mater. 2007;19:4292–6.

89. Ruiz-Rosas R, Bedia J, Lallave M, Loscertales IG, Barrero A, Rodriguez-Mirasol J, Cordero T. The production of submicron diameter carbon fibers by the electrospinning of lignin. Carbon. 2010;48:696–705.

90. Baker DA, Rials TG. Recent advances in low-cost carbon fiber manufacture from lignin. J Appl Polym Sci. 2013;130:713–28.

91. Frank E, Steudle LM, Ingildeev D, Spörl JM, Buchmeiser MR. Carbon fibers: precursor systems, processing, structure, and properties. Angew Chem Int Ed Engl. 2014;53:5262–98.

92. Ragauskas AJ, Beckham GT, Biddy MJ, Chandra R, Chen F, Davis MF, Davison BH, Dixon RA, Gilna P, Keller M, Langan P, Naskar AK, Saddler JN, Tschaplinski TJ, Tuskan GA, Wyman CE. Lignin valorization: improving lignin processing in the biorefinery. Science. 2014;344:1246843.

93. Otani S, Fukuoka Y, Igarashi B, Sasaki K. Method for producing carbonized lignin fiber. US 3461082 A. 1969.
94. Fukuoka Y. Method for producing carbonized lignin fiber. Jpn Chem Q. 1969;5:63–6.
95. Mikawa S. Lignin-based carbon fiber. Chem Econ Eng Rev. 1970;2:43–6.
96. Mansmann M. Stable lignin fibers. GB 1359764 A. 1974.
97. Bissett PJ, Herriott CW. Lignin/polyacrylonitrile-containing dopes, fibers and production methods. US 20120003471 and WO 2012003070. 2012.
98. Maradur SP, Kim CH, Kim SY, Kim B-H, Kim WC, Yang KS. Preparation of carbon fibers from a lignin copolymer with polyacrylonitrile. Synth Met. 2012;162:5–6.
99. Seydibeyoglu MO. A novel partially biobased PAN-lignin blend as a potential carbon Fiber precursor. J Biomed Biotechnol. 2012;2012:1–8.
100. Sudo K, Shimizu K. Production of lignin-based carbon fiber. JP 62–110922. 1987.
101. Uraki Y, Hubo S, Nigo N, SanoY Sasaya T. Preparation of carbon fibers from organosolv lignin obtained by aqueous-acetic-acid pulping. Holzforschung. 1995;49:343–50.
102. Uraki Y, Kubo S, Kurakami H, Sano Y. Activated carbon fibers from acetic acid lignin. Holzforschung. 1997;51:188–92.
103. Uraki Y, Nakatani A, KuboS SY. Preparation of activated carbon fibers with large specific surface area from softwood acetic acid lignin. J Wood Sci. 2001;47:465–9.
104. Kubo S, Uraki Y, Sano Y. Preparation of carbon fibers from soft-wood lignin by atmospheric acetic acid pulping. Carbon. 1998;36:1119–24.
105. Luo J, Genco J, Cole BJW, Fort RC. Lignin recovered from the near-neutral hemicelluloses extraction process as a precursor for carbon fiber. Bioresources. 2011;6:4566–93.
106. Lin J, Kubo S, Yamada T, Koda K, Uraki Y. Chemical thermostabilization for the preparation of carbon fibers from soft wood lignin. Bioresources. 2012;7:5634–46.
107. Kadla JF, Kubo S, Venditti RA, Gilbert RD, Compere AL, Griffith W. Lignin-based carbon fibers for composite fiber applications. Carbon. 2002;40:2913–20.
108. Baker DA, Gallego NC, Baker FS. Carbon fiber production from a Kraft hard wood lignin. In: Book of abstracts of the fiber society. Québec: Fall Conference 2008; 2008. p. 106–7.
109. Baker FS, Gallego NC. Low cost carbon fiber from renewable resources. In: DOEFY2010 progress report for light weighting materials, Part 3.C. Washington, DC: US Department of Energy; 2010. p. 32.
110. Baker DA, Harper DP, Rials TG. Carbon fiber from extracted commercial softwood lignin. In Book of abstracts of the fiber society. Boston: Fall Conference; 2012. p. 17.
111. Nordström Y, NorbergI SE, Drougge R. A new softening agent for melt spinning of soft wood Kraft lignin. J Appl Polym Sci. 2012;129:1274–9.
112. Kadla JF, Kubo S, Venditti RA, Gilbert RD. Novel hollow core fibers prepared from lignin polypropylene blends. J Appl Polym Sci. 2002;85:1353–5.
113. Kadla JF, Kubo S. Lignin-based polymer blends: analysis of intermolecular interactions in lignin-synthetic polymer blends. Compos A Appl Sci Manuf. 2004;35:395–400.
114. Kubo S, Kadla JF. Poly(ethyleneoxide)/organosolv lignin blends: relationship between thermal properties, chemical structure and blend behavior. Macromolecules. 2004;37:6904–11.
115. Kubo S, Kadla JF. Kraft lignin/poly(ethyleneoxide) blends: effect of lignin structure on miscibility and hydrogen bonding. J Appl Polym Sci. 2005;98:1437–44.
116. Kubo S, Kadla JF. The formation of strong intermolecular interactions in immiscible blends of poly(vinylalcohol) (PVA) and lignin. Biomacromolecules. 2003;4:561–7.
117. Baker FS, Gallego NC, Baker DA. Low cost carbon fiber from renewable resources. In: DOEFY2008 progress report for light weighting materials, Part 7.A. Washington, DC: US Department of Energy; 2008. p. 1.
118. Warren CD. Future lower cost carbon fiber for autos: international scale-up & what is needed. In: 8th-Annual Automotive Composites Conference and Exhibition (ACCE2008): the road to light weight performance. Troy: SPE Automotive and Composites Divisions; 2008. p. 50.
119. Sevastyanova O, Qin W, Kadla JF. Effect of nanofillers as reinforcement agents for lignin composite fibers. J Appl Polym Sci. 2010;117:2877–81.

120. Qin W, Kadla JF. Effect of organoclay reinforcement on lignin-based carbon fibers. Ind Eng Chem Res. 2011;50:12548–55.
121. Baker FS, Baker DA, Menchhofer PA. Carbon nanotube enhanced precursor for carbon fiber production and method of making a CNT-enhanced continuous lignin fiber. US Patent 2011285049 A1. 2011.
122. Sudo K, Shimizu K. A new carbon fiber from lignin. J Appl Polym Sci. 1992;44:127–34.
123. Sudo K, Shimizu K, Nakashima N, Yokoyama A. A new modification method of exploded lignin for the preparation of a carbon fiber precursor. J Appl Polym Sci. 1993;48:1485–91.
124. Sudo K, Shimizu K. Method for manufacturing lignin for carbon fiber spinning. US Patent 5344921 A. 1994.
125. Gould AM. Manufacture of Carbon Fibre. Patent GB 1358164A. 1974.
126. Eckert RC, Abdullah Z. Carbon Fibers from Kraft Soft wood Lignin. US Patent 20080317661. 2008.
127. Wohlmann B, Woelki M, Ebert A, Engelmann G, Fink HP. Lignin derivative, shaped body comprising the derivative, and carbon fibers produced from the shaped body. Patent WO2010081775. 2010.
128. Shen Q, Zhang T, Zhang WX, Chen S, Mezgebe M. Lignin-based activated carbon fibers and controllable pore size and properties. J Appl Polym Sci. 2011;121:989–94.
129. Thunga M, Chen K, Grewell D, Kessler MR. Bio-renewable precursor fibers from lignin/polylactide blends for conversion to carbon fibers. Carbon. 2014;68:159–66.
130. Sen S, Sadeghifar H, Argyropoulos DS. Kraft lignin chain extension chemistry via propargylation, oxidative coupling and Claisen rearrangement. Biomacromolecules. 2013;14:3399–408.
131. Berenguer R, Garcia-Mateos FJ, Ruiz-Rosas R, Cazorla-Amoros D, Morallon E, Rodriguez-Mirasol J, Cordero T. Biomass-derived binderless fibrous carbon electrodes for ultrafast energy storage. Green Chem. 2015. doi:10.1039/C5GC02409A.
132. Dallmeyer I, Ko F, Kadla JF. Electrospinning of technical lignins for the production of fibrous networks. J Wood Chem Technol. 2010;30:315–29.
133. Hosseinaei O, Baker DA. Electrospun carbon nanofibers from Kraft lignin. In: Book of abstracts of the fiber society. Boston, Fall Conference; 2012. p. 19.
134. Montero GA, Peresin MS, Rojas OJ. Lignins in the production of nanofibers via elecrospinning. In: The abstract book of the 82nd ACS colloid and surface science symposium; 2008.
135. Dallmeyer I, Ko F, Kadla JF. Correlation of elongational fluid properties to fiber diameter in electrospinning of softwood Kraft lignin solutions. Ind Eng Chem Res. 2014;53:2697–705.
136. Seo DK, Jeun JP, Kim HB, Kang PH. Preparation and characterization of the carbon nanofiber mat produced from electrospun PAN/lignin precursors by electron beam irradiation. Rev Adv Mater Sci. 2011;28:31–4.
137. Choi DI, Lee JN, Song J, Kang PH, Park JK, Lee YM. Fabrication of polyacrylonitrile/lignin-based carbon nanofibers for high-power lithium ion battery anodes. J Solid State Electrochem. 2013;17:2471–5.
138. Lai C, Zhou Z, Zhang L, Wang X, Zhou Q, Zhao Y, Wang Y, Wu XF, Zhu Z, Fong H. Free-standing and mechanically flexible mats consisting of electrospun carbon nanofibers made from a natural product of alkali lignin as binder-free electrodes for high-performance supercapacitors. J Power Sources. 2014;247:134–41.
139. Lin L, Li Y, Ko FK. Fabrication and properties of lignin based carbon nanofiber. J Fiber Bioeng Inform. 2013;6:335–47.
140. Teng NY, Dallmeyer I, Kadla JF. Incorporation of multiwalled carbon nanotubes into electrospun softwood Kraft lignin-based fibers. J Wood Chem Technol. 2013;33:299–316.
141. Hu S, Hsieh YL. Ultrafine microporous and mesoporous activated carbon fibers from alkali lignin. J Mater Chem A. 2013;1:11279–88.
142. Hu S, Zhang S, Pan N, Hsieh YL. High energy density supercapacitors from lignin derived submicron activated carbon fibers in aqueous electrolytes. J Power Sources. 2014;270:106–12.

143. Braun JL, Holtman KM, Kadla JF. Lignin-based carbon fibers: oxidative thermostabilization of Kraft lignin. Carbon. 2005;43:385–94.
144. Foston M, Nunnery GA, Meng X, Sun Q, Baker FS, Ragauskas A. NMR a critical tool to study the production of carbon fiber from lignin. Carbon. 2013;52:65–73.
145. Brodin I, Ernstsson M, Gellerstedt G, Sjöholm E. Oxidative stabilization of Kraft lignin for carbon fibre production. Holzforschung. 2012;66:141–7.
146. Gellerstedt G, Sjoeholm E, Brodin I. The wood-based biorefinery: a source of carbon fiber? Open Agric J. 2010;4:119–24.
147. Dallmeyer I, Lin LT, Li Y, Ko F, Kadla JF. Preparation and characterization of interconnected Kraft lignin-based carbon fibrous materials by electrospinning. Macromol Mater Eng. 2014;299:540–51.
148. Baker DA, Baker FS, Gallego NC. Thermal engineering of lignin for low-cost production of carbon fiber. In: Book of abstracts of the fiber society. Georgia, Fall Conference; 2009. p. 54.
149. Kubo S, Kadla JF. Lignin-based carbon fibers: effect of synthetic polymer blending on fiber properties. J Polym Environ. 2005;13:97–105.
150. Compere AL. Evaluation of lignin from alkaline-pulped hardwood black liquor. Reports of the Oak Ridge National Laboratory; 2005.
151. Johnson DJ, Tomizuka I. The fine structure of lignin- and pitch-based carbon fibers. In: Mountifield J, editor. Carbon fibres: their place in modern technology, Plastics and polymers conference supplement no. 6. London: Plastics Institute; 1974. p. 20.
152. Rodríguez-Mirasol J, Cordero T, Rodriguez JJ. High temperature carbons from lignin. Carbon. 1996;34:43–52.
153. McCarthy JL, Islam A. Lignin chemistry, technology and utilization: a brief history. In: Glasser WG, Northey RA, Schultz TP, editors. Lignin: historical, biological, and materials perspectives, ACS symposium series, vol. 742. Washington, DC: American Chemical Society; 2000. p. 2.
154. Capanema EA, Balakshin MY, Kadla JF. A comprehensive approach for quantitative lignin characterization by NMR spectroscopy. J Agric Food Chem. 2004;52:1850–60.
155. Compere AL, Griffith WL, Leitten CF, Petrovan S. Improving the fundamental properties of lignin-based carbon fiber for transportation applications. In: Proceedings of the 36th International SAMPE technical conference, society for the advancement of material and process engineering. Covina; 2004. p. 2246.
156. Hurt RH, Chen ZY. Liquid crystals and carbon materials. Phys Today. 2000;53:39–44.
157. Kubo S, Yoshida T, Kadla JF. Surface porosity of lignin/PP blend carbon fibers. J Wood Chem Technol. 2007;27:257–71.
158. Wang SX, Yang L, Stubbs LP, LiX HC. Lignin-derived fused electrospun carbon fibrous mats as high performance anode materials for lithium ion batteries. ACS Appl Mater Interfaces. 2013;5:12275–82.
159. Kyotani T, Nagai T, Inoue S, Tomita A. Formation of new type of porous carbons by carbonization in zeolite nanochannels. Chem Mater. 1997;9:609–15.
160. Rodriguez-Mirasol J, Cordero T, Radovic LR, Rodriguez JJ. Structural and textural properties of pyrolytic carbon formed within a microporous zeolite template. Chem Mater. 1998;10:550–8.
161. Fierro CM, Górka J, Zazo JA, Rodriguez JJ, Ludwinowicz J, Jaroniec M. Colloidal templating synthesis and adsorption characteristics of microporous–mesoporous carbons from Kraft lignin. Carbon. 2013;62:233–9.
162. Saha D, Warren KE, Naskar K. Soft-templated mesoporous carbons as potential materials for oral drug delivery. Carbon. 2014;71:47–57.
163. Valero-Romero MJ, Márquez-Franco EM, Bedia J, Rodríguez-Mirasol J, Cordero T. Hierarchical porous carbons by liquid phase impregnation of zeolite templates with lignin solution. Microporous Mesoporous Mater. 2014;196:68–78.

164. Ruiz-Rosas R, Valero-Romero MJ, Salinas-Torres D, Rodríguez-Mirasol J, Cordero T, Morallón E, Cazorla-Amorós D. Electrochemical performance of hierarchical porous carbon materials obtained from the infiltration of lignin into zeolite templates. ChemSusChem. 2014;7:1458–67.

165. Wang N, Fan H, Ai S. Lignin-templated synthesis of porous carbon-CeO_2 composites and their application for the photocatalytic desulphuration. Chem Eng J. 2015;260:785–90.

166. Zhang W, Yin J, Lin Z, Lin H, Lu H, Wang Y, Huang W. Facile preparation of 3D hierarchical porous carbon from lignin for the anode material in lithium ion battery with high rate performance. Electrochim Acta. 2015;176:1136–42.

167. Zhang W, Zhao M, Liu R, Wang X, Lin H. Hierarchical porous carbon derived from lignin for high performance supercapacitor. Colloids Surf A Physicochem Eng Asp. 2015;484:518–27.

168. Hata T, Yamane K, Kobayashi E, Imamura Y, Isihara S. MMicrostructural investigation of wood charcoal made by spark plasma sintering. J Wood Sci. 1998;44:332–4.

169. Rodriguez-Mirasol J, Cordero T, Rodriguez JJ. High-temperature carbons from kraft lignin. Carbon. 1996;34:43–52.

170. Jones LE, Thrower PA. Influence of boron on carbon fiber microstructure, physical properties and oxidation behavior. Carbon. 1991;29:251–69.

171. Pimenta M, Dresselhaus M, Dresselhaus MSD, Cancado L, Jorio A, Saito L. Studying disorders in graphite-based systems by Raman spectroscopy. Phys Chem Chem Phys. 2007;9:1276–90.

172. Johnson DJ, Tomizuka I, Watanabe O. The fine structure of lignin-based carbon fibres. Carbon. 1975;13:321–5.

173. Kubo S, Uraki Y, Sano Y. Catalytic graphitization of hardwood acetic acid lignin with nickel acetate. J Wood Sci. 2003;49:188–92.

174. Popova OV, Servinovskii MY. Graphite from hydrolysis lignin: preparation procedure, structure, properties and application. Russ J Appl Chem. 2014;87:818–23.

175. Popova OV, Servinovskiy MY, Abramova AG. Development of technology for production and application of graphite from hydrolytic lignin. Eur J Wood Prod. 2015;73:369–75.

176. Demir M, Kahveci Z, Aksoy B, Palapati NKR, Subramanian A, Cullinan HT, El-Kaderi HM, Harris CT, Gupta RB. Graphitic biocarbon from metal-catalyzed hydrothermal carbonization of lignin. Ind Eng Chem Res. 2015;54:10731–9.

Chapter 9
Biofuels and Chemicals from Lignin Based on Pyrolysis

Xianglan Bai and Kwang Ho Kim

9.1   Introduction

Pyrolysis is thermal depolymerization technology and has been widely applied to convert biomass for biofuels and chemicals. During pyrolysis, biomass is heated in the absence of oxygen at temperatures ranging from 300 to 600 °C [1]. Pyrolysis includes slow pyrolysis and fast pyrolysis. The major product of slow pyrolysis of biomass is char whereas the primary product of fast pyrolysis is liquid, generally called pyrolysis oil or bio-oil, whose yield can be as high as 70 % for lignocellulosic biomass. To obtain high yields of bio-oil, rapid heating of biomass (usually >100 °C/s) followed by rapid cooling of the volatile is essential [2]. In general, fast pyrolysis takes less than two seconds. To achieve high heat transfer rate and uniform heating, the moisture content of dry biomass must be controlled to be below 10 % and particle size of biomass should be reduced. A proper reactor design is also required to ensure a minimal temperature gradient inside the reactor. Bio-oil derived from lignocellulosic biomass is a complex mixture of various organics such as anhydrosugars, aldehydes, ketones, acids, furans and phenols. This intermediate liquid can be further upgraded to biofuels and chemicals. Other pyrolysis products include char (or biochar) and light gases. Biochar has potential applications as a solid fuel, soil amendment or activated carbon precursor. Due to the simplicity of pyrolysis, potential for scaling up the process and the convenience of storing and transporting bio-oil, fast pyrolysis of biomass has been studied extensively [3].

Lignin is an important component of biomass and accounts for 10–30 % of biomass. In addition to biomass, technical lignin is available as a byproduct from pulp,

X. Bai (✉)
Department of Mechanical Engineering, Iowa State University, 50011 Ames, IA, USA
e-mail: bxl9801@iastate.edu

K.H. Kim
Deconstruction Division, Joint BioEnergy Institute, 94608 Emeryville, CA, USA

paper industry as well as emerging biorefinery process. It is expected that more lignin will become available in coming years as the production capability of second generation of biofuels increases [4, 5]. Accordingly, thermal depolymerization of lignin to aromatics and other value-added products through fast pyrolysis is of great interest.

Lignin is a phenylpropane-based polymer made of three precursor monomers through random polymerization. Through pyrolysis, the macropolyaromatic structure of lignin is depolymerized to phenolic compounds with various molecular sizes and functionalities. The volatilized lignin is quenched and recovered as a mixture of monomeric phenols such as phenol, guaiacols, syringols, alkyl phenols and catechols, and phenolic oligomers. Employing catalysts can selectively increase targeted phenols or produce deoxygenated aromatics such as benzene, toluene and xylene (BTX) or other alkylated aromatics. These compounds could be used as platform chemicals or fuel additives to replace petrochemicals [4, 5]. Lignin-derived phenolic oligomers have potential use as biocomposites and biopolymers. However, pyrolytic conversion of lignin needs to deal with high char yield and low-quality, complex oil products. Catalytic upgrading of lignin or lignin-derived pyrolysis oil also suffers from low conversion and catalyst deactivation. These problems are attributed to the structural complexity and recalcitrance of lignin. Lignin has striking abilities to self-associate due to the strong electronic stabilization energies between the various subunits [6]. Technical lignin is difficult to pyrolyze in reactors due to its thermoplastic behavior [7]. For these reasons, commercial-scale lignin pyrolysis for products is rarely reported in spite of its great potential for renewable sources. However, growing interest in the utilization of lignin has prompted the development of new reactor designs, catalysts and other related techniques since lignin is the only natural aromatic source that can replace petroleum derived aromatic compounds. In this chapter, fundamentals of lignin pyrolysis and the recent advances in lignin pyrolysis and product upgrading are discussed (Fig. 9.1).
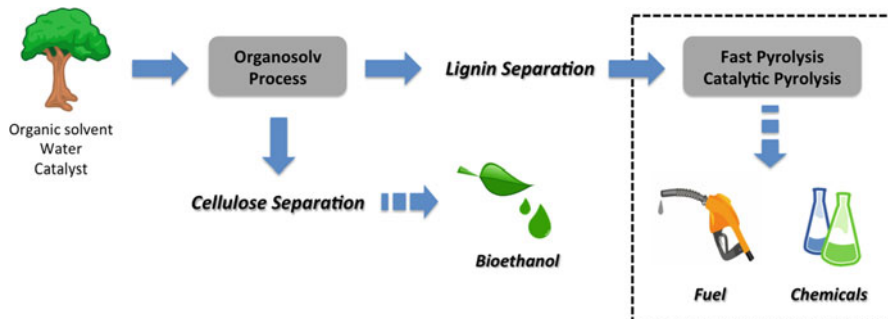
Fig. 9.1 Biorefinery concept of the integrated bio- and thermal conversion of biomass

9.2   Fundamentals of Lignin Pyrolysis

9.2.1   Lignin Structures Related to Complexity of Pyrolysis

Three major precursors of lignin are *p*-coumaryl alcohol, coniferyl alcohol and sina-pyl alcohol. Thus, the structure of the heterogeneous aromatic polymer of lignin is designated as *p*-hydroxyphenyl (H unit), guaiacyl (G unit) and syringyl (S unit). The different aromatic units are connected through various linkages including β-O-4, β-5, α-O-4, β-β, 5-5, 4-O-5 and β-1. Among them, β-O-4 is the most abundant in lignin, accounting 40–60 % of the total linkages. The main functionalities in lignin are methoxyl, benzyl alcohol, phenolic and aliphatic hydroxyl, noncyclic benzyl ether, carboxyl and carbonyl groups [8]. The relative ratios of these linkages and functionalities depend on biomass type. Hardwood lignin contains G and S units, whereas softwood lignin contains mostly G units, and herbaceous lignin contains H, G and S units. The lignin isolation method also has significant influence on lignin structure because it is difficult to separate lignin from biomass without modifying its natural structure. Not only are covalent bonds between lignin and carbohydrates cleaved, but the cleavage and reforming of intra molecular bonds of lignin polymer also occur during isolation. It is considered that the structure of milled wood lignin (MWL) most resembles natural lignin compared with other types of technical lig-nin. The complexity of the chemical structure of lignin and the variation of lignin origin bring unique challenges in understanding pyrolysis reactions of lignin.

9.2.2   Pyrolysis Kinetics of Lignin

Pyrolysis behavior of lignin is usually studied using thermogravimetric analysis (TGA). In TGA, milligram quantities of lignin are pyrolyzed in a sample cup with pre-defined heating rates (5–50 °C/min), and the mass loss and differential thermo-gravimeteric (DTG) are recorded. The TGA results show that the depolymerization of biomass starts with hemicellulose, followed by lignin, and finally cellulose. Among the three major compositions of biomass, lignin is found to be the most thermally resistant component, gradually decomposing over the temperature range of 200–900 °C [9]. Lignin produces a char yield that could be over 40 %, which is greater than any other component of biomass. Although the majority of the mass loss of lignin usually occurs at 300~450 °C, the decomposition rate differs with lignin type. It has been reported that the temperatures for maximum mass loss rate were 346 °C for alkali lignin, 359 °C for MWL, 396 °C for organosolv lignin and 405 °C for kraft lignin [10]. The models of pyrolysis kinetics were developed based on TGA profiles of lignin. According to first order reaction models, the values of apparent activation energy of lignin decomposition ranged from 25 up to 300 kJ/mol, varied by biomass origin and lignin isolation method [8]. Due to the broader temperature region for thermal decomposition, the range of activation energy is also

relatively large. The mass loss of lignin observed in TGA is a complex mixture of volatiles that could be derived from different stages of lignin pyrolysis. Thus, the time–resolved devolatilization of lignin was characterized using a TGA-FTIR or TGA-MS method [9, 11] to improve the kinetic models. It was found that lignin initially releases absorbed water at 100 °C and then starts to form some volatiles and light gases at higher temperatures. Water was also produced when aliphatic hydroxyl groups dehydrate. Other volatile products include phenols, alcohols, aldehydes and acids. The main gaseous products were CO, CO_2, and CH_4, produced from decarbonylation, decarboxylation and demethylation, respectively [12]. Two-step pyrolysis kinetic models have been proposed to describe the complex pyrolysis kinetics of lignin [10, 13]. In Cho's model [13], lignin first decomposed to solid polyaromatics and volatiles at low temperatures (first step). Above 327 °C, the polyaromatics further decomposed to light gases and condensable liquid, consisting of phenolic monomers and oligomers (second step). According to the model, the activation energy of enzymatic lignin derived from maple wood was 74 kJ/mol at the first step of the reaction, then increased to 110 kJ/mol at the second step. Wang et al. [10] later combined the modified distributed activation energy model (DAEM) introduced by Chen [14] and the double Gaussian function model to develop a two-step pyrolysis kinetic of lignin. In their model, lignin decomposes to volatiles through the breakage of ether linkages and side branches in reaction I. Reaction II is the polymerization and cross linking of the primary products to char. This model was used to predict the pyrolysis behavior of several different types of lignin. The activation energy of reaction I was 140 kJ/mol for alkali lignin, 146 kJ/mol for MWL, both lower than 151 kJ/mol for organosolv lignin and 166 kJ/mol for kraft lignin.

9.2.3   Py-GC/MS of Lignin

Identification of pyrolysis products of lignin is frequently investigated using a micropyrolyzer equipped with gas chromatography and mass spectroscopy (Py-GC/MS) method. Py-GC/MS method is often used to probe the primary reactions of biomass pyrolysis. Typically, a sample cup containing about 500 µg of sample is dropped into a preheated micropyrolysis reactor, where lignin is rapidly pyrolyzed and the volatile products are directly swept into online GC and MS for instant identification and quantification [15]. Figure 9.2 shows a GC/MS chromatogram with identification of phenolic monomers obtained from pyrolysis of corn stover derived organosolv lignin. As shown, 4-vinylphenol, 2-methoxy-4-vinylphenol, phenol, 2-methoxyphenol (guaiacol) and 2,6-dimethoxyphenol (syringol) are the main pyrolysis products from lignin pyrolysis. These phenolic monomers are produced from the cleavage of various lignin linkages. For example, β-O-4 linkages are readily cleaved at temperatures as low as 200 °C due to its lower bond dissociation energy, forming free radicals which induce bond cleavage at different positions of lignin side chains [16]. Free radical-initiated depolymerization is an
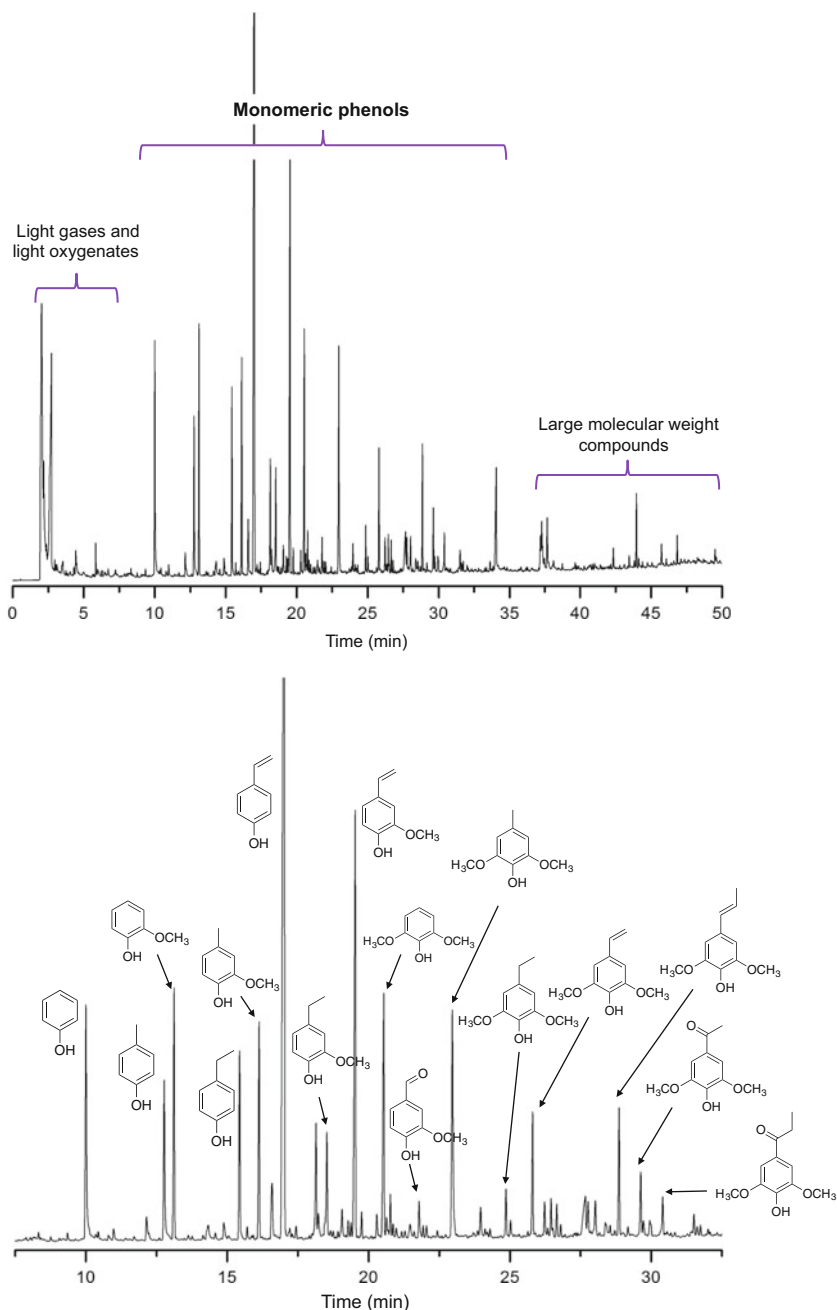
Fig. 9.2 Full chromatogram (*top*) resulting from the pyrolysis of corn stover derived lignin and zoomed chromatogram with species identification (*bottom*). Pyrolysis temperature: 500 °C, GC injection temperature: 300 °C, GC oven temperature: 50–280 °C, Column: UA-5 (30 m×0.25 mm×0.25 μm)

important feature of lignin depolymerization. Coupling the pyrolyzer with a cold finger electron paramagnetic resonance (EPR) spectroscopy was able to detect the free radicals and further determined methoxyl, phenoxy, and substituted phenoxy radicals as the intermediate products [17]. These intermediate species continue to undergo secondary reactions such as decarboxylation, demethylation or demethoxylation to form various phenolic products. The reactive free radicals also contribute to polymerization and char forming reactions [18].

Py-GC/MS of lignin usually detects volatiles including light oxygenates and phenolic monomers with a molecular weight (MW) less than 220 Da. Jiang et al. [16] were able to identify over 50 different types of phenolic monomers from pyrolysis of alkali lignin and found the yields of most individual compounds to be less than 1 %. The total yield of the GC/MS detectable monomers is low, usually around 10–17 % of lignin. Previously, Patwardhan et al. [15] reported up to 83 % of mass balance by pyrolyzing corn stover-derived organosolv lignin in the micropyrolyzer. The identified products included about 16 % phenolic monomers and 37 % of pyrolysis char. The other quantified products were carbon oxides, acetaldehyde, carboxylic acids and furan. The missing mass balance is attributed to GC/MS non-detectable phenolic oligomers and water. In fact, non-volatile phenolic oligomers are important part of lignin pyrolysis oil. It has been thought that these large MW compounds are partly decomposed lignin fragments that are thermally ejected and entrained in the carrier gas flow. However, characterization of phenolic oligomers has shown that the native lignin structures such as β-aryl ether, phenylcoumaran and resinol were not present in the phenolic oligomers [19]. Instead, newly formed phenolic structures are found among phenolic oligomers [20, 21]. Thus, an alternative theory is that lignin initially depolymerizes to monomers, but the monomers repolymerize, catalyzed by carboxylic acids [15]. Recently, Bai et al. [22] collected the primary pyrolysis vapor of lignin in a cold solvent and analyzed it using two high resolution MS spectroscopies (APPI-FTICR and Orbitrap). As a result, the authors were able to detect 569 different types of phenolic compounds, mainly consisting of phenolic monomers and dimers. However, the exact structures of phenolic oligomers still remain unknown due to the limitation of analytical methods.

Light gases and char are also produced from pyrolysis. The CO_2 and CO results from decarboxylation and decarbonylation, and CH_4 is formed through demethoxylation of benzene ring. Hydrogen and other hydrocarbon gases, such as C_2H_6 and C_3H_6, are also produced in low yields. The light gases are produced when aromatic side chain cleavages. Char is carbonized material formed through the random cross linking of partly decomposed free radical intermediates and repolymerization of primary phenols in solid matrix [18].

It should be noted that pyrolysis conditions of lignin in lab-scale reactors can be varied compared with that of lignin in PY-GC/MS. The vapor residence times are usually longer in lab-scale reactors, and pyrolysis vapor is condensed downstream. While PY-GC/MS uses helium as the carrier gas, lab-scale reactors use nitrogen for economic reason. Compared to helium, nitrogen has a lower thermal conductivity and its pyrolysis products have lower mass diffusivity in a nitrogen environment.

For these reasons, a number of secondary reactions of pyrolysis products, such as cracking, repolymerization and condensation, can occur in both the vapor phase and condensed pyrolysis oil. It is usually expected that the yields of pyrolysis oil, especially the yields of phenolic monomers, are lower when lignin is pyrolyzed in lab-scale reactors compared to when lignin is pyrolyzed using the PY-GC/MS method. Nevertheless, PY-GC/MS is still an efficient way to characterize the lignin materials and a great tool to study fundamental reaction mechanisms.

9.2.4   Factors Affecting Lignin Pyrolysis

Pyrolysis behavior of lignin and composition of pyrolysis products are affected by a number of factors, such as lignin origin, pyrolysis conditions, and presence of impurities and carbohydrates. The effects of several common factors are discussed in below:

Lignin Source   The origin of biomass from which lignin is derived, and lignin isolation method can greatly affect the pyrolysis behavior of lignin and composition of pyrolysis products. Asmadi et al. [23] pyrolyzed beech wood (hardwood) MWL and cedar wood (softwood) MWL and found that hardwood lignin decomposes at lower temperatures than softwood lignin. They also reported that hardwood lignin produces fewer amounts of phenolic monomers and more char compared to softwood lignin. Due to the variation of building block units, hardwood lignin produces mostly alkylated syringols (syringol, vinyl syringol etc.), whereas softwood lignin tends to produce more alkylated guaiacols. Herbaceous lignin produces similar amounts of alkylated phenols, alkylated guaiacol and alkylated syringols. The order of pyrolysis char was herbaceous MWL < hardwood MWL < softwood MWL in a recent experiment conducted by the authors.

The lignin structure is modified from its natural structure depending on how the lignin was isolated from the biomass. Severe isolation method cleaves more intra molecular bonds of lignin polymer to form a thermally-stable lignin structure through free radical reactions and repolymerization reactions. Such structural change is reflected on the yield of pyrolysis char. For example, kraft lignin produced the maximum yield of char (49.86%), followed by alkaline lignin (49.43%) and organosolv lignin (44.69%) despite the fact that all were derived the same biomass species [10]. In comparison, MWL produced the least amount of char, which is 41.86%.

The GC/MS pyrogram of MWL and organosolv lignin, both derived from red oak, are compared in Fig. 9.3. Not only does MWL produce significantly less char than oragnosolv lignin, but it also tends to produce phenolic monomers with multi-functionalities and longer side chain lengths. Since an increased amount of the phenolic side chains are cleaved during the organosolv extraction process, organosolv lignin produced simpler phenols upon pyrolysis. MWL also produced more CO and CO_2 and less CH_4 compared to organosolv lignin.

Pyrolysis Temperature   Temperature has a significant influence on product yield and composition. Different linkages in lignin have different levels of resistance for
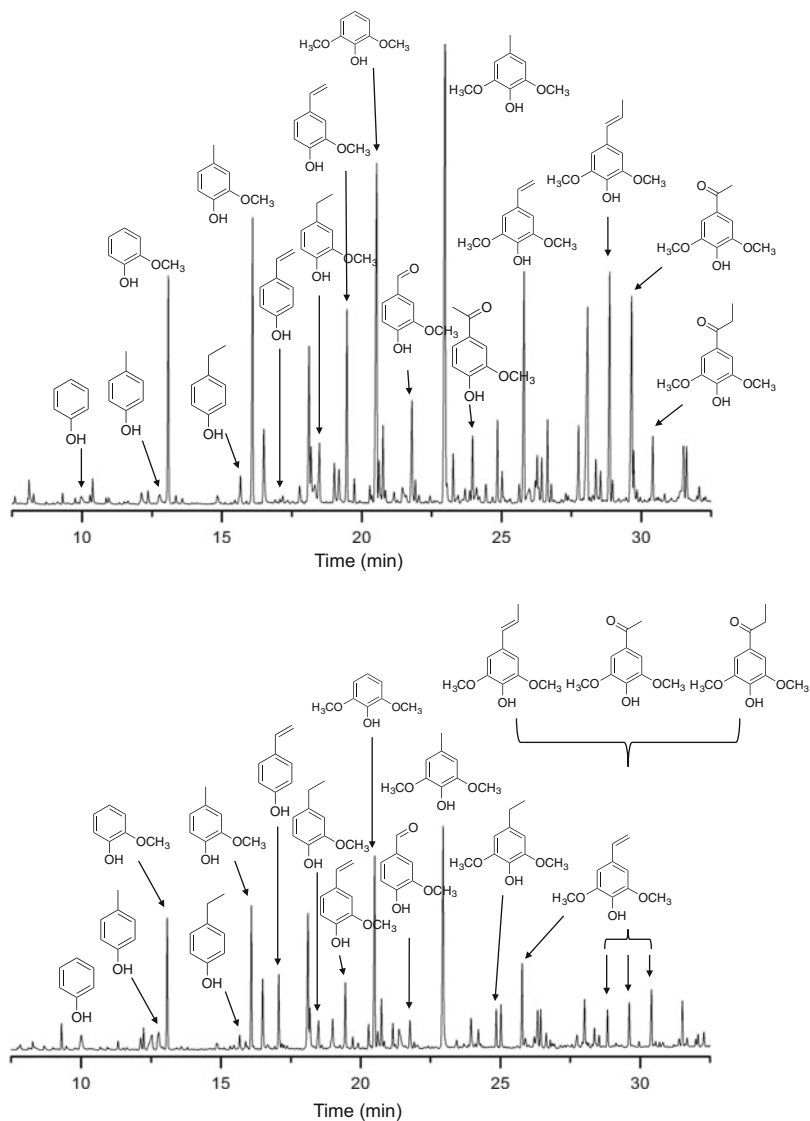
Fig. 9.3 Pyrogram of red oak lignin; milled wood lignin (*top*); organosolv lignin (*bottom*). Pyrolysis temperature: 500 °C, GC injection temperature: 300 °C, GC oven temperature: 50~280 °C, Column: UA-5 (30 m×0.25 mm×0.25 μm)

thermal cleavage. Usually, C-O bonds containing β-O-4 and α-O-4 linkages are cleaved at relatively low temperatures. In comparison, C-C bond containing linkages, such as 5-5 linkage, are relatively difficult to cleave and require high pyrolysis temperatures. The bond dissociation energy is also related to functional groups. For example, the value of bond dissociation energy is 463.6 kJ/mol for HO-Ph, which is much higher than the value of 268.6 kJ/mol for CH$_3$-OPh [16]. In

general, higher pyrolysis temperatures increase gas yield and decrease char yield. While higher temperatures enhance the volatility of products, it also causes secondary reactions of primary products, such as repolymerization and cracking. Thus, the optimum temperature for maximum yield of pyrolytic oil is usually an intermediate temperature. Garcia-Perez et al. [24] previously pyrolyzed biomass in a fluidized bed between 350 and 580 °C and found that the increase in bio-oil yield between 350 and 500 °C is attributed to the increase in lignin-derived oligomers. Further increasing the temperature beyond the optimum temperature would increase gas formation at the expense of pyrolysis oil and char due to cracking.

The composition of pyrolysis oil depends on pyrolysis temperature and its change can reveal the pyrolysis reaction pathway. Previously, Alcell lignin and Asian lignin were pyrolyzed to find that the maximum yields of phenolic monomers both occur at 600 °C, which are 17.2 % and 15.5 %, respectively [16]. Among all of the products, 5-hydroxyvanillin was found to be the most abundant monomer produced from Alcell lignin (4.3 %), whereas it was 2-methoxy-4-vinylphenol from Asian lignin (4.2 %). It was also found that phenol, catechol, pyrogallol and methylphenols increase, while guaiacol and syringol decrease as the pyrolysis temperature increases, suggesting that an increasing temperature promotes demethoxylation, demethylation, and alkylation. Catechol and pyrogallol were present in high concentrations, since it is difficult to cleave the HO-Ph bond, even at high temperatures. On the other hand, carboxylic acids were only found to decrease at 800 °C. Thus, it was suggested that decarboxylation reactions occurred at this temperature. Corn stover organosolv lignin was also pyrolyzed at different temperatures and both phenols and gases were monitored [15]. The major pyrolysis products of lignin at 300 °C were CO_2, 4-vinyl phenol and 2-methoxy-4-vinyl phenol, indicating that β-O-4 cleavage and decarboxylation are predominant in the initial steps of the lignin degradation. As temperature further increased, the yields of CO and CO_2 both increased from 8.8 % at 300 °C to 25.9 % at 700 °C. Among phenolic monomers, vinyl- or methoxy phenols reached maximum yields at 600 °C, whereas phenol, methyl phenols and ethyl phenols were found to increase with temperature. Therefore, it was concluded that demethoxylation became the prevailing reaction at higher temperatures. A linear decrease in char yields from 60 % at 300 °C to 22 % at 700 °C was accompanied by the increase in low MW volatiles and gases. While the optimum temperature for a maximum pyrolysis oil yield depends on the lignin source, it could be higher than 500 °C. For example, Ben et al. [25] previously reported 600 °C to be the optimum pyrolysis temperature for softwood kraft lignin. They also found that the increased amount of gas is similar to the decreased amount of char when temperature increased from 600 to 700 °C. It is likely that cracking of lignin char at higher temperatures mostly produces gaseous products instead of phenols.

Inorganic Impurities Biomass-inherent alkaline and alkaline earth metals strongly catalyze fragmentation of pyranose and furanose rings in carbohydrates rather than cleavage of glycosidic bonds. As a result, a minimal amount of inorganic impurities can greatly diminish sugar yields [26]. Other than the inherent inorganics, various forms of inorganic salts could also be present in lignin due to the carryover of

chemicals used in lignin isolation process. The effect of inorganic salts on lignin pyrolysis has also been investigated, revealing that the influence of inorganic salts on lignin is less straightforward than it was when observed with carbohydrates. Previously, Patwardhan et al. [15] doped organosolv lignin with 1 % of NaCl, KCl, MgCl$_2$ and CaCl$_2$ and found that there is no apparent change in the pyrolysis products. Based on the results, they suggested that inorganics do not affect lignin pyrolysis due to the absence of coordination bond positions in lignin polymers. However, other researchers have shown that inorganic salts can enhance the depolymerization of lignin and promote production of phenolic monomers. For example, Gray et al. [27] found that calcium-ion exchanged wood produces twice as much guaiacol than untreated wood. Alkali metals, such as K and Na, were much more effective than alkali earth metals. The effect of inorganic salts also depends on the form of anion. Di Blasi et al. [28] previously reported that addition of NaOH or KOH increases the yields of phenols from 2.10 to 4.19 % or 3.83 %, respectively. Carbonate salts increased the yield of phenols less significantly, as the yields were 2.89 % for Na$_2$CO$_3$ and 2.34 % for K$_2$CO$_3$. In comparison, CH$_3$COOK increased the yield to 2.50 %, whereas the addition of NaCl decreased the yield to 1.70 %. The selectivity of phenols also changed when inorganic salts present. NaOH tends to increase phenols with propyl, methoxy, hydroxyl, and propenyl groups. KOH and Na$_2$CO$_3$ increase ethyl phenols, but NaOH reduces these phenols. It was also found that both KOH and K$_2$CO$_3$ increase aldehyde groups, though they were not significant with sodium salts. In general, the addition of inorganic salts promotes the formation of light gases and char and reduces the yield of liquid products. TGA studies also showed that the presence of inorganic salts lowers the temperature for maximum mass loss rate. Inorganic salts promote dehydration, decarboxylation, demethoxylation and carbonization reactions, and thermally instable or basic salts have stronger catalytic effects than thermally stable and neutral salts [29]. It was suggested that alkali metals catalyze the cleavage of linkages between aromatic rings in lignin structures, and the reactivity of the salts is a function of atomic mass and corresponding electropositivity of cation metals [29].

Influence of Carbohydrate In biomass, ether and ester covalent bonds hold lignin and carbohydrates (i.e., cellulose and hemicellulose) together. Although the lignin isolation process removes carbohydrates, technical lignin (such as enzymatic lignin) could still contain a significant amount of carbohydrate residues (up to 50 %) [7]. The possible interactions between lignin and carbohydrates have been studied previously. Pyrolyzing lignin and carbohydrates independently or as a mixture in TGA and comparing their mass loss and DSC profiles often suggest that there is a negligible interaction between lignin and carbohydrates [30]. This finding led to the conclusion that the product yields of biomass pyrolysis is a mathematical addition of product yields of individual components in biomass [31]. However, the analysis of vapor composition revealed that there is in fact a significant interaction among lignin and carbohydrates [32–34]. Hosoya et al. [33] pyrolyzed lignin and cellulose in a dual-space, closed ampoule reactor to investigate the liquid/solid and the vapor phase interactions separately and reported that the pyrolysis oil yield increases

whereas the char yield decreases when lignin is co-pyrolyzed with cellulose. They also found that cellulose-derived organics suppress secondary char formation of lignin-derived phenols in the vapor phase. A significant increase in the yields of methane and catechols from lignin was also observed. Similarly, Wang et al. [34] also observed that the presence of cellulose and hemicellulose has positive effects on lignin decomposition by increasing the yields of phenolic products, such as phenol and 2,6-dimethoxy phenol. It was suggested that cellulose-derived oxygenates stabilize lignin-derived phenolic free radicals by donating hydrogen [33]. The stabilized phenolic free radicals are less likely to polymerize to form char.

Gaseous Environment Although pyrolysis is supposed to occur at a pure inert environment, it was found that pyrolysis with controlled amounts of oxygen could be beneficial. Kim et al. [35] found that adding 0.525 and 1.05 vol.% of oxygen to carrier gas can increase the total yield of phenolic monomers especially phenolic aldehydes, such as vanillin and syringaldehyde. Li et al. [36] also reported that partial oxidative pyrolysis of kraft lignin increases the yields of simpler phenols at the expense of heavy phenolic oligomers. Small amounts of oxygen can promote the cracking of lignin to enhance side chain cleavage. Oxygen can also react with lignin-derived phenols to form phenolic aldehydes and ketones. While pyrolysis is an endothermic reaction, oxidative pyrolysis can reduce the required process heat and even achieve autothermal pyrolysis through combustion of pyrolysis char or the introduction of other oxidative exothermic reactions. However, excessive oxygen content also promotes decomposition and combustion of smaller phenols to increase the yields of CO_2 and CO.

9.3   Pyrolysis of Technical Lignin

9.3.1   *Pyrolysis of Lignin in Lab-Scale Reactors*

There are two ways to obtain lignin-derived phenols. One is to pyrolyze the entire plant biomass and then wash the bio-oil using cold water to separate water-insoluble phenols. Another way is to pyrolyze technical lignin. While biomass pyrolysis has already reached commercial scale, pyrolysis of technical lignin has mostly been conducted in bench-scale reactors (including Py-GC/MS) for scientific research in the lab. For example, Ben et al. [25] pyrolyzed a few grams of kraft lignin in a tube reactor in the range of 400~700 °C and recovered heavy oil and light oil using two condensers. At 700 °C, char and gas yields were 38.14% and 17.59%, respectively. NMR analysis of pyrolysis oil suggests that primary thermal depolymerization of lignin is related to the aliphatic hydroxyl, carboxyl, and methoxyl groups in addition to the ether bond cleavage in the lignin.

There has been a significant effort to continuously pyrolyze lignin using lab-scale pyrolyzers, such as fluidized bed reactors or entrained flow reactors [7].
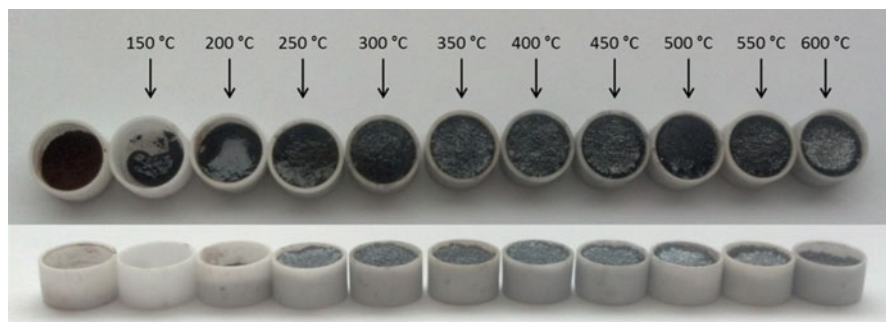
Fig. 9.4 Thermal decomposition of lignin at varying final temperatures using a thermogravimetric analyzer (TGA)

Nevertheless, the attempts often fail due to the clogging of lignin in the feeder and the collapse of the fluidization caused by molten lignin, char and sand agglomeration [37, 38]. This is because lignin displays "thermoplastic" behavior upon heating, which causes various problems in continuous reactors. Lignin melts below 200 °C (Fig. 9.4) and ultimately proceeds to a stage of decomposition into small molecules to release volatiles. During this process, cross linking, repolymerization and dehydration reactions among the melts lead to a hard-shelled carbonized char (Fig. 9.5). The extent of lignin agglomeration depends on lignin types. For example, ETEK lignin, which is enzymatic lignin, is less likely to agglomerate compared with high purity lignin, probably because of its high carbohydrate content (up to 50 % cellulose) [7]. Alkaline lignin also agglomerates less significantly compared with acetosolv lignin [38]. Nevertheless, pyrolyzing lignin continuously for hours is difficult. Several approaches have been developed in recent years to address this technical challenge. De Wild et al. [37] pyrolyzed wheat straw-derived organosolv lignin in the bubbling bed with its feeder cooled with a water jacket and reported 40–60 % of pyrolysis oil and 30–40 % of char. The pyrolysis oil contained 7–11 % phenolic monomers and 14–24 % of phenolic oligomers. However, it was noted that the reactor was partially clogged with char and sand agglomerates, even with a minimal lignin feeding rate. Gooty et al. [39] later improved the reactor design by installing a stir bar (spinning rate of 1 Hz) inside of the fluidized bed reactor to break the char agglomerates.

Instead of modifying the reactor, lignin can be pretreated prior to pyrolysis to reduce agglomeration. Pelletizing lignin alone was less effective as the pellets still agglomerated during pyrolysis. Thus, lignin was mixed with other materials. Wiberink et al. [40] extruded the slurry of lignin and clay mixed in 1:1 ratio as pellets and then dewatered. Pyrolyzing the lignin-clay pellets was able to overcome agglomeration inside the fluidized reactor. The yields of pyrolysis oil, char and gas were approximately 44 %, 36 % and 15 %, respectively, for three different types of lignin and the yield of phenolic monomers accounted for 6–7 % of lignin [41]. Formate salt pretreatment was also effective [42]. Wheat straw lignin was mixed with a large amount of formate salts in two-step process and dewatered. The

Fig. 9.5 Char agglomerates and molten lignin collected from a fluidized bed reactor after pyrolysis
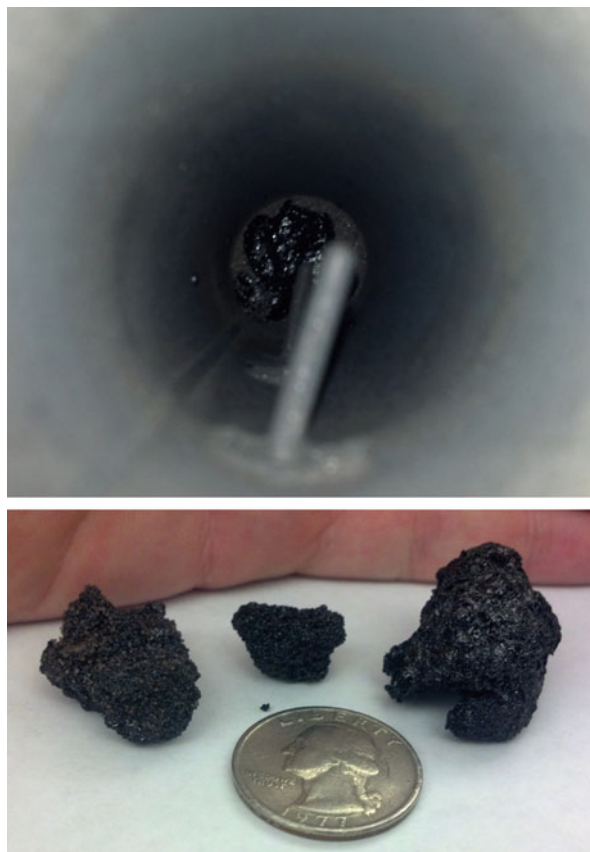
pretreated lignin was pyrolyzed in a fluidized reactor to yield 32.5 % of pyrolysis-oil. Since formate salt decomposes and releases hydrogen during pyrolysis, a significant decrease in methoxy and hydroxy functionalities was found.

Zhou et al. [38] found that pretreating lignin with as low as 5 % of $Ca(OH)_2$ can completely inhibit the melting of lignin and agglomeration of char. This method was successfully applied to organosolv lignin and enzymatic hydrolysis lignin, both derived from corn stover, hardwood hydrolysis lignin and softwood alkaline lignin. Phenolic hydroxyl and carbonyl groups in lignin are likely responsible for the "thermoplastic" behavior of lignin whereas the $Ca(OH)_2$ pretreatment reduced or eliminated these functionalities by forming hydroxylcalcium phenoxides, phenolic alcohols, and phenolic carboxylate salts. After pyrolysis, $Ca(OH)_2$ is recovered in char as CaO. At 500 °C, the yield of pyrolysis oil was approximately 38 wt % for the organosolv lignin and the char and gas yields were 33.4 and 15.3 %, respectively. The yield of phenolic monomers was about 6 % of lignin. The previous studies about lignin pyrolysis in continuous reactors are summarized in Table 9.1.

Table 9.1 Pyrolysis of lignin in fluidized bed reactors

Lignin type	T (°C)	Conditions	Products yield (%)			Refs.
			Liquid	Gas	Char	
Wheat straw and glass, soda pulping	400	Pretreated (pelletized, additive)	42 (21)*	17	30	[5]
Hardwood organosolv	400	Pretreated (pelletized, additive)	37 (24)	20	35	[5]
Herbaceous soda pulping	530	agglomerate	31.2 (11.4)	5.7	48.8	[7]
Softwood, hydrolysis	500	agglomerate	57.7 (12.4)	10.3	27.2	[7]
Pines Kraft	500–550	Various % of oxygen	Dry oil <26	>23	42<	[36]
			Aqueous oil >9			
Wheat straw organosolv A	500	agglomerate	54.7 (23.9)	15.1	35.6	[37]
Wheat straw organosolv B	500	agglomerate	51.0 (19.9)	17.4	30.9	[37]
Wheat straw/grass soda pulping	500	agglomerate	47.6 (17.1)	15.2	39.0	[37]
Hardwood organosolv	500	agglomerate	38.9 (14.5)	20.7	43.0	[37]
Organosolv (cornstover)	500	Pretreated 5 % $Ca(OH)_2$	38.3 (13.3)	19.5	32.8	[38]
Kraft	450–600	Modified reactor	36–37 (12)	NA	NA	[39]
Wheat straw organosolv, Biolignin, Kraft		Pretreated (pelletized, additive)	~44	~15	~36	[41]
Acid hydrolyzed kraft	500	Sand removal	23	39	41	[42]
Acid hydrolyzed kraft	500	Pretreated (1:1 formate salt)	32.5	32.7	34.8	[42]

*Inside parentheses are water yield per lignin

9.3.2　Properties of Lignin Pyrolysis Oil

Phenolic oil separated from the bio-oil produced from pyrolysis of whole plant bio-mass is also called pyrolytic lignin. The pyrolytic lignin accounts for up to 35 % of bio-oil and mostly consists of phenolic oligomers and smaller fractions of phenolic monomers. It should be noted that the lignin pyrolysis oil described in the literature mostly indicates pyrolytic lignin. Previously, Meier's group conducted an extensive characterization of pyrolytic lignin [21, 43–45]. They found that functional groups in pyrolytic lignin are somehow similar to technical lignin [43]. It was also found that pyrolytic lignin has an average degree of polymerization (DP) between 4 and 9 (MW of 600–1300 Da) [44] and consists of oligomeric alkylated aromatic units linked by newly formed bonds, especially stable C-C linkages [21]. Due to the dif-ficulty of pyrolyzing technical lignin in reactors, a comprehensive characterization

of pyrolysis oil of technical lignin is seldom available. Ben et al. [25] analyzed heavy phenolic-oil and light phenolic-oil produced from softwood kraft lignin using NMR to quantify the content of different functionalities. They also reported the average MW of heavy oil to be in the range of 200–360 Da, much lower than that of pyrolytic lignin. Gooty et al. [39] analyzed the pyrolytic oil of kraft lignin, but mainly reported water content and heating values of the pyrolysis oil. A relatively comprehensive characterization of the pyrolysis oil's properties has recently been provided for the pyrolysis of pretreated corn stover lignin [38]. The average MW of total pyrolysis oil was 288 Da and GPC results showed that the phenols are mostly monomers and dimers. GC/MS detectable phenolic monomers such as 4-vinylphenol, 2-methoxy-4-vinylphenol, guaiacol and syringol accounted for 16 % of the total pyrolysis oil (the combination of heavy oil and light oil) in the study. Other properties of pyrolysis oil determined by Zhou et al. are listed in Fig. 9.6 and Table 9.2.

Regardless of whether it is pyrolytic lignin or lignin pyrolysis oil, lignin-derived phenolic oil is thermally unstable during storage. Not only does the viscosity of phenolic oil increase, but the water content also increases due to condensation. The yields of most phenolic monomers decrease during aging, with vinylphenols decreasing most significantly. Polymerization of reactive functionalities such as vinyl, aldehyde, are responsible for increasing the molecular weight of the phenolic oil [46]. The phenolic oil also contains free radicals, but these stable, carbon or oxygen centered radicals do not contribute to polymerization.

Converting reactive functionalities to more stable forms can improve the stability of the lignin-derived phenolic oil. Rover et al. [47] were able to stabilize the pyrolytic lignin using mild hydrogenation. Pyrolytic lignin extracted from red oak bio-oil and corn stover bio-oil were hydrogenated at room temperature and 1 atm using 5 % Pt/C as the catalyst for 24 h. Hydrogenated pyrolytic lignin had excellent
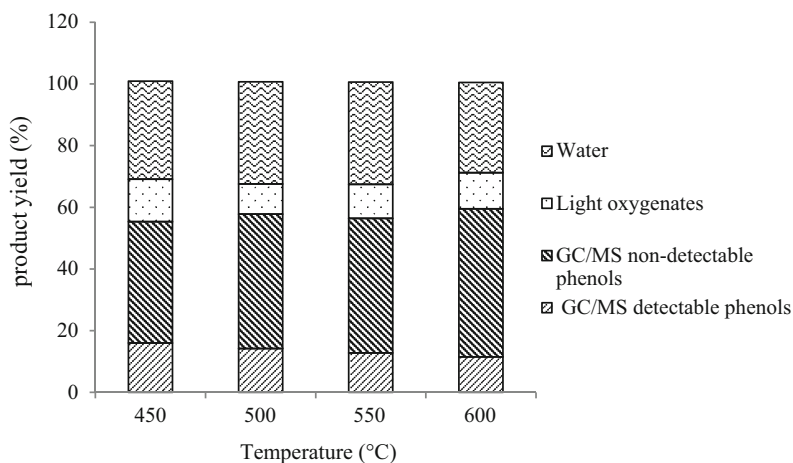
Fig. 9.6 Composition of pretreated lignin pyrolysis-oil as a function of pyrolysis temperature [38] (Reprinted with permission of Royal Society of Chemistry)

Table 9.2 Properties of pretreated lignin pyrolysis oil [38]

Temperature (°C)	450	500	550	600
Water (% in bio-oil)	31.78	33.11	34.18	29.23
Molecular weight distribution				
Mw (Da)	274	288	268	252
Mn (Da)	167	174	170	157
PD	1.66	1.66	1.56	1.58
MAN (mg KOH/g)	119.52	104.78	118.13	145.50
Elemental composition (%)				
C	43.90	46.18	42.69	41.87
H	6.92	7.55	6.84	6.55
O[a]	47.66	44.51	48.57	49.54
N	1.50	1.73	1.86	2.02
S	0.03	0.03	0.02	0.02
Heating value (MJ/kg)				
As-is pyrolysis-oil	18.35	19.11	16.29	15.41
Dry pyrolysis-oil	23.92	27.52	23.64	20.91

Reprinted with permission of Royal Society of Chemistry
[a]By difference

stability during the aging test and also a significantly lower viscosity than untreated pyrolytic lignin. The NMR analysis revealed that the vinyl groups were converted to ethyl groups and carbonyl groups to alcohol groups. The low viscosity is probably due to the formation of phenolic alcohol.

9.4 Catalytic Upgrading of Lignin

9.4.1 Catalytic Upgrading of Pyrolysis Vapor of Lignin

Catalytic pyrolysis upgrades pyrolysis vapor by introducing catalyst in the reactor. Depending on whether the feedstock and catalyst physically contact or not, catalytic pyrolysis can be defined as an *in-situ* or *ex-situ* catalytic pyrolysis. Catalytic pyrolysis of biomass has received increasing attention as it could produce partly deoxygenated bio-oil or ideally hydrocarbons in a single step conversion. Various zeolite and transition or noble metal catalysts have shown excellent catalytic activity for producing hydrocarbons from biomass for biofuels and platform chemicals. Due to its intrinsic aromatic structure, lignin can be a great source of aromatic hydrocarbons, such as benzene, toluene, xylene and ethyl benzene (BTXE). However, lignin is found to be the most challenging component of biomass to deoxygenate. Low conversion yield, severe catalytic coke and rapid deactivation of catalyst are commonly found in catalytic pyrolysis of lignin and lignin-derived phenols [8].

Zeolite catalyst is frequently used in biomass pyrolysis because of its excellent deoxygenation capability without the need of external hydrogen. Zeolite is a porous, acidic catalyst and its active sites are mostly located inside of the pores where cracking, dehydration, decarboxylation, decarbonylation, oligomerization, isomerization and aromatization occur [8]. Zeolite is also highly shape selective and ZSM-5 is found to be the most effective catalyst in deoxygenating biomass [48]. It is considered that ZSM-5 outperforms other zeolite catalysts because it has the right balance between its pore size and acidity. When cellulose and hemicellulose were converted by ZSM-5 at 650 °C, the aromatic hydrocarbon yields reach 28.8 % and 19.4 %, respectively [49]. In comparison, switchgrass-derived MWL produced only 7.4 % of aromatics. Instead, up to 60 % of the lignin was converted to solid residue (char and catalytic coke). The conversion mechanism of lignin over zeolite catalyst is not clearly understood. It was suggested that the narrow pores of zeolite could selectively pass or convert phenols within its small volume and reduce polymerization reactions among molecules [8]. However, the molecule sizes of the majority of phenols derived from the thermal decomposition of lignin are too large to enter the zeolite pores in the first place. Thus, Mullen et al. [50] suggested that the surface acidic sites of zeolite promotes the depolymerization of lignin and only the aliphatic linkers among the different aromatic units of lignin are deoxygenated inside the pores to form olefins and then aromatize. They also suggested that simpler phenols are difficult to be deoxygenated by zeolite and eventually polymerize and become coke and char to poison catalysts. Catalytic conversion of lignin with a higher concentration of H units produces an increased amount of solid residue since phenol has low conversion and stronger adsorption on zeolite compared to guaiacol and syringol. It was suggested that the latter two are less bonded to active sites due to the steric bulk around the hydroxyl provided by the methoxy groups on the *ortho* positions of the planar benzene ring [50]. On the other hand, Yu et al. [51] suggested that the thermal expansion of zeolite pore size at elevated temperatures and the ability to adjust molecular orientation when a molecule enters the enlarged pores could allow a molecular size larger than the static pore size to access active sites and be converted. Regardless of the proposed reaction pathways, significant coke deposition on the catalyst indicates that lignin-derived phenols have a strong tendency for adsorption and polymerization. In addition to zeolite, metal oxides such as Co, Mo, Ni and Ti have also been explored in an effort to produce aromatic compounds from lignin pyrolysis [8, 50]. However, deoxygenation efficiencies of these catalysts are usually inferior to zeolite catalysts.

Catalytic hydropyrolysis of lignin with HZSM-5 has been carried out using hybrid polar wood-derived Klason lignin. It was found that increasing the partial pressure of H_2 can result in a significantly higher amount of aromatic hydrocarbons compared to catalytic pyrolysis under an inert environment [52]. Incorporating a hydrogenation catalyst was even more effective as the yield of aromatic hydrocarbons reached 40 % when the lignin was converted by 1 % Pd/HZSM-5 at 650 °C and 1.72 MPa. This value corresponds to a 44 % increase compared to when lignin is converted using HZSM-5 at the same reaction conditions. The formation of cycloalkanes was observed with the bifunctional catalyst, indicating that aromatic ring

saturation occurred due to a strong hydrogenation. The H_2 environment plays an important role in the production of hydrocarbons from lignin as hydrogen provides a suitable reaction medium for reducing the amount of coke on the catalyst surface. Hydrogen can stabilize reactive free radicals produced from thermal depolymerization of lignin and also saturate the side chain functionalities of phenols to reduce polymerization and cross linking. As a result, hydrogen reduces the formation of thermal char and also suppresses the adsorption of the phenols on catalyst surfaces to decrease the formation of coke precursors. Hydrogen also promotes hydrodeoxygenation rather than decarbonylation and decarboxylation, thus reducing limiting carbon loss through forming carbon oxides.

Some hydrogen donor agents supply hydrogen without needing a high reaction pressure. Waste plastics, such as polyethylene and polypropylene are cheap hydrogen sources and readily produce hydrogen radicals when they thermally decompose at atmospheric pressure. It has been shown that co-pyrolyzing with polyethylene (PE) produced up to 43 % more phenolic monomers since strong hydrogen abstraction by lignin-derived phenols and free radicals facilitates the depolymerization of both lignin and plastics [53]. When co-converted using HZSM-5 catalyst, total aromatics yield increased by 50 % whereas catalytic coke decreased due to the synergistic effect among lignin and PE. Alkanes were nearly absent in the products, suggesting that lignin effectively utilizes hydrogen donors to promote hydrodeoxygenation. The synergistic increase in the yield of aromatics and olefins was also observed when lignin and plastics were co-converted over other catalysts, such as LOSA-1, spent FCC and Gamma-Al_2O_3 [54].

9.4.2   Catalytic Upgrading of Phenolic Oil

Catalytic upgrading of condensed phenolic oil can be carried out at conditions that totally differ from lignin pyrolysis (such as reaction time, pressure and reaction gas). However, this upgrading approach requires the reheating of phenolic oil that has low volatility (i.e., tendency for charring) and high viscosity (i.e., low fluidity). To avoid rapid deactivation of catalyst caused by phenols in bio-oil, Gayubo et al. [55] previously proposed a two-step upgrading of bio-oil. Crude bio-oil was first heated to 400 °C to remove pyrolytic lignin using a bed of glass spheres. The rest of the volatilized bio-oil (mostly carbohydrate-derived compounds) was then upgraded by HZSM-5 zeolite catalyst at a second reactor. The different properties of phenolic oil compared to the rest fraction of bio-oil suggest that upgrading pyrolytic lignin independently is preferred.

Pyrolytic lignin separated from rice husk bio-oil was converted over several different types of zeolite catalysts and ZSM-5 was found to be the most effective catalyst [56]. The carbon yield of aromatics (including phenols and aromatic hydrocarbons) was 39 %, with 85 % selectivity for aromatic hydrocarbons.

Low temperature, low pressure hydrotreating of pyrolytic lignin separated from hardwood bio-oil was also tested using a Ru/TiO_2 catalyst in the temperature range

of 25–150 °C [19]. Although the mild reaction condition was not sufficient to produce hydrocarbons, a decrease in the percentages of carbonyl and aromatic carbons and increasing percentages of aliphatic C-O and C-C moieties were observed. It was also noted that a higher MW fraction in pyrolytic lignin produces much more coke than the lower MW phenols.

The most promising results to date were reported by Elliot et al. [57]. In their study, pyrolytic lignin extracted from corn stover bio-oil and red oak bio-oil was hydrotreated using precious metal catalysts and sulfided base metal catalysts in two-stages. The operating pressure was 12 MPa and the reaction temperatures were 140 °C and 375 °C, respectively. The approach was highly effective, as they were able to obtain up to 81 % (carbon based) of the liquid products containing a nearly no oxygen. The liquid hydrocarbon consisted of 42–52 % of gasoline range molecules and 43 % of diesel range molecules. However, the authors also reported that the pyrolytic lignin had to be filtered to remove particulate matter prior to hydrotreating, otherwise it would cause plugging in the reactor.

Few studies reported catalytic upgrading of lignin pyrolysis oil due to the technical difficulty of pyrolyzing lignin for liquid products. De Wild et al. [5] hydrotreated phenolic oil produced from pyrolyzing an organosolv lignin or soda pulping lignin. The reaction was conducted at 350 °C for 1 h with 10 MPa of hydrogen pressure using Ru/C as the catalyst. At the end of the reaction, the liquid products were separated into an organic phase and water phase. Due to the short reaction time, deoxygenation was incomplete as the organic phase included alkyl-substituted cyclohexanols and cyclohexanol in addition to cycloalkanes and linear alkanes.

9.5 Application of Lignin Pyrolysis Products

Lignin-derived phenolic oil is a mixture and the yields of most individual compounds are very low. However, the concentrations of certain phenols in pyrolysis oil could be high enough to consider extraction. For example, vinylphenols are usually the most predominant phenolic monomers found in pyrolysis of various lignin. The concentration of 4-vinylphenol and 2-methoxyl-4-vinylphenol accounted for 20 % of the heavy oil when pretreated lignin was pyrolyzed [38]. Vinylphenols have application in polymer and electronic industries. Poly-4-vinylphenol, commonly called polyvinylphenol or PVP, is produced by thermal polymerization of 4-vinylphenol [58]. In electronics, PVP is used as a gate insulating layer in an organic thin film transistor [59]. The liquid hydrocarbons produced from catalytic upgrading of lignin can be used as biofuels or biofuel additives. BTXE has the highest selectivity among lignin-derived aromatic hydrocarbons and they are also important petrochemicals [49].

Other than being used as liquid fuels and chemicals, pyrolysis products of lignin have several other applications. Pyrolytic lignin can be used as the mixture for producing biobased composite materials, binder or solid fuels [60]. Pyrolytic lignin was blended with bitumen in 3–9 % to produce bio-asphalt [61], which was

successfully applied to pavement. The bio-asphalt is overall similar to petroleum-derived asphalt, while it had higher stiffness. Pyrolytic lignin was also mixed with coal to make co-firing pellets in power plant to reduce greenhouse gas emissions and air pollution [62]. The high heating value of the co-firing pellets was about 28 MJ/kg, similar to that of parent coal. Pyrolytic lignin can be used to replace phenol in production of phenol-formaldehyde resins, which serve as adhesives for plywood, chipboard, medium-density fiberboard and oriented strand board [63, 64]. Carbon fiber was prepared from pyrolytic lignin. Qin et al. [65] demonstrated that pyrolytic lignin-based carbon fiber is comparable to it produced from kraft lignin. Pyrolytic lignin has a lower melting temperature and glass transition temperature than lignin when it is used as a low-cost carbon fiber precursor.

Pyrolysis char can account for $30\sim50\%$ of initial lignin. Although it is commonly considered a residue, exploring potential applications of the char in addition to pyrolysis oil would greatly boost the economic feasibility of lignin pyrolysis. However, the potential value of lignin pyrolysis char is largely unknown [66]. While lignin-based activated carbon has been extensively studied, such processes do not produce more valuable phenolic oil. Thus this section will briefly describe the properties of lignin pyrolysis char and discuss its potential application. Pyrolysis char of raw lignin produces a hard-shelled carbonaceous chunk, which can be mechanically milled into fine powders. The lignin char recovered from the pyrolysis of pretreated lignin is powder, similar to the original lignin because no melting and agglomeration occur during pyrolysis. However, micropores commonly found in biochar are absent in lignin char [38]. The ratios of the elemental compositions of the char produced from the (pretreated) corn stover lignin and the raw corn stover lignin are shown in Fig. 9.7 (calculated based on reference [38]). The lignin char is a carbon rich solid. It contained less oxygen and hydrogen compared to the raw lignin since dehydration and deoxygenation occurred during pyrolysis. Increasing the pyrolysis temperature reduced both the H/C ratio and the O/C ratio since the carbon concentration in lignin char increased.

The properties of the (pretreated) corn stover lignin char were also compared with the biochar derived from pyrolysis of corn stover in literature [38]. The lignin char was found to contain a lesser amount of ash than the biochar, probably because some soluble ash in corn stover was removed during the lignin isolation process. The lignin char was also richer in nitrogen and other inorganics such as K, S, P, N and Fe compared to the biochar. For example, the concentration of N and S were 1.14 and 0.2 % for the lignin char versus 0.6 and 0.02 % for the biochar. According to the FTIR analysis, the lignin char has condensed the polyaromatic structure combined with the phenolic OH as well as C-C, C-H and C-O containing functionalities [38, 66]. The corn stover lignin char was basic (pH value of 8–9) and its HHV value was about 18 MJ/kg. However, the BET surface area of the lignin char was about 1 m²/g, lower than the biochar due to the lack of micropores. It is also suggested that the lignin char has small, dead-ended pores (versus open micropores found in biochar), preventing the adsorption of gas [67]. However, post activation of the lignin char can significantly increase its surface area [36]. Overall, lignin char could have potential applications similar to biochar, such as soil amendment, activated carbon
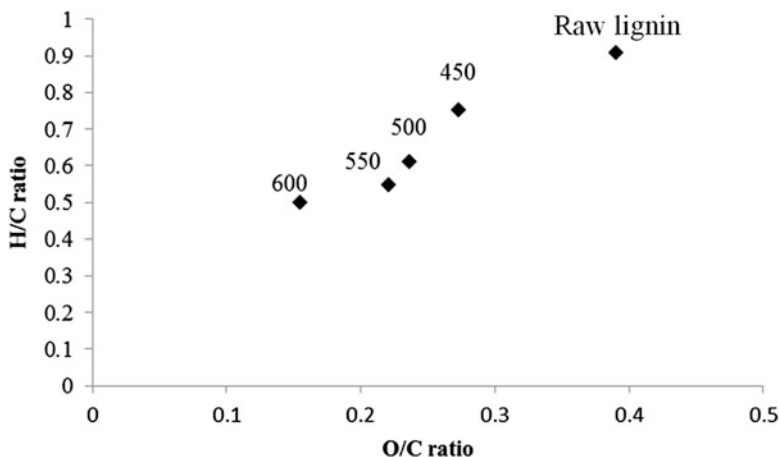
Fig. 9.7 H/C and O/C ratio of the char produced from pretreated corn stover lignin at different pyrolysis temperatures compared with the raw lignin. Calculated based on reference [38]

and solid fuel. The potential applications of lignin pyrolysis products are summarized in Table 9.3.

9.6 Conclusions and Future Outlook

Fast pyrolysis has gained great interest due to its potential for producing biofuels and chemicals through a simple and cost-effective process. Although this technology potentially provides renewable aromatics from lignin, the pyrolysis of lignin for products has yet to be reported mainly due to the low yield and poor quality of liquid product, and the difficulty of continuously pyrolyzing lignin in large reactors. Lignin-derived phenolic oil is also a mixture of hundreds of different phenolic monomers and oligomers, and it is thermally unstable. Catalytic deoxygenation of lignin and lignin-derived phenolic oil is also problematic due to its low conversion and catalyst deactivation. The complex molecular structure of lignin, the variation of lignin source and inability to fully characterize lignin pyrolysis products analytically create significant challenges in understanding the pyrolysis reaction mechanism of lignin and optimizing the technology.

To improve the technical feasibility of fast pyrolysis-based utilization of lignin, future studies in following areas are strongly recommended:

1. Development of comprehensive analytical techniques to fully characterize lignin and lignin products;
2. Determination of deoxygenation mechanisms of lignin and lignin-derived phenols over catalysts and developing newly designed and tailored catalysts;

Table 9.3 Potential applications of pyrolysis products of lignin

Products	Form of use	Applications	Refs.
Pyrolysis oil	Chemicals (extraction required)	Vinyl phenols, vanillin, phenol etc.	[38, 58]
	Catalytic upgrading	BTX or other hydrocarbons; chemicals or biofuels	[49, 57]
	Crude oil (post treatment required)	Bioasphalt	[61]
		Solid fuel	[62]
		Resin	[63, 64]
		Carbon fiber	[65]
Char	As is	Solid fuel	[38]
	Treatment may required	Soil amendment	[3]
	Treatment required	Activated carbon	[36]
Gas	As is	Flue gas	[68]

3. Development of methods for pyrolysis of lignin in reactors in cost-effective ways and improving yield and quality of liquid product;
4. Development of extraction techniques for chemicals in phenolic oil;
5. Development of applications that can use bulky phenolic oil and pyrolysis char.

References

1. Venderbosch RH, Prins W. Fast pyrolysis. In: Thermochemical processing of biomass: conversion into fuels, chemicals and power. Chichester: Wiley; 2011.
2. Van de Velden M, Baeyens J, Brems A, Janssens B, Dewil R. Fundamentals, kinetics and endothermicity of the biomass pyrolysis reaction. Renew Energy. 2010;35:232–42.
3. Brown RC, Brown TR. Why are we producing biofuels?: shifting to the ultimate source of energy. Ames: Brownia LLC; 2012.
4. Ragauskas AJ, Beckham GT, Biddy MJ, Chandra R, Chen F, Davis MF, Davison BH, Dixon RA, Gilna P, Keller M. Lignin valorization: improving lignin processing in the biorefinery. Science. 2014;344:1246843.
5. De Wild P, Van der Laan R, Kloekhorst A, Heeres E. Lignin valorisation for chemicals and (transportation) fuels via (catalytic) pyrolysis and hydrodeoxygenation. Environ Prog Sustainable Energy. 2009;28:461–9.
6. Davin LB, Patten AM, Jourdes M, Lewis NG. Lignins: a twenty-first century challenge. Oxford: Blackwell Publishing; 2008.
7. Nowakowski DJ, Bridgwater AV, Elliott DC, Meier D, de Wild P. Lignin fast pyrolysis: results from an international collaboration. J Anal Appl Pyrolysis. 2010;88:53–72.
8. Li C, Zhao X, Wang A, Huber GW, Zhang T. Catalytic transformation of lignin for the production of chemicals and fuels. Chem Rev. 2015;115:11559–624.
9. Yang H, Yan R, Chen H, Lee DH, Zheng C. Characteristics of hemicellulose, cellulose and lignin pyrolysis. Fuel. 2007;86:1781–8.
10. Wang S, Ru B, Lin H, Sun W, Luo Z. Pyrolysis behaviors of four lignin polymers isolated from the same pine wood. Bioresour Technol. 2015;182:120–7.
11. Faix O, Jakab E, Till F, Székely T. Study on low mass thermal degradation products of milled wood lignins by thermogravimetry-mass-spectrometry. Wood Sci Technol. 1988;22:323–34.

12. Liu Q, Wang S, Zheng Y, Luo Z, Cen K. Mechanism study of wood lignin pyrolysis by using TG–FTIR analysis. J Anal Appl Pyrolysis. 2008;82:170–7.
13. Cho J, Chu S, Dauenhauer PJ, Huber GW. Kinetics and reaction chemistry for slow pyrolysis of enzymatic hydrolysis lignin and organosolv extracted lignin derived from maplewood. Green Chem. 2012;14:428–39.
14. Chen D, Zheng Y, Zhu X. In-depth investigation on the pyrolysis kinetics of raw biomass. Part I: kinetic analysis for the drying and devolatilization stages. Bioresour technol. 2013;131:40–6.
15. Patwardhan PR, Brown RC, Shanks BH. Understanding the fast pyrolysis of lignin. ChemSusChem. 2011;4:1629–36.
16. Jiang G, Nowakowski DJ, Bridgwater AV. Effect of the temperature on the composition of lignin pyrolysis products. Energy Fuel. 2010;24:4470–5.
17. Kibet J, Khachatryan L, Dellinger B. Molecular products and radicals from pyrolysis of lignin. Environ Sci Technol. 2012;46:12994–3001.
18. Mu W, Ben H, Ragauskas A, Deng Y. Lignin pyrolysis components and upgrading—technology review. Bioenergy Res. 2013;6:1183–204.
19. Chen W, McClelland DJ, Azarpira A, Ralph J, Luo Z, Huber GW. Low temperature hydrogenation of pyrolytic lignin over Ru/TiO 2: 2D HSQC and 13 C NMR study of reactants and products. Green Chem. 2016;18:271–81.
20. Mullen CA, Boateng AA. Characterization of water insoluble solids isolated from various biomass fast pyrolysis oils. J Anal Appl Pyrolysis. 2011;90:197–203.
21. Bayerbach R, Meier D. Characterization of the water-insoluble fraction from fast pyrolysis liquids (pyrolytic lignin). Part IV: structure elucidation of oligomeric molecules. J Anal Appl Pyrolysis. 2009;85:98–107.
22. Bai X, Kim KH, Brown RC, Dalluge E, Hutchinson C, Lee YJ, Dalluge D. Formation of phenolic oligomers during fast pyrolysis of lignin. Fuel. 2014;128:170–9.
23. Asmadi M, Kawamoto H, Saka S. Pyrolysis reactions of Japanese cedar and Japanese beech woods in a closed ampoule reactor. J Wood Sci. 2010;56:319–30.
24. Garcia-Perez M, Wang S, Shen J, Rhodes M, Lee WJ, Li C-Z. Effects of temperature on the formation of lignin-derived oligomers during the fast pyrolysis of mallee woody biomass. Energy Fuel. 2008;22:2022–32.
25. Ben H, Ragauskas AJ. NMR characterization of pyrolysis oils from kraft lignin. Energy Fuel. 2011;25:2322–32.
26. Patwardhan PR, Satrio JA, Brown RC, Shanks BH. Influence of inorganic salts on the primary pyrolysis products of cellulose. Bioresour Technol. 2010;101:4646–55.
27. Gray MR, Corcoran WH, Gavalas GR. Pyrolysis of a wood-derived material. Effects of moisture and ash content. Ind Eng Chem Process Des Dev. 1985;24:646–51.
28. Di Blasi C, Galgano A, Branca C. Influences of the chemical state of alkaline compounds and the nature of alkali metal on wood pyrolysis. Ind Eng Chem Res. 2009;48:3359–69.
29. Dalluge DL. Optimization of biomass fast pyrolysis for the production of monomers. Thesis/dissertation, Iowa State University; 2013.
30. Yang H, Yan R, Chen H, Zheng C, Lee DH, Liang DT. In-depth investigation of biomass pyrolysis based on three major components: hemicellulose, cellulose and lignin. Energy Fuel. 2006;20:388–93.
31. Qu T, Guo W, Shen L, Xiao J, Zhao K. Experimental study of biomass pyrolysis based on three major components: hemicellulose, cellulose, and lignin. Ind Eng Chem Res. 2011;50:10424–33.
32. Hosoya T, Kawamoto H, Saka S. Cellulose–hemicellulose and cellulose–lignin interactions in wood pyrolysis at gasification temperature. J Anal Appl Pyrolysis. 2007;80:118–25.
33. Hosoya T, Kawamoto H, Saka S. Solid/liquid-and vapor-phase interactions between cellulose- and lignin-derived pyrolysis products. J Anal Appl Pyrolysis. 2009;85:237–46.
34. Wang S, Guo X, Wang K, Luo Z. Influence of the interaction of components on the pyrolysis behavior of biomass. J Anal Appl Pyrolysis. 2011;91:183–9.

35. Kim KH, Bai X, Rover M, Brown RC. The effect of low-concentration oxygen in sweep gas during pyrolysis of red oak using a fluidized bed reactor. Fuel. 2014;124:49–56.

36. Li D, Briens C, Berruti F. Oxidative pyrolysis of kraft lignin in a bubbling fluidized bed reactor with air. Biomass Bioenergy. 2015;76:96–107.

37. De Wild P, Huijgen W, Heeres H. Pyrolysis of wheat straw-derived organosolv lignin. J Anal Appl Pyrolysis. 2012;93:95–103.

38. Zhou S, Brown RC, Bai X. The use of calcium hydroxide pretreatment to overcome agglomeration of technical lignin during fast pyrolysis. Green Chem. 2015;17:4748–59.

39. Gooty AT, Li D, Berruti F, Briens C. Kraft-lignin pyrolysis and fractional condensation of its bio-oil vapors. J Anal Appl Pyrolysis. 2014;106:33–40.

40. Wilberink R, Van DLR, De WPJ. Pyrolysis of lignin. 2011. Google Patents.

41. De Wild PJ, Huijgen WJ, Gosselink RJ. Lignin pyrolysis for profitable lignocellulosic biorefineries. Biofuels Bioprod Biorefin. 2014;8:645–57.

42. Mukkamala S, Wheeler MC, van Heiningen AR, DeSisto WJ. Formate-assisted fast pyrolysis of lignin. Energy Fuel. 2012;26:1380–4.

43. Scholze B, Meier D. Characterization of the water-insoluble fraction from pyrolysis oil (pyrolytic lignin). Part I. PY–GC/MS, FTIR, and functional groups. J Anal Appl Pyrolysis. 2001;60:41–54.

44. Scholze B, Hanser C, Meier D. Characterization of the water-insoluble fraction from fast pyrolysis liquids (pyrolytic lignin): Part II. GPC, carbonyl goups, and 13C-NMR. J Anal Appl Pyrolysis. 2001;58:387–400.

45. Bayerbach R, Nguyen VD, Schurr U, Meier D. Characterization of the water-insoluble fraction from fast pyrolysis liquids (pyrolytic lignin): Part III. Molar mass characteristics by SEC, MALDI-TOF-MS, LDI-TOF-MS, and Py-FIMS. J Anal Appl Pyrolysis. 2006;77:95–101.

46. Kim KH, Bai X, Cady S, Gable P, Brown RC. Quantitative investigation of free radicals in bio-oil and their potential role in condensed-phase polymerization. ChemSusChem. 2015;8:894–900.

47. Rover MR, Hall PH, Johnston PA, Smith RG, Brown RC. Stabilization of bio-oils using low temperature, low pressure hydrogenation. Fuel. 2015;153:224–30.

48. Jae J, Tompsett GA, Foster AJ, Hammond KD, Auerbach SM, Lobo RF, Huber GW. Investigation into the shape selectivity of zeolite catalysts for biomass conversion. J Catal. 2011;279:257–68.

49. Wang K, Kim KH, Brown RC. Catalytic pyrolysis of individual components of lignocellulosic biomass. Green Chem. 2014;16:727–35.

50. Mullen CA, Boateng AA. Catalytic pyrolysis-GC/MS of lignin from several sources. Fuel Process Technol. 2010;91:1446–58.

51. Yu Y, Li X, Su L, Zhang Y, Wang Y, Zhang H. The role of shape selectivity in catalytic fast pyrolysis of lignin with zeolite catalysts. Appl Catal A Gen. 2012;447:115–23.

52. Jan O, Marchand R, Anjos LC, Seufitelli GV, Nikolla E, Resende FL. Hydropyrolysis of Lignin Using Pd/HZSM-5. Energy Fuel. 2015;29:1793–800.

53. Xue Y, Kelkar A, Bai X. Catalytic co-pyrolysis of biomass and polyethylene in a tandem micropyrolyzer. Fuel. 2016;166:227–36.

54. Zhang H, Xiao R, Nie J, Jin B, Shao S, Xiao G. Catalytic pyrolysis of black-liquor lignin by co-feeding with different plastics in a fluidized bed reactor. Bioresour Technol. 2015;192:68–74.

55. Gayubo A, Valle B, Aguayo A, Olazar M, Bilbao J. Pyrolytic lignin removal for the valorization of biomass pyrolysis crude bio-oil by catalytic transformation. J Chem Technol Biotechnol. 2010;85:132–44.

56. Zhao Y, Deng L, Liao B, Fu Y, Guo Q-X. Aromatics production via catalytic pyrolysis of pyrolytic lignins from bio-oil. Energy Fuel. 2010;24:5735–40.

57. Elliott DC, Wang H, Rover M, Whitmer L, Smith R, Brown R. Hydrocarbon liquid production via catalytic hydroprocessing of phenolic oils fractionated from fast pyrolysis of red oak and corn stover. ACS Sustain Chem Eng. 2015;3:892–902.

58. Kaneko S, Yamaoka S, Mizuno M, Okabe Y. Crosslinked resin of epoxy compound and isocyanate and process for producing same. Google Patents. 1983.
59. Kim GH, Yoon SM, You IK, Kang SY, Ahn SD, Baek KH, Suh KS. Composition for thermosetting organic polymeric gate insulating layer and organic thin film transistor using the same. Google Patents. 2009.
60. Effendi A, Gerhauser H, Bridgwater AV. Production of renewable phenolic resins by thermochemical conversion of biomass: a review. Renew Sust Energ Rev. 2008;12:2092–116.
61. Peralta J, Raouf MA, Tang S, Williams RC. Bio-renewable asphalt modifiers and asphalt substitutes. In: Sustainable bioenergy and bioproducts. London: Springer; 2012. p. 89–115.
62. Friend A. Development of a co-firing fuel from biomass-derived binder and crushed coal. Dissertation, Iowa State University; 2013.
63. Calvo-Flores FG, Dobado JA. Lignin as renewable raw material. ChemSusChem. 2010;3:1227–35.
64. Chum H, Diebold J, Scahill J, Johnson D, Black S, Schroeder H, Kreibich RE, Hemingway R, Conner A, Branham S. Biomass pyrolysis oil feedstocks for phenolic adhesives. In: Adhesives from renewable resources. Washington, DC: American Chemical Society; 1989. p. 135–51.
65. Qin W, Kadla J. Carbon fibers based on pyrolytic lignin. J Appl Polym Sci. 2012;126:E204–13.
66. Sharma RK, Wooten JB, Baliga VL, Lin X, Chan WG, Hajaligol MR. Characterization of chars from pyrolysis of lignin. Fuel. 2004;83:1469–82.
67. Carrott P, Carrott MR. Lignin–from natural adsorbent to activated carbon: a review. Bioresour Technol. 2007;98:2301–12.
68. Hu X, Dong CQ, Yang YP, Zhang JJ. The effect of biomass pyrolysis gas reburning on N_2O emission in a coal-fired fluidized bed boiler. Chin Sci Bull. 2011;56:1429–33.

Chapter 10
Lignin Depolymerization (LDP) with Solvolysis for Selective Production of Renewable Aromatic Chemicals

Dekui Shen, Chongbo Cheng, Nana Liu, and Rui Xiao

10.1 Introduction

Lignin

Lignin, which is one of the three major constituents in lignocellulosic biomass, consists of *p*-hydroxyphenyl (H), guaiacyl (G) and syringyl (S) units polymerized by ether bonds or carbon-carbon linkages. The content and chemical structure of lignin is substantially influenced by its origin and the separation methods used for its isolation. The difference in chemical structure for the lignin from different sources changes the content and ratio of *p*-coumaryl-, coniferyl-, and sinapyl-alcohols (C_9 unit) (Fig. 10.1a). The C_9 unit of softwood lignin is estimated to be dominated by coniferyl-alcohol (more than 95 %), while that of hardwood lignin has high coniferyl-alcohols and sinapyl-alcohols in roughly equal proportions. The chemical structure of straw (herbaceous biomass) lignin is different from that of woody lignin due to the extra content of H-type unit mainly in forms of hydroxycinnamic acid (up to 15 % in rice straw). The proportions of *p*-coumaryl alcohol, coniferyl alcohol and sinapyl alcohol in lignin depend main on the source.

Lignin monolignols are linked either by ether or by C–C bonds. In native lignin, two-thirds or more of the total linkages are ether bonds, while the other linkages are C–C bonds [32]. In general, the carbon atoms in the aliphatic side chains of the monolignols are labeled as α, β, and γ and those in the aromatic moieties are numbered 1–6 to distinguish between the various types of linkages between two monolignols. The major linkages between the structural units of lignin are β-O-4, α-O-4 (α-aryl ether), β-β (resinol), and β-5 (phenylcoumaran) [68]. Other linkages include 4-O-5 (diaryl ether), 5–5, α-O-γ (aliphatic ether), and β-1 (spirodienone), etc.

D. Shen • C. Cheng • N. Liu • R. Xiao (✉)

Key Lab of Thermal Energy Conversion and Control of MoE, Southeast University, Nanjing, China

e-mail: 101011398@seu.edu.cn; ruixiao@seu.edu.cn
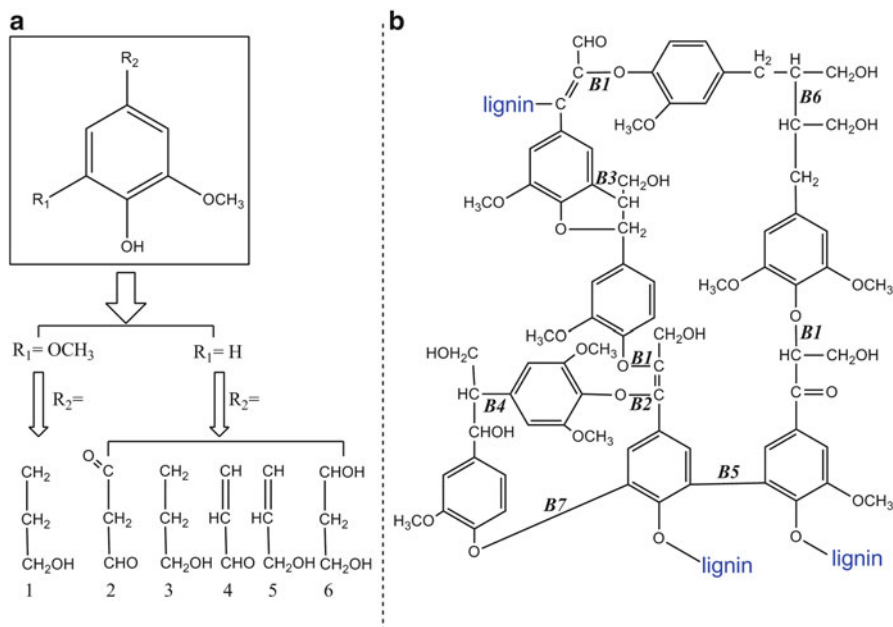
Fig. 10.1 Schematics for the chemical structure of lignin (B1: β-O-4, B2: α-O-4, B3: β-5, B4: β-1, B5: 5–5, B6: β-β, B7: 4-O-5). (**a**) The structure of monomer C9 units; (**b**) The chemical structure of woody lignin

Representative structures of these linkages are shown in Fig. 10.1b. Typical proportion values of these linkages and the functional groups in lignin are also depending on the source [10].

Solvolysis

Solvolysis is one of the promising methods to convert lignin into different kinds of value-added aromatic chemicals. The process involves the depolymerization of lignin macromolecule and repolymerization of the fragments in the solvent system using various heating methods, experimental conditions, catalysts and solvent systems. The goal of solvolys is is to selectively form specific compounds. In this chapter, lignin depolymerization in solvent is overviewed regarding the following fundamental issues (Fig. 10.2):

1. Lignin depolymerization (LDP) strategies; Liquid products and distribution of aromatic compounds are greatly influenced by the technology of lignin depolymerization. Three kinds of LDP strategies are used that are termed as hydrogenolysis, oxidativelysis and two-step LDP.
2. Effect of heating method on lignin depolymerization (LDP); Yield of liquid products and distribution of aromatic compounds from LDP under conventional heating and microwave heating is influenced by reaction temperature, reaction time, species and the addition of catalyst.
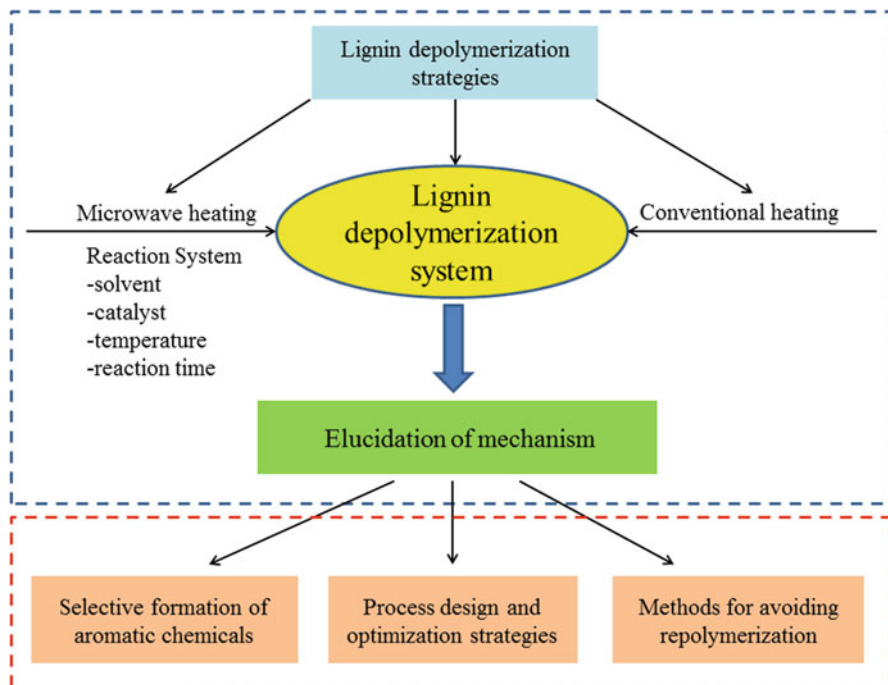
Fig. 10.2 Target and main contents of this work

3. Inherent mechanism of LPD process; Cleavage of specific inter-unit linkages and the kinetics for the depolymerization of lignin macromolecule allow formation of specific aromatic compounds. New strategies to avoid repolymerization of lignin fragments are introduced.

Issues of LDP concerning the above three fundamental issues are discussed and outlook of this field is given. This chapter provides a conceptual guide for solvolysis of lignin utilization and optimization of LDP process for value-added chemical production.

10.2 Lignin in Conventional Heating

10.2.1 Hydrogenolysis

Hydrogenolysis is a reductive reaction that occurs between hydrogen or a hydrogen-donor reactant and a target compound, usually in presence of catalyst. It is one of the most popular and efficient strategies applied to lignin depolymerization for producing aromatic compounds and especially for promoting the cleavage of C–O

bond (mainly inter-unit β-O-4 linkage). Harsh hydrogenolysis conditions will lead to undesirable concurrent cleavage of aliphatic C–O bonds and hydrogenation of aromatic rings. A number of studies concerning the depolymerization of lignin and its model compounds through hydrogenolytic cleavage of C–C and C–O bonds have been conducted using (1) hydrogen-donor solvent system and (2) the direct use of hydrogen in high pressure system [68]. Corresponding references on hydrogenolysis are summarized in Table 10.1.

Table 10.1 Selected lignin depolymerization studies on hydrogenolysis of lignin

Materials Main products	Catalyst	Reaction conditions	LDP yield	Refs.
Kraft lignin; low-molecular weight products	none	300 °C, 60 min, 2 MPa N_2; Hydrogen donor: formic acid; Water/ethanol	90 wt %	[22]
Switchgrass lignin; p-propylguaiacol	Pt/C	350 °C, 1,4,8,20 h; Hydrogen donor: formic acid; Ethanol	21 wt %	[69]
Alcell lignin; aromatics and phenolics	Ru/C	400 °C, 4 h, 20 MPa N_2; Hydrogen donor: formic acid; Iso-propanol	68 % (11 % alkylphenolics and 19 % aromatics)	[28]
Birch sawdust; propylguaiacol and propylsyringol	Ni/C	200 °C, 6 h, 0.1Mpa Ar; CH_3OH/i-PrOH/1,4-Dioxane/Glycerol/Cyclohexane	Selectivity (Propylguaiacol and propylsyringol) >90 %; Conversion about 50 %	[55]
Organosolv lignin; saturated alcohols	Cu-PMO	300 °C, 24 h; Hydrogen donor: supercritical methanol	No aromatics	[4]
Wood and cellulosic solids; methylated derivatives	Cu-PMO	300–320 °C, 8 h, 16–22 MPa N_2; Hydrogen donor: supercritical methano	98 % conversion	[36]
Organosolv lignin; catechol	Cu-PMO	180 °C, 14 h, 4 MPa H_2; Hydrogen donor: supercritical methanol	>70 % (methanol-soluble products)	[5]
Kraft lignin; abundant liquid products(LP25)	α-MoC_{1-x}/AC	280 °C, 6 h, 10.5 MPa N_2; supercritical ethanol	82 wt %	[35]
KL/AL/EL lignin; monomers	Ru/Al_2O_3; Rh/Al_2O_3; Pd/Al_2O_3	340–380 °C, 2–6 h Hydrogen donor: formic acid; water	95 % conversion	[42]
Spruce lignin; guaiacol, pyrocatechol and resorcinol	Palladium-Nafion SAC-13	300 °C, 2 h; Hydrogen donor: formic acid; Water	7.7 wt %	[34]

Table 10.1 (continued)

Materials Main products	Catalyst	Reaction conditions	LDP yield	Refs.
Phenols; arenes	Raney Ni and β-zeolite	160 °C, 4 h; Hydrogen donor: 2-propanol n-$C_{16}H_{34}$	82 % (benzene)	[62]
Phenols; propylcyclohexane	Pt/AC(N)	280 °C, 1 h, 4 MPa H_2; Water	97 % (propylcyclohexane)	[40]
Corn stalk/Bamboo/ Klason lignin; 4-ethylphenolics	5 % Ru/C or Pd/C or Pt/C	200–275 °C, 60–180 min, 2 MPa H_2; Ethanol/water	3.1 % (4-Ethylphenol) and 1.3 % (4-ethylguaiacol)	[70]
Alkali lignin	Pd/C	80–180 °C, 3 h, 1–5 MPa H_2; Dioxane and water	Hydroxyl, phenolic hydroxyl and alcoholic hydroxyl increase 64.23 %, 37.10 % and 89.67 %	[24]
Lignin monomer guaiacol; cyclohexane	Rh/ SiO_2-Al_2O_3 or Ru/ SiO_2-Al_2O_3	50 °C, 1 h, 4 MPa H_2; n-decane	60 % (cyclohexane)	[30]
Guaiacol; phenol, catechol, 3-methylcatechol	Pt/γ-Al_2O_3	300 °C, 1 h, 0.14 MPa H_2	~75 % conversion	[39]
β-O-4 lignin molecules; aromatic fragments	Pd/C and $ZnCl_2$	150 °C, 4 h, 0.2–2 MPa H_2; Methanol or CH_2Cl_2	80–90 %	[48]
Birch wood; guaiacylpropane, syringylpropane	Ni-W_2C/AC	235 °C, 4 h, 6 Mpa H_2; Methanol or ethylene glycol	46.5 %	[33]
Organosolv lignin; monomers	NiRu or NiRh	130 °C, 1–12 h, 1 MPa H_2; Water	6.8 wt %	[71]
Lignin model compounds; monomers	Sulfided CoMo/Al_2O_3	300 °C, 4 h, 5 MPa H_2; Dodecane	90 % conversion	[27]
Guaiacol; phenol, cresols	W_2C/CNF or Mo_2C/CNF	300–375 °C, 4 h, 5.5 MPa H_2; Dodecane	>99 % conversion (methylated phenolics)	[26]
Organosolv/kraft lignin/sugarcane bagasse; aromatics	Pt/γ-Al_2O_3 and NaOH; CoMo/Al_2O_3 or Mo_2C/ CNF	225 °C, 2 h, 5.8 MPa Ar, ethanol-water; 300 °C, 4 h, 5 MPa H_2, Dodecane	9 %	[25]
C–O bonds in ethers; arenes, alcohols	Ni(COD)$_2$ and SIPr·HCl	80–120 °C, 16–32 h, 0.1 MPa H_2; m-xylene, NaO^{t}Bu	95 % conversion	[52]

10.2.2   *Hydrogen-Donor Solvent System*

To improve the control of hydrogenation process by external pressurized hydrogen, solvents as the hydrogen donor (such as formic acid or levulinic acid from cellulose depolymerisation or methanol, ethanol and 2-propanol) are used for lignin depolymerization. Hydrogen donor solvents play an important role in the hydrogenolysis process for LDP. Wang and Rinaldi [63] studied the effect of solvents on the hydrogenolysis of lignin and diphenyl ether as a model compound, where the solvents were classified into four groups: (1) *protic solvents displaying Lewis basicity* (both good H-bond donor and good H-bond acceptor and Lewis-based solvent such as methanol, ethanol, 2-propanol,1-butanol,2-butanol, and *tert*-butanol); (2) *protic solvent displaying no Lewis basicity* which is considered as the best H-bond donor but not an H-bond acceptor or a Lewis base such as Hex-F-2-PrOH, or 1,1,1,3,3,3-hexa fluoro-2-isopropanol; (3) *aprotic polar solvents* as an H-bond acceptor, and a Lewis base such as ethyl acetate, tetrahydrofuran (THF), 2-methyltetrahydrofuran (2-Me-THF), and 1,4-dioxane; (4) *aprotic nonpolar solvents* which is not an H-bond donor, H-bond acceptor or Lewis acid such as methylcyclohexane (MCH), decaline, and *n*-heptane.

Huang and co-workers [22] reported on the reductive depolymerization of Kraft lignin (KL) with formic acid (FA) as an in-situ hydrogen donor. Under 300 °C, 18.6 wt% substrate concentration and water-ethanol medium with FA, Kraft lignin was effectively depolymerized. It was found that FA is a more reactive hydrogen source than the external hydrogen. However, use of FA is not enough to produce specific aromatic compounds, so catalysts should be involved in the reaction to improve the selectivity of products. Most reported systems involve the use of heterogeneous catalysts (e.g. metal catalysts, synergic catalysts) with in situ generated hydrogen. Noble metal catalysts, such as Pd, Pt, Ru and Rh possess outstanding catalytic properties in hydroprocessing reactions. Xu and co-workers [69] reported that organosolv switchgrass lignin could be successfully depolymerized and hydrodeoxygenated to yield phenolic monomers and improved H/C and O/C molar ratios by treatment in ethanol at 350 °C. The *p*-propylguaiacol was the dominant product after 4 h reaction and the reaction time could be varied to tailor the properties of the products obtained from lignin. The combined presence of both formic acid and Pt/C catalyst yielded the highest fraction of lower molecular weight liquid products and the least amount of char formed. Kloekhorst and co-workers [28] also reported a similar work, catalytic conversion of Alcell (organosolv) lignin in iso-propanol/formic acid mixtures (1:1 mass ratio) on Ru/C catalyst at 400 °C was studied. Compared to a catalytic hydrotreatment using molecular hydrogen, catalytic solvolysis resulted in the highest oil yield, the lowest O/C ratio of the lignin oil, and highest yield in valuable chemical compounds (alkylphenolics, and aromatics).

Nickel-based catalysts have been used for lignin hydrogenolysis/hydrogenation for a long time. Song and co-workers [55] studied the hydrogenolys is of native birch wood lignin for conversion into monomeric phenols over Ni/C catalysts with alcohols (CH₃OH, i-PrOH, 1,4-dioxane, glycerol, cyclohexane) as solvents were
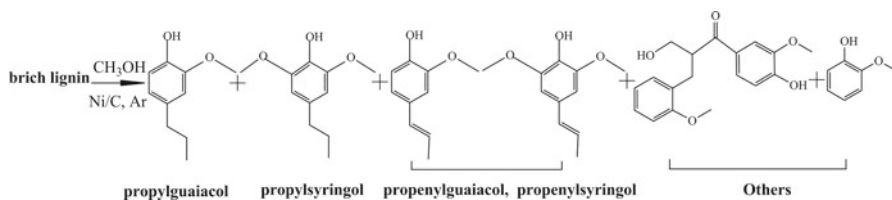
Fig. 10.3 Prominent aromatic products from LDP in presence of Ni/C catalyst (Adapted with permission from Ref. [55], Copyright 2013 Royal Society of Chemistry. http://dx.doi.org/10.1039/C2EE23741E)

used. The dominant products found were propylguaiacol, propylsyringol, propenyl-guaiacol and propenylsyringol after 6 h at 200 °C (Fig. 10.3). The low efficiency of reaction in i-PrOH was attributed to low lignin dissolution, and 1,4-dioxane, glycerol, cyclohexane could not produce hydrogen under the reaction conditions which lead to poor hydrogenolysis of lignin.
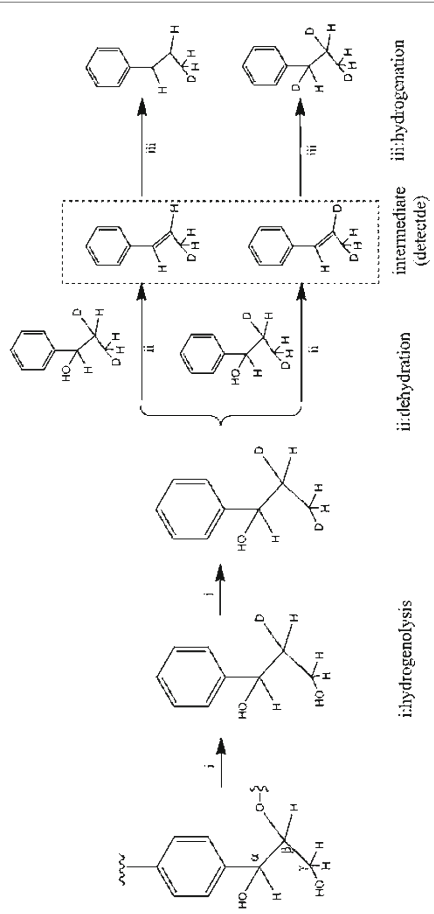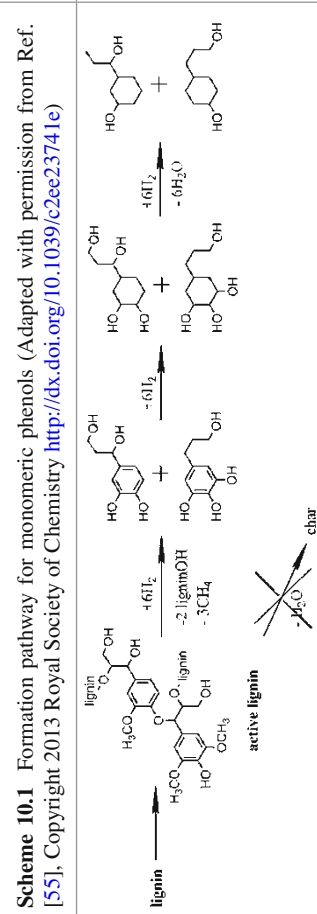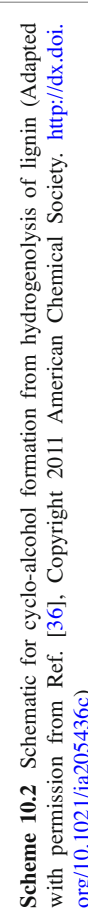
Song and co-workers [55] proposed that the LDP reaction is a fragmentation-hydrogenolysis process. The initial step involves the fragmentation of a long lignin polymer chain into a range of smaller fragments. The second step involves the hydrogenolysis of lignin fragments into monomeric phenols. Conversion of smaller lignin fragments into monomeric phenols undergo β-elimination dehydration coupled with the hydrogenation process for C_α and C_β, and subsequent hydrogenolysis reaction for C_γ (Table 10.2: Scheme 10.1).

The Barta group [4, 5, 36] have studied Cu-doped porous metal oxides as catalyst and have obtained different products from lignin (saturated alcohols with low oxygen content, C_2–C_6 aliphatic alcohols , methylated derivatives, catechol). Organosolv lignin was disassembled to monomeric units with little or no formation of insoluble char by hydrogen transfer from supercritical methanol and Cu catalyst leading to a continuous operation with high yield. In 2010, complete hydrogenolysis of phenyl ether bonds, coupled with the hydrogenation of aromatic rings in the depolymerisation of organosolv lignin was achieved at 300 °C. Then catalytic conversion of wood and cellulosic solids to liquid and gaseous products in a single stage reactor operating was obtained at 300–320 °C (Table 10.2: Scheme 10.2). In 2014, using the same system but with the addition of H_2 at 180 °C catalytic conversions of organosolv lignin into catechol was carried out. Cu played an important role, minimizing char formation and apparently favoring the required hydrogenolysis, dehydration, and hydrogenation steps without reducing the aromatic rings, to obtain catechols from lignin biopolymer.

However, ethanol did not act as hydrogen donor at the reaction conditions. Ma and co-workers [35] reported the complete ethanolysis of Kraft lignin over an α-MoC$_{1-x}$/AC catalyst in pure ethanol at 280 °C to give chemicals of low molecular weight with a maximum overall yield of the 25 most abundant liquid products of 1.64 g per gram of lignin. Ethanol was a reactant and gave rise to ethyl esters or other products through esterification or alkylation reaction routes.

Bengoechea and co-workers [42] reported on the catalytic solvolys is of three lignins of different sources (alkali lignin, acid lignin and enzymatic lignin) in a

Table 10.2 Summary of the proposed mechanisms for lignin depolymerization
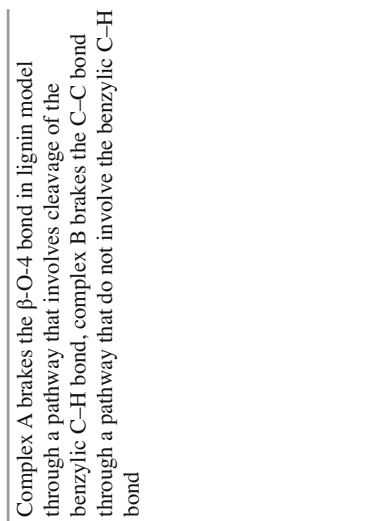
Description	Notes
 i:hydrogenolysis ii:dehydration intermediate (detectde) iii:hydrogenation **Scheme 10.1** Formation pathway for monomeric phenols (Adapted with permission from Ref. [55], Copyright 2013 Royal Society of Chemistry http://dx.doi.org/10.1039/c2ee23741e) **Scheme 10.2** Schematic for cyclo-alcohol formation from hydrogenolysis of lignin (Adapted with permission from Ref. [36], Copyright 2011 American Chemical Society. http://dx.doi.org/10.1021/ja205436c)	Conversion of smaller lignin fragments into monomeric phenols undergoes β-elimination dehydration coupled with the hydrogenation process for C_α and C_β, and subsequent hydrogenolysis reaction for $C\gamma$ Complete hydrogenolysis of phenyl ether bonds (α-O-4 and β-O-4), coupled with the hydrogenation of aromatic rings in the depolymerisation of organosolv lignin

The pathway is different from the well-known pathway (guaiacol→phenol→hydrodeoxygenated products)

Scheme 10.3 Catalytic hydrogenation pathway of guaiacol to cyclohexane (Adapted from Ref. [30], Copyright 2012, with permission from Elsevier. http://dx.doi.org/10.1016/j.catcom.2011.10.011)

Pathway A involves substrate binding to Zn^{2+} sites and hydrogen spillover from Pd sites. Pathway B represents desorption of Zn^{2+} into solution, activation of substrate via binding, and it is the Zn bound substrate that reacts with Pd sites on the catalyst's surface

Scheme 10.4 Mechanistic hypothesis for the synergy between Zn^{2+} and Pd (Adapted with permission from Ref. [48], Copyright 2012 Royal Society of Chemistry. http://dx.doi.org/10.1039/c2sc21657d)

(continued)

Table 10.2 (continued)

Description	Notes
	Complex A brakes the β-O-4 bond in lignin model through a pathway that involves cleavage of the benzylic C–H bond, complex B brakes the C–C bond through a pathway that do not involve the benzylic C–H bond

Scheme 10.5 Oxidation of phenolic lignin model compounds in presence of catalyst A and B (Adapted with permission from Ref. [21], Copyright 2012 by John Wiley & Sons, Inc. http://dx.doi.org/10.1002/anie)
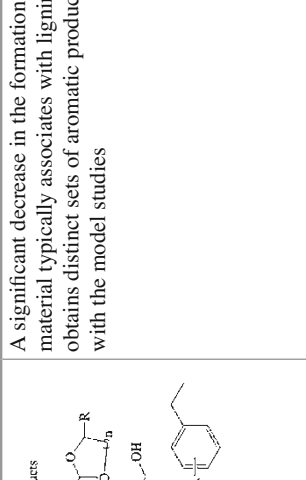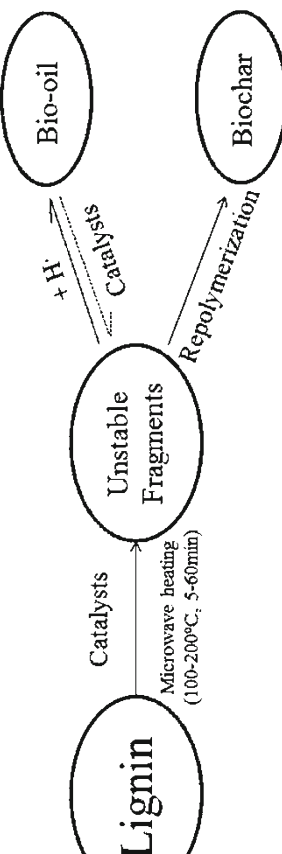
A rate-limiting elimination step involves both a base (formate) to remove the proton and an acid (formic acid) to assist in the loss of the formate as a leaving group
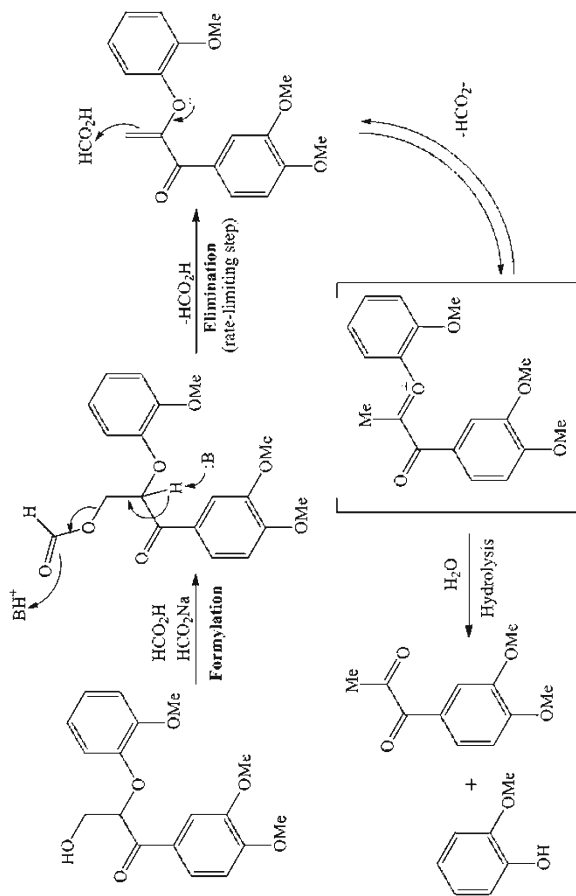
Scheme 10.6 Mechanism for cleavage of C–O linkage (Adapted by permission from Macmillan Publishers Ltd: Nature Ref. [50], Copyright 2014. http://dx.doi.org/10.1038/nature13867)

(continued)

Table 10.2 (continued)

Description	Notes
Model compound studies **Application for lignin**	A significant decrease in the formation of insoluble material typically associates with lignin acidolysis and obtains distinct sets of aromatic products in agreement with the model studies

Scheme 10.7 Formation of aromatic monomers from lignin and model compounds by in situ conversion of reactive intermediates in the acid (Adapted with per-mission from Ref. [11], Copyright 2015 American Chemical Society. http://dx.doi.org/10.1021/jacs.5b03693)

	Some unstable fragments are hydrogenated by the solvent-derived hydrogen to liquid products (bio-oil), while a part of liquid products are converted into the unstable fragments again in the reaction conditions

Scheme 10.8 Schematic for hydrogenolysis of lignin assisted by microwave heating (Adapted with permission from Ref. [58], Copyright 2012 by John Wiley & Sons, Inc. http://dx.doi.org/10.1002/cctc.201200616)

formic acid/water reaction system using bifunctional Ru/Al$_2$O$_3$, Rh/Al$_2$O$_3$, Pd/Al$_2$O$_3$ catalysts. The alumina support played an important role in the de-polymerization of lignin due to its Lewis acid sites that lead to an increase in the amount of low molecular weight compounds. Ru gave the highest amount of highly hydrodeoxygenated monomers compared with Rh and Pd. Only lignins used in acid reaction media were suitable for these bifunctional catalyst.

Liguori and Barth [34] used formic acid as the hydrogen source in combination with a palladium catalyst and Nafion® SAC-13 as a solid acid catalyst with water as reaction medium for catalysed depolymerisation of lignin to phenols. The dominant products were guaiacol, pyrocatechol and resorcinol after 2 h reaction at 300 °C. It was found that Nafion SAC-13, acted as a Brønsted acid favouring hydrogenolysis over aromatic ring hydrogenation and had a synergic effect with palladium. However, under identical reaction conditions, the model compounds were hydrodeoxygenated and hydrogenated. Wang and Rinaldi [62] carried out the hydrodeoxygenation of phenols into arenes in the presence of Raney Ni and β-zeolite using 2-propanol as an H-donor in n-C$_{16}$H$_{34}$ as solvent.

Almost all the catalysts used for hydrogen-donor solvent system are heterogeneous catalysts. The hydrogenolysis over noble metal catalysts like Pt, Ru, Rh, Pd always lead to fully hydrogenated aromatic rings in lignin-model compounds leading to cyclic alcohols and cycloalkanes and is often carried out in high temperature and high pressure. However, the hydrogenolysis of lignin over cheap and active transition metals (e.g. Ni, Cu) catalyst mainly involve hydrogenolysis reaction in mild conditions (selectively cleavage of C–C and C–O bonds in lignin without affecting the aromatic rings). Both zeolite and Al$_2$O$_3$ have a synergic effect with metals in lignin depolymerisation and this leads to a higher yield of target products. High hydrogen pressures in the hydrogen-donor solvent system do not seem to have any significant influence on lignin depolymerisation yields. Basic solvents (e.g., methanol, 1,4-dioxane, and THF) markedly reduce the catalytic activity for hydrogenation of aromatic products, but do not affect the hydrogenolysis of ether bonds, and improve the selectivity for phenols from lignin [63]. It can be concluded that the solvent system greatly influence the product distribution in lignin depolymerization.

10.2.3 Hydrogen-Involved System

Noble metal catalysts, such as Pd, Pt, Ru and Rh, exhibit outstanding catalytic properties in hydrogen-involved pressurized systems. Ohta and co-workers [40] reported aqueous-phase hydrodeoxygenation of phenols on carbon-supported Pt catalysts at 280 °C with the addition of H$_2$. The Pt/AC(N) could be reused without loss of the catalytic activity and gave yields of propylcyclohexane as high as 97 %. Ye and co-workers [70] reported on the hydrogenolysis of lignin (Corn stalk lignin/Bamboo lignin/Klason lignin) to 4-ethylphenolics that was carried out in ethanol/water as solvent, with Ru/C, Pd/C and Pt/C as catalysts at 275 °C in the presence of H$_2$. It

was found that 2.0 MPa initial hydrogen pressure was enough for hydrogenolysis of monomeric intermediates, *p*-hydroxyphenyl (H) type units and complex linkages resulting in higher yield of 4-ethylphenolics from corn stalk lignin. Ye and co-workers [24] also reported the hydrogenation of alkali lignin in dioxane/water in the presence of Pd/C catalyst under hydrogen atmosphere. The total hydroxyl, phenolic hydroxyl and alcoholic hydroxyl was increased about 64.2%, 37.1% and 89.6%, respectively, while carbonyl and carboxyl was decreased as 43.5% and 53.4%.

Lee and co-workers [30] reported on the hydrodeoxygenation of guaiacol using bifunctional catalysts of metal nanoparticles supported on acidic matrices (Rh/SiO$_2$-Al$_2$O$_3$ and Ru/SiO$_2$-Al$_2$O$_3$) in *n*-decane solvent with the addition of H$_2$. The amount of the remaining 2-methoxycyclohexanol with a hydrogenated cyclohexyl ring increased as the acidity of catalyst decreased. Thus, hydrogenation of aromatic rings on metal catalysts and the deoxygenation on metal-deposited acidic supports were occurred and a chemical pathway for guaiacol to hydrodeoxygenated products was proposed from the well-known pathway (guaiacol→phenol→hydrodeoxygena ted products) (Table 10.2: Scheme 10.3). Nimmanwudipong and co-workers [39] determined an extensive reaction network for the conversion of guaiacol into phenol, catechol, and 3-methylcatechol catalyzed by Pt/γ-Al$_2$O$_3$ with H$_2$ at 300 °C. Three major reactions occurred: hydrogenolysis (including hydrodeoxygenation), hydrogenation, and transalkylation. Metal functionalized catalyst of the two former reactions, while alumina support promoted the latter at the high temperatures (ca. 300 °C). The selectivity for hydrodeoxygenation increased as the partial pressure of H$_2$ increased.

Parsell and co-workers [48] described a bimetallic Pd/C and Zn catalytic system that could achieve selective hydrodeoxygenation of monomeric lignin surrogates, together with the cleavage of β-O-4 linkages in dimeric lignin model complexes and synthetic lignins. The benzyl alcohol and aldehyde groups could be selectively deoxygenated in good yields without hydrogenation of the phenyl ring in presence of both Pd/C and Zn^{2+}. The hydrogenation of the aromatic ring in methanol was suppressed while aromatic ring was hydrogenated to cyclohexanol in CH$_2$Cl$_2$. A mechanistic hypothesis for the synergy between Zn^{2+} and Pd is presented in Table 10.2: Scheme 10.4.

Li and co-workers [33] reported on catalytic conversion of raw woody biomass into chemicals over a carbon supported Ni-W$_2$C catalyst at 235 °C in methanol/ethylene glycol as a solvent with H$_2$. Lignin component was selectively converted to different monophenols with a yield of 46.5% (based on lignin). Pd-based catalysts favored lignin hydrogenation to the hydroxyl group contained products (such as guaiacylpropanol, and syringylpropanol), while NiW$_2$C/AC and other catalysts facilitated the dehydroxylation to produce guaiacylpropane and syringylpropane.

Zhang and co-workers [71] reported on a series of bimetallic Ni$_{85}$M$_{15}$ (M=Ru, Rh, and Pd) catalysts that were effective in the hydrogenolysis of lignin model compounds and organosolv lignin in water at 130 °C with H$_2$. The Ni$_{85}$M$_{15}$ bimetallic catalyst was more active and selective compared with the single-metal catalysts as
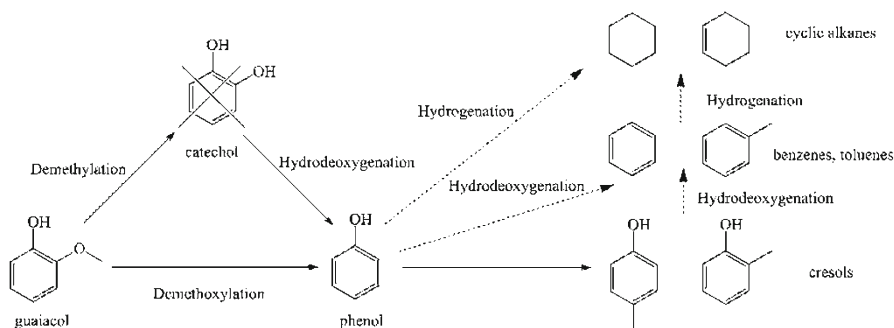
Fig. 10.4 Hydrogenolysis pathways of guaiacol (Adapted with permission from Ref. [26], Copyright 2013 by John Wiley & Sons, Inc.)

evident from the high fraction of surface atoms and turn-over-frequency (TOF). The hydrogenation of the aromatic ring was greatly inhibited by $Ni_{85}Ru_{15}$ catalyst compared with that of the pure Ru catalyst since the former gave high yields of aromatic monomeric compounds. When H_2 pressure was larger than 15 bar, yield of both monomer and dimer decreased due to the high coverage of hydrogen on catalyst surface that most likely inhibited the adsorption of substrates.

Jongerius' group [25–27] achieved a two-step approach for lignin depolymerization by different catalysts. The hydrodeoxygenation (HDO) of mono-aromatic lignin model compounds on a sulfided $CoMo/Al_2O_3$ catalyst in dodecane at 300 °C and 50 bar H_2 gave the products of low oxygen content as well as demethylated and ring methylated products. Hydrodeoxygenation of guaiacol on carbon-nanofiber-supported (CNF) W_2C and Mo_2C catalysts at 55 bar hydrogen pressure in dodecane gave products of phenol and cresols were proposed. As observed for the conversion of guaiacol to phenol on sulfided $CoMo/Al_2O_3$, the reaction involved sequential demethylation (DME) and HDO steps. However, the conversion of guaiacol to phenol on carbon-nanofiber-supported (CNF) W_2C and Mo_2C catalysts did not involve sequential DME and HDO steps but a direct demethoxylation pathway (Fig. 10.4). It was confirmed that Lewis acid sites on alumina-supported catalysts gave rise to catalytic DME activity.

A two-step approach for the conversion of organosolv, Kraft and sugarcane bagasse lignin to aromatics was proposed [25]. The first step is the lignin depolymerization in a liquid phase reforming (LPR) reaction over a Pt/γ-Al_2O_3 and NaOH in ethanol-water under Ar. The second step was hydrodeoxygenation (HDO) of the lignin-derived oil in dodecane under 50 bar hydrogen over $CoMo/Al_2O_3$ and Mo_2C/CNF. 25 % of the total collected monomeric products (9 %) was composed of the oxygen-free products, most of which cannot be obtained through direct HDO process of lignin.

Sergeev and Hartwig [52] reported on the hydrogenolysis of aromatic C–O bonds in alkyl aryl and diaryl ethers that form exclusively arenes and alcohols. This process was catalyzed by a soluble nickel carbene complex in *m*-xylene and NaO'Bu solvent under 1 bar of hydrogen at temperatures of 80–120 °C. The favorable effect of the strong base in the hydrogenolysis could lead to the formation of anionic nickel complexes that were more active for the cleavage of the C–O bonds or for activation of coordinated dihydrogen. No detectable products from hydrogenation of the arene ring were observed.

Both heterogeneous catalysts and homogeneous catalysts can be efficient for lignin depolymerisation in hydrogen-involved systems. The hydrogenolysis over noble metal catalysts leads to fully hydrogenate the aromatic rings giving cyclic alcohols and cycloalkanes of high temperatures and high pressures. The hydrogenolysis of lignin over active transition metals mainly involves hydrogenolysis reaction in mild conditions. The Lewis acid sites of Al_2O_3 or other supports may have an important effect on lignin depolymerisation, leading to the change of pathway and product distribution. The synergistic and bimetallic catalysts seem to be more efficient due to synergistic effects. The results also underpin the importance of H_2 as a reagent for deoxygenation. Hydrogenation of the aromatic ring in methanol is suppressed due to the competitive donor for hydrogen from methanol and H_2 which emphasizes that the solvent is important for molecular hydrogen reaction systems.

10.2.4   Oxidativelysis

Oxidative depolymerization of lignin is an efficient strategy applied to lignin depolymerization for producing polyfunctional aromatic compounds. The oxidative cracking reaction includes the cleavage of the aryl ether bonds, carbon-carbon bonds, or other linkages within the lignin. A number of studies have concentrated on the cleavage of the aryl ether bonds, carbon-carbon bonds in the oxidative depolymerization of lignin model compounds. Nitrobenzene, metal oxides, molecular oxygen, and hydrogen peroxide have been considered as effective oxidative reagents. Aromatic aldehydes and carboxylic acids are the main products in oxidative depolymerization of lignin with different kinds of catalyst being used for homogeneous systems. Catalysts used in most oxidative depolymerization reactions to produce specific products even achieve chemoselective oxidation of specific linkages for which the most widely used for lignin oxidation can be divided into four types: organometallic catalysts, metal-free-organic catalysts, acid/base catalysts, metal salts catalysts.

10.2.5 Organometallic Catalysts

A ligand is an ion or molecule (functional group) binded to a central metal atom to form a coordination complex. In comparison with some ligands, salen complexes are cheap, easy to synthesize and are relatively stable. Son and Toste [54] used a series of vanadium (V) complexes (e.g. A in Table 10.2: Scheme 10.5) bearing Schiff base ligands and air for the oxidative degradation of lignin model compounds at 80 °C in CD_3CN solvent. The reaction was a non-oxidative reaction, thus oxygen was not essential for the reaction. The catalyst favored benzylic oxidation to form the oxidation product over the desired C–O bond cleavage to form the phenol. Chan and Toste [8] used this vanadium-based chemistry to degrade organosolv lignin (from *M. giganteus*) into vanillin, syringic acid and syringaldehyde at 80 °C in air. Hanson's group [20] used a series of dipicolinate vanadium(V) complexes (e.g. B in Table 10.2: Scheme 10.5) to oxidize lignin model complexes at 100 °C in air, but this reaction was oxidative. It was also found that solvent had a big influence on reaction. The products of oxidation of 1, 2-diphenyl-2-methoxyethanol depended on the solvent: benzaldehyde and methanol were the major products in DMSO, while benzoic acid and methyl benzoate were the major products in pyridine solvent.

Hanson's group [21] compared the differences between the Toste studies and their own studies. It was found that Toste's catalyst A broke the C–O bond in lignin model through a pathway that involved cleavage of the benzylic C–H bond; complex B broke the C (alkyl)–C (phenyl) bond through a pathway that did not involve the benzylic C–H bond (Table 10.2: Scheme 10.5).

Hanson's group [19] used a $CuCl_2$ and 2,2,6,6-tetramethylpiperidine-1-oxyl radical (TEMPO) to oxidize lignin model complexes at 100 °C in air. Unlike the vanadium systems, the copper-catalyzed reactions were generally characterized by direct C–C bond cleavage of the lignin model compound without ketone or aldehyde intermediates. The phenolic group played an important role in the reaction pathway. In the absence of phenolic groups, vanadium catalyst B operated with high selectivity for C–H bond cleavage, whereas the copper catalyst system operated by C–C bond cleavage (Fig. 10.5a). The introduction of a phenolic functional group in the substrate enabled cleavage of the C_α–C_{aryl} bond with help of both vanadium and copper catalysts (Fig. 10.5b).

Parker and co-workers [47] worked for understanding the role of ligand structure on the activity of vanadium Schiff-base catalysts towards a non-phenolic β-O-4 model dimer. Electron-donating ligand substituents could produce the most selective catalyst. Catalytic activity was increased by the addition of bulky aliphatic substituents such as tert-butyl and adamantyl groups at the 3′-position of the phenolate ring in catalyst. However, the trityl-substituted complex was less active as a result of increased steric hindrance that prevented the model compound access to the metal center of catalyst.
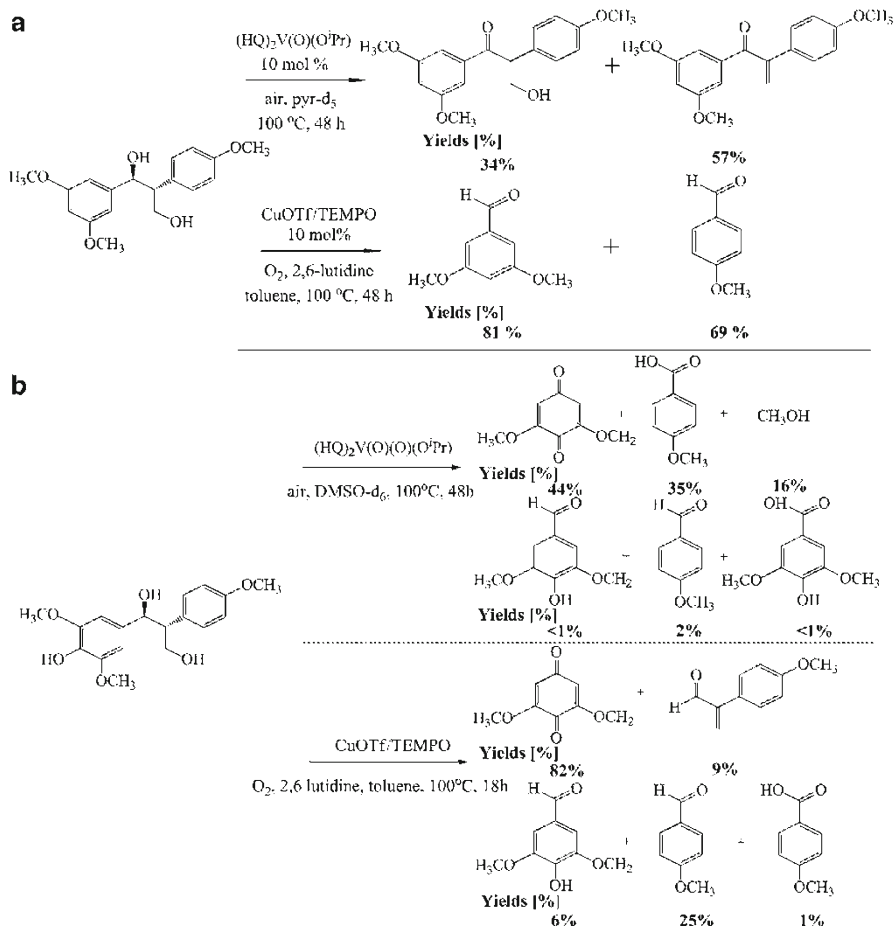
Fig. 10.5 (**a**) The aerobic oxidation of non-phenolic β-1 linkage lignin model compound in presence of vanadium and copper catalysts (Adapted with permission from Ref. [19], Copyright 2015 American Chemical Society); (**b**) The aerobic oxidation of phenolic β-1 linkage lignin model compound in presence of vanadium and copper catalysts (Adapted with permission from Ref. [19], Copyright 2015 American Chemical Society)

Haibach and co-workers [18] reported on the dehydroaryloxylation of aryl alkyl ethers using pincer iridium catalysts. This method represented a rare fully atom-economical method for ether C–O bond cleavage and high conversion (ca. 95 %) for a variety of substituted alkyl aryl ethers. Stein and co-workers [56] used ruthenium-triphos complexes in the redox-neutral C–C bond cleavage of the β-O-4 lignin linkage of 1,3-dilignol model compounds. The catalysts exhibited excellent catalytic activity and selectivity in toluene at 140 °C for various substitution patterns of the aromatic rings in the model compounds. It should be noted that the phenolic group

played an important role: (1) the secondary hydroxyl group (link with C_γ) was required for both the C–C and the C–O bond cleavage, and (2) the primary alcohol group (link with C_α) was essential for accessing to the C–C bond cleavage.

10.2.6 Metal-Free-Organic Catalysts

Rahimi and Stahl [49] proposed an efficient organocatalytic method for chemoselective aerobic oxidation of benzylic 2° alcohols (link with C_α) in the presence of unprotected 1° alcohols (link with C_γ) in lignin and a wide range of lignin model compounds. AcNH-TEMPO in combination with HNO_3 and HCl was used as co-catalysts in CH_3CN/H_2O solvent at 45 °C with 0.1 MPa O_2. Gao and co-workers [14] used nitrogen-containing graphene material (LCN) as an effective catalyst for the oxidation of β-O-4 and α-O-4 types of lignin model compounds in the presence of tertbutyl hydroperoxide (0.1 MPa O_2, 80 °C), to provide aromatic aldehydes, acids and other organic chemicals in high yield. This reaction followed a free-radical mechanism. O*rtho*-methoxy substituents weakened the stability of the aromatic ring, which was evidenced by the free-radical trapping experiments.

10.2.7 Acid/Base Catalysts

NaOH and KOH are used most frequently in the alkaline oxidation of lignin. Maziero and co-workers [37] reported that the lignin oxidized over NaOH catalyst (pH = 13.3) with H_2O_2 at 98 °C had the highest fragmentation, oxidation degree and stability. Demesa and co-workers [9] studied the partial wet oxidation of alkali lignin over NaOH catalyst (pH = 11) with O_2. A maximum total yield of products (formic acid, acetic acid, succinic acid, oxalic acid, and glutaconic acid) of 44 % was obtained at 200 °C. It was found that a higher reaction temperature and oxygen partial pressure improved the yield of the products formed but also leaded to the repolymerizarion of lignin fragments. Wu and co-workers [65] reported that the aromatic components of lignin model compounds and lignins were degraded in KOH with H_2O_2 or $K_2S_2O_8$ as solvent. A maximum total yield of products (MeOH, formate, carbonate, and oxalate) of 15 % was obtained at 60 °C.

Azarpira and co-workers [1] reported that β-ether dimer and oligomer model compounds and a milled wood lignin sample from Loblolly pine were catalytically oxidized by 1,10-phenanthroline and copper (II) sulfate pentahydrate and NaOH. The reaction was conducted in the presence of O_2 at 80 °C in methanol. Different mechanisms were possibly involved in the alkaline oxidation reaction of the compounds due to the phenolic hydroxyl group *para* to the side chain (link with 4′-position C).

10.2.8 Metal Salt Catalysts

Rohr's group [60, 61] studied lignin oxidation by polyoxometalate (POMs) catalysts. POMs are soluble in aqueous and organic media and its redox potential is high enough to oxidize typical lignin subunits and low enough to be reoxidized by molecular oxygen. Voitl and Rohr [61] developed a novel method to oxidatively degrade lignin using aqueous POMs in the presence of alcohols for the purpose of converting Kraft lignin into chemicals. The oxidation of Kraft lignin in acidic media using oxygen yielded twice as many monomers in the presence of the catalyst $H_3PMo_{12}O_{40}$. Then, the depolymerization of Kraft lignin with $H_3PMo_{12}O_{40}$ as a homogeneous catalyst was carried out at 170 °C in methanol/water as the solvent [60]. Extracted products containing vanillin (3.5 wt %) and methyl vanillate (3.5 wt %) were recovered with a yield of 65 wt %. The sum of all quantified products, as well as the amount of consumed oxygen, reached constant levels after five runs, and no indication of catalyst deactivation was found.

Transition metal salts are another sort of homogeneous catalysts for lignin oxidation due to the broad spectrum of cation redox potential. Werhan and Rohr [64] started to study the performance of different transition metal salts ($CuSO_4$, $FeCl_3$, $CuCl_2$, $CoCl_2$) in the acidic oxidation of kraft lignin. The maximum yield of vanillin obtained in the experiments was always higher for the transition metal salts than for the POM. $CoCl_2$ turned out to be the best of the investigated catalysts regarding the total yield of vanillin and methyl vanillate, with a maximum yield of 6.3 % at 170 °C. Napoly and co-workers [38] reported on the oxidation of Kraft lignin using different metal salt catalysts ($Fe_2(SO_4)_3$, $Fe(NO_3) \cdot 9H_2O$, $Mn(SO_4) \cdot H_2O$, $Bi_2(SO_4)_3$, $Bi(NO_3)_3 \cdot 5H_2O$, H_2WO_4, and $Na_2WO_4 \cdot 2H_2O$)/H_2O_2 in acetone/water at 45 °C. The $Na_2WO_4 \cdot 2H_2O$ catalyst yielded four vanillin-based monomers (vanillin, acetovanillone, vanillic acid, and guaiacol). It should be noted that the effect of ultrasound irradiation in the reaction leads to high oxidative coupling of phenoxy radicals issuing from lignin polymerization.

Oxidativelysis strategies can be useful in the production aromatic aldehydes and carboxylic acids. However, the effect of ligand structure of different metal complex catalysts is still uncertain along with interaction in the solvent system. The method for chemoselective aerobic oxidation of secondary benzylic alcohols within lignin model compounds and natural lignins proposed by Rahimi and Stahl [49] can be a potential method for understanding the mechanisms.

10.2.9 Two-Step LDP

Two-step strategies, such as oxidation followed by a bond cleavage, are attracting much attention due to the high yields of low-molecular-weight aromatics from lignin. Rahimi and Stahl reported on the depolymerization of an oxidized lignin in aqueous formic acid under mild conditions to give yields of low-molecular-weight aromatics [50]. The yield of structurally identified, monomeric aromatics was 52 %
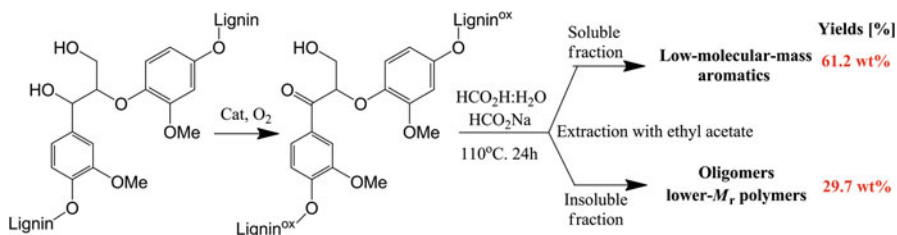
Fig. 10.6 Depolymerization of Aspen lignin in formic acid/formate reaction conditions (Adapted by permission from Macmillan Publishers Ltd: Nature Ref. [50], Copyright 2014. http://dx.doi.org/10.1038/nature13867)
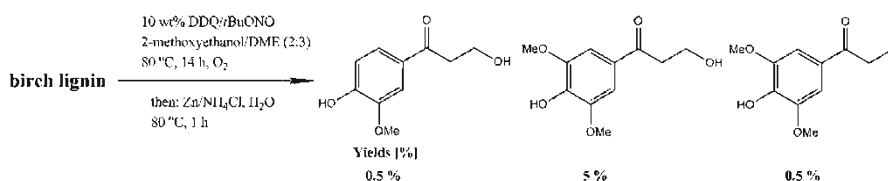
Fig. 10.7 Catalytic hydrothermal depolymerization of lignin and product distribution (Adapted with permission from Ref. [29], Copyright 2014 by John Wiley & Sons, Inc.)

of the original lignin that was converted to well-defined aromatic compounds which is the highest value reported to date [6]. The strategy involved: (1) initial selective oxidation of a secondary benzylic alcohol to a ketone, followed by activation of the linkage in the second step [49], (2) mediation by formate and formic acid, that was redox-neutral, that was, no formic acid was consumed in the process (Fig. 10.6). The C_α ketone was crucial in the extent of the reaction: no products from LDP were observed when the non-oxidized model compounds were subjected to the formic acid/formate reactions. The beneficial effect of lignin oxidation might be attributed to the ability of the benzylic carbonyl group to polarize the C–H bond and lower the barrier for the rate-limiting E2 elimination reaction. A rate-limited elimination step in Table 10.2: Scheme 10.6 was proposed, involving both a base (formate) to remove the proton and an acid (formic acid) to assist the loss of the formate.

Lancefield and Westwood reported the chemoselective catalytic oxidation of β-O-4 linkages in polymeric models and an actual lignin promoted by the DDQ/tBuONO/O_2 system. The oxidized β-O-4 linkage was then cleaved through the reaction with zinc [29]. The results showed that guaiacyl (G) units were oxidized more readily than syringyl (S) units, consistent with the reaction proceeding through a benzylic cation (Fig. 10.7).

Two advantages of this strategy are: (1) high selectivity for pure compounds production, (2) retention of functional groups in the major phenolic product. Jiang and co-workers [23] developed an approach to selectively convert lignin to monophenols in corncob residue, avoiding significant degradation of the cellulose component. High delignification was achieved in the H_2O-THF co-solvent system, and the conversion of lignin reached up to 89.8 % at 200 °C for 1.0 h. High yields of

monophenols (24.3 wt%) were obtained by the further reaction of the filtrate at 300 °C for 8.0 h without hydrogen addition.

Due to the formation of radicals in high temperature and pressure and/or C–C bond forming self-condensation reactions in acidic media, lignin depolymerisation usually generates a complex pool of re-condensed aromatics.

Toledano and co-workers [57] studied boric acid and phenol as capping agents in base-catalyzed lignin depolymerization. Phenol capping agent was used to prevent oligomerization reaction without inhibiting the demethoxylation and dealkylation reactions. Boric acid trapped base catalyzed depolymerization intermediates and restricted product formation and produced oligomers. Phenol capping agent was proved to favor phenolic compounds formation and avoid the repolymerization of produced fragments. Deuss and Barta [11] used the reactive intermediates in the acid-catalyzed depolymerization of lignin in situ conversion to aromatic monomers (Table 10.2: Scheme 10.7). Unstable compounds (mainly aldehyde products) were captured by the reaction with diols and in-situ catalytic hydrogenation or decarbonylation. Three kinds of aromatic compounds as acetals, ethanol and ethyl aromatics, and methyl aromatics were achieved in high yields.

Acetal formation with diols (Fig. 10.8a) and metal-catalyzed approaches to provide desirable simpler aromatics (Fig. 10.8b) and catalytic decarbonylation to obtain methyl-aromatics (Fig. 10.8c) confirm the methods for aldehyde stabilization. This strategy has potential for the production of renewable aromatic compounds from lignin and to stabilize fragments.

10.3 LDP Assisted by microwave Heating

Compared with conventional heating, microwave heating assists lignin depolymerization process through electromagnetic vibration [2, 7, 26]. Heat triggered by microwave irradiation penetrates into the bulk of the lignin sample, accelerating the degradation rate of the material at moderate conditions [41]. Low energy consumption, of microwave heating allows LDP to occur that can be classified as hydrogenolysis and oxidative processes (Table 10.3).

10.3.1 Hydrogenolysis

Different kinds of hydrogen-donor solvents such as indane, tetrahydronaphthalene, decahydronaphthalene, cyclohexane and isopropanol, glycol have been reported in hydrogenolysis of lignin by microwave heating. Li [31] studied the microwave-assisted degradation of wheat straw alkali lignin with glycol as solvent. A maximum yield of 13.5 % for monophenolic products was obtained and guaiacyl (G)-type phenolic compounds were the main product with 2-methoxy-4-methyl phenol yield being more than 50 % of the total monophenolic products. The monophenolic
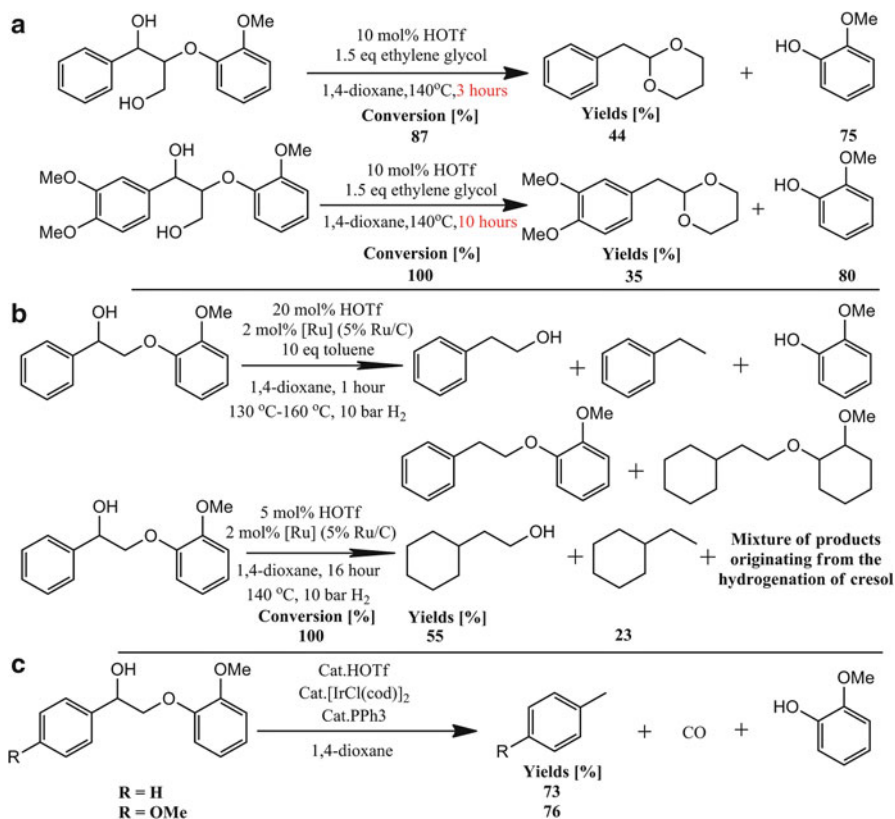
Fig. 10.8 (**a**) In situ acetal formation with ethylene glycol upon triflic acid-catalyzed cleavage of lignin model compounds (Adapted with permission from Ref. [11], Copyright 2015 American Chemical Society); (**b**) Catalytic in situ hydrogenation upon triflic acid-catalyzed cleavage of lignin model compounds (Adapted with permission from Ref. [11], Copyright 2015 American Chemical Society); (**c**) Catalytic in situ decarbonylation upon triflic acid-catalyzed cleavage of lignin model compounds (Adapted with permission from Ref. [11], Copyright 2015 American Chemical Society)

products yield increased first and then decreased with the reaction temperature increasing, more *p*-hydroxyphenyl (H)-type and syringyl (S)-type phenolic compounds observed at a relatively lower temperature (110 °C). Fu and co-workers [13] reported on a method for producing phenolic compounds with low molecular weight with hydrogen-donor solvents under microwave irradiation. The selected hydrogen-donor solvents were indane, tetrahydronaphthalene, decahydronaphthalene, cyclohexane and iso-propanol, the yield of phenolic compounds with low molecular weight could achieve respectively 18.1 %, 28.7 %, 1.8 %, 10.7 % and 9.1 %, analyzed by GC-FID. There is some other reports support the results. Xiong [67] studied lignin model compound benzyl phenyl ether (BPE) degradation with the assistance of microwave and hydrogen-donor solvents. The conversation rate of

Table 10.3 Lignin depolymerization in solvent systems assisted by microwave heating

Materials/Main products	Catalyst	Reaction conditions	LDP yield	Refs.
Black-liquor lignin; phenolic monomeric products	none	600 W, 110–180 °C, 5–90 min; Hydrogen donor: formic acid	64.08 %	[12]
Wheat straw alkali lignin; monophenol	none	800 W, 140 °C, 40 min; Hydrogen donor: formic acid; Ethanol	Ethanol improved the dissolution or dispersion of lignin	[43]
Wheat straw alkali lignin; monophenolic	H_2SO_4	120 °C, 30 min; glycol	13.47 % (G-type phenolic compounds)	[31]
Lignin; monophenolic compounds	Sulphuric/hydrochloric/p-toluene sulfonic acid	140–200 °C, 20–60 min; Hydrogen donor: indane/tetrahydronaphthalene/decahydronaphthalene/cyclohexane/isopropanol	18.1 %, 28.7 %, 1.8 %, 10.7 % and 9.1 % (in different solvent)	[13]
Lignin model compound benzyl phenyl ether (BPE)	Formic/benzoic/sulfuric acid/p-toluene sulfonic acid	150 °C, 10–40 min; Hydrogen donor: indane/tetrahydronaphthalene/isopropanol/glycol/cyclohexane/DMF	~90 % conversation (indane or tetrahydronaphthalene as solvent)	[67]
Wheat straw alkali lignin; monophenol	H_2SO_4	300 W, 120 °C, 40 min; Hydrogen donor: phenol; Ethylene glycol	13.61 %	[41]
Organosolv olive tree pruning lignin; monophenol	H_2SO_4	130/155/180 °C, 5/10/15 min; Hydrogen donor: polyethylene glycol and glycerol	A liquefaction yield of 99.07 %	[51]
Corn stover	H_2SO_4	600 W, 160 °C, 5–30 min; Hydrogen donor: ethylene glycol	20 min is optimal reaction time for microwave assisted liquefaction with the minimal residue content of 4.85 %	[66]
Organosolv olive tree pruning lignin; phenolic products	Ni 10 % Al-SBA-15	400 W, 150 °C, 30 min; Hydrogen donor: tetralin/isopropanol/glycerol/formic acid	$5.9 \text{ mg/g}_{lignin}^{-1}$	[58]

Feedstock	Catalyst	Conditions	Results	Reference
Organosolv olive tree pruning lignin; phenolic products	Ni/Pd/Pt/Ru AlSBA-15	400 W, 150 °C, 30 min; Hydrogen donor: tetralin/formic acid	A maximum yield of 30 % bio-oil	[59]
Black-liquor lignin; monophenol	Modified HUSY	600 W, 130 °C, 30 min; Hydrogen donor: formic acid	Liquid products yield : 88.28 %	[53]
Soda lignin	NaOH	300 W, 75 °C, pH=11.0, 30 min, H_2O_2	Degraded lignin contained higher content of phenolic hydroxyl and lower content of methoxyl	[44]
Lignin model compound: apocynol	SBA-15	300 W, 150 °C, 5–45 min, H_2O_2; Acetonitrile	SBA-15 was an efficient catalyst for oxidation of apocynol	[2]
Lignin model compound: apocynol	La/SBA-15	300 W, 150 °C, 5–40 min, H_2O_2; Acetonitrile	Apocynol complete degradation in 40 min	[3]
3-methoxy-4-hydroxybenzyl alcohol	La/SBA-15	200 W, 5–40 min, H_2O_2; Acetonitrile	68 % conversion	[15]
4-hydroxy-1-phenylpropane	La/SBA-15	200 W, 5–40 min, H_2O_2; Acetonitrile	70.5 % conversion	[17]
Organosolv beech wood lignin	La/SBA-15	200 W, 5–30 min, H_2O_2; NaOH solution	Vanillin: 9.94%; Syringaldehyde: 15.66 %	[16]
lignin model compounds	14 types of metal salts	50 W, 80 °C, 10 min, H_2O_2; Acetonitrile/dioxane/methanol/ethanol	88 % conversion	[46]

BPE was close to 90 % in 40 min when indane or tetrahydronaphthalene as solvent was used which was higher than isopropanol and glycol, whereas cyclohexane and DMF were ineffective.

Formic acid is the most common hydrogen-donor solvent. Dong and co-workers [12] studied microwave-assisted degradation of black-liquor lignin with formic acid and achieved the maximum liquid products yield of 64.1 %. It was found that ethanone, 1-(4-hydroxy-3-methoxyphenyl), vanillin and ethanone, 1-(4-hydroxy −3, 5-methoxyphenyl) were the main phenolic monomeric products and the bio-oil was primarily composed of monomers, dimers and trimers analyzed by MALDI-TOF MS. Ouyang and co-workers [43] studied liquefaction of wheat straw lignin in formic acid with the presence of ethanol. Ethanol could improve the dissolution or dispersion of lignin and make the reaction mixture a homogeneous phase, resulting in an enhancement of the liquefaction efficiency.

Different acids (sulphuric acid, hydrochloric acid and *p*-toluene sulfonic acid) have been employed for lignin degradation in dihydroanthracene [13], for which yields of phenolic compounds with low molecular weights could be achieved as 12.4 %, 13.2 %, and 21.5 % respectively. Xiao and Han [66] reported a comparative study on conventional and microwave-assisted liquefaction of corn stover by using ethylene glycol (EG) as liquefacient and sulfuric acid as catalyst. It was found that the depolymerisation reaction of lignocellulosic components in corn stover was greatly accelerated by microwave heating compared to that of LDP by conventional heating.

Many different kinds of catalysts also have been involved in the hydrogen-donor solvents system, which could promote the degradation of lignin. Acid have been extensively studied as catalyst in the degradation of lignin due to strongly acidic condition favoring β-ether linkage cleavage [45]. Sequeiros and co-workers [51] studied organosolv olive tree pruning lignin liquefied under microwave heating by using glycerol and polyethylene glycol (PEG) as solvents and sulphuric acid as catalyst to produce polyols with high content of reactive hydroxyl groups. The maximum liquefaction yield achieved 99.1 % and the liquefaction products had a hydroxyl number of 811.8 mg KOH/g. Ouyang and co-workers [45] studied the liquefaction of wheat straw alkali lignin with H_2SO_4 as catalyst and phenol as the hydrogen-donor reagent using different heating methods. They found that microwave irradiation could promote the cleavage of C–C bonds (such as an extra 29 % of C_{aryl}–C_α bond cleavage), enhancing the yield of monophenolic compounds from 0.92 to 13.6 % under the same conditions. The bond cleavage of the side chain mainly commenced on the C_α–C_β position of the lignin intermediates. Self-condensation of lignin-derived intermediates was inhibited by phenol as a hydrogen donor.

Toledano and co-workers [58] studied the depolymerisation of lignin under microwave irradiation with a series of hydrogen-donor solvents catalysed by Ni 10 % Al-SBA-15. The selected solvents were tetralin, isopropanol, glycerol and formic acid. The obtained phenolic monomeric products (including syringol, syringaldehyde, vanillin and aspidinol) were remarkably affected by the type of hydrogen-donor solvent and the optimal result obtained with formic acid (5.9 mg/

g_{lignin}^{-1}), where no biochar was produced compared to a maximum of 38 % biochar derived from LDP in tetralin. The relevant mechanism of microwave-assisted hydrogenolysis of lignin is shown in Table 10.2: Scheme 10.8 [58]. A number of unstable fragments were produced through the cleavage of ether linking to the carbon atom on α, β and γ position of side chain, the position 4 of a phenolic ring in an adjacent unit or carbon-carbon linkage at α, β and α, γ sites [58]. The produced unstable fragments were hydrogenated by the solvent donated hydrogen to generate liquid products (bio-oil) partially acting as the precursor for production of the unstable fragments.

Toledano and co-workers [59] studied lignin depolymerisation to simple aromatics assisted by microwave heating in presence of different metal supported nanoparticles on mesoporous Al-SBA-15 including nickel, palladium, platinum and ruthenium. A maximum yield of 30 wt% bio-oil primarily composed of monomers, dimers and trimers was obtained using formic acid as hydrogen-donor with the catalyst of Ni 10 % Al-SBA-15 solvent. Demethoxylation reactions did not take place when formic acid was employed as hydrogen-donor solvent in lignin depolymerisation reactions and no bio-char was generated in the experiments with formic acid as hydrogen-donor solvent. Shen and co-workers [53] studied the microwave-assisted catalytic solvolysis of lignin in formic acid concerning the addition of HUSY catalysts modified by oxalic acid. All the modified catalysts could promote the yield of bio-oil, achieving the maximum value of 88.3 % for HUSY-0.2 M catalyst.

Microwave heating in the hydrogenolysis of lignin or lignin model compounds in solvent systems can produce value-added aromatics with or without catalysts. It was reported that microwave irradiation might facilitate the repolymerization reactions of the unstable fragments to generate tar or biochar [58]. The liquefaction rate and production was highly improved by microwave heating compared to that of conventional heating. The distribution of product molecular weight from LDP assisted by microwave is remarkably narrower than that by the conventional heating.

10.3.2 Oxidativelysis

Oxidative degradation of lignin or lignin model compounds assisted by microwave heating is considered to be another important alternative for aromatic compounds production. Ouyang and co-workers [44] studied the oxidative degradation of soda lignin assisted by microwave using H_2O_2 as oxidant. The microwave irradiation efficiently facilitated the degradation of the lignin to produce the compounds with high molecular weight. Sushanta and Badamali [2, 3] studied the oxidative degradation of a lignin model phenolic monomer (apocynol) catalyzed by SBA-15 or Co (salen)/SBA-15 using H_2O_2 as oxidant. SBA-15 and Co (salen)/SBA-15 were highly efficient for catalytic oxidation, of apocynol (nearly 100 % conversion) after 40 min microwave heating, compared to a poor conversion of 57 % after 24 h under conventional heating. Gu and co-workers [15–17] studied the oxidative degradation of

organosolv beech wood lignin and two lignin model phenolic monomers (3-methoxy-4-hydroxybenzyl alcohol and 4-hydroxy-1-phenylpropane) catalysed by La/SBA-15 using H_2O_2. The highest yield of vanillin obtained was 9.9 % and that of syringaldehyde was 15.7 %. A 68 % conversion of 3-methoxy-4-hydroxybenzyl alcohol to vanillin or other undetectable by-products was obtained with microwave heating.

Pan and co-workers [46] reported that microwave heating could promote the oxidation of lignin model compounds (such as 2-phenoxy-1-phenylethanol, vanillyl alcohol, and 4-hydroxybenzyl alcohol) in presence of 14 metal salts. The degradation of the lignin model compounds was found to O.K. as is by the acidity of the solution containing metal salts. The conversion of 2-phenoxy-1-phenylethanol was 88 % in the mixed solvent of acetonitrile and H_2O. $CrCl_3$ and $MnCl_2$ were estimated to be the effective metal-salt catalysts for the degradation of 2-phenoxy-1-phenylethanol, vanillyl alcohol, and 4-hydroxybenzyl alcohol.

10.4 Conclusions and Future Outlook

Lignin depolymerization (LDP) in solvent systems is attracting much attention for producing value-added chemicals. Relevant methods either hydrogenolysis or oxidativelysis of lignin concentrate on the selection of heating method, solvent, catalyst and reaction conditions for production of specific aromatic compounds. Two-step LDP technologies are proposed for enhancing the production of aromatic compounds and avoiding the repolymerization of the derived fragments. Considering the ambiguity of LDP mechanism and the limited yield of aromatic compounds from LDP, several issues are needed to be addressed for the application of LDP technology: (1) identification of oligomers from LDP for specifying the inherent depolymerization mechanism; (2) synthesis of lignin model compounds representing the natural information in the fragments (both monomers and oligomers) derived from LDP, (3) identification of the precursors from LDP contributing to be repolymerized to tar or char; (4) new strategies to restrict the repolymerization of the fragments from LDP; (5) separation of specific aromatic compounds from LDP system; (6) stability of the catalyst involved and how to maintain its activity during LDP.

References

1. Azarpira A, Ralph J, Lu F. Catalytic alkaline oxidation of lignin and its model compounds: a pathway to aromatic biochemicals. BioEnergy Res. 2013;7:78–86.
2. Badamali S, Clark J, Breeden S. Microwave assisted selective oxidation of lignin model phenolic monomer over SBA-15. Catal Commun. 2008;9:2168–70.

3. Badamali S, Luque R, Clark J, Breeden S. Microwave assisted oxidation of a lignin model phenolic monomer using Co(salen)/SBA-15. Catal Commun. 2009;10:1010–3.

4. Barta K, Matson TD, Fettig ML, Scott SL, Iretskii AV, Ford PC. Catalytic disassembly of an organosolv lignin via hydrogen transfer from supercritical methanol. Green Chem. 2010;12:1640.

5. Barta K, Warner GR, Beach ES, Anastas PT. Depolymerization of organosolv lignin to aromatic compounds over Cu-doped porous metal oxides. Green Chem. 2014;16:191–6.

6. Bruijnincx PCA, Weckhuysen BM. Biomass conversion: lignin up for break-down. Nat Chem. 2014;6:1035–6.

7. Bu Q, Lei H, Ren S, Wang L, Zhang Q, Tang J, Ruan R. Production of phenols and biofuels by catalytic microwave pyrolysis of lignocellulosic biomass. Bioresour Technol. 2012;108:274–9.

8. Chan JMW, Bauer S, Sorek H, Sreekumar S, Wang K, Toste FD. Studies on the vanadium-catalyzed nonoxidative depolymerization of Miscanthus giganteus-derived lignin. ACS Catal. 2013;3:1369–77.

9. Demesa AG, Laari A, Turunen I, Sillanpää M. Alkaline partial wet oxidation of lignin for the production of carboxylic acids. Chem Eng Technol. 2015;38:2270–8.

10. Deuss PJ, Barta K. From models to lignin: transition metal catalysis for selective bond cleavage reactions. Coord Chem Rev. 2016;306:510–32.

11. Deuss PJ, Scott M, Tran F, Westwood NJ, De Vries JG, Barta K. Aromatic monomers by in situ conversion of reactive intermediates in the acid-catalyzed depolymerization of lignin. J Am Chem Soc. 2015;137:7456–67.

12. Dong C, Feng C, Liu Q, Shen D, Xiao R. Mechanism on microwave-assisted acidic solvolysis of black-liquor lignin. Bioresour Technol. 2014;162:136–41.

13. Fu J, Peng J, Li X. A method of producing phenolic compounds with low molecular weight with hydrogen-donating solvents under microwave irradiation. 2012.

14. Gao Y, Zhang J, Chen X, Ma D, Yan N. A metal-free, carbon-based catalytic system for the oxidation of lignin model compounds and lignin. ChemPlusChem. 2014;79:825–34.

15. Gu X, He M, Shi Y, Li Z. LA-containing SBA-15/H2O2 systems for the microwave assisted oxidation of a lignin model phenolic monomer. Maderas Ciencia y Tecnología. 2010;12:181–8.

16. Gu X, He M, Shi Y, Li Z. La-modified SBA-15/H2O2 systems for the microwave assisted oxidation of organosolv beech wood lignin. Maderas Ciencia y Tecnología. 2012;14:31–41.

17. Gu X, He M, Shi Y, Li Z. Production of aromotic aldehyde by microwave catalytic oxidation of a lignin model compound with La-containing SBA-15/H_2O_2 systems. BioResources. 2010;5:2029–39.

18. Haibach MC, Lease N, Goldman AS. Catalytic cleavage of ether C–O bonds by pincer iridium complexes. Angew Chem. 2014;53:10160–3.

19. Hanson SK, Baker RT. Knocking on wood: base metal complexes as catalysts for selective oxidation of lignin models and extracts. Acc Chem Res. 2015;48:2037–48.

20. Hanson SK, Baker RT, Gordon JC, Scott BL, Thorn DL. Aerobic oxidation of lignin models using a base metal vanadium catalyst. Inorg Chem. 2010;49:5611–8.

21. Hanson SK, Wu R, Silks AL. C–C or C–O bond cleavage in a phenolic lignin model compound: selectivity depends on vanadium catalyst. Angew Chem Int Ed. 2012;51:3410–3.

22. Huang S, Mahmood N, Tymchyshyn M, Yuan Z, Xu C. Reductive depolymerization of Kraft lignin for chemicals and fuels using formic acid as an in-situ hydrogen source. Bioresour Technol. 2014;171:95–102.

23. Jiang Z, He T, Li J, Hu C. Selective conversion of lignin in corncob residue to monophenols with high yield and selectivity. Green Chem. 2014;16:4257.

24. Jie-Wang Y, Gui-Zhen F, Chun-De J. Hydrogenation of alkali lignin catalyzed by Pd/C. APCBEE Procedia. 2012;3:53–9.

25. Jongerius AL, Bruijnincx PCA, Weckhuysen BM. Liquid-phase reforming and hydrodeoxygenation as a two-step route to aromatics from lignin. Green Chem. 2013;15:3049.

26. Jongerius AL, Gosselink RW, Dijkstra J, Bitter JH, Bruijnincx PCA, Weckhuysen BM. Carbon nanofiber supported transition-metal carbide catalysts for the hydrodeoxygenation of guaiacol. ChemCatChem. 2013;5:2964–72.

27. Jongerius AL, Jastrzebski R, Bruijnincx PCA, Weckhuysen BM. CoMo sulfide-catalyzed hydrodeoxygenation of lignin model compounds: an extended reaction network for the conversion of monomeric and dimeric substrates. J Catal. 2012;285:315–23.

28. Kloekhorst A, Shen Y, Yie Y, Fang M, Heeres HJ. Catalytic hydrodeoxygenation and hydrocracking of Alcell® lignin in alcohol/formic acid mixtures using a Ru/C catalyst. Biomass Bioenergy. 2015;80:147–61.

29. Lancefield CS, Ojo OS, Tran F, Westwood NJ. Isolation of functionalized phenolic monomers through selective oxidation and C–O bond cleavage of the β-O-4 linkages in lignin. Angew Chem Int Ed. 2015;54:258–62.

30. Lee CR, Yoon JS, Suh Y-W, Choi J-W, Ha J-M, Suh DJ, Park Y-K. Catalytic roles of metals and supports on hydrodeoxygenation of lignin monomer guaiacol. Catal Commun. 2012;17:54–8.

31. Li B. Study on liquefaction and degradation of wheat straw alkali lignin assisted by microwave irradiation. Guangzhou: South China University of Technology; 2013.

32. Li C, Zhao X, Wang A, Huber GW, Zhang T. Catalytic transformation of lignin for the production of chemicals and fuels. Chem Rev. 2015;115:11559–624.

33. Li C, Zheng M, Wang A, Zhang T. One-pot catalytic hydrocracking of raw woody biomass into chemicals over supported carbide catalysts: simultaneous conversion of cellulose, hemicellulose and lignin. Energy Environ Sci. 2012;5:6383–90.

34. Liguori L, Barth T. Palladium-Nafion SAC-13 catalysed depolymerisation of lignin to phenols in formic acid and water. J Anal Appl Pyrolysis. 2011;92:477–84.

35. Ma R, Hao W, Ma X, Tian Y, Li Y. Catalytic ethanolysis of kraft lignin into high-value small-molecular chemicals over a nanostructured α-molybdenum carbide catalyst. Angew Chem Int Ed. 2014;53:7310–5.

36. Matson TD, Barta K, Iretskii AV, Ford PC. One-pot catalytic conversion of cellulose and of woody biomass solids to liquid fuels. J Am Chem Soc. 2011;133:14090–7.

37. Maziero P, Neto MDO, Machado D, Batista T, Cavalheiro CCS, Neumann MG, Craievich AF, et al. Structural features of lignin obtained at different alkaline oxidation conditions from sugarcane bagasse. Ind Crop Prod. 2012;35:61–9.

38. Napoly F, Kardos N, Jean-Gérard L, Goux-Henry C, Andrioletti B, Draye M. H2O2-mediated Kraft lignin oxidation with readily available metal salts: what about the effect of ultrasound? Ind Eng Chem Res. 2015;54:6046–51.

39. Nimmanwudipong T, Runnebaum RC, Block DE, Gates BC. Catalytic conversion of guaiacol catalyzed by platinum supported on alumina: reaction network including hydrodeoxygenation reactions. Energy Fuel. 2011;25:3417–27.

40. Ohta H, Kobayashi H, Hara K, Fukuoka A. Hydrodeoxygenation of phenols as lignin models under acid-free conditions with carbon-supported platinum catalysts. Chem Commun. 2011;47:12209.

41. Oliver Kappe C. Microwave dielectric heating in synthetic organic chemistry. Chem Soc Rev. 2008;37:1127–39.

42. Oregui Bengoechea M, Hertzberg A, Miletić N, Arias PL, Barth T. Simultaneous catalytic depolymerization and hydrodeoxygenation of lignin in water/formic acid media with Rh/Al2O3, Ru/Al2O3 and Pd/Al2O3 as bifunctional catalysts. J Anal Appl Pyrolysis. 2015;113:713–22.

43. Ouyang X, Huang X, Zhu Y, Qiu X. Ethanol-enhanced liquefaction of lignin with formic acid as an in situ hydrogen donor. Energy Fuel. 2015;29:5835–40.

44. Ouyang X, Lin Z, Deng Y, Yang D, Qiu X. Oxidative degradation of soda lignin assisted by microwave irradiation. Chin J Chem Eng. 2010;18:695–702.

45. Ouyang X, Zhu G, Huang X, Qiu X. Microwave assisted liquefaction of wheat straw alkali lignin for the production of monophenolic compounds. J Energy Chem. 2015;24:72–6.

46. Pan J, Fu J, Lu X. Microwave-assisted oxidative degradation of lignin model compounds with metal salts. Energy Fuel. 2015;29:4503–9.

47. Parker HJ, Chuck CJ, Woodman T, Jones MD. Degradation of β-O-4 model lignin species by vanadium Schiff-base catalysts: influence of catalyst structure and reaction conditions on activity and selectivity. Catal Today. 2015;269:40–7.

48. Parsell TH, Owen BC, Klein I, Jarrell TM, Marcum CL, Haupert LJ, Amundson LM, et al. Cleavage and hydrodeoxygenation (HDO) of C–O bonds relevant to lignin conversion using Pd/Zn synergistic catalysis. Chem Sci. 2013;4:806–13.

49. Rahimi A, Azarpira A, Kim H, Ralph J, Stahl SS. Chemoselective metal-free aerobic alcohol oxidation in lignin. J Am Chem Soc. 2013;135:6415–8.

50. Rahimi A, Ulbrich A, Coon JJ, Stahl SS. Formic-acid-induced depolymerization of oxidized lignin to aromatics. Nature. 2014;515:249–52.

51. Sequeiros A, Serrano L, Briones R, Labidi J. Lignin liquefaction under microwave heating. J Appl Polym Sci. 2013;130:3292–8.

52. Sergeev AG, Hartwig JF. Selective, nickel-catalyzed hydrogenolysis of aryl ethers. Science. 2011;332:439–43.

53. Shen D, Liu N, Dong C, Xiao R, Gu S. Catalytic solvolysis of lignin with the modified HUSYs in formic acid assisted by microwave heating. Chem Eng J. 2015;270:641–7.

54. Son S, Toste FD. Non-oxidative vanadium-catalyzed C–O bond cleavage: application to degradation of lignin model compounds. Angew Chem. 2010;49:3791–4.

55. Song Q, Wang F, Cai J, Wang Y, Zhang J, Yu W, Xu J. Lignin depolymerization (LDP) in alcohol over nickel-based catalysts via a fragmentation–hydrogenolysis process. Energy Environ Sci. 2013;6:994.

56. Stein TV, Hartog T, Buendia J, Stoychev S, Mottweiler J, Bolm C, Leitner W. Ruthenium-catalyzed C–C bond cleavage in lignin model substrates. Angew Chem. 2015;54:5859–63.

57. Toledano A, Serrano L, Labidi J. Improving base catalyzed lignin depolymerization by avoiding lignin repolymerization. Fuel. 2014;116:617–24.

58. Toledano A, Serrano L, Labidi J, Pineda A, Balu AM, Luque R. Heterogeneously catalysed mild hydrogenolytic depolymerisation of lignin under microwave irradiation with hydrogen-donating solvents. ChemCatChem. 2013;5:977–85.

59. Toledano A, Serrano L, Pineda A, Romero AA, Luque R, Labidi J. Microwave-assisted depolymerisation of organosolv lignin via mild hydrogen-free hydrogenolysis: catalyst screening. Appl Catal B Environ. 2014;145:43–55.

60. Voitl T, Rohr PRV. Demonstration of a process for the conversion of kraft lignin into vanillin and methyl vanillate by acidic oxidation in aqueous methanol. Ind Eng Chem Res. 2010;49:520–5.

61. Voitl T, Rohr PRV. Oxidation of lignin using aqueous polyoxometalates in the presence of alcohols. ChemSusChem. 2008;1:763–9.

62. Wang X, Rinaldi R. A route for lignin and bio-oil conversion: dehydroxylation of phenols into arenes by catalytic tandem reactions. Angew Chem Int Ed. 2013;52:11499–503.

63. Wang X, Rinaldi R. Solvent effects on the hydrogenolysis of diphenyl ether with Raney nickel and their implications for the conversion of lignin. ChemSusChem. 2012;5:1455–66.

64. Werhan H, Mir JM, Voitl T, Rudolf Von Rohr P. Acidic oxidation of kraft lignin into aromatic monomers catalyzed by transition metal salts. Holzforschung. 2011;65:703–9.

65. Wu A, Lauzon JM, Andriani I, James BR. Breakdown of lignins, lignin model compounds, and hydroxy-aromatics, to C1 and C2 chemicals via metal-free oxidation with peroxide or persulfate under mild conditions. RSC Adv. 2014;4:17931.

66. Xiao W, Han L, Zhao Y. Comparative study of conventional and microwave-assisted liquefaction of corn stover in ethylene glycol. Ind Crop Prod. 2011;34:1602–6.

67. Xiong J. Studies on catalytic degradation of lignin model compounds with the assistance of microwave and hydrogen-donor solvents. Hangzhou: Zhejiang University; 2012.

68. Xu C, Arancon RD, Labidid J, Luque R. Lignin depolymerisation strategies- towards valuable chemicals and fuels. Chem Soc Rev. 2014;43:7485–500.

69. Xu W, Miller SJ, Agrawal PK, Jones CW. Depolymerization and hydrodeoxygenation of switchgrass lignin with formic acid. ChemSusChem. 2012;5:667–75.
70. Ye Y, Zhang Y, Fan J, Chang J. Selective production of 4-ethylphenolics from lignin via mild hydrogenolysis. Bioresour Technol. 2012;118:648–51.
71. Zhang J, Teo J, Chen X, Asakura H, Tanaka T, Teramura K, Yan N. A series of NiM (M=Ru, Rh, and Pd) bimetallic catalysts for effective lignin hydrogenolysis in water. ACS Catal. 2014;4:1574–83.

Chapter 11
Molecular Mechanisms in the Thermochemical Conversion of Lignins into Bio-Oil/Chemicals and Biofuels

Haruo Kawamoto

11.1 Introduction

Lignin accounts for 20–30 % by weight of lignocellulosic biomass, and is a promising renewable resource for the production of aromatic chemicals and bio-fuels [1]. It is composed of phenylpropane units containing three different aromatic ring substitution patterns: *p*-hydroxyphenyl (H), guaiacyl (4-hydroxy-3-methoxyphenyl, G) and syringyl (3,5-dimethoxy-4-hydroxyphenyl, S) [1]. Softwoods contain a greater proportion of G units and smaller amounts of the H type, whereas hardwoods consist of G and S units while herbaceous species contain G, S and H units [1]. These monomers are linked together through ether (C–O) and condensed (C–C) bonds. Accordingly, lignin pyrolysis proceeds heterogeneously, depending on the plant species. This is in contrast to the pyrolysis of cellulose, a homogeneous polymer of D-glucose units connected via β-1 → 4 linkages.

In this chapter, molecular mechanisms involved in lignin pyrolysis are discussed with the focus being primarily on G-lignin after the brief analysis of the devolatilization temperature of lignin and the product compositions. Although many papers have reported theoretical investigations of specific pyrolysis reactions of lignins, this chapter concentrates on the results of experimental investigations conducted by the author's research group.

H. Kawamoto (✉)
Graduate School of Energy Science, Kyoto University,
Yoshida-honmachi, Sakyo-ku, Kyoto 606-8501, Japan
e-mail: kawamoto@energy.kyoto-u.ac.jp

11.2 Lignin Devolatilization Temperature

The devolatilization behavior of lignins during pyrolysis has been studied based on thermogravimetric (TG) analyses of lignins isolated from lignocellulosic biomasses [2–5]. Figure 11.1 presents TG and derivative thermogravimetric (DTG) data obtained from milled wood lignin (MWL) isolated from Japanese cedar (*Cryptmeria japonica*), a softwood [6]. Generally, the mass loss of lignins starts at approximately 200 °C, a temperature that is below those associated with the pyrolysis of cellulose and hemicellulose, and the major mass loss is observed between 200 and 400 °C, representing the primary pyrolysis step. Nuclear magnetic resonance (NMR) [4] and model compound [7–11] studies have confirmed that the ether linkages between the phenylpropane units are cleaved in this temperature range. In the case of hardwood lignins consisting of G and S units, the DTG peaks are shifted to slightly lower temperatures (compare 353 °C for Japanese cedar, a softwood, to 326 °C for Japanese beech, a hardwood) [6]. Although the mechanisms responsible for this difference are not presently known, several papers report similar relations [5, 12–14]. The lignin preparation methods are also reported to affect the devolatilization behavior [15].

In the higher temperature range of 400–800 °C, the mass loss rates are reduced and a relatively large amount of residue remains even at 800 °C, a much greater amount than is observed during the pyrolysis of cellulose or hemicellulose. In general, softwood lignins tend to generate larger amounts of residue than hardwood
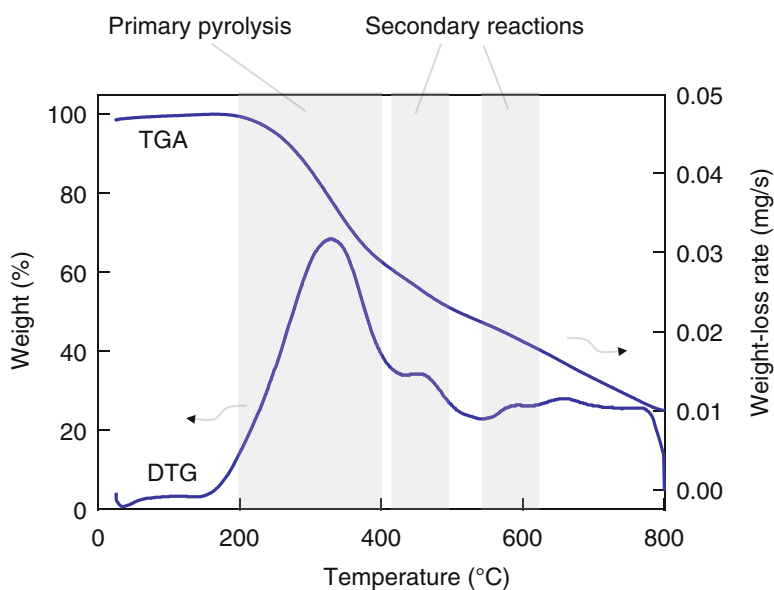
Fig. 11.1 Thermogravimetric analysis of milled wood lignin isolated from Japanese cedar (*Cryptmeria japonica*) (Adapted with permission from Ref. [6], Copyright © 2011 Elsevier)

lignins [3, 12]. This is explained by the greater proportion of condensed type link-ages in softwood lignins, which preferentially consist of G units, because these condensed structures are relatively resistant to pyrolytic depolymerization. The C5 positions of the guaiacyl units are involved in the formation of various condensed linkages, such as the 5-5′ and β-5′ types, during lignin biosynthesis, whereas increas-ing proportions of syringyl units, in which the C5 positions are already substituted by methoxyl groups, makes the contributions of the condensed-type linkages less important.

Even in the high temperature region, several DTG peaks are observed, at approx-imately 450, 550–600 and 650 °C. These peaks suggest that various temperature-dependent secondary reactions take place upon increasing the pyrolysis temperature. While the TG/DTG plots directly reflect the solid/liquid phase pyrolytic reactions, similar reactions are also considered to proceed in the gas phase, as discussed in Sect. 11.5. Based on the gas phase reactions, these DTG peaks are believed to result from reactions initiated by the homolytic cleavage of the methoxyl C–O bonds and side-chain C–C bonds (at 450 °C) as well as the decomposition of aromatic rings (at 550–600 °C).

11.3 Pyrolysis Products and Effects of Temperature

The chemical structures of the volatile products obtained from lignins have been determined on the basis of gas chromatography/mass spectrometry (GC/MS) [16–18], NMR [4, 18–23] and infrared (IR) [2, 11, 20, 24] analyses of the pyrolysis products from wood and isolated lignin fractions. In addition, other studies have employed pyrolysis directly coupled with GC/MS [25–29] and IR [2, 14] analyses (Py-GC/MS, Py-IR). The volatile products from the pyrolysis of lignins have been found to include aromatic compounds (phenols and aromatic hydrocarbons), low molecular weight (MW) aliphatic compounds (formaldehyde, formic acid, metha-nol and others) and non-condensable gases such as methane, CO, CO_2 and H_2.

Figure 11.2 summarizes the changes in the aromatic ring and side-chain struc-tures of the GC/MS-detectable products derived from G-type lignin during the pyrolysis of Japanese cedar MWL, under N_2 in a closed ampoule in a furnace pre-heated to 600 °C [18]. In this pyrolysis system, the temperature inside the ampoule reached 600 °C in 120 s [30], and hence these data show the structural changes of the volatile pyrolysis products as the sample is heated to the pyrolysis temperature.

At 40 s (450 °C) and 60 s (530 °C) points (Fig. 11.2), where the values in paren-theses are the associated temperatures, the only aromatic ring in the pyrolysis prod-ucts is guaiacol (2-methoxyphenol), which is the original repeating unit in the Japanese cedar lignin. In the early stage (40 s) of the pyrolysis (corresponding to the DTG peak at 350 °C), the side chains are primarily unsaturated alkyl (>C=C<, >C=O and conjugated >C=O) groups. The major volatile products in this stage include coniferyl alcohol (R: –CH=CH–CH₂OH), coniferyl aldehyde (R: –CH=CH–CHO), isoeugenol (R: –CH=CH–CH₃), 4-vinylguaiacol (R: –CH=CH₂), vanillin (R:
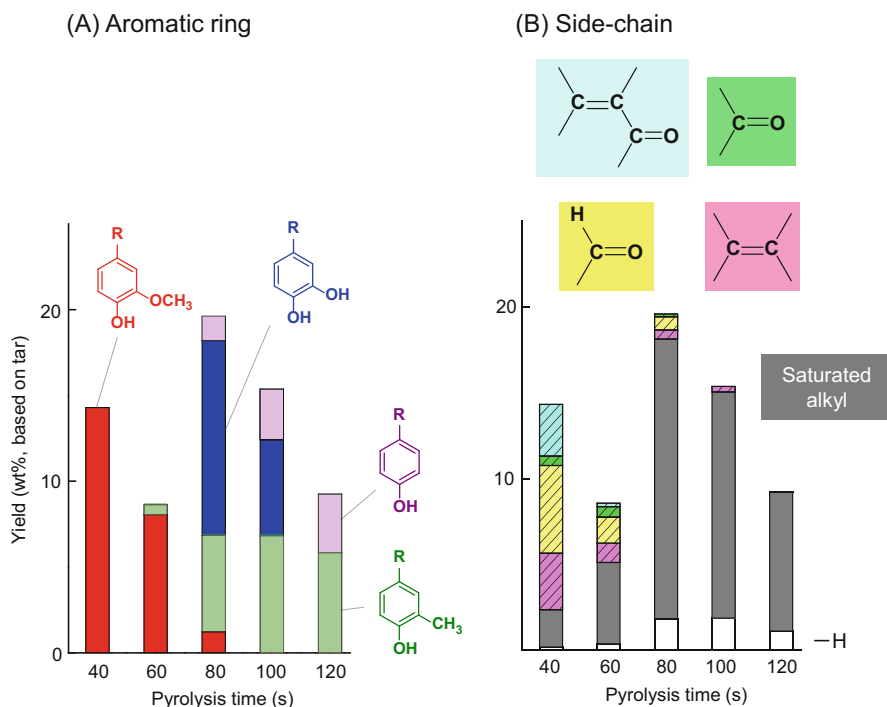
Fig. 11.2 Changes in the aromatic ring and side chain structures of the GC/MS-detectable volatile products from Japanese cedar (*Cryptmeria japonica*) MWL during pyrolysis in a closed ampoule (under N₂) in a furnace preheated to 600 °C. Here pyrolysis time is defined as the total time span over which the ampule is in the furnace (Adapted with permission from Ref. [18], Copyright © 2008 Elsevier)

–CHO) and acetovanillone (R: –CO–CH₃). The unsaturated alkyl side chains gradually transition to saturated alkyls (methyl, ethyl, propyl, 3-hydroxypropyl and others) and non-substituted (–H) types upon increasing the pyrolysis time and temperature. S-lignin is found to generate the corresponding syringol (2,6-dimethoxyphenol) derivatives. These primary products undergo re-polymerization and side chain conversions, as discussed in Sect. 11.4.4, and this re-polymerization reduces the yields of volatile products, as observed between 40 and 60 s.

During the pyrolysis period from 60 to 80 s, the aromatic ring structures undergo rapid transition from guaiacol to catechol (2-hydroxyphenol), *o*-cresol (2-methylphenol) and phenol types, along with an increase in the total yield of the GC/MS-detectable products. These changes result from homolytic cleavage of the side chain C–C bonds of the condensation products as well as from reactions of methoxyl groups, as discussed in Sect. 11.5. In this stage, the unsaturated side chains are almost completely replaced by saturated alkyl groups (methyl, ethyl and propyl). Dealkylation through the addition of hydrogen radicals to the aromatic

rings also proceeds. These events are all associated with the secondary pyrolysis stage at the DTG temperature in the vicinity of 450 °C (Fig. 11.1).

The yields of catechol-type products rapidly diminish between 80 and 120 s (corresponding to the DTG peak at 550–600 °C), at which point the ring-opening of the catechol rings to form non-condensable gases such as CO takes place, as discussed in Sect. 11.5. Polyaromatic hydrocarbons (PAHs), including naphthalene, fluorene, phenanthrene and anthracene, also start to form over this temperature range.

On the basis of the above, it is evident that the pyrolysis temperature is a very important factor determining the chemical composition of the volatile products obtained from lignins. It can also be seen that the product compositions are reasonably explained on the basis of primary and secondary pyrolysis reactions.

11.4   Primary Pyrolysis Reactions

As noted, lignin is a heterogeneous polymer including various ether and condensed type linkages between phenylpropane units. As an example, spruce (a softwood) MWL is reported to include 63–67% ether linkages (such as 48% β-ether and 11.5–15% α-ether) and 30–35% condensed linkages (including 9.5–11% 5-5′ [biphenyl] and 9–12% β-aryl) [1]. The proportions of ether linkages in hardwood lignins including S and G units are normally higher than those of the softwood lignins, as can be seen from the 60% β-ether linkage proportion in birch (a hardwood) MWL [1]. Accordingly, the roles of these linkages (or substructures) during pyrolysis in the temperature range of 200–400 °C are quite important with regard to understanding the primary pyrolysis step of lignins.

In this section, the reaction mechanisms involved in the primary pyrolysis step are described, based on data obtained using model compounds.

11.4.1   Model Compound Reactivity

The use of model dimers that represent the lignin ether and condensed type linkages is an effective means of understanding the pyrolytic reactions of lignins having heterogeneous chemical structures. Figure 11.3 summarizes the degradation pathways of various phenolic (Ph) and non-phenolic (Non-ph) model dimers during treatment at 400 °C in an open-top reactor [10]. The model phenolic dimers represent the end groups of lignin macromolecules, while the non-phenolic dimers represent the repeating units. This system allows the pyrolysis products to quickly escape from the heated zone, thus favoring primary reactions over secondary ones. As discussed in Sect. 11.4.4, the primary pyrolysis products from lignins are normally quite unstable even at temperatures lower than their formation temperatures.

Biphenyl (5-5′) dimers in both the phenolic and non-phenolic compounds are quite stable, even at 400 °C. The non-phenolic β-aryl dimer tends to undergo
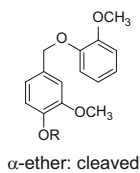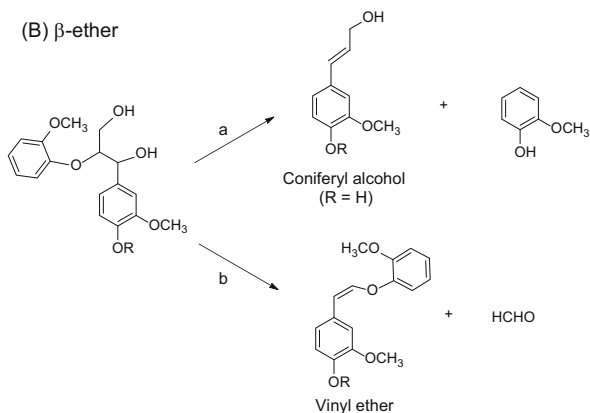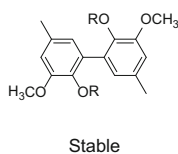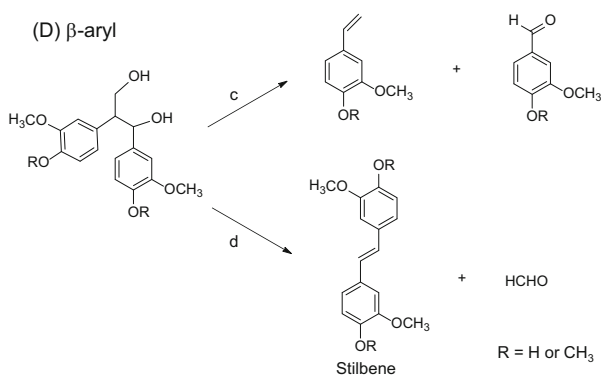
Fig. 11.3 Degradation pathways of ether and condensed linkage lignin model dimers under N_2 following immersion in a salt bath preheated to 400 °C for 1 min (Adapted with permission from Ref. [10], Copyright © 2007 Springer)

transition to a stilbene along with the fragmentation products formed through the cleavage of C_α–C_β bonds. The latter reaction leads to the depolymerization of the lignin macromolecule, although this reaction proceeds minimally even at 400 °C. The phenolic β-aryl dimer is very reactive and selectively generates a stilbene in approximately 50 mol% yield. Because stilbenes are formed through the elimination of the side chain (C_γ), the contributions of condensed linkages appear to be very limited during the pyrolytic depolymerization of lignin macromolecules.

Conversely, the ether linkages are cleaved quite effectively at 400 °C, a process that contributes to lignin depolymerization. The α-ether dimers were cleaved effectively, although this was followed by re-polymerization to form higher MW products. The β-ether dimer in phenolic form (guaiacylglycerol-β-guaiacyl ether) gave coniferyl alcohol in a 30.4 mol% yield, representing 60 mol% of the decomposition products of this dimer. Accordingly, the phenolic β-ether structures must be cleaved

to selectively form cinnamyl alcohols, such as coniferyl alcohol from the G lignin. Interestingly, these are the monomers that are utilized in lignin biosynthesis during the cell wall lignification process [31]. As discussed in Sect. 11.4.4, coniferyl alcohol is further degraded into various substances, including condensation products. Elimination of the C_γ-carbon, likely as formaldehyde, also proceeds to give vinyl ether, as observed in the formation of stilbenes from the β-aryl dimers. These results contradict those of an earlier study by Brežný et al. [7], which reported a complex mixture of products from the same β-ether dimers. This difference might have resulted from the use of a closed type reactor in the case of the earlier work, possibly allowing secondary reactions of the primary products to proceed. Consequently, the primary pyrolysis reactions of these substructures are evidently not as complicated as might be expected from the final pyrolysis product mixtures obtained from lignins.

The formation of coniferyl alcohol (from the β-ether structure) and stilbene (from the β-aryl structure) during the pyrolysis of natural lignins has also been confirmed by ultraviolet (UV) and IR spectroscopic analyses of the pyrolyzates of Japanese cedar MWL [11].

Phenolic dimers are normally more reactive than the corresponding non-phenolic dimers. As an example, the onset temperatures obtained during model dimer pyrolysis over a 1 min timespan are: α-ether (<200 °C [Ph], 350 °C [Non-ph]), β-ether (250–300 °C [Ph], 400 °C [Non-ph]) and β-aryl (300–350 °C [Ph], 400 °C [Non-ph]) [11]. Thus, the phenolic end groups in lignin macromolecules are expected to serve as reactive sites for the pyrolytic decomposition of lignins at relatively low temperatures. This is confirmed by the methylation of the phenolic hydroxyl groups of Japanese cedar MWL, which effectively inhibits pyrolytic conversion in the relatively low temperature region below 300 °C [11].

The TG data in Fig. 11.1 are evidence that Japanese cedar MWL undergoes efficient depolymerization at temperatures above the range of 300–350 °C (heating period: 1 min), even though the phenolic end-groups are expected to be reactive at lower temperatures based on the reactivities of the dimers and MWL described above. These apparently contradictory results can be explained by the re-polymerization of the primary products generated by the depolymerization reactions (see Sect. 11.4.4). This is confirmed by the onset temperature range (300–350 °C) for the formation of the depolymerization products, a range that is not affected by the methylation of the hydroxyl groups in Japanese cedar MWL [11].

11.4.2   Ether Cleavage Mechanisms

Several heterolytic and homolytic mechanisms have been proposed for the pyrolytic cleavage of the β-ether bond, which is the most abundant linkage type in lignin macromolecules. With regard to heterolysis, Klein and Virk [9] proposed a six membered retro-ene mechanism based on an analysis of the kinetics of the formation of styrene and phenol from phenethyl phenyl ether, representing the simplest

model compound without any aromatic ring substituents or side chains. Brežný et al. [7] explained the pyrolysis products obtained from guaiacylglycerol-β-guaiacyl ether and its methylated derivative using an oxirane mechanism. Homolysis via C_α-radicals has also been suggested, based on the pyrolytic reactivity of phenethyl phenyl ether [32–34].

However, these mechanisms are not completely supported by reliable experimental evidence, and do not address the effects of aromatic ring substituent groups or side chains. As described above, the α- and β-ether bonds in phenolic dimers are cleaved at much lower temperatures than those in the corresponding non-phenolic dimers. In addition, elimination of the side chain hydroxyl groups significantly alters the reactivity for the cleavage of the β-ether bond in the phenolic form, as noted below in this section [35, 36]. Accordingly, the roles of such substituent groups must be explained when developing a complete set of molecular mechanisms.

It is helpful to study the effects of substituents on the cleavage reactivities of the α- and β-ether bonds in lignin model compounds, substituted at aromatic ring *para* positions, when elucidating the ether cleavage mechanisms (that is, heterolysis and homolysis) during pyrolysis [37]. The associated mechanisms are clearly indicated by plots of the cleavage reactivities against Hammett's substituent constant (σ_p) and against ΔBDE, a parameter that indicates the reduction in the bond dissociation energy (BDE) brought about by the substituent.

Assuming a heterolytic reaction, the ether linkage is cleaved to form a *para* substituted phenolate anion, and thus the reactivity should increase directly with the electron-attracting ability of the substituent group, as this stabilizes the anion. This property of the *para* position substituent may be quantified using Hammett's substituent constant, σ_p. Consequently, in the case of heterolysis, a positive correlation would be expected between cleavage reactivity and σ_p (Fig. 11.4).

In contrast, homolysis of the ether bond forms a phenoxy radical, and so the reactivity will vary depending on the stability of this species. When a stable radical is formed, cleavage of the ether linkage tends to proceed efficiently, because the increased stability of the radical reduces the BDE of the aromatic O–C bond. The stabilization obtained from a substituent is therefore reflected in the ΔBDE value. Thus, in the case of homolysis, a positive relationship is expected between reactivity and ΔBDE (Fig. 11.4). Fortunately, because the phenoxy radical is stabilized by electron donating substituents, σ_p, ΔBDE values tend to be increase in the opposite order: σ_p in the order of $-COCH_3 > -Cl > -H > -OCH_3$ and ΔBDE in the order of $-OCH_3 > -Cl > -H > -COCH_3$. Accordingly, the cleavage mechanism is clearly indicated by comparing plots of reactivities (the amounts of model compound reacted) against σ_p and ΔBDE.

Based on the substituent effects observed for α-ether type dimers with $-COCH_3$, –Cl, –H and $-OCH_3$ groups at the *para* positions of the C_α-phenoxyl group, the α-ether bond in the non-phenolic (methylated) form is confirmed to undergo homolytic cleavage (Fig. 11.5A) [37]. This is consistent with the relatively high temperature (350 °C) required for the cleavage of this bond. However, in the phenolic form, the substituent effects exhibit a heterolytic mechanism (Fig. 11.5B) [37]. The push
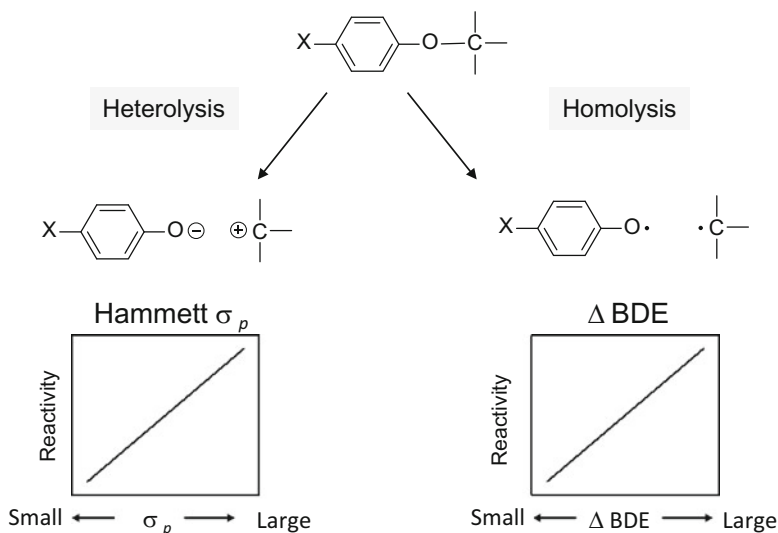
Fig. 11.4 Effect of the *para* substituent on the ether cleavage reactivity of lignin model compounds utilized for the elucidation of the ether cleavage mechanisms (heterolysis and homolysis) in pyrolysis. BDE: bond dissociation energy

and pull reaction that generates a quinone methide intermediate results in very efficient heterolysis of the C_α–O bond in the phenolic dimer. This reduces the cleavage temperature to <200 °C, significantly lower than the 350 °C required to cleave the non-phenolic α-ether bond, which cannot form a stable quinone methide intermediate.

The cleavage mechanisms associated with β-ether bonds are more complicated, because the reactivity varies depending on the side-chain hydroxylation pattern and the reactor type (see Sect. 11.4.3), as well as the use of phenolic or non-phenolic compounds.

Unexpectedly, the reactivity of a phenolic β-ether dimer was lowered to the level of a non-phenolic dimer by eliminating one of the hydroxyl groups from the C_α and C_γ of the guaiacylglycerol-β-guaiacyl ether [35, 36]. The effect of eliminating the C_α–OH is attributed to the inhibition of quinone methide formation, as illustrated in Fig. 11.5C. Low temperature homolysis of the C_β–O bond via a quinone methide intermediate during aqueous phase delignification [38–40] and steam-explosion [41] conditions has previously been postulated. Ponomarev [42] calculated the BDE of the C_β–O bond in the quinone methide form to be 44.1 kcal/mol, a value that is much lower than that of the phenolic form (57.0 kcal/mol). The reactivity for the cleavage of the β-ether bond of guaiacylglycerol-β-guaiacyl ether is not affected by the addition of tetralin as a radical scavenger, indicating that the rate-determining step is not the homolysis of the C_β–O bond but rather the formation of the quinone methide via a heterolysis reaction [43].
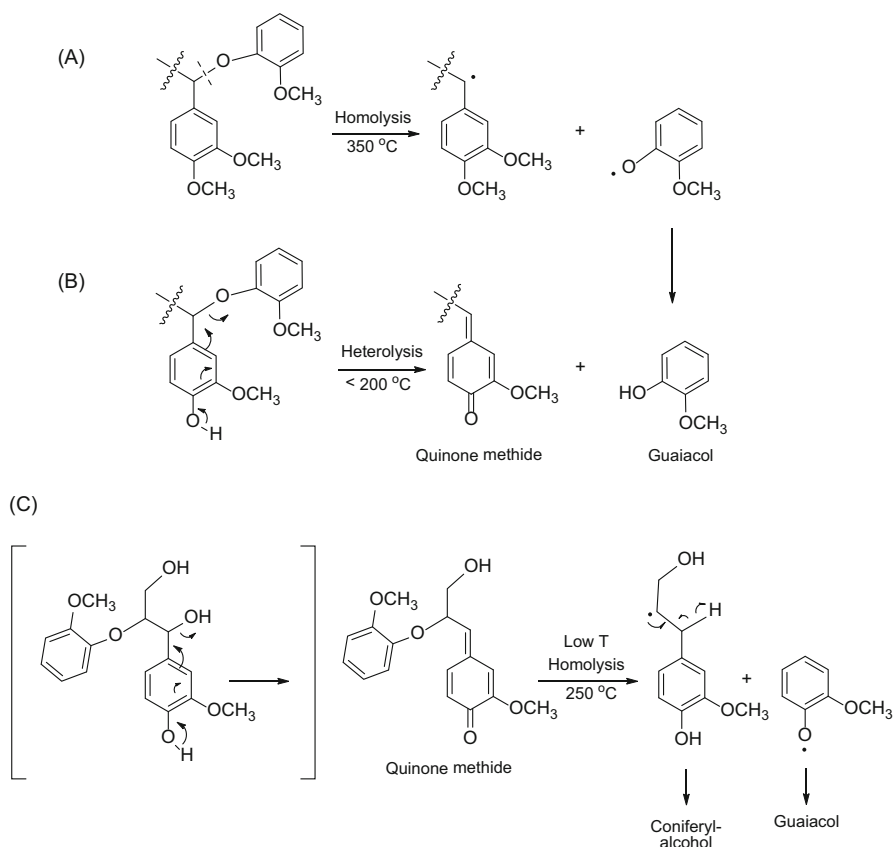
Fig. 11.5 Ether cleavage mechanisms proposed for the α- and β-ethers in lignins

The role of the quinone methide intermediate in the cleavage of the C_β–O bond in the phenolic end group can also be deduced from the reactivities of phenolic α,β-diether trimers that include various substituents at the *para* positions of the C_α-phenoxyl groups [37]. The reactivities of the β-ether bonds depend solely on those of the α-ether bonds, demonstrating that the cleavage of the α-ether bond acts as the rate-determining step. As noted, the α-ether bond in phenolic compounds is cleaved heterolytically to form the quinone methide intermediate. Furthermore, the substituent effect observed for a trimer incorporating a –OCH_3 group, which has a large ΔBDE value, are changed to those associated with a homolytic mechanism for the α-ether bond in the α,β-diether-type trimer. Radical species produced by the homolytic cleavage of the β-ether bond of the quinone methide intermediate would be expected to abstract hydrogen from the phenolic hydroxyl group. The resulting phenoxy radical would subsequently cleave the α-ether linkage in the trimer through β-scission to form the quinone methide intermediate (see Sect. 11.4.3, Fig. 11.6 pathway a).

(A)

Guaiacol

$C_\alpha=O$ type

$C_\alpha=C_\beta$ type

β-scission

Homolysis

• OH

Quinone methide

Pathway b

Pathway a

R '-H

R ' •

Dimer

R=H or CH₃

Radical chain reactions
(wood)

(B)

16–20 nm

Lignin-hemicellulose matrix
• Lignin decomposition starts at 200-250°C.
                                    (max. 300-350 °C)
• Strong interactions with hemicelluloses

Cellulose
microfibril

Xylan   Activation

R •   R-H

Lignin   Lignin   Depolymerization
                              (radical)   products

R •   R-H

Inhibition

Cellulose – lignin interaction
Cellulose: inhibits (< 300°C)

Glucomannan (for nonphenolic repeating units)

Fig. 11.6 (**a**) Summary of *in situ* method for studying the radical chain reactions of lignin using model dimers and (**b**) the interactions indicated between the constituent polymers of the cell wall, suggesting strong interactions between lignin and hemicellulose/cellulose (Adapted with permission from Ref. [44], Copyright © 2015 Elsevier)

During the pyrolysis of a non-phenolic α,β-diether trimer, the cleavage of the α-ether bond also serves as the rate-determining step for the scission of the β-ether bond. A β-scission type reaction with the $C_α$–radical, formed by the homolytic cleavage of the $C_α$–O bond, simultaneously cleaves the $C_β$–O bond homolytically [37].

The unexpected role of the $C_γ$–OH group of guaiacylglycerol-β-guaiacyl ether is explained by the stabilization effect on the transition state of the quinone methide formation (a heterolytic reaction) [35, 36]. Although the details of the mechanism are not known, hydrogen bonding between the $C_α$ and $C_γ$ hydroxyl groups may stabilize the transition state, promoting the elimination of the hydroxyl group from the $C_α$ under pyrolysis conditions without requiring any stabilization effects via solvation. Similar stabilization effects have been proposed to explain the higher reactivities of β-hydroxy ketones compared with other ketones during retro-aldol condensation [45]. Intermolecular hydrogen bonding, which acts as an acid catalyst, is also a key factor in activating the transglycosylation and dehydration reactions during the molten phase pyrolysis of carbohydrates [46–48]. Accordingly, carbohydrates are quite stable in the gas phase, in which intermolecular hydrogen bonding is not important [49].

As discussed above, the heterolysis of the $C_α$–OR bonds is an important reaction that tends to accelerate the homolytic cleavage of the β-ether linkage via the quinone methide intermediate. However, the unexpected effects of $C_γ$–OH groups on the formation of the quinone methide suggest that the heterolysis of the $C_α$–OR bonds is greatly affected by the three-dimensional structure of the lignin. The DTG peak temperature (approximately 350 °C) corresponding to the primary pyrolysis of Japanese cedar lignin suggests that cleavage of the β-ether linkages via the quinone methide mechanism, as observed for dimers and trimers, does not proceed very efficiently in lignins [11].

The β-ether linkages of the non-phenolic dimers are comparatively stable, even at 400 °C in an open-top reactor, although the reactivity increases in a sealed reactor (see Sect. 11.4.3). Direct homolysis of the $C_β$–O bonds are clearly indicated based on the substituent effects of non-phenolic β-ether dimers substituted in varying manners at the *para* positions of the $C_β$-phenoxyl groups (–H, –OCH₃, –Cl) [43].

Based on this evidence, the majority of the ether linkages between phenylpropane units are considered to be cleaved homolytically, except for the α-ether bonds in the phenolic end groups. This process leads to the formation of a large number of radical species during the primary devolatilization step. It is important to consider this new information, especially when assessing the interactions between lignin and cellulose/hemicellulose during pyrolysis, because the volatile products from cellulose and hemicellulose are non-radical species, generated through the heterolytic cleavage of glycosidic C–O bonds [47, 48].

11.4.3 Radical Chain Reactions

It has been suggested that radical chain reactions take place during the pyrolytic devolatilization of lignins during the primary pyrolysis stage. This is evident from the reactivities of the C_γ–deoxy β-ether dimers that vary substantially depending on the reactor type [43]. To avoid any uncertainty arising from the effects of the C_γ–OH groups on the formation of the quinone methide when working with phenolic model dimers, C_γ–deoxy type dimers are frequently employed for the investigation of radical chain reactions. Many papers also have reported radical chain mechanisms for the pyrolytic cleavage of phenethyl phenyl ether and its derivatives [32–34].

In the case of an open-top reactor, which allows volatile products to readily exit the heated zone, the majority of phenolic and non-phenolic dimers can be recovered without undergoing pyrolysis reactions. However, the reactivities of these compounds are dramatically increased in a sealed reactor, especially that of the phenolic dimers, giving β-ether cleavage products, including isoeugenol and 4-O-methyl isoeugenol from phenolic and non-phenolic (methylated) dimers, respectively [43]. These compounds correspond to coniferyl alcohol and its methyl ether derivative, as obtained from C_γ–OH type dimers. Furthermore, the addition of tetralin as a radical scavenger has been shown to effectively suppress the reactivities, such that the level of reactivity becomes comparable to that in an open-top reactor at a tetralin/dimer ratio of 20 (mol/mol) [43]. These observations clearly indicate that radical chain reactions occur in a sealed reactor.

Based on analyses of the pyrolyzates from C_γ–deoxy dimers, the two pathways shown in Fig. 11.6 are believed to be involved in the radical chain reactions [50]. One path proceeds via the phenoxy radical formed by the abstraction of hydrogen from the phenolic hydroxyl group, which is further converted to the quinone methide intermediate through a β-scission type reaction. The C_β–O bond is subsequently cleaved to give isoeugenol (pathway a). The alternate pathway (b) proceeds via the C_α–radical, which further fragments into a C_α=O type monomer along with guaiacol through a β-scission reaction. These pathways have been confirmed by studying kinetic deuterium isotope effects during the formation of these products from regio-specifically deuterated dimers [51].

It was noted in the previous section that the C_α–O linkage (representing a benzyl ether) in lignin α-ether structures is least resistant to homolysis. Accordingly, the role of this bond in the radical chain reactions has also been investigated, using an α,β-diether trimer [1-(4-(3,4-dimethoxybenzoyloxy)-3-methoxyphenyl)-2-(2-methoxyphenoxy)-1-propanol] representing the benzyl ether derivative (R: −CH_2–C_6H_5) of the model dimer in Fig. 11.6. This trimer (320 °C) exhibited reactivity intermediate between those of the phenolic (260 °C) and non-phenolic (methylated, 360 °C) dimers, where the values in parentheses indicate the onset temperature of pyrolytic decomposition in a sealed reactor over a heating period of 2 min [50]. The higher reactivity of the trimer relative to the methylated dimer can be explainable by considering the homolysis of the C_α–O bond of the trimer as an initial step.

The extremely high reactivity of the phenolic dimer, which does not include any bonds that readily undergo homolysis, can be attributed to the formation of three radicals from the phenoxy radical intermediate through the homolytic cleavage of the C_β–O bond and the quinone methide formation (pathway a in Fig. 11.6) [50]. In contrast, the number of radical species does not change in pathway b because the C_α–radical is fragmented into one radical and one non-radical species. Thus, radical coupling reactions may terminate the chain reactions, as suggested by the formation of C-benzylated products from the pyrolyzates of the α,β-diether-type trimer [50]. These species are formed from the coupling of benzyl radicals and aromatic C radicals as a result of rearrangements of the phenoxy radical.

Consequently, the phenolic end-groups are expected to act as radical sensitizers in native lignin pyrolysis. As such, adding the phenolic dimer increases the reactivity of the non-phenolic dimers, while that of the phenolic dimer is decreased. This results in the pyrolytic decomposition of the two species taking place over essentially the same temperature region (between 300 and 400 °C), which is close to the DTG peak temperature (350 °C) corresponding to the primary pyrolysis of Japanese cedar lignin [51].

This model dimer system has also been applied to the investigation of the interactions of lignin with hemicellulose and cellulose in plant cell walls [44]. The cell walls in wood samples (with thicknesses of 1–10 μm) consist of heterogeneous layered structures, in which cellulose microfibrils (16–20 nm across) are filled with a matrix consisting of hemicellulose and lignin [52]. Accordingly, the heterogeneous nature of the wood cell wall structure should be considered when assessing the pyrolysis reactions of wood constituent polymers, including lignins. Lignins in this matrix will undergo pyrolysis while being affected by the pyrolysis of hemicellulose. Lignins are also expected to be pyrolyzed differently in softwoods and hardwoods, because these woods have different hemicellulose compositions; xylan is the major hemicellulose in hardwoods, while glucomannan accounts for the majority in softwoods.

To allow for the study of radical chain reactions of lignins in wood and other lignocellulosic biomass resources, an *in situ* dimer probe method has been developed, based on the changes in the reactivity of dimers in the presence of wood and its constituent polymers (MWL, hemicelluloses [xylan or glucomannan] and cellulose) [44]. As shown in Fig. 11.6, phenolic and non-phenolic dimers having similar chemical structures to native lignins can be utilized as models of the terminal phenolic and non-phenolic repeating phenylpropane units in lignins, respectively. It is also possible to follow the pyrolysis reactions (that is, the radical chain reactions) of dimers under the influence of co-existing substances by assessing the chemical compositions of the dimer-derived products.

The radical chain reactions (pathways a and b) responsible for the cleavage of the β-ether linkages in lignins begin in the temperature range of 200–250 °C, in which the pure dimers are stable, and become particularly frequent in the range of 300–350 °C [44]. This is consistent with the DTG peak temperature (350 °C) corresponding to the primary pyrolysis of Japanese cedar lignin.

Strong interactions between lignin and wood polysaccharides are indicated based on the significant effects of wood polysaccharides on the reactivity of dimers, which are also dependent on the type of polysaccharide and the pyrolysis temperature [44]. Two different types of hemicellulose exhibit very different effects on the reactivity; xylan activates the radical chain reactions of dimers, whereas glucomannan strongly inhibits the non-phenolic dimer. Based on these results, depolymerization of the lignin via radical chain reactions is expected to occur more effectively in hardwoods than in softwoods. This hypothesis is supported by the results obtained from studies of Japanese cedar wood (a softwood) and Japanese beech wood (a hardwood) [6].

The effect of cellulose is greatly dependent on the pyrolysis temperature [44]. Cellulose inhibits the radical chain reactions of lignins at temperatures below 300 °C, although these effects are minimal at temperatures above 350 °C, at which cellulose rapidly decomposes. Taking into account the heterogeneous nature of the cell wall structure, these interactions are expected to occur at the boundary surfaces between the cellulose microfibrils and the lignin-hemicellulose matrix.

11.4.4   Re-polymerization and Side Chain Conversion

As discussed in the previous sections, cinnamyl alcohols such as coniferyl alcohol are believed to be the most important primary products in lignin pyrolysis, and are formed from the cleavage of the β-ether bonds in lignins. In contrast, the contributions of cinnamyl alcohols in the pyrolyzates from wood and isolated lignins are much smaller than expected from studies using model compounds. Coniferyl aldehyde, isoeugenol, dihydroconiferyl alcohol, 4-vinylguaiacol and vanillin have been reported as more important products from the pyrolysis of G-lignin. Only direct mass spectrometric analysis of the pyrolyzates from wood and lignin samples without cooling indicates the significant contributions of coniferyl alcohol (MW: 180) and sinapyl alcohol (MW: 210), based on intense peaks observed at *m/z* 180 and 210 [53]. These apparently contradictory observations arise from the propensity of coniferyl alcohol and sinapyl alcohol to undergo secondary reactions, especially condensation (polymerization). Once cooled to an oily state, the pyrolyzates (including these compounds) do not subsequently evaporate completely. In addition, even at temperatures (<300 °C) lower than those used for pyrolysis, secondary reactions of these compounds have been found to occur quite efficiently.

The evaporation and degradation of *trans*-coniferyl alcohol and other monomeric products have been studied using an open-top reactor system made of a Pyrex glass tube (internal diameter 8.0 mm, length 300 mm) under nitrogen [54]. After the heat treatment of a small amount (5.0 mg) of coniferyl alcohol added to the bottom of the reactor, the reactor wall was sectioned approximately 1.5 cm from the bottom of the reactor to produce two regions. The compounds recovered from the upper part of the reactor wall represented the volatile substances that are evaporated from the bottom section. Using this system, the evaporation of coniferyl alcohol, which competes with the secondary reactions, was studied over the temperature range of

200–350 °C, a range that is lower than the DTG peak temperature (350 °C) corresponding to the primary pyrolysis of Japanese cedar lignin.

The evaporation and degradation of coniferyl alcohol were determined to start at 200 to 250 °C (heating period: 5 min), and polymerization was found to be a more important process than the evaporation and side chain conversion processes [54]. Coniferyl aldehyde (**2**, R: –CH=CH–CHO) (an oxidation product), dihydroconiferyl alcohol (**3**, R: –CH$_2$–CH$_2$–CH$_2$OH) and isoeugenol (**4**, R: –CH=CH–CH$_3$) (reduction products) were all formed as side chain conversion products, together with *cis*-coniferyl alcohol and 4-vinylguaiacol (**5**, R: –CH=CH$_2$) (Fig. 11.7). Accordingly, some redox reactions evidently take place during the pyrolysis of coniferyl alcohol (see Sect. 11.4.5). Furthermore, these products are quite similar to the pyrolyzates obtained from the pyrolysis of Japanese cedar wood and MWL under similar conditions [55]. This finding supports the hypothesis that guaiacols with various side chains are formed via coniferyl alcohol during the pyrolysis of lignins.

Nevertheless, the total yields of compounds **2–5** were less than 15 wt% of the coniferyl alcohol used for the experiment, although these yields increased with an increase in the pyrolysis temperature (Fig. 11.7). The evaporation efficiency of the coniferyl alcohol (**1**) also directly increased with the pyrolysis temperature, although the levels were only approximately 15% at 300 and 350 °C, at which point the coniferyl alcohol recovered from the bottom of the reactor wall was negligible.
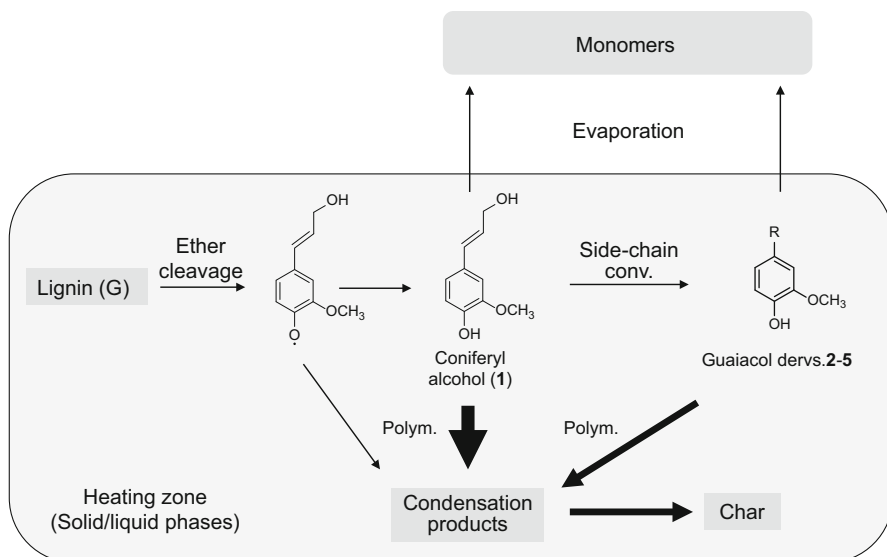
Fig. 11.7 Primary pyrolysis step, including depolymerization of the lignin macromolecule through ether cleavage, followed by two competing processes: evaporation of the monomeric products and re-polymerization to condensation products and char (Adapted with permission from Ref. [54], Copyright © 2014 Elsevier and [55], Copyright © 2013 Elsevier)

Based on the results of gel permeation chromatographic (GPC) analyses of the pyrolyzates, the remainder of the yield (approximately 70%) was found to consist of polymerization products. These results suggest that the coniferyl alcohol yield is low even when it is formed during the pyrolysis of G-type lignin.

The evaporation and polymerization behavior of compounds **2–5**, evaluated with a similar experimental system, demonstrate that **2**, **4** and **5**, all bearing conjugated $C_\alpha = C_\beta$ structures, were also prone to polymerization, although the reactivities for polymerization were much lower than that of coniferyl alcohol [54]. Because compound **3**, which does not contain a conjugated double bond, was selectively evaporated before condensation, the presence of conjugated $C_\alpha = C_\beta$ bonds is evidently the key to polymerization.

Methylation of the phenolic hydroxyl group of coniferyl alcohol (**1**) significantly suppresses the condensation reactivity [54, 56], although methylation does not alter the polymerization reactivity of 4-vinylguaiacol (**5**) [56]. From the chemical structure of the dimeric product obtained from **5**, a radical chain vinyl condensation mechanism has been proposed for the polymerization of 4-vinylguaiacol and its methyl ether derivative [56]. In the case of coniferyl alcohol, the bulky C_γ–hydroxymethyl group is believed to suppress the vinyl condensation reactivity.

Although a dimer fraction could not be isolated from the pyrolyzates of coniferyl alcohol at 250 °C, pyrolysis in the presence of creosol (4-methylguaiacol) gave two dimers (**6** and **7**, Fig. 11.8) [56]. Based on these results, a quinone methide mechanism can be proposed for the thermal condensation of coniferyl alcohol. Similar mechanisms have also been considered for the polymerization of coniferyl aldehyde (**2**) and isoeugenol (**4**). The reactivities for quinone methide formation from the guaiacol derivatives with conjugated $C_\alpha = C_\beta$ units are much more efficient than those of compounds with C_α–OR groups, which are the original structures observed in natural lignins. For these reasons, the primary pyrolysis products are more reactive for thermal polymerization than are natural lignins.

Fig. 11.8 Mechanisms for the condensation of coniferyl alcohol with 4-methylguaiacol through reactive quinone methide intermediates as a proposed explanation for the condensation products **6** and **7** obtained at 250 °C
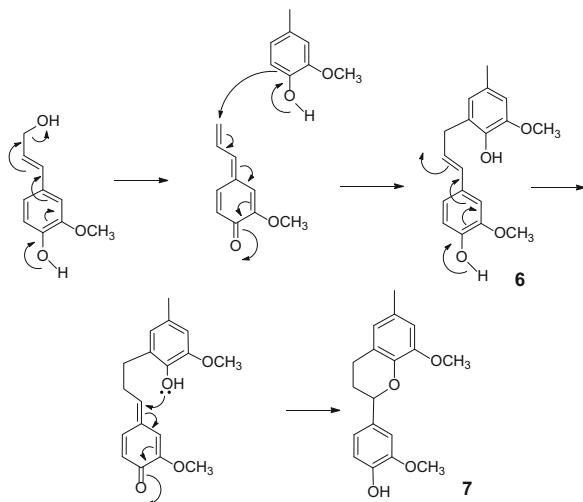
The compound 4-*O*-methyl coniferyl alcohol is relatively stable against thermal polymerization although, in the presence of coniferyl alcohol, this compound was incorporated into the condensation process of coniferyl alcohol [54]. This result provides some insight into the pyrolysis of natural lignins, showing that coniferyl alcohol structures can also add to the repeating phenylpropane units.

Sinapyl alcohol, the corresponding primary product from S-type lignins, exhibits similar reactions to those observed for coniferyl alcohol, except for the radical sensitivity at a relatively high pyrolysis temperature of 350 °C [57], as discussed below.

11.4.5 Side-Chain Conversion Mechanism

The mechanisms proposed for the formation of *cis*-coniferyl alcohol (**1**), coniferyl aldehyde (**2**), dihydroconiferyl alcohol (**3**), isoeugenol (**4**), and 4-vinylguaiacol (**5**) are shown in Fig. 11.9 [54]. These mechanisms include the quinone methide (A) and radical chain (B) pathways.

Isomerization from trans to cis coniferyl alcohol is possible via both quinone methide intermediate A (pathway a) and C_α- and C_γ-radicals (pathways d and e). Higher trans/cis ratios are usually observed during pyrolysis, with the equilibrium tending towards the more stable trans isomer for steric reasons.

Coniferyl aldehyde (**2**) would be formed via the C_γ-radical intermediate (pathway c). Two pathways are considered for the formation of this radical intermediate, involving either homolytic cleavage of the C_γ–H bond or hydrogen abstraction (H-abstraction) from the C_γ–H bond by a radical species. The relatively large calculated BDE (79.9 kcal/mol, density functional theory (DFT)/B3LYP/6-311+G**) suggests that the later H-abstraction pathway is more probable. The β-scission-type reaction from the C_γ-radical would give a coniferyl aldehyde and a hydrogen radical (H-radical). This H-radical could be used for addition to a double bond and hydrogen donation (H-donation) to stabilize other radical species.

Dihydroconiferyl alcohol (**3**) is a hydrogenation product of coniferyl alcohol. The direct addition of a H-radical to the double bond of coniferyl alcohol (pathways d and e) and hydrogenation to form quinone methide intermediate A (pathway a) are both plausible reaction pathways. 4-*O*-Methyl coniferyl alcohol also gives a dihydroconiferyl alcohol type derivative, which indicates that direct H-radical addition pathways d and e are involved in this transformation. Formation of a H-radical would be necessary for both pathways. Formation of this type of compound could therefore be used as a probe for the H-radical in the pyrolysis environment, as well as formation of isoeugenol.

Both the quinone methide (pathway b) and radical (pathway e) mechanisms are considered for the formation of isoeugenol (**4**) from coniferyl alcohol. Quinone methide intermediate B formed by elimination of the hydroxy group from the C_γ atom of coniferyl alcohol would be hydrogenated. In the radical mechanism, elimination of the C_γ-hydroxy group could proceed in two different ways: by β-scission-type elimination of the OH radical from the C_β-radical intermediate or by direct
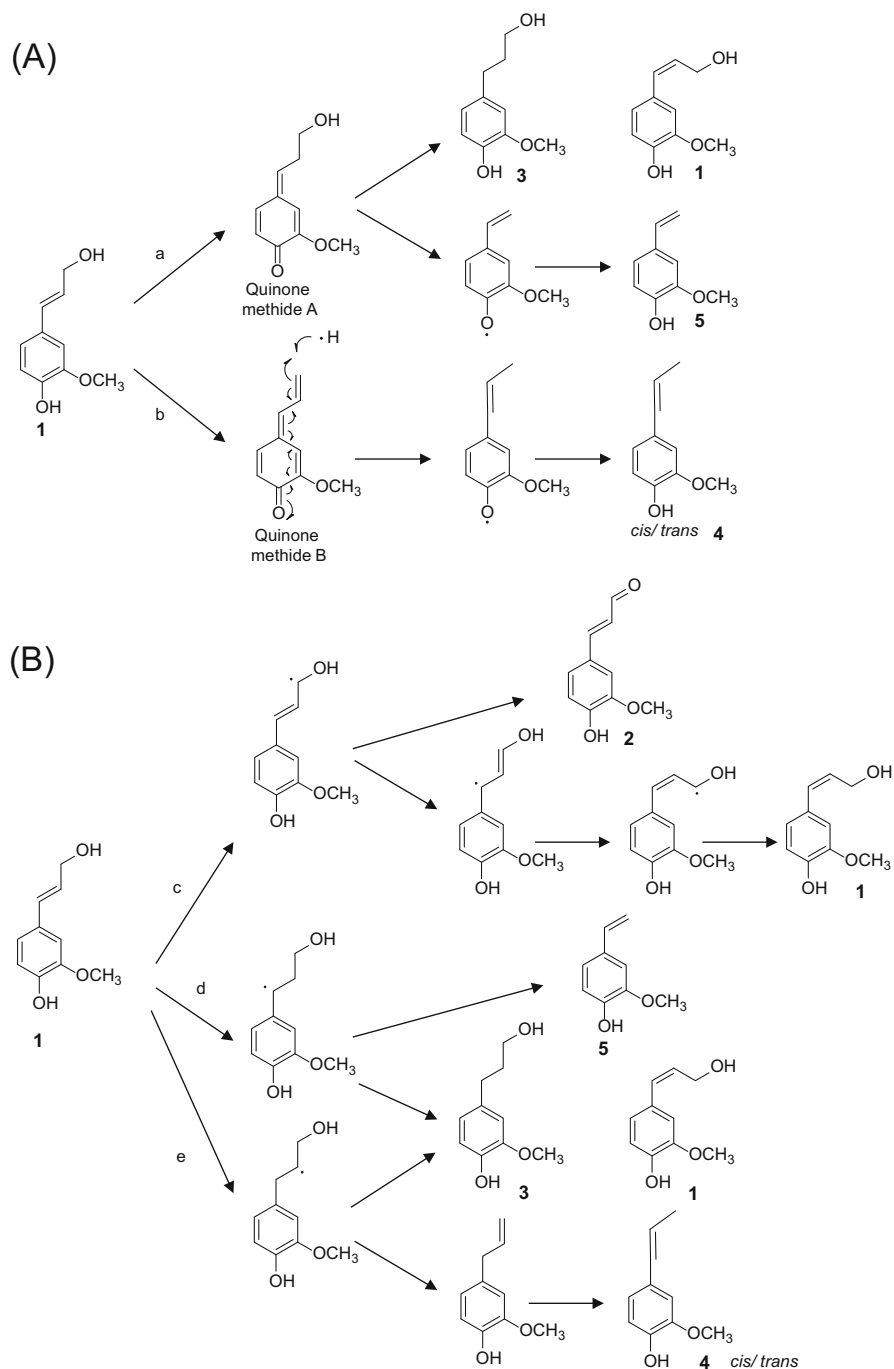
Fig. 11.9 Side-chain conversion mechanisms of coniferyl alcohol in the temperature range 200–350 °C to give compounds **2–5** (Adapted with permission from Ref. [54], Copyright © 2013 Elsevier)

homolysis of the C_γ–OH bond. However, the calculated BDE (72.2 kcal/mol, DFT/B3LYP/6-311+G**) would be too large for the homolysis pathway at pyrolysis temperature less than 350 °C. The C_β-radical pathway would therefore be more probable. In a manner analogous to the dihydroconiferyl alcohol formation mechanism, formation of the isoeugenol-type structure from 4-O-methyl coniferyl alcohol suggests that pathway e is involved in this conversion process.

4-Vinylguaiacol (**5**) would be formed via C_α-radical (pathway d) and quinone methide intermediate A (pathway a). Homolytic C_β–C_γ bond cleavage of the quinone methide intermediate A would occur. The electron-withdrawing quinone methide moieties attached to the C_β positions would reduce the BDE of the C_β–C_γ bonds to 51.8 kcal/mol (DFT/B3LYP/6-311+G**). Formation of this type of products from 4-O-methyl coniferyl alcohol suggests that radical pathway d is involved in the formation of **5**.

11.4.6   Role of Cinnamyl Alcohol in Lignin Primary Pyrolysis

The roles of the characteristic features of coniferyl alcohol and sinapyl alcohol in lignin pyrolysis have been carefully investigated using Japanese cedar, Japanese beech, and their MWL fractions in the temperature range 250–350 °C [55, 57]. As described above, the product compositions from wood and MWL samples are similar to those from pyrolysis of coniferyl alcohol and sinapyl alcohol. Because large parts of the lignin ether linkages are homolytically cleaved, the influences of diphenoxybenzene (DPB) (an aprotic solvent) and 1,2,3,10b-tetrahydrofluoranthene (a hydrogen donor, H-donor) on the monomer formation are different for wood/MWL and coniferyl alcohol/sinapyl alcohol [55, 57]. The following discussion mainly focuses on G-type lignin [55].

Pyrolysis in DPB is very effective to increase the recovery of coniferyl alcohol during pyrolysis of coniferyl alcohol by suppression of thermal polymerization [55]. This is probably because of inhibition of proton-transfer, which is as an important step in formation of quinone methide intermediates (heterolysis reaction).

In contrast to coniferyl alcohol, both DPB and H-donors are required for effective formation of the monomer from lignin contained in Japanese cedar and the MWL fraction [55]. Such differences can be explained by stabilization of the coniferyl alcohol radical with the H-donor as a primary product from homolytic cleavage of the β-ether linkages in lignin (Fig. 11.7). The amount of H-donor is usually not sufficient to stabilize all of the radical species formed through cleavage of ether linkages. Under these conditions, primary radicals tend to undergo radical coupling reactions. For pyrolysis in DPB containing a H-donor, the yields of monomeric guaiacols reach 8.3 and 12.8 wt% (lignin-based) from MWL and wood samples, respectively, and the side-chain reduction products (dihydroconiferyl alcohol and isoeugenol) are the main components of the monomers. These are produced by addition of a H-radical (from H-donor thermal decomposition) to the C=C double bond of the side-chain of coniferyl alcohol.

The polymer effect is also suggested to promote the secondary reactions of lignin primary pyrolyzates [55]. Cleavage of the ether linkages at the terminal end-groups of the lignin macromolecule leads to direct formation of monomers. This is similar to the pyrolysis reactions of coniferyl alcohol and model dimers. In contrast, the secondary reactions proceeded more effectively in pyrolysis of MWL/wood. Cleavage of ether linkages within the polymer would not lead to immediate formation of monomers from lignin because of its polymeric nature. In these circumstances, pyrolyzates would remain in the heating zone and undergo secondary reactions prior to the formation of monomers through cleavage of their ether linkages. These polymer effects would reduce the monomer yield and increase the contributions of the side-chain conversion products, including compounds **2–5**.

In pyrolysis of MWL/wood, the relative efficiency of oxidation/reduction of the side-chain of coniferyl alcohol varies depending on the pyrolysis temperature [55]. At the relatively low temperature of 250 °C, coniferyl aldehyde (**2**), an oxidation product, is the main monomer from lignin. This can be explained by the H-donor/radical balance. During the early stage of primary pyrolysis of lignin, the pyrolysis environment is considered to be under radical conditions through homolytic cleavage of lignin ether linkages. Under such H-donor-deficient conditions, these radical species would tend to condense or abstract hydrogen atoms from other molecules. The C_γ-hydrogen atom of coniferyl alcohol, which is at the conjugated allyl position, would be the site of H-abstraction, and this abstraction leads to production of coniferyl aldehyde (Fig. 11.9). In contrast, at a relatively high pyrolysis temperature of 350 °C, the pyrolysis environment would be richer in H-donor species (H-radicals). H-radicals are formed during charring reactions, which effectively promote pyrolytic radical chain reactions of guaiacol and syringol [30] (see Sect. 11.5.1). The presence of high levels of H-donor (H-radical) species would increase the monomer yield and the selectivity for side-chain reduction products, such as dihydroconiferyl alcohol (**3**) and isoeugenol (**4**).

Oligomeric products should also be considered as initial products along with monomers, because condensed (C–C) linkages are stable during primary pyrolysis of lignin [55]. Consequently, the monomer yield is estimated to be as low as ∼30% from a schematic softwood lignin structure composed of 16 C9 units, even without considering secondary polymerization. The rest of the products should be obtained as oligomeric products with relatively low volatilities, which preferentially condense under neat conditions. The use of DPB and H-donors significantly increases the yields of oligomers, as observed for monomer formation from lignin.

In summary (Fig. 11.7), two competitive reactions (i.e., H-addition and the radical coupling reaction to form condensation products) occur for the coniferyl alcohol radical following its formation during primary pyrolysis of lignin (DTG peak temperature ∼350 °C). This temperature would be sufficiently high to cause the secondary reaction of coniferyl alcohol. Although evaporation and the secondary degradation process are competitive under such conditions, the most important reaction is the condensation reaction, followed by side-chain conversion reactions. The relative efficiencies of the evaporation/polymerization/side-chain conversion

processes would determine the yield of monomeric products and their composition.

For condensation of coniferyl alcohol, the quinone methide intermediate is an important intermediate. The electropositive carbon atoms of quinone methides tend to react with electronegative aromatic and double-bonded carbon atoms rather than with oxygen atoms of the side-chain and phenolic groups. This reactivity can be explained by the hard and soft acid and base rule. Given that condensed (C–C) linkages are much more stable than ether linkages during the lignin pyrolysis process, re-depolymerization would not be effective for the condensation products. Together with the high condensation reactivity of the primary products, this would explain why lignin pyrolysis tends to preferentially form solid products (char).

Concerning the role of sinapyl alcohol in the pyrolysis of S-type lignins, analogous to coniferyl alcohol, sinapyl alcohol preferentially gives condensation products, along with similar side-chain conversion products [57]. The formation behavior of monomeric guaiacols and syringols from pyrolysis of Japanese beech wood and the MWL fraction can be explained by the reactivities of coniferyl alcohol and sinapyl alcohol as the pyrolysis intermediates formed as radical species. Remarkable differences are only observed for the evaporation efficiency and radical sensitivity of sinapyl alcohol [57].

The recovery of sinapyl alcohol (expected boiling point 385 °C) by evaporation is lower than that of coniferyl alcohol (expected boiling point 332 °C), most likely because of its low evaporation efficiency compared with the condensation reactivity [57]. Pyrolysis of sinapyl alcohol in DPB increases the recovery of sinapyl alcohol at 250 and 300 °C by suppression of the condensation reactivity. However, unlike coniferyl alcohol pyrolysis, DPB is insufficient to increase the recovery at 350 °C, and the additional use of a H-donor is required to increase the monomeric syringol recovery [57]. Based on these results, it is suggested that sinapyl alcohol is more susceptible to free radical reactions than coniferyl alcohol at 350 °C. These results also suggest that formation of monomeric syringols is less effective than monomeric guaiacols.

Although addition of a H-donor significantly increases the monomer yields from Japanese cedar wood (a softwood) and its MWL fraction, the influence on pyrolysis of Japanese beech wood (a hardwood) is very limited, and relatively large amounts of monomers are produced even without addition of any H-donors [57]. Based on these results, we proposed that pyrolysis of other wood constituents (probably hemicellulose) of beech wood acts as a source of H-donors and H-radicals to stabilize the intermediate radicals. Together with activation of lignin radical chain reactions by pyrolysis of xylan (Sect. 11.4.3, Fig. 11.6), these results indicate the different influences of softwood and hardwood hemicelluloses.

11.5 Secondary Reactions

As shown in Fig. 11.10, by increasing the pyrolysis temperature to ~450 °C, methoxyl groups attached to the lignin aromatic rings become very reactive for homolytic cleavage of the O–CH$_3$ bond. Radical-induced rearrangement of the methoxyl group also simultaneously occurs. Owing to these reactions, the aromatic substituent changes from –OCH$_3$ to –OH and –CH$_3$. Demethoxylation also proceeds via the formyl intermediate during the rearrangement pathway, along with formation of coke, a solid carbonized substance formed from volatile products.

When the pyrolysis temperature is further increased to 550–600 °C, formation of PAHs, demethylation of the aromatic moiety, and decomposition of catechols and pyrogarolls into non-condensable gases (mainly CO) occurs.
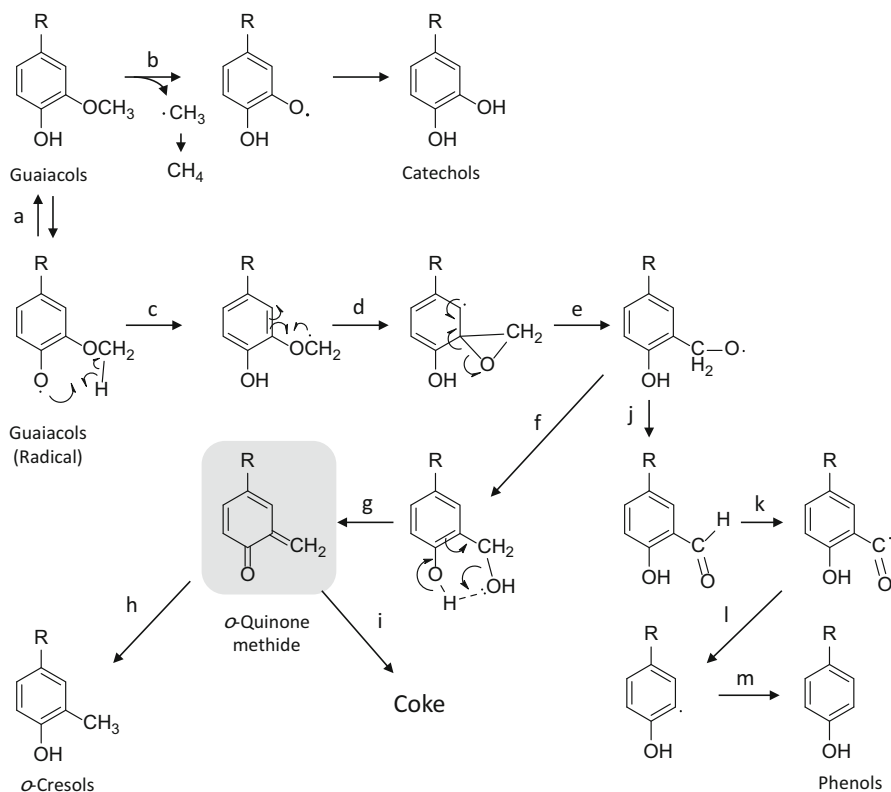
Fig. 11.10 Conversion mechanisms of guaiacol-type aromatic rings to catechols, *o*-cresols, and phenols, which proceed effectively at pyrolysis temperatures higher than 450 °C

11.5.1 Homolysis and Rearrangement of Methoxyl Groups

H-Abstraction and H-donation play important roles in the homolysis and rearrangement pathways. Catechol and methyl radicals formed by homolysis reaction b are stabilized by formation of catechol and methane, respectively, when two H-donors can donate hydrogen atoms to these radicals. Otherwise, these radicals would be consumed by radical coupling reactions. Methylation of aromatic rings by coupling of the methyl radical and C-centered radicals formed as resonance structures of phenoxy radicals also occurs [30].

The rearrangement pathway starts from the phenoxy radical of guaiacol [58], which is formed by H-abstraction from the phenolic hydroxyl group of guaiacol. Intramolecular H-abstraction at the methyl group by the phenoxy radical (reaction c) and subsequent 1,2-aryl migration (reaction e) have been proposed for the ether-rearrangement mechanism [58, 59]. This type of 1,2-aryl migration is supported by the high-yield formation of *o*-hydroxybenzaldehyde (reaction j) from guaiacol in the presence of cumene (a H-donor) [58]. This 1,2-aryl migration product is further converted into *o*-quinone methide (reaction g, a key intermediate) [60, 61], which is subsequently hydrogenated to *o*-cresol (reaction h).

Demethoxylation occurs by α-scission of the formyl radical (reaction l) formed by H-abstraction from *o*-hydroxybenzaldehyde (reaction k) [30, 58]. This type of reaction converts syringols formed as primary pyrolysis products of S-type lignins to guaiacols and finally phenols [30].

These pathways would be influenced by the concentrations of H-acceptors (radicals) and H-donors [62]. For catechol/CH_4 formation, only H-donors are required, because catechol and methyl radicals are supplied by unimolecular decomposition of guaiacol ($O–CH_3$ bond homolysis). In contrast, formation of other products by the OCH_3 rearrangement pathway starting from the guaiacol radical requires both H-acceptors and H-donors. The numbers of H-acceptors/H-donors required for formation of *o*-quinone methide, *o*-cresol, and phenol from guaiacol are 1/1, 1/3, and 3/1, respectively. Accordingly, the selectivity for the homolysis and rearrangement pathways can be controlled by changing the concentrations of H-acceptors/H-donors in the pyrolysis environment [63] (see Sect. 11.5.5).

Asmadi et al. [62] suggested that polyaromatization during the charring reaction activates the pyrolysis reactions in Fig. 11.10 by acting as a source of H-radicals, which can act as both H-acceptors and H-donors. A combination of guaiacol and syringol markedly suppressed coking in an ampoule reactor (N_2/600 °C/40–600 s), although the mechanism of the mixing effect is unknown. This also reduced the $O–CH_3$ bond homolysis products in the early stage of pyrolysis, while it enhanced the formation of condensation products. This can be explained by the decrease in the concentration of the H-donor stabilizing phenoxy radicals. To confirm this hypothesis, pyrolysis of the guaiacol/syringol mixture was performed in the presence of guaiacol coke, which drastically enhanced most of the products in Fig. 11.10.

Stereoelectronic effects are known for H-donation to radical species because all of the intermediates favor a linear transition state, which maximizes the interaction

between the radical orbital and the vacant σ* orbital of the bond that is going to be cleaved. H-donation by a small H-radical would be effective for steric reasons.

From the S-type lignin in Japanese beech wood, pyrogallol, 3-methoxycatechol, 3-methylcatechol, and 2,6-xylenol are produced as O–CH₃ bond homolysis and rearrangement products via syringol primary pyrolysis products [30]. 2,6-Xylenol is also produced from the G-type lignin by coupling of *o*-cresol with methyl radicals, and other pyrogallol and catechol derivatives disappear because of gasification, as discussed in Sect. 11.5.4. Accordingly, the lignin-derived products are different only in the primary pyrolysis stage, while the compositions for S- and G-type lignins are similar after the secondary reactions [30, 64].

11.5.2   Coke and Polyaromatic Hydrocarbon Formation

Coke and PAH formation are important because of the tar problem in biomass gasification. Issues related to tar formation represent a challenge that must be overcome to allow establishment of reliable gasification systems. Tar causes clogging of the pipeline from the outlet of the gasifier and can damage engines and turbines used for power generation by condensing and coking on walls.

The coke formation behavior of volatiles formed during the primary pyrolysis stage is different for lignin and polysaccharides [65]. In pyrolysis of wood polysaccharides, coking primarily occurs by condensation of volatile intermediates on the reactor wall at lower temperatures. Thus, cooling of volatile intermediates during gasification would lead to clogging of the pipeline from the gasifier. This stability of polysaccharide-derived volatiles in the gas phase has been explained by intermolecular hydrogen bonding, which can act as an acid catalyst only in the liquid (molten) phase to promote liquid-phase reactions leading to polymerization and dehydration to form coke [49, 65–67]. These reactions have been extensively studied using levoglucosan (1,6-anhydro-β-D-glucopyranose) as the important intermediate of cellulose pyrolysis along with other low MW glycosides [47–49, 67, 68]. In contrast, volatiles from lignin are subject to vapor-phase reactions that continuously produce coke materials from the bottom, where lignin is placed for pyrolysis, to the top of the reactor wall.

Coking of lignin-derived volatile intermediates has been suggested to be closely related to the *o*-quinone methide intermediate formed by rearrangement of the OCH₃ group (Fig. 11.10). Hosoya et al. [69] compared the coking behavior of various types of pyrolysis products with guaiacol-, cresol-, catechol- and phenol-type aromatic nuclei. They found that only guaiacols with methoxyl groups exhibited high reactivities for coke formation (in closed ampoule/N₂/600 °C/80 s, the final temperature reached 569 °C). Interestingly, the ethoxyl group was not effective in such coke formation. 2-Ethoxyphenol gave 2,3-benzofuran rather than formation of coke. This can be reasonably explained by the different reactivities of the *o*-quinone methide intermediates: the *o*-quinone methide intermediate formed from 2-ethoxyphenol has a reactive allyl moiety, which tends to be converted to

2,3-benzofuran by addition of the allyl radical formed by H-abstraction to the carbonyl oxygen of the *o*-quinone methide intermediate. The coking mechanism for the *o*-quinone methide intermediate (Fig. 11.10, reaction i) is not clear, although Diels–Alder type reactions proceed to form 9*H*-xanthene and its derivatives with OH/CH$_3$. Similar reactions are also expected in char formation, although the details are not known.

Even though the reactivities of cresols/xylenols and catechols/pyrogallols are much lower than those of guaiacols (in closed ampoule/N$_2$/600 °C), they also give coke substances by increasing the pyrolysis period and temperature to 600 s and 600 °C [70]. Thus, coking reactions of guaiacols/syringols occur in two stages: guaiacols/syringols with methoxyl groups simultaneously give coke during rearrangement of the methoxyl group, while coke formation from cresols/xylenols and catechols/pyrogallols occurs at higher pyrolysis temperatures. The same *o*-quinone methide intermediate can be formed from *o*-cresol by abstraction of phenolic and benzylic hydrogen atoms. It should be noted that the coke yield increases with increasing number of methyl groups: *o*-cresol (6.1 wt%)<2,4-xylenol (12.8 wt%), 2,6-xylenol (9.2 wt%)<2,4,6-trimethylphenol (23.5 wt%) (in closed ampoule/ N$_2$/600 °C) [70]. Phenol and 2-ethylphenol do not form any coke materials. Therefore, methoxyl and methyl groups are the key structural elements for coke formation.

At the stage where cresols/xylenols and catechols/pyrogallols become reactive for coke formation, PAHs start to form from guaiacol/syringol via their pyrolysis products, which include biphenyl and naphthalene (two aromatic rings), and phenanthrene and anthracene (three aromatic rings) at temperatures up to 600 °C [6, 30, 64]. There are many papers that deal with PAH formation by thermal decomposition of catechol and phenol at much higher temperatures [71–74]. Reactive intermediates such as the cyclopentadienyl radical formed by decomposition of aromatic rings are considered to be involved in PAH formation.

Regarding the reactivities of guaiacol and syringol as the primary pyrolysis products from G- and S-type lignins, the most significant difference is observed in the first-stage coke yield, which is almost two times higher for syringol [30]. This effective coking can be explained by the influence of the additional OCH$_3$ group in syringol, which doubles the opportunity for coke formation. Consequently, the yields of GC/MS-detectable low MW products are two times higher for guaiacol than for syringol. Because the reactivities of cresols/xylenols and catechols/pyrogallols tend to be enhanced by increasing the number of substituent groups on phenol, syringol-derived intermediates are more reactive than the corresponding guaiacol-derived intermediates [70]. These characteristic features for the pyrolysis of guaiacol and syringol are confirmed by the pyrolysis of Japanese cedar, Japanese beech, and their MWL fractions [6, 64].

From the results of stepwise pyrolysis of the char and coke fractions from MWLs at 450 and 600 °C, methoxyl group-related reactions (Fig. 11.10) (450 °C) and intermediate gasification (600 °C) have been confirmed to occur in the solid/liquid phase [6]. In the case of solid/liquid-phase reactions, tar formation, especially catechols/pyrogallols and PAHs, is significantly suppressed. Thus, gas-phase secondary reactions would be a source of PAHs at 600 °C.

11.5.3 Dealkylation

Several papers have described the hydrogen-transfer reaction in the aromatic ring during coal liquefaction in H-donor solvents such as tetralin, which is followed by cleavage of the strong bond between the aromatic ring and the aliphatic side-chain [75, 76]. Lignin pyrolyzates obtained at the secondary reaction stage include methylated aromatic compounds such as cresols and xylenols, which are formed by OCH_3 rearrangement (Fig. 11.10), methylation by radical coupling with the methyl radical, and homolysis of C–C bonds in ethyl and propyl side-chains of the intermediates. These methylated phenols are subject to demethylation reactions [70, 77, 78].

Demethylation is the main reaction for cresols/xylenols at 600 °C along with coke formation (second stage) [70]. For pyrolysis of o-cresol and 2,6-xylenol at 600 °C (in ampoule/600 s), the total yields of the monomers formed by demethylation reach 18.0 and 18.2 wt%, respectively, although gas formation is very limited. Thus, o-cresol is converted to phenol, and 2,6-xylenol is converted to o-cresol.

The 2,3-xylenol selectively gives m-cresol (32.6 wt%) in preference to o-cresol (1.4 wt%) [70]. As indicated by this example, demethylation reactions proceed regioselectively and methyl groups at the o- and p-positions with respect to the phenolic hydroxyl group are selectively cleaved. The higher reactivities of the o- and p-methyl groups are explained by the following two mechanisms [70]. First, because of the relative stability of the intermediate cyclohexadienyl radicals formed by attack of the H-radical to the aromatic ring-carbons, the resonance structure with the radical on the carbon atom adjacent to the OH group stabilizes the radicals. The second proposed mechanism is based on radical coupling of C-centered radicals (selectively formed at the o- and p-positions) as resonance structures of phenoxy radicals with H-radicals. These coupling reactions lead to formation of cyclohexanedienones, which have weaker C–CH_3 bonds. The calculated BDEs of the o- and p-derivatives are 60.3 and 62.5 kcal/mol, respectively (DFT/B3LYP/6-311++G**), which are much lower than the BDEs of the corresponding phenols (110.5 and 108.7 kcal/mol). As described for low-temperature homolysis of the β-ether linkage of the quinone methide intermediate (Sect. 11.4.2), the strong electron-withdrawing ability of the conjugated carbonyl moiety significantly decreases the BDE of the C–CH_3 bond.

11.5.4 Gasification

Gasification reactivities of lignin-derived volatile and charred intermediates have been compared with those of cellulose-derived products at 600 °C in ampoule reactors under nitrogen [21]. The cellulose-derived volatile intermediates from primary pyrolysis are efficiently gasified to form CO-rich gas, while the gasification reactivity significantly decreases by converting to the coke and char materials. In contrast, lignin is much less reactive for gasification under these pyrolysis conditions at

600 °C. Interestingly, the gasification reactivity is not considerably different for the lignin-derived volatile and char/coke materials. This can be explained by the above description that similar secondary reactions proceed for both phases of the intermediates (Sect. 11.5.2).

Methane content is generally higher in the gas produced from lignin than in that produced from cellulose. This is related to O–CH$_3$ bond homolysis and demethylation, both of which proceed at the secondary reaction stage. Based on comparison of the gas yields from MWLs and guaiacol/syringol, gas formation at the primary pyrolysis stage is more pronounced for MWLs. Part of the lignin side-chain would be transformed to gaseous products, which is supported by formation of C6–C2 structures during the primary pyrolysis of lignins and model dimers.

From the pyrolysis reactivities of cresols/xylenols and catechols/pyrogallols as the intermediates converted from guaiacols/syringols at 600 °C, catechol- and pyrogallol-moieties are efficiently converted into gaseous products containing CO as the main component [70]. Pyrogallol derivatives tend to be more reactive than catechol derivatives and produced CO$_2$ as well as CO, although the mechanism is not well understood. Nevertheless, S-type lignin produces more CO$_2$ than G-type lignin.

Composition of the gaseous products formed from cresols/xylenols are different from that produced from catechols/pyrogallols, in addition to the lower gasification reactivities [70]. Cresols/xylenols tend to produce CH$_4$ and H$_2$ rather than CO and CO$_2$, along with demethylation products and coke. These gas compositions can be explained by the secondary reactions described in Sects. 11.5.2 and 11.5.3. Methane is the product of H-donation to the methyl radical formed during demethylation. The coking process would produce H-radicals during polyaromatization, which leads to formation of H$_2$. Accordingly, the CH$_4$ yield is related to the number of methyl groups in cresols/xylenols, where the yield increased in the order o-cresol (2.8 wt%) < 2,4-xylenol (5.9 wt%) and 2,6-xylenol (6.0 wt%) < 1,3,5-trimethylphenol (9.5 wt%). The H$_2$ yield also increased in this order because the coke yield varied in this order (see Sect. 11.5.2).

11.5.5 Interaction Between Lignin and Polysaccharide Pyrolysis

As discussed above, radical reactions play important roles in the primary and secondary reactions of lignins, while heterolysis reactions to form non-radical intermediates dominate in pyrolysis of the polysaccharide components of wood and other lignocellulosic biomass. These features cause significant interactions between the pyrolysis of lignin and polysaccharides.

Polysaccharide-derived pyrolysis intermediates stabilize the lignin-derived intermediate radicals produced by primary pyrolysis, which increases the yields of GC/MS-detectable monomers from lignin [63, 79]. This is accomplished by stabili-

zation of radical intermediates by H-donation from polysaccharide-derived non-radical intermediates, probably aldehydes and other reactive hydrogen atoms in the molecules. Consequently, the secondary reactions are accelerated for the polysaccharide-derived intermediates (products). For example, conversion of anhydrosugars (including levoglucosan, an important intermediate in cellulose pyrolysis) to C2 and C3 fragmentation products is enhanced under the influence of lignin pyrolysis [63].

Anhydrosugars such as levoglucosan efficiently polymerize into polysaccharides by converting the vapor into a molten substance under cooling [49, 66]. This polymerization reaction is suppressed in the presence of lignin-derived products [68, 79]. This can be explained by general hydrogen-bonding theory, in which intermolecular hydrogen bonding acts as an acid catalyst. Hydrogen bonding between aromatic π-electrons and OH groups of anhydrosugars inhibits intermolecular hydrogen bonding between anhydrosugars. Consequently, both yields of anhydrosugar and C2/C3 fragments from cellulose increase in the presence of lignin pyrolysis, while the water-soluble polysaccharide yield decreases [79].

By increasing the pyrolysis temperature to >450 °C, coexisting polysaccharide pyrolysis significantly increases the selectivity for O–CH$_3$ bond homolysis products (i.e., catechols/pyrogallols and CH$_4$) over OCH$_3$ rearrangement products (e.g., cresols/xylenols and coke) [63]. For example, the yield of GC/MS-detectable monomers from Japanese cedar MWL increased from 5.3 to 20.2 wt% because of the influence of cellulose pyrolysis, and the selectivity of catechols over cresols/xylenols also increased from 0.9 to 5.5. These results are reasonably explained by the roles of H-acceptors and H-donors, as described in the discussion relating to the pathways in Fig. 11.10. Cellulose-derived intermediates, which can act as H-donors, suppress the OCH$_3$ rearrangement pathway by inhibiting formation of the phenoxy radical, which is the key intermediate in this pathway. This enhances conversion of cellulose-derived intermediates to gaseous products.

11.6   Conclusions and Future Outlook

The chemical structures of lignin are more complex than the polysaccharide components in lignocellulosic biomass because of the heterogeneity arising from the existence of several linkage types between the phenylpropane units in lignin. Although investigations using model dimers, which represent lignin linkage types, have clarified the molecular mechanisms underlying primary and secondary pyrolysis of lignin, many uncertainties still remain to be clarified, which include the influences of conformational mobility of lignin macromolecules, types of aromatic ring substitution patterns, minerals, other co-existing substances such as hemicellulose. Uncovering the molecular mechanisms of lignin and other components in lignocellulosic biomass would help to improve the existing thermochemical conversion processes for production of biofuels and biochemical.

References

1. Adler E. Lignin chemistry – past, present and future. Wood Sci Technol. 1977;11(3):169–218.
2. Fenner RA, Lephardt JO. Examination of the thermal-decomposition of kraft pine lignin by fourier-transform infrared evolved gas-analysis. J Agric Food Chem. 1981;29(4):846–9.
3. Gardner DJ, Schultz TP, McGinnis GD. The pyrolytic behavior of selected lignin preparations. J Wood Chem Technol. 1985;5(1):85–110.
4. Haw JF, Schultz TP. ^{13}C CP MAS NMR and FT-IR study of low-temperature lignin pyrolysis. Holzforschung. 1985;39(5):289–96.
5. Jakab E, Faix O, Till F. Thermal decomposition of milled wood lignins studied by thermogravimetry mass spectrometry. J Anal Appl Pyrolysis. 1997;40–1:171–86.
6. Asmadi M, Kawamoto H, Saka S. Gas- and solid/liquid-phase reactions during pyrolysis of softwood and hardwood lignins. J Anal Appl Pyrolysis. 2011;92(2):417–25.
7. Brežný R, Mihálov V, Kováčik V. Low-temperature thermolysis of lignin 1. Reactions of β-O-4 model compounds. Holzforschung. 1983;37(4):199–204.
8. Brežný R, Šurina I, Košik M. Low-temperature thermolysis of lignin 2. Thermofractography and thermal-analysis of β-O-4 model compounds. Holzforschung. 1984;38(1):19–24.
9. Klein MT, Virk PS. Model pathways in lignin thermolysis 1. Phenthyl phenyl ether. Ind Eng Chem Fund. 1983;22(1):35–45.
10. Kawamoto H, Horigoshi S, Saka S. Pyrolysis reactions of various lignin model dimers. J Wood Sci. 2007;53(2):168–74.
11. Nakamura T, Kawamoto H, Saka S. Pyrolysis behavior of Japanese cedar wood lignin studied with various model dimers. J Anal Appl Pyrolysis. 2008;81(2):173–82.
12. Faix O, Jakab E, Till F, Székely T. Study on low mass thermal-degradation products of milled wood lignins by thermogravimetry-mass-spectrometry. Wood Sci Technol. 1988;22(4):323–34.
13. Li J, Li B, Zhang X. Comparative studies of thermal degradation between larch lignin and manchurian ash lignin. Polym Degrad Stab. 2002;78:279–85.
14. Liu Q, Wang S, Zheng Y, Luo Z, Cen K. Mechanism study of wood lignin pyrolysis by using TG-FTIR analysis. J Anal Appl Pyrolysis. 2008;82(1):170–7.
15. Kuno S, Kadla J. Thermal decomposition study of isolated lignin using temperature modulated TGA. J Wood Chem Technol. 2008;28:106–21.
16. Sipilä K, Kuoppala E, Fagernäs L, Oasmaa A. Characterization of biomass-based flash pyrolysis oils. Biomass Bioenerg. 1998;14(2):103–13.
17. Branca C, Giudicianni P, Di Blasi C. GC/MS characterization of liquids generated from low-temperature pyrolysis of wood. Ind Eng Chem Res. 2003;42(14):3190–202.
18. Hosoya T, Kawamoto H, Saka S. Secondary reactions of lignin-derived primary tar components. J Anal Appl Pyrolysis. 2008;83(1):78–87.
19. Pindoria RV, Lim JY, Hawkes JE, Lazaro MJ, Herod AA, Kandiyoti R. Structural characterization of biomass pyrolysis tars/oils from eucalyptus wood waste: effect of H-2 pressure and sample configuration. Fuel. 1997;76(11):1013–23.
20. Sharma RK, Wooten JB, Baliga VL, Lin X, Geoffrey Chan W, Hajaligol MR. Characterization of chars from pyrolysis of lignin. Fuel. 2004;83(11–12):1469–82.
21. Hosoya T, Kawamoto H, Saka S. Pyrolysis gasification reactivities of primary tar and char fractions from cellulose and lignin as studied with a closed ampoule reactor. J Anal Appl Pyrolysis. 2008;83(1):71–7.
22. Dufour A, Castro-Diaz M, Brosse N, Bouroukba M, Snape C. The origin of molecular mobility during biomass pyrolysis as revealed by in situ ^{1}H NMR spectroscopy. ChemSusChem. 2012;5(7):1258–65.
23. Dufour A, Castro-Díaz M, Marchal P, Brosse N, Olcese R, Bouroukba M, et al. In situ analysis of biomass pyrolysis by high temperature rheology in relations with ^{1}H NMR. Energy Fuels. 2012;26(10):6432–41.

24. Scholze B, Meier D. Characterization of the water-insoluble fraction from pyrolysis oil (pyrolytic lignin). Part I. PY-GC/MS, FTIR, and functional groups. J Anal Appl Pyrolysis. 2001;60(1):41–54.
25. Genuit W, Boon JJ, Faix O. Characterization of beech milled wood lignin by pyrolysis-gas chromatography photoionization mass-spectrometry. Anal Chem. 1987;59(3):508–13.
26. Ralph J, Hatfield RD. Pyrolysis-Gc-Ms characterization of forage materials. J Agric Food Chem. 1991;39(8):1426–37.
27. Arias ME, Polvillo O, Rodríguez J, Hernández M, González-Pérez JA, González-Vila FJ. Thermal transformations of pine wood components under pyrolysis/gas chromatography/mass spectrometry conditions. J Anal Appl Pyrolysis. 2006;77(1):63–7.
28. Greenwood PF, van Heemst JDH, Guthrie EA, Hatcher PG. Laser micropyrolysis GC-MS of lignin. J Anal Appl Pyrolysis. 2002;62(2):365–73.
29. Alen R, Kuoppala E, Oesch P. Formation of the main degradation compound groups from wood and its components during pyrolysis. J Anal Appl Pyrolysis. 1996;36(2):137–48.
30. Asmadi M, Kawamoto H, Saka S. Thermal reactions of guaiacol and syringol as lignin model aromatic nuclei. J Anal Appl Pyrolysis. 2011;92(1):88–98.
31. Higuchi T. Lignin biochemistry: biosynthesis and biodegradation. Wood Sci Technol. 1991;24(1):23–63.
32. Autrey ST, Alnajjar MS, Nelson DA, Franz JA. Absolute rate constants for the β-scission reaction of the 1-phenyl-2-phenoxypropyl radical – a model for radical reactions of lignin. J Org Chem. 1991;56(6):2197–202.
33. Britt PF, Buchanan AC, Malcolm EA. Thermolysis of phenethyl phenyl ether – a model for ether linkages in lignin and low-rank coal. J Org Chem. 1995;60(20):6523–36.
34. Beste A, Buchanan III AC, Britt PF, Hathorn BC, Harrison RJ. Kinetic analysis of the pyrolysis of phenethyl phenyl ether: computational prediction of alpha/beta-selectivities. J Phys Chem A. 2007;111(48):12118–26.
35. Kawamoto H, Horigoshi S, Saka S. Effects of side-chain hydroxyl groups on pyrolytic β-ether cleavage of phenolic lignin model dimer. J Wood Sci. 2006;53(3):268–71.
36. Kawamoto H, Saka S. Role of side-chain hydroxyl groups in pyrolytic reaction of phenolic β-ether type of lignin dimer. J Wood Chem Technol. 2007;27(2):113–20.
37. Kawamoto H, Nakamura T, Saka S. Pyrolytic cleavage mechanisms of lignin-ether linkages: a study on *p*-substituted dimers and trimers. Holzforschung. 2008;62(1):50–6.
38. Sano Y. Reactivity of β-O-4 linkages in lignin during solvolysis pulping – degradation of β-O-4 lignin model compounds. Mokuzai Gakkaishi. 1989;35(9):813–19.
39. Kishimoto T, Sano Y. Delignification mechanism during high-boiling solvent pulping – Part 2. Homolysis of guaiacylglycerol-β-guaiacyl ether. Holzforschung. 2002;56(6):623–31.
40. Li S, Lundquist K. Reactions of the β-aryl ether lignin model 1-(4-hydroxy-3-methoxyphenyl)-2-(2-methoxyphenoxy)-1-propanol on heating in aqueous solution. Holzforschung. 2001;55(3):296–301.
41. Tanahashi M, Karina M, Tamabuchi K, Higuchi T. Degradation mechanism of lignin accompanying steam explosions 1. Degradation products of lignin and β-O-4 lignin substructure model dimers. Mokuzai Gakkaishi. 1989;35(2):135–43.
42. Ponomarev DA. Formation of quinone methides: an alternative pathway of thermal degradation of some β-O-4-ethers as compounds modeling lignin. Russ J Appl Chem. 1997;70(5):824–6.
43. Kawamoto H, Ryoritani M, Saka S. Different pyrolytic cleavage mechanisms of β-ether bond depending on the side-chain structure of lignin dimers. J Anal Appl Pyrolysis. 2008;81(1):88–94.
44. Kawamoto H, Watanabe T, Saka S. Strong interactions during lignin pyrolysis in wood – a study by in situ probing of the radical chain reactions using model dimers. J Anal Appl Pyrolysis. 2015;113:630–7.
45. Smith GG, Yates BL. Pyrolysis studies 15. Thermal retrograde aldol condensation of β-hydroxy ketones. J Org Chem. 1965;30(6):2067–8.

46. Matsuoka S, Kawamoto H, Saka S. Retro-aldol-type fragmentation of reducing sugars preferentially occurring in polyether at high temperature: role of the ether oxygen as a base catalyst. J Anal Appl Pyrolysis. 2012;93:24–32.

47. Kawamoto H, Ueno Y, Saka S. Thermal reactivities of non-reducing sugars in polyether—role of intermolecular hydrogen bonding in pyrolysis. J Anal Appl Pyrolysis. 2013;103:287–92.

48. Kawamoto H, Hosoya T, Ueno Y, Shoji T, Saka S. Thermal stabilization and decomposition of simple glycosides in the presence of aromatic substances in closed ampoules: the role of OH center dot center dot center dot pi hydrogen bonding. J Anal Appl Pyrolysis. 2014;109:41–6.

49. Fukutome A, Kawamoto H, Saka S. Processes forming gas, tar, and coke in cellulose gasification from gas-phase reactions of levoglucosan as intermediate. ChemSusChem. 2015;8(13):2240–9.

50. Watanabe T, Kawamoto H, Saka S. Radical chain reactions in pyrolytic cleavage of the ether linkages of lignin model dimers and a trimer. Holzforschung. 2009;63(4):424–30.

51. Watanabe T, Kawamoto H, Saka S. Pyrolytic reactivities of deuterated β-ether-type lignin model dimers. J Anal Appl Pyrolysis. 2015;112:23–8.

52. Salmén L. Micromechanical understanding of the cell-wall structure. C R Biol. 2004;327(9–10):873–80.

53. Evans RJ, Milne TA. Molecular characterization of the pyrolysis of biomass. 1. Fundamentals. Energy Fuels. 1987;1(2):123–37.

54. Kotake T, Kawamoto H, Saka S. Pyrolysis reactions of coniferyl alcohol as a model of the primary structure formed during lignin pyrolysis. J Anal Appl Pyrolysis. 2013;104:573–84.

55. Kotake T, Kawamoto H, Saka S. Mechanisms for the formation of monomers and oligomers during the pyrolysis of a softwood lignin. J Anal Appl Pyrolysis. 2014;105:309–16.

56. Nakamura T, Kawamoto H, Saka S. Condensation reactions of some lignin related compounds at relatively low pyrolysis temperature. J Wood Chem Technol. 2007;27(2):121–33.

57. Kotake T, Kawamoto H, Saka S. Pyrolytic formation of monomers from hardwood lignin as studied from the reactivities of the primary products. J Anal Appl Pyrolysis. 2015;113:57–64.

58. Dorrestijn E, Mulder P. The radical-induced decomposition of 2-methoxyphenol. J Chem Soc Perkin Trans. 1999;2(4):777–80.

59. Vuori A. Pyrolysis studies of some simple coal related aromatic methyl ethers. Fuel. 1986;65(11):1575–83.

60. Dorrestijn E, Epema OJ, van Scheppingen WB, Mulder P. o-Quinone methide as a common intermediate in the pyrolysis of o-hydroxybenzyl alcohol, chroman and 1,4-benzodioxin. J Chem Soc Perkin Trans. 1998;2(5):1173–8.

61. Dorrestijn E, Pugin R, Nogales MVC, Mulder P. Thermal decomposition of chroman. Reactivity of o-quinone methide. J Org Chem. 1997;62(14):4804–10.

62. Asmadi M, Kawamoto H, Saka S. The effects of combining guaiacol and syringol on their pyrolysis. Holzforschung. 2012;66(3):323–30.

63. Hosoya T, Kawamoto H, Saka S. Solid/liquid- and vapor-phase interactions between cellulose- and lignin-derived pyrolysis products. J Anal Appl Pyrolysis. 2009;85(1–2):237–46.

64. Asmadi M, Kawamoto H, Saka S. Pyrolysis reactions of Japanese cedar and Japanese beech woods in a closed ampoule reactor. J Wood Sci. 2010;56(4):319–30.

65. Hosoya T, Kawamoto H, Saka S. Pyrolysis behaviors of wood and its constituent polymers at gasification temperature. J Anal Appl Pyrolysis. 2007;78(2):328–36.

66. Hosoya T, Kawamoto H, Saka S. Different pyrolytic pathways of levoglucosan in vapor- and liquid/solid-phases. J Anal Appl Pyrolysis. 2008;83(1):64–70.

67. Fukutome A, Kawamoto H, Saka S. Gas- and coke-forming reactivities of cellulose-derived tar components under nitrogen and oxygen/nitrogen. J Anal Appl Pyrolysis. 2014;108:98–108.

68. Hosoya T, Kawamoto H, Saka S. Thermal stabilization of levoglucosan in aromatic substances. Carbohydr Res. 2006;341(13):2293–7.

69. Hosoya T, Kawamoto H, Saka S. Role of methoxyl group in char formation from lignin-related compounds. J Anal Appl Pyrolysis. 2009;84(1):79–83.

70. Asmadi M, Kawamoto H, Saka S. Thermal reactivities of catechols/pyrogallols and cresols/xylenols as lignin pyrolysis intermediates. J Anal Appl Pyrolysis. 2011;92(1):76–87.
71. Ledesma EB, Marsh ND, Sandrowitz AK, Wornat MJ. An experimental study on the thermal decomposition of catechol. Proc Combust Inst. 2002;29:2299–306.
72. Lomnicki S, Truong H, Dellinger B. Mechanisms of product formation from the pyrolytic thermal degradation of catechol. Chemosphere. 2008;73(4):629–33.
73. Marsh ND, Ledesma EB, Sandrowitz AK, Wornat MJ. Yields of polycyclic aromatic hydrocarbons from the pyrolysis of catechol [ortho-dihydroxybenzene]: temperature and residence time effects. Energy Fuels. 2004;18(1):209–17.
74. Ledesma EB, Marsh ND, Sandrowitz AK, Wornat MJ. Global kinetic rate parameters for the formation of polycyclic aromatic hydrocarbons from the pyrolysis of catechol, a model compound representative of solid fuel moieties. Energy Fuels. 2002;16(6):1331–6.
75. McMillen DF, Malhotra R, Hum GP, Chang SJ. Hydrogen-transfer-promoted bond scission initiated by coal fragments. Energy Fuels. 1987;1(2):193–8.
76. McMillen DF, Malhotra R, Chang SJ, Ogier WC, Nigenda SE, Fleming RH. Mechanisms of hydrogen transfer and bond scission of strongly bonded coal structures in donor solvent systems. Fuel. 1987;66(12):1611–20.
77. Jones BW, Neuworth MB. Thermal cracking of alkyl phenols – mechanism of dealkylation. Ind Eng Chem. 1952;44(12):2872–6.
78. Buryan P. Thermal-decomposition of dimethylphenol. J Anal Appl Pyrolysis. 1991;22(1–2):83–93.
79. Hosoya T, Kawamoto H, Saka S. Cellulose–hemicellulose and cellulose–lignin interactions in wood pyrolysis at gasification temperature. J Anal Appl Pyrolysis. 2007;80(1):118–25.

Chapter 12
Depolymerization Mechanisms and Product Formation Rules for Understanding Lignin Pyrolysis

Gaojin Lyu, Shubin Wu, and Rui Lou

12.1 Introduction

Lignin is a highly branched aromatic polymer of three phenylpropanoid monomers (conifer alcohol, coumaryl alcohol, and sinapyl alcohol) linked by a variety of C-O and C-C bonds, accounting for 15–35 % weight of plant cell wall [1]. Lignin provides physical strength and protection from pathogens to plants; on the other hand, it is a major source of recalcitrance to the bioconversion of lignocelluloses and needs to be removed. Current biological-platform technologies only use carbohydrates for fuels and chemicals and leave lignin as a residue. The most common proposal for lignin is use as a low-value solid fuel. Therefore, valorization of lignin to value-added products is crucial to the commercial success of any bioconversion technology [2, 3].

Structurally, lignin is a 3-D networked polymer that is biosynthesized in plants from three phenylpropane moieties by a radical combinatorial process. Considering the aromatic nature and associated properties of lignin, it has been identified as a promising feedstock for producing aromatic chemicals. Diverse technologies have been investigated and adopted to convert lignin into useful petroleum-like byproducts

G. Lyu
Key Lab of Pulp and Paper Science and Technology of the Ministry of Education, Qilu University of Technology, 250353 Jinan, China

State Key Laboratory of Pulp and Paper Engineering, South China University of Technology, 381 Wushan Road, 510640 Guangzhou, China

S. Wu (✉)
State Key Laboratory of Pulp and Paper Engineering, South China University of Technology, 381 Wushan Road, 510640 Guangzhou, China
e-mail: shubinwu@scut.edu.cn

R. Lou
Key Laboratory of Papermaking Technology and Special Paper Development of Shaanxi Provence, Shaanxi University of Science and Technology, 710021 Xi'an, China

and aromatics, such as pyrolysis, hydrogenolysis, and oxidation etc. [4–6]. Among all of these processes and technologies, pyrolysis is an attractive way to produce high-grade transportation fuels and value-added chemicals from lignin. Pyrolysis of different types of lignin with or without catalyst at elevated temperatures (400–600 °C) at short times (≤2 s) in the absence of oxygen is now widely studied [7, 8]. All of these studies that have been carried out in the past decades have achieved good results and provided a wealth of information in many aspects, such as thermal behavior and kinetic parameters of lignin pyrolysis [9, 10], release profiles of some volatile products [11, 12], effect of pyrolysis equipment, pyrolysis parameters, catalysts, and lignin sources on the products yields [7, 13–15]. However, the detailed depolymerization mechanisms of lignin are still insufficiently understood.

Studying the pyrolysis mechanism of lignin will not only help to obtain an understanding of biomass pyrolysis, but also provide guidance for the utilization of this byproduct. For example, Faravelli et al. [16] described the thermal degradation of lignin under pyrolysis conditions with a semi-detailed kinetic model. Approximately 100 molecular and radical species and pseudo-species were introduced and were involved in the reaction mechanism. Wang et al. [17–19] and Luo et al. [20] investigated and compared the pyrolysis behaviors of varied lignin polymers isolated ether from the same wood plant or from different tree species by using a variety of analytical methods. However, because of the complex structure of lignin, it is difficult to analyze detailed mechanisms through experiments. In recent years, it is popular to study the thermal decomposition mechanism of lignin and forecast possible reaction pathways by using its model compounds and employing theoretical methods [21–24]. To attempt a fundamental description of lignin thermolysis, Klein and Virk [25] simulated lignin pyrolyses at temperatures from 300 to 600 °C by a mathematical model that simulated the temporal evolution of lignin thermolysis products in each of four categories. The modest disagreements between simulated and experimental results can be traced to structural differences between the respective lignin substrates. Hou et al. [26] further developed integrated approaches and software tools for modeling lignin pyrolysis, which simplifies the complex lignin pyrolysis model and allows for engineering simulation of a wide range of lignins.

The monolignols in lignin are interlinked by a variety of linkages, such as β-O-4, α-O-4, 4-O-5, β-1, α-1, 5-5, etc., and the β–O–4 linkage usually accounts for 48–60 % of the total linkages depending on the type of the plants and the lignin isolation methods [1, 2]. The theoretical investigation of lignin pyrolysis mechanisms thus mainly studies model compounds (mostly monomers and dimers) that contains these linkages, especially ether bonds (β-O-4, α-O-4, 4-O-5) [27, 28]. Our previous work has been concerned with elucidating the pyrolysis behavior of lignins isolated from non-woody materials, with focus on the product formation and distribution rules, as well as computational methods for its thermal decomposition mechanism [29–32].

The scope of this chapter is to illustrate the depolymerization mechanism and product formation rules for two kinds of non-woody lignin that have been carefully isolated from *moso* bamboo and rice straw. First, reviews of the structural

characterization as well as qualitative and quantitative identification the major chemical bonds of two enzymatic/mild acidolysis lignin (EMAL) are given. Then, pyrolysis of the EMAL examines product identification and distribution as they vary with temperature. Density functional theory (DFT) studies of bond dissociation energies for EMAL model compounds are shown. Finally, the pyrolysis mechanism of EMAL is deduced and presented through a combination of experimental research and theoretical simulations.

12.2 Experimentation and Computational Calculation

12.2.1 Materials and Characterization

Bamboo (*moso* bamboo) and rice straw collected from Hunan Province (China) with leaves removed, were ground and screened with 40–60 mesh sizes (0.28–0.45 mm) for lignin preparation. The compositions of bamboo and rice straw analyzed according to National Standards Methods and literatures [33] are listed in Table 12.1.

The enzymatic/mild acidolysis lignin (EMAL) were isolated and purified from bamboo and rice straw according to methods described in literature [34, 35]. In summary, the ball milled bamboo or rice straw power (10 g) was subjected to enzymatic treatment by using industrial cellulase with an activity of 8000 U/mL carboxyl methyl cellulose (40 °C, 48 h, pH 4.5), after which the resulting impure lignin was centrifuged, washed, and freeze-dried. The impure lignin (5 g) was then suspended in 100 mL of dioxane//acidified deionized water solutions (85:15 v/v, 0.01 mol/L HCl) and extracted at 87 °C with sparging nitrogen gas for 2 h. The resulting

Table 12.1 Chemical composition of bamboo and rice straw used for enzymatic/mild acidolysis lignin (EMAL) isolation

Composition	Content (w_{db}%)	
	Bamboo	Rice straw
Hot water extractive	14.14	10.10
1%NaOH extractive	22.88	38.12
Acetone extractive	2.73	3.72
Benzene-alcohol extractive	4.34	2.34
CH_2Cl_2 extractive	1.13	2.35
Alcohol nitrocellulose	43.19	34.38
Holocellulose	70.67	58.93
Pentosan	17.50	19.61
Acid-insoluble lignin	23.77	21.34
Acid soluble lignin	3.46	1.57
Ash	0.62	13.53

mixture solution was filtered and the combined filtrate solutions were neutralized with sodium bicarbonate. The neutralized solutions were then rotary evaporated to obtain a thick solution. Then, the thick solution was carefully added into excessive acidified deionized water (pH 2.0, HCl) and the precipitated lignin was isolated by centrifuging, washing and freeze-drying. The obtained lignin was washed with HPLC grade hexane and dried in a vacuum oven at room temperature.

Detailed analysis of the chemical composition and structure of the two lignins were firstly carried out to benefit follow-up research on its depolymerization mechanism. The organic elements were determined using an elemental analyzer (Vario EL, Elementar, Germany). The weight-averaged molecular weight (M_w) and number-averaged molecular weight (M_n) of two EMAL were estimated by gel permeation chromatography (GPC) on a HPLC system (ICS 3000, Dionex, Sunnyvale, CA) with a UV detector. The structural characterization of bamboo and rice straw EMAL were investigated by FT-IR, ^{1}H NMR, ^{13}C NMR, and quantitative ^{31}P NMR techniques. Details on the analysis procedures can be found in previous publications [29].

12.2.2   Pyrolysis and Product Analysis

EMAL was first pyrolyzed with a TG–FTIR setup, which consists of a thermogravimetric analyzer (TGA, NETZSCH STA 499C, Germany) and a FTIR spectrometer (TENSOR 27, BRUKER, Germany). About 8–10 mg EMAL sample was pyrolyzed under a nitrogen stream (40 mL/min) from 40 to 800 °C at a heating rate of 20 °C/min. Data on the mass loss were collected automatically with an integrated thermal gravimetric analyzer. The released volatiles were purged immediately to a gas cell via a Teflon tube (preheated to 180 °C), followed by the FTIR analysis using mercury cadmium telluride (MCT) detector. The spectrum scanning range was 4000–400 cm^{-1} and the resolution factor was 4 cm^{-1}.

Fast pyrolysis of the prepared EMAL was carried out in a Py–GC/MS system that includes a JHP–3 model Curie–point pyrolyzer (CDS 5200, USA) and a Shimadzu QP 2010 Plus gas chromatograph/mass spectrometer (Japan). Based on the pyrolysis behavior of EMAL obtained from TGA, the pyrolysis temperature here was set at 250 °C, 320 °C, 400 °C, 600 °C, and 800 °C, respectively.

Approximately 0.1 mg of samples were pyrolyzed with an event time of 0.5 s, and the obtained pyrolysis products were separated with an Agilent DB–5MS column (30 m×0.25 mm I.D., 0.25 μm film). Helium was used as carrier gas with a flow rate of 1.2 mL/min. The oven temperature was programmed from 50 °C (2 min) to 250 °C (5 min) at 10 °C/min. The injector temperature was set at 230 °C in split mode with split ratio of 50:1. The MS detector was operated in electron impact (EI, 70 eV) ionization mode with the ion source temperature and quadrupole temperature set to be 230 °C and 150 °C, respectively. Scanning ion range was set to be between m/z 45–550.

The detected ion peaks were analyzed and compared with the database (NIST 08 library), and the peak similarity (SI) ≥90 was selected to integrate on the area of peaks. After area normalization, the obtained peak area percentage acts as the yield of pyrolysis products.

12.2.3 Theoretical Study of Bond Dissociation Energies

To study the mechanism of EMAL pyrolysis and the formulate rules for its main products, , density functional theory B3P86 method was adopted for calculation of bond dissociation energies (E_B) of the major types of linkage in EMAL. The equilibrium geometries of reactants and free radicals were fully optimized by employing the hybrid density functional at B3LYP/6-31G(d, p) level. Standard thermodynamic parameters at 298 K were obtained by vibrational frequency calculations, including the zero-point energy correction (ZPE). The multiple conformers were fully optimized to find the energy minima. Then, the global energy minimum (without imaginary frequency) was identified through comparisons of these energy minima, and was selected as the research object. Bond dissociation energy, E_B, was calculated as:

$$E_B(R-X) = E(R) + E_{ZP}(R) + E(X) + E_{ZP}(X) - E(RX) - E_{ZP}(RX) \qquad (12.1)$$

where E_B refers to bond dissociation energy; E is molecular energy and E_{ZP} is zero-point energy; RX refers to a molecule which is consist of group R and group X; R-X is the chemical bond between group R and group X; R and X refer to the intermediate radicals formed by RX molecule homolytic cleavage. All calculations were performed using the Gaussian 03 suite of programs.

12.3 Results and Discussion

12.3.1 Characterization of EMAL

Elemental analysis of the lignin from bamboo and rice straw is summarized in Table 12.2. As shown in Table 12.2, lignin had high C content (50–60 %) and low O and H content, thus has a low H/C and O/C ratio. Compared with rice straw lignin, bamboo lignin had higher C content and lower H and O content.

As shown in Table 12.3, the weight-averaged molecular weight (M_w) and number-averaged molecular weight (M_n) of the bamboo lignin were 9000 and 6000, respectively, while those of rice straw lignin were a little lower, i.e. 8300 and 4700, respectively. The large molecular weight of EMAL indicates that the original lignin structure was less damaged than industrial residual lignin and its typical chemical bonds were retained during isolation.

Table 12.2 Elemental analysis of enzymatic/mild acidolysis lignins (EMALs) isolated from bamboo and rice straw

Samples	Elements (w_{daf}%)					O/C^b	H/C	HHV (MJ/kg)^c	Formula
	C	H	O^a	N	S				
Bamboo EMAL	58.74	5.72	32.90	2.58	0.06	0.42	1.17	24.15	$CH_{1.17}O_{0.42}N_{0.037}$
Rice straw EMAL	50.42	6.24	42.90	0.35	0.09	0.64	1.49	20.35	$CH_{1.49}O_{0.64}N_{0.006}$

^{a}Calculated by difference
^{b}Atomic ratio
^{c}Higher heating value, evaluated using the Dulong's formula

Table 12.3 Molecular weights of enzymatic/mild acidolysis lignins (EMALs) isolated from bamboo and rice straw

Sample	$\overline{Mn}$	$\overline{Mp}$	$\overline{Mw}$	$\overline{Mz}$	PD
Bamboo EMAL	6019	10,721	9036	12,472	1.50
Rice straw EMAL	4732	10,643	8295	12,319	1.75
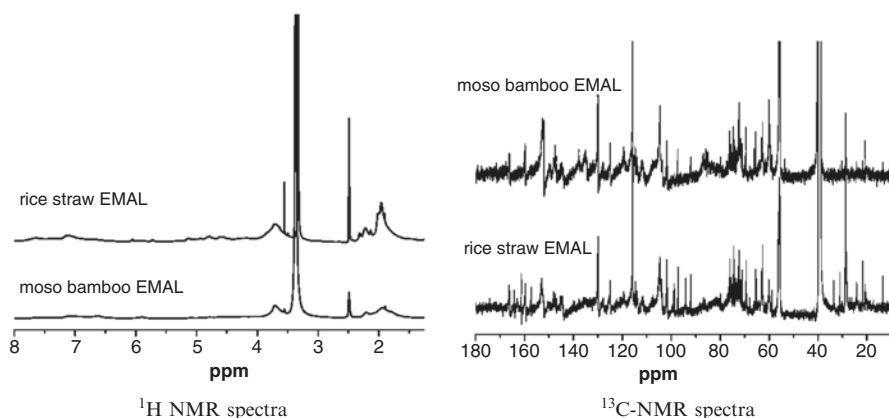
Fig. 12.1 ^{1}H NMR spectra, ^{13}C-NMR spectra of bamboo and rice straw enzymatic/mild acidolysis lignins (EMALs)

According to the FT-IR spectra of bamboo and rice straw EMAL (spectra were not shown here) [36], the IR absorbance of the two non-woody biomass lignin were roughly the same except for some absorption peak intensity were varied. The absorbance at 1330 and 1125 cm^{-1} indicates that the two EMAL contained guaiacyl and syringyl units, and the band at 1260 cm^{-1} represent p-hydroxyphenyl unit.

The structural features of the two EMAL were further explored with ^{1}H-NMR and ^{13}C-NMR. The results are presented in Fig. 12.1. In addition to the three kinds of units in lignin, both of the two EMAL have characteristics of β-O-4 structures
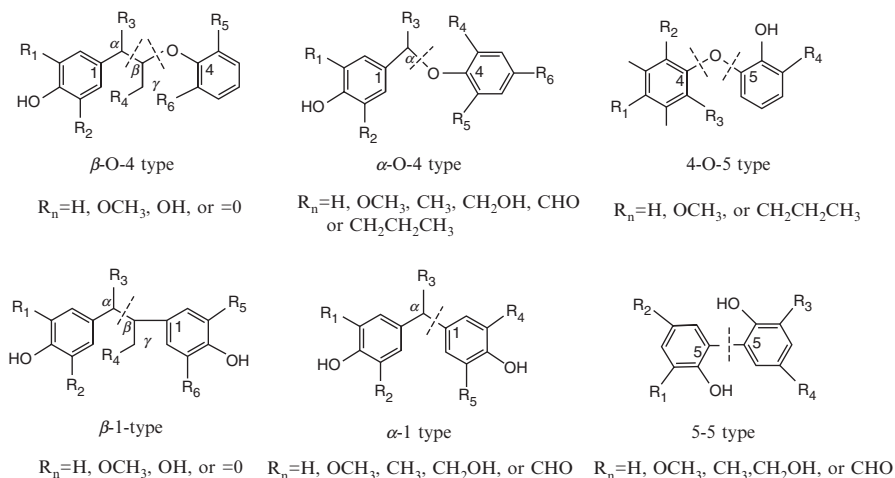
Fig. 12.2 Chemical structure of six linkages present in bamboo and rice straw enzymatic/mild acidolysis lignin (EMAL) and their homolytic cleavage ways (Reprinted with permission from Ref. [42], Copyright © 2015 Elsevier)

(signals at 4.6 and 6.0 ppm in ^{1}H NMR and 61.0–57.0 ppm in ^{13}C NMR), some carbon–carbon linked (condensed) structures such as β-1 (75.2 ppm), β-5 (63.2 and 87.6 ppm), β-β (70.5 and 72.6 ppm), and 5–5 (83.7 ppm) were still present in the EMAL, although their intensities varied depending on the lignin preparation procedure and the raw materials. Compared with bamboo EMAL, which contains more methoxy group and syringyl units, and β-1, β-5 and α-O-4 linkages, the rice straw EMAL has more guaiacyl units and β-β, 5-5 linkages. The identified typical substructures of both bamboo and rice straw EMAL are shown in Fig. 12.2.

The ^{31}P NMR spectra were used to distinguish the phenolic hydroxyl from aliphatic hydroxyl in lignin because the peaks between phenolic hydroxyl and aliphatic hydroxyl are overlapped in ^{1}H NMR. Quantitative ^{31}P NMR of the two EMAL before and after derivatization followed by reductive cleavage (DFRC) were carried out (spectra not shown here). Table 12.4 shows the content of non-condensed and/or condensed phenolic hydroxyl of bamboo and rice straw EMAL. The results illustrate that the carboxyl and total phenolic hydroxyl content of rice straw EMAL were 0.091 mmol/g and 3.085 mmol/g, respectively, which are higher than the corresponding content of bamboo EMAL (0.027 mmol/g and 1.996 mmol/g). The guaiacyl hydroxyl and *p*-hydroxyphenyl hydroxyl of rice straw EMAL were also higher than those of bamboo EMAL. These results are consistent with the FTIR and ^{1}H NMR results.

Table 12.4 Functional groups content of enzymatic/mild acidolysis lignin (EMAL) determined by quantitative ^{31}P-NMR

Shift δ (ppm)	Functional group	Content (mmol/g)	
		Rice straw EMAL	Bamboo EMAL
147.4~145.8	Aliphatic hydroxy	5.353	6.339
144.8~143.1, 142.34~141.5	Total condensed phenol hydroxyl	0.575	1.228
143.1~142.4	Syringyl hydroxyl	0.282	0.146
140.0~138.8	Guaiacyl hydroxyl	1.041	0.302
138.2~137.4	p-hydroxyphenyl hydroxyl	1.187	0.321
135.5~134.5	Hydroxyl in carboxylic acid	0.091	0.027
	G:S	3.69	2.07
	Total phenol hydroxyl	3.085	1.996

12.3.2 Thermal Analysis

Pyrolysis characteristics of EMAL isolated from bamboo and rice straw were firstly investigated by TG–FTIR. Both thermogravimetric (TG) and differential thermogravimetric (DTG) curves of the two EMAL, obtained at heating rate of 20 °C/min, are plotted in Fig. 12.3. Thermogravimetric analysis has manifested that the decomposition of the EMAL occurred over a wide temperature range from approximately 150–800 °C and the generated solid residue was 34 % and 32 % for rice straw and bamboo EMAL, respectively. Both the two EMAL curves recorded a maximum weight loss peak at 384 °C and a visible shoulder peak at 270 °C, which the rice straw was bigger. This indicates that the rice straw and bamboo EMAL pyrolysis experience two rapid reactions in the major mass loss temperature range. It has been shown from the structural characterization that both rice straw and bamboo EMAL contain abundant aromatic rings as well as various branches, and the different activities of these diverse chemical bonds and the functional groups in EMAL led to its degradation in a wide temperature range and even at different pyrolysis temperature.

For engineering applications, understanding pyrolysis kinetics is necessary for predicting the pyrolysis behavior as well as for the design of suitable reactor. Thus, Eq. (12.2) obtained by the integral Coats–Redfern [11, 35, 37] method was adopted to estimate the kinetic parameters of bamboo and rice straw EMAL, where β is the heating rate, T is the absolute temperature and R is the universal gas constant. The reaction rate was determined by both the activation energy (E) and the pre-exponential factor (A) based on Arrhenius theory. In order to avoid unnecessary
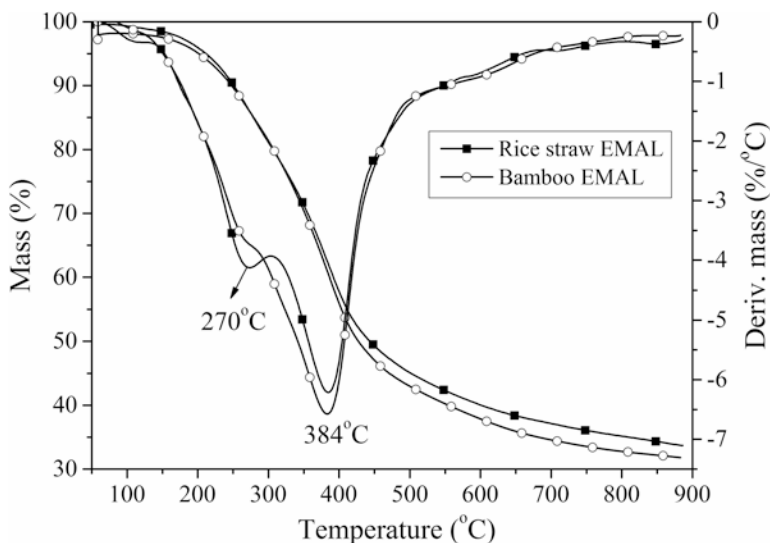
Fig. 12.3 TG and DTG curves of bamboo and rice straw enzymatic/mild acidolysis lignin (EMAL) at heating rate of 20 °C/min
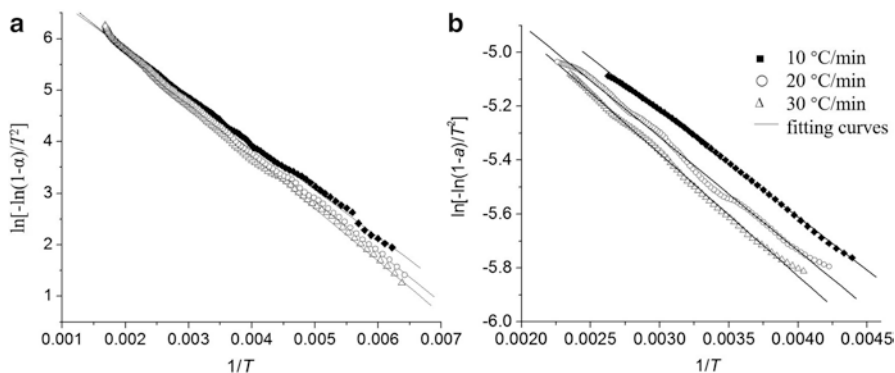
Fig. 12.4 Arrhenius plots of rice straw (**a**) and bamboo (**b**) enzymatic/mild acidolysis lignin (EMAL) pyrolysis at different heating rates

experimental errors because of the initial and the end of pyrolysis process, the kinetic evaluations mainly focus on the main decomposition temperature ranges (200–600 °C).

$$\ln\left[\frac{-\ln\left(1-\alpha\right)}{T^2}\right] = \ln\frac{AR}{\beta E}\left[1 - \frac{2RT}{E}\right] - \frac{E}{RT} \qquad (12.2)$$

The Arrhenius plots of rice straw and bamboo EMAL pyrolysis at different heating rates are displayed in Fig. 12.4 and the obtained kinetic parameters are listed in

Table 12.5 Kinetic parameters of rice straw and bamboo enzymatic/mild acidolysis lignin (EMAL) pyrolysis at different heating rates

	Rice straw EMAL			Bamboo EMAL		
β (°C/min)	E (kJ·mol^{-1})	ln$A$ (min^{-1})	R^2	E (kJ·mol^{-1})	ln$A$ (min^{-1})	R^2
10	17.40	17.53	0.999	24.81	10.10	0.999
20	18.79	17.85	0.999	31.38	21.19	0.998
30	19.55	17.99	0.999	34.07	24.89	0.999

Table 12.5. This indicates that the kinetic parameters derived by global activation energy model here are linearly correlated, and all correlation coefficients (R^2) are higher than 0.99. The whole activation energy distribution for rice straw EMAL pyrolysis is located in the lower range (17.4–19.6 kJ/mol) than that of bamboo EMAL (24.8–34.1 kJ/mol), implying poor thermal stability for rice straw EMAL. In addition, the average activation energies for both rice straw and bamboo EMALs increased with heating rate increases.

Volatiles released from bamboo and rice straw EMAL pyrolysis were detected on–line using FTIR, and their FTIR spectra varied with pyrolysis temperature are plotted in Fig. 12.5. As shown in Fig. 12.5, as the pyrolysis time and temperature increases, the infrared absorption peak in the range of 1000–2000 cm^{-1} varied the most significantly. The characteristic bands in this range are mainly attributed to C-H stretching, C-C skeleton, C=O stretching, C-O-C and OH stretching vibrations, indicating the resulting products are mainly phenolic compounds and small molecule carboxylic acids, aldehydes, and alcohols etc. [12, 38]. All of these products released abundantly in the temperature range of 200–600 °C, wherein methanol, carboxylic acids and phenols have a maximum releasing rate at 415 °C, 330 °C, and 380 °C, respectively; while that of CH_4, CO_2 and CO usually released in a wider temperature range with maximum rates close to 430 °C, 270 °C and 520 °C, respectively. Peak at 3017 cm^{-1} was the characteristic absorption of CH_4, indicating the yield of CH_4 increases with increasing pyrolysis temperature. The CO_2 has characteristic absorption at 2200 cm^{-1}, which probably arose from the decomposition of carboxyl, carbonyl and ether groups in the phenylpropane side chains [11, 12]. As the pyrolysis temperature rises, CO_2 evolution rate from bamboo EMAL pyrolysis showed an increasing trend, while that of rice straw EMAL had a maximum evolution rate between 270 and 380 °C. The difference in evolution behavior of the two EMALs is attributed to the differences in their chemical structures.

12.3.3   Pyrolysis Products of EMAL

To reliably identify the individual pyrolysis products generated from bamboo and rice straw lignin, the two EMALs were further subjected to pyrolysis by using Py-GC/MS at 250, 320, 400, 600, and 800 °C respectively [30, 31, 39, 40]. Table 12.6
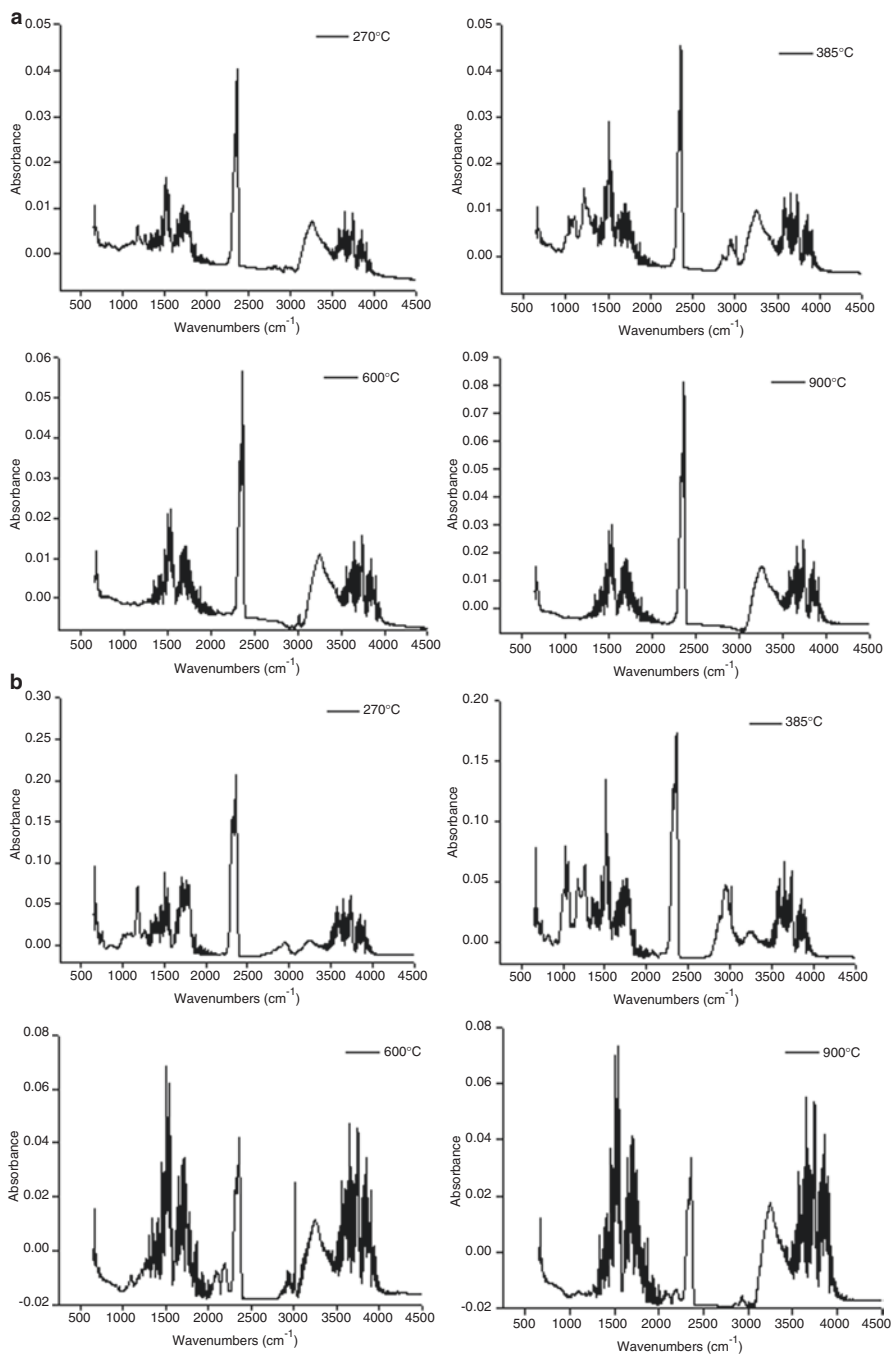
Fig. 12.5 FTIR spectra of pyrolysis volatiles of bamboo (**a**) and rice straw (**b**) enzymatic/mild acidolysis lignin (EMAL) varied with temperature

Table 12.6 Products identification from bamboo and rice straw enzymatic/mild acidolysis lignin (EMAL) pyrolyzed at 600 °C

R.T (min)	Compounds	SI	MF	Mw	Yield (Area %) Bamboo	Rice straw
1.971	Acetic acid	96	$C_2H_4O_2$	60	–	2.69
4.285	Furfural	98	$C_5H_4O_2$	96	–	1.34
8.682	Phenol	98	C_6H_6O	94	1.61	1.42
10.578	p-Cresol	98	C_7H_8O	108	1.01	2.36
10.688	Guaiacol	97	$C_7H_8O_2$	124	3.78	3.77
11.875	2,4-xylenol	97	$C_8H_{10}O$	122	–	3.00
12.175	p-Ethylphenol	98	$C_8H_{10}O$	122	0.74	2.27
12.562	p-Methylguaiacol	93	$C_8H_{10}O_2$	138	1.45	3.33
12.979	2,3-Dihydrobenzofuran	91	C_8H_8O	120	36.05	31.11
13.921	p-Ethylguaiacol	96	$C_9H_{12}O_2$	152	–	1.55
14.065	4-Allylphenol	90	$C_9H_{10}O$	134	–	1.45
14.250	2-Methyl-4-hydroxyacetophenone	94	$C_9H_{10}O_2$	150	–	11.04
14.373	4-Vinylguaiacol	91	$C_9H_{10}O_2$	150	7.23	–
14.773	Syringol	92	$C_8H_{10}O_3$	154	9.69	5.61
15.027	Eugenol	95	$C_{10}H_{12}O_2$	164	-	1.16
15.334	Vanillin	94	$C_8H_8O_3$	152	2.64	2.40
16.114	Methylsyringol	90	$C_9H_{12}O_3$	168	2.98	4.04
16.242	E-isoeugenol	93	$C_{10}H_{12}O_2$	164	2.66	2.64
17.206	2,6-Di-tert-butyl-p-cresol	96	$C_{15}H_{24}O$	220	2.10	2.16
17.576	1-(3,5-dimethoxyphenyl)-Ethanone	90	$C_{11}H_{24}$	180	6.63	4.06
18.528	Syringaldehyde	94	$C_9H_{10}O_4$	182	2.42	–
19.169	Methoxyeugenol	90	$C_{11}H_{14}O_3$	194	5.06	3.10
19.400	Acetosyringone	91	$C_{10}H_{12}O_4$	196	-	2.22
19.445	Coniferyl alcohol	90	$C_{10}H_{12}O_3$	180	9.49	–
21.901	Sinapylaldehyde	91	$C_{11}H_{12}O_4$	208	1.96	–
22.116	Pentadecylic acid	95	$C_{15}H_{30}O_2$	242	-	1.21
23.760	p-p′-Isopropylidenebisphenol	94	$C_{15}H_{16}O_2$	228	4.46	–
24.796	Allylphthalate	90	$C_{14}H_{14}O_4$	246	1.37	–

summarizes the pyrolysis products of the EMAL pyrolyzed at 600 °C (TIC and products of other temperatures were not shown).

As shown in Table 12.6, pyrolysis products of EMAL were mainly aromatics, wherein mostly were different kinds of phenolic compounds and 2,3-dihydrobenzofuran (DHBF). There was a small amount of furfural, esters, acetic acid,, benzene, and toluene present that were mostly generated at high temperatures. There were a total of 33 kinds of products from bamboo EMAL pyrolysis at different pyrolysis temperatures, among which 2,3-dihydrobenzofuran, 6-di-tert-butyl-p-cresol, and allylphthalate possess a larger proportion under low temperature pyrolysis (250 °C, 320 °C). However, the thermal stability of these products was poor, and many may undergo depolymerization into other phenolics, so their content

was reduced rapidly and even disappeared (except for DHBF) as temperature increased further. For pyrolysis temperatures of 320–600 °C, the major monophenols from bamboo EMAL pyrolysis were methoxyeugenol, 4-ethenylguaiacol, syringol, and 1-(3,5-dimethoxyphenyl)-ethanone etc. At 800 °C, acetic acid,, phenol, and alkyl-substituted phenol such as o-cresol, p-cresol and p-ethylphenol that potentially originated from secondary depolymerization of pyrolysis volatiles increased. Roughly speaking, the product species from rice straw lignin pyrolysis are similar to those of bamboo lignin except for their relative content and variation with temperature that differ slightly.

According to its structural features, the identified mono phenolic compounds from bamboo and rice straw EMAL pyrolysis can be classified into G-phenols (derived from guaiacyl), S-phenols (derived from syringyl), and H-phenols (derived from p-hydroxyphenyl) [38, 40]. The grouped compounds and their structure are illustrated in Fig. 12.6.

12.3.4   Products Distribution

The variation of yields of grouped compounds with pyrolysis temperature is presented in Fig. 12.7. As shown in Fig. 12.7, the pyrolysis temperature has a distinct impact on the yield of G-, S- and H-phenols. The trends of total phenols from bamboo and rice straw EMAL have some differences. As the pyrolysis temperature increased, the total phenols yield of bamboo EMAL reached a maximum of 63 % at 600 °C and then reduced gradually, while that of rice straw EMAL increased. Although slightly different on total phenols, the overall trends of G- and S-phenols between bamboo and rice straw EMAL were consistent, i.e. both of them reached their highest yield at 600 °C and S-phenol was slightly higher than G-phenols. H-phenols increased rapidly at high temperatures, and was more than the other two types of phenols when temperature exceeds 700 °C. The amount of DHBF occupied a large proportion in the pyrolysis products from EMAL pyrolysis, especially at lower temperatures. As temperature increased, DHBF may further depolymerize into simple phenols. Compared with bamboo EMAL, rice straw EMAL produced more DHBF. According to the hypothesis suggested by Takashi et al. [41], DHBF is formed through the recombination of allyl radical intermediate compound during pyrolysis. It is worth noting that, different results would be obtained from different lignin types. DHBF content from herbaceous lignin pyrolysis was higher than from woody lignin, meanwhile proto lignin with well-preserved structure such as EMAL and milled wood lignin (MWL) usually produced more DHBF than industrial lignin or other lignin model compounds [17, 19, 30, 31]. This is related to the structure and chemical bonding of lignin. EMAL from plants has more phenyl coumaran structure (connected from α-O-4 and β-5 bonds) that is the main precursor to form DHBF [40].

Yields of major mono phenols from bamboo and rice straw EMAL pyrolysis varying with pyrolysis temperature are plotted in Fig. 12.8. Figure 12.8a and b show the

H-phenols

phenol   o-cresol   p-cresol   2,4-xylenol   4-ethylphenol   4-allylphenol

G-phenols

guaiacol   p-methylguaiacol   4-vinylguaiacol   vanillin

p-propylguaiacol   eugenol   (E)-isoeugenol   coniferylalcohol

S-phenols

syringol   methylsyringol   syringaldehyde

acetosyringone   methoxyeugenol   sinapylaldehyde
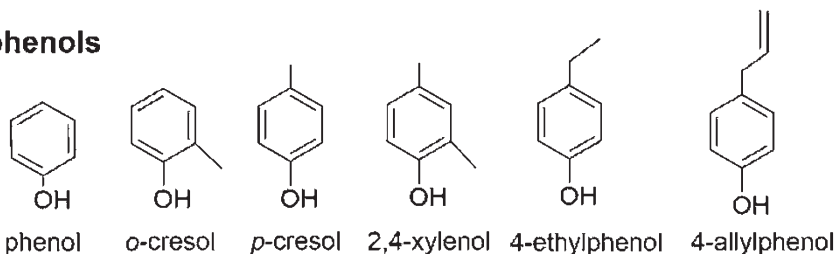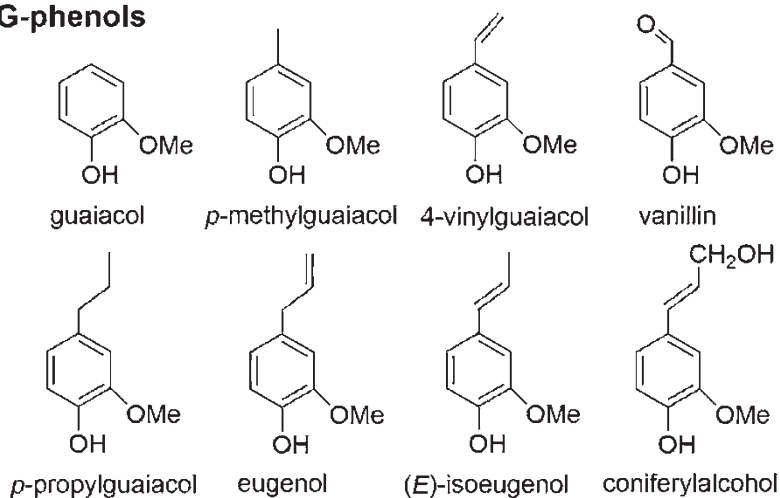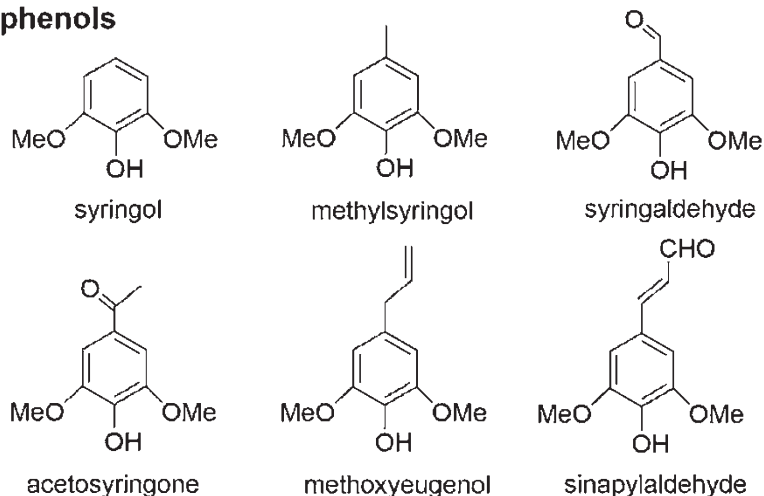
Fig. 12.6 Chemical structures of identified mono phenols from enzymatic/mild acidolysis lignin (EMAL) pyrolysis (Adapted with permission from Ref. [31], Copyright © 2010 Elsevier)
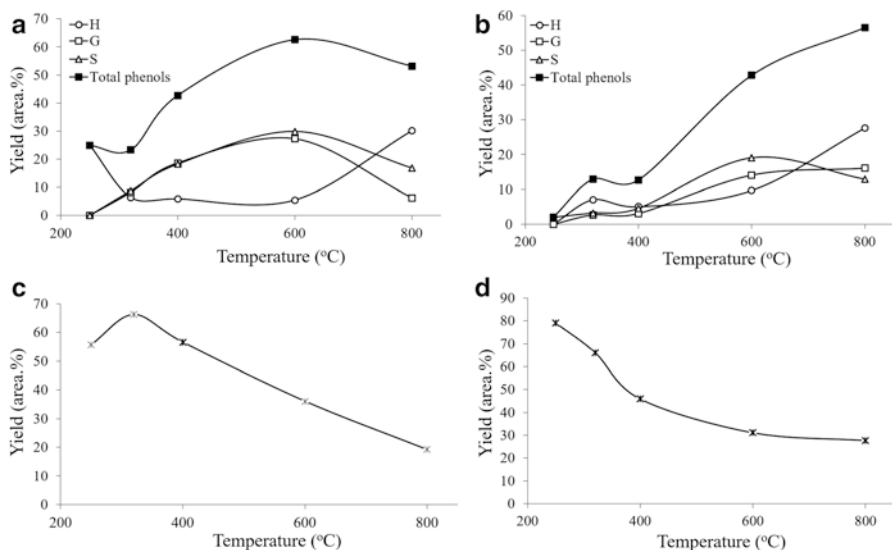
Fig. 12.7 Grouped products yields varied with pyrolysis temperature: (**a**) H-, G- and S-phenols of bamboo enzymatic/mild acidolysis lignin (EMAL), (**b**) H-, G- and S-phenols of rice straw EMAL, (**c**) 2,3-dihydrobenzofuran (DHBF) of bamboo EMAL, (**d**) DHBF of rice straw EMAL

major G-type phenols as functions of the pyrolysis temperature. Bamboo EMAL produced more 4-vinylguaiacol,, vanillin and *E*-isoeugenol at 320 °C–400 °C. These products predominating at low temperature are originated from directly depolymerization of lignin guaiacyl units and usually retain relatively complex functional groups on side chains such as aldehyde and unsaturated vinyl groups [11, 22]. As pyrolysis temperature increases, the side chains of the first depolymerization products began peeling off and reform to generate 4-methylguaiacol and guaiacol. At 600 °C, the pyrolysis products 4-methylguaiacol and guaiacol reached their highest yields. As the temperature further increased to 800 °C, guaiacol and its derivatives undergo demethylation and demethoxylation reactions to form phenol and simple substituted phenols [21, 27, 39]. Since the molecular structure of bamboo and rice straw EMAL has some differences, the thermal cracking pathways may not be exactly the same, but guaiacol and their derivatives distribution with temperature are consistent.

Syringol, methoxyeugenol, 4-methylsyringol, and sinapylaldehyde have syringly structure (Fig. 12.8c and d). When temperature is below 400 °C, only methoxyeugenol emerged as S-type phenols in EMAL pyrolysis. As temperature is increased to 600 °C, syringol and 4-methylsyringol reach their maximum yields, then undergo demethylation and demethoxylation as temperature is further increased. These trends are similar to those of guaiacol and its derivatives. From Fig. 12.8e and f, it can be seen that there are no simple substituted H-phenols from both bamboo and rice straw EMAL pyrolysis at low temperature. Until temperature is increased to 600 °C, generation of a large number of H-type phenols occurs, and continues to increase with further increases in temperature. It can be understood from the above analysis that the EMAL has its strongest first pyrolysis reaction and generates most
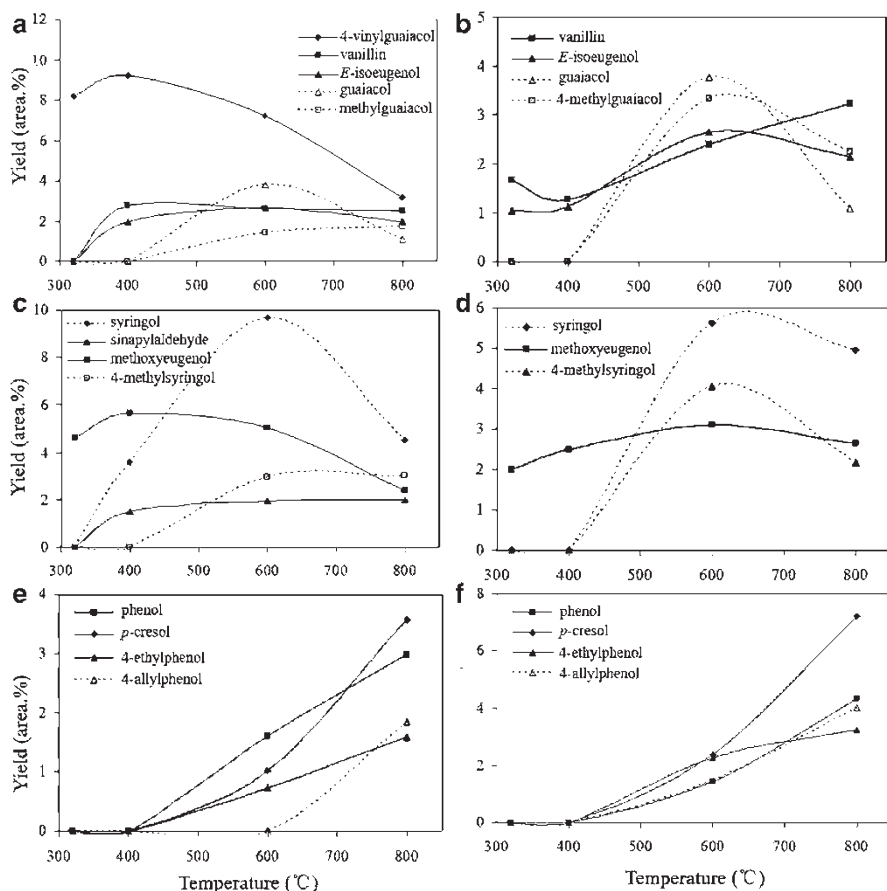
Fig. 12.8 Influence of temperature on products distribution: (**a**) G-phenols, (**c**) S-phenols, (**e**) H-phenols from bamboo enzymatic/mild acidolysis lignin (EMAL) pyrolysis, (**b**) G-phenols, (**d**) S-phenols, (**f**) H-phenols from rice straw EMAL pyrolysis

abundant kinds and yields of G- and S-type phenolic compounds at 600 °C. When the pyrolysis temperature increases further, those phenolic compounds having various functional groups begin secondary cracking and form small molecular gases along with benzene, phenol or simple substituted phenols.

12.3.5 Bond Dissociation Energies of Lignin Model Compounds

Because of the complexity of its structure, the lignin pyrolysis mechanism is usually explored and investigated by using diverse of lignin model compounds. Radical reactions are considered to be the dominant reactions in the pyrolysis of lignin
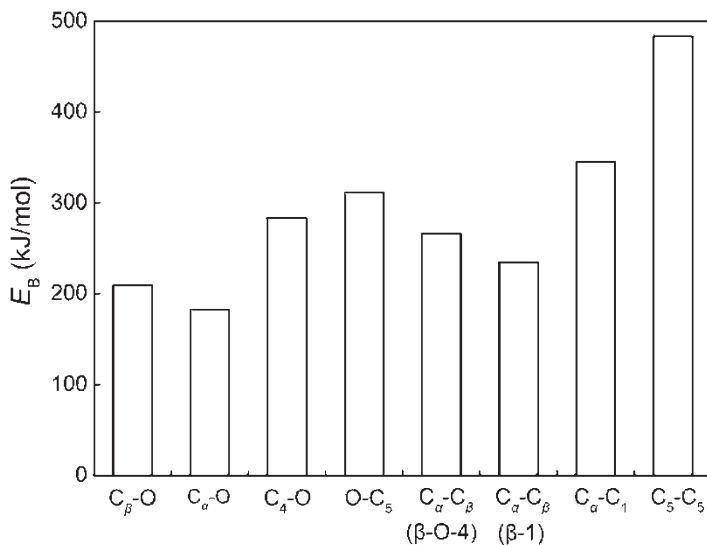
Fig. 12.9 Comparison of average E_B of C-O and C-C bonds of various linkages from lignin model compounds (Reprinted with permission from Ref. [42], Copyright © 2015 Elsevier)

[21, 32]. Bond dissociation energy is an important parameter which can exemplify the chemical activity of free radical reactions, i.e. the smaller of the bond dissociation energy, the easier that the chemical bond can be broken [22]. So the research on bond dissociation energy will benefit the further understanding of EMAL pyrolysis mechanism. Based on the aforementioned chemical structure interpretation of the two EMAL, 63 lignin model compounds that contain six prevalent linkages (i.e. β–O–4, α–O–4, 4–O–5, β–1, α–1 and 5–5) were selected (see Fig. 12.2) for theoretically calculation by using density functional theory method. Detailed information on the bond dissociation energies (E_B) and bond lengths of each linkage in 63 lignin model compounds, as well as the effect of various substituents on E_B and the correlation between the bond lengths and the corresponding E_B are illustrated in previous work [32, 42].

Figure 12.9 shows a comparison of average E_B of C–O and C–C bonds of various linkages in lignin model compounds. Figure 12.9 shows that the E_B of C–O bond is generally lower than that of C–C bond, while the E_B of $C_{aromatic(4,5)}$–O bond and $C_{aromatic(1,5)}$–$C_{(\alpha,5)}$ bond that is connected to the benzene ring is high. In all the types of linkages, the average E_B of C_α–O in α–O–4 linkage model compound is the lowest (182.7 kJ/mol), that is followed by the average E_B of C_β–O in β–O–4 linkage (209.4 kJ/mol). The C_5–C_5 in 5–5 linkage model compounds has the highest average E_B of 483.4 kJ/mol. The order of the average E_B is as follows: C_α–O $< C_\beta$–O $< C_\alpha$–C_β (β–1) $< C_\alpha$–C_β (β–O–4) $< C_4$–O $<$ O–C_5 $< C_\alpha$–C_1 $< C_5$–C_5.

The above analysis shows that during the process of lignin pyrolysis, C_α–O and C_β–O bonds are easily cracked, and the homolytic cleavage of C_α–O and C_β–O bonds is the dominant pyrolysis pathway. Almost all kinds of phenolic compounds,

especially the above-mentioned G- and S- type phenols (see Fig. 12.6), can be formed through the homolytic cleavage of C_α–O and C_β–O bonds. The C_α–C_β (both in β–1 and β–O–4) bond is also easy to be fractured, and the homolytic cleavage of C_α–C_β bond is the main competitive pyrolysis pathway. Cleavage of the C_α–C_β bond in the β–O–4 linkage often occurs in the secondary depolymerization of some pyrolysis products, thus forming simple alkanes substituted H-type phenolic compounds. The E_B of C_5–C_5 was so high that it was hard to be fractured. So the 5–5 linkage was easy to undergo cyclization during lignin pyrolysis and further transform into coke. These computational analyses are consistent with the previous experimental results [30, 39].

12.3.6 Pyrolysis Mechanism of EMAL

Based on the above analysis of various linkages of EMAL structure and their bond dissociation energies, as well as the dominating products of EMAL pyrolysis and the distribution laws vary with pyrolysis temperature, the formation mechanism can be discussed. Figure 12.10 shows a proposed formation mechanism of EMAL pyrolysis products.

When EMAL is pyrolyzed, the ether bond and C-C bonds connected between lignin phenylpropane monomers are first cleaved, such as cracking of β–O–4, α–O–4, 4-O-5, and β-1, and generate relatively high molecular weight aromatic compounds (mostly as intermediates) as well as some small molecule gases (CO_2, CO) [31, 40]. Then, as the pyrolysis temperature is increased to moderate temperatures (400–600 °C), the side-chain functional groups of lignin and/or unstable intermediate are split or undergo homolytic cleavage to form many G- and S-phenols, such as guaiacol, 4-vinylguaiacol, and syringol (Fig. 12.10a). At higher temperatures (800 °C), further rupturing of the G- and S- phenols causes the methyl and methoxy groups to be removed and thus the H-phenols become dominant in the products. Most of the pyrolysis products are generated through radical-induced reactions and homolysis reactions [42]. The intermediate, o-quinone methide is important, because it has an allyl-methyl group with comparably weak C-H bonds. In the EMAL pyrolysis process, weak C-H bonds dissociate to form the ally radical intermediate through H-abstraction. The following cyclization gives 2,3-benzofuran, that is followed by H-reduction reaction to produce 2,3-dihydrobenzofuran (Fig. 12.10b) [40, 41].

12.4 Conclusions and Future Outlook

The depolymerization mechanism and products formation rules of two kinds of enzymatic/mild acidolysis lignins (EMAL) from bamboo and rice straw were investigated through the combination of experimental research and theoretical
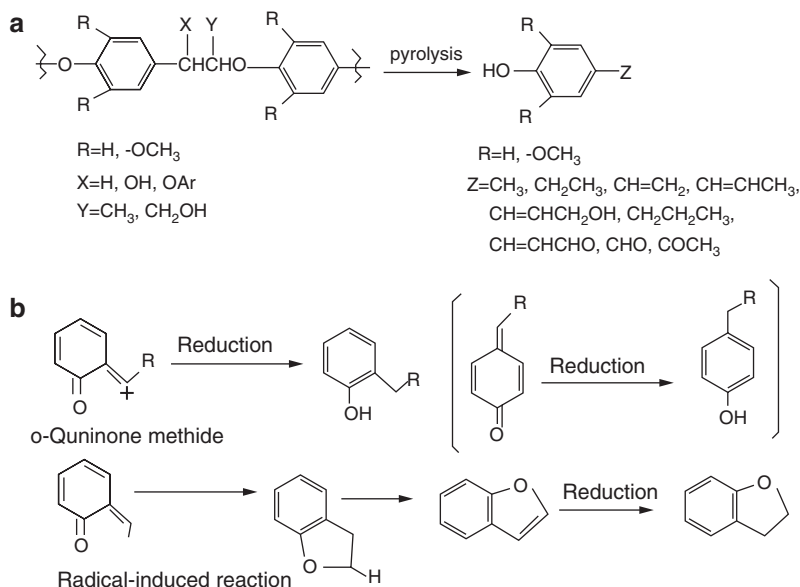
Fig. 12.10 Proposed formation mechanism of enzymatic/mild acidolysis lignin (EMAL) pyrolysis products

simulation. Identification followed by theoretical calculation of the bond dissociation energies (E_B) of the prevalent linkages in EMAL gives the order of the average E_B as follows: C_α–O < C_β–O < C_α–C_β (β–1) < C_α–C_β (β–O–4) < C_4–O < O–C_5 < C_α–C_1 < C_5–C_5. This determination allows one to understand the formation and distribution rules of lignin pyrolysis products. The results indicate that during the process of lignin pyrolysis, the C-O-C ether bonds and C-C bonds coupled between lignin monomers cleaves first. This is followed by side-chain functional groups peeling off or undergoing homolytic cleavage and then radical-induced rearrangements form many types of phenols. Pyrolysis temperature plays a vital role in the yields of many kinds of phenolic compounds. Both bamboo and rice straw EMAL pyrolysis have maximum G- and S-type phenols at 600 °C. As pyrolysis temperature is elevated beyond 600 °C, secondary depolymerization of the G- and S- phenols occurs which makes the methyl and methoxy groups leave and thus the methyl, ethyl, vinyl and allyl groups are substituted to be H-phenol dominant in the products. The final data set of this chapter is of interest for further studies on pyrolysis mechanism and regulation of the target products during lignin pyrolysis.

Pyrolysis is one of the most important technologies for lignin conversion into substitute transportation fuels and chemicals. In-depth investigations on the mechanism of pyrolysis of lignin and its product formation rules are still needed for the improvement of bio-oil properties. Experimental research together with theoretical simulations is a very efficient means of studying lignin pyrolysis mechanism and laws, which can allow estimation or prediction of product distribution and trends

with temperature variation. Thus, the combination of experimental mapping and theoretical studies of the thermal degradation of lignins needs more attention in the future.

References

1. Vanholme R, Demedts B, Morreel K, Ralph J, Boerjan W. Lignin biosynthesis and structure. Plant Physiol. 2010;153(3):895–905.
2. Ragauskas AJ, Beckham GT, Biddy MJ, Chandra R, Chen F, Davis MF, Davison BH, Dixon RA, Gilna P, Keller M, Langan P, Naskar AK, Saddler JN, Tschaplinski TJ, Tuskan GA, Wyman CE. Lignin valorization: improving lignin processing in the biorefinery. Science. 2014;344(6185):709–19.
3. Ma R, Xu Y, Zhang X. Catalytic oxidation of biorefinery lignin to value-added chemicals to support sustainable biofuel production. ChemSusChem. 2015;8(1):24–51.
4. Venderbosch RH. A critical view on catalytic pyrolysis of biomass. ChemSusChem. 2015;8(8):1306–16.
5. Besse X, Schuurman Y, Guilhaume N. Hydrothermal conversion of lignin model compound eugenol. Catal Today. 2015;258:270–5.
6. Wu A, Lauzon JM, Andriani I, James BR. Breakdown of lignins, lignin model compounds, and hydroxy-aromatics, to C1 and C2 chemicals via metal-free oxidation with peroxide or persulfate under mild conditions. RSC Adv. 2014;4(34):17931–4.
7. De Wild PJ, Huijgen WJJ, Gosselink RJA. Lignin pyrolysis for profitable lignocellulosic biorefineries. Biofuels Bioprod Biorefin. 2014;8(5):645–57.
8. Demirbas A. Biorefineries: current activities and future developments. Energy Convers Manag. 2009;50(11):2782–801.
9. Jiang G, Nowakowski DJ, Bridgwater AV. A systematic study of the kinetics of lignin pyrolysis. Thermochim Acta. 2010;498(1–2):61–6.
10. Jankovic B. The comparative kinetic analysis of Acetocell and Lignoboost (R) lignin pyrolysis: The estimation of the distributed reactivity models. Bioresour Technol. 2011;102(20):9763–71.
11. Liu Q, Wang S, Zheng Y, Luo Z, Cen K. Mechanism study of wood lignin pyrolysis by using TG–FTIR analysis. J Anal Appl Pyrolysis. 2008;82(1):170–7.
12. Yang H, Yan R, Chen H, Lee DH, Zheng C. Characteristics of hemicellulose, cellulose and lignin pyrolysis. Fuel. 2007;86(12–13):1781–8.
13. Bahrle C, Custodis V, Jeschke G, van Bokhoven JA, Vogel F. In situ observation of radicals and molecular products during lignin pyrolysis. ChemSusChem. 2014;7(7):2022–9.
14. Rajić N, Logar NZ, Rečnik A, El-Roz M, Thibault-Starzyk F, Sprenger P, Hannevold L, Andersen A, Stöcker M. Hardwood lignin pyrolysis in the presence of nano-oxide particles embedded onto natural clinoptilolite. Microporous Mesoporous Mater. 2013;176:162–7.
15. Guo D, Wu S, Liu B, Yin X, Yang Q. Catalytic effects of NaOH and Na_2CO_3 additives on alkali lignin pyrolysis and gasification. Appl Energy. 2012;95:22–30.
16. Faravelli T, Frassoldati A, Migliavacca G, Ranzi E. Detailed kinetic modeling of the thermal degradation of lignins. Biomass Bioenergy. 2010;34(3):290–301.
17. Wang S, Wang K, Liu Q, Gu Y, Luo Z, Cen K, Fransson T. Comparison of the pyrolysis behavior of lignins from different tree species. Biotechnol Adv. 2009;27(5):562–7.

18. Wang S, Lin H, Ru B, Sun W, Wang Y, Luo Z. Comparison of the pyrolysis behavior of pyrolytic lignin and milled wood lignin by using TG–FTIR analysis. J Anal Appl Pyrolysis. 2014;108:78–85.
19. Wang S, Ru B, Lin H, Sun W, Luo Z. Pyrolysis behaviors of four lignin polymers isolated from the same pine wood. Bioresour Technol. 2015;182(1):120–7.
20. Luo Z, Wang S, Guo X. Selective pyrolysis of organosolv lignin over zeolites with product analysis by TG-FTIR. J Anal Appl Pyrolysis. 2012;95:112–7.
21. Elder T. A computational study of pyrolysis reactions of lignin model compounds. Holzforschung. 2010;64(4):435–40.
22. Parthasarathi R, Romero RA, Redondo A, Gnanakaran S. Theoretical study of the remarkably diverse linkages in lignin. J Phys Chem Lett. 2011;2(20):2660–6.
23. Kijima M, Hirukawa T, Hanawa F, Hata T. Thermal conversion of alkaline lignin and its structured derivatives to porous carbonized materials. Bioresour Technol. 2011;102(10):6279–85.
24. Huang X, Liu C, Huang J, Li H. Theory studies on pyrolysis mechanism of phenethyl phenyl ether. Comput Theor Chem. 2011;976(1–3):51–9.
25. Klein MT, Virk PS. Modeling of lignin thermolysis. Energy Fuel. 2008;22(4):2175–82.
26. Hou Z, Bennett CA, Klein MT, Virk PS. Approaches and software tools for modeling lignin pyrolysis. Energy Fuel. 2010;24(1):58–67.
27. Zhang J, Jiang X, Ye X, Chen L, Lu Q, Wang X, Dong C. Pyrolysis mechanism of a β-O-4 type lignin dimer model compound. J Therm Anal Calorim. 2016;123:501–10.
28. Younker JM, Beste A, Buchanan Iii AC. Computational study of bond dissociation enthalpies for lignin model compounds: β-5 Arylcoumaran. Chem Phys Lett. 2012;545:100–6.
29. Yang Q, Wu S, Lou R, Lv G. Structural characterization of lignin from wheat straw. Wood Sci Technol. 2011;45(3):419–31.
30. Lou R, Wu S. Products properties from fast pyrolysis of enzymatic/mild acidolysis lignin. Appl Energy. 2011;88(1):316–22.
31. Lou R, Wu S, Lv G. Effect of conditions on fast pyrolysis of bamboo lignin. J Anal Appl Pyrolysis. 2010;89(2):191–6.
32. Huang J, He C, Liu C, Tong H, Wu L, Wu S. A computational study on thermal decomposition mechanism of β-1 linkage lignin dimer. Comput Theor Chem. 2015;1054:80–7.
33. Shi S, He F. Measurement and analysis of pulp and papermaking. Beijing: Light Industrial Press of China; 2003. p. 117–58.
34. Wu S, Argyropoulos DS. An improved method for isolating lignin in high yield and purity. J Pulp Pap Sci. 2003;29(7):235–40.
35. Lou R, Wu S. Pyrolysis characteristics of rice straw EMAL. Cellul Chem Technol. 2008;42(7–8):371–80.
36. Wu S, Lou R, Zhao Z. Study on the Characteristics of Crop Stalks EMAL Isolated. Pap Sci Technol. 2008;6(27):87–92.
37. Coats AW, Redfern JP. Kinetic parameters from thermogravimetric data. Nature. 1964;201:68–9.
38. Lv G, Wu S, Lou R, Yang Q. Analytical pyrolysis characteristics of enzymatic/mild acidolysis lignin from sugarcane bagasse. Cellul Chem Technol. 2010;44(9):335–42.
39. Lou R, Wu S, Lv G, Guo D. Pyrolytic products from rice straw and enzymatic/mild acidolysis lignin (EMAL). BioResources. 2010;5(4):2184–94.
40. Lou R, Wu S, Lv G. Fast pyrolysis of enzymatic mild acidolysis lignin from moso bamboo. BioResources. 2010;5(2):827–37.
41. Takashi H, Kawamoto H, Saka S. Role of methoxyl group in char formation from lignin-related compounds. J Anal Appl Pyrolysis. 2009;84(1):79–83.
42. Huang J, Wu S, Cheng H, Ming L, Liang J, Hong T. Theoretical study of bond dissociation energies for lignin model compounds. J Fuel Chem Technol. 2015;43(4):429–36.

Part IV
Techno-economics

Chapter 13
Integrated Lignin-Kraft Pulp Biorefinery for the Production of Lignin and Its Derivatives: Economic Assessment and LCA-Based Environmental Footprint

Marzouk Benali, Olumoye Ajao, Jawad Jeaidi, Banafsheh Gilani, and Behrang Mansoornejad

13.1 Introduction

Kraft pulping processes are the predominant technology for producing pulp and paper products and account for 92 % of chemical-based pulping in the world and for 61 % in Canada. Black liquor is the spent solution obtained after delignification in the pulping digester. It contains many chemicals and dissolved wood substances, including lignin (polyaromatic), saccharinic acids (hydroxyl acids), formic and acetic acids, and inorganic components. The chemical composition of black liquor varies considerably between different mills and depends on the cooking process and the type of biomass used (i.e. softwood or hardwood). It is estimated that about 98 % of the lignin in liquor is combusted as low-cost fuel in the chemical recovery boiler. The economic viability of a Kraft pulp mill is highly dependent upon the performance of its recovery boiler, which should be operated at maximum thermal efficiency.

The production capacity of about 70 % of Kraft pulp mills in North America is constrained by the operational limits of the recovery boilers. Although most have similar configurations, the recovery boiler at each mill has a unique set of operating conditions and limitations. Limited capacity of the installed boiler's configuration, restrictive air system configuration, and economic constraints are some of the elements to consider when optimizing the performance of a recovery boiler. In many cases, installed recovery boilers are originally designed for a possible upgrade to a higher capacity. Although upgrading is often conducted by mill decision-makers, it remains cost-intensive. Another quite remarkable aspect is that over the last 10 years, most North American Kraft pulp mills have progressively increased their pulp production, to the point where the calorific load on their respective recovery

M. Benali (✉) • O. Ajao • J. Jeaidi • B. Gilani • B. Mansoornejad
Natural Resources Canada, CanmetENERGY, Varennes, QC, Canada
e-mail: marzouk.benali@canada.ca

boilers has reached the design limits. Therefore, offloading the recovery boiler by precipitating a portion of the lignin in the Kraft mill black liquor is a cost-effective solution to consider, since it leads to immediate benefits from the resulting incremental increase of pulp production by up to 25 % (depending on the installed equipment capacity), along with lignin as a new final product at the mill. This has been the focus of much of the work done in the last decade and has resulted in the first commercial installations, referred to as the LignoBoost™ platform, in the U.S.A. (2013) and in Finland (2014) [1].

The extraction of lignin from black liquor containing between 30 % and 40 % of dissolved solids reduces the higher heating value of the gas-fired black liquor, and this has a huge impact on the steam generation rate and the maximum pulp production rate that the recovery boiler can sustain. Consequently, the implementation of a lignin recovery process into a Kraft mill, combined with full heat integration, certainly offers new opportunities to improve the competitiveness of a Kraft mill. However, major impacts on resource utilization (e.g. biomass, water, chemicals, process energy, utilities, etc.) must be evaluated to determine its technical feasibility [2]. A Canadian softwood Kraft mill with a production capacity of about 1000 air-dry-tonnes per day of pulp is considered in this chapter as the receptor mill for a lignin recovery process, producing up to 100 dry-tonnes of two grades of lignin: Low-Residue Content Lignin (LRCL) or High-Residue Content Lignin (HRCL). LRCL refers to lignin that has undergone washing, filtration, and purification, while none of these steps are required for HRCL. Many useful applications of lignin have been identified and demonstrated, including active ingredients in adhesives, resins, rubber products, plastics, asphalt, casting resins, and as feedstocks for the production of specialty chemicals and carbon fiber [3]. Some of the highest potential has been found in the conversion of lignin to carbon fiber, as well as its utilization as a renewable component in polyurethane-based insulating products [4]. Combustion, gasification, and pyrolysis can also be used to convert lignin to heat, power, liquid fuel, chemicals, or syngas, depending on process economics and lignin availability.

High-purity lignin with ash content <0.1 % and sulphur content <1 % [5, 6], can be obtained by fractionation of biomass using supercritical treatment [7], deep eutectic solvents (DES) [8], or the ethanol-based organosolv process and other modified organosolv processes, such as that demonstrated by Lignol in Canada [9]. Lignol Innovations has been acquired, and the technology is being further developed by Fibria, a South American pulp and paper company [10, 11].

This chapter is based on the results of a research and development project on Integrated Forest Biorefinery through Product Diversity: Modeling, Optimization, Prefeasibility, and Multi-Criteria Decision-Making Tool, funded by Natural Resources Canada, which aims at:

- Developing and validating practical integrated biorefinery models as well as retrofit/design solutions to enable successful transformation of the forest industry towards integrated biorefineries.
- Developing, demonstrating, and disseminating integrated decision-making tools to support the selection of a viable biorefinery solution, and assessing the benefits and risks of implementing available biorefinery technologies.

This chapter is divided into five sections. It starts with an introduction in which the operational challenges of Kraft pulping mills and related technological solutions are addressed. Then, the key processes to recover lignin from weak black liquor are described, followed by the presentation of lignin derivatives, with an emphasis on their production pathways, energy, and economic profiles. The global markets of lignin derivatives are also provided. The third section focuses on multi-criteria analysis methodology, and how economic[1] and environmental assessments are performed to obtain the corresponding evaluation criteria and metrics. An industrial case study is discussed in the fourth section, and the fifth section describes results obtained from integrating a LignoBoost™ process or LignoForce System™ with capacities of 100 t/day within a Canadian softwood Kraft pulp mill, with a production capacity of about 1000 air-dry-tonnes per day of bleached pulp.

13.2 Process Descriptions: Lignin Recovery and Production of Derivatives

The first patents on precipitation of lignin from black liquor were granted between 1919 and 1958 [12–15]. In the late 1940s, MeadWestvaco in North Charleston (South Carolina, U.S.A.) became the pioneer in producing lignin, first by recovery from lignosulfonates and then from Kraft weak black liquor. MeadWestvaco was the only manufacturer able to produce proven pure lignin with well-defined structural, chemical, and mechanical properties. Pure lignin production from black liquor was based on a batch process in which black liquor was acidified using mineral acids such as sulphuric or hydrochloric acid, under continuous mechanical agitation. The typical annual production capacity of high-purity lignin was about 60,000 tonnes [16]. Interest began to grow in Sweden, in the early nineties, and culminated in the development of the LignoBoost™ technology. Afterwards, other developments were initiated in Canada and the United States, where researchers came up with novel ideas and developed the LignoForce System™ and SLRP™ technologies, respectively. Other lignin recovery processes from black liquor, such as membrane and electrochemical-based processes, are also being investigated at present.

13.2.1 *LignoBoost™ Process*

The LignoBoost™ process, which is now commercially available, was developed and patented for lignin recovery from Kraft black liquor, using acid precipitation with CO_2 as the agent. This process is an innovation that originated in 1997 from research conducted by Professor Hans Theliander at the chemical and biological

---

[1] All economic assessments are based on US dollars.

engineering department of Chalmers University (Sweden). The first laboratory tests were conducted in 1999, followed by pilot trials and a demonstration-scale unit in 2003 and 2006, respectively [1]. International and American patents cover the technology and processes related to LignoBoost [17, 18]. Figure 13.1a. illustrates the separation process of lignin from Kraft black liquor, comprising:

– A black liquor reservoir, a multiple-effect evaporator from which black liquor is withdrawn at about 30–40 % solids.
– An acidification reactor to precipitate lignin using CO_2 as an acidic reactant for lowering the pH from 12–14 to 9–10 at 72–75 °C.
– A lignin coagulation vessel in which the temperature and pH are maintained respectively at 60–70 °C and 9–10.
– A washing-filtration train in which the liquor containing coagulated lignin is filtered and the cake is washed with H_2SO_4 and water.

LignoBoost technology has already been commercialized on different continents. In February 2013, Domtar successfully started up the first ever commercial installation of a LignoBoost™ plant, trademarked as "BioChoice™," at its pulp and paper mill located in Plymouth (North Carolina, U.S.A.). The first washed (high-purity) lignin was produced 17 days after start-up [1]. Full production capacity was reached after a year, equivalent to an average annual production of about 25,000 tonnes of dry lignin (~54 kg of lignin per one air-dry-tonne of pulp) with 65 % solid content. In 2015, the second commercial installation of a LignoBoost plant started up at Stora Enso Sunila mill in Kotka (Finland), with an annual production capacity of about 50,000 tonnes of lignin (~135 kg of lignin per one air-dry-tonne of pulp) at 95 % solid content. The average black liquor feed for the plant is about 82 t/h. The first washed (high-purity) lignin was produced 10 days after start-up [1].

13.2.2 LignoForce System™

Research and development efforts led by FPInnovations (Canada) focused on: (a) improving the washing-filtration train of conventional processes such as the LignoBoost™ process [1, 2, 19, 20] and (b) integrating a black liquor oxidation step prior to lignin precipitation to eliminate the total reduced sulphur compounds (i.e. hydrogen sulphide, methyl mercaptan, dimethyl sulphide, and dimethyl disulfide) and to convert a part of the organic compounds into carboxylic acids. Following successful results on the laboratory and pilot scales, FPInnovations developed a novel technology called the LignoForce System™ that has been commercialized by NORAM Engineering and Constructors (Canada). The first commercial installation of a LignoForce System™ started in the first quarter of 2016 at the West Fraser mill, located in Hinton (Alberta, Canada), and an average annual production of about 10,000 tonnes of dry lignin is targeted. Figure 13.1b. depicts a general view of the LignoForce System™. In comparison to the LignoBoost™ process, the LignoForce System™ incorporates an oxidation reactor for black liquor that, as claimed in the
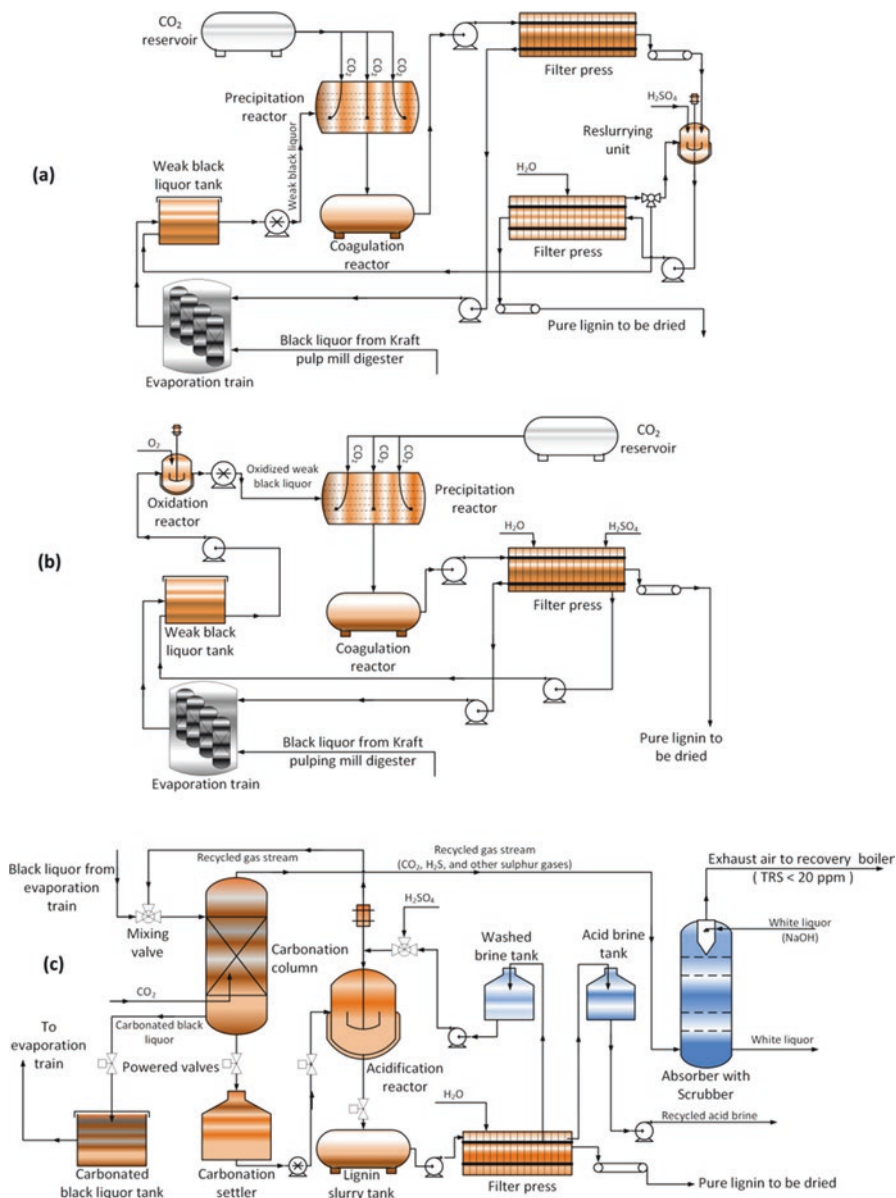
Fig. 13.1 Process diagrams for (**a**) LignoBoost™, (**b**) LignoForce System™, and (**c**) SLRP™

patents [19] and [20], will result in a reduction of sulphur compounds in recovered lignin and CO_2 consumption during the precipitation step, as well as in increased lignin purity. These improvements have been identified during laboratory and pilot-scale trials, but no data on commercial-scale performance is available yet.

One remarkable aspect to mention is that all Kraft pulping processes generate significant amounts of total reduced sulphur (TRS) compounds that end up in the digester condensates and black liquor. The TRS gases are usually a mixture of hydrogen sulphide (H_2S), carbon disulphide (CS_2), carbonyl sulphide (COS), methyl mercaptan (CH_3SH), dimethyl sulphide (CH_3SCH_3), and dimethyl disulphide ($CH3S•SCH_3$). In black liquor, the TRS concentration is essentially the sum of CH_3SH and CH_3SCH_3 concentrations [21]. When recovering lignin with the LignoBoost™ process or LignoForce System™, the management of sulphur is crucial to guarantee high levels of lignin purity and low sulphurous gas emissions.

13.2.3   Sequential Liquid-Lignin Recovery and Purification (SLRP™)

The SLRP™ technology was developed in South Carolina (U.S.A.) and a U.S. patent application has been submitted [22]. The SLRP™ also enables separation and purification of the lignin contained in Kraft-based black liquor. In this process, the black liquor is first pressurized (preferred operating pressure is about 1035 kPa, but could be as low as 345 kPa). The soluble lignin at a pH ranging from 12 to 14 is precipitated by introducing the pressurized black liquor into an absorption column and treating the black liquor counter-currently with CO_2, which is at an elevated temperature (80–120 °C) [22, 23]. The pH is then reduced to 9–10 to partially neutralize the NaOH and other basic components within the black liquor. As the acidification agent, CO_2 enables conversion of the sodium phenolic groups on the lignin molecules to hydrogen, causing the lignin to become insoluble. This is followed by a separation and the formation of a dense lignin-rich phase called "liquid lignin" and a light lignin-depleted phase [22]. Figure 13.1c. depicts the key unit operations involved in the SLRP™.

The operating parameters of these three processes are compared and the results are summarized in Table 13.1.

13.2.4   Other Lignin Isolation Methods: Ultrafiltration, Electrolysis, and Electrodialysis Membranes

Pressure-driven membrane techniques such as ultrafiltration (UF), nanofiltration (NF) or reverse osmosis (RO) membranes have low energy intensity and have been utilized alone or combined in different configurations to treat Kraft black liquor [24]. Some of the noted advantages of employing UF or NF techniques for lignin recovery are that black liquor can be withdrawn at different points in the receptor mill, without requiring temperature adjustment or the addition of chemicals to adjust the pH [25, 26]. Also, lignin with a narrow and defined molecular weight

Table 13.1 Operating parameters and chemical costs per tonne of lignin produced

Operating parameters and costs	LignoBoost™ process [17, 18]	LignoForce system™ [19, 20]	SLRP™ [22, 23]
CO_2 consumption (t/t)	0.15–0.25	0.20–0.30	0.14–0.18
O_2 consumption (t/t)	0	0.15–0.25	0
Incremental NaOH (t/t)	0.05–0.08	0.08–0.16	0
Water (t/t)	2.00–2.50	4.0–5.00	1.20
H_2SO_4 (t/t)	0.09–0.25	0.10–0.20	0.09
Precipitation yield (%)	70.00	67.00	55.00
Precipitation reactor pressure (kPa)	101.33	101.33	345–1380
Precipitation reactor temperature (°C)	60–70	60–70	80–120
Lignin ash content (%, w/w)	0.02–1.00	0.10–0.70	≤1
Lignin sulphur content (%, w/w)	1.30–3.40	1.40–1.70	2.00–3.00
Chemical costs[a] ($/t of lignin)	100–150	129–227	Not available

[a]The costs are based on the following prices: CO_2 ($300/t); H_2SO_4 ($150/t); NaOH ($600/t); O_2 ($35/t)

distribution can be obtained [27, 28]. In practice, the temperature at which the black liquor can be filtered is dependent on the type of membrane material. Typical organic membranes have a maximum temperature that is lower than 50 °C, as well as a specific pH range and molecular weight cut-off [29]. Therefore, ceramic membranes are the most suitable for a wide range of black liquor recovery temperatures from the Kraft process. Challenges associated with the use of membranes include identification of suitable membranes that will result in high yield and lignin purity for host mill operating conditions and black liquor composition variations. All membranes are prone to flux decline, which can be reversible or irreversible. Flux decline might be encountered as a result of fouling or volume reduction during lignin recovery and should be addressed to make the process economically feasible.

Electrochemical processes differ from pressure-based membranes in that the separation is driven by an electric potential gradient between the anode (+) and cathode (−) of the system. Electrolysis and electrodialysis are two common electrochemical methods for lignin recovery from black liquor that have been investigated. During electrolysis, the black liquor is fed into the anode compartment, and a cation exchange membrane (CEM) in the compartment is employed to selectively enable the migration of Na^+ ions to the cathode when electrical current is supplied at the electrodes [30]. This leads to a lowering of the pH that facilitates lignin precipitation. Caustic is recovered and the production of hydrogen takes place at the cathode [30–32].

Electrodialysis, in contrast, requires two types of selectively permeable membranes, anion exchange membrane (AEM) and CEM, that are placed alternately for the treatment of black liquor [33]. These permit the migration of anions such as OH^-, HS^-, HCO^{3-}, and SO_4^{2-} to the anode, in addition to Na^+ migration to the

cathode. The use of bipolar membranes (BPM), which are combined layers of AEM and CEM on the same matrix, has been reported as a means of obtaining lower operating costs and energy demands than that of conventional electrolysis. The most important operating variables that have been identified for electrodialysis systems are black liquor concentration and current density [34].

Similar to the pressure-driven membrane processes, fouling could limit the application of electrodialysis systems. Hence, pre-treatment of the black liquor prior to electrochemical treatment might be necessary in many cases.

13.2.5   Molecular Structure of Lignin

Considering the complexity of lignin obtained using different methods and conditions, established analytical protocols have been adapted for the chemical characterization of lignins. The heterogeneity of lignin is caused by variations in the polymer composition, size of the molecular chain, cross linking, and functional groups. The most important characteristics that must be considered for any potential industrial application of recovered lignin are the purity, molecular structure, and thermal properties. The purity is determined by measuring the ash, sulphur, extractives, and carbohydrate content. The molecular structure refers to the molecular mass, molecular distribution, molecular size, and functional groups present. Thermal properties are determined by measuring the glass transition temperature, decomposition temperature, and viscosity. The molecular structure has a significant effect on lignin degradation. The structural features of lignin also significantly affect the efficiency of the postprocessing pathways. Existing analytical protocols can be used for the determination of purity and thermal properties of lignin with a good confidence level and repeatability. However, determining molecular weight is challenging, since the established analytical tools are sensitive to the wide variability of lignin's molecular structure. The molecular weight parameters are provided by M_n (Number-average molecular weight), M_w (Weight-average molecular weight), M_z, and the polydispersity index (Pd) defined by the ratio M_w/M_n. The larger the polydispersity index, the broader the molecular weight distribution. These molecular weight averages can be determined by Gel Permeation Chromatography (GPC) and Size Exclusion Chromatography (SEC). To give accurate and reproducible results, the GPC method requires that the baseline be well defined. Published data on molecular weight of lignin from various biomass sources (softwood *versus* hardwood) indicate that M_n, M_w, and Pd vary respectively from 2400 to 8300 g/mol, 5900 to 23,500 g/mol, and 1.65 to 3.7, depending on the lignin source [35]. This study is based on lignin extracted from softwood-based Kraft processes. The softwood biomass used is composed of balsam fir, white spruce, and jack pine.
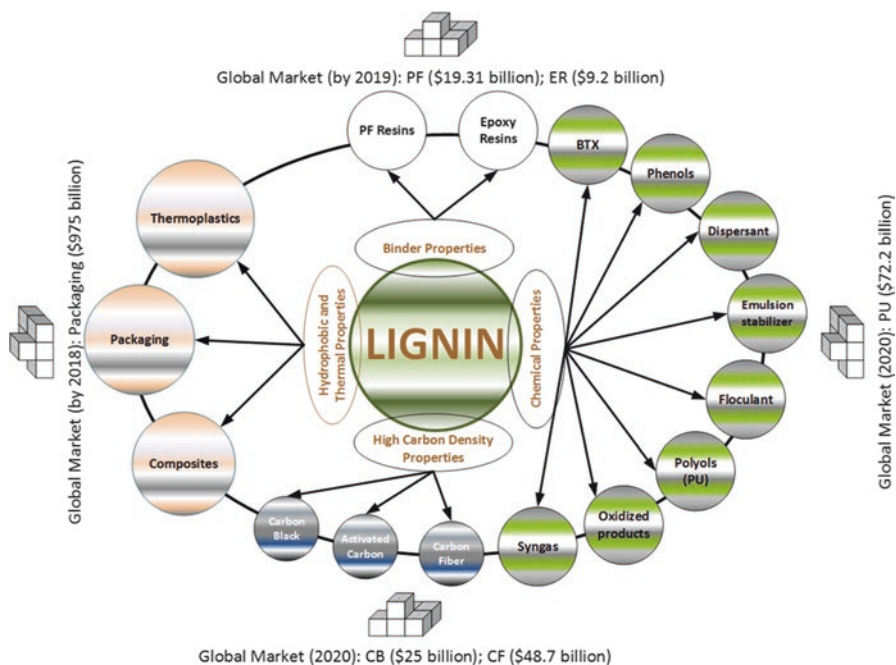
Fig. 13.2 Lignin properties, potential derivatives, and scope of the global markets

13.2.6   Emerging Innovative Applications of Lignin

Advances in understanding the physical chemistry of lignin have led to the development of innovative applications to replace a wide range of petroleum-derived monomers, polymers, as well as composites. As shown in Fig. 13.2, the key characteristics of lignin that determine its areas of application and type of derivatives are its binding, chemical, hydrophobic and thermal, and high-carbon density properties. Possible derivatives include PF and epoxy resins, thermoplastics, activated carbon, carbon black, carbon fiber, polyols, phenols, BTX, dispersants, flocculants, syngas, etc. The molecular structure of lignin along with its functional group content (e.g. β-ether bonds, phenolic OH groups, and aliphatic OH groups) also play an important role in targeting lignin derivatives (e.g. low M_n favors monomers, while high M_n enables the production of biopolymers). It is also expected that, by 2019–2020, high-purity lignin is ready to dominate major markets, regardless of fluctuations on the gas and petroleum markets. The global markets of the petrochemical-based products, in which high-purity lignin will be able to be incorporated in proportions varying from 20 to 100 %, range from 9 to 180 billion dollars. In the total market of binders, high-purity lignin is already able to replace up to 35 % of phenol contained in phenol-formaldehyde resins and epoxy resins commercially (i.e., by 2019, the market size for lignin could represent 10 billion dollars). Due to its high carbon density, lignin is a good candidate to enter the carbon fiber reinforced plastics

market (expected to reach 48.7 billion dollars by 2020), as well as the flexible and rigid polyurethane foams market (expected to reach 72.2 billion dollars by 2020). Considering the possibility of a 20 % incorporation of lignin in these two petrochemical-based products, the potential market size for high-purity lignin could reach 24 billion dollars. Based on year 2012, the total market of polyols, bioplastics, and biocomposites represent 28 billion dollars [36].

By taking advantage of its four key properties, lignin can be used unmodified or with modification. Compared to unmodified lignin, modified lignin is expected to reach a higher degree of substitution when replacing a fossil-fuel product. When deciding whether or not to modify lignin, the following critical factors should be taken into consideration: the cost of the product to be substituted, the substitution ratio, and the cost of the lignin modification process. Lignin modifications can be broadly categorized based on their objective: those that enhance existing targeted functionalities, and those that change the polymeric structure, including the molecular weight distribution.

Two approaches exist for enhancing existing functionalities: changing an existing reactive group to obtain targeted functional groups, which would increase the targeted functional group content in the lignin or open up the lignin structure to increase its reactivity to existing targeted groups, by making them more accessible. For instance, lignin phenolation consists of increasing the aromatic content of lignin by adding phenol that will react with the aliphatic reactive group. Phenolated lignin exhibits better heat insulation properties and hydrophobicity. Demethylation of lignin aims to remove oxygen-methyl groups to obtain the hydroxyl group and make the lignin more phenolic. For example, oxypropylation is an addition of propylene oxide into lignin to make the hydroxyl functional groups more accessible, while the number of hydroxyl groups remains unchanged [37, 38]. Modification of the lignin structure can be done with depolymerization pathways that will create more monomers and reduce the molecular weight.

Table 13.2 provides the inventory of promising lignin derivatives, their associated pathways, competitive fossil-based products, and technology readiness levels (TRL).

Considering that the technologies for all the potential lignin derivatives shown in Fig. 13.2 are not available at the industrial scale or commercially, this chapter focuses on flexible polyurethane foams and carbon fibers with projected global markets worth 72.2 billion and 48.7 billion dollars, respectively, by 2020. Typical lignin-based polyol replacement in conventional polyurethane foams ranges from 20 to 25 %, while typical lignin-based carbon fiber replacement in precursors of carbon fibers is in the range of 50–100 %.

13.2.6.1 Lignin-Based Polyols for Polyurethanes

Polyurethanes (PU) are one of the most widely used classes of organic polymers. They can be produced by the polyaddition reaction between a polyol and di- or polymeric isocyanate, which is favored by the presence of a catalyst or an additive

Table 13.2 Potential lignin derivatives and respective production pathways

End product	Pathway	Competitive fossil–based product	TRL
Vanillin	Oxidation	Vanillin	9
Syngas	Thermal	Syngas	9
Thermoplastics	Thermo-mechanical	Polypropylene or Polyethylene	9
Packaging	Thermo-chemical	Polypropylene or polyethylene	9
Carbon Black	Thermal	Carbon Black	8
Phenol formaldehyde resins	Thermo-chemical	Phenol	7
Phenols	Thermo-chemical or Biological	Phenol	7
Polyurethane	Thermo-chemical	Polyol	7
Epoxy resins	Thermo-chemical	Bisphenol A	6
Activated carbon	Thermo-chemical	Carbon	6
Carbon fiber	Thermal	Polyacrylonitrile (PAN)	4

[39]. The chemical reaction below (Eq. 13.1) illustrates the reaction that occurs during polyurethane formation. The properties of polyurethanes can be manipulated through the use of polyols and polyisocyanates with different molecular weights, functionality, degree of polymerization, formulations, or processing techniques [40]. The key types of polyurethane include flexible foam, rigid foam, coatings, adhesives, sealants, and elastomers (CASE), thermoplastic polyurethane (TPU), reaction injection molding (RIM), binders, and waterborne polyurethane dispersions (PUDs).

$$NCO - R_1 - OCN + HO - R_2 - OH \rightarrow R_1 - NHC(O)O - R_2 \qquad (13.1)$$
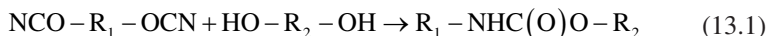
Increased interest in valorizing isolated Kraft lignin has led to its identification as a promising feedstock for polyurethane production. However, the application of lignin is still constrained by inconsistency of lignin quality, due to varying molecular weight, degree of crosslinking, and hydroxyl functional groups. Lignin can be used directly in the production of polyurethanes or after chemical modification, such as prior conversion into polyols. Partial replacement of polyols directly with lignin in PU formulations is possible, because it has abundant phenolic hydroxyls [41], which can serve as reaction sites for polyisocyanates. Due to the resulting crosslinked network, the derived PU exhibits some native characteristics of lignin, such as improved moisture and flame resistance. Importantly, it has also been shown that there is a limit to the lignin content, beyond which the PU will be rigid, irrespective of the lignin's molecular weight. To create flexible PU from lignin without prior modification, the current practice is to introduce a linear polyol in the formulation [42]. The usefulness of this approach depends on the lignin and polyol characteristics (type, molecular weight, and functional groups). Chemical modification to

transform lignin into polyols can be carried out using two different approaches, oxypropylation, and liquefaction [41, 43, 44]. Oxypropylation is a polymerization reaction in the presence of an acid or base catalysts and requires the addition of propylene oxide onto lignin to make the hydroxyl functional groups more accessible and, at the same time, transform the solid lignin into liquid polyols [37].

The key process parameters for oxypropylation include the type of feedstock, the catalyst employed, and the ratio of propylene oxide to lignin. Liquefaction is an acid- or base-catalyzed degradation and decomposition of lignin into polyols and other smaller molecules by using solvolytic reactions or polyhydric alcohols [45]. The key process parameters for liquefaction include the type of solvent employed, the biomass-to-solvent ratio, catalysts, residence time, and temperature. An important difference between oxypropylation and liquefaction is that the number of hydroxyl groups remains unchanged during oxypropylation, while for liquefaction, the number of hydroxyl groups decreases as a result of oxidation and dehydration [38]. In some cases, the properties of the lignin-derived PU was comparable or superior to those of conventional sources [46]. Although polyols can be derived from lignin, the choice of polyisocyanate sources is limited and most bio-derived PU are produced from formulations of biobased polyols, together with petroleum-derived isocyanates [38].

13.2.6.2   Lignin-Based Precursor for Carbon Fibers

Carbon fiber (CF) is an engineered fibrous material made from a bundle of filaments. Carbon atoms are bonded together in an imperfect graphite crystalline structure that gives the material remarkable properties [47]. The number of thousands of agglomerated filaments defines the tow grade, which typically ranges from 2 to 80 K. CF tows are sold directly and in various forms including: cord, chopped fibers, textile, and pre-impregnated. Most of the manufactured CF are further processed to CF composites, which have fibers embedded in the polymeric matrix [48]. In principle, any fibrous material with a carbon atom back-bone can be used as a precursor [47]. However, only a few precursors have been identified for making CF with attractive mechanical properties: viscose rayon, which is regenerated cellulose produced in dissolving pulp mills; mesophase pitch, which is derived from petroleum; polyacrylonitrile (PAN), which is derived from propylene; and to a lesser extent, lignin precursors. Lignin-based precursors have been investigated over the last 50 years because they are cheaper and greener alternatives to most common PAN precursors [49]. Lignin-based carbon fibers are made with modified or unmodified lignin, with the option of blending with additives [49]. Lignin has been successfully blended with PAN [50], polylactic acid (PLA) [51], cellulose [52], polyethylene oxide [4], polyethylene glycol [53], and polyethylene terephthalate [54]. Between the 1967 and 1973, the Japanese company Kayaku Co. commercialized carbon fiber based on lignosulfonates.

Lignin derived from CF manufacturing processes can generally be broken down into six main operations [55–57]:

1. *Lignin-based precursor preparation.* Lignin powder is dried to remove water and volatile organic compounds, and then compounded with additives in a twin-screw pelletizer to obtain the precursor.
2. *Precursor spinning.* The thermoplastic behaviour of the precursor is used to form filaments. Lignin is usually converted into precursor fibers by melt-spinning, but other techniques, such as solvent-assisted spinning and electrospinning have been investigated [52, 58].
3. *Stabilization.* The thermoplastic behaviour of the filaments is removed to obtain thermoset behaviour and ensure that the filaments will not fuse upon further heating. Oxidative treatment is used, and the biggest challenge is being able to achieve homogenous stabilization with fast heating rates.
4. *Carbonization.* Heat treatment under inert atmospheres and temperatures between 1000 and 2000 °C for removing non-carbon atoms.
5. *Graphitization.* When using lignin as a precursor, this is a mandatory heat treatment step at temperatures between 2000 and 3000 °C for improving mechanical proprieties through the formation of a graphite-like layered structure.
6. *Surface treatment and sizing.* For carbon fiber composites, the surface adhesion between fiber and matrix can be improved by oxidative treatment on the fiber.

Lignin-based precursors for carbon fiber are promising, because of their high yield (between 45 and 55 % [49]), lower cost, and process similarities with conventional PAN-based carbon fiber. The main challenges are associated with lignin thermal properties, especially glass and softening temperatures. Softwood lignin is more difficult to melt, but it is better for crosslinking during carbonization, in comparison with hardwood lignin. To date, the mechanical properties for 100 % lignin-based carbon fiber have not been able to match the quality of PAN-based carbon fiber. However, due to their low cost, lignin-based CF can serve mass applications where light weight and moderate mechanical properties are required.

13.3 Multi-criteria Analysis Methodology: Technical, Economic, and Environmental Assessments

13.3.1 Foundations of Multi-criteria Analysis

Multi-criteria analysis (MCA) is a widely used tool to support decision-making, when there is a choice to be made between competing options in biorefinery, or when a series of options from different biopathways are possible. It is specifically relevant as a tool for the integrated assessment of large-scale production systems with complex and inter-connected ranges of technological, environmental, and

economic issues, as well as operational constraints and data uncertainty. All these aspects must be simultaneously taken into account for making trade-offs between various unavoidable competing criteria. In the context of biorefinery implementation in existing infrastructure, the multi-criteria analysis tool utilizes different metrics to reflect conflicting issues and objectives.

The MCA is a panel-based decision-making technique that is applied through an integrated assessment, consisting of a set of interdependent components (e.g. models, process operating and market data, metrics, and critical assumptions, when data is unavailable). A structured framework is submitted to a panel of experts in process design, biorefinery, and pulp and paper, who will define the veto criteria and preference rules. Reaching a consensus among experts is a priority throughout the procedure. The procedure includes multiple steps and continuously involves the members of the expert panel. Overall, an MCA is performed by following several steps within two phases (pre-panel and panel). These steps are as follows:

- Pre-panel phase

  - Reviewing the decision context.
  - Defining the objectives of the decision-making.
  - Providing the definition of the various biorefinery alternatives.
  - Introducing all of the criteria that have been considered.

- Panel phase

  - Evaluating all of the criteria and their respective interpretation and metrics.
  - Analyzing the preferred interpretation of panel members.
  - Quantifying the relative importance of the decision criteria.
  - Calculating the final scores that represent the performance of the design alternatives.
  - Ranking the alternatives, interpreting results, and making a final decision.
  - The number of criteria should be kept as low as is consistent with making a well-founded decision. There is no hard-and-fast rule to guide this judgement, and it will certainly vary from one industrial process to another. In this study, economic, competitiveness, and sustainability criteria were considered.

13.3.2 Technical Assessment

The models incorporated in Natural Resources Canada's I-BIOREF software as well as the multi-criteria analysis methodology described above were applied to the Canadian softwood Kraft mill considered in this industrial case study. A series of combinations of operating parameters were examined to obtain significant improvements in recovery boiler performance and a reduction of fresh water intake and energy use by up to 30 % and 15 %, respectively, all the while boosting pulp production by up to 20 % and producing up to 100 tonnes of dry lignin per day. The impact assessment of the resources (e.g. steam, water, chemicals, biomass, fuel, electricity)

used in the Kraft pulping mill as well as the impact on the effluent generated (i.e. additional load on installed wastewater plant) were examined.

13.3.3 Economic Assessment

The objective of an economic analysis is to quantify the economic performance of a project. Such quantification is carried out using economic metrics that indicate the profitability of the project. These metrics involve traditional indices that measure the rate of return, such as return on investment (ROI) or payback period, and modern metrics that take into account the value of money over time, such as net present value (NPV) or internal rate of return (IRR) [59, 60]. To quantify the economic metrics, two main cost items must be estimated: total product cost and total capital investment [60].

13.3.3.1   Total Product Cost

Total product cost is the aggregation of all costs related to plant operation, product sales, and corporate functions such as management and research and development. It is generally calculated on a daily basis, a product unit basis, or an annual basis. The total product cost has two components: manufacturing (also referred to as production or operating costs) and general expenses. Operating costs are directly linked with plant operation. These expenses can be classified into three categories: variable production costs, fixed charges, and plant overhead costs. On the other hand, general expenses include administrative expenses, distribution and marketing expenses, and research and development expenses. A portion of the variable operating costs is attributable to the cost of resources that are used directly in the production process. These costs comprise the cost of feedstock, chemicals, utilities (including water, steam, and electricity), direct operating labor, supervisory and clerical labor directly related to the manufacturing operation, maintenance and repairs, operating supplies, laboratory supplies, royalties, catalysts, and solvents. Fixed charges represent the expenses that are independent of the production rate, such as expenditures for depreciation, property taxes, and insurance. Finally, plant overhead costs cover expenses related to general plant maintenance and overhead, safety services, payroll overhead, employee insurance, salvage services, quality-control laboratories, property protection, warehouse, and storage facilities.

13.3.3.2   Total Capital Investment

Total capital investment (TCI) is the amount needed to acquire land, purchase and install equipment, maintain service facilities, piping, and controls, as well as cover plant operational expenses, before sales revenue becomes available. TCI consists of

two components: fixed capital investment (FCI) and working capital (WC). FCI is further comprised of the manufacturing fixed capital investment (direct costs) and the non-manufacturing fixed capital investment, also known as indirect costs [61]. Direct costs include the capital necessary for (a) purchasing equipment, (b) installing equipment, (c) instrumentation and controls, (d) piping and insulation, (e) electrical systems, (f) buildings associated with the process (e.g. substructures and superstructures, auxiliary buildings such as administration and office space, maintenance buildings such as electrical, piping, and building services including heating and dust collection), (g) yard improvements, (h) service facilities, including utility facilities, non-process equipment such as offices, and distribution and packaging facilities, and (i) land. The items covered under direct costs can be estimated based on the installed equipment cost (i.e. the summation of equipment purchase and installation costs). To calculate the installed equipment cost of a given piece of equipment, the cost for a reference capacity, along with several other parameters, is needed. The other parameters required for installed equipment cost calculation are the capacity exponent, year indices (Marshall and Swift cost index or Chemical Engineering Plant cost index), and installation factors. Eq. 13.2 is used for either estimating the cost of a plant at the conceptual design level, or estimating the cost of a single unit.

$$C = C_{ref} \, I \left(\frac{M}{M_{ref}} \right)^{\alpha} \left(\frac{y}{y_{ref}} \right) \qquad (13.2)$$

where C is the cost of new equipment, I is the installation coefficient, M is the capacity of equipment, α is the capacity exponent, and y is the year index. The subscript "*ref*" corresponds to values related to the reference equipment data.

The calculation of other direct cost items is carried out based on experience or "rules of thumb." These costs can be estimated as a percentage of the total purchased equipment cost (TPEC) or total installed cost (TIC). Indirect costs represent construction overhead costs and, as with some direct cost items, they are estimated based on different aggregate cost items, based on TIC or FCI. The summation of direct and indirect costs gives the FCI. The other part of TCI is the working capital that represents the total amount of money invested in raw material, supplies, etc. Working capital is also estimated as a percentage of TCI.

13.3.3.3 Economic Metrics

The economic metrics used in evaluating the performance of industrial projects include the payback period, NPV, IRR, ROI, return on capital employed (ROCE), and earnings before interest, taxes, depreciation, and amortization (EBITDA). The formulas for these metrics are presented in Table 13.3.

Payback period is a metric for evaluating investment opportunities and product development projects based on the time taken to recoup the investment. IRR and

Table 13.3 Economic metrics

Metric	Formulation
PP (Payback Period)	$\dfrac{Capital\ investment}{Cash\ flow}$
IRR (Internal Rate of Return)	$\displaystyle\sum_{Project\ lifetime}^{Year=i} \dfrac{Cash\ flow_i}{\left(1+IRR\right)^i}$
NPV (Net Present Value)	$\displaystyle\sum_{Project\ lifetime}^{Year=i} \dfrac{Cash\ flow_i}{\left(1+IRR\right)^i}$
ROI (Return On Investment)	$\dfrac{Revenue - product\ cost\ including\ depreciation - tax}{Capital\ investment}$
ROCE (Return On Capital Employed)	$\dfrac{Revenue - product\ cost\ including\ depreciation}{Capital\ investment}$
EBITDA (Earnings Before Interest, Taxes, Depreciation, and Amortization)	$EBITDA = Revenue - Operating\ cost$
CAB (Competitive Access to Biomass)	$\dfrac{EBITDA}{Tonne\ of\ biomass}$
RTMU (Resistance To Market Uncertainty)	$\dfrac{Revenue - product\ cost\ including\ depreciation}{Cost\ of\ raw\ material + cost\ of\ energy}$

NPV take into account the time value of money via a discounted cash flow. IRR is the rate of return equivalent to the maximum interest rate at which money could be borrowed to finance the project under conditions where the net cash flow to the project over its life would be just sufficient to pay all principal and interest accumulated on the outstanding principal. IRR shows the amount of unreturned investment at the end of each year during the project lifetime, and when applied to the yearly cash flow, it makes the net present value equal to zero at the end of the project lifetime. NPV is the aggregation of the discounted cash flows at a specific interest rate (i). It represents the difference between the present value of annual cash flows and the initial investment. ROI represents earning power of assets that is measured as the ratio of the net income to the average capital invested in a project. It is a measure of profitability that indicates whether or not a project is utilizing its resources in an efficient manner. ROCE measures the returns that a company is realizing from its capital. It represents the efficiency with which capital is being utilized to generate revenues. EBITDA is used to analyze and compare profitability between companies and industries, by eliminating the effects of financing and accounting decisions. Competitive access to biomass (CAB) refers to the ability to guarantee a supply of biomass over the long term and simultaneously provide competitive value to biomass producers. Lastly, the resistance to market uncertainty (RTMU) is the sensitivity of a given biorefinery option to market value fluctuations, as a result of varying raw material and energy prices.

13.3.4 Environmental Assessment Methodology

It is now commonly accepted that biorefinery products are instrumental for displacing numerous fossil-derived products, reducing greenhouse gas emissions, and ultimately mitigating climate change. The most suitable feedstock choice, processing technology, and potential bioproducts have to be determined on a case-by-case basis. The environmental aspects, benefits, and impact of biorefinery processes are usually assessed by performing environmental impact assessment (EIA), best available technology (BAT) analysis, life cycle assessment (LCA) or estimation and analysis of process emissions for regulatory compliance. An LCA investigation boundary that spans from the raw material up to the product end disposal is often used for evaluating biorefinery projects and is referred to as "cradle-to-grave." Alternatively, a "cradle-to-gate" boundary is also employed in some cases, for which the end point is considered to be the factory gate. LCA results can be employed by biorefinery stakeholders to help make well-informed decisions [62].

Approaches to LCA can be categorized as attributional (ALCA) and consequential (CLCA) [63]. ALCA takes into account the environmental impacts (pollutants, resources, and exchange between processes) based on the history of a product. CLCA extends further to describe the potential environmental consequences, which result due to changes between alternative raw materials, processes, or products. In CLCA, the impacts and environmental consequences considered are not limited to the "cradle-to-grave" investigation boundaries of a product system. Hence, reliable assumptions must be made for forecasting, modeling, and quantifying impacts to avoid uncertainties. The choice of approach is usually guided by the study context and the results required for decision-making. For integrated biorefinery projects in particular, the use of CLCA is suitable, because numerous consequences occur outside the life cycle of a given biorefinery process or product.

In this study, potential environmental consequences and incremental impacts of integrating lignin precipitation processes at an existing Kraft pulp and paper mill are calculated. CLCA is used as an analytical tool, and environmental analysis is performed following the standard practices defined by ISO 14040 [64], including goal and scope definition, inventory analysis, impact assessment, and interpretation. The goal in this study was to compare the environmental results of lignin precipitation technologies, using the consequential impact perspective. The implemented approach for defining system boundaries in this work is the CLCA, along with the system boundary expansion and cut-off procedure. To perform the cut-off procedure for eliminating similar processes from the system boundary, it is assumed that the capacity of the existing pulp production line is maintained constant, and the case study mill will produce the same amount of products, before and after lignin precipitation. Moreover, the analysis scope was considered as "cradle-to-gate," since it was assumed that the precipitated lignin from LignoBoost™ and LignoForce System™ technologies have the same post-processing and end-use application, the same end-of-life treatment, and the same final disposal. The system boundary encompassed the lignin precipitation process from black liquor, all the input mate-
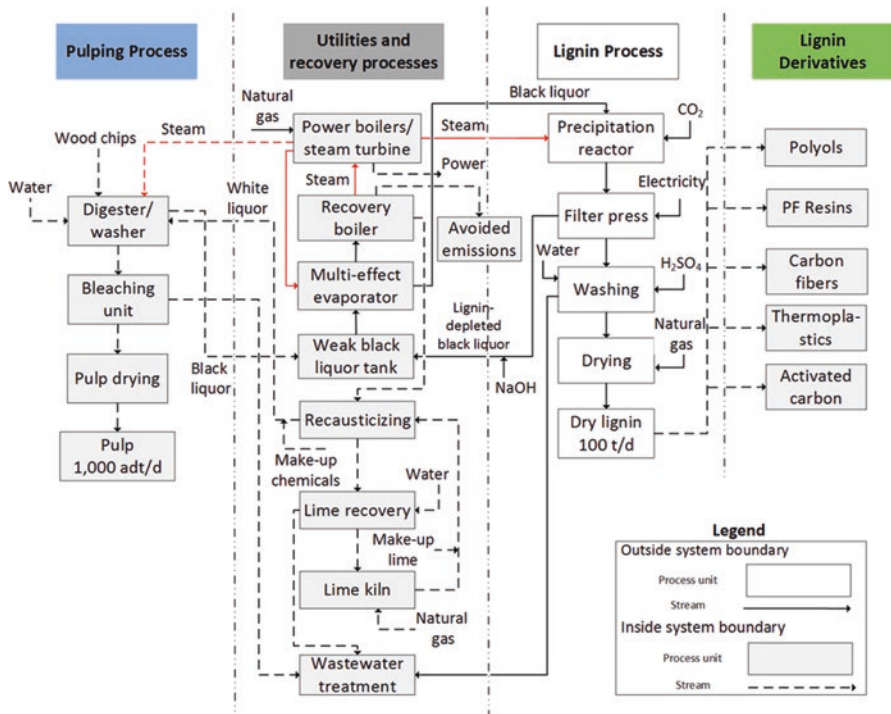
Fig. 13.3 LCA system boundaries and functional units

rial and potential emissions, as well as incremental changes on the mill's process, particularly on the existing evaporators, recovery boiler, and energy plant, after biorefinery integration. Figure 13.3. illustrates the system boundary that is defined for this analysis.

In this study, the functional unit was defined as 100 t/day of dry-lignin (95 % dryness) produced from both LignoBoost™ and LignoForce System™ technologies. Due to the cut-off procedure selected, the existing pulp and paper mill product was not included in the functional unit. Life cycle inventory (LCI), including biomass, chemicals, energy, water, other resource consumptions and emissions were calculated. Available data from the Kraft mill, mass, and energy balance results of lignin precipitation technologies, results associated with incremental impacts on the exiting Kraft process, and published information from technology providers were used as references for characterization of the LCI. In the last step, which is the life cycle impact assessment (LCIA), inventory results were converted into environmental impacts. The objective is to aggregate the relative contribution of inventory data in terms of emissions and resource consumption to the equivalent environmental impacts. In this study, end-point or damage impact categories were selected as environmental metrics to quantify the environmental performance of lignin precipitation technologies. Table 13.4 presents a summarized description of the selected environmental metrics.

Table 13.4 LCA metrics based on damage categories [65]

LCA metric	Definition
Climate change	Global warming potential (GWP) indicates the contribution of GHG to climate change
	$$GWP = \frac{\int_{T}^{0} I_{gas}(t) \times M_{gas(t)} dt}{\int_{T}^{0} I_{CO_2}(t) \times M_{CO_2(t)} dt}$$
	(I: instantaneous radiative forcing by gas at a time t; M: mount of added gas remaining at a time T; T: time horizon)
	Unit of measurement: kilo-tonne CO_2 equivalent
Human health	Includes human toxicity (carcinogenic and non-carcinogenic effects), respiratory effects, ionizing radiation, and ozone layer depletion. Damage to human health expressed as the number of years lost and the number of years lived disabled
	Unit of measurement: disability-adjusted life years per kg emission (DALY/ kg emitted)
Ecosystem quality	Includes terrestrial acidification, terrestrial nitrification, and land occupation.
	Unit of measurement: potentially disappeared fraction over a certain area and during a certain time per kg of emitted substance (PDF·m²·year/kg emitted)
Resources	Includes mineral extraction and non-renewable energy consumption. Modelling is based on size of reserves, extraction rates, demand, and substitution potential of the resources.
	Unit of measurement: amount of additional primary energy required per unit of mineral and total non-renewable primary energy for energy carriers (MJ/ unit consumed)

All of these environmental metrics are incorporated in the I-BIOREF software developed by Natural Resources Canada. The software enables modeling of any established biorefinery process or pathway and the simultaneous assessment of technical performance, economic viability, and environmental footprint. This tool also facilitates benchmarking of the selected biorefinery option against other well-established options. In addition, the incorporation of graphical capabilities makes it possible to develop the process flow diagram of a biorefinery that is integrated into an existing mill or on a standalone basis. The incorporation of pulp and paper process models and a comprehensive library of well-established biorefinery technologies – independently or in combination – enables the simulation of a wide range of plausible "what-if" scenarios. Models available in I-BIOREF include: pulp and paper processes (Kraft pulp and thermomechanical mills); biomass pretreatment processes (steam explosion, liquid hot water, acid hydrolysis, instant controlled pressure, organosolv, subcritical and supercritical fluids, ionic liquids, torrefaction); pre-extraction processes (supercritical fluids, hot water, enzymatic hydrolysis); lignin recovery processes (LignoBoost™, LignoForce System™, SLRP™); conversion processes of sugars from lignocellulosic biomasses (detoxification, fermentation, separation/purification); and thermochemical processes (gasification, pyrolysis,

catalysis). Each model is supported by a detailed mass and energy balance and related key process characteristics, including electricity, steam, water, biomass, fuel, chemicals, and effluents. Process flow diagrams of the selected pulp and paper process and biorefinery technology are also provided to help visualize the main unit operations involved. Pre- and post-evaluation rules exist to verify the consistency of data and calculations. The inconsistencies are diagnosed and the user is informed about the invalid data, so that only valid data is used when creating process flow diagrams.

13.4 Industrial Case Study Description

13.4.1 Host Mill for Lignin Recovery Processes

The industrial case study mill is a Canadian Kraft mill that aims at extracting up to 100 t/day of lignin from its black liquor stream (about 33,300 dry-t/year). The mill produces 1000 odt of pulp per day, for 333 operational days of the year. It consumes 2300 adt per day of softwood biomass, a mix of fir, spruce, and pine. The mill also generates around 13,800 t/day of black liquor, with a 14 % solid content. Cooking chemicals used in the mill are provided mainly through recovery of spent chemicals and by purchasing makeup chemicals, such as lime and sodium hydroxide if necessary. The chemical recovery is efficient, so the amount of purchased makeup chemicals is low. The water consumption is about 3 410 m^3/h, and the process water is procured from the nearby river. The mill has two power boilers, each with a maximum hourly capacity of 230 tonnes of steam. Natural gas and hog fuel can be used as fuel for the power boilers. The recovery boiler can produce up to 280 t/h. The overall steam consumption in the mill is 37.5 GJ/t of produced pulp. The mill is electrically self-sufficient, as the electricity required by the process is produced in the mill. There are three steam-turbines: two back-pressure turbines that produce 32 MW of electricity combined, and one condensing turbine that produces 25 MW of electricity. The electricity production exceeds the mill requirements, and the surplus electricity is sold to the grid. A general overview of the Kraft pulping mill is shown in Fig. 13.4. Reported greenhouse gas emissions for the case study mill were approximately 99,200 tonnes CO_2-eq in 2013.

13.4.2 Lignin Recovery

By extracting lignin from black liquor, a portion of the load on the recovery boiler will be lifted, and pulp production can be increased. However, the amount of lignin that can be extracted is limited, because it is necessary to maintain the higher heating value (HHV) of the liquor entering the recovery boiler within its operational range for high thermal efficiency. Based on this operational constraint, the
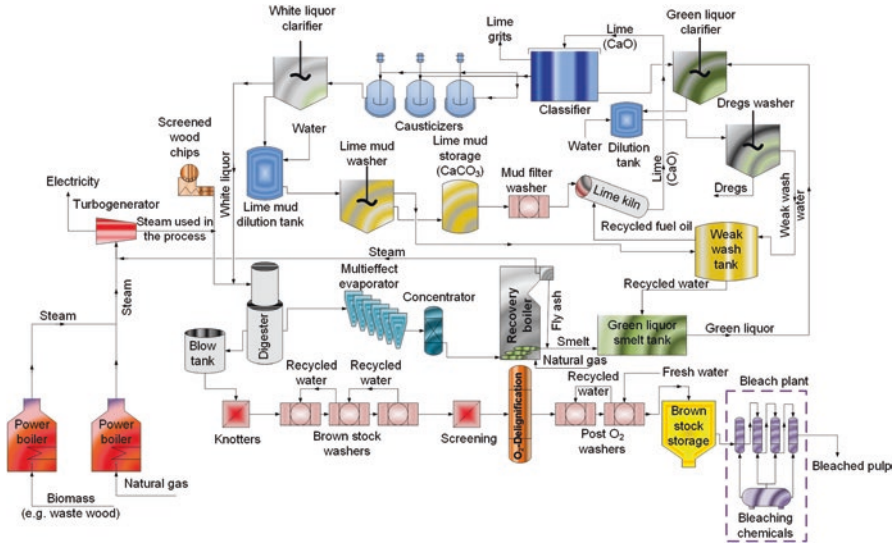
Fig. 13.4 General overview of Kraft pulping process
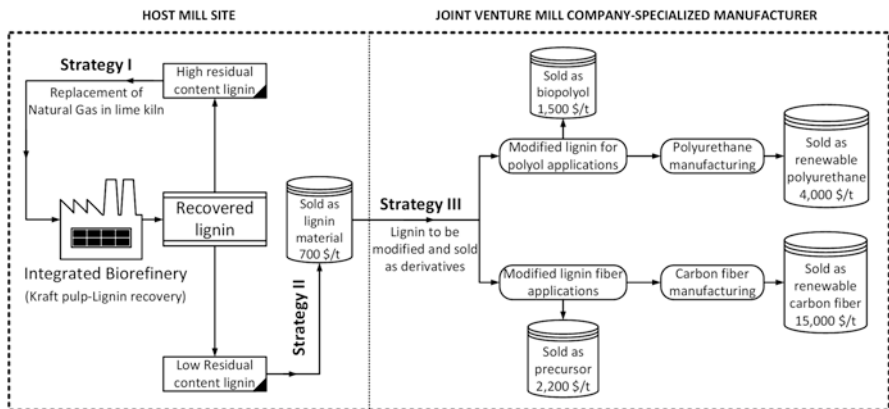
Fig. 13.5 Lignin recovery and lignin valorization pathways

maximum lignin extraction in this case study equals 125 t/day of lignin. Figure 13.5 illustrates the various strategies for large-scale valorization of lignin recovered from black liquor. It also provides the selling prices of the targeted lignin derivatives. As shown in Fig. 13.5, three major strategies can be considered. The first strategy (I) is to recover lignin from black liquor and use it internally to replace natural gas consumed in the lime kiln. Thus, the mill will improve its environmental footprint, while gaining experience in lignin recovery. More specifically, an average lignin heating value of 25 MJ/kg is assumed for the recovered lignin. The second strategy (II) involves modifications of the lignin at the mill for producing intermediate

Table 13.5 Implementation scenario over the project lifetime

Recovered lignin applications	0–1 year	1–2 year	2–5 year	5–10 year	10–15 year
Fuel	100%	40%	–	–	–
High-purity lignin	–	60%	60%	–	–
Polyols	–	–	20%	50%	20%
CF precursors	–	–	20%	50%	10%
PU	–	–	–	–	30%
CF	–	–	–	–	40%

products, namely carbon fiber precursors and biopolyols. The third strategy (III) consists of establishing a joint venture (JV) with a specialized manufacturer to produce and retail carbon fibers and polyurethane, along with biopolyols and carbon fiber precursors. A JV partnership enables the pulp and paper mill to share the investment costs, as well as enjoy complementary intellectual property and know-how, while externalizing the risks associated with manufacturing new products.

Based on the strategies described above, an illustrative plausible implementation scenario was developed. In the first year after construction, the lignin recovery process is expected to run at 70% of its full capacity, and the recovered lignin is combusted as fuel in the lime kiln of the Kraft pulp process. After 12 months of operation, full production capacity (100 t/day) is reached. The diversification of the product portfolio commences with sales of 60% of the high purity lignin, while the remaining 40% is combusted. A joint venture, established in the third year, has the mandate to manufacture and sell polyurethane (PU) and carbon fiber (CF) derived from high-purity lignin, along with biopolyols and precursors. Half of the equity for the joint venture company belongs to the mill company. Both capital investments and benefits are shared equally. From the third to the fifth year of production, the sales targets are: 60% for high-purity lignin, 20% for polyols, and 20% for CF precursors. From the sixth to the tenth year, the new intermediate product sales represent 50% of the lignin sold as biopolyols and 50% as CF precursors. The final phase is reached after 10 years, and the product portfolio comprises biopolyols (25%), CF precursors (25%) and high-purity lignin (50%). Table 13.5 summarizes the expected end-use of recovered lignin during the project lifetime.

13.4.3 Lignin Derivatives

For PU manufacturing, which involves the chemical modification of lignin, about 0.6 kg of polyols suitable for PU flexible foam production is obtained for each kg of lignin. The maximum amount of conventional polyol that is substituted is 20%. It is assumed that the quality of PU foam produced is unchanged. Based on published data [36], the typical formulation selected to produce 1 kg of flexible polyurethane foam is 0.021 kg of water, 0.71 kg of polyol blend, 0.28 kg of toluene diisocyanate

(TDI), 0.011 kg of surfactant and additives. In addition to the polyurethane foam, 0.019 kg of solid waste and 0.051 kg of gaseous emissions are produced from the process. The feed of polyol, isocyanate, and other constituents into a mixing system is controlled, and the product is discharged into a foam mold after a predetermined residence time. The foam, in the form of a block, is cut into the desired dimension. Although different types of polyurethane can be produced from a common feedstock, the production economics depend on the stoichiometric ratio of the polyols to polyisocyanates, equipment costs (mainly molds and cutting machines), the catalysts for controlling the reactions, the blowing agents, and the amount of additives used. Common additives include pigments, flame retardants, anti-bacterial agents, UV stabilizers, and density-improving fillers.

The CF case study involves the manufacturing of a lignin-based carbon fiber, composed of high-purity lignin and PAN for the automotive market. Data availability on the equipment and operation costs is limited. The most detailed source of information is the Oak Ridge National Laboratory (ORNL), which operates a state-of-the-art demonstration facility and provides manufacturing costs for several precursors. In addition to an enhanced green profile, lignin-based precursors are cost-competitive in comparison to conventional PAN precursors [66–70]. An Excel spreadsheet model was developed for calculating mass and energy balances and estimating OPEX and CAPEX costs. Overall, 1 kg of melt-spinnable lignin yields 0.75 kg of lignin-based carbon fiber composed of high-purity lignin (65 %, w/w) and PAN (35 %, w/w). Based on published data [69], the production of 1 kg of CF from a lignin-based precursor requires 460 MJ. Therefore, the avoided CO_2 emissions due to lignin content of carbon fiber were estimated to be about 4.55 kg of $CO_{2\text{-eq}}$ per kg of CF or 3.41 kg of $CO_{2\text{-eq}}$ per kg of melt-spinnable lignin consumed. Carbon fiber manufacturing is operated continuously and requires between 8 and 12 main pieces of equipment, including creel stations, winders, oxidation ovens, medium- and high-temperature furnaces, surface treatment units, and waste gas treatment units.

13.5 Process Impacts, Economic and Environmental Assessment

The extraction of lignin from black liquor reduces the Kraft process recovery boiler load. This in turn makes it possible to increase the biomass throughput and the pulp production, provided that there is enough capacity in the existing process facilities, particularly in the recovery boiler. Another major impact that lignin extraction has on the Kraft process relates to steam consumption and generation. Due to the lignin extraction, the heating value of the black liquor going to the recovery boiler decreases, which results in less steam production. On the other hand, the recycled stream from the lignin extraction technology dilutes the stream going to the evaporator system. Therefore, to achieve the same level of concentration at the outlet of the evaporator system, more steam is needed. These two factors, along with steam

requirements of the lignin extraction technology, increase the overall steam demand. If the level of steam production is held constant, a large portion of the produced steam will be needed for the evaporator system and for compensating the steam production decrease in the recovery boiler. Thus, less steam will be available for turbines, and the electricity generation will drop. For the case study mill, at a fixed pulp production rate, the steam production must increase by 15% to provide the steam required for the LignoBoost™ technology, and to keep the same level of electricity generation. The consumption of other resources due to an increase in pulp production was studied as well. Figure 13.6a, b depict the increase in biomass, electricity, steam, and fuel (natural gas) used in the power boilers as a result of pulp production increase. Typically, an increase of pulp production by up to 20% leads to higher biomass, electricity, steam, natural gas, and water consumption by 20%, 20%, 10%, 10%, and 20%, respectively.

13.5.1 Economic Assessment Result of Lignin Recovery

In this section, the economic assessment of the LignoBoost™ and LignoForce System™ is presented. Since SLRP and membrane-based lignin recovery processes are not yet commercially implemented, industrial data are not available. Therefore, they are not considered in economic and environmental assessments. The assessment includes the estimation of capital cost, product cost, and economic metrics. For capital cost, the chemical engineering plant cost index was used to adjust the cost of equipment. Moreover, the impact of the lignin market price on the economic metrics is analyzed in the case of the LignoBoost™ technology. Similar analysis can also be carried out for the LignoForce System™ technology.

To estimate the capital cost, the installed cost of equipment was calculated. The capacity of process equipment was estimated based on a comprehensive mass and energy balance. Other parameters involved in calculating the cost of process equipment include the reference price and reference capacity, the year index for the year-of-quote and the year-of-project, the scaling factor, and the installation factor. All equipment costs were indexed to 2015. The total installed equipment cost (TIEC) and the total purchased equipment cost (TPEC), which excludes the installation factor, were used in estimating other direct capital cost items, comprising piping (20% of TPEC), electrical (15% of TPEC), instrumentation and controls (20% of TPEC), service facilities and yard improvements (40% of TPEC), and capital spares (5% of TIEC). The sum of all direct cost items gives the direct cost or total installed cost (TIC). Indirect cost items were estimated based on either TIC or fixed capital investment (FCI): engineering and supervision (5% of TIC), construction expenses and contractor fees (6% of TIC), legal expenses (1% of FCI), and contingency (12% of FCI). Finally, start-up and working expenses are considered as 8% of FCI and 10% of total capital investment (TCI), respectively. The sum of direct costs, indirect costs, start-up expenses and working capital yields the TCI. The breakdown of capital investment for both technologies is presented in Table 13.6.
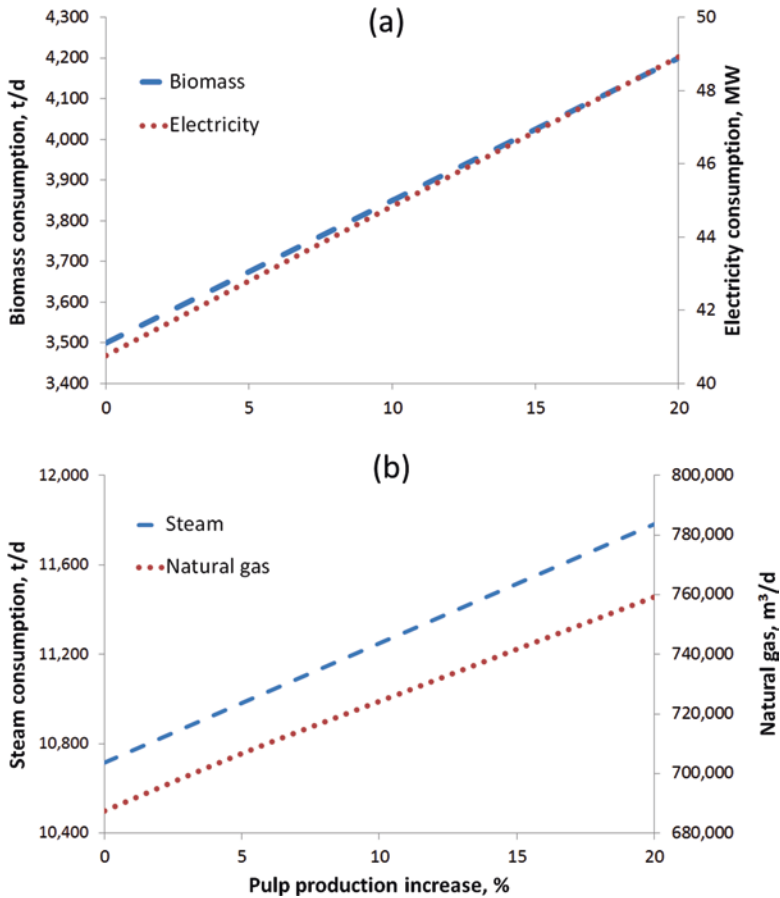
Fig. 13.6 Technical impact of pulp production increase on resource utilization: (**a**) biomass and electricity, (**b**) steam and natural gas

Product costs consist of direct costs and indirect costs. Direct costs comprise the cost of chemicals, including carbon dioxide, sulfuric acid, sodium hydroxide, and oxygen in the case of the LignoForce System™, as well as the cost of steam, electricity, water, and fuel (in this case study, natural gas is considered as the fuel for drying lignin). These costs were calculated based on the specific consumption of each resource by the process and the mass and energy balance calculations. Specifically, the steam cost calculation considered three cost contributors: the cost of steam for lignin extraction technology; the cost of extra steam required in the mill evaporator system to concentrate the black liquor stream diluted by the recycled stream from the lignin extraction process; and the cost associated with the additional steam that must be produced to compensate the steam production loss in the recovery boiler, due to partial lignin removal from the black liquor.

Table 13.6 Breakdown of capital cost (2015 USD) for two lignin recovery technologies

Cost item ($) (2015 USD)	LignoBoost™	LignoForce™
Total purchased equipment costs	6,692,000	9,296,000
Total installed equipment costs	10,202,000	13,462,000
Total direct costs	18,408,000	24,825,000
Total indirect costs	5,078,000	6,848,000
Fixed capital investment	23,486,000	31,673,000
Total capital investment	28,184,000	38,007,000
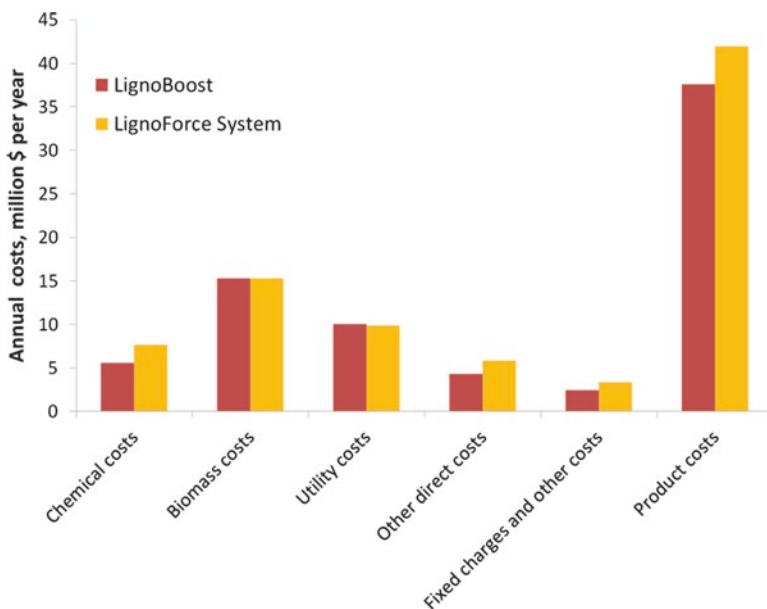
Fig. 13.7 Breakdown of annual operating expenses for LignoBoost™ and LignoForce System™ based on publicly available data

Other direct cost items were estimated as follows: labor costs including operating labor, operating supervision, and clerical assistance (11% of product cost), maintenance and repairs (8% of fixed capital investment), operating supplies (15% of maintenance costs), laboratory charges (2% of product cost), and patents and royalties (3% of product cost). Indirect costs include fixed charges and other costs. Fixed charges in this study included depreciation (linear over project lifetime) and insurance (0.8% of fixed capital investment). Finally, other indirect costs related to plant overhead (5% of product cost), administrative costs (2% of product cost), distribution and marketing (5% of product cost), and research and development (5% of product cost). Product cost breakdown is shown in Fig. 13.7.

The revenue was calculated for each technology based on a lignin price of $700/t. Incremental revenue from a 15% pulp production increase was also considered,

Table 13.7 Economic benchmarking of the LignoBoost™ process and LignoForce System™

	PP (year)	IRR (%)	NPV ($)	ROI (%)	ROCE (%)	EBITDA (M$)	RTMU	CAB ($/t)
LignoBoost™	2.3	32	41.2	42	62	18.9	0.53	46,250
LignoForce System™	4.2	19	16.5	24	31	13.8	0.36	36,830
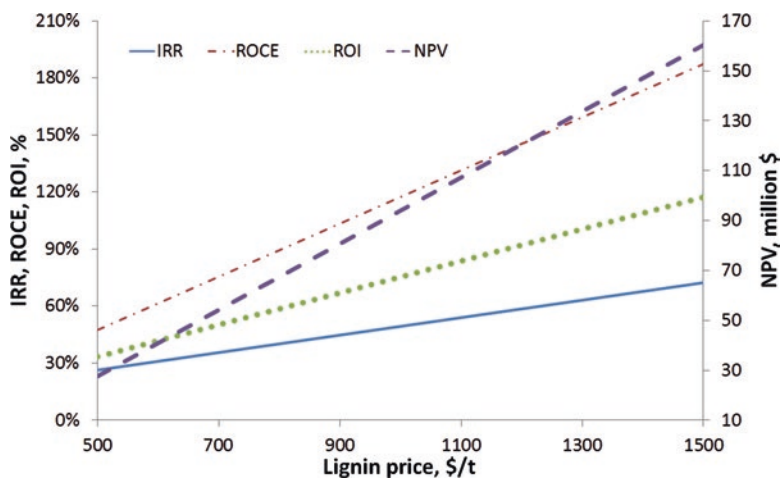
Fig. 13.8 Key economic metrics as a function of lignin price for the LignoBoost™ process. See Table 13.4 for definitions of economic metrics

based on a pulp price of $750/odt. Table 13.7 illustrates the economic metrics calculated for the two technologies.

Figure 13.8 shows the impact of the market price of lignin on the economic performance of LignoBoost™ technology for a recovery rate of 100 t/day of lignin and a pulp production increase of 15 %. It also illustrates that lignin extraction coupled with a pulp production increase offers strong economic performance. Even with a lignin market price of $500/t, the project's IRR is above 20 %, which is considered to be a threshold for biorefinery investment. However, if there is no pulp production increase, the IRR drops to 15 %. In this case, to meet the 20 % IRR threshold, the lignin price must be $780/t, which is above the base case price (i.e. $700/t). Similar analysis can be carried out for the LignoForce System™, and no difference in the observed trends is expected for the technology.

The improvement of economic metrics due to government subsidies (federal and provincial combined) is illustrated in Fig. 13.9. In this case, 43 % of the total capital cost is funded by the government. Subsidies become crucial in cases where the mill does not have the capacity to increase its pulp production. Considering the case study mill without an increase in pulp production, the subsidies improve the IRR from 15 to 32 %, which is higher than the minimum acceptable 20 % threshold.
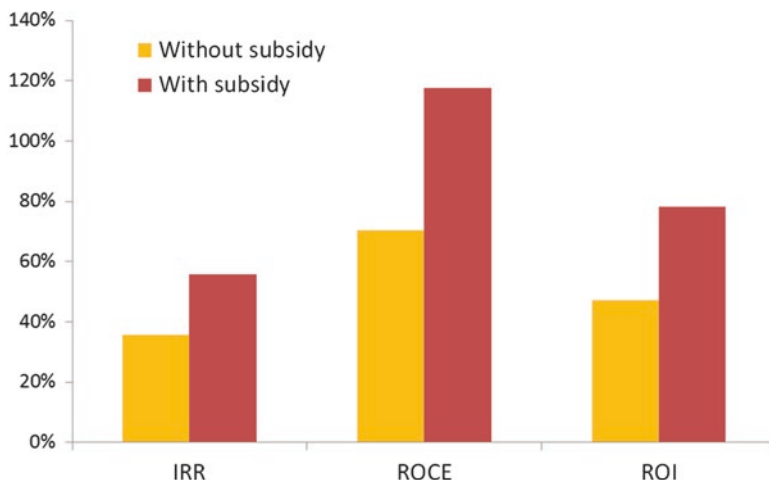
Fig. 13.9 Economic metrics with and without government subsidies (LignoBoost™). See Table 13.4 for economic definitions

13.5.2   Environmental Assessment Results

Consequential LCA results were evaluated for analyzing the incremental environmental impacts of integrating lignin precipitation processes into an existing Kraft pulp and paper mill. The system boundary that is presented in Fig. 13.3 was the basis for the results evaluation. The main assumptions for implementing the cut-off procedure, defining the system boundary, and quantifying the life cycle inventory for LignoBoost™ and LignoForce System™ technologies are as follows:

- Lignin from both technologies has similar application and end-of-life.
- Combustion credit at the recovery boiler following the lignin precipitation is considered to be identical for both technologies.
- Recovered sodium from the electrostatic precipitator and bleaching plant (make-up sodium) are considered sufficient to compensate for the process losses. However, sodium hydroxide required for neutralizing the recycled stream from the lignin process to the existing evaporators is included in the LCA inventory.
- CO_2 that is used in the precipitation reactor is recycled back to the evaporator and the recovery boiler. The CO_2 reacts with Na at the recovery boiler, leading to an increase of Na_2CO_3 in the smelt stream.
- The waste water treatment plant (WWTP) installed at the Kraft pulp mill has adequate capacity for treating the incremental effluent streams.
- The capacity of the mill's existing evaporator system is sufficient to concentrate the spent and filtrate streams, which are recycled from the lignin recovery process and mixed with the weak black liquor.
- Natural gas is used for lignin drying.
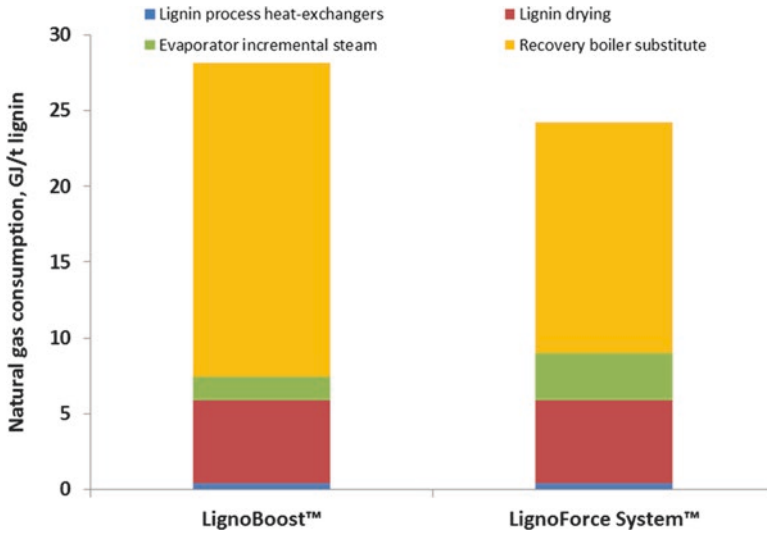
Fig. 13.10 Energy balance results and natural gas consumption for integrated LignoBoost™ and LignoForce System™ technologies (GJ/t lignin)

- Incremental steam demand for the Kraft process and lignin technologies is supplied by a natural gas power boiler.
- Required electricity for the Kraft and biorefinery processes is provided by the grid. However, the case study mill generates power from existing steam turbines, which is then sold to the grid.
- The transportation distance for chemicals and consumables transferred to the mill gate is 200 km.
- Differences in the biorefinery process units for both lignin technologies are considered in the analysis, specifically two filter presses in LignoBoost™ and one press in the LignoForce System™.
- The LCA analysis considers a decrease of TRS emissions in the LignoForce System™ technology as a result of using an oxidation reactor prior to lignin precipitation.

Calculations of energy and steam demand include three major components: lignin technologies, incremental steam demand for the existing evaporators, and additional steam that must be produced to compensate for steam production loss in the recovery boiler. Recovery and power boilers are used to produce high-pressure (HP) steam in the industrial case study mill. The HP steam is sent to the existing steam turbines for generating power, which is sold to the power gird, and medium- and low-pressure steam required for the Kraft and lignin processes. The incremental energy requirement for the mill after integration of lignin recovery processes was analyzed, and the results in terms of natural gas consumption are presented in Fig. 13.10. The increase in fuel demand at the mill evaporator (5 % of the total fuel demand for the LignoBoost™ process and 9 % for the LignoForce System™) is due

to the additional steam required for concentrating the black liquor, which has been diluted by the recycled spent liquor and filtrate streams from the lignin recovery process. Since it is mandatory for the mill to maintain its power production capacity, the compensatory steam demand is met by combusting more natural gas in the existing power and recovery boilers. The results illustrated in Fig. 13.10 indicate that natural gas consumption for the recovery boiler in the integrated Kraft mill-LignoBoost™ process is similar to the integrated Kraft mill-LignoForce System™. To compensate the steam production loss at the existing recovery boiler, the additional fuel demand accounts for approximately 75 % of the total required natural gas for both lignin recovery technologies.

Both lignin recovery technologies have comparable fuel consumption: about 17 % of the total natural gas consumption for the integrated Kraft mill-LignoBoost™ process and about 16 % for the integrated Kraft mill-LignoForce System™. When both lignin recovery technologies are compared independently to the host Kraft mill, about 93 % of the natural gas consumption in each is attributed to the lignin dryer. However, the natural gas consumption for the LignoForce System™ is 5 % higher than the LignoBoost™ process, due to higher natural gas demand at the Kraft mill evaporation train to compensate for steam loss at the existing recovery boiler.

A breakdown of the cradle-to-gate (i.e. gate of the mill) environmental results for the integrated LignoBoost™ and LignoForce System™ technologies is presented in Table 13.8. Both technologies have similar impact trends. Natural gas consumption for producing the steam required for the process is the most important contributor to climate change and resource consumption, while chemical consumption has the highest contribution to human health and ecosystem quality. More specifically, natural gas contribution to climate change impacts is 79 % of the total for the LignoBoost™ process and 70 % for the LignoForce System™. Chemicals make up 54 % of the ecosystem quality impacts for the LignoBoost™ process and 60 % for the LignoForce System™. Higher electricity consumption in the LignoForce System™ resulted in impacts that were twice as high as those of the LignoBoost™ process. The effect of electricity consumption on the overall environmental results was less than 10 % for both lignin recovery technologies. In this analysis, the avoided impacts due to reduced TRS emissions in the LignoForce System™ were considered. As illustrated in Table 13.8, the main impact of the reduced TRS emissions was on ecosystem quality.

13.5.3 Economic Assessment for Lignin Derivative Production

It is estimated that up to 425 t/day of PU can be produced from the 100 t/day of lignin recovered from black liquor. At such a production scale, the production process will be operated continuously. The estimated CAPEX for the PU plant to be up and running is $2000/t of installed annual capacity.

The cost of PU foam mainly reflects the cost of the raw materials (polyol at $3500/t, toluene diisocyanate at $2350/t, surfactant at $500/t, and additives at

Table 13.8 Summary of LCA results for LignoBoost™ and LignoForce System™ technologies

		Chemicals	Natural gas	Dewatering unit	Electricity	Avoided TRS	Transport	Total
LignoBoost™	Climate change (kg CO_{2-eq})	52,140	228,123	2274	5398	–	2183	290,118
	Human health (DALY[a])	0.053	0.029	0.003	0.005	–	0.002	0.092
	Ecosystem quality (PDF[b] m²·yr)	10,349	5616	1415	796	–	863	19,038
	Resources (MJ primary)	8.48E+05	4.33E+06	3.26E+04	9.18E+04	–	3.55E+04	5.34E+06
LignoForce System™	Climate change (kg CO_{2-eq})	81,294	238,438	1783	12,956	0	3668	338,139
	Human health (DALY)	0.077	0.03	0.003	0.011	−0.003	0.003	0.12
	Ecosystem quality (PDF·m²·yr)	15,150	5870	1109	1909	−60	1450	25,428
	Resources (MJ primary)	1.33E+06	4.53E+06	2.56E+04	2.20E+05	0	5.97E+04	6.16E+06

[a]DALY stands for the disability-adjusted life year
[b]PDF stands for the potentially disappeared fraction of species

$10,000/t), which represents 80 % of the total production cost in this case. The use of lignin as the polyol source can potentially reduce costs and avoid emissions. Specifically, the market price for conventional polyols is about $3500/t, while the price of lignin could be as low as $700/t. Assuming the transformation cost for lignin into polyols requires at least $800/t more, the cost margin is an incentive for the use of lignin-derived polyols in PU foam manufacturing. Even if the transformation cost were twice as high, significant cost savings could still be achieved. The key to economic feasibility is thus the cost-efficient transformation of the lignin into polyols. The CO_2 emissions associated with the production of 1 kg of flexible polyurethane foam from petroleum-derived polyols and TDI is about 3.9 kg [36]. It is estimated that after substitution of 20 % of the petroleum with lignin-derived polyols, the CO_2 emissions reduction will total about 14 %.

The sensitivity of the ROCE for flexible PU production with respect to the key cost drivers is illustrated in Fig. 13.11a. The ROCE threshold, below which investment in PU production will not be cost-effective, must be determined on a case-by-case basis. A threshold of 20 % was considered in the case of PU production. The high and low bounds for the cost of polyols and polyisocyanates were selected to reflect historic price trends due to oil price fluctuations. The lignin-derived polyol price is the sum of the lignin price and the cost of lignin transformation into a suitable polyol. Given that the raw material cost represents about 80 % of the total production cost, the higher priced petroleum-derived polyol has a greater influence on the profitability of a production process. An increase in the PU foam price would lead to increased profitability, but the price is market-dependent. The effect of introducing bio-polyols is less dominant, because of the substitution ratio maximum value of 25 %. The development of formulations that can tolerate a higher amount of bio-polyols without modifying the morphological and mechanical properties of PU foam would lead not only to significant price reductions, but also to the decoupling of costs from oil price and currency fluctuations.

Using the ROCE metric, economic performance was examined for carbon fibers with different high-purity lignin fractions relative to PAN: CF_{65} (65 %; 35 %) and CF_{100} (100 %; 0 %). Considering the availability of melt-spinnable Kraft lignin (100 t/day), 15,346 t/year of CF_{65} and 9975 t/year of CF_{100} can be produced. As illustrated in Fig. 13.11b, the base case is expected to have a ROCE of 31 %. This figure also presents the results from the sensitivity analysis for critical parameters. CAPEX intensity for conventional technologies ranges from $15,000 to $19,235/(t/year) and is as low as $9423/(t/year) for emerging technologies, such as microwave-assisted plasma carbonization [66, 70]. Manufacturing costs were evaluated at $11.83/kg with the following breakdown: raw materials ($6.73/kg), utilities ($1.41/kg), labor ($1.41/kg) and depreciation ($1.08/kg). Manufacturing costs and especially the raw material component have the greatest impact on profitability, whereas CAPEX has a moderate impact on ROCE. Fluctuations in the selling price of lignin-based carbon fibers have been studied in the range $11–$17/kg, which represents the targeted price for automotive manufacturers [55]. Considering the importance of the market and the technology risks, a threshold of 30 % is expected for this process. For a better return–to-risk ratio, a phased implementation and a joint-venture partnership is considered in the next section.
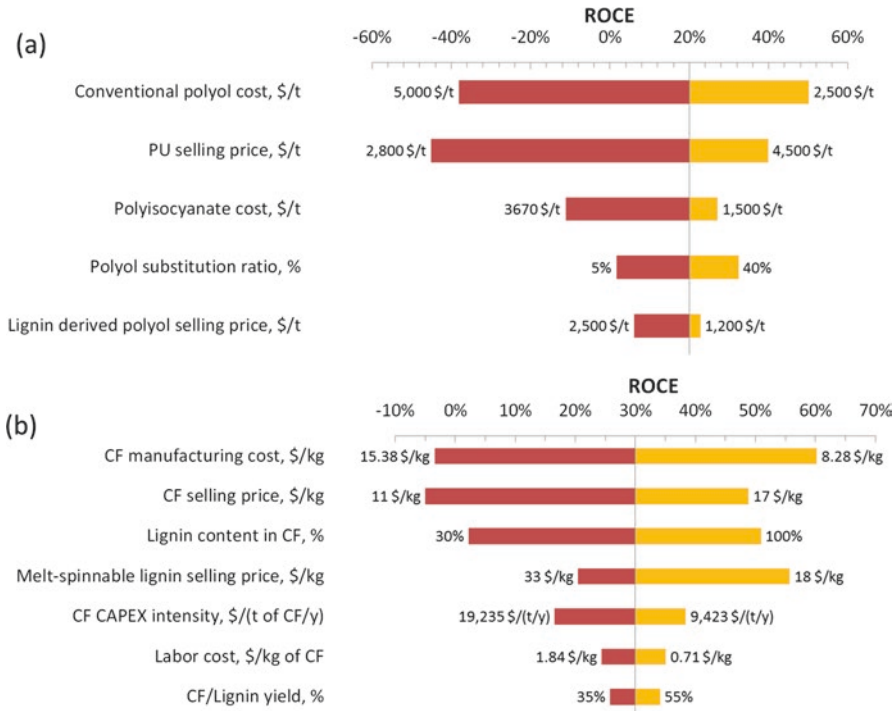
Fig. 13.11 Sensitivity of return on capital employed (ROCE) to process yield and operating costs for (**a**) flexible PU foam production; (**b**) CF production

13.5.3.1 Economic Results for the Implementation Scenario

The cumulative cash position for an integrated biorefinery was evaluated for the same phased-implementation scenario discussed in section 13.4.2, under three different conditions, and is illustrated in Fig. 13.12a–c. It represents the cash that a mill company generates, spends, and accumulates while it diversifies its product portfolio by retrofitting new biorefining processes. It is often correlated to the NPV, which represents the project's value-added for shareholders. However, the cash flow in this study is not discounted (i.e. it does not consider the time value of money). The overall capital investment over the project timeline is about US$398 million, but due to the established joint venture, the mill company will only have to invest 53.5 % of the total sum for all five phases.

For implementation with no increase in pulp production and the absence of government support (Fig. 13.12a), the IRR on the invested capital is 9 %, when the duration of the project is 15 years. Also, the ROCE is negative during the first phase, but positive and increasing for phases 2–5. However, the cash position is negative for most of the project lifetime, due to multiple high investments in years 1, 2, 3, 6, and 11. Although the investments lead to a negative cash position throughout the project lifetime, they are critical for the survival of the mill company.
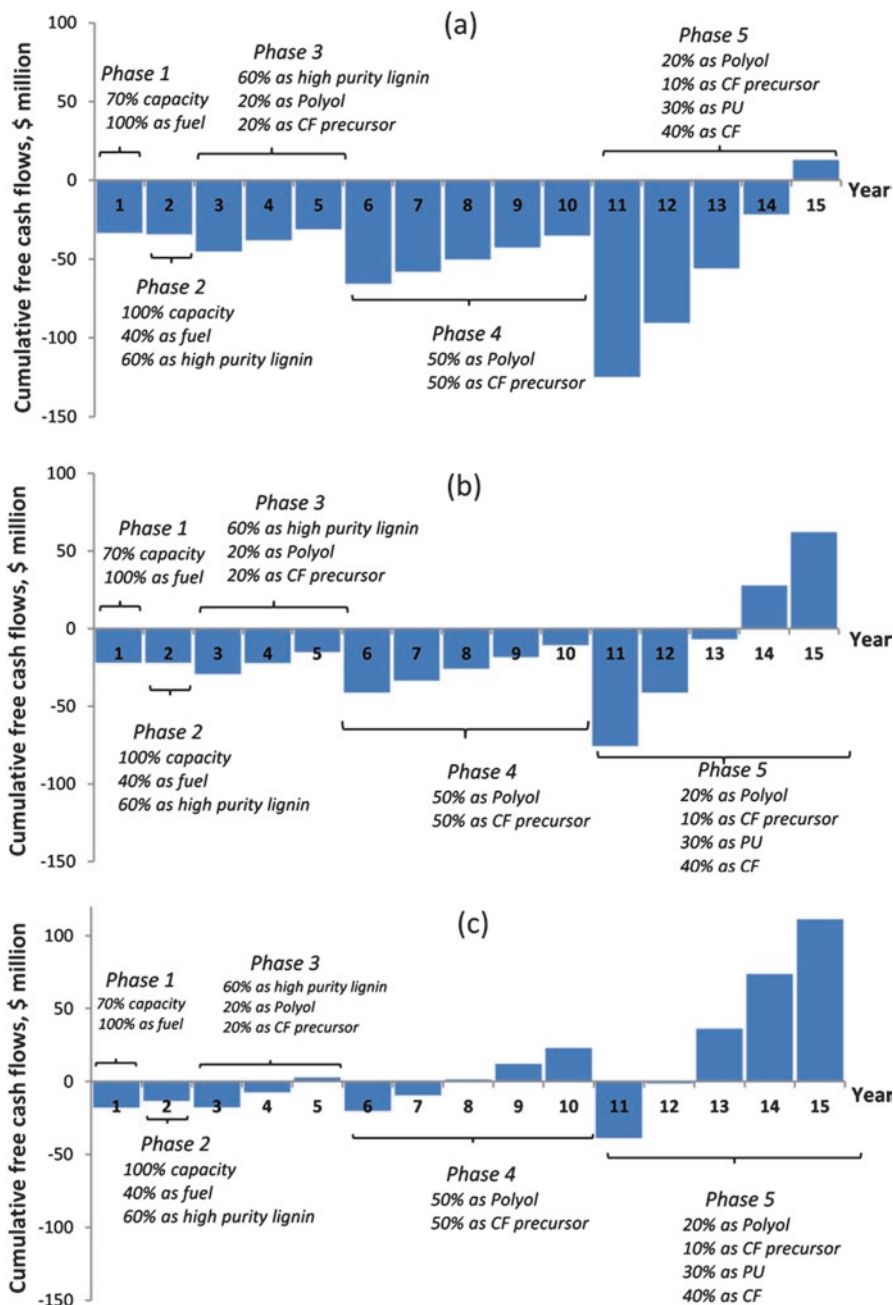
Fig. 13.12 Cumulative cash flow positions over 15 years for the implementation scenario considering (**a**) no pulp production increase without subsidies; (**b**) no pulp production increase with subsidies; and (**c**) 15 % pulp increase with subsidies

When government subsidies totaling US$49.2 million are made available (Fig. 13.12b), gross earnings remain the same as in the previous condition, but the capital invested by the mill company is lower. Consequently, the cash position is substantially improved (by at least 34 % in year 1 and as much as 84 % in year 13), thereby mitigating bankruptcy risk. For the same project duration, the IRR for case (b) is higher than for case (a) by 8 %, and the ROCE for each phase exhibits similar trends.

With a 15 % pulp production increase in addition to government funding, higher revenues are generated, and the cash position for phased implementation is the highest (Fig. 13.12c) Specifically, the cash position is positive in years 5 and 8, as well as from year 12 onward. This implies that the investment in the preceding years has been recouped, and the deficit in year 11 (US$38.8 million) is lower than in the previous cases. This case also has the highest IRR (32 %).

13.6 Conclusion and Future Outlook

Lignin, which is one of the primary components of wood, is dissolved into the black liquor during the pulping process. It is mainly burned to recover pulping chemicals and provide part of the steam needed in any Kraft pulp mill. Lignin recovery from black liquor using the LignoBoost™ process has already been demonstrated in the U.S.A. and Finland as a cost-effective technological solution for producing pure lignin. The lignin can be used either as a solid fuel to replace the natural gas consumed in the lime kiln of the Kraft pulp process, or as feedstock to produce a series of chemicals and materials, such as polyurethane and carbon fibers. The energy intensity and environmental footprint can be reduced by about 15–20 % and 30–50 %, respectively, depending on the targeted lignin markets.

Depending on lignin purity and its specific properties, four major applications can be considered: (a) binder (e.g. PF resins, epoxy resins); (b) chemicals (e.g. phenols, polyols, oxidized products, flocculants, dispersants, syngas); (c) high carbon density (e.g. carbon black, activated carbon, carbon fibers); and (d) hydrophobic and thermal (e.g. thermoplastics, packaging, composites). Considering the various technology readiness levels associated with these lignin derivatives, short- and long-term decision-making should be considered for implementing the biorefinery strategy in phases, to mitigate market and technology risks. Such a strategy may help the company efficiently change its operating culture, as it enters new markets with new partners. One of the ultimate corporate goals of any forest-based company is to improve the ability of its biorefinery strategy to generate cash flow from the capital invested in order to produce higher margins, thereby meeting growth targets and improving the company's value through strategic investment.

The results emphasize the importance of a market shift – from low value applications of lignin to higher value products that generate higher earnings – for the successful transformation of pulping mills into integrated biorefineries. Furthermore, phased implementation, coupled with higher revenue and margins from an increase in pulp production, enables the mill company to lower market risk related to price

volatility, as the revenue source is diversified. At the end of the planned transformation, the Kraft mill will produce about 100 t/day of high-purity lignin. The lignin will be transformed by the joint-venture company into about 11.4 t/day of biopolyols, 9.5 t/day of lignin-based CF precursors, as well as 69.1 t/day of PU and 28.5 t/day of lignin-based PAN-CF over 8000 h of operation in a year. The target production capacities for PU and CF represent 1.3 % of the projected global PU market and 6.8 % of the CF market in 2020.

Different purity grades and molecular structures of lignin lead to different industrial and agricultural applications. Therefore, further developments on the functional reactivity of lignin are critical to ensure a wide spectrum of suitable commercial applications.

Clearly, the future commercialization of lignin is assured if international collaborative efforts are made to enable the mobilization of sufficient resources and accelerate the development of pathways for innovative lignin derivatives and their penetration in the industry.

References

1. Björk M, Rinne J, Nikunen K, Kotilainen A, Korhonen V, Wallmo H, Karlsson H. Successful start-up of lignin extraction at Stora Enso Sunila mill. In: VTT (ed) 6th Nordic wood biorefinery conference VTT, Helsinki, Finland; 2015. p. 185–92.
2. Benali M, Périn-Levasseur Z, Savulescu L, Kouisni L, Jemaa N, Kudra T, Paleologou M. Implementation of lignin-based biorefinery into a Canadian softwood kraft pulp mill: optimal resources integration and economic viability assessment. Biomass Bioenergy. 2014;67:473–82. doi:10.1016/j.biombioe.2013.08.022.
3. Lora JH, Glasser WG. Recent industrial applications of lignin: a sustainable alternative to nonrenewable materials. J Polym Environ. 2002;10:39–48. doi:10.1023/A:1021070006895.
4. Kadla J, Kubo S, Venditti R, Gilbert R, Compere A, Griffith W. Lignin-based carbon fibers for composite fiber applications. Carbon. 2002;40:2913–20. doi:10.1016/S0008-6223(02)00248-8.
5. Lin SY. Commercial spent pulping liquors. In: Lin SY, Dence CW, editors. Methods in lignin chemistry. Berlin/Heidelberg: Springer; 1992. p. 75–80.
6. Kannangara M, Marinova M, Fradette L, Paris J. Effect of mixing hydrodynamics on the particle and filtration properties of precipitated lignin. Chem Eng Res Des. 2016;105:94–106. doi:10.1016/j.cherd.2015.11.003.
7. Pasquini D, Pimenta MTB, Ferreira LH, da Curvelo AAS. Extraction of lignin from sugar cane bagasse and Pinus taeda wood chips using ethanol–water mixtures and carbon dioxide at high pressures. J Supercrit Fluids. 2005;36:31–9.
8. Domínguez de María P. Recent trends in (ligno)cellulose dissolution using neoteric solvents: switchable, distillable and bio-based ionic liquids. J Chem Technol Biotechnol. 2014;89:11–8.
9. Arato C, Pye EK, Gjennestad G. The lignol approach to biorefining of woody biomass to produce ethanol and chemicals. Appl Biochem Biotechnol. 2005;123:0871–82.

10. Leaf Resources. Leaf Resources announces cellulosic sugar patent application. Biomass Mag. 2015. http://biomassmagazine.com/articles/11809/leaf-resources-announces-cellulosic-sugar--patent-application. Accessed 8 Apr 2016.
11. Leaf Resources. The business case for the Glycell TM process. Aust. Stock Exch. (ASX). 2015. http://www.asx.com.au/asxpdf/20150309/pdf/42x4ym52g7yf3m.pdf. Accessed 8 Apr 2016.
12. Drewsen V. Ligno-tanning material and process of producing the same from waste sulfite liquor. US Patent 1,303,176 A. 1919.
13. Tomlinson Jr GH, Tomlinson GH. Method of treating lignocellulosic material. US Patent 2,406,867. 1946.
14. Pollak A, Drum LF, Keilen Jr JJ. Method of producing lignin from black liquor. US Patent 2,464,828 A. 1949.
15. Giesen J. Method of treating lignocellulosic material. US Patent 2,828,297 A. 1958.
16. Smolarski N. High-value opportunities for lignin: ready for liftoff. Paris: Frost & Sullivan; 2014.
17. Öhman F, Theliander H, Norgren M, Tomani P, Axegård P. Method for separating lignin from a lignin containing liquid/slurry. US Patent 8,815,052, B2. 2009.
18. Öhman F, Theliander H, Tomani P, Axegard P. Method for separating lignin from black liquor. US Patent 8,486,224 B2. 2013.
19. Kouisni L, Paleologou M. Method for separating lignin from black liquor. US Patent 9,091,023 B2. 2015.
20. Kouisni L, Maki K, Holt-Hindle P, Chan C, Paleologou M. Sulphur profile of the LignoForce System as compared to conventional lignin recovery processes. In: 6th Nordic wood biorefinery conference; 2015. p. 193–200.
21. Zhu JY, Chai X-S, Pan XJ, Luo Q, Li J. Quantification and reduction of organic sulfur compound formation in a commercial wood pulping process. Environ Sci Technol. 2002;36:2269–72.
22. Lake MA, Blackburn JC. Process for recovering lignin. US Patent 20110294991 A1. 2011.
23. Lake MA, Blackburn JC. SLRP™ – an innovative lignin-recovery technology. Cellul Chem Technol. 2014;48:799–804.
24. Bhattacharjee C, Sen D. Treatment of Kraft black liquor using membrane-based separation process. In: Membrane technologies and applications. Boca Raton: CRC Press; 2011. p. 107–19.
25. Jönsson A-S, Nordin A-K, Wallberg O. Concentration and purification of lignin in hardwood kraft pulping liquor by ultrafiltration and nanofiltration. Chem Eng Res Des. 2008;86:1271–80. doi:10.1016/j.cherd.2008.06.003.
26. Arkell A, Olsson J, Wallberg O. Process performance in lignin separation from softwood black liquor by membrane filtration. Chem Eng Res Des. 2014;92:1792–800. doi:10.1016/j.cherd.2013.12.018.
27. Toledano A, García A, Mondragon I, Labidi J. Lignin separation and fractionation by ultrafiltration. Sep Purif Technol. 2010;71:38–43. doi:10.1016/j.seppur.2009.10.024.
28. Satyanarayana S, Bhattacharya P, De S. Flux decline during ultrafiltration of kraft black liquor using different flow modules: a comparative study. Sep Purif Technol. 2000;20:155–67. doi:10.1016/S1383-5866(00)00086-1.
29. Ajao O, Rahni M, Marinova M, Chadjaa H, Savadogo O. Retention and flux characteristics of nanofiltration membranes during hemicellulose prehydrolysate concentration. Chem Eng J. 2015;260:605–15. doi:10.1016/j.cej.2014.09.007.
30. Blanco MA, Negro C, Tijero J, De Jong ACMP, Schmal D. Electrochemical treatment of black liquor from straw pulping. Sep Sci Technol. 1996;31:2705–12.
31. Ghatak HR, Kumar S, Kundu PP. Electrode processes in black liquor electrolysis and their significance for hydrogen production. Int J Hydrogen Energy. 2008;33:2904–11. doi:10.1016/j.ijhydene.2008.03.051.

32. Lora J, Caro R, Cloutier J. Treatment of nonwood black liquors by electrolysis and lignin precipitation. In: TAPPI engineering. Pulping environmental conference. Atlanta: TAPPI Press; 2005. p. 267–71.

33. Rapp H-J, Pfromm PH. Electrodialysis field test for selective chloride removal from the chemical recovery cycle of a kraft pulp mill. Ind Eng Chem Res. 1998;37:4761–7. doi:10.1021/ie980376+.

34. Haddad M, Cloutier J, Labrecque R, Savadogo O, Paris J. Effect of operating parameters on electrodialysis acidification of Kraft black liquor using bipolar membranes. In: International chemical recovery conference; 2014. p. 263–71.

35. Tolbert A, Akinosho H, Khunsupat R, Naskar AK, Ragauskas AJ. Characterization and analysis of the molecular weight of lignin for biorefining studies. Biofuels Bioprod Biorefin. 2014;8:836–56.

36. Boustead I. Polyurethane flexible foam. Brussels: Association of Plastics Manufacturers in Europe-PlasticsEurope; 2005.

37. Cateto CA, Barreiro MF, Rodrigues AE, Belgacem MN. Optimization study of lignin oxypropylation in view of the preparation of polyurethane rigid foams. Ind Eng Chem Res. 2009;48:2583–9. doi:10.1021/ie801251r.

38. Li Y, Luo X, Hu S. Bio-based polyols and polyurethanes. Cham: Springer; 2015. doi:10.1007/978-3-319-21539-6.

39. Prisacariu C. Polyurethane elastomers. Vienna: Springer; 2011.

40. Mills N. Polymer foams handbook. Burlington: Butterworth-Heinemann; 2007.

41. Cui C, Sadeghifar H, Sen S, Argyropoulos DS. Toward thermoplastic lignin polymers; Part II: thermal & polymer characteristics of kraft lignin & derivatives. BioResources. 2013;8:864–86. doi:10.15376/biores.8.1.864-886.

42. Borges da Silva EA, Zabkova M, Araújo JD, Cateto CA, Barreiro MF, Belgacem MN, Rodrigues AE. An integrated process to produce vanillin and lignin-based polyurethanes from Kraft lignin. Chem Eng Res Des. 2009;87:1276–92. doi:10.1016/j.cherd.2009.05.008.

43. D'Souza J, George B, Camargo R, Yan N. Synthesis and characterization of bio-polyols through the oxypropylation of bark and alkaline extracts of bark. Ind Crops Prod. 2015;76:1–11. doi:10.1016/j.indcrop.2015.06.037.

44. Hatakeyama H, Hatakeyama T. Lignin structure, properties, and applications. In: Abe A, Dusek K, Kobayashi S, editors. Biopolym. SE – 12. Berlin/Heidelberg: Springer; 2009. p. 1–63.

45. Jin Y, Ruan X, Cheng X, Lü Q. Liquefaction of lignin by polyethyleneglycol and glycerol. Bioresour Technol. 2011;102:3581–3. doi:10.1016/j.biortech.2010.10.050.

46. Li Y, Ragauskas AJ. Kraft lignin-based rigid polyurethane foam. J Wood Chem Technol. 2012;32:210–24. doi:10.1080/02773813.2011.652795.

47. Bahl O, Shen Z, Lavin J, Ross R. Manufacture of carbon fibers. In: Carbon fibers. 3rd ed. New York: Marcel Dekker Inc.; 1998. p. 1–84.

48. Witten E, Kraus T, Kühnel M. Composites market report 2015. Germany: Federation of Reinforced Plastics; 2015.

49. Chatterjee S, Saito T. Lignin-derived advanced carbon materials. ChemSusChem. 2015;8:3941–58.

50. Maradur SP, Kim CH, Kim SY, Kim B-H, Kim WC, Yang KS. Preparation of carbon fibers from a lignin copolymer with polyacrylonitrile. Synth Met. 2012;162:453–9.

51. Wang S, Li Y, Xiang H, Zhou Z, Chang T, Zhu M. Low cost carbon fibers from bio-renewable Lignin/Poly(lactic acid) (PLA) blends. Compos Sci Technol. 2015;119:20–5. doi:10.1016/j.compscitech.2015.09.021.

52. Garoff N. A novel concept for carbon fiber from renewable resources. 2015. In: 6th Nordic wood biorefinery conference. Helsinki, Finland. 2015. p. 235–8.

53. Lin J, Koda K, Kubo S, Yamada T, Enoki M, Uraki Y. Improvement of mechanical properties of softwood lignin-based carbon fibers. J Wood Chem Technol. 2013;34:111–21.

54. Kubo S, Kadla J. Lignin-based carbon fibers: effect of synthetic polymer blending on fiber properties. J Polym Environ. 2005;13:97–105.

55. Mainka H, Täger O, Körner E, Hilfert L, Busse S, Edelmann FT, Herrmann AS. Lignin – an alternative precursor for sustainable and cost-effective automotive carbon fiber. J Mater Res Technol. 2015;4:283–96. doi:10.1016/j.jmrt.2015.03.004.

56. Mainka H, Hilfert L, Busse S, Edelmann F, Haak E, Herrmann AS. Characterization of the major reactions during conversion of lignin to carbon fiber. J Mater Res Technol. 2015;4:377–91.

57. Norberg I. Carbon fibres from Kraft lignin. PhD thesis, KTH Royal Institute of Technology, Sweden; 2012.

58. Dallmeyer I, Lin L-T, Li Y, Ko FK, Kadla JF. Preparation and characterization of interconnected, Kraft lignin-based carbon fibrous materials by electrospinning. Macromol Mater Eng. 2014;299:540–51.

59. Sprague JC, Whittaker JD. Economic analysis for engineers and managers: the Canadian context. Scarborough: Prentice-Hall Canada Inc.; 1986.

60. Dimian A. Integrated design and simulation of chemical processes. Amsterdam: Elsevier Science B.V; 2003.

61. Peters M, Timmerhaus K, West R. Plant design and economics for chemical engineers. 5th ed. New York: McGraw-Hill Education; 2003.

62. Sandin G, Røyne F, Berlin J, Peters GM, Svanström M. Allocation in LCAs of biorefinery products: implications for results and decision-making. J Clean Prod. 2015;93:213–21.

63. Curran MA. Life cycle assessment: principles and practice. Cincinnati: National Risk Management Research Laboratory Office of Research and Development, U.S. Environmental Protection Agency; 2006.

64. International Organization for Standardization. ISO 14040: environmental management – life cycle assessment – principles and framework; 2006.

65. Jolliet O, Margni M, Charles R, Humbert S, Payet J, Rebitzer G, Rosenbaum R. IMPACT 2002+: a new life cycle impact assessment methodology. Int J LCA. 2003;8:324–30.

66. Warren C. Low cost carbon fiber overview, Presentation at 2010 DOE hydrogen program and vehicle technologies annual merit review and peer evaluation meeting.

67. Paulaskas F, Warren C, Eberle CC, Naskar AK, Ozcan S. Novel Precursor materials and approaches for producing lower cost carbon fiber for high volume industries. In: 17th international conference on composite materials; 2009.

68. Baker DA, Rials TG. Recent advances in low-cost carbon fiber manufacture from lignin. J Appl Polym Sci. 2013;130:713–28.

69. Das S. Life cycle assessment of carbon fiber-reinforced polymer composites. Int J Life Cycle Assess. 2011;16:268–82.

70. Chen M. Commercial viability analysis of lignin based carbon fibre. MBA thesis, Simon Fraser University, Canada; 2014.

Index